Einfluss von neutralen Co-Liganden auf die Struktur und die magnetischen Eigenschaften von Koordinationspolymeren

Kumulative Dissertation

zur Erlangung des Doktorgrades

der Mathematisch-Naturwissenschaftlichen Fakultät

der Christian-Albrechts-Universität

zu Kiel

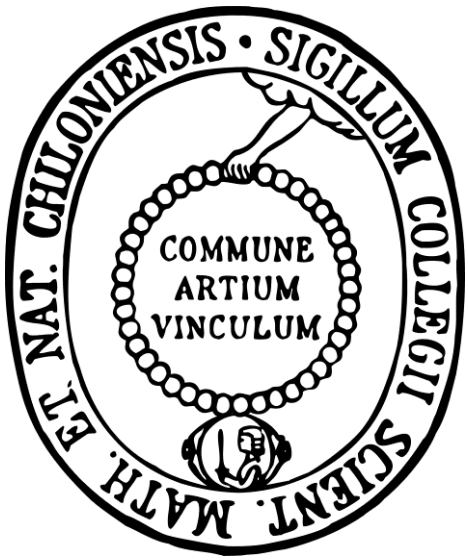

Vorgelegt von

Julia Werner

Kiel, Juli 2015

Referent/in:	Prof. Dr. Christian Näther
Korreferent/in:	Prof. Dr. Wolfgang Bensch
Tag der mündlichen Prüfung:	04.09.2015
Zum Druck genehmigt:	04.09.2015
Gez. der Dekan:	

Kurzzusammenfassung

Den Ausgangspunkt dieser Arbeit bildeten frühere Untersuchungen zur Synthese von ausgewählten Übergangsmetallthiocyanat-Koordinationspolymeren, mit dem Ziel den Einfluss einer chemischen Modifizierung auf die strukturellen und magnetischen Eigenschaften dieser Verbindungsklasse zu untersuchen. Neben der Synthese von Verbindungen mit neuartigen Koordinationsnetzwerken waren insbesondere Verbindungen mit 1D-Strukturen und Kobalt(II) als Metallkation von Interesse, da frühere Untersuchungen belegen, dass diese das seltene Phänomen des Einzelkettenmagnetismus aufweisen. Hier galt es insbesondere den Einfluss des Co-Liganden auf die Parameter zu untersuchen, welche die Leistungsfähigkeit derartiger Materialien beschreiben. Hierzu wurden eine Vielzahl neuer Koordinationsverbindungen mit den Metallkationen Mn(II), Fe(II), Co(II) und Ni(II) sowie unterschiedlichen neutralen Co-Liganden synthetisiert und hinsichtlich ihrer strukturellen, thermischen und magnetischen Eigenschaften systematisch untersucht.

Im Verlauf dieser Untersuchungen wurde eine Reihe von Verbindungen synthetisiert, in denen Schichtstrukturen mit einer für Thiocyanat-Koordinationsverbindungen neuartigen Topologie der Koordinationsnetzwerke beobachtet werden. Diese weisen in Abhängigkeit des Metallkations antiferromagnetisches oder ferromagnetisches Verhalten auf. Des Weiteren wurden auch 1D-Koordinationspolymere erhalten, welche nicht aus den für diese Verbindungen typischen Metallthiocyanat-Ketten aufgebaut sind. In Abhängigkeit der Synthesebedingungen wurden auch für einige Metallkationen Verbindungen mit isomeren Koordinationsnetzwerken erhalten und hinsichtlich ihrer magnetischen Eigenschaften sowie ihrer thermodynamischen Stabilität und ihres Umwandlungsverhaltens untersucht.

Von besonderer Bedeutung sind die hier vorgestellten Untersuchungen an Kobalt-Verbindungen mit Kettenstrukturen, da diese eine langsame Relaxation der Magnetisierung zeigen, welche bislang immer als Einzelkettenmagnetismus interpretiert wurde. Insgesamt wurden drei unterschiedliche Verbindungen erhalten, wobei diese die vorangegangenen Ergebnisse komplettieren und zum ersten Mal allgemeine Schlussfolgerungen zulassen. Ganz offensichtlich lassen sich all diese Verbindungen in zwei Gruppen aufteilen, von denen die eine einen antiferromagnetischen, die anderen einen ferromagnetischen Grundzustand aufweisen. Die Analyse der maßgeblichen magnetischen Parameter ergibt, dass die in den Verbindungen mit einem antiferromagnetischen Grundzustand auftretenden Relaxationen auf die von Einzelketten zurückgeführt werden können, diese daher Einzelkettenmagneten sind. Für die Verbindungen mit einem ferromagnetischen Grundzustand wird ein zu kleiner Mydosh-Parameter, ein zu kleiner präexponentieller Faktor sowie eine ungewöhnlich hohe Energiebarriere für die Spininversion und eine sehr breite und temperaturunabhängige Verteilung der Relaxationszeiten beobachtet. Dies legt den Schluss nahe, dass die in diesen Verbindungen beobachteten Relaxationen nicht auf die von Einzelketten zurückgeführt werden können, sondern dass diese Verbindungen „gewöhnliche“ Ferromagneten sind in denen eine frequenzabhängige Bewegung der Domänenwände auftritt. Diese Ergebnisse sind insofern von Bedeutung, da diese nahe legen, dass die Interpretation der magnetischen Eigenschaften der Stammverbindung $[Co(NCS)_2(Pyridin)_2]_n$ als Einzelkettenmagnetismus gegebenenfalls unvollständig sind und daher erneut untersucht werden müssen. Die Ergebnisse der hier vorgestellten Untersuchungen ergaben auch, dass für all diese Verbindungen nur zwei unterschiedliche Strukturmotive beobachtet werden, die jedoch nicht mit dem magnetischen Grundzustand korrelieren.

Abstract

The origin of this thesis was based on previous investigations on the synthesis of selected transition metal thiocyanato coordination polymers. The major goal of these investigations consists of the influence of a chemical modification onto the structural and the magnetic properties of this class of compounds. In this context, not only the synthesis of compounds with new coordination networks was of interest. First of all compounds with 1D structures and Co(II) as cation were of special importance because previous investigations indicated that they show single chain magnetism. The influence of the co-ligand on those parameters that describe the performance of such materials should be investigated. Therefore, several new compounds with Mn(II), Fe(II), Co(II) and Ni(II) as metal cations as well as different neutral co-ligands were prepared and systematically investigated for their structural, thermal and magnetic properties.

In the course of these investigations several new compounds with layered structures were obtained, in which a completely new topology of the thiocyanato coordination network was observed. Depending on the nature of the metal cation antiferromagnetic or ferromagnetic behavior was observed. Furthermore 1D coordination polymers were obtained that are not formed by the typical metal thiocyanato chains usually observed for such compounds. Depending on the synthesis conditions, compounds with isomeric coordination networks were obtained that were investigated for their magnetic properties, their thermodynamic stability, and for their transition behavior.

The investigations on cobalt compounds with chain structures are of special importance because they showed a slow relaxation of the magnetization, which was previously always discussed as single chain magnetism. Altogether three different compounds were obtained that complete the previous results and that for the first time allow general conclusions. Obviously all of these compounds can be divided into two different groups, of which the first group consists of compounds with an antiferromagnetic ground state, whereas the ground state of the compounds of the second group is ferromagnetic. The analyses of the important magnetic parameters reveal that the relaxations observed in the antiferromagnetic compounds can be traced back to the relaxation of single chains. In contrast, for the compounds with a ferromagnetic ground state, a very small Mydosh-parameter and prefactor as well as an unusual high energy barrier for the spin reversal and a very broad and temperature independent distribution of the relaxation times is observed. This strongly indicates that the relaxations observed in these compounds might not be traced back to the relaxation of single chains and that it is more likely that they originate from the domain behavior of conventional ferromagnets. These results are of extreme importance because they indicate that the interpretation of the magnetic properties of the stem compound $[Co(NCS)_2(pyridine)_2]_n$ as single chain magnet are incomplete and must be reinvestigated. Finally, it is noted that for all of these compounds only two different structural motifs are observed, that do not correlate with their magnetic ground state.

Gewidmet

Karlheinz Werner

Danksagung

Diese Dissertationsschrift wurde in der Zeit von April 2012 bis Juni 2015 am Institut für Anorganische Chemie der Christian Albrechts Universität zu Kiel, im Arbeitskreis von Prof. Dr. Christian Näther angefertigt. An dieser Stelle möchte ich all denen danken, die mich bei der Durchführung und Fertigstellung meiner Arbeit unterstützt haben.

Ein besonderer Dank geht an meinem Doktorvater Herrn Christian Näther, der mir jederzeit zur Seite stand und mich mit vielen Ratschlägen sowie bereichernden Gesprächen unterstützt hat und somit die Entwicklung meiner Arbeit immer positiv beeinflusst hat.

Danken möchte ich Frau Inke Jeß, die mit großer Einsatzbereitschaft unzählige Einkristalle gemessen hat.

Für die Nutzung der experimentellen Ausstattung möchte ich an dieser Stelle herzlichst Herrn Prof. Dr. Bensch danken.

Ein herzlicher Dank geht an Maren Rasmussen und Henning Lühmann für die Durchführung zahlreicher Magnetmessungen und die hilfreichen Diskussionen. Außerdem möchte ich mich bei der Spektroskopischen Abteilung für die Anfertigung zahlreicher Spektren bedanken.

Mein Dank gilt meinen Kooperationspartnern Prof. Dr. Robert E. Dinnebier, Tomče Runčevski, Prof. Dr. Stefan G. Ebbinghaus. Ein besonderer Dank geht an Herrn Dr. Zbigniew Tomkowicz und Herrn Dr. Michał Rams für ihr großes Engagement und Unterstützung bei der Interpretation der magnetischen Phänomene.

Bedanken möchte ich mich bei Stefan Suckert und Tristan Neumann für die freundschaftliche Zusammenarbeit im Laboraltag.

Ein besonderer Dank gilt meiner Familie und meinen Freunden, die mich immer unterstützt haben.

Inhaltsverzeichnis

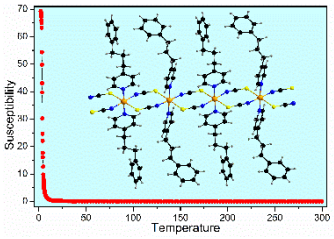

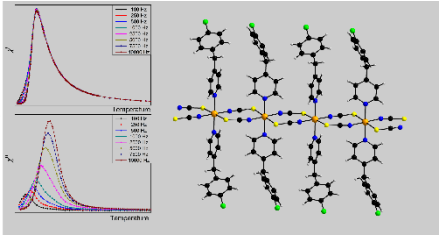

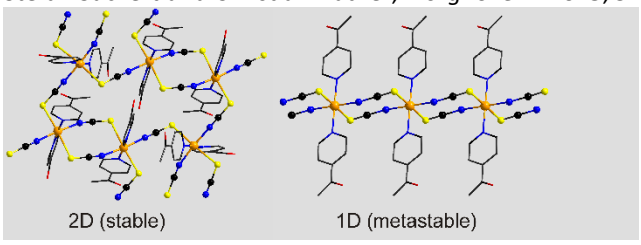

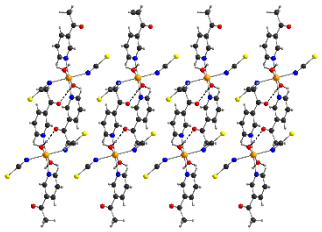

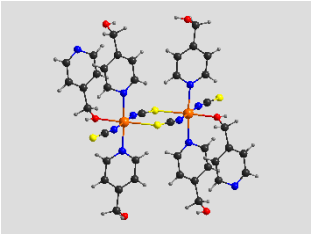

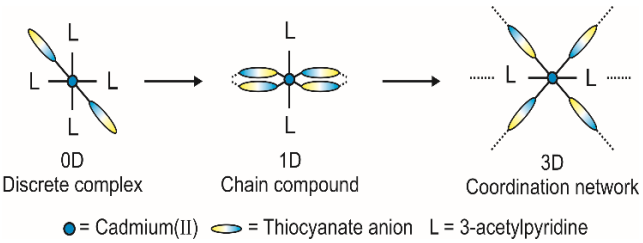

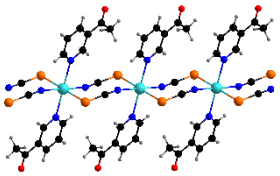

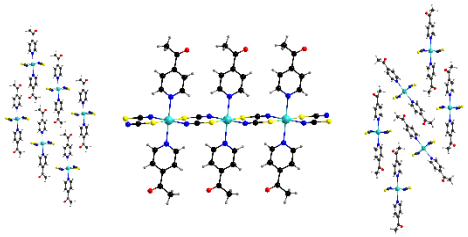

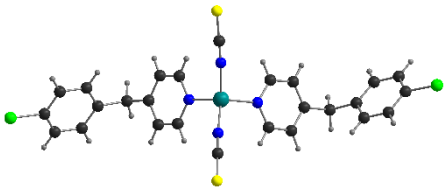

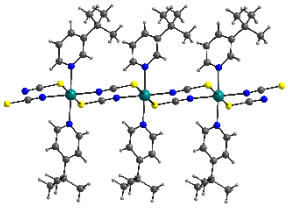

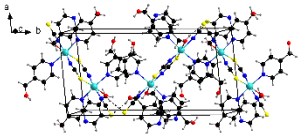

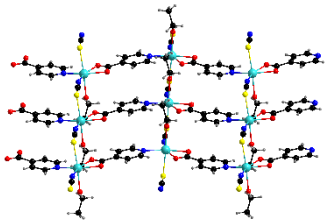

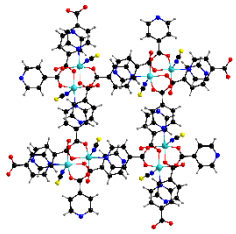

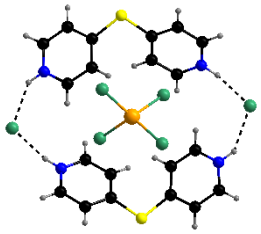

1. Einleitung

1.1 Bedeutung von Koordinationspolymeren

Die Erforschung von Koordinationspolymeren hat in den letzten zwei Jahrzehnten stark zugenommen. Dies liegt zum einen daran, dass für diese Art von Verbindungen bereits auf der Basis einfachster Überlegungen hinsichtlich der Koordinationseigenschaften der Metallkationen, sowie der anionischen und neutralen Liganden Vorhersagen über die Topologie der auftretenden Koordinationsnetzwerke getroffen werden können. Zum anderen können dadurch ihre physikalischen Eigenschaften gezielt beeinflusst werden. Damit verbunden ist der Begriff „Crystal Engineering“, ein Forschungsbereich, indem versucht wird auf der Basis der in Kristallen auftretenden Wechselwirkungen, Strategien zu entwickeln, mit denen chemische Verbindungen mit vorgegebenen Strukturen und definierten physikalischen Eigenschaften dargestellt werden können.[1-4] Zu den bekanntesten Vertretern dieser Verbindungsklasse gehören die sog. Metallorganischen-Gerüstverbindungen (engl. Metal-Organic-Framework MOF), die aufgrund ihrer vielfältigen Anwendungsmöglichkeiten mittlerweile auch in der chemischen Industrie intensiv untersucht werden. So ließen sich auf der Basis von Struktur-Eigenschaftsbeziehungen gezielt Verbindungen herstellen, die eine definierte Anwendung ermöglichen[2, 5-6]. Unter anderem werden diese Verbindungen als Katalysatoren oder zur Gasspeicherung eingesetzt und neuste Forschungen legen eine mögliche Anwendung als elektrische Leiter nahe.[7]

Koordinationspolymere sind definiert als Koordinationsverbindungen, deren sich wiederholende Einheiten sich in ein, zwei oder drei Dimensionen erstrecken.[8] In diesen Verbindungen ist ein Metallkation von neutralen und/oder anionischen Liganden umgeben, wobei die Wahl des Kations die Geometrie des Komplexes beeinflusst und die Koordinationseigenschaften der Liganden die Topologie, d.h. die Verknüpfung der Koordinationsnetzwerke in Koordinationspolymere festlegt.[9] Diese Eigenschaften von Koordinationspolymeren sind sehr gute Voraussetzungen für systematische Untersuchungen von Struktur-Eigenschafts-Beziehungen. Neben den Metallorganischen-Gerüstverbindungen finden sich auch immer mehr Arbeiten die sich mit der Synthese von „magnetischen“ Koordinationspolymeren beschäftigen (Molekularer Magnetismus).[10-13] In vielen Fällen werden die Übergangsmetallkationen Mangan, Eisen, Kobalt und Nickel zur Darstellung derartiger Koordinationspolymere verwendet, da deren unterschiedlichen Elektronenkonfigurationen das Auftreten von interessanten magnetischen Phänomenen, wie zum Beispiel spin crossover, eine langsame Relaxation der Magnetisierung oder Metamagnetismus ermöglichen.[14-18] In der Regel weisen diese Kationen die Oxidationsstufe 2+ auf und bevorzugen eine oktaedrische Geometrie. Damit ein effektiver magnetischer Austausch zwischen den Metallzentren möglich wird, müssen diese durch möglichste kleinen Liganden verbrückt werden. Pseudohalogenide Anionen wie Cyanide, Azide oder NCX (X = O, S, Se) eigenen sich sehr gut zur Verknüpfung und sind darüber hinaus in der Lage unterschiedlichste Verknüpfungsmodi einzugehen.[19-22] Das Hauptinteresse des Arbeitskreises von Professor Dr. Näther liegt in der Erforschung der Struktur-Eigenschafts-Beziehungen von Übergangsmetall-Koordinationspolymeren, wobei das Hauptaugenmerk auf der Erforschung der magnetischen Eigenschaften liegt.[23-24]

1.2 Darstellung von Koordinationspolymeren auf Basis von Übergangsmetallkationen und Thio- bzw. Selenocyanat-Anionen.

Kleine dreiatomige, anionische Liganden wie Azide oder NCX (X = O, S, Se) eigenen sich sehr gut, um Übergangmetalle zu verknüpfen und somit einen magnetischen Austausch zwischen den Metallzentren zu vermitteln.[25-26] Diese Liganden können sowohl eine terminale als auch unterschiedliche verbrückende Koordinationsmodi aufweisen, wobei bei den Thio- und Selenocyanaten sowie den oben genannten Metallkationen die terminale Koordination energetisch bevorzugt ist und daher am meisten beobachtet wird. Nichts desto trotz weisen gerade Thiocyanatanionen eine große Vielfalt an Koordinationsmodi auf, welche zu ein-, zwei- oder dreidimensionalen Strukturen führen können, da die Anionen auf unterschiedliche Art und Weise koordinieren können (Abbildung 1).[27]

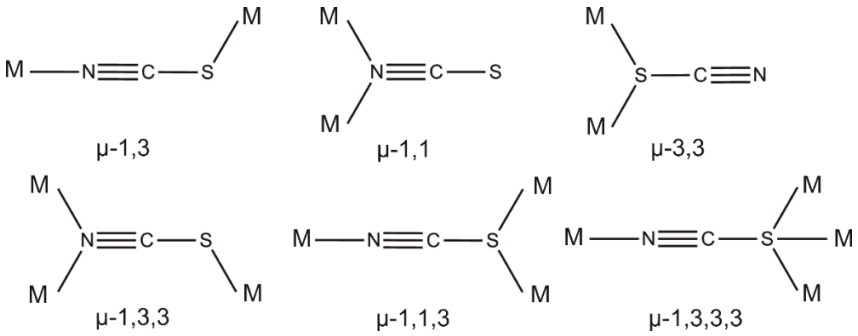

Abbildung 1. Schematische Darstellung unterschiedlicher verbrückender Koordinationsmodi von Thiocyanatanionen.

Was nun die Häufigkeit der unterschiedlichen Koordinationsmodi von Thiocyanatanionen anbelangt, so zeigt eine Recherche in der Cambridge Structural Database (CSD), dass der terminale gegenüber dem μ-1,3 verbrückenden Modus bevorzugt ist (Abbildung 2). Thiocyanatanionen können sowohl über das Stickstoffatom als auch über das Schwefelatom terminal verbrücken, jedoch ist der Koordination über ein Stickstoffatom fünf Mal häufiger aufzufinden.[28] Wenn nun Schwefel gegen Selen ausgetauscht wird sinkt die Anzahl der bekannten Strukturen dramatisch, was auf eine schwierigere Synthese und geringere Stabilität dieser Verbindungen hindeutet. Obwohl sich die Anzahl der Strukturen in den letzten Jahren stark erhöht hat, ist die Verteilung der Koordinationsmodi weitgehend gleich geblieben.

Die Ergebnisse der CSD-Recherche legen nahe, dass für die Metallkationen Mn(II), Fe(II), Co(II) und Ni(II) der terminale Koordinationsmodus energetisch günstiger als die verschiedenen verbrückenden Koordinationsmodi ist und daher die Darstellung von Koordinationspolymeren, in denen die Metallkationen durch Thiocyanatanionen verknüpft sind, schwierig sein wird, wenn diese Verbindungen aus Lösung synthetisiert werden sollen.[29]

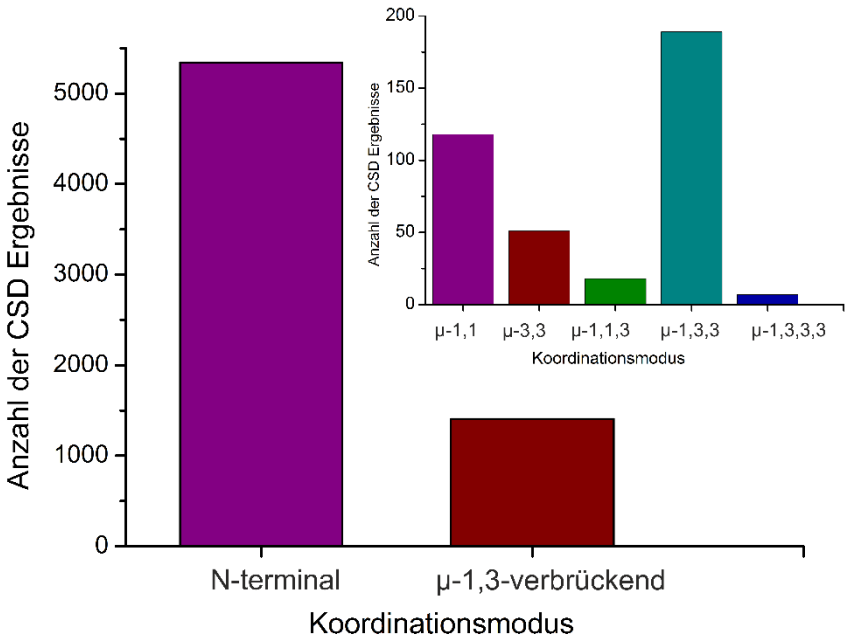

Abbildung 2. Häufigkeitshistogramm der unterschiedlichen Koordinationsmodi in Thiocyanat-Koordinationsverbindungen, welche in der Cambridge Struktural Database hinterlegt sind (Stand: März 2015).[29]

Für diesen Fall, dass eine Synthese von Verbindungen mit verbrückenden Thiocyanatanionen nicht möglich ist, kann ein alternatives Syntheseverfahren verwendet werden, welches bereits seit Jahren in der Arbeitsgruppe von Herrn Näther verwendet wird.[30-31] Dieses beruht auf dem thermischen Abbau ligandenreicher Vorläuferverbindungen, in denen die Übergangsmetallkationen oktaedrisch von zwei terminal gebundenen Thio- oder Selenocyanatanionen sowie vier Stickstoffliganden umgeben sind. Werden diese erhitzt, kommt es in der Regel zu einem stufenweisen Verlust der Stickstoffliganden und die dabei freiwerdenden Koordinationsstellen werden von den Schwefelatomen der Thiocyanatanionen besetzt, die zuvor nicht an der Metallkoordination beteiligt waren (Abbildung 3).[32] Da die Stickstoffliganden emittiert werden, ist diese Reaktion irreversibel und die verbrückende Koordination wird erzwungen. Ein weiterer Vorteil dieses Verfahrens besteht darin, dass die Dimensionalität der Produkte gezielt eingestellt werden kann, da monodentate Co-Liganden zu 1D-Koordinationspolymeren führen, wohingegen einfache verbrückende Co-Liganden zu 2D-Netzwerken führen.[33-34] Für einige Metallkationen, wie beispielsweise Co(II) könnte im Prinzip auch die Bildung einer Verbindung mit einer tetraedrischen Koordination erfolgen, wobei diese von weitaus geringerem Interesse ist als die oktaedrische Koordination (Abbildung 3).[35-36]

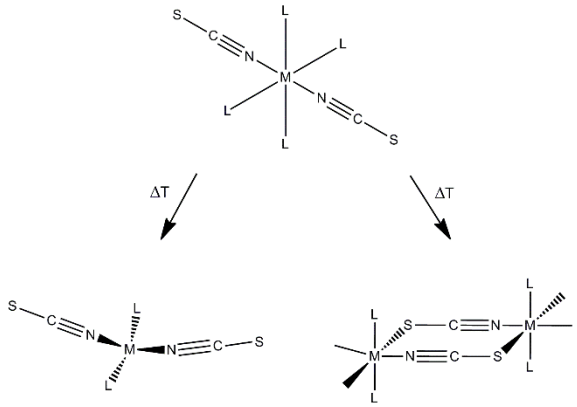

Abbildung 3. Mögliche strukturelle Änderungen beim thermischen Abbau einer oktaedrisch koordinierten Vorläufer Verbindung mit terminal koordinierten Thiocyanatanionen der Zusammensetzung $M(NCS)_2(L)_2$. (M = Mn, Fe, Co, Ni, L = Pyridinderivat).

Ein weiterer Aspekt des thermischen Abbaus ist die Synthese thermodynamisch metastabiler Verbindungen, welche aus Lösung nur schwer zugänglich sind, jedoch mittels thermischen Abbaus isoliert werden können.[37-38]

Nun besteht ein Nachteil dieses Verfahrens darin, dass nur mikrokristalline Pulver erhalten werden, deren Struktur nicht durch Einkristallstrukturanalyse bestimmt werden kann. Erste Hinweise ob sich eine Verbindung mit terminalen oder verbrückenden Thiocyanatanionen gebildet hat, kann die IR-Spektroskopie liefern, da der Wert der asymmetrischen C-N-Streckschwingung von der Koordination des anionischen Liganden abhängt.[39-41] Die asymmetrische Streckschwingung von terminalen Thiocyanatanionen liegt in vielen Fällen unterhalb von 2100 cm^{-1} und die von verbrückenden Thiocyanatanionen oberhalb von 2100 cm^{-1}.[42] Eine Vielzahl von Untersuchungen hat jedoch gezeigt, dass diese Bereiche oftmals überlappen und nicht immer eine eindeutige Unterscheidung getroffen werden kann.[41]
Es wird außerdem versucht die gewünschten Verbindungen mit Mangan, Eisen, Kobalt und Nickel sowie einem bestimmten Liganden aus Lösung zu kristallisieren. In vielen Fällen verhalten sich diese Verbindungen isotyp, sodass die Struktur der anderen Verbindung mittels Rietveld-Verfeinerung bestimmt werden kann.[43] Oft ist es jedoch so, dass in dem Fall, indem eine Verbindung mit drei der vier Kationen nicht aus Lösung zugänglich ist, diese dann auch nicht mit dem vierten Kation kristallisiert werden kann.
Eine weitere Möglichkeit besteht darin zu versuchen eine Struktur *ab-initio* aus Pulverdaten zu lösen. Auch wenn dies nur in wenigen Fällen gelingt, so wird auch in dieser Arbeit über ein derartiges Beispiel berichtet.[44]
Für den Fall, dass all diese Methoden zu Strukturaufklärung versagen, wurde in der Arbeitsgruppe von Herrn Näther ein alternatives Verfahren entwickelt. Es wurde bereits zu Beginn erwähnt, dass für die paramagnetischen Metallkationen die terminale gegenüber einer verbrückenden Koordination energetisch bevorzugt ist, was daran liegt, dass diese Metallkationen wenig chalcophil sind und versuchen eine Schwefelkoordination zu vermeiden. Im Gegensatz hierzu ist Cadmium weitaus chalcophiler und weist in den meisten Fällen ebenfalls eine oktaedrische Koordination auf. Die Darstellung von Verbindungen mit einer verbrückenden Koordination der Thio- oder Selenocyanatanionen gestaltet sich daher mit Cadmium wesentlich einfacher.[45-48] Derartige Verbindungen können leicht kristallisiert werden und sind in vielen Fällen isotyp zu den paramagnetischen Analoga, sodass deren Strukturbestimmung durch Rietveld-Verfeinerung erfolgen kann.[43]

Ähnliche Vorteile bietet auch die Untersuchung entsprechender Zinkverbindungen, welche in den meisten Fällen tetraedrisch koordiniert. Diese Verbindungen eigenen sich daher zur Identifizierung von Intermediaten, welche beim thermischen Abbau auftreten und in denen die Metallkationen eine tetraedrische Koordination aufweisen.[35, 49-51]

1.3 Grundlagen des Magnetismus sowie die Auswertung von magnetischen Messungen

Die Magnetochemie beschäftigt sich mit verschieden Erscheinungsformen des Magnetismus, wie zum Beispiel dem Diamagnetismus, Paramagnetismus und weiteren kooperativen magnetischen Eigenschaften. Eine Verbindung, welche diamagnetisches Verhalten aufweist, besitzt keine ungepaarten Elektronen und wird aus einem angelegten Magnetfeld abgestoßen. Alle Stoffe besitzen einen diamagnetischen Anteil, dieser wird jedoch durch den Paramagnetismus überlagert. Stoffe mit ungepaarte Elektronen besitzen paramagnetisches Verhalten und deren Eigendrehimpuls sowie Bahndrehimpuls sorgt für das Auftreten eines permanenten magnetischen Gesamtmoments. Paramagnetische Stoffe werden von einem angelegten magnetischen Feld angezogen, da sich die magnetischen Momente entsprechend dem magnetischen Feld ausrichten wenn die Magnetfeldliniendichte erhöht wird.[52-53]

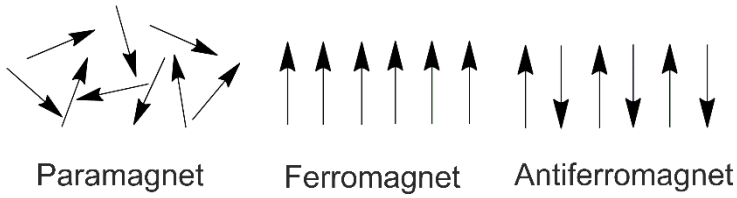

Abbildung 4. Schematische Darstellung der Spinanordnung im Paramagnet, Ferromagnet und Antiferromagnet.

Die Basis für die Messung von magnetischen Eigenschaften bildet die Messung der magnetischen Suszeptibilität in Abhängigkeit der Temperatur, welche für einen einfachen Paramagneten mit abnehmender Temperatur zunimmt und dessen Verlauf durch das Curie- oder Curie-Weiss-Gesetz beschrieben werden kann (Gleichung 1).[53-54]

$$\chi_M = \frac{C}{T} \qquad \chi_M = \frac{C}{T-\theta}$$

Gleichung 1. Gleichung zur Bestimmung Curie-Gesetz (links) und Curie-Weiss-Gesetz (rechts); C = Curie-Konstante, θ = Weiss-Konstante und T = Temperatur.

Die Art der magnetischen Austauschwechselwirkungen kann zum einen durch eine Auftragung des Produkts von χ und T gegen Temperatur ermittelt werden (Temperaturunabhängige Suszeptibilität). Wird zu tieferen Temperaturen hin ein Anstieg der χT Werte beobachtet, liegen ferromagnetische, nehmen diese Werte ab, liegen antiferromagnetische Austauschwechselwirkungen vor. Zur quantitativen Auswertung wird in der Regel die reziproke molare Suszeptibilität gegen die Temperatur aufgetragen. Dabei wird eine Gerade erhalten, die für den Fall, indem keine magnetischen Austauschwechselwirkungen vorliegen durch den Nullpunkt geht (Curie-Gesetz, Gleichung 1). Liegen hingegen ferromagnetische Austauschwechselwirkungen vor, schneidet diese Gerade die Temperaturachse im positiven, liegen antiferromagnetische Austauschwechselwirkungen vor schneidet diese Gerade die Temperaturachse im negativen Bereich (Curie-Weiss-Gesetz,

Gleichung 1). Die Größe und das Vorzeichen der Weiss-Konstante θ, sind ein Maß für die Stärke und die Art der Wechselwirkungen. Eine positive Weiss-Konstante deutet auf ferromagnetische und eine negative auf antiferromagnetische Wechselwirkungen hin. Aus der Steigung der Geraden kann das effektive magnetische Moment μ_{eff} berechnet werden, dessen Vergleich mit berechneten Werten eine Bestimmung der Anzahl an ungepaarten Elektronen erlaubt.[52-55]

$$\mu_{eff} = 2.828 \cdot \sqrt{C}$$

Gleichung 2. Gleichung zur Bestimmung des effektiven magnetischen Moments aus der reziproken Auftragung der Suszeptibilität gegen die Temperatur.

Neben diesem einfachen magnetischen Phänomen, gibt es weitere, die immer dann auftreten können wenn die paramagnetischen Metallkationen entweder direkt oder über Liganden miteinander wechselwirken (Kooperative magnetische Phänomene). Hierbei kann u.a. zwischen Antiferromagnetismus oder Ferromagnetismus unterschieden werden. Beim Antiferromagnetismus steigt die Suszeptibilität beim Abkühlen zunächst an, durchläuft ein Maximum, an dem es zu einer spontanen antiparallelen Ausrichtung der Spins kommt. Die Temperatur am Maximum der Kurve wird als Néel Temperatur (T_N) bezeichnet. Im Gegensatz hierzu ordnen sich die Spins beim Abkühlen eines Ferromagneten unterhalb der sog. Curie-Temperatur (T_C) parallel. Dies führt zu einem enormen Anstieg der Suszeptibilitätswerte, welche bei weiterem Abkühlen in eine Sättigung laufen (Abbildung 5).[55]

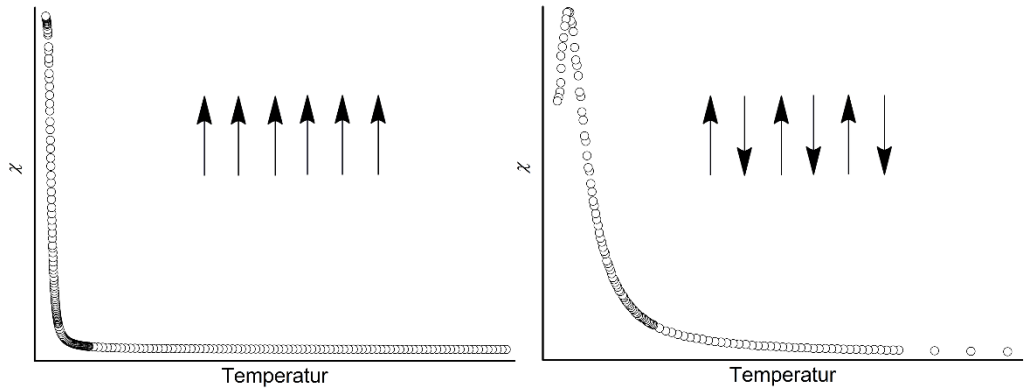

Abbildung 5. Verlauf der molaren Suszeptibilität χ als Funktion der Temperatur für einen Ferromagneten (links) und einen Antiferromagneten (rechts).

Zu den sog. feldabhängigen Phänomenen gehört der Metamagnetismus, er kann in Stoffen mit einem antiferromagnetischen Grundzustand auftreten.[52] Wenn nun ein externes Magnetfeld angelegt wird, kann die antiparallele Anordnung der Spins aufgebrochen werden und die Spins ordnen sich parallel zueinander an. Die Verbindung geht in eine gesättigte paramagnetische Phase über.[54] Mit Hilfe einer Neukurve kann man die kritische Feldstärke (H_C), oberhalb derer die Verbindung in die gesättigte paramagnetische Phase übergeht, bestimmen.[56] Es ist jedoch zu beachten, dass sowohl der antiferromagnetische Ordnungspunkt (T_N) als auch der ferromagnetische Ordnungspunkt (T_C) feldabhängig sind und die Magnetisierung eine Temperaturabhängigkeit aufweist. Die Néel Temperatur (T_N) verschiebt sich mit höherem angelegtem Magnetfeld zu kleineren Temperaturwerten, wohingegen sich die Curie Temperatur zu größeren Werten verschiebt. Die kritische Feldstärke hingegen sinkt bei ansteigenden Temperaturen. Die Abhängigkeit der einzelnen Parameter kann genutzt werden, um ein Phasendiagramm zu erstellen (Abbildung 6).[53-55, 57]

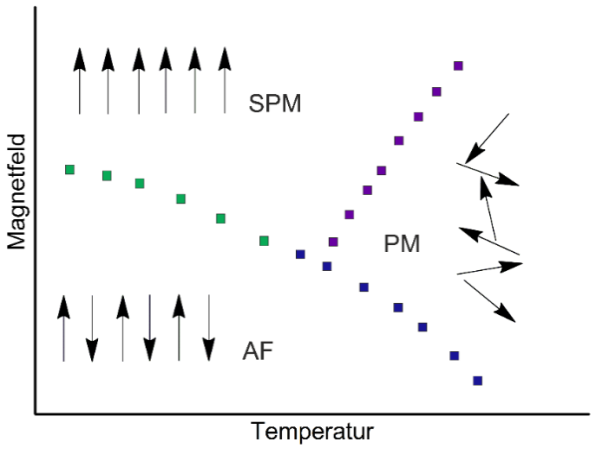

Abbildung 6. Schematisches Phasendiagramm eines Metamagneten. AF: Antiferromagnetische Phase; SPM: Gesättigte paramagnetische Phase; PM: Paramagnetische Phase.

Ein weiteres magnetisches Phänomen, welches in den letzten Jahren intensiv beforscht und auch Gegenstand der hier vorgestellten Untersuchungen ist, ist der Einzelkettenmagnetimus. Derartige Verbindungen zeigen unterhalb der sog. Blocking-Temperatur eine langsame Relaxation der Magnetisierung und sind somit in der Lage unterhalb dieser Temperatur ein magnetisches Moment permanent zu speichern. Im Gegensatz zu herkömmlichen Ferromagneten, in denen eine dreidimensionale parallele Ordnung der Spins auftritt, sind diese in Einzelkettenmagneten nur in einer Dimension parallel ausgerichtet. Damit eine Verbindung ein derartiges Verhalten aufweisen kann, müssen einige Voraussetzungen erfüllt sein. Zum einen dürfen die Spinträger nur entlang einer Kette parallel geordnet sein. Im Prinzip können auch 2-dimensionale Koordinationsverbindungen ein derartiges Verhalten zeigen, wenn die ferromagnetischen Ketten beispielsweise durch Liganden zu Schichten verknüpft sind, die keinen magnetischen Austausch vermitteln. Darüber hinaus werden Metallkationen mit hoher magnetischer Anisotropie wie Mn(III), Fe(II), Co(II), Ni(II) oder Lanthanoid-Kationen benötigt.[58-63] Außerdem werden Anionen oder Moleküle zur Verbrückung der Metallzentren verwendet, die eine starke Intrakettenwechselwirkung hervorrufen. Die Interkettenwechselwirkung zwischen den Ketten sollte hingegen klein sein, was zum Teil durch sterisch anspruchsvolle neutrale Liganden erzielt wird.[64] In diesem Zusammenhang sei erwähnt, dass immer mehr Verbindungen bekannt sind, die Metamagnetismus und langsame Relaxation vereinen.[13, 58, 60, 65-66]

Das Phänomen des Einzelkettenmagnetismus wurde bereits 1963 von Glauber vorhergesagt, jedoch konnte dieses erst 2001 von der Arbeitsgruppe um A. Caneschi experimentell nachgewiesen werden.[67-69] Die dort beschriebene Verbindung besteht aus Co(II) Kationen, die über NITPhOMe-Liganden (4'-methoxy-phenyl-4,4,5,5-tetramethylimidazoline-1-oxyl-3-oxide) zu einer Kette verbrückt sind. Wenn man nun die Verbindungen der letzten Jahre betrachtet, die Einzelkettenmagnetismus aufweisen, fällt auf, dass es nur wenig systematische Untersuchungen gibt und in den meisten Fällen ausschließlich nach neuen Verbindungen gesucht wird, die ein derartiges Verhalten zeigen.[58, 70-71]

Um zu prüfen, ob Einzelkettenmagnetismus vorliegt und die Parameter zu bestimmen, welche die Leistungsfähigkeit derartiger magnetischer Materialien bestimmen, müssen eine Reihe von Messungen ausgeführt werden. Wie zuvor schon erwähnt sind die Intra- (J_{intra}) und Interkettenwechselwirkungen (J_{inter}) ein sehr wichtiger Parameter zur Beschreibung derartiger Verbindungen. Eine Möglichkeit die Intrakettenwechselwirkung zu bestimmen besteht darin die Steigung der $\ln\chi T$ gegen T^{-1}–Kurve zu bestimmen. Die Steigung des linearen Teils der Auftragung

entspricht der Energie, die zur Ausbildung einer Domänenwand benötigt wird ($\Delta\xi$) und aus dem Zusammenhang kann auch die Intrakettenwechselwirkung bestimmt werden (Gleichung 3).[54, 72]

$\Delta\xi = 4S^2J$ (Heisenberg System) $\Delta\xi = 2S^2J$ (Ising-System)

Gleichung 3. Gleichung zur Bestimmung der Intrakettenwechselwirkung nach Heisenberg und Ising.

Daneben kann auch der Verlauf der χT- gegen T-Kurve mit Hilfe eines Fisher-Modells angepasst werden, wobei neben der Intrakettenwechselwirkung auch Informationen über das Vorzeichen sowie der Größe der Interkettenwechselwirkungen erhalten werden. Austauschwechselwirkungen mit einem positiven Vorzeichen bezeichnen eine ferromagnetische Kopplung während ein negatives Vorzeichen antiferromagnetische Austauschwechselwirkungen bezeichnet (Gleichung 4).[73]

$$\chi_{\parallel}^{chain} = \frac{N_A {\mu_B}^2 {g_{\parallel}}^2}{4k_BT}\exp\left(\frac{J}{2k_BT}\right)$$

$$\chi_{\perp}^{chain} = \frac{N_A g_{\perp}^2 \mu_B^2}{2J}[\tanh(\frac{J}{4kT}) + \frac{J}{4kT}\operatorname{sech}^2(\frac{J}{4kT})]$$

Gleichung 4. Lösung des Hamiltonians eines Ising-Systems nach Fisher.

Mit Hilfe von frequenzabhängigen AC-Suszeptibilitätamesungen (AC= Alternating Current; Wechselstrom) kann geprüft werden, ob eine langsame Relaxation der Magnetisierung oder lediglich antiferromagnetisches oder ferromagnetisches Verhalten vorliegt. Ein Antiferromagnet zeigt im Realteil (χ‘) frequenzunabhängige Maxima, die der Néel -Temperatur (T_N) entsprechen, im Imaginärteil (χ‘) hingegen wird kein Signal beobachtet. Werden sowohl im Realteil als auch im Imaginärteil frequenzunabhängige Maxima beobachtet, handelt es sich um einen Ferromagneten. Die hier beobachteten Maxima entsprechen der Curie-Temperatur (T_C). Wenn sowohl im Realteil als auch im Imaginärteil der AC-Suszeptibilitätsmessungen ein frequenzabhängiger Versatz der Maxima auftritt, kann dies auf eine langsame Relaxation der Magnetisierung zurückgeführt werden. Dieses Phänomen tritt beispielsweise in Einzelkettenmagneten (SCMs), Einzelmolekülmagneten (SMMs) oder Spingläsern auf (Abbildung 7). Jedoch könnte ein Versatz der Maxima auch auf das „Wackeln‘‘ der Domänenwände eines gewöhnlichen Ferromagneten zurückgeführt werden.[74]

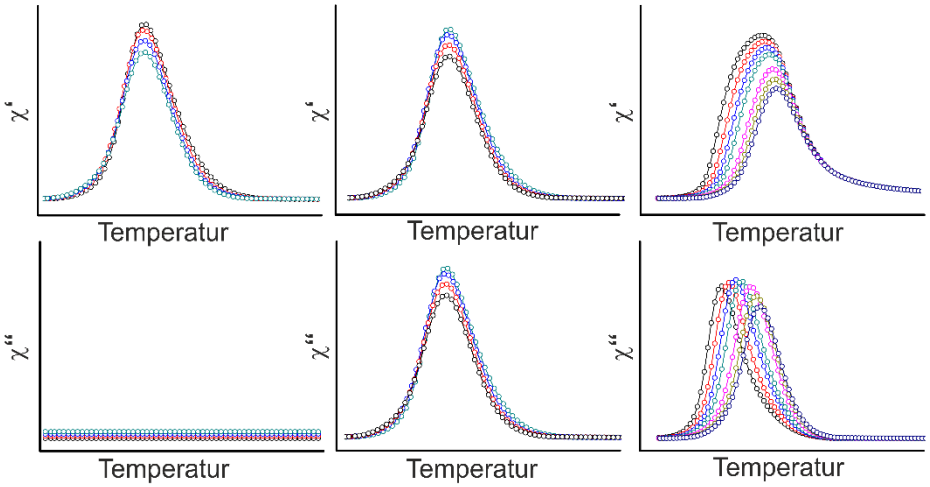

Abbildung 7. Schematische Darstellung von AC-Susceptibilitätsmessungen für einen Antiferromagneten (links), einen Ferromagneten (Mitte) und eines Einzelkettenmagneten, eines Spinglas oder eines SMM (rechts).

Der Mydosh Parameter (φ) ist ein Maß für den frequenzabhängigen relativen Temperatur-Versatz der Suszeptibilitätsmaxima und mit Hilfe dieses Parameters kann eine Aussage darüber getroffen werden, ob die zu untersuchende Verbindung superparamagnetisches Verhalten (wie in Einzelkettenmagneten oder SMMs) oder Spinglas-Verhalten aufweist. Ein Superparamagnet weist einen Mydosh-Parameter zwischen $0.1 > \varphi < 0.3$ auf, wohingegen ein Wert unterhalb von 0.1 ($\varphi < 0.1$) auf Spinglas-Verhalten hindeutet (Gleichung 5).[75]

$$\varphi = \Delta T_m/[T_m \Delta(\log f)]$$

Gleichung 5. Gleichung zur Bestimmung des Mydosh-Parameters.

Die Relaxationszeit τ ($\tau = 1/(2\pi f)$) ist ein temperaturabhängiger Parameter, der aus den AC-Suszeptibilitätsmessungen bestimmt wird (Gleichung 6). Durch Anwendung des Arrhenius-Gesetzes können aus den Relaxationszeiten die effektive anisotrope Energiebarriere ΔE für die Spininversion sowie der prä-exponentielle Faktor τ_0 bestimmt werden.[74]

$$\tau = \tau_0 = \exp(\Delta E/k_B T)$$

Gleichung 6. Gleichung zur Bestimmung der Energiebarriere nach dem Arrhenius-Gesetz (τ_0 = prä-exponentielle Faktor, ΔE = Energiebarriere der Spininversion, k_B = Boltzmann-Konstante und T = Temperatur).

Der prä-exponentielle Faktor τ_0 korreliert mit der Kettenlänge des Systems und beschreibt die Eigendynamik der Spins innerhalb dieses Systems. Der Wert des prä-exponentiellen Faktors sollte im Fall eines Superparamagneten nicht unterhalb $\tau_0 < 10^{-12}$ sein, da ein zu niedriger Wert physikalisch unrealistisch ist. Die Energiebarriere, die zur Spinumkehr überwunden werden muss, wird durch die effektive anisotrope Energiebarriere ΔE beschrieben, die mit Hilfe von temperaturabhängigen oder isothermen, frequenzabhängigen AC-Suszeptibilitätsmessungen bestimmt werden kann. Die zweite Methode bietet den Vorteil, dass in diesem Fall eine simultane Anpassung an allen Messwerten durchgeführt wird. Der Cole-Exponent α lässt sich ebenfalls aus den isothermen AC-Suszeptibilitätsmessungen bestimmen. Dieser gibt Aufschluss über die Verteilung der Relaxationszeiten. Für einen idealen SCM wird nur ein Relaxationsmechanismus beobachtet und α sollte einen Wert von nahezu 0 aufweisen, auch wenn in der Literatur auch Werte von bis zu 0.4 auf Einzelkettenmagnetismus zurückgeführt werden. Spingläser haben eine breite Verteilung von Relaxationsprozessen und weisen deutlich größere Werte auf.[76]

Die Energiebarriere hängt mit noch einem weiteren Faktor zusammen, der Korrelationslänge ξ der Kette. Die Korrelationslänge beschreibt den Bereich der Kette, in dem alle Spins die gleiche Ausrichtung aufweisen. Bei hohen Temperaturen ist die Korrelationslänge wesentlich kleiner als die Kettenlänge L und die Kette besteht aus verschiedenen Segmenten in denen die Spins die gleiche Ausrichtung haben. Die Spininversion findet innerhalb der Kette statt, wofür ein bestimmter Energiebetrag (ΔE) notwendig ist.

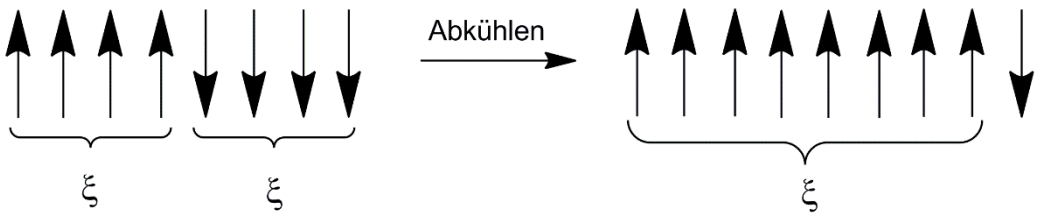

Abbildung 8. Zusammenhang zwischen der Kettenlänge L, der Korrelationslänge ξ und der Energiebarriere ΔE in Abhängigkeit der Temperatur.

$$\Delta E = (2J + |D|)S^2 \qquad \Delta E = (4J + |D|)S^2$$

unendliche Kette endliche Kette

Gleichung 7. Abhängigkeit der Energiebarriere ΔE von der Kettenlänge des Systems. J = Austauschkonstante, D = Anisotropiekonstante, S = Gesamtspin.

Mit sinkender Temperatur nimmt die Korrelationslänge immer weiter zu und entspricht dann der Kettenlänge. In diesem Fall findet die Spininversion jedoch am Ende einer Kette statt und da dieser Spin nur einen Nachbarspin hat, ist die zu überwindende Energiebarriere nur halb so groß (Abbildung 8 und Gleichung 7).

Die beschriebenen Parameter geben die Möglichkeit die zu untersuchenden Verbindungen einzuschätzen und zu prüfen, ob Einzelkettenmagnetismus vorliegt. Die Erkenntnisse, die im Rahmen dieser Arbeit gewonnen wurden, deuten darauf hin, dass der magnetische Grundzustand der Verbindungen einen starken Einfluss auf das magnetische Verhalten hat.

1.4 Magnetische Eigenschaften von 1D und 2D Koordinationspolymeren auf der Basis von Thio- und Selenocyanaten

Aufbauend auf den zuvor vorgestellten Ergebnissen der CSD-Recherche wurde zunächst versucht, Thiocyanat-Koordinationspolymere mit Mn, Fe, Co und Ni sowie einfachen verbrückenden Co-Liganden aus Lösung oder durch thermischen Abbau herzustellen. Dabei wurden eine Reihe von Verbindungen erhalten, in denen die Kationen durch die anionischen Liganden zu Ketten verknüpft wurden. Systematische Untersuchungen zu deren magnetischen Eigenschaften ergaben jedoch Hinweise darauf, dass auch die verbrückenden Co-Liganden am magnetischen Austausch beteiligt sind. Um deren Einfluss auszuschalten, wurden daraufhin monodentate Co-Liganden zur Synthese verwendet.[30, 77-78]

Hierzu wurde zunächst Pyridin als Co-Ligand verwendet. Dabei wurden Verbindungen der Zusammensetzung $[M(NCS)_2(Pyridin)_2]_n$ (M = Mn, Fe, Co, Ni) erhalten, in denen die Metallkationen durch die Thiocyanatanionen zu Ketten verknüpft sind und die einen Austausch zwischen den Metallkationen vermitteln. Im Gegensatz zu den diskreten Komplexen der Zusammensetzung $M(NCS)_2(Pyridin)_4$, welche nur paramagnetisches Verhalten aufzeigen, konnten für die verbrückenden Verbindungen kooperative magnetische Phänomene beobachtet werden.[79-81] Die Auswertung der magnetischen Messungen ergab, dass für die Verbindung mit Mangan antiferromagnetisches Verhalten und für die mit Kobalt ferromagnetisches Verhalten gefunden werden konnte. Die Verbindungen mit Eisen und Nickel weisen Metamagnetismus auf (Tabelle 1).

Tabelle 1. Magnetische Eigenschaften bekannter 1D Koordinationspolymere mit dem Ligand Pyridin.

Verbindung	Magnetische Eigenschaft
$[Mn(NCS)_2(Pyridin)_2]_n$	Antiferromagnetismus[80]
$[Fe(NCS)_2(Pyridin)_2]_n$	Metamagnetismus[81]
$[Co(NCS)_2(Pyridin)_2]_n$	Ferromagnetismus/ SCM Verhalten[79]
$[Ni(NCS)_2(Pyridin)_2]_n$	Metamagnetismus[80]

Die weiteren magnetischen Untersuchungen der Verbindung $[Co(NCS)_2(Pyridin)_2]_n$ ergaben Hinweise darauf, dass diese Verbindung das bis dato für diese Verbindungtyp unbekannte Verhalten des

Einzelkettenmagneten (engl. Single-Chain-Magnet, SCM) aufwies. Die weiteren Literaturrecherchen zeigten, dass es eine Reihe von Verbindungen gibt, die dieses Verhalten aufweisen.[82-84] Im Folgenden wurde sowohl der Einfluss der neutralen Co-Liganden als auch der, der verbrückenden Anionen auf das magnetische Verhalten untersucht. Diese Untersuchungen zeigten, dass die Thiocyanatanionen durch Selenocyanatanionen ausgetauscht werden konnten, ohne dass sich das magnetische Verhalten änderte, denn auch $[Co(NCSe)_2(Pyridin)_2]_n$ zeigte das Phänomen des Einzelkettenmagnetismus.[77] Im Gegensatz zur Thiocyanat-Verbindung wurde eine Erhöhung der Intrakettenwechselwirkungen beobachtet. Darüber hinaus konnte auch für die Verbindung $[Fe(NCSe)_2(Pyridin)_2]_n$ Einzelkettenmagnetismus nachgewiesen werden. Da die entsprechende Thiocyanatverbindung dieses Verhalten nicht zeigt, wird hier offensichtlich die im Vergleich zu Co(II)-Kationen niedrigere Anisotropie der Fe-Kationen durch die höheren Intrakettenwechselwirkungen kompensiert.[23] In weiteren Untersuchungen konnte mit der Verbindung $[Co(NCS)_2(4\text{-bpe})]_n$ eine Verbindung synthetisiert werden, die ein zweidimensionales Koordinationsnetzwerk aufweist und in der sowohl Metamagnetismus als auch eine langsame Relaxation der Magnetisierung beobachtet werden konnte (Abbildung 9). Auch in dieser Verbindung sind die Kobaltzentren mittels μ-1,3 verbrückender Thiocyanatanionen zu Ketten verbrückt, jedoch sind diese Ketten durch den Liganden 1,2-Bis(4-pyridyl)-ethylen (4-bpe) zu Schichten verknüpft. Die Suszeptibilitätsmessungen dieser Verbindung zeigen einen antiferromagnetischen Ordnungspunkt oberhalb von $H_C = 650$ Oe. Offensichtlich sind die ferromagnetischen Kobalthiocyanat-Ketten durch die bpe-Liganden antiferromagnetisch gekoppelt und diese Wechselwirkung wird oberhalb der kritischen Feldstärke überkompensiert (Abbildung 9).[85]

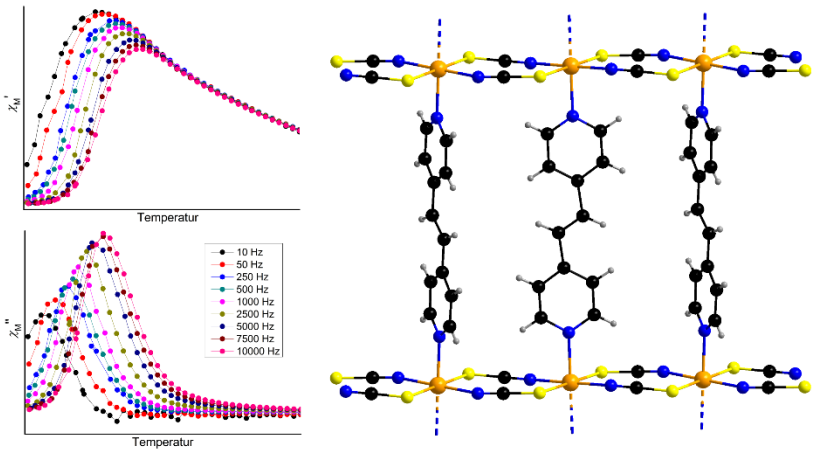

Abbildung 9. AC Suszeptibilitätsmessungen (χ‘ = Realteil; χ‘‘ = Imagniärteil) der Verbindung $[Co(NCS)_2(4\text{-bpe})]_n$ (links) und Ausschnitt aus der Kristallstruktur (rechts).[85]

Zu diesem Zeitpunkt war dies die erste zweidimensionale Thiocyanat-Koordinationsverbindung Verbindung die sowohl Metamagnetismus als auch SCM Verhalten aufwies. In weiteren Synthesen wurden die Thiocyanatanionen durch Selenocyanatanionen ersetzt und die magnetischen Untersuchungen ergaben, dass auch für diese Verbindung ein identisches magnetisches Verhalten beobachtet wird, wobei es zu einer Erhöhung der Intrakettenwechselwirkungen sowie der Energie für die Spininversion kommt.[17] Neben großen bidentaten Liganden wurden auch kleinere monodentate Liganden wie beispielsweise 4-Ethylpyridin verwendet. Mit $Co(NCS)_2$ und 4-Ethylpyridin konnte eine Verbindung synthetisiert werden, die wie bereits zuvor das Pyridin eine eindimensionale Struktur aufweist. Die Kobaltkationen sind durch μ-1,3 verbrückende Thiocyanatanionen zu Ketten verbrückt. Die Auswertung der Magnetmessungen zeigte, dass auch diese Verbindung Metamagnetismus und eine langsame Relaxation aufweist. Somit konnte gezeigt werden, dass sowohl das Anion als auch der neutrale Ligand ausgetauscht werden können, ohne dass das

magnetische Phänomen des Einzelkettenmagnetismus verloren geht.[86] Ganz offensichtlich wurde eine Verbindungsklasse entdeckt, in der systematisch der Einfluss einer chemischen sowie einer strukturellen Modifizierung auf die Parameter untersucht werden kann, welche die Leistungsfähigkeit von Einzelkettenmagneten beschreiben.

In weiteren systematischen Untersuchungen wurden auch Verbindungen mit anderen Übergangsmetallen dargestellt und untersucht. So wurden beispielsweise mit $Mn(NCS)_2$ und verschiedenen Co-Liganden eine Vielzahl von Verbindungen mit unterschiedlichen Strukturen synthetisiert (Abbildung 10).[24, 33, 87] Die magnetischen Messungen ergaben, dass in den Verbindungen, in denen die Mangankationen durch die anionischen Liganden zu Ketten verknüpft sind entweder Antiferromagnetismus oder Paramagnetismus beobachtet wird, was auch in Literaturbekannten Verbindungen beobachtet werden kann.[21, 88]

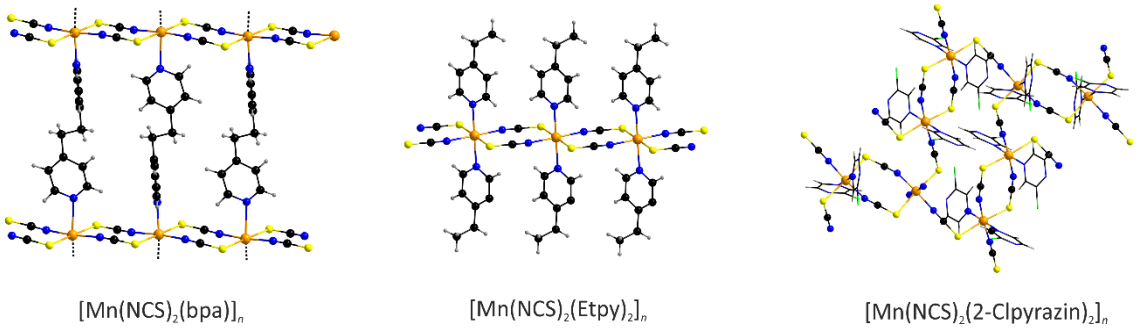

Abbildung 10. Koordinationsmodi verschiedener Verbindungen mit $Mn(NCS)_2$ und den Liganden (bpa), 4-Ethylpyridin (Etpy) und 2-Chlorpyrazin.[24, 33, 87]

Auch Verbindungen mit dem Übergangsmetall Nickel zeigen eine große Strukturvielfalt und es werden neben ein- und zweidimensionale Strukturen auch Dimere beobachtet. Magnetische Messungen ergaben, dass ein ferromagnetischer Austausch über Thiocyanatanionen auftritt und dass in der Regel Para- oder Metamagnetismus beobachtet wird.[24, 33, 89]

Literatur

[1] G. R. Desiraju, *Crystal Engineering - The Design of Organic Solids*, Elsevier, Amsterdam - Oxford - New York - Tokio, **1989**.

[2] M. J. Zaworotko, *Nat. Chem.* **2011**, *3*, 653-653.

[3] A. Schoedel, L. Wojtas, S. P. Kelley, R. D. Rogers, M. Eddaoudi, M. J. Zaworotko, *Angew. Chem.* **2011**, *123*, 11623-11626.

[4] C. V. K. Sharma, *Cryst. Growth Des.* **2002**, *2*, 465-474.

[5] G. Férey, *Dalton Trans.* **2009**, 4400-4415.

[6] S. K. Henninger, F. Jeremias, H. Kummer, C. Janiak, *Eur. J. Inorg. Chem.* **2012**, *2012*, 2625-2634.

[7] C. Janiak, J. K. Vieth, *New J. Chem.* **2010**, *34*, 2366-2388.

[8] R. Batten Stuart, R. Champness Neil, X.-M. Chen, J. Garcia-Martinez, S. Kitagawa, L. Öhrström, M. O'Keeffe, M. Paik Suh, J. Reedijk, in *Pure Appl. Chem., Vol. 85*, **2013**, p. 1715.

[9] A. Y. Robin, K. M. Fromm, *Coord. Chem. Rev.* **2006**, *250*, 2127-2157.

[10] M. Wriedt, C. Näther, *Z. Anorg. Allg. Chem.* **2009**, *635*, 1115-1122.

[11] B. Gil-Hernandez, J. K. Maclaren, H. A. Hoppe, J. Pasan, J. Sanchiz, C. Janiak, *CrystEngComm* **2012**, *14*, 2635-2644.

[12] M. Dey, N. Gogoi, *Angew. Chem.* **2013**, *125*, 13014-13016.

[13] H. L. Sun, Z. M. Wang, S. Gao, *Coord. Chem. Rev.* **2010**, *254*, 1081-1100.

[14] G. S. Matouzenko, E. Jeanneau, A. Y. Verat, Y. de Gaetano, *Eur. J. Inorg. Chem.* **2012**, *2012*, 969-977.

[15] K. Bhar, S. Khan, J. S. Costa, J. Ribas, O. Roubeau, P. Mitra, B. K. Ghosh, *Angew. Chem. Int. Ed.* **2012**, *51*, 2142-2145.

[16] Y.-L. Bai, X. Bao, S. Zhu, J. Fang, J. Tao, *Dalton Trans.* **2013**, *42*, 1033-1038.

[17] S. Wöhlert, U. Ruschewitz, C. Näther, *Cryst. Growth Des.* **2012**, *12*, 2715-2718.

[18] X.-J. Song, M. Muddassir, Y. Chen, H.-S. Wang, Y. Song, X.-Z. You, *Dalton Trans.* **2013**, *42*, 1116-1121.

[19] O. Sengupta, Y. Song, P. S. Mukherjee, *Dalton Trans.* **2009**, 10343-10352.

[20] Y. Wang, R. Cao, W. Bi, X. Li, D. Yuan, D. Sun, *Microporous Mesoporous Mater.* **2006**, *91*, 215-220.

[21] E. Shurdha, C. E. Moore, A. L. Rheingold, S. H. Lapidus, P. W. Stephens, A. M. Arif, J. S. Miller, *Inorg. Chem.* **2013**, *52*, 10583-10594.

[22] J.-Q. Tao, Z.-G. Gu, T.-W. Wang, Q.-F. Yang, J.-L. Zuo, X.-Z. You, *Inorg. Chim. Acta* **2007**, *360*, 4125-4132.

[23] J. Boeckmann, M. Wriedt, C. Näther, *Chem. Eur. J.* **2012**, *18*, 5284-5289.

[24] S. Wöhlert, T. Runčevski, R. E. Dinnebier, S. G. Ebbinghaus, C. Näther, *Cryst. Growth Des.* **2014**, *14*, 1902-1913.

[25] Y.-Q. Wang, Q. Sun, Q. Yue, A.-L. Cheng, Y. Song, E.-Q. Gao, *Dalton Trans.* **2011**, *40*, 10966-10974.

[26] R.-Y. Li, B.-W. Wang, X.-Y. Wang, X.-T. Wang, Z.-M. Wang, S. Gao, *Inorg. Chem.* **2009**, *48*, 7174-7180.

[27] F. A. Mautner, M. Scherzer, C. Berger, R. C. Fischer, R. Vicente, S. S. Massoud, *Polyhedron* **2015**, *85*, 20-26.

[28] Gerard P. M. v. Klink, T. Nomoto, M. Lutz, Anthony L. Spek, Otto S. Akkerman, F. Bickelhaupt, *Eur. J. Inorg. Chem.* **2004**, *2004*, 154-159.

[29] F. Allen, *Acta Cryst.* **2002**, *B58*, 380-388.

[30] C. Näther, S. Wöhlert, J. Boeckmann, M. Wriedt, I. Jeß, *Z. Anorg. Allg. Chem.* **2013**, *639*, 2696-2714.

[31] M. Wriedt, I. Jeß, C. Näther, *Eur. J. Inorg. Chem.* **2009**, 1406-1413.

[32] M. Wriedt, S. Sellmer, C. Näther, *Dalton Trans.* **2009**, 7975-7984.

[33] S. Wöhlert, L. Fink, M. Schmidt, C. Näther, *Z. Anorg. Allg. Chem.* **2013**, *639*, 2186-2194.
[34] M. Wriedt, S. Sellmer, C. Näther, *Inorg. Chem.* **2009**, *48*, 6896-6903.
[35] L. Kong, W.-J. Li, X.-L. Li, W.-Q. Geng, F.-Y. Hao, J.-Y. Wu, H.-P. Zhou, J.-X. Yang, Y.-P. Tian, B.-K. Jin, *Polyhedron* **2010**, *29*, 1575-1582.
[36] J. Boeckmann, B. Reimer, C. Näther, *Z. Naturforsch.* **2011**, *66b*, 819-827.
[37] C. Näther, G. Bhosekar, I. Jeß, *Inorg. Chem.* **2007**, *46*, 8079-8087.
[38] S. Wöhlert, J. Boeckmann, I. Jess, C. Näther, *CrystEngComm* **2012**, *14*, 5412-5420.
[39] M. Wriedt, C. Näther, *Chem. Commun.* **2010**, *46*, 4707-4709.
[40] R. A. Bailey, S. L. Kozak, T. W. Michelsen, W. N. Mills, *Coord. Chem. Rev.* **1971**, *6*, 407-445.
[41] G. A. Van Albada, R. A. G. De Graaff, J. G. Haasnoot, J. Reedijk, *Inorg. Chem.* **1984**, *23*, 1404-1408.
[42] P. O. Kinell, B. Strandberg, *Acta Chem. Scand.* **1959**, *13*, 1607-1622.
[43] H. Rietveld, *Acta Cryst.* **1967**, *22*, 151-152.
[44] Y. G. Andreev, G. S. MacGlashan, P. G. Bruce, *Phys. Rev. B* **1997**, *55*, 12011-12017.
[45] QI Ma, M. Zhu, C. Yuan, S. Feng, L. Lu, Q. Wang, *Cryst. Growth Des.* **2009**, *Vol. 10*, 1706-1714.
[46] S. Banerjee, B. Wu, P.-G. Lassahn, C. Janiak, A. Ghosh, *Inorg. Chim. Acta* **2005**, *358*, 535-544.
[47] A. Tahli, J. K. Maclaren, I. Boldog, C. Janiak, *Inorg. Chim. Acta* **2011**, *374*, 506-513.
[48] I. N. B. Machura, K. Michalik *Polyhedron* **2011**, *Vol. 30*, 2619–2626.
[49] L. Y. Zhu, D. Xu, X. Q. Wang, G. Yu, *J. Chem. Crystallogr.* **2008**, *38*, 609-612.
[50] Q.-H. Jin, J.-J. Sun, J.-Q. Wu, Y.-C. Dai, C.-L. Zhang, *J. Chem. Crystallogr.* **2009**, *Vol. 40* 310–315.
[51] S. Wöhlert, I. Jess, U. Englert, C. Näther, *CrystEngComm* **2013**, *15*, 5326-5336.
[52] H. Lueken, *Magnetochemie*, B. G. Teubner Stuttgart Stuttgart - Leipzig, **1999**.
[53] E. Jäger, R. Perthel, *Magnetische Eigenschaften von Festkörpern, Vol. 2*, Akademie Verlag GmbH, Berlin, **1996**.
[54] R. L. Carlin, *Magnetochemistry*, Springer-Verlag, Berlin Heidelberg New York Tokyo, **1986**.
[55] A. F. Hollemann, E. Wiberg, *Lehrbuch der Anorganischen Chemie, Vol. 101*, de Gruyter, Berlin - New York, **1995**.
[56] E. Stryjewski, N. Giordano, *Advances in Physics* **1977**, *26*, 487 - 650.
[57] H. Miyasaka, K. Takayama, A. Saitoh, S. Furukawa, M. Yamashita, R. Clérac, *Chem. Eur. J.* **2010**, *16*, 3656-3662.
[58] D. Zhang, Y. Bian, J. Qin, P. Wang, X. Chen, *Dalton Trans.* **2014**, *43*, 945-949.
[59] J. Ru, F. Gao, T. Wu, M.-X. Yao, Y.-Z. Li, J.-L. Zuo, *Dalton Trans.* **2014**, *43*, 933-936.
[60] P. Hu, X. Wang, Y. Ma, Q. Wang, L. Li, D. Liao, *Dalton Trans.* **2014**, *43*, 2234-2243.
[61] Q. Zhang, H. Zhang, S. Zeng, D. Sun, C. Zhang, *Chemistry – An Asian Journal* **2013**, *8*, 1985-1989.
[62] D.-F. Weng, B.-W. Wang, Z.-M. Wang, S. Gao, *Coord. Chem. Rev.* **2013**, *257*, 2484-2490.
[63] D.-P. Dong, Y.-J. Zhang, H. Zheng, P.-F. Zhuang, L. Zhao, Y. Xu, J. Hu, T. Liu, C.-Y. Duan, *Dalton Trans.* **2013**, *42*, 7693-7698.
[64] G. Bhargavi, M. V. Rajasekharan, J. P. Costes, J. P. Tuchagues, *Dalton Trans.* **2013**, *42*, 8113-8123.
[65] X.-B. Li, G.-M. Zhuang, X. Wang, K. Wang, E.-Q. Gao, *Chem. Comm.* **2013**, *49*, 1814-1816.
[66] T. Han, W. Shi, Z. Niu, B. Na, P. Cheng, *Chem. Eur. J.* **2013**, *19*, 994-1001.
[67] R. J. Glauber, *J. Math. Phys.* **1963**, *4*, 294-308.
[68] A. Caneschi, D. Gatteschi, N. Lalioti, C. Sangregorio, R. Sessoli, G. Venturi, A. Vindigni, A. Rettori, M. G. Pini, M. A. Novak, *Angew. Chem. Int. Ed.* **2001**, *40*, 1760-1763.
[69] R. J. Glauber, *J. Math. Phys.* **1963**, *4*, 294-307.
[70] R. Ishikawa, K. Katoh, B. K. Breedlove, M. Yamashita, *Inorg. Chem.* **2012**, *51*, 9123-9131.
[71] F. Luo, Z.-w. Liao, Y.-m. Song, H.-x. Huang, X.-z. Tian, G.-m. Sun, Y. Zhu, Z.-Z. Yuan, M.-b. Luo, S.-j. Liu, W.-y. Xu, X.-F. Feng, *Dalton Trans.* **2011**, *40*, 12651-12655.
[72] O. Kahn, *Molecular Magnetism*, Wiley VCH, New York, **1993**.
[73] M. E. Fisher, *J. Math. Phy.* **1963**, *4*, 124-135.

[74] W.-X. Zhang, R. Ishikawa, B. Breedlovea, M. Yamashita, *RSC Adv.* **2013**, *3*, 3772-3798.
[75] J. A. Mydosh, *Spin Glasses: An Experimental Introduction*, Taylor and Francis, London, **1993**.
[76] C. Coulon, H. Miyasaka, R. Clérac, *Struct. Bond.* **2006**, *122*, 163-206.
[77] J. Boeckmann, C. Näther, *Chem. Commun.* **2011**, *47*, 7104-7106.
[78] M. Wriedt, C. Näther, *Z. Anorg. Allg. Chem.* **2011**, *637*, 666-671.
[79] J. Boeckmann, C. Näther, *Dalton Trans.* **2010**, *39*, 11019-11026.
[80] J. Boeckmann, C. Näther, *Polyhedron* **2012**, *31*, 587-595.
[81] S. Foner, R. B. Frankel, J. E. J. McNiff, W. M. Reiff, B. F. Little, G. J. Long, *AIP Conf. Proc.* **1975**, *24*, 363-364.
[82] V. Costa, R. Lescouëzec, J. Vaissermann, P. Herson, Y. Journaux, M. H. Araujo, J. M. Clemente-Juan, F. Lloret, M. Julve, *Inorg. Chim. Acta* **2008**, *361*, 3912-3918.
[83] E. Pardo, R. Ruiz-García, F. Lloret, J. Faus, M. Julve, Y. Journaux, M. Novak, F. Delgado, C. Ruiz-Pérez, *Chem. Eur. J.* **2007**, *13*, 2054-2066.
[84] D. Visinescu, A. M. Madalan, M. Andruh, C. Duhayon, J.-P. Sutter, L. Ungur, W. Van den Heuvel, L. F. Chibotaru, *Chem.-Eur. J.* **2009**, *15*, 11808-11814.
[85] S. Wöhlert, J. Boeckmann, M. Wriedt, C. Näther, *Angew. Chem., Int. Ed.* **2011**, *50*, 6920–6923.
[86] S. Wöhlert, T. Fic, Z. Tomkowicz, S. G. Ebbinghaus, M. Rams, W. Haase, C. Näther, *Inorg. Chem.* **2013**, *52*, 12947-12957.
[87] S. Wöhlert, T. Runčevski, R. E. Dinnebier, C. Näther, *Z. Anorg. Allg. Chem.* **2013**, *639*, 2648-2656.
[88] M. G. Barandika, M. L. Hernandez-Pino, M. K. Urtiaga, R. Cortes, L. Lezama, M. I. Arriortua, T. Rojo, *J. Chem. Soc., Dalton Trans.* **2000**, 1469-1473.
[89] S. Wöhlert, C. Näther, *Eur. J. Inorg. Chem.* **2013**, *2013*, 2528-2537.

2. Zielsetzung und Gliederung

Die vorangegangenen Untersuchungen im Arbeitskreis Näther ergaben, dass thermische Abbaureaktionen durchaus geeignet sind um gezielt niederdimensionale Koordinationspolymere zu synthetisieren, die nicht aus Lösung zugänglich sind. Des Weiteren konnte gezeigt werden, dass diese Koordinationspolymere bestehend aus den Metallkationen (Mn(II), Fe(II), Co(II) und Ni(II)) und Thio- oder Selenocyanatanionen kooperative magnetische Eigenschaften aufweisen. Für die Verbindungen mit Mangan wurde ausschließlich Para- und Antiferromagnetismus beobachtet, wohingegen für die Verbindungen mit Nickel entweder Para- oder Metamagnetismus beobachtet wurde. Im Gegensatz hierzu zeigten Verbindungen mit Kobalt Einzelkettenmagnetismus, ein Verhalten das auch mit Eisen beobachtet werden kann, wenn durch den Austausch der Thio- gegen Selenocyanatanionen die Intrakettenwechselwirkungen erhöht werden. Dennoch bleiben eine Reihe von Fragen offen und die Datenbasis ist zu gering, um zu allgemeinen Schlussfolgerungen zu gelangen. Insbesondere weitere systematische Untersuchungen zum Einfluss von monodentaten Co-Liganden auf die magnetischen Eigenschaften derartiger Verbindungen sind vonnöten. Im Rahmen dieser Arbeit sollen daher weitere Verbindungen synthetisiert und untersucht werden, die ggf. Aufschluss über die Zusammenhänge zwischen der Struktur derartiger Koordinationspolymere und deren magnetischen Verhalten geben.

Die Ergebnisse dieser Promotionsarbeit werden in Form einer kumulativen Dissertation vorgestellt.

Einen wesentlichen Teil dieser Arbeiten bildet die Synthese neuer eindimensionaler Verbindungen mit Co(II) als Metallkation, welche über Thiocyanatanionen verbrückt sind. Da derartige Verbindungen eine langsame Relaxation der Magnetisierung aufweisen, welche auf Einzelkettenmagnetismus zurückzuführen ist. Hier gilt es vor allem den Einfluss der Co-Liganden auf die magnetischen Eigenschaften weiter zu untersuchen. Dabei stellt sich zum einen die Frage, ob dieses seltene magnetische Verhalten erhalten bleibt, und sollte dies der Fall sein, welchen Einfluss dies insbesondere auf die Interkettenwechselwirkungen ausübt. Hierzu sollen vor allem „große“ Liganden verwendet werden, welche die Ketten ggf. effektiver voneinander abschirmen. Hierüber wird in Kapitel 3 berichtet.
Im Zuge von systematischen Untersuchungen sind auch die entsprechenden Verbindungen mit Mn(II), Fe(II) und Ni(II) von Interesse. Hier wurde ebenfalls der Einfluss der Co-Liganden auf die Struktur sowie die magnetischen Eigenschaften im Detail untersucht. Dabei stellt sich beispielsweise die Frage, ob die Verwendung monodentater Liganden für alle Metallkationen immer zu den typischen Ketten führt, oder ob auch andere Koordinationstopologien beobachtet werden können und welche magnetischen Eigenschaften damit verbunden sind. Da für derartige Verbindungen keine langsame Relaxation der Magnetisierung beobachtet werden kann, werden diese in einem gesonderten Kapitel (Kapitel 4) vorgestellt. Einige diese Arbeiten enthalten auch Untersuchungen zu Kobalt-Verbindungen, welche aufgrund ihrer Struktur keinen Einzelkettenmagnetismus zeigen können.
Wie bereits erwähnt, sind auch Verbindungen mit Cadmium und Zink von Interesse, da diese in vielen Fällen Rückschlüsse auf die Struktur der paramagnetischen Analoga zulassen. Diese Arbeiten werden in Kapitel 5 vorgestellt.
In den hier vorgestellten Untersuchungen sind immer wieder Kristalle von Verbindungen angefallen, die beispielsweise nicht in einen direkten thematischen Zusammenhang zu dieser Arbeit stehen oder für die keine größeren phasenreinen Mengen dargestellt werden konnten. Deren Strukturen wurden daher in Form von Strukturmitteilungen bei Acta Crystallographica E veröffentlicht (Kapitel 4, 5 und 6).

Zuletzt wurden auch weitere Ergebnisse erhalten, die auf Grund der zeitaufwendigen magnetischen Messungen noch nicht publiziert werden konnten. Diese werden daher in der Zusammenfassung kurz vorgestellt.

3. Der Einfluss neutraler Co-Liganden auf die Struktur und die magnetischen Eigenschaften von 1D Kobalt-Thiocyanat-Koordinationsverbindungen mit einer langsamen Relaxation der Magnetisierung

3.1. A Co(II) Thiocyanato Coordination Polymer with 4-(3-phenylpropyl)pyridine: The Influence of the Co-Ligand on the Magnetic Properties

Julia Werner, Michał Rams, Zbigniew Tomkowicz und Christian Näther, *Dalton Trans.* **2014**, *43*, 17333-17342.

DOI: 10.1039/C4DT02271H

Motivation

In früheren Arbeiten des Arbeitskreises Näther wurden eine Reihe von ein- sowie zweidimensionalen Verbindungen der Zusammensetzung $[Co(NCS)_2(L)_2]_n$ und Zusammensetzung $[Co(NCS)_2(L)]_n$ (L = monodentater oder bidentater Co-Ligand) untersucht, die alle eine langsame Relaxation der Magnetisierung aufweisen, die vermutlich auf Einzelkettenmagnetismus zurückgeführt werden kann. Um den Einfluss der Interkettenwechselwirkung auf das magnetische Verhalten genauer zu untersuchen, wurde 4-(3-Phenylpropyl)pyridin als Co-ligand verwendet. Dieser Ligand sollte aufgrund seiner Größe auch einen größeren Interkettenabstand hervorrufen und damit zu einer Verringerung der Interkettenwechselwirkungen führen. Um diese Annahme zu bestätigen, wurde $Co(NCS)_2$ und 4-(3-Phenylpropyl)pyridin zur Reaktion gebracht und es konnte die gewünschte 1D Verbindung mit *trans* verbrückenden Thiocyantanionen erhalten werden. Der Intrakettenabstand liegt wie erwartet mit 5.639 Å in dem Bereich, der auch für bereits bekannte Verbindungen dieses Typs gefunden wird. Die Interkettenabstände sind mit 11.261 und 12.973 Å wie erwartet wesentlich größer als bei den bisher bekannten Verbindungen.
Die Auswertung der magnetischen Untersuchungen ergaben jedoch Unterschiede zu denen analoger Verbindungen. Im Gegensatz zu den bekannten Verbindungen, die fast alle einen antiferromagnetischen Grundzustand aufweisen, besitzt diese Verbindung einen ferromagnetischen Grundzustand. Auch in dieser Verbindung wird eine langsame Relaxation der Magnetisierung beobachtet. Die Verbindung weist jedoch einen sehr kleinen Mydosh Parameter auf, welcher eher in dem Bereich liegt der für Spingläser zu erwartet ist. Darüber hinaus führt die Analyse der Relaxationszeiten zu einer Energiebarriere, die deutlich höher ist als die vergleichbarer Verbindungen und es wird ein präexponentieller Faktor erhalten, welcher zu klein ist als der, welcher für Einzelkettenmagneten erwartet wird. Zuletzt wird eine sehr breite Verteilung der Relaxationszeiten beobachtet, welche im Gegensatz zu der in anderen Verbindungen nahezu temperaturunabhängig ist. Die Summe all dieser Beobachtungen legt daher nahe, dass die in dieser Verbindung beobachteten Relaxationen nicht auf die von Einzelketten zurückgeführt werden können. Diese Verbindung verhält sich daher eher wie ein Ferromagnet und die hier beobachteten Relaxationen könnten dann auf die Relaxation der Domänenwände zurückgeführt werden.

Dalton Transactions

PAPER

View Article Online
View Journal | View Issue

Cite this: *Dalton Trans.*, 2014, **43**, 17333

A Co(II) thiocyanato coordination polymer with 4-(3-phenylpropyl)pyridine: the influence of the co-ligand on the magnetic properties†‡

Julia Werner,[a] Michał Rams,[b] Zbigniew Tomkowicz[b] and Christian Näther*[a]

Received 25th July 2014,
Accepted 15th September 2014

DOI: 10.1039/c4dt02271h

www.rsc.org/dalton

Three new coordination compounds with the composition $Co(NCS)_2$(4-(3-phenylpropyl)pyridine)$_4$ (**1**), $Co(NCS)_2$(4-(3-phenylpropyl)pyridine)$_4(H_2O)_2$ (**2**) and $[Co(NCS)_2$(4-(3-phenylpropyl)pyridine)$_2]_n$ (**3**) were prepared and investigated. The crystal structures of compounds **1** and **2** consist of discrete complexes, in which the Co(II) cations are coordinated by only terminal N-bonded thiocyanato anions. In the crystal structure of **3** the Co(II) cations are linked into chains by pairs of μ-1,3-bridging thiocyanato anions. DTA-TG measurements on compound **1** show decomposition without the formation of **3** as an intermediate. In contrast, on heating compound **2** two water molecules are removed in the first step leading to the formation of compound **3** in the second step. Magnetic measurements on **3** reveal ferromagnetic interactions between Co(II) ions along chains with J = 29.5(1) K, and also ferromagnetic interactions between chains with zJ' = 0.38(1) K. The ferromagnetic transition is observed at 3.3 K, which is confirmed by specific heat measurements. The temperature dependent ac susceptibility shows slow relaxations above and below 3.3 K. The results for this quasi-one dimensional Ising ferromagnet, having also some features of a cluster spin-glass, are compared with those of related compounds.

Introduction

Investigation on the synthesis and the magnetic properties of new coordination polymers is still a major field in coordination chemistry.[1–17] In this context, compounds with 1D magnetic alignment of ferro- or ferri-magnetically coupled magnetic moments are of special interest when they can retain their magnetization upon removal of an external magnetic field and thus are able to store a magnetic moment permanently.[18–21] These compounds, known as single chain magnets (SCMs), show a slow relaxation of the magnetization and have been investigated in detail in the last decade. In most cases they consist of cations being a source of large easy axis anisotropy that are connected into chains with a large ratio of intrachain to interchain interactions, but the same phenomenon can also be observed in layered coordination networks in which ferromagnetic chains are linked by ligands that possibly do not participate in the magnetic exchange and, thus, are 1D magnetic compounds. Because such materials are of general scientific interest and additionally have some potential for future application, an increasing number of such compounds with different cationic, anionic and neutral co-ligands have recently been reported.[22–37] In this context also thio- or selenocyanato anions can be used for the preparation of magnetic coordination compounds and polymers; some selected examples are given in the reference list.[38–52]

We have reported as well on several such compounds with the composition $[M(NCS)_2(L)_2]_n$ (M = Fe(II), Co(II); L = monodentate co-ligand) and $[M(NCS)_2(L)]_n$ (M = Fe(II), Co(II); L′ = bridging co-ligand), with some of them showing magnetic relaxations, indicative of SCM behavior.[53–58] In all of these compounds the Co(II) cations are linked by pairs of anionic ligands into chains. These chains can be terminated by monodentate ligands L leading to 1D coordination networks or can be linked by bidentate ligands L′ into 2D coordination networks. We have shown that the anionic ligands can be exchanged by selenocyanato anions and that in this case Co(II) can be replaced by Fe(II) without a change of the overall magnetic behavior. Finally, also the neutral N-donor co-ligand can be varied to some extent. In most of these compounds magnetic relaxations are observed.

However, detailed investigations on $[Co(NCS)_2$(4-ethylpyridine)$_2]_n$ revealed that the distribution of the relaxation times,

[a]*Institut für Anorganische Chemie, Christian-Albrechts-Universität zu Kiel, Max-Eyth-Straße 2, 24118 Kiel, Germany. E-mail: cnaether@ac.uni-kiel.de; Fax: +49 431-8801520; Tel: +49 431-880 1520*
[b]*Institute of Physics, Jagiellonian University, 30-059 Kraków, Reymonta 4, Poland*
† Dedicated to Professor Gerd Meyer on the occasion of his 65th birthday.
‡ Electronic supplementary information (ESI) available: X-Ray powder pattern and IR-spectra of compounds **1**, **2** and **3**. DTA, DTG and TG curves for compounds **1** and **2**. Additional specific heat and magnetic measurements for compound **3**. CCDC 1015898 and 1015899. For ESI and crystallographic data in CIF or other electronic format see DOI: 10.1039/c4dt02271h

expressed by the Cole–Cole parameter α, is relatively broad and depends on the temperature.[59] Moreover, the relaxation time that could be traced back to the relaxation of single chains was too fast to explain the hysteresis and bifurcations observed in experiments. Thus, the magnetism of this family of compounds seems to be more complicated, in particular interchain interactions cannot be neglected. To reduce the interchain interactions and to study its influence on the magnetic properties we prepared similar compounds based on 4-(3-phenylpropyl)pyridine as a co-ligand for which larger interchain distances are expected. In this context the question arises, *e.g.* whether the relaxations are retained on ligand exchange.

Results and discussion

Synthetic aspects

$Co(NCS)_2$ and 4-(3-phenylpropyl)pyridine were reacted in different ratios and in different solvents (water, ethanol, methanol and acetonitrile) and the products isolated were characterized by elemental analysis, IR-spectroscopy and X-ray powder diffraction (XRPD). In these experiments three samples of composition $Co(NCS)_2$(4-(3-phenylpropyl)pyridine)$_4$ (**1**), $Co(NCS)_2$(4-(3-phenylpropyl)pyridine)$_2(H_2O)_2$ (**2**) and $[Co(NCS)_2$(4-(3-phenylpropyl)pyridine)$_2]_n$ (**3**) were obtained. Compound **1** is accessible in all solvents if the ratio between $Co(NCS)_2$ and PPP is 1 : 4 or larger. Compound **2** can be prepared using stoichiometric ratios in water but also from other solvents if some extra amount of water is added. If solvents are used with practically no water content, compound **3** will form.

The asymmetric ν(as) CN stretching vibrations are observed at 2071 cm^{-1} for **1**, at 2109 cm^{-1} for **2** and at 2098 cm^{-1} for **3**, indicating that in **1** and **2** the thiocyanato anions are only terminal N-bonded, whereas in **3** they act as μ-1,3-bridging ligands (Fig. S1–S3 in the ESI‡). The crystal structures of **1** and **3** were determined by single crystal structure analysis (see below). Compound **2** is isotypic to the corresponding Mn compound reported recently,[60] which is obvious if the experimental X-ray powder pattern of this compound is compared with that calculated from the single crystal data for the Mn compound (Fig. S4 in the ESI‡). Moreover, a Pawley fit reveals that this compound is obtained as a pure phase (Fig. S5 in the ESI‡). Comparison of the experimental patterns of **1** and **3** with those calculated from the single crystal data also proves that these compounds are obtained as pure samples, which additionally was proven for the more important compound **3** by a Pawley fit (Fig. S6–S8 in the ESI‡).

To investigate if compound **3** can also be obtained by thermal decomposition of compound **1** or **2**, or if a different crystalline modification is obtained as frequently observed for this class of compounds, **1** and **2** were investigated by simultaneous differential thermoanalysis (DTA) and thermogravimetry (DTG). For compound **1** only one distinct mass step is observed in the TG curve that corresponds to the removal of all co-ligands in one step (Fig. S9 in the ESI‡). In contrast, for compound **2** two mass steps are observed of which the first corresponds to that calculated if only the water molecules are removed (Fig. S10 in the ESI‡). If the TG experiment is repeated and stopped after water removal and the residue is investigated by IR-spectroscopy and XRPD, it is proved that it consists of **3** exclusively, thus, no different crystalline phase has been formed (Fig. S11 and S12 in the ESI‡).

Crystal structures

$Co(NCS)_2$(4-(3-phenylpropyl)pyridine)$_4$ (**1**) crystallizes in the triclinic space group $P\bar{1}$ with one crystallographically independent molecule which is situated on a center of inversion. The crystal structure consists of discrete complexes, in which the Co centers are octahedrally coordinated by two terminal anions and four neutral 4-(3-phenylpropyl)pyridine ligands (Fig. 1). Bond lengths and angles around the Co centers are in the usual range for similar compounds (Table S1‡).

Compound **2** is isotypic to $Mn(NCS)_2$(4-(3-phenylpropyl)-pyridine)$_2(H_2O)_2$ reported recently and also consists of discrete complexes, in which the metal cations are octahedrally coordinated.[60]

$[Co(NCS)_2$(4-(3-phenylpropyl)pyridine)$_2]_n$ (**3**) crystallizes in the monoclinic space group $P2_1/n$ with four formula units in the unit cell. The asymmetric unit consists of two crystallographically independent cobalt cations located on centers of inversion as well as two thiocyanato anions and two 4-(3-phenylpropyl)pyridine ligands in general positions. The cobalt cation is coordinated by two N-bonded 4-(3-phenylpropyl)pyridine ligands and four μ-1,3 bridging thiocyanato anions within a slightly distorted octahedral coordination geometry.

The cobalt cations are linked in chains by pairs of *trans* oriented μ-1,3-bridging thiocyanato anions (Fig. 2). In the crystal structure the Co thiocyanato chains extend in the direc-

Fig. 1 View of the coordination sphere of **1**. An ORTEP plot of this structure can be found in Fig. S13 in the ESI.‡

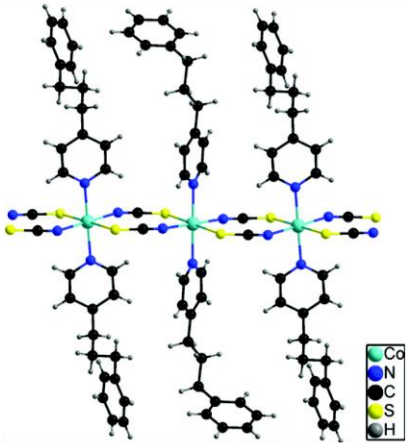

Fig. 2 View of the Co thiocyanato chains in 3. An ORTEP plot of this structure can be found in Fig. S14 in the ESI.‡

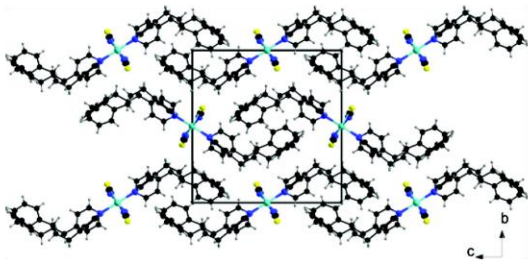

Fig. 3 Crystal structure of 3 shown along the crystallographic *a*-axis.

tion of the crystallographic *a*-axis and are arranged in such a way that the co-ligands of neighboring chains fit perfectly into the aperture formed by the co-ligands of neighboring chains (Fig. 3). There are no indications for specific, *e.g.* π···π or C–H···π interactions and it is more likely that this arrangement leads to a more dense packing of the building blocks. The intrachain Co···Co distance amounts to 5.639 Å, and the $N_{co\text{-}ligand}$–$N_{co\text{-}ligand}$ vector between the two neighbored Co atoms (Co1 and Co2) amounts to 6.7° (Table 1). The shortest interchain Co···Co distances are 11.261 and 12.973 Å (Table 1). Therefore, as mentioned in the Introduction, the shortest Co1···Co1 interchain distance is significantly longer than those reported for the similar coordination polymers with pyridine and 4-ethylpyridine (Table 1). It is noted that Co complexes in neighboring chains are canted and that their $N_{co\text{-}ligand}$–$N_{co\text{-}ligand}$ angles amount to 83.8° (N–Co1–N/N–Co1–N), 116.6° (N–Co1–N/N–Co2–N) and 58.9° (N–Co2–N/N–Co2–N).

Magnetic investigations

The magnetic susceptibility of 3 at 300 K gives χT = 3.1 cm^3 K mol^{-1}, corresponding to an effective magnetic moment of 4.98 μ_B. This value is within the range 4.7–5.2 μ_B, typical for

Table 1 Intra and shortest interchain Co···Co distances in 1D thiocyanato coordination polymers of composition $[Co(NCS)_2(L)_2]_n$ and $[Co(NCS)_2(L')]_n$ (bpe = 1,2-bis(-4-pyridyl)-ethylene; bpa = 1,2-bis(-4-pyridyl)-ethane; PPP = 4-(3-phenylpropyl)pyridine: the numbers in parentheses refer to the Co···Co distance along the bpe or bpa co-ligand

L/L′	Intrachain distances	Interchain distances
Pyridine	5.626/5.640 Å	8.675/8.950 Å
Ethylpyridine	5.623/5.659 Å	8.658/9.186 Å
PPP	5.639 Å	12.973/11.261 Å
bpe	5.648 Å	9.514 (13.716) Å
bpa	5.611 Å	9.569 (13.681) Å

the room temperature magnetic moment of the Co(II) ion in an octahedral surrounding.[10,61] The decrease of $\chi T(T)$ below room temperature (see Fig. 4) is an effect of Co(II) single ion properties.

Below 50 K a further decrease, expected for an isolated Co ion, is overwhelmed by a strong increase due to a ferromagnetic exchange interaction between Co magnetic moments. A similar behavior was also observed in related Co–NCS–Co and Co–NCSe–Co chain compounds.[53,54] Temperature dependence of magnetization measured using a low field (inset of Fig. 4) has the maximum slope at 3.4 K. Zero-field cooled and field cooled curves bifurcate at 3.2 K pointing to an irreversibility of magnetization below this temperature and a kind of freezing of magnetic moments.

The magnetization reaches an elevated value even at low fields applied, and for this reason it is necessary to take the demagnetization effect into account in further analysis. Neglecting this effect led in our preliminary measurements and data analysis to inconsistent results, in disagreement with the ferromagnetic ground state (see further text).

To estimate the demagnetization effect, magnetic measurements were performed using the powder sample pressed into a pellet of ϕ5 mm × 2 mm. For most of the measurements, the pellet was oriented along the magnetic field, and only for a test measurement it was oriented perpendicular to the field

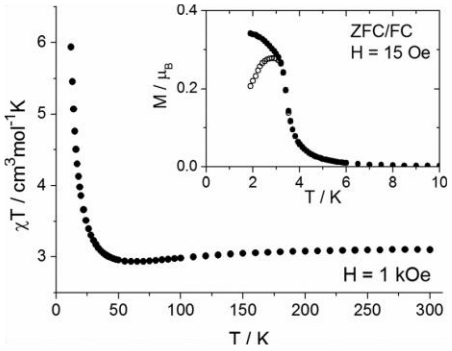

Fig. 4 Temperature dependence of χT for 3 measured at H = 1 kOe. Data above 6 cm^3 mol^{-1} K are cut. Inset: zero-field cooled (open symbols) and field cooled (solid symbols) magnetization per f.u. measured at H = 15 Oe.

(Fig. S15 in the ESI‡). The demagnetization factor N was estimated approximating the cylindrical shape of the sample by an ellipsoid and using the appropriate analytical formula,[62] obtaining

$$N_\perp = 0.60 \times 4\pi, N_\parallel = 0.20 \times 4\pi$$

for two orientations of the sample. The demagnetization field

$$H_{\text{demag}} = -N \cdot M/V,$$

where M/V is the magnetic moment of the sample per volume, adds to the applied field. This affects the dimensionless susceptibility (magnetic moment per volume) as

$$\frac{1}{\chi} = \frac{1}{\chi_a} - N$$

where χ is the true susceptibility, and χ_a is the measured apparent susceptibility. The same equation holds in the case of ac measurements, with the complex susceptibility

$$\chi = \chi' - i\chi''.$$

Explicit equations to calculate χ' and χ'' using χ'_a and χ''_a are given *e.g.* in ref. 63 The influence of demagnetization in the case of **3** is shown in Fig. S15 in ESI.‡ In further text the corrected susceptibility is presented and analyzed.

In the case of Co^{II}, it is safe to assume that each Co has an effective spin s = 1/2 below 20 K, due to the Kramers doublet as the ground state of the ion in an axially distorted octahedral crystal field. A model chain of s = 1/2 Ising spins with the exchange interaction described by the Hamiltonian

$$H = -J\sum_i s_i^z s_{i+1}^z \quad (1)$$

is solved exactly[64] giving the expression for the magnetic zero-field susceptibility

$$\chi_\parallel^{\text{chain}} = \frac{N_A g_\parallel^2 \mu_B^2}{4kT} \exp\left(\frac{J}{2kT}\right), \quad (2)$$

where the index ∥ denotes the value parallel to the easy axis of Ising spins.[64,65] The exponential dependence is responsible for the strong increase of $\chi T(T)$. The susceptibility of **3** measured at low field and low temperature is presented in Fig. 5 as $\ln(\chi T)$ *vs.* $1/T$. The linear dependence is observed in the 5–20 K temperature range, but below 5 K χT increases more strongly than predicted by eqn (2). This can be explained by introducing a ferromagnetic interaction between chains zJ' in the mean field model approximation

$$\chi_\parallel = \frac{\chi_\parallel^{\text{chain}}}{1 - zJ'\chi_\parallel^{\text{chain}}/N_A g_\parallel^2 \mu_B^2} \quad (3)$$

$$\chi = \chi_\parallel/3$$

The last equation takes into account averaging over angles for the powder sample, assuming that the perpendicular susceptibility of the Ising chain $\chi_\perp^{\text{chain}}$ is much smaller than the $\chi_\parallel^{\text{chain}}$. Fitting the parameters of eqn (2) and (3) to the corrected

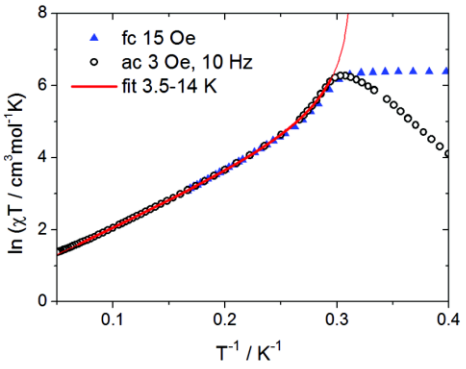

Fig. 5 Low field susceptibility, shown as $\ln(\chi T)$, *versus* inverse temperature. Triangles denote field cooled dc susceptibility, circles denote ac susceptibility, both corrected for demagnetization. The solid line is a fit (see text).

ac susceptibility in the temperature range from 3.5 to 14 K, we obtained $g_\parallel$ = 7.53(3), J = 29.5(1) K, zJ' = +0.38(1) K. The curve calculated using these parameters diverges at T = 3.1 K (see Fig. 5). For the $g_\parallel$ value of 7.5, $g_\perp$ is in the range 1.5–2.5 (see ref. 64 for the plot showing the relation between ground state $g_\parallel$ and $g_\perp$ values of Co in an axially deformed octahedron). This justifies neglecting in our analysis the $\chi_\perp^{\text{chain}}$ that is proportional to $g_\perp^2$.

The magnetization of compound **3** measured as a function of the field at 1.8 K, shown in Fig. 6, is typical for a ferromagnet with a strong single-ion anisotropy. The rapid increase of magnetization to 1.65μ_B at 1 kOe is due to the alignment of domains and, possibly, the influence of the magnetic field on canted magnetic moments. Such an influence is possible because the energy $g_\parallel s\mu_B H$ for H = 1 kOe is 0.25 K, which is of the order of the zJ' interaction constant. The almost linear increase of the magnetization at higher fields is related to the single-ion anisotropy of Co(II). The hysteresis loop is observed

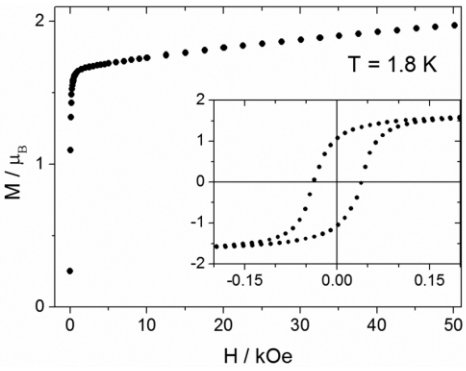

Fig. 6 Magnetization of **3** per f.u. measured at T = 1.8 K. The field was corrected for the demagnetization effect.

only at low fields, and has a coercive field of about 40 Oe at 1.8 K.

The ac susceptibility of compound **3** is shown in Fig. 7. The ac susceptibility curves were also corrected for demagnetization, because the demagnetization effect mixes χ' and χ'' components shifting slightly the peaks of apparent susceptibility. The peaks of $\chi'(T)$ are accompanied by peaks of out-of-phase susceptibility χ''. With decreasing ac frequency f all maxima shift to lower temperatures, which is indicative of a slow relaxation of the magnetization as observed in, *e.g.*, single chain magnets or spin glasses. The Mydosh parameter is defined as the relative temperature shift of the susceptibility peak on a decade of frequency

$$\Delta T_m/[T_m \Delta(\log f)],$$

where T_m is the position of the χ' maximum, equals 0.018. If positions of χ'' maxima are used, the value of 0.059 is obtained.

This is below the range typical for superparamagnets and single chain magnets, but falls in the range typical for spin glasses (0.01–0.08). The temperature dependence of the relaxation time τ for SCMs should follow the Arrhenius law

$$\tau = \tau_0 \exp(E_a/kT),$$

where $\tau = 1/(2\pi f)$. From the $\chi''(T)$ maxima, the values $E_a = 116$ K and $\tau_0 = 10^{-19}$ s are obtained. Such low τ_0 is unphysical, and the E_a value differs a lot from the ~40 K obtained for compounds of the same family that demonstrate SCM behavior. On the other hand, for cluster spin-glasses the Vogel–Fulcher law

$$\tau = \tau_0 \exp[E_a/k(T_m - T_0)] \quad (4)$$

is frequently fulfilled. T_0 is a measure of interparticle or intercluster interaction. The application of eqn (4) in the case of **3** leads to reasonable values of the parameters $E_a = 19(2)$ K, $T_0 = 2.6(4)$ K, and $\tau_0 = 5 \times 10^{-15}$ s (see Fig. S17‡). Thus compound **3** might not show SCM behavior and in contrast to all other compounds of this family the relaxation properties seem to be more complex.

The magnetic measurements presented so far do not answer the important question of whether there is a long range magnetic order in **3**. The lack of an obvious source of a crystal disorder and the positive zJ' suggest a ferromagnetic ordering, but slow relaxations resemble those of a cluster spin-glass. To answer this important question, specific heat measurements were performed.

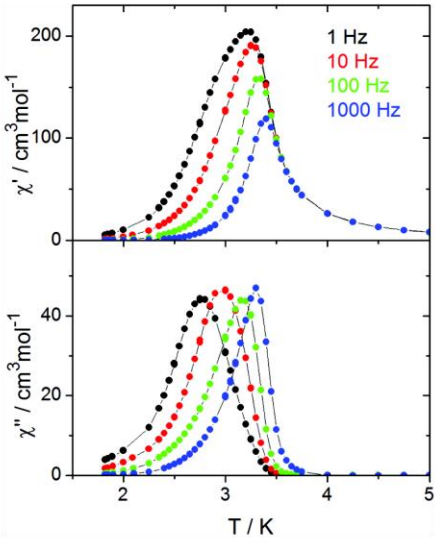

Fig. 7 Temperature dependence of the ac susceptibility for **3** measured using different frequencies, the driving field H_{ac} = 3 Oe, and H_{dc} = 0 Oe. The χ' and χ'' values were corrected for the demagnetization.

Specific heat

To check if there is a magnetic ordering transition in compound **3** the specific heat C was measured in the range from 2 to 20 K. The data measured without an applied magnetic field are presented in Fig. 8, while data for different fields, from 0.4 to 90 kOe, are shown in Fig. S16 in the ESI.‡ A peak is present at T_c = 3.3 K in the zero field $C(T)$ dependence, denoting an ordering transition around this temperature. It is noted that this peak is not visible at higher fields, which is typical for a ferromagnetic transition.

For compound **3** the phonon contribution to the specific heat is significant even below 5 K, due to a number of atoms in the formula unit, and the softness of the material. To analyze the data we approximated the phonon contribution using the single mode Debye model. Since this is a crude approximation of the real phonon density of states, the applicability of such a method is limited to low temperatures.

For the chain of Ising spins $s = 1/2$, as defined by (1), the magnetic contribution to the specific heat is

$$C_{chain} = R(J/4kT)^2 \operatorname{sech}^2(J/4kT),$$

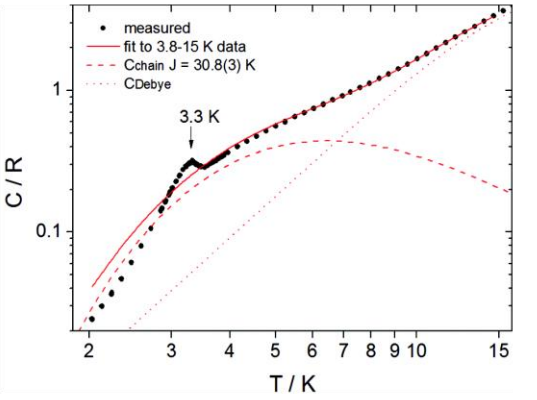

Fig. 8 Molar specific heat of **3** in units of R (the gas constant). The lines were calculated as described in the text.

where the gas constant $R = N_A k$.[64,65] This model does not include inter-chain interactions, and therefore, does not account for the ordering transition. For this reason the equation

$$C(T) = C_{\text{chain}}\ (J, T) + AC_{\text{Debye}}\ (\theta_D, T)$$

was fitted in the range 3.8–15 K, *i.e.* above T_c. We obtained the parameters J = 30.8(3) K, the effective Debye temperature θ_D = 84(1) K and the factor A = 0.43(1). The sign of J cannot be determined purely on the basis of specific heat data. The positive sign was assigned based on the magnetic measurements. The fitted $C(T)$ is drawn in Fig. 8 and extrapolated to lower temperatures. Also both contributions, calculated for the fitted parameters, are shown. Almost identical results were obtained assuming simply that the phonon contribution is proportional to T^3 and limiting the temperature range up to 10 K. This is also visible in Fig. 8 where the marked $C_{\text{Debye}}(T)$ dependence starts to deviate from the T^3 law only above 10 K. It is noted that the value for the intrachain interaction J of 29.5(1) K estimated from magnetic measurements is in very good agreement with that estimated from the specific heat measurements J = 30.8(3) K.

Above 3.8 K the fitted $C(T)$ follows experimental points, confirming that magnetic properties of **3** can be described above this temperature using the one dimensional model. However, at lower temperatures, the fitted $C(T)$ deviates from measured data, which denotes a crossover from the 1D to the 3D system, due to the magnetic interaction between the chains. The critical entropy, *i.e.* the entropy change from 0 to T_c quantifies how ideal the 1D magnetic system is. It is zero for the 1D system, about $0.805R \ln 2$ for 1/2 Ising spins on the simple cubic 3D lattice,[64,66] and reaches $R \ln 2$ for the mean-field model. For **3** the entropy change from 2 to 3.3 K (which is close to the critical entropy) is only $0.060R \ln 2$, close to the 1D case.

The specific heat data unambiguously show that compound **3** undergoes a true phase transition to a magnetically ordered state.

Comparison of the magnetic properties with those for related compounds

As mentioned in the Introduction, the new compound **3** is a member of a family of compounds that are strongly related, because in all of these compounds the Co(II) cations are linked by the anionic ligands into chains. This includes $[Co(NCS)_2(pyridine)_2]_n$,[53] $[Co(NCS)_2(4\text{-ethylpyridine})_2]_n$,[58] $[Co(NCS)_2(bpe)]_n$ (bpe = 1,2-bis(4-pyridyl)-ethylene)[55,59] and $[Co(NCS)_2(bpa)]_n$ (bpa = 1,2-bis(4-pyridyl)-ethane),[20] all of them showing ferromagnetic interactions within the Co thiocyanato chains. The intrachain distances in all of these compounds are comparable (see Table 1) and therefore, similar values for the intrachain interactions are obtained from fittings of magnetic data (4-ethylpyridine: 25.2 K, bpe: 25.9 K, and bpa: 28.1 K).

However, as concerns interchain interactions, the situation is not so obvious. Likewise compound **3**, the compound with pyridine also shows ferromagnetic interchain interactions and a ferromagnetic transition, whereas the other three compounds are metamagnets and therefore, show an antiferromagnetic transition below their critical field. For $[Co(NCS)_2(bpe)]_n$ this can be rationalized because in this compound the ferromagnetic Co thiocyanato chains are antiferromagnetically coupled by the bpe co-ligands. The reason why $[Co(NCS)_2(bpa)]_n$ also shows antiferromagnetic canted interchain coupling is more difficult to understand because it can be assumed here that the co-ligand does not participate in the magnetic exchange. Therefore, dipolar interactions should play a role.

In compound **3** there is also no exchange path between the chains, which means that also here dipolar interactions are important, and that they are responsible for the coupling of the chains into the 3D magnetic ordering. In such a case the arrangement of chains and their easy axes decide on the ground state magnetic structure. In this context it is noted that the Co thiocyanato chains are differently arranged in the crystal structures of these compounds. Unfortunately, we still have no experimental proof on the direction of the easy axis, which would be needed to understand the magnetic properties in more detail.

However, in all compounds relaxations are observed, which means that this behavior does not disappear on the ligand exchange. For all these compounds except compound **3** these relaxations might be related to the relaxation of single chains, even if the overall magnetic behavior is more complex. In contrast, the origin of the relaxations in compound **3** is not proven and its magnetic behavior seems to be more complicated.

Conclusion

In the present contribution the magnetic properties of a new Co(II) thiocyanato coordination polymer **3** are reported. **3** belongs to a family of compounds that are structurally strongly related, and for which slow relaxations were observed in the ac magnetic measurements indicative of single chain magnetism.

Both specific heat measurements and magnetic measurements consistently show that compound **3** is a quasi-one dimensional ferromagnet with T_c = 3.3 K. The values of the intra-chain exchange interaction J obtained from both types of measurements are very close to each other and are in agreement with those values obtained for all related compounds. Interestingly, on the ligand exchange the magnetic relaxations are retained, but because the relaxation properties of **3** are more complex it is still not proved whether they can be traced back to the same origin. According to our findings this seems to be unlikely. These magnetic relaxations are present not only above but also below the ordering transition, and this effect is similar to the SCM relaxational behavior observed in, *e.g.*, the antiferromagnetically ordered compounds reported recently.[67–69] However the relaxation dynamics of **3** follows the Vogel–Fulcher equation much better than the Arrhenius activation law, which excludes SCM behavior and rather points to

a glassy behaviour of 3. Such effects may result from clusters that evolve, with decreasing temperature, from single chains to a higher dimension, as shown by Etzkorn *et al.* for quasi-one dimensional systems.[70] The slow relaxation in 3 may be due to SCM-like behavior far above T_c and the cluster (domain) relaxation below T_c. The ac measurements in a much wider frequency range are needed to explore such a scenario.

In principle, such a behavior can also originate from disordered, frustrated interactions between ferromagnetic nanoparticles, but in our opinion this can be excluded. First of all our XRPD investigations gave no hint of the presence of such particles, which should lead to a broadening of the reflection profiles. This is a bit different for samples prepared by thermal decomposition, where poorly crystalline powders with much smaller particles and relatively broad reflection profiles are observed. This is also obvious from SEM investigations of different batches shown in Fig. S18,‡ which show that the samples obtained by crystallization consist of relatively large particles, which is not the case for batches prepared by thermal decomposition. More importantly, independent of the synthetic method the same magnetic behavior with relaxations is always observed, and therefore, this possibility can be excluded.

In any case our results indicate that obviously a relatively stable chemical system was discovered, in which the relaxations are always retained and that therefore, allows detailed investigations on the relation between the structure and composition of these compounds and their relaxational properties.

Experimental section

$Co(NCS)_2$ and 4-(3-phenylpropyl)pyridine (PPP) were obtained from Alfa Aesar. KNCS and $Co(NO_3)_2{\cdot}6H_2O$ were obtained from Merck. Solvents were used without further purification. The crystalline powders of all compounds were prepared by stirring the reactants in the respective solvents at room temperature. The purity of the compounds was checked by X-ray powder diffraction and elemental analysis.

Synthesis of $Co(NCS)_2$(4-(3-phenylpropyl)pyridine)$_4$ (1)

Single crystals suitable for single crystal X-ray diffraction were prepared by the reaction of $Co(NCS)_2$ (0.25 mmol, 43.8 mg) and 4-(3-phenylpropyl)pyridine (1.00 mmol, 192.6 μL) in 1.5 mL ethanol at 80 °C. After 1 day pink block-shaped crystals were obtained. A pink crystalline powder was synthesized by stirring $Co(NCS)_2$ (0.25 mmol, 43.8 mg) and 4-(3-phenylpropyl)pyridine (1.00 mmol, 192.6 μL) in 1.5 mL H_2O for 3 days. Yield: 87.2%. Elemental analysis for $C_{58}H_{60}CoN_6S_2$: calcd C 72.25, H 6.27, N 8.72, S 6.65; found: C 72.37, H 6.44, N 8.63, S 6.39. IR (ATR): ν_{max} = 3023 (w), 2942 (w), 2860 (w), 2071 (s), 1610 (m), 1420 (m), 1012 (m), 750 (m), 702 (m), 515 (m).

Synthesis of $Co(NCS)_2$(4-(3-phenylpropyl)pyridine)$_2(H_2O)_2$ (2)

A light pink colored crystalline powder was synthesized by stirring $Co(NO_3)_2{\cdot}6H_2O$ (1.00 mmol, 291 mg), KNCS (2.00 mmol, 194 mg) and 4-(3-phenylpropyl)pyridine (2.00 mmol, 385.2 μL) in 5 mL MeCN and 2 mL H_2O for 3 days. Yield: 70%. Elemental analysis for $C_{30}H_{34}CoN_4O_2S_2$ in %: calcd C 59.49, H 5.66, N 9.25, S 10.59; found: C 59.67, H 5.62, N 9.16, S 10.24. IR (ATR): ν_{max} = 3436 (b), 3347 (b), 3024 (w), 2945 (w), 2855 (w), 2109 (s), 1613 (s), 1425 (m), 1225 (m), 1019 (m), 824 (m), 755 (s), 697 (m), 498 (m).

Synthesis of $[Co(NCS)_2$(4-(3-phenylpropyl)pyridine)$_2]_n$ (3)

Single crystals suitable for single crystal X-ray diffraction were prepared by the reaction of $Co(NCS)_2$ (0.25 mmol, 43.8 mg) and 4-(3-phenylpropyl)pyridine (0.50 mmol, 96.3 μL) in 1.5 mL ethanol. After one week pink block-shaped crystals were obtained. A light pink colored crystalline powder was synthesized by stirring $Co(NCS)_2$ (1.00 mmol, 175.1 mg) and 4-(3-phenylpropyl)pyridine (1.00 mmol, 192.6 μL) in 5 mL H_2O for 3 d. Yield: 85.7%. Elemental analysis for $C_{30}H_{30}CoN_4S_2$ in %: calcd C 63.25, H 5.31, N 9.84, S 11.26; found: C 63.18, H 5.26, N 9.79, S 11.15. Co content determined by AAS: 10.31% (calc.: 10.35%). IR (ATR): ν_{max} = 3017 (w), 2943 (w), 2857 (w), 2098 (s), 1615 (m), 1422 (m), 1226 (m), 1016 (m), 748 (m), 699 (s), 495 (m).

Elemental analysis

CHNS analysis was performed using an EURO EA elemental analyzer fabricated by EURO VECTOR Instruments and Software.

IR-spectroscopy

All IR data were obtained using an ATI Mattson Genesis Series FTIR Spectrometer, control software: WINFIRST, from ATI Mattson.

Single crystal structure analysis

The data collection was performed with imaging plate diffraction systems (STOE IPDS-1 (1), STOE IPDS-2 (3)) using MoK_α radiation. The structure solution was done with direct methods using SHELXS-97 and structure refinement was performed against F^2 using SHELXL-97.[71] For compound 1 a numerical absorption correction was applied using X-red and X-shape of the Program Package X-area.[72] All non-hydrogen atoms were refined with anisotropic displacement parameters. All hydrogen atoms were positioned with idealized geometry and were refined isotropically with $U_{eq}(H) = -1.2U_{eq}(C)$ using a riding model with d_{C-H} = 0.93 Å. Details of the structure determination are given in Table 2.

The crystal of compound 2 is non-merohedrally twinned. Both individuals were indexed separately and from their orientation matrix, the twin law was calculated (−1 0 0 0 1 0 0.3 0 1). Afterwards the structure was refined in the HKLF5 format (BASF parameter: 0.156 (2)). Because in this procedure symmetry equivalent reflections cannot be merged, which would lead to an artificially high ratio between reflections and parameters, all reflections were merged before generating the file in HKLF-5 format. Because some symmetry equivalent reflections are affected by the second individuum, absorption

Table 2 Selected crystal data and details on the structure determination of compounds **1** and **3**

Compound	1	3
Formula	$C_{58}H_{60}CoN_6S_2$	$C_{30}H_{30}CoN_4S_2$
M_w/g mol^{-1}	964.17	569.63
Crystal system	Triclinic	Monoclinic
Space group	$P\bar{1}$	$P2_1/n$
Z	1	4
D_{calc}/mg cm^{-3}	1.261	1.331
μ/mm^{-1}	0.464	0.776
a/Å	9.4597(7)	11.2774(6)
b/Å	11.3800(9)	16.0343(8)
c/Å	13.1332(10)	15.8148(10
α/°	72.399(9)	90
β/°	82.890(9)	96.240(5)
γ/°	70.483(9)	90
V/Å^3	1269.78(17)	2842.8(3)
T/K	200(2)	293(2)
Scan range 2θ/°	2.51 to 27.00	1.81 to 25.27
Measured refl.	13 385	26 128
R_{int}	0.0577	0.0794
Min/max transm.	0.8083, 0.9544	—
Unique reflns	5439	5039
Refl. [$F_0 > 4\sigma(F_0)$]	4171	3014
Parameters	304	338
R_1 [$F_0 > 4\sigma(F_0)$]	0.0410	0.0540
wR_2 [all data]	0.1069	0.1789
GOF	0.955	0.937
$\Delta\rho_{max/min}$/e Å^{-3}	0.277 and −0.641	0.845 and −0.275

correction was performed using data for which the overlapping reflections were omitted.

CCDC 1015898 (**1**) and CCDC 1015899 (**3**) contain the supplementary crystallographic data for this paper.

Differential thermal analysis and thermogravimetry (DTA-TG)

The DTA-TG measurements were performed under a nitrogen atmosphere (purity: 5.0) in Al_2O_3 crucibles using a STA-409CD instrument from Netzsch. All measurements were performed with a flow rate of 75 mL min^{-1} and were corrected for buoyancy and current effects. The instrument was calibrated using standard reference materials.

X-Ray powder diffraction (XRPD)

The measurements were performed using (1) a PANalytical X'Pert Pro MPD Reflection Powder Diffraction System with CuK_α radiation (λ = 154.0598 pm) equipped with a PIXcel semiconductor detector from PANalytical and (2) a Stoe Transmission Powder Diffraction System (STADI P) with CuK_α radiation (λ = 154.0598 pm) that was equipped with a linear position-sensitive detector from STOE & CIE.

Magnetic measurements

Magnetic measurements were performed using a QD MPMS-5XL magnetometer. The powder sample was pressed into a pellet. During most of measurements the sample was oriented with the flat surface parallel to the magnetic field, to minimize the demagnetization effect. This effect was estimated and taken into account correcting apparent susceptibility, or applied field. We checked also for the absence of ferromagnetic impurities at room temperature. Some additional measurements were also performed using a PPMS (Physical Property Measurement System) from Quantum Design. The data were corrected for core diamagnetism.

Specific heat

Specific heat measurements were performed using the relaxation technique with QD PPMS equipment. The powder sample was pressed into a pellet with no binder, and 3 mm diameter, 6.2 mg. The heat capacity of the microcalorimeter, including a drop of Apiezon N grease used to fix the sample, was measured earlier and subtracted. It was also checked that the influence of magnetic field on the calorimeter heat capacity was negligible in this case.

Atomic absorption spectroscopy (AAS)

AAS measurements were performed using an AAnalyst 300 spectrometer from Perkin Elmer. Calibration curves were measured using standard reference materials. For each sample at least three different measurements were performed, in which the Co content differs by a maximum of about 0.3%.

Scanning electron microscopy (SEM)

The SEM measurements were performed with a Philips Environmental Scanning Electron Microscope ESEM XL30, which is equipped with an EDAX detector.

Acknowledgements

This project was supported by the Deutsche Forschungsgemeinschaft (project no. Na 720/5-1) and the State of Schleswig-Holstein. We thank Prof. Dr Wolfgang Bensch for access to his experimental facilities. The research was in part carried out with the equipment purchased with the support of European Regional Development Fund within the Polish Innovation Economy Operational Program (POIG.02.01.00-12-023/08).

References

1 S. R. Batten and K. S. Murray, *Coord. Chem. Rev.*, 2003, **246**, 103–130.
2 C. Janiak, *Dalton Trans.*, 2003, 2781–2804.
3 D. Maspoch, D. Ruiz-Molina and J. Veciana, *J. Mater. Chem.*, 2004, **14**, 2713–2723.
4 D. Braga, L. Maini, M. Polito, L. Scaccianoce, G. Cojazzi and F. Grepioni, *Coord. Chem. Rev.*, 2001, **216**, 225–248.
5 S. L. James, *Chem. Soc. Rev.*, 2003, **32**, 276–288.
6 X.-B. Li, Y. Ma, X.-M. Zhang, J.-Y. Zhang and E.-Q. Gao, *Eur. J. Inorg. Chem.*, 2011, **2011**, 4738–4744.
7 Y.-F. Zeng, X. Hu, F.-C. Liu and X.-H. Bu, *Chem. Soc. Rev.*, 2009, **38**, 469–480.
8 D.-F. Weng, Z.-M. Wang and S. Gao, *Chem. Soc. Rev.*, 2011, **40**, 3157–3181.

9 J. Ferrando-Soria, R. Ruiz-García, J. Cano, S.-E. Stiriba, J. Vallejo, I. Castro, M. Julve, F. Lloret, P. Amorós, J. Pasán, C. Ruiz-Pérez, Y. Journaux and E. Pardo, *Chem. – Eur. J.*, 2012, **18**, 1608–1617.

10 M. Kurmoo, *Chem. Soc. Rev.*, 2009, **38**, 1353–1379.

11 M. Wriedt and H.-C. J. Zhou, *Dalton Trans.*, 2012, **41**, 4207–4216.

12 G. Aromi, D. Aguila, P. Gamez, F. Luis and O. Roubeau, *Chem. Soc. Rev.*, 2012, **41**, 537–546.

13 W. L. Leong and J. J. Vittal, *Chem. Rev.*, 2011, **111**, 688–764.

14 X.-Y. Wang, Z.-M. Wang and S. Gao, *Chem. Commun.*, 2008, 281–294.

15 J. Vallejo, I. Castro, L. Canadillas-Delgado, C. Ruiz-Perez, J. Ferrando-Soria, R. Ruiz-Garcia, J. Cano, F. Lloret and M. Julve, *Dalton Trans.*, 2010, **39**, 2350–2358.

16 J. S. Miller, *Adv. Mater.*, 2002, **14**, 1105–1110.

17 C. Näther, S. Wöhlert, J. Boeckmann, M. Wriedt and I. Jeß, *Z. Anorg. Allg. Chem.*, 2013, **639**, 2696–2714.

18 A. Caneschi, D. Gatteschi, N. Lalioti, C. Sangregorio, R. Sessoli, G. Venturi, A. Vindigni, A. Rettori, M. G. Pini and M. A. Novak, *Angew. Chem., Int. Ed.*, 2001, **113**, 1810–1813.

19 H.-L. Sun, Z.-M. Wang and S. Gao, *Coord. Chem. Rev.*, 2010, **254**, 1081–1100.

20 W.-X. Zhang, R. Ishikawa, B. Breedlovea and M. Yamashita, *RSC Adv.*, 2013, **3**, 3772–3798.

21 R. Mas-Ballesté, J. Gómez-Herrero and F. Zamora, *Chem. Soc. Rev.*, 2010, **39**, 4220–4233.

22 K. Bernot, J. Luzon, A. Caneschi, D. Gatteschi, R. Sessoli, L. Bogani, A. Vindigni, A. Rettori and M. G. Pini, *Phys. Rev. B: Condens. Matter*, 2009, **79**, 134419.

23 S. Hu, L. Yun, Y.-Z. Zheng, Y.-H. Lan, A. K. Powell and M.-L. Tong, *Dalton Trans.*, 2009, 1897–1900.

24 T. D. Harris, M. V. Bennett, R. Clérac and J. R. Long, *J. Am. Chem. Soc.*, 2010, **132**, 3980–3988.

25 A. V. Palii, O. S. Reu, S. M. Ostrovsky, S. I. Klokishner, B. S. Tsukerblat, Z.-M. Sun, J.-G. Mao, A. V. Prosvirin, H.-H. Zhao and K. R. Dunbar, *J. Am. Chem. Soc.*, 2008, **130**, 14729–14738.

26 Z. Tomkowicz, M. Rams, M. Bałanda, S. Foro, H. Nojiri, Y. Krupskaya, V. Kataev, B. Büchner, S. K. Nayak, J. V. Yakhmi and W. Haase, *Inorg. Chem.*, 2012, **51**, 9983–9994.

27 M.-X. Yao, Q. Zheng, K. Qian, Y. Song, S. Gao and J.-L. Zuo, *Chem. – Eur. J.*, 2013, **19**, 294–303.

28 J.-P. Zhao, Q. Yang, Z.-Y. Liu, R. Zhao, B.-W. Hu, M. Du, Z. Chang and X.-H. Bu, *Chem. Commun.*, 2012, **48**, 6568–6570.

29 I. Bhowmick, E. A. Hillard, P. Dechambenoit, C. Coulon, T. D. Harris and R. Clerac, *Chem. Commun.*, 2012, **48**, 9717–9719.

30 M. G. Pini, A. Rettori, L. Bogani, A. Lascialfari, M. Mariani, A. Caneschi and R. Sessoli, *Phys. Rev. B: Condens. Matter*, 2011, **84**, 094444.

31 F. Luo, Z.-w. Liao, Y.-m. Song, H.-x. Huang, X.-z. Tian, G.-m. Sun, Y. Zhu, Z.-Z. Yuan, M.-b. Luo, S.-j. Liu, W.-y. Xu and X.-F. Feng, *Dalton Trans.*, 2011, **40**, 12651–12655.

32 X.-B. Li, G.-M. Zhuang, X. Wang, K. Wang and E.-Q. Gao, *Chem. Commun.*, 2013, **49**, 1814–1816.

33 T. Han, W. Shi, Z. Niu, B. Na and P. Cheng, *Chem. – Eur. J.*, 2013, **19**, 994–1001.

34 J. H. Yoon, D. W. Ryu, S. Y. Choi, H. C. Kim, E. K. Koh, J. Tao and C. S. Hong, *Chem. Commun.*, 2011, **47**, 10416–10418.

35 M. Ding, B. Wang, Z. Wang, J. Zhang, O. Fuhr, D. Fenske and S. Gao, *Chem. – Eur. J.*, 2012, **18**, 915–924.

36 M. Bałanda, M. Rams, S. K. Nayak, Z. Tomkowicz, W. Haase, K. Tomala and J. V. Yakhmi, *Phys. Rev. B: Condens. Matter*, 2006, **74**, 224421.

37 J. Ferrando-Soria, D. Cangussu, M. Eslava, Y. Journaux, R. Lescouëzec, M. Julve, F. Lloret, J. Pasán, C. Ruiz-Pérez, E. Lhotel, C. Paulsen and E. Pardo, *Chem. – Eur. J.*, 2011, **17**, 12482–12494.

38 E. Shurdha, S. H. Lapidus, P. W. Stephens, C. E. Moore, A. L. Rheingold and J. S. Miller, *Inorg. Chem.*, 2012, **51**, 9655–9665.

39 M. Wriedt and C. Näther, *Chem. Commun.*, 2010, **46**, 4707–4709.

40 J. M. Shi, J. N. Chen, C. J. Wu and J. P. Ma, *J. Coord. Chem.*, 2007, **60**, 2009–2013.

41 S. Wöhlert, L. Fink, M. Schmidt and C. Näther, *CrystEngComm*, 2013, **15**, 945–957.

42 S. Wöhlert, M. Wriedt, T. Fic, Z. Tomkowicz, W. Haase and C. Näther, *Inorg. Chem.*, 2013, **52**, 1061–1068.

43 S. Wöhlert, L. Peters and C. Näther, *Dalton Trans.*, 2013, **42**, 10746–10758.

44 C. J. Adams, M. C. Muñoz, R. E. Waddington and J. A. Real, *Inorg. Chem.*, 2011, **50**, 10633–10642.

45 S. Wöhlert and C. Näther, *Eur. J. Inorg. Chem.*, 2013, **2013**, 2528–2537.

46 M. Wriedt, I. Jeß and C. Näther, *Eur. J. Inorg. Chem.*, 2009, 1406–1413.

47 C. J. Adams, M. F. Haddow, D. J. Harding, T. J. Podesta and R. E. Waddington, *CrystEngComm*, 2011, **13**, 4909–4914.

48 P. Bhowmik, S. Chattopadhyay, M. G. B. Drew, C. Diaz and A. Ghosh, *Polyhedron*, 2010, **29**, 2637–2642.

49 B. Machura, J. Palion, M. Penkala, T. Groń, H. Duda and R. Kruszynski, *Polyhedron*, 2013, **56**, 189–199.

50 B. Machura, A. Świtlicka, J. Mroziński, B. Kalińska and R. Kruszynski, *Polyhedron*, 2013, **52**, 1276–1286.

51 J. G. Małecki, T. Groń and H. Duda, *Polyhedron*, 2012, **36**, 56–68.

52 C. J. Adams, J. A. Real and R. E. Waddington, *CrystEngComm*, 2010, **12**, 3547–3553.

53 J. Boeckmann and C. Näther, *Dalton Trans.*, 2010, **39**, 11019–11026.

54 J. Boeckmann and C. Näther, *Chem. Commun.*, 2011, **47**, 7104–7106.

55 S. Wöhlert, J. Boeckmann, M. Wriedt and C. Näther, *Angew. Chem., Int. Ed.*, 2011, **50**, 6920–6923.

56 S. Wöhlert, U. Ruschewitz and C. Näther, *Cryst. Growth Des.*, 2012, **12**, 2715–2718.

57 J. Boeckmann, M. Wriedt and C. Näther, *Chem. – Eur. J.*, 2012, **18**, 5284–5289.

58 S. Wöhlert, T. Fic, Z. Tomkowicz, S. G. Ebbinghaus, M. Rams, W. Haase and C. Näther, *Inorg. Chem.*, 2013, **52**, 12947–12957.

59 S. Wöhlert, Z. Tomkowicz, M. Rams, S. G. Ebbinghaus, L. Fink, M. U. Schmidt and C. Näther, *Inorg. Chem.*, 2014, **53**, 8298–8310.

60 J. Werner, I. Jess and C. Näther, *Z. Anorg. Allg. Chem.*, 2014, **640**, 2161–2168.

61 O. Kahn, *Molecular Magnetism*, Wiley VCH, New York, 1993.

62 H. A. Farach, R. J. Creswick and C. P. Poole, *Superconductivity*, Academic Press, San Diego, 1995.

63 J. A. Quilliam, L. R. Yaraskavitch, H. A. Dabkowska, B. D. Gaulin and J. B. Kycia, *Phys. Rev. B: Condens. Matter*, 2011, **83**, 094424.

64 R. L. Carlin, *Magnetochemistry*, Springer Verlag, Berlin - Heidelberg - New York - Tokyo, 1986.

65 M. E. Fisher, *J. Math. Phys.*, 1963, **4**, 124–135.

66 L. J. de Jongh and A. R. Miedema, *Adv. Phys.*, 1974, **23**, 1.

67 I. Bhowmick, E. A. Hillard, P. Dechambenoit, C. Coulon, T. D. Harris and R. Clerac, *Chem. Commun.*, 2012, **48**, 9717–9719.

68 H. Miyasaka, K. Takayama, A. Saitoh, S. Furukawa, M. Yamashita and R. Clérac, *Chem. – Eur. J.*, 2010, **16**, 3656–3662.

69 C. Coulon, R. Clérac, W. Wernsdorfer, T. Colin and H. Miyasaka, *Phys. Rev. Lett.*, 2009, **102**, 164204–164207.

70 S. J. Etzkorn, W. Hibbs, J. S. Miller and A. J. Epstein, *Phys. Rev. Lett.*, 2002, **89**, 207201.

71 G. M. Sheldrick, *Acta Crystallogr., Sect. A: Fundam. Crystallogr.*, 2008, **A64**, 112–122.

72 *X-Area, Version 1.44, Program Package for Single Crystal Measurements*, STOE & CIE GmbH, Darmstadt, Germany, 2008.

3.2. Synthesis, Structure and Properties of $[Co(NCS)_2(4\text{-}(4\text{-Chlorobenzyl})pyridine)_2]_n$, that shows Slow Relaxations of the Magnetization and a Metamagnetic Transition

Julia Werner, Zbigniew Tomkowicz, Stefan G. Ebbinghaus, Tristan Neumann und Christian Näther, *Dalton Trans.* **2015**, *44*, 14149-14158.

Motivation

Da die Ergebnisse aus Kapitel 3.1 ergaben, dass die Verbindung mit 4-(3-Phenylpropyl)pyridin als Co-Liganden vermutlich keine Einzelkettenrelaxation zeigt, wurde bewiesen, dass es keinen einfachen Zusammenhang zwischen den Interkettenabständen und dem gewählten Liganden gibt. Um den Einfluss des neutralen Co-Liganden weiter zu untersuchen, wurde mit 4-(4-chlorobenzyl)pyridin ein weiterer großer monodentater Ligand ausgewählt.
In der Reaktion von 4-(4-chlorobenzyl)pyridin und $Co(NCS)_2$ konnte eine Verbindung synthetisiert werden, in der die typischen Kobaltthiocyanat-Ketten gefunden werden. Die Auswertung der magnetischen Messungen zeigt, dass diese Verbindung, so wie die meisten anderen auch einen antiferromagnetischen Grundzustand besitzt und einen metamagnetischen Übergang zeigt (H_C = 258±5 Oe bei 2 K). Die Auswertung der magnetischen Daten ergab, dass wiederum eine langsame Relaxation der Magnetisierung auftritt, die jedoch in diesem Fall wieder auf die Relaxation von Einzelketten zurückgeführt werden kann. Ganz offensichtlich findet sich kein einfacher Zusammenhang zwischen der Art und Größe des Co-Liganden sowie den magnetischen Eigenschaften der daraus resultierenden Verbindungen.

Journal Name

Dynamic Article Links ►

Cite this: DOI: 10.1039/c0xx00000x

www.rsc.org/xxxxxx

ARTICLE TYPE

Synthesis, Structure and Properties of $[Co(NCS)_2(4\text{-}(4\text{-Chlorobenzyl})pyridine)_2]_n$, that shows Slow Magnetic Relaxations and a Metamagnetic Transition

Julia Werner[a], Zbigniew Tomkowicz[b], Michał Rams[b], Stefan G. Ebbinghaus[c], Tristan Neumann[a] and Christian Näther[a]*

Received (in XXX, XXX) Xth XXXXXXXXX 2014, Accepted Xth XXXXXXXXX 20XX

DOI: 10.1039/b000000x

Reaction of $Co(NCS)_2$ with 4-(4-chlorobenzyl)pyridine (ClBP) leads to the formation of $Co(NCS)_2$(4-(4-chlorobenzyl)pyridine)$_4$ (**1**) and $[Co(NCS)_2(4\text{-}(4\text{-chlorobenzyl})pyridine)_2]_n$ (**2**). In the crystal structure of **1** the Co(II) cations are octahedrally coordinated by two terminal bonded thiocyanato anions and four ClBP ligands, whereas in **2** the Co(II) cations are linked into chains by pairs of μ-1,3-bridging thiocyanato anions. Magnetic measurements on **2** show an antiferromagnetic phase transition with T_N = 3.9 K. A metamagnetic transition is observed at the critical magnetic field of 260 Oe. Magnetic relaxations in zero field are consistent with single chain magnetic behavior. These results are compared with those obtained for similar compounds reported recently.

Introduction

Low-dimensional magnetic materials because of their unusual properties attracted wide interest of researches through several decades. The last wave of interest is related with the discovery of the so called Single Chain Magnets (SCM) and an increasing number of such compounds are continuously reported.[1-9] In this regard compounds that show a slow relaxation of the magnetization that can be traced back to the relaxation of single chains are of special interest because of their potential for future applications as high-density storage material.[10-27] To get more insight into the influence of a chemical and a structural modification onto the magnetic properties of such compounds systematic investigations using strongly related compounds are needed.

For the creation of such materials, it is necessary that cations of large magnetic anisotropy are linked into chains by small ligands like, e.g. azido anions that can mediate strong magnetic exchange along the chains.[28-31] In this context thiocyanato ligands are also useful because they offer a broad number of different bonding modes, which allows the selective preparation of coordination compounds with a different dimensionality of the coordination network.[32-53]

In our ongoing project on the synthesis, structure and properties of thio- or selenocyanato coordination polymers we are especially interested in compounds, in which Co(II) or Fe(II) cations are connected by pairs of these anionic ligands into chains, because several of them show a slow relaxation of the magnetization, indicative for SCM behavior. For the first time we observed such relaxations in $[Co(NCS)_2(pyridine)_2]_n$.[54] A similar behavior is observed for the corresponding selenocyanato coordination polymer $[Co(NCSe)_2(pyridine)_2]_n$, with significantly stronger intrachain interactions.[55] In contrast, the analogous Fe(II) compound $[Fe(NCS)_2(pyridine)_2]_n$ reported by Foner *et al.* is a metamagnet that shows no relaxations but this behavior can be induced by exchange of the anionic ligand.[56-57] $[Fe(NCSe)_2(pyridine)_2]_n$ is also a metamagnet but it shows slow relaxation of the magnetization and it is assumed that the lower magnetic anisotropy of Fe(II) cations is compensated by stronger intrachain interactions.[58]

To study the influence of the co-ligand onto the relaxation properties, compounds with different co-ligands were prepared that also consist of 1D $Co(NCS)_2$ chains and also show these relaxations. This includes, e.g., $[Co(NCS)_2(4\text{-acetylpyridine})_2]_n$ that exhibit a ferromagnetic ground state.[59] In contrast, $[Co(NCS)_2(4\text{-ethylpyridine})_2]_n$, has an antiferromagnetic ground state and shows a metamagnetic transition.[60] A similar behavior is also observed for $[Co(NCS)_2(bis\text{-}(4\text{-pyridyl})ethylene)_2]_n$ and for $[Co(NCS)_2(bis\text{-}(4\text{-pyridyl})ethane)_2]_n$.[39, 61] We also tried to investigate the influence of the interchain interactions by using the relatively large 4-(3-phenylpropyl)pyridine as co-ligand. $[Co(NCS)_2(4\text{-}(3\text{-phenylpropyl})pyridine)_2]_n$ exhibits a ferromagnetic ground state and also shows magnetic relaxations that, however, cannot be clearly attributed to single chain relaxations.[62]

To investigate the influence of the co-ligand onto the magnetic properties in more detail we tried to prepare a compound based on

the relatively large co-ligand 4-(4-chlorobenzyl)pyridine, in which the Co cations are linked by pairs of μ-1,3-bridging thiocyanato anions into chains. Here we report on our investigations.

Results and Discussions

Synthesis and Crystal structures

Reaction of different ratios of $Co(NCS)_2$ and 4-(4-chlorobenzyl)pyridine leads to the formation of two different compounds as indicated by X-ray powder diffraction. The results of the elemental analysis reveal a composition of $Co(NCS)_2(ClBP)_4$ (**1**) and of $Co(NCS)_2(ClBP)_2$ (**2**). In compound **1** the asymmetric stretching vibration $\nu_{as}(CN)$ is observed at 2064 cm^{-1}, which proves that only N-terminally bonded thiocyanato anions are present. In contrast, in compound **2** the asymmetric stretching vibration $\nu_{as}(CN)$ is shifted to 2105 cm^{-1}, which indicates that μ-1,3 bridging thiocyanato anions are present (Figure S1 and S2 in the Supporting Information). Based on these results it can be concluded that compound **1** consists of octahedrally coordinated discrete complexes, whereas in compound **2** the cations are linked by the anionic ligands into a coordination polymer. To verify if compound **1** could be used as a precursor to prepare a ligand deficient phase by thermal decomposition, measurements using simultaneous differential thermoanalysis and thermogravimetry were performed. This shows that compound **1** decompose in only one step at about 120°C, without the formation of any further intermediate (Figure S3 in the Supporting Information). Single crystals were obtained from acetonitrile (**1**) or methanol (**2**) and were characterized by single crystal x-ray diffraction.

$Co(NCS)_2(ClBP)_4$ (**1**) crystallizes in the monoclinic space group *C*2/c with four formula units in the unit cell. The asymmetric unit consists of one cobalt cation which is located on a center of inversion as well as of one thiocyanato anion and two 4-(4-chlorobenzyl)pyridine ligands in general position. The metal center is octahedrally surrounded by two thiocyanato anions and four 4-(4-chlorobenzyl)pyridine ligands (Figure 1).

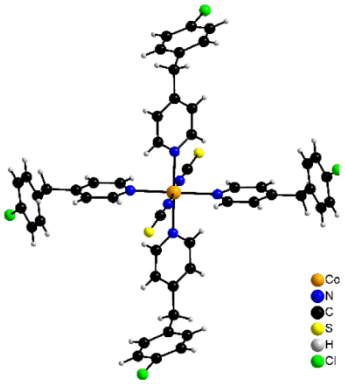

Figure 1. Coordination sphere of **1**. An ORTEP plot of this structure can be found in Figure S4 in the Supporting Information.

The cobalt nitrogen distances range between 2.0943(15) and 2.241(2) Å and the bond angles have values between 88.66(6) and 91.34(6)° and of 180.00(8)° (Table S1 in the Supporting Information).

$[Co(NCS)_2(ClBP)_2]_n$ (**2**) crystallizes in the triclinic space group *P*-1 with two formula units in the unit cell. The asymmetric unit consists of two crystallographically independent cobalt cations which are located on centers of inversion as well as of two thiocyanato anions and two 4-(4-chlorobenzyl)pyridine ligands in general positions. The cobalt cations are in an octahedral environment and are coordinated by two ClBP ligands and by two N and two S atoms of four thiocyanato anions in *trans* position (Figure 2). The cobalt nitrogen distances range from 2.060(2) to 2.165(2) Å and the Co-S distances are between 2569(1) and 2.607(1) Å (Table S2 in the Supporting Information). The overall coordination of both crystallographically independent Co cations is almost identical.

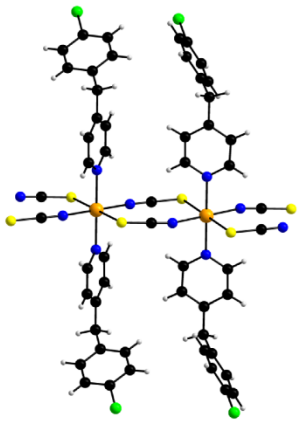

Figure 2. View of the coordination sphere of **2**. An ORTEP plot of **2** can be found in Figure S5 in the Supporting Information.

The Co cations are linked by pairs of μ-1,3-bridging thiocyanato anions into chains with an interchain distance of 5.6348 Å between neighboring Co cations (Figure 2). The shortest interchain Co···Co distance amounts to 8.2413 Å. In the crystal structure the cobalt thiocyanato chains are orientated parallel to each other and this arrangement is similar to that in $[Co(NCS)_2(pyridine)_2]_n$ and $[Co(NCS)_2(4\text{-Acpy})_2]_n$ reported recently.[54]

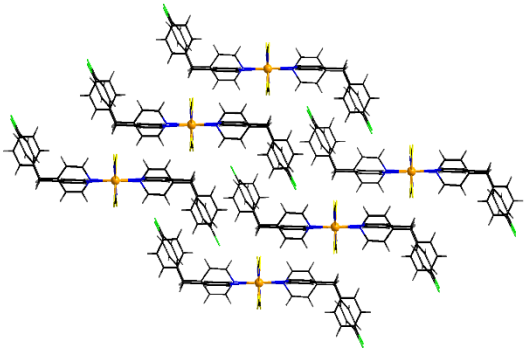

Figure 3. View of the arrangement of the chains in the crystal structure of **2**.

Based on the crystallographic data powder pattern were calculated for compound **1** and **2** and were compared with those measured, which proves that both compounds were obtained as pure phases (Figure S6 and S7 in the Supplemental). Scanning electron microscopy shows that for **2** crystalline particles of several μm were obtained (Figure S8 in the Supplemental).

Magnetic investigations

DC study

As already mentioned in the introduction, the main topic of this work focus on single chain magnetism and therefore, especially the chain compound **2** is of interest. However, for completeness

we also measured the magnetic susceptibility of the discrete complex **1** as a function of temperature T in the temperature range 2 – 300 K. The χT vs. T dependence for **1** is shown in Figure S9. The value of χT monotonically decreases with decreasing temperature starting from 3.16 K·emu/mol at 290 K and ending at 1.77 K·emu/mol at 2.0 K. This behavior is well described by the simultaneous action of the spin-orbit coupling and the axial crystal field. The fit and fit parameters are given in Figure S9.

For the chain compound **2** the magnetic susceptibility was measured in the temperature range 2 – 300 K. The $\chi(T)$ dependence is presented in Figure 4. It has a sharp maximum at 3.9 K characteristic for an antiferromagnetic transition. In the inset the temperature dependence of the χT product is shown. The room temperature value of χT equals 3.3 emu·K/mol and is much greater than the spin only value 1.87, expected for s = 3/2, pointing to the orbital contribution in Co(II) which is also responsible for a small decrease of χT with decreasing temperature (not seen in the scale of the figure). However, below about 20 K a strong increase of χT is observed due to ferromagnetic intrachain interactions. Thus, the above mentioned antiferromagnetic transition can only be caused by weak antiferromagnetic interchain interactions.

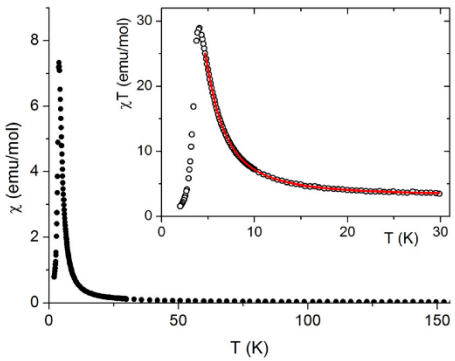

Figure 4. Temperature dependence of magnetic susceptibility χ and the χT product (inset) measured for **2** at 50 Oe. Solid line is a fit; see text.

For quasi one-dimensional anisotropic magnetic systems the temperature dependence of χT is often presented in the form of ln χT vs. reciprocal temperature plot (Figure S10 in the Supplemental). The slope of the linear part of this plot Δ_ξ/k_B = 11.9 K equals the energy for the creation of a domain wall and is a measure of the intrachain exchange interaction J. The value of J may be estimated from the relation $\Delta_\xi = 2s^2J$,[27] thus, assuming s = 1/2 one obtains J/k_B ~23.8 K. The rounding down near the maximum may indicate antiferromagnetic interchain interactions. This behavior may be well described by the Ising hamiltonian adequate for linear chain of Co(II) ions in an axially distorted octahedral coordination

$$\mathcal{H} = -J\sum_i s_i^z s_{i+1}^z + \mu_B \sum_i H\cdot\hat{g}\cdot s_i, \qquad (1)$$

where the effective spin 1/2 is assumed at low temperatures in agreement with the Kramers doublet ground state of Co(II). The expression for susceptibility derived for $H \sim 0$ has the form[63]

$$\chi_\parallel^{chain} = \frac{N_A\mu_B{}^2 g_\parallel{}^2}{4k_BT}\exp\left(\frac{J}{2k_BT}\right), \qquad (2)$$

where $g_\parallel$ is the g-factor for H parallel to the easy axis of anisotropy. The perpendicular component of susceptibility $\chi_\perp^{chain}$ is negligible at low temperatures. The interchain interaction zJ' may be accounted for in the mean field approximation

$$\chi_\parallel = \frac{\chi_\parallel^{chain}}{1 - zJ'\chi_\parallel^{chain}/(N_A g_\parallel{}^2\mu_B{}^2)}, \qquad (3)$$

and susceptibility averaged for a powder sample calculated as

$$\chi = \chi_\parallel/3 + \chi_{tip}. \qquad (4)$$

The term χ_{tip} takes into account the increasing population of excited Kramers doublets of single Co(II) centers at elevated temperatures. Fitting such model to experimental data in the 5-30 K temperature range leads to the following values: J = 29.8(2) K, zJ' = –0.43(2) K, g = 7.2(1) and χ_{tip} = 0.034(1) emu/mol (Figure 4).

Such small interchain interaction zJ' may be easily overcome by magnetic field. To show this effect, the temperature dependent magnetic susceptibility was measured in various magnetic fields. The data obtained prove that a metamagnetic transition occurs between 200 and 400 Oe (Figure 5). It is noted that the fields given in the figure refer to the external fields and therefore, at 300 Oe an antiferromagnetic–like maximum is still visible especially, considering the fact that the sample is powdered and not all crystallites undergo metamagnetic transition at the same field.[64]

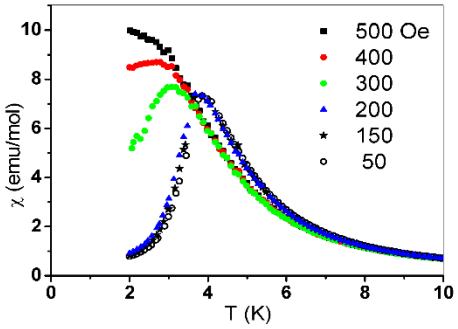

Figure 5. Magnetic susceptibility vs. temperature registered in various magnetic fields.

This transition is also clearly visible in field dependent magnetization measured at 2.0 K (Figure 6). The rapid increase of M below 2 kOe is followed by a slower increase up to 2.4 μ_B at 90 kOe. There is no saturation, seemingly because of the high anisotropy of Co(II) ions. No hysteresis loop is observed. The inset in Figure 6 shows $M(H)$ in the vicinity of the metamagnetic transition. The critical field H_c = 258±5 Oe at 2.0 K was determined from crossing of tangents to $M(H)$ curve below and above the transition. The values for H_c at higher temperatures were determined in the same way and used for the construction of the magnetic phase diagram (Figure 7). The additional points at higher temperatures were taken from the DC measurements at different fields (Figure 5).

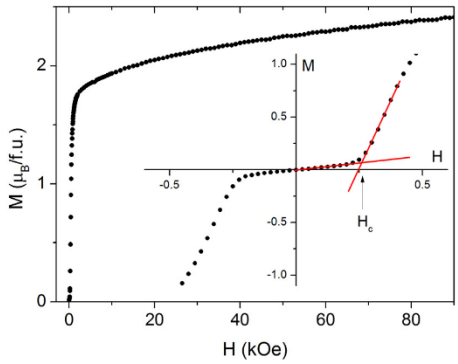

Figure 6. Magnetization vs. field measured at T = 2.0 K for **2**. The inset magnifies the low-field region and shows the way of critical field determination.

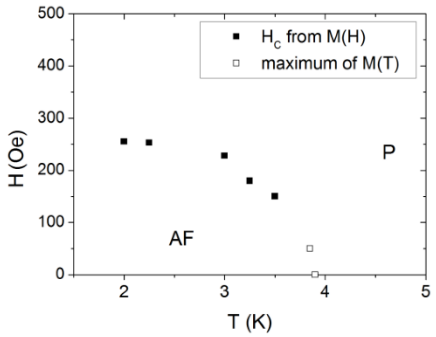

Figure 7. Magnetic phase diagram of **2**.

Additional temperature dependent DC measurements, were performed under the field cooling (FC) and zero-field cooling (ZFC) regimes. Only small bifurcation between FC and ZFC curves in the limits of experimental uncertainties was observed, which does not clearly prove the presence of long time magnetic relaxations (Figure S11 in the Supplemental).

AC study

Figure 8 presents the temperature dependent AC magnetic susceptibility measured with the AC field amplitude of 5 Oe for various frequencies in a small DC field of 5 Oe. The measurements in higher DC fields: an intermediate field 360 Oe just above H_c and 1000 Oe far above H_c were also done for comparison. At 5 Oe a maximum at 3.89 K is observed in the χ' curve, that does not depend on frequency and originates from the antiferromagnetic phase transition. At lower temperatures the frequency dispersion appears in the antiferromagnetic state. However, χ'' component is observed in the wider temperature range up to 4.5 K. The χ'' maxima depend on frequency and show a temperature shift of their T_m positions. The Mydosh parameter φ determined according to equation

$$\varphi = \Delta T_m / [T_m \Delta(\log f)]. \qquad (5)$$

is equal to 0.14, which is in the range expected for superparamagnets or single chain magnets. Above the critical field strong relaxations are observed. The $\chi'(T)$ maxima change their character and are not more a sign of the antiferromagnetic transition. This behavior is characteristic for the mixed phase in which 3D ferromagnetic domains appear.[64-66] Therefore, it cannot be described by a single relaxation process. In a still higher field the mixed phase fades and the chains are nearly decoupled. Because the object of our interest are single chain magnets, in the following we focus only on the relaxation behavior that is observed in fields below H_c.

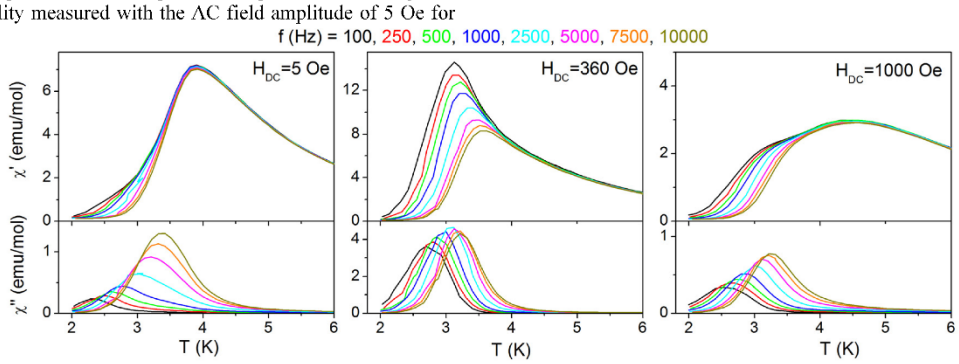

Figure 8. Temperature dependent AC magnetic susceptibilities for **2** measured for various frequencies in different DC magnetic fields.

In Figure 9 frequency dependent AC susceptibility measured at various temperatures in DC field of 5 Oe is presented. All frequency dependencies can be well described by the generalized Debye model with one mean relaxation time according to the equation

$$\chi = \chi' - i\chi'' = \chi_\infty + \frac{\chi_0 - \chi_\infty}{1+(i2\pi f\tau)^{1-\alpha}}, \qquad (6)$$

where χ_0 and χ_∞ are AC susceptibilities in the limit of zero and infinite frequency, respectively, τ is the mean relaxation time, f is the frequency of the AC field, α is a parameter related with the width of the relaxation times distribution ($0 \le \alpha \le 1$; $\alpha = 0$ means a unique relaxation time, $\alpha = 1$ means an infinity of relaxations times).

The table with the best fit parameters is given in the Supporting Information (Table S3). As seen in the Table, τ strongly increases with decreasing temperature. The simultaneous increase of α means that the width of relaxation time distribution increases with decreasing temperature, which should be caused by interchain interactions. The Cole-Cole plots, which present χ'' vs. χ' dependence are shown in Figure 10. They are arc of circles which are shifted down with respect to the χ' axis according to the non-zero α parameter.

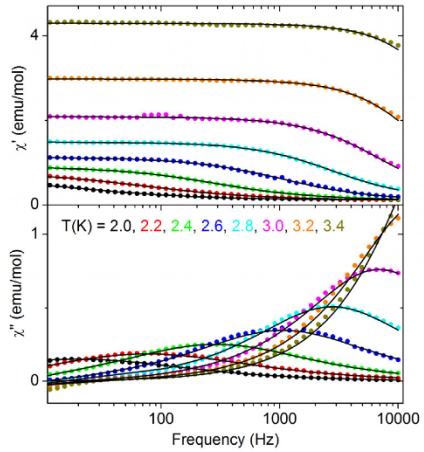

Figure 9. Frequency dependent AC susceptibility for **2** measured at various temperatures. Solid lines are fits with the generalized Debye model.

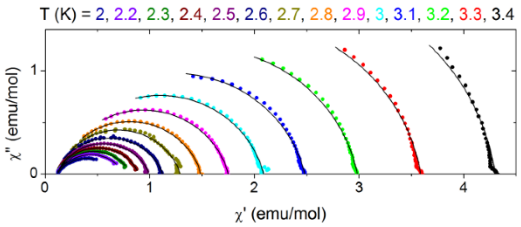

Figure 10. Cole-Cole plots for **2** at various temperatures. Solid lines are fits with the generalized Debye model.

The temperature dependence of τ is shown in Figure 11 as a plot of ln τ *vs.* $1/T$, from which the energy barrier ΔE and prefactor τ_0 in the Arrhenius equation

$$\tau = \tau_0 \exp(\Delta E/k_B T) \qquad (7)$$

can be determined. Their values are: $\Delta E/k_B = 37.1 \pm 0.5$ K and $\tau_0 = (9.5 \pm 1.0) \cdot 10^{-11}$ s.

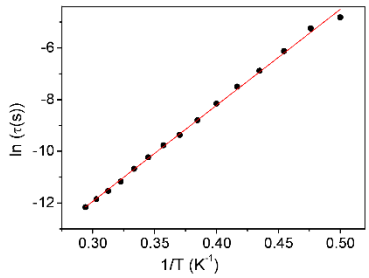

Figure 11. Logarithm τ vs. reciprocal temperature for **2**. Solid line is a linear fit.

Discussion of the magnetic properties

Compound **2**, built from ferromagnetic Co-$(NCS)_2$-Co chains, shows an antiferromagnetic transition at a Néel temperature of 3.8 K. It undergoes a metamagnetic transition in field of ~260 Oe. The magnetic relaxations existing in the antiferromagnetic state are well described with one mean relaxation time and single energy barrier for thermal activation $\Delta E/k_B = 37.1$ K, which may originate from single chain relaxations[67]

According to Coulon *et al.*[27] the activation energy of the relaxation time may be discussed using the following equation

$$\Delta E = k\Delta_\xi + \Delta_A , \qquad (8)$$

where Δ_ξ is the creation energy of the domain wall (here equal to $J/2$), k is a factor equal to 1 or 2, depending on whether we are dealing with finite or infinite chains, respectively, and Δ_A is the activation energy of a single uncoupled anisotropic spin. Assuming $k = 1$, a Δ_A value of 22.6 K is obtained for compound **2**. Thus the Glauber criterion $\Delta_A > \Delta_\xi$ is satisfied for $Co(NCS)_2(ClBP)_2$ chains in accordance with their Ising nature.

A crossover from $k = 1$ to $k = 2$ is expected with increasing temperature around T^*, that can be related to the chain length n[27]

$$2n\exp(-2Js^2/k_B T^*) = 1. \qquad (9)$$

However no change of slope (change of ΔE) is visible in Figure 11. If $k = 1$ and all points in the figure are below T^*, $1/T^* < 0.29$ K^{-1}, then $n < 50$ Co atoms for our sample of **2**. It is an acceptable limit.

As mentioned in the introduction compound **2** is a member of a family of compounds we have investigated in the past. All of these compounds of the general composition $[Co(NCS)_2(L_2)]_n$ (L = co-ligand) consist of octahedrally coordinated Co(II) cations that are linked into chains by pairs of thiocyanato anions. When the magnetic properties of these compounds are compared always similar values for the intrachain interaction are noted, which can be traced back to the fact that always the same thiocyanato chains are involved (Table 2). It is not clear if the small differences between the J values originate from the influence of the co-ligand.

Table 1: Selected magnetic parameters for compound **2** and related 1D compounds of composition $[Co(NCS)_2(L)_2]_n$ with (L = 4-Ethylpyridine (Etpy), 4-acetylpyridine (Acpy), 4-(3-phenylpropyl)pyridine (PPP), 1,2-bis(4-pyridiyl)-ethylene (bpe) and 1,2-bis(4-pyridiyl)-ethane (bpa). The parameters zJ' and J given below differ slightly from the values given in ref.[59-62] This is due to different models used to fit $\chi T(T)$ in some of these reports, particularly different definitions of zJ' and the temperature range used in the fitting procedures. To be able to compare directly between zJ' parameters for all compounds of this family, we estimated the parameters zJ' and J again, fitting $\chi T(T)$ data, but using the identical model as for **2**. For better comparison the value if Δ_A for the compound with Etpy was recalculated assuming k=1. Thus, it deviates from that given in ref.[60] where arbitrarily k=2 was selected. J = intrachain interaction; zJ' = interchain interaction; T_c = critical temperature; AF = antiferromagnetic ground state; FO = ferromagnetic ground state; H_c = critical field; ΔE = Arrhenius law energy; τ_0 = prefactor; Δ_A = see equation 8; α = distribution of the relaxation times determined at different temperatures; φ = Mydosh parameter.

	2	Etpy	bpe	bpa	Acpy	PPP
ground state	AF	AF	AF	AF	FM	FM
H_c (Oe)	~260 (2 K)	~175 (1.5 K)	~400 (2 K)	~40 (2K)	-	-
T_c (K)	3.9	3.4	4.0	3.1	3.8	3.3
J/k_B (K)	29.8	27.0	26.8	27.8	30.2	28.4
zJ'/k_B (K)	−0.43	−0.42	−0.66	−0.22	+0.17	+0.15
$\Delta E/k_B$ (K)	37.1	45.3	33.3	39.2	74	116
τ_0 (s)	9.5×10^{-11}	2×10^{-12}	1.2×10^{-11}	1.2×10^{-11}	6×10^{-13}	10^{-19}
Δ_A/k_B (K)	22.2 (k=1)	31.8 (k=1)	19.9 (k=1)	25.3 (k=1)	-	-
α	0.09 - 0.37	0.1 - 0.4	0.10 - 0.46	0.06 - 0.41	0.4 - 0.52	-
φ	0.14	0.14	0.16	0.11	0.074	0.059

However, all of these compounds can be divided into two different groups. The first group consists of compounds that exhibit an antiferromagnetic ground state and show a metamagnetic transition as it is the case for compound **2**. For all of these compounds the Mydosh parameter points to superparamagnetic behaviour, the magnetic relaxations can be well fitted using the Debye model leading to similar values for the anisotropy energy Δ_A and the Glauber criterion is also fulfilled. In this context it is noted that Δ_A can be also calculated in a more general way, without assuming the Fisher model restrictions, by using the Δ_ξ values obtained from the ln(chi*T*)(1/*T*) dependence. The values of Δ_A obtained in such a way do not differ very much from those given in table 2. Therefore, their relaxations seem to originate from the relaxation of single chains. However, for α, which is a measure for the distribution of the relaxation times, relatively large values are observed (Table 1). Even if such high values are frequently discussed in literature in context of single chain magnetic behaviour the question raises if this might always be adequate. With decreasing temperatures α increases dramatically which suggests that at higher temperatures single chain relaxations are observed, whereas at lower temperatures interchain interactions must come into play.

The second group consists of compounds with a ferromagnetic ground state. For these two compounds with 4-(3-phenylpropyl)pyridine (PPP) and 4-acetylpyridine (Acpy) as co-ligand a relatively small Mydosh parameter is observed indicating for spin glass-like behaviour (Table 2). Interestingly, for the Acpy compound the frequency dependent AC data can be fitted using the Debye model but in this case relatively high values of α and $\Delta E/k_B$ are obtained together with much smaller τ_0 value, which clearly shows that this compound behaves differently to that with the AF ground state. Moreover, temperature dependent AC data obtained for the compound with PPP lead to an unrealistic small τ_0, so obtained ΔE cannot be linked with the relaxation process of single chains. All these findings indicate that for the ferromagnetic compounds the relaxation might not be traced back to the relaxation of single chains and that it is more reasonable to assume that these are relaxations of walls of 3-dimensional ferromagnetic domains.

The reason why some of these compounds exhibits an antiferromagnetic whereas some others exhibits a ferromagnetic ground state is still unclear. There is, e.g., no simple correlation between the interchain distances and their magnetic properties. It is noted that two different arrangements of the $Co(NCS)_2$ chains are observed in their crystal structures. In some of these compounds the N-N vector of the two coordinating pyridine ligands of neighboring chains are parallel, whereas in some others they are canted. Unfortunately this does not correlate with the magnetic ground state of these compounds. Most probably, the type of the magnetic ground state is due to different arrangements of the anisotropic Co chains in the crystal structures, which lead to different dipolar interactions changing the sign of effective *zJ'*. The basis for the simulations of dipolar interactions and expected ground state is however single ion Co anisotropy and its direction, which is not obvious. To gain such information magnetic investigations with a single crystal would be desirable.

Conclusions

In the present contribution a new thiocyanato compound with the relatively large co-ligand 4-(4-chlorobenzyl)pyridine was prepared, in which the Co(II) cations are linked by pairs of thiocyanato anions into chains. This new compound is a member of a family of compounds that we have recently investigated to examine the influence of a chemical and a structural modification onto the magnetic properties in detail. For some of these compounds the magnetic properties can be discussed as single chain magnetic behavior, while for some other compounds this seems to be inadequate. Within this family, compound **2** presented in this report, in spite of undergoing an antiferromagnetic transition, most clearly demonstrates the relaxation behavior characteristic for single chain magnets.

In this context it is noted that the stem compound $Co(NCS)_2$(pyridine) mentioned in the introduction obviously also exhibits a ferromagnetic ground state but shows relaxations which were interpreted as SCM relaxations on the basis of the Mydosh parameter, α and the analysis of the relaxation times.[54] In this work these parameters were determined by a different procedure and the temperature dependence of α was not investigated and therefore, these results cannot be compared here. However, in the light of the results of this work the question araises how this compound can be classified and what the real nature of its relaxations is. Consequently, these questions must be answered in future investigations.

Experimental Section

$Co(NCS)_2$ and 4-(4-chlorobenzyl)pyridine (ClBP) were obtained from Alfa Aesar. Solvents were used without further purification. The crystalline powders of all compounds were prepared by stirring the reactants in the respective solvents at room temperature. The purity of the compounds was checked by X-ray powder diffraction and elemental analysis.

***Synthesis of $Co(NCS)_2$(4-(4-chlorobenzyl)pyridine)$_4$* (1):**
Single crystals suitable for single crystal X-ray diffraction were prepared by $Co(NCS)_2$ (26.3 mg, 0.15 mmol) 4-(4-chlorobenzyl)pyridine (105.4 µL, 0.60 mmol) in 1.5 mL acetonitrile. A crystalline powder was synthesized by stirring $Co(NCS)_2$ (175.1 mg, 1.00 mmol) and 4-(4-chlorobenzyl)pyridine (702.3 µL, 4.00 mmol) in 5 mL acetonitril for 6 d. Yield: 85 % elemental analysis calcd (%) for $C_{50}H_{40}Cl_4CoN_6S_2$: C 60.67, H 4.07, N 8.49; S 6.48; found C 59.33, H 4.24, N 8.31, S 6.89. IR (ATR): ν_{max} = 3075 (w), 3039 (w),2915 (w), 2064 (s), 2084 (s), 1615 (s), 1558 (m), 1488 (s), 1422 (s), 1348 (w), 1311 (w), 1222 (m), 1091 (m), 1048 (m), 1014 (s), 923 (w), 855 (s), 805 (s), 799 (s), 733 (m), 714 (m), 675 (w), 592 (s), 490 (s), 423 (m).

***Synthesis of [Co(NCS)$_2$(4-(4-chlorobenzyl)pyridine)$_2$]$_n$* (2):**
Single crystals suitable for single crystal X-ray diffraction were prepared by $Co(NCS)_2$ (52.5 mg, 0.30 mmol) 4-(4-chlorobenzyl)pyridine (26.4 µL, 0.15 mmol) in 1.5 mL methanol. A crystalline powder was synthesized by stirring $Co(NCS)_2$ (175.1 mg, 1.00 mmol) and 4-(4-chlorobenzyl)pyridine (93.8 µL, 0.50 mmol) in 5 mL water for 3 d. Yield: 77 % elemental analysis calcd (%) for $C_{26}H_{20}Cl_2CoN_4S_2$: C 53.62, H 3.46, N 9.62; S 11.01; found C 53.36, H 3.35, N 9.40, S 10.86. IR (ATR): ν_{max} = 3086 (w), 3027 (w),2905 (w), 2105 (s), 2084 (s), 1692 (w), 1612 (s), 1558 (m), 1488 (s), 1423 (s), 1274 (w), 1223 (m), 1094 (m), 1068 (m), 1014 (s), 919 (w), 852 (m), 805 (s), 787 (s), 733 (m), 656 (w), 597 (s), 503 (s), 489 (s), 423 (m).

Elemental Analysis
CHNS analysis was performed using an EURO EA elemental analyzer fabricated by EURO VECTOR Instruments and Software.

IR-Spectroscopy
All IR data were obtained using an ATI Mattson Genesis Series FTIR Spectrometer, control software: WINFIRST, from ATI Mattson.

Differential Thermal Analysis and Thermogravimetry (DTA-

TG)
The DTA-TG measurements were performed in a nitrogen atmosphere (purity: 5.0) in Al_2O_3 crucibles using a STA-409CD instrument from Netzsch. All measurements were performed with a flow rate of 75 mL·min^{-1} and were corrected for buoyancy and current effects. The instrument was calibrated using standard reference materials.

Scanning electronmicroscopy (SEM)
The SEM measurements were performed with a Philips Environmental Scanning Electron Microscope ESEM XL30, which is equipped with an EDAX detector.

Magnetic measurements
Magnetic measurements were performed using a PPMS (Physical Property Measurement System) from Quantum Design. All AC data were obtained with the amplitude of the AC field equal to 5 Oe. The data were corrected for core diamagnetism.

X-Ray Powder Diffraction (XRPD)
The measurements were performed using 1) a PANalytical X'Pert Pro MPD Reflection Powder Diffraction System with CuKα radiation (λ = 154.0598 pm) equipped with a PIXcel semiconductor detector from PANanlytical and 2) a Stoe Transmission Powder Diffraction System (STADI P) with CuKα radiation (λ = 154.0598 pm) that was equipped with a linear position-sensitive detector from STOE & CIE.

Single Crystal Structure analysis
The data collection was performed with imaging plate diffraction systems (STOE IPDS-1 (**1**), STOE IPDS-2 (**2**)) using MoKα radiation. The structure solution was done with direct methods using SHELXS-97 and structure refinement was performed against F2 using SHELXL-97.[68] For both compounds a numerical absorption correction was applied using X-red and X-shape of the Program Package X-area.[69-71] All non-hydrogen atoms were refined with anisotropic displacement parameters. All hydrogen atoms were positioned with idealized geometry and were refined isotropically with U_{iso}(H) = −1.2 U_{eq}(C) (1.5 for methyl H). Selected crystal data and details of the structure determinations are given in Table .

CCDC-1401785 (**1**) and CCDC-1401784 (**2**) contain the supplementary crystallographic data for this paper. These data can be obtained free of charge from the Cambridge Crystallographic Data Centre via http://www.ccdc.cam.ac.uk/data_request/cif.

Table 2: Selected crystal data and details on the structure determination of compounds **1** and **2**.

Compound	**1**	**2**
formula	$C_{50}H_{40}Cl_4CoN_6S_2$	$C_{26}H_{20}Cl_2CoN_4S_2$
MW / g mol^{-1}	989.73	582.41
crystal system	*monoclinic*	*triclinic*
space group	*C*2/c	*P*-1
Z	4	2
D_{calc} / mg cm^{-3}	1.382	1.482
μ / mm^{-1}	0.715	1.045
a / Å	18.8098(13)	9.0456(15)
b / Å	9.5685(5)	10.8405(16)
c / Å	27.6126(17)	14.941(3)
α / °	90	73.393(19)
β / °	106.867(7)	83.37(2)
γ / °	90	68.356(17)
V / Å^3	4756.0(5)	1304.9(4)
T / K	293(2)	200(2)
scan range 2θ / deg	2.26 to 25.97	2.10 to 26.99
measured refl.	20774	18952
R_{int}	0.0389	0.0413
min/max. transm.	0.7998, 0.8759	0.7951, 0.9070
unique reflns.	4584	5692
refl.[F_0>4σ(F_0)]	3894	4342
parameters	296	320
R_1 [$F_0 > 4\sigma(F_0)$]	0.0357	0.0441
wR_2 [all data]	0.0946	0.1021
GOF	1.057	1.034
$\Delta\rho_{max/min}$/e Å^{-3}	0.428 and -0.394	0.380 and -0.437

Acknowledgements

This project was supported by the Deutsche Forschungsgemeinschaft (Project No. Na 720/5-1) and the State of Schleswig-Holstein. We thank Prof. Dr. Wolfgang Bensch for access to his experimental facilities. ZT thanks National Science Centre Poland for financial support granted under decision DEC-2013/11/B/ST3/03799.

† Electronic Supplementary Information (ESI) available: X-Ray powder pattern and IR-spectra of compound **1** and **2**. DTA, DTG and TG curves for compound **1** and **2**. Additional magnetic measurements for compound **2**.

Notes

[a] *Institut für Anorganische Chemie, Christian-Albrechts-Universität zu Kiel, Max-Eyth-Straße 2, 24118 Kiel, Germany. Fax: +49 431-880 1520; Tel: +49 431-880 1520; E-mail: cnaether@ac.uni-kiel.de*

[b] *Institute of Physics, Jagiellonian University, 30-348 Kraków, Łojasiewicza 11, Poland.*

[c] *Martin-Luther-Universität Halle-Wittenberg, Institut für Chemie, Kurt-Mothes-Straße 2, 06120 Halle / Saale, Germany.*

ReferencesUncategorized References

[1] W. L. Leong, J. J. Vittal, *Chem. Rev.* **2011**, *111*, 688-764.
[2] H. Arora, F. Lloret, R. Mukherjee, *Inorg. Chem.* **2009**, *48*, 1158-1167.
[3] L. Bogani, C. Sangregorio, R. Sessoli, D. Gatteschi, *Angew. Chem.* **2005**, *117*, 5967-5971.
[4] S. W. Choi, H. Y. Kwak, J. H. Yoon, H. C. Kim, E. K. Koh, C. S. Hong, *Inorg. Chem.* **2008**, *47*, 10214-10216.
[5] E. Shurdha, C. E. Moore, A. L. Rheingold, S. H. Lapidus, P. W. Stephens, A. M. Arif, J. S. Miller, *Inorg. Chem.* **2013**, *52*, 10583-10594.
[6] X. Shen, Q. Zhang, H. Zhou, H. Zhou, A. Yuan, *New J. Chem.* **2012**, *36*, 1180-1186.
[7] P. P. Chakrabarty, S. Saha, D. Schollmeyer, A. K. Boudalis, A. D. Jana, D. Luneau, *J. Coord. Chem.* **2012**, *66*, 9-17.
[8] C. Näther, S. Wöhlert, J. Boeckmann, M. Wriedt, I. Jeß, *Z. Anorg. Allg. Chem.* **2013**, *639*, 2696-2714.
[9] M. Balanda, Z. Tomkowicz, W. Haase, M. Rams, *J. Phys.: Conf. Ser.* **2010**, *303*, 012036.
[10] A. Caneschi, D. Gatteschi, N. Lalioti, C. Sangregorio, R. Sessoli, G. Venturi, A. Vindigni, A. Rettori, M. G. Pini, M. A. Novak, *Angew. Chem.* **2001**, *113*, 1810-1813.
[11] E. Pardo, R. Ruiz-García, F. Lloret, J. Faus, M. Julve, Y. Journaux, M. Novak, F. Delgado, C. Ruiz-Pérez, *Chem. Eur. J.* **2007**, *13*, 2054-2066.

[12] H.-L. Sun, Z.-M. Wang, S. Gao, *Coord. Chem. Rev.* **2010**, *254*, 1081-1100.

[13] L. Bogani, A. Vindigni, R. Sessoli, D. Gatteschi, *J. Mater. Chem* **2008**, *18*, 4733–4880.

[14] W.-X. Zhang, R. Ishikawa, B. Breedlovea, M. Yamashita, *RSC Adv.* **2013**, *3*, 3772-3798.

[15] J. Ru, F. Gao, T. Wu, M.-X. Yao, Y.-Z. Li, J.-L. Zuo, *Dalton Trans.* **2014**, *43*, 933-936.

[16] E. V. Peresypkina, A. M. Majcher, M. Rams, K. E. Vostrikova, *Chem. Commun.* **2014**, *50*, 7150-7153.

[17] H. Miyasaka, R. Clérac, *Bull. Chem. Soc. Jpn.* **2005**, *78*, 1725-1748.

[18] A. V. Palii, O. S. Reu, S. M. Ostrovsky, S. I. Klokishner, B. S. Tsukerblat, Z.-M. Sun, J.-G. Mao, A. V. Prosvirin, H.-H. Zhao, K. R. Dunbar, *J. Am. Chem. Soc.* **2008**, *130*, 14729-14738.

[19] M. Bałanda, M. Rams, S. K. Nayak, Z. Tomkowicz, W. Haase, K. Tomala, J. V. Yakhmi, *Phys. Rev. B* **2006**, *74*, 224421.

[20] Z. Tomkowicz, M. Rams, M. Bałanda, S. Foro, H. Nojiri, Y. Krupskaya, V. Kataev, B. Büchner, S. K. Nayak, J. V. Yakhmi, W. Haase, *Inorg. Chem.* **2012**, *51*, 9983-9994.

[21] S.-Y. Zhang, W. Shi, Y. Lan, N. Xu, X.-Q. Zhao, A. K. Powell, B. Zhao, P. Cheng, D.-Z. Liao, S.-P. Yan, *Chem. Commun.* **2011**, *47*, 2859-2861.

[22] X. Feng, T. David Harris, J. R. Long, *Chem. Sci.* **2011**, *2*, 1688-1694.

[23] R. Liu, L. Li, X. Wang, P. Yang, C. Wang, D. Liao, J.-P. Sutter, *Chem. Commun.* **2010**, *46*, 2566-2568.

[24] V. Mougel, L. Chatelain, J. Hermle, R. Caciuffo, E. Colineau, F. Tuna, N. Magnani, A. de Geyer, J. Pécaut, M. Mazzanti, *Angew. Chem.* **2014**, *126*, 838-842.

[25] Y.-L. Hou, R.-R. Cheng, G. Xiong, J.-Z. Cui, B. Zhao, *Dalton Trans.* **2014**, *43*, 1814-1820.

[26] H. Miyasaka, T. Madanbashi, A. Saitoh, N. Motokawa, R. Ishikawa, M. Yamashita, S. Bahr, W. Wernsdorfer, R. Clérac, *Chem. Eur. J.* **2012**, *18*, 3942-3954.

[27] C. Coulon, H. Miyasaka, R. Clérac, *Struct. Bond.* **2006**, *122*, 163-206.

[28] J. H. Yoon, J. W. Lee, D. W. Ryu, S. W. Yoon, B. J. Suh, H. C. Kim, C. S. Hong, *Chem. Eur. J.* **2011**, *17*, 3028-3034.

[29] J. H. Yoon, W. R. Lee, D. W. Ryu, J. W. Lee, S. W. Yoon, B. J. Suh, H. C. Kim, C. S. Hong, *Inorg. Chem.* **2011**, *50*, 10777-10785.

[30] X.-B. Li, G.-M. Zhuang, X. Wang, K. Wang, E.-Q. Gao, *Chem. Commun.* **2013**, *49*, 1814-1816.

[31] A. Escuer, G. Vlahopoulou, F. A. Mautner, *Inorg. Chem.* **2011**, *50*, 2717-2719.

[32] F. A. Mautner, M. Scherzer, C. Berger, R. C. Fischer, R. Vicente, S. S. Massoud, *Polyhedron* **2015**, *85*, 20-26.

[33] B. Machura, A. Świtlicka, P. Zwoliński, J. Mroziński, B. Kalińska, R. Kruszynski, *J. Solid State Chem.* **2013**, *197*, 218-227.

[34] B. Machura, A. Świtlicka, J. Mroziński, B. Kalińska, R. Kruszynski, *Polyhedron* **2013**, *52*, 1276-1286.

[35] J. G. Małecki, T. Groń, H. Duda, *Polyhedron* **2012**, *36*, 56-68.

[36] Q. Ma, M. Zhu, L. Lu, S. Feng, J. Yan, *Inorg. Chim. Acta* **2011**, *370*, 102-107.

[37] M. Wriedt, C. Näther, *Chem. Commun.* **2010**, *46*, 4707-4709.

[38] J. Boeckmann, C. Näther, *Polyhedron* **2012**, *31*, 587-595.

[39] S. Wöhlert, J. Boeckmann, M. Wriedt, C. Näther, *Angew. Chem., Int. Ed.* **2011**, *50*, 6920–6923.

[40] P. Bhowmik, S. Chattopadhyay, M. G. B. Drew, C. Diaz, A. Ghosh, *Polyhedron* **2010**, *29*, 2637-2642.

[41] S. Wöhlert, U. Ruschewitz, C. Näther, *Cryst. Growth Des.* **2012**, *12*, 2715-2718.

[42] S. Wöhlert, J. Boeckmann, I. Jess, C. Näther, *CrystEngComm* **2012**, *14*, 5412-5420.

[43] S. Wöhlert, L. Peters, C. Näther, *Dalton Trans.* **2013**, *42*, 10746-10758.

[44] C. J. Adams, M. F. Haddow, D. J. Harding, T. J. Podesta, R. E. Waddington, *CrystEngComm* **2011**, *13*, 4909-4914.

[45] A. Barasiński, P. Sobczak, A. Drzewiński, G. Kamieniarz, A. Bieńko, J. Mroziński, D. Gatteschi, *Polyhedron* **2010**, *29*, 1485-1491.

[46] S. Wöhlert, T. Runčevski, R. E. Dinnebier, S. G. Ebbinghaus, C. Näther, *Cryst. Growth Des.* **2014**, *14*, 1902-1913.

[47] S. Wöhlert, M. Wriedt, T. Fic, Z. Tomkowicz, W. Haase, C. Näther, *Inorg. Chem.* **2013**, *52*, 1061-1068.

[48] J. G. Małecki, P. Zwoliński, *Polyhedron* **2012**, *39*, 85-90.

[49] J.-F. Létard, S. Asthana, H. J. Shepherd, P. Guionneau, A. E. Goeta, N. Suemura, R. Ishikawa, S. Kaizaki, *Chem. Eur. J.* **2012**, *18*, 5924-5934.

[50] S. Das, K. Bhar, S. Chattopadhyay, P. Mitra, V. J. Smith, L. J. Barbour, B. K. Ghosh, *Polyhedron* **2012**, *38*, 26-35.

[51] J. G. Małecki, B. Machura, A. Świtlicka, T. Groń, M. Bałanda, *Polyhedron* **2011**, *30*, 746-753.

[52] J. Palion-Gazda, B. Machura, F. Lloret, M. Julve, *Cryst. Growth Des.* **2015**, *15*, 2380-2388.

[53] R. González, A. Acosta, R. Chiozzone, C. Kremer, D. Armentano, G. De Munno, M. Julve, F. Lloret, J. Faus, *Inorg. Chem.* **2012**, *51*, 5737-5747.

[54] J. Boeckmann, C. Näther, *Dalton Trans.* **2010**, *39*, 11019-11026.

[55] J. Boeckmann, C. Näther, *Chem. Commun.* **2011**, *47*, 7104-7106.

[56] S. Foner, R. B. Frankel, W. M. Reiff, B. F. Little, G. J. Long, *Solid State Commun.* **1975**, *16*, 159-161.

[57] S. Foner, R. B. Frankel, W.M. Reiff, H. Wong, G. J. Long, *J. Chem. Phys.* **1978**, *68*, 4781-4783.

[58] J. Boeckmann, M. Wriedt, C. Näther, *Chem. Eur. J.* **2012**, *18*, 5284-5289.

[59] M. R. Julia Werner, Zbigniew Tomkowicz, Tomče Runčevski, Robert E. Dinnebier, Stefan Suckert and Christian Näther, *Inorg. Chem.* **2015**, *54*, 2893.

[60] S. Wöhlert, T. Fic, Z. Tomkowicz, S. G. Ebbinghaus, M. Rams, W. Haase, C. Näther, *Inorg. Chem.* **2013**, *52*, 12947-12957.

[61] S. Wöhlert, Z. Tomkowicz, M. Rams, S. G. Ebbinghaus, L. Fink, M. U. Schmidt, C. Näther, *Inorg. Chem.* **2014**, *53*, 8298–8310.

[62] J. Werner, M. Rams, Z. Tomkowicz, C. Nather, *Dalton Trans.* **2014**, *43*, 17333-17342.

[63] M. E. Fisher, *J. Math. Phys.* **1963**, *4*, 124-135.

[64] R. L. Carlin, A. J. van Duyneveldt, *Acc. Chem. Res.* **1980**, *13*, 231-236.

[65] R. Hoogerbeets, S. A. J. Wiegers, A. J. van Duyneveldt, R. D. Willett, U. Geiser, *Physica B* **1984**, *125*, 135-149.

[66] C. Coulon, R. Clérac, W. Wernsdorfer, T. Colin, H. Miyasaka, *Phys. Rev. Lett.* **2009**, *102*, 164204-164207.

[67] H. Miyasaka, K. Takayama, A. Saitoh, S. Furukawa, M. Yamashita, R. Clérac, *Chem. Eur. J.* **2010**, *16*, 3656-3662.

[68] G. M. Sheldrick, *Acta Cryst.* **2008**, *A64*, 112-122.

[69] *X-Area, Version 1.44, Program Package for Single Crystal Measurements*, STOE & CIE GmbH, Darmstadt, Germany, **2008**.

[70] *X-Red, Version 1.11, Program for Data Reduction and Absorption Correction*, STOE & CIE GmbH, Darmstadt, Germany, **1998**.

[71] *X-Shape, Version 1.03, Program for the Crystal Optimization for Numerical Absorption Correction*, STOE & CIE GmbH, Darmstadt, Germany, **1998**.

9

Synthesis, Structure and Properties of $[Co(NCS)_2(4\text{-}(4\text{-Chlorobenzyl})pyridine)_2]_n$, that shows Slow Magnetic Relaxations and a Metamagnetic Transition

Julia Werner, Zbigniew Tomkowicz, Michał Rams, Stefan G. Ebbinghaus, Tristan Neumann and Christian Näther

Dalton Trans., 2015, ...

DOI: ....

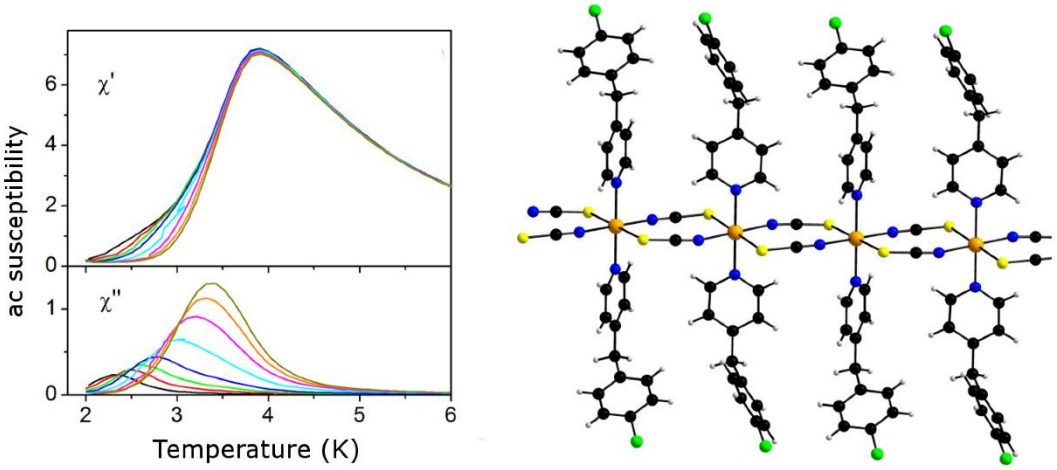

$[Co(NCS)_2(4\text{-}(4\text{-Chlorobenzyl})pyridine)_2]_n$ shows metamagnetic behavior and slow relaxations of the magnetization indicative for single chain magnet behavior.

3.3. Thermodynamically Metastable Thiocyanato Coordination Polymer that Shows Slow Relaxations of the Magnetization

Julia Werner, Michał Rams, Zbigniew Tomkowicz, Tomče Runčevski, Robert E. Dinnebier, Stefan Suckert und Christian Näther, *Inorg. Chem*. **2015**, *54*, 2893-2901.

DOI: 10.1021/ic503029t

Motivation

Die in Kapitel 3.1 und 3.2 vorgestellten Untersuchungen belegen, dass der neutrale Co-Ligand durchaus einen Einfluss auf die magnetischen Eigenschaften der Verbindung ausübt und dass kein einfacher Zusammenhang zwischen der Art und Größe des Co-Liganden und den magnetischen Eigenschaften gefunden wurde. Was jedoch auffällt, ist die Tatsache, dass alle Verbindungen, die Einzelkettenmagnetismus zeigen, einen antiferromagnetischen Grundzustand aufweisen. Im Gegensatz hierzu weist formell $[Co(NCS)_2(4\text{-}(3\text{-Phenylpropyl})pyridin)_2]_n$ einen ferromagnetischen Grundzustand auf und die magnetischen Messungen deuten darauf hin, dass diese Verbindung kein SCM-Verhalten zeigt. Um den Einfluss des neutralen Co-Liganden genauer zu untersuchen wurde versucht eine weitere Verbindung mit 4-Acetylpyridin zu synthetisieren.
Überraschenderweise wird aus Lösung eine Verbindung gewünschter Zusammensetzung erhalten, in der jedoch an Stelle der sonst üblichen Ketten ein zweidimensionales Koordinationsnetzwerk gefunden wird. Weitere Untersuchungen ergaben, dass die 1D-Zielverbindung jedoch durch thermischen Abbau eines Hydrat-Vorläuferkomplexes dargestellt werden kann und dass dieses Isomer thermodynamisch metastabil ist, wohingegen das 2D-Isomer die zwischen Raum- und Zersetzungstemperatur thermodynamisch stabile Phase darstellt. So wie die Verbindung mit 4-(3-Phenylpropyl)pyridin weist auch diese Verbindung einen ferromagnetischen Grundzustand auf und die hier beobachteten Relaxationen können nicht auf Einzelkettenmagnetismus zurückgeführt werden.

Inorganic Chemistry

Article

pubs.acs.org/IC

Thermodynamically Metastable Thiocyanato Coordination Polymer That Shows Slow Relaxations of the Magnetization

Julia Werner,[†] Michał Rams,[‡] Zbigniew Tomkowicz,[‡] Tomče Runčevski,[§] Robert E. Dinnebier,[§] Stefan Suckert,[†] and Christian Näther*[,†]

[†]Institut für Anorganische Chemie, Christian-Albrechts-Universität zu Kiel, Max-Eyth-Straße 2, 24118 Kiel, Germany

[‡]Institute of Physics, Jagiellonian University, Łojasiewicza 11, 30-348 Kraków, Poland

[§]Max Planck Institute for Solid State Research, Heisenbergstraße 1, 70569 Stuttgart, Germany

Supporting Information

ABSTRACT: Reaction of cobalt thiocyanate with 4-acetylpyridine leads to the formation of $[Co(NCS)_2(4\text{-acetylpyridine})_2]_n$ (**3/I**). In its crystal structure the Co cations are connected by pairs of μ-1,3-bridging thiocyanato ligands into dimers that are further connected into layers by single anionic ligands. DTA-TG measurements of $Co(NCS)_2(4\text{-acetylpyridine})_4$ (**1**) led to the formation of **3/I**. In contrast, when the hydrate $Co(NCS)_2(4\text{-acetyl-pyridine})_2(H_2O)_2$ (**2**) is decomposed, a mixture of **3/I** and a thermodynamically metastable form **3/II** is obtained. Further investigations reveal that thermal annealing of **2** leads to the formation of **3/II**, that contains only traces of the stable form **3/I**. DSC and temperature dependent X-ray powder diffraction (XRPD) measurements prove that **3/II** transforms into **3/I** on heating. The crystal structure of **3/II** was determined ab initio from XRPD data. In its crystal structure the Co cations are linked by pairs of bridging thiocyanato anions into a 1D coordination polymer, and thus, **3/II** is an isomer of **3/I**. Magnetic measurements disclose that the stable form **3/I** only shows paramagnetism without any magnetic anomaly down to 2 K. In contrast, the metastable form **3/II** shows ferromagnetic behavior. The phase transition into ordered state at T_c = 3.8 K was confirmed by specific heat measurements. Alternating current susceptibility measurements show frequency dependent maxima in χ' and χ'', which is indicative for a slow relaxation of the magnetization.

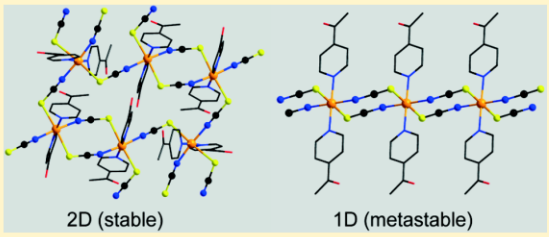

INTRODUCTION

Investigations on a rational synthesis of new compounds with desired, e.g., magnetic properties are an important field in chemical research.

This approach, often called "crystal engineering", is based on investigations on the structure−property relationships of crystalline solids and on considerations for how a specific structure can be prepared.[1] In this context one has to be aware of the phenomena of polymorphism or isomerism that are frequently observed, which makes the prediction of a coordination network challenging.[2]

Recently, we have reported on the synthesis of new coordination polymers based on transition metal thiocyanates and neutral N-donor coligands. In the course of these investigations we prepared a number of compounds in which the metal cations are octahedrally coordinated by four μ-1,3-bridging anionic ligands and two N-donor coligands. In those cases where monodentate coligands are used, 1D coordination polymers are frequently obtained, whereas using bidentate coligands mostly leads to the formation of 2D structures.[3] In all of these compounds the metal cations are connected by μ-1,3-bridging anionic ligands into chains (Figure 1), which obviously corresponds to a relatively stable arrangement, usually observed in such compounds.[4] In a few cases, 2D thiocyanato coordination networks are obtained, in which two metal cations are μ-1,3-bridged into dimers by pairs of thiocyanato anions which are then further connected into layers by μ-1,3-bridging single anionic ligands.[5]

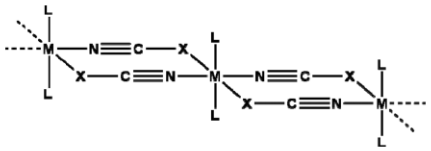

Figure 1. View of the metal thiocyanato chains usually observed in compounds of composition $M(NCX)_2(L)_2$ with M = Mn, Fe, Co, and Ni, X = S, Se and L = monodentate N-donor coligand.

Magnetic investigations on the 1D compounds $[M(NCS)_2(pyridine)_2]_n$ with M = Mn^{II}, Fe^{II}, Co^{II}, and Ni^{II} reveal that the Mn compound shows antiferromagnetic ordering, whereas for the Ni and for the Fe compounds reported in the literature, a metamagnetic transition is observed.[6] Instead, $[Co(NCS)_2$-

Received: December 18, 2014
Published: March 5, 2015

DOI: 10.1021/ic503029t
Inorg. Chem. 2015, 54, 2893−2901

$(pyridine)_2]_n$ shows a slow relaxation of the magnetization indicating a single chain magnetic (SCM) behavior.[7] This is a relatively rare magnetic behavior with potential for future applications, and this is one of the reasons why an increasing number of such compounds were recently reported in the literature.[8]

In further work we have prepared a large number of such μ-1,3-bridging thiocyanato coordination polymers and investigated the influence of the metal cation, the anionic ligand, and the coligand on their structural and magnetic properties. Surprisingly, in $[Co(NCS)_2(pyridine)_2]_n$, the anionic ligand can be exchanged by selenocyanato anions and the coligand by, e.g., 4-ethylpyridine without losing the magnetic relaxations.[9] A similar magnetic behavior was also observed in $[Fe(NCSe)_2(pyridine)_2]_n$ that compared to the thiocyanato analog exhibits stronger intrachain interactions.[10] Because of the actual interest in such magnetic behavior our research mainly focused on compounds that contain cations of large magnetic anisotropy like, e.g., Fe^{II} and Co^{II}. In this context it is noted that the compounds with a 2D thiocyanato network do not show slow relaxations and, therefore, are of minor importance.[5]

To study the influence of the substitution of the pyridine coligands on the magnetic properties we tried to prepare compounds based on cobalt(II) thiocyanate with 4-acetylpyridine as a ligand. Two discrete complexes of composition $Co(NCS)_2(4\text{-acetylpyridine})_4$ (1) and $Co(NCS)_2(4\text{-acetylpyridine})_2(H_2O)_2$ (2) are already reported in literature; however, the desired compound $[Co(NCS)_2(4\text{-acetylpyridine})_2]_n$ was unknown.[11] We have found that a compound of this chemical composition can easily be prepared in solution, but instead of the 1D structure, a 2D thiocyanato network was obtained, which showed only paramagnetic behavior. In a consecutive work, we were able to prepare the desired 1D compound that showed relaxations of the magnetization, and we have found that it is metastable at room temperature with the 2D polymorph being the thermodynamically stable form. Herein we report on these investigations.

EXPERIMENTAL SECTION

Synthesis. 4-Acetylpyridine and $Co(NCS)_2$ were obtained from Alfa Aesar. Solvents were used without further purification. Crystalline powders of compounds **1**, **2**, and **3/I** were prepared by stirring the reactants in appropriate solvents at room temperature. Compound **3/II** was prepared by annealing at 70 °C. The purity of all compounds was proved by XRPD and elemental analysis.

Synthesis of Compound 1. $Co(NCS)_2$ (43.8 mg, 0.25 mmol), and 4-acetylpyridine (275.3 μL, 2.50 mmol) were stirred in 2.0 mL of water for 3 d. Yield: 60.8%. Anal. Calcd (%) for $C_{30}H_{28}CoN_6O_4S_2$: C 54.62, H 4.28, N 12.74; S 9.72. Found: C 54.39, H 4.13, N 12.68, S 9.61. IR (ATR): ν_{max} = 3043 (w), 2905 (w), 2060 (s), 1693 (s), 1555 (m), 1412 (m), 1361 (m), 1262 (s), 1011 (m), 828 (s), 591 (s), 483 (m).

Synthesis of Compound 2. $Co(NCS)_2$ (43.8 mg 0.25 mmol), and 4-acetylpyridine (55.1 μL, 0.50 mmol) were stirred in 1.5 mL of water for 3 d. Yield: 92.6%. Anal. Calcd (%) for $C_{16}H_{18}CoN_4O_4S_2$: C 42.38, H 4.00, N 12.36; S 14.14. Found: C 42.50, H 3.95, N 12.42, S 14.50. IR (ATR): ν_{max} = 3314 (b), 3228 (b), 3046 (w), 2088 (s), 1680 (s), 1557 (m), 1412 (m), 1362 (m), 1276 (s), 1060 (m), 1012 (m), 831 (s), 595 (s), 471 (s).

Synthesis of Compound 3/I. $Co(NCS)_2$ (43.8 mg, 0.25 mmol), and 4-acetylpyridine (55.1 μL, 0.50 mmol) were stirred in 1.5 mL of ethanol for 3 d. Yield: 80.4%. Single crystals suitable for single crystal X-ray diffraction were prepared by the same method in acetonitrile. After 2 weeks dark red single crystals were obtained. Anal. Calcd (%) for $C_{16}H_{14}CoN_4O_2S_2$: C 46.04, H 3.38, N 13.42; S 15.37. Found: C 46.07, H 3.32, N 13.47, S 15.39. IR (ATR): ν_{max} = 3131 (w), 3083 (w), 3046 (w), 2102 (s), 1687 (s), 1555 (m), 1413 (s), 1361 (m), 1270 (s), 1138 (b), 1059 (m), 815 (s), 594 (s), 465 (m).

Synthesis of Compound 3/II. A 60 mg portion of compound **2** was annealed at 70 °C for 1 day. Anal. Calcd (%) for $C_{16}H_{14}CoN_4O_2S_2$: C 46.04, H 3.38, N 13.42; S 15.37. Found: C 46.35, H 3.30, N 13.44, S 14.93. IR (ATR): ν_{max} = 3116 (w), 3078 (w), 2359 (w), 2098 (s), 1697 (s), 1555 (m), 1411 (m), 1360 (m), 1263 (s), 1060 (m), 1014 (m), 818 (s), 593 (s), 469 (m).

Elemental Analysis. CHNS analysis was performed using an EURO EA elemental analyzer, fabricated by EURO VECTOR Instruments and Software.

IR Spectroscopy. FT IR spectra were recorded on a Genesis series FTIR spectrometer, by ATI Mattson, in KBr pellets, as well with an Alpha IR spectrometer from Bruker equipped with a Platinum ATR QuickSnap sampling module between 4000 and 375 cm^{-1}.

Single Crystal X-ray Diffraction. Data collection for **3/I** was performed with an imaging plate diffraction system IPDS-2 with Mo Kα radiation from STOE & CIE. The structure solution was performed with direct methods using SHELXS-97, and structure refinements were performed against F^2 using SHELXL-97. All non-hydrogen atoms were refined with anisotropic displacement parameters. The hydrogen atoms were positioned with idealized geometry and were refined with fixed isotropic displacement parameters [$U_{iso}(H) = -1.2 \cdot U_{eq}(C_{aromatic})$] using a riding model. Selected crystal data are shown in Table 1. CCDC 1030910 (**3/I**) and CCDC 1030911 (**3/II**) contain the supplementary crystallographic data for this Article. These data can be obtained free charge from the Cambridge Crystallographic Data Centre via http://www.ccdc.cam.ac.uk/data_request/cif.

Table 1. Selected Crystal Data and Details of the Structure Refinement for Compound 3/I

	3/I
formula	$C_{16}H_{14}CoN_4O_2S_2$
MW/g mol^{-1}	417.36
cryst syst	*orthorhombic*
space group	*Pbca*
a/Å	9.5315(3)
b/Å	15.8242(4)
c/Å	24.3712(6)
α/deg	90
β/deg	90
γ/deg	90
V/Å^3	3675.87(17)
T/K	293(2)
Z	8
D_{calc}/g cm^{-3}	1.508
μ/mm^{-1}	1.177
θ_{max}/deg	2.57−28.07
measured refins	32 860
unique refins	4408
refins [$F_0 > 4\sigma(F_0)$]	3747
parameter	228
R_{int}	0.0462
R1 [$F_0 > 4\sigma(F_0)$]	0.0539
wR2 [all data]	0.0962
GOF	1.262
$\Delta\rho_{max}$, $\Delta\rho_{min}$/e Å^{-3}	0.281/−0.302

X-ray Powder Diffraction. For checking samples' phase purity, XRPD experiments were performed using a Stoe Transmission Powder Diffraction System (STADI P) with Cu Kα radiation (λ = 154.0598 pm) that is equipped with a linear position-sensitive detector (6.5−7° simultaneous; scan range overall = 2−130°) from STOE & CIE, an Image Plate Detector (scan range overall = 0−127°), and a

DOI: 10.1021/ic503029t
Inorg. Chem. 2015, 54, 2893−2901

PANalytical X'Pert Pro MPD Reflection Powder Diffraction System with Cu Kα radiation (λ = 154.0598 pm) equipped with a PIXcel semiconductor detector from PANalytical.

For the crystal structure solution of **3/II** and for the in situ measurements a D8 Advance powder diffractometer was used [Bruker, Cu Kα1, radiation from primary Ge(111)-Johannson-type monochromator, Vantag-1 position sensitive detector (PSD), with an opening angle of 6° in Debye–Scherrer geometry]. The powdered sample was sealed in a borosilicate glass capillary (0.5 mm diameter Hilgenberg glass capillary No. 50), which was spun during the measurement for better data statistics. For the crystal structure, solution data were taken from 6° to 43° 2θ for a period of 24 h. For the temperature-variable measurements data were collected at 5 K temperature intervals, from 8° to 28° 2θ for a period of 15 min.

The powder pattern of **3/II** was analyzed with TOPAS 4.2.[12] The indexing was performed from first-principles by the iterative use of singular value decomposition. The indexing indicated the phase crystallizes in a triclinic unit cell. Precise lattice parameters were determined by a Pawley fit.[13] The crystal structure determination was performed in the $P1$ and $P\bar{1}$ space groups with the simulated annealing approach where the cation was positioned at 1/2 1/2 1/2 special position and the organic ligands were allowed to freely rotate and translate.[14] For the final Rietveld refinement,[15] all profile and lattice parameters were subjected to free unconstrained refinement, and the final plot is shown in Figure S1 in the Supporting Information. Selected crystallographic data are listed in Table 2. The positions of the hydrogen atoms were calculated.

Table 2. Selected Crystal Data and Details of the Rietveld Refinement for Compound 3/II

	3/II
formula	$C_{16}H_{14}CoN_4O_2S_2$
cryst syst	triclinic
space group	$P\bar{1}$
a/Å	5.628 03(64)
b/Å	8.4717(14)
c/Å	10.3170(19)
α/deg	76.7846(97)
β/deg	87.540(15)
γ/deg	73.483(17)
V/Å^3	458.988
T/K	297.15
Z	1
start to finish angle/deg 2θ	6–43
λ/Å	1.540 596
R_{wp}/%[a]	7.40
R_p/%[a]	11.54
R_{exp}/%[a]	10.27
R_{Bragg}/%[a]	0.25

[a]Background corrected values. The lower R_{wp} value compared to R_p is attributed to an inappropriate weighting scheme for data collected with Mythen PSD.

Differential Thermoanalysis and Thermogravimetry. The DTA-TG measurements were performed in a nitrogen atmosphere (purity: 5.0) in Al_2O_3 crucibles using a STA-409CD instrument from Netzsch. The DTA-TG-MS measurements were performed with the same instrument, which is connected to a quadrupole mass spectrometer from Balzers via Skimmer coupling from Netzsch. The MS measurements were performed in analog and trend scan mode in Al_2O_3 crucibles in a dynamic nitrogen atmosphere (purity: 5.0) using heating rates of 4 K/min. All measurements were performed with a flow rate of 75 mL/min. The instrument was calibrated using standard reference materials.

Magnetic Measurements. Magnetic measurements of **1**, **2**, and **3/I** were performed using Quantum Design PPMS equipped in 7 T magnet, using samples mounted in a gelatin capsule.

For **3/II** the magnetic measurements were performed using a Quantum Design MPMS-5XL magnetometer. The powder sample was pressed into 5 mm × 0.8 mm pellet together with a bag made of PTFE tape. The pellet was oriented along the magnetic field to minimize the demagnetization effect. The diamagnetic response of the PTFE and the core diamagnetic response were subtracted.

Specific Heat. Specific heat measurements were performed using the relaxation technique in Quantum Design PPMS cryostat. The powder sample was pressed into 2.4(1) mg, 3 mm diameter pellet with no binder. The heat capacity of the microcalorimeter, together with a drop of ApiezonN grease used to fix the sample, was measured before the sample measurement and subtracted. The influence of the magnetic field on this background signal is negligible above 2 K.

RESULTS AND DISCUSSIONS

Synthetic Aspects. In the beginning of our investigations, cobalt(II) thiocyanate was reacted in various solvents with different stoichiometric ratios of 4-acetylpyridine, and the products obtained were characterized by elemental analysis, IR spectroscopy, and X-ray powder diffraction (XRPD). We have found that in water only a 6-fold excess of the coligand leads to the formation of $Co(NCS)_2(4\text{-acetylpyridine})_4$ (**1**) whereas all other stoichiometric ratios led to the formation of the hydrate $Co(NCS)_2(4\text{-acetylpyridine})_2(H_2O)_2$ (**2**) (Table S1 in the Supporting Information). IR spectroscopic investigations show that the asymmetric $\nu_{(as)}$ C–N stretching vibration is observed at 2060 cm^{-1} for **1** and at 2088 cm^{-1} for **2** indicating that the anionic ligands are only terminal N-bonded (Figures S2 and S3 in the Supporting Information).[16] In contrast, in ethanol, methanol, and acetonitrile in most cases a new crystalline compound (**3/I**) crystallized. The results of elemental analysis showed that a compound of composition $Co(NCS)_2(4\text{-acetylpyridine})_2$ was formed, and in the IR spectra its asymmetric $\nu_{(as)}$ C–N stretching vibration was observed at 2102 cm^{-1}, indicating that μ-1,3 bridging thiocyanato anions are present (Figure S4 in the Supporting Information).[16] Investigations with XRPD revealed that compounds **1** and **2** were obtained as pure crystalline phases and that in the powder pattern of compound **3** no reflections of **1** or **2** are present, indicating that this compound is also obtained as phase pure (Figures S5–S7 in the Supporting Information). Later on, single crystals of compound **3/I** were prepared by reaction of $Co(NCS)_2$ with 4-acetylpyridine in a ratio of 1:2 in acetonitrile, and single crystal X-ray structure analysis confirmed the composition of this compound as $Co(NCS)_2(4\text{-acetylpyridine})_2$ (see Experimental Section).

Crystal Structure of Form 3/I. Compound **3/I** crystallizes in the orthorhombic space group *Pbca* with 8 formula units in the unit cell. The asymmetric unit consists of one Co cation, two crystallographically independent thiocyanato anions, and two distinct 4-acetylpyridine ligands (Figure S8 in the Supporting Information). In the crystal structure, the Co cations are always *trans* coordinated by two coligands as well as two N- and two S-bonding thiocyanato anions. The Co–N bond lengths between 2.064(2) and 2.174(2) Å and the Co–S bond lengths of 2.572(1) and 2.647(1) Å are in the typical range for similar compounds, and the bonding angles show a slight distortion from the octahedral geometry (Table S2 in the Supporting Information). Each of the two Co cations is linked by pairs of μ-1,3-bridging thiocyanato anions into dimers, that are further connected by single μ-1,3-bridging anionic ligands

DOI: 10.1021/ic503029t
Inorg. Chem. 2015, 54, 2893–2901

into layers parallel to the *a*-/*b*-plane (Figure 2, top). The layers are stacked perpendicular to the *c*-axis with the acetyl group of

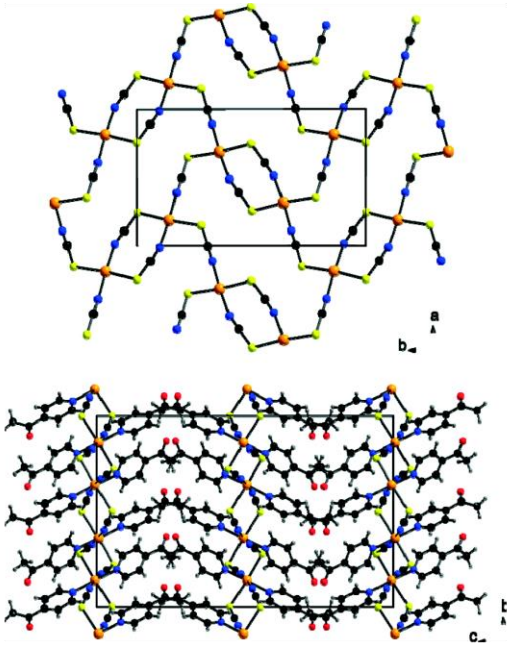

Figure 2. Crystal structure of the compound **3/I** with view of the cobalt thiocyanato network along the *c*-axis (top) and perpendicular to the layers with view along the *a*-axis (bottom). An ORTEP plot of this compound is given in Figure S8 in the Supporting Information.

the coligands pointing to each other. It is noted that the phenyl rings of neighboring chains are shifted relative to each other, which means that no $\pi\cdots\pi$ interactions are observed.

On the basis of the structural data, the powder pattern was calculated, which shows that compound **3/I** was obtained as a pure crystalline phase (Figure S9 in Supporting Information). Surprisingly, this structure is completely different from that expected as no cobalt thiocyanato chains are observed, which is the most common structural motif for such coordination polymers. Considering the 2D structure, it is highly unlikely that this compound will show a slow relaxation of the magnetization of single chains. Since **3/I** is formed by crystallization from solution, it can be assumed that it is the thermodynamic stable product at room temperature. Consequently, the 1D compound (if it exists) must be metastable and therefore not observed by recrystallizations. This modification might be formed by thermal decomposition of suitable precursor compounds like, e.g., the discrete complexes **1** and **2**. Therefore, both compounds were investigated by simultaneous differential thermoanalysis and thermogravimetry (DTA-TG) and temperature dependent XRPD.

Thermoanalytical Measurements of Compounds 1 and 2. If $Co(NCS)_2(4\text{-acetylpyridine})_4$ (**1**) is heated in a thermobalance, a mass step is observed at about 118 °C, which is accompanied by an endothermic event in the DTA curve (Figure 3 and Figure S10 in the Supporting Information). The experimental mass loss of this step of 36.0% is in good agreement with that calculated for the removal of two of the four 4-acetylpyridine ligands. On further heating, a second step

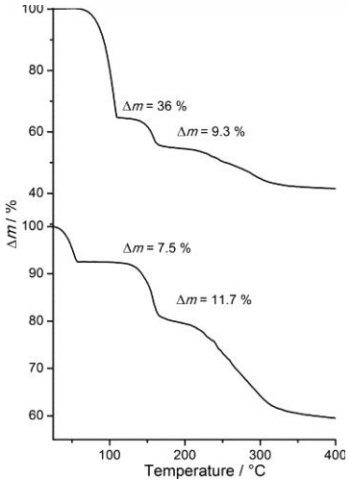

Figure 3. Thermogravimetric curve for compound **1** (top) and **2** (bottom) at 1 K/min.

of 9.3% is observed that cannot be assigned to any reasonable reaction. This result suggests that in the first TG step a compound of composition $Co(NCS)_2(4\text{-acetylpyridine})_2$ has formed. To investigate the nature of this intermediate in more detail, a second TG run was performed at 4 K/min and stopped after the first mass loss. XRPD investigations of this residue proved that it is amorphous (Figure S11 in the Supporting Information). When the experiment was repeated with 1 K/min, a crystalline product was obtained, which unfortunately corresponds to the 2D compound **3/I**.

DTA-TG measurements on the hydrate complex **2** show a well-resolved TG step of 7.5% at about 78 °C, which is accompanied by an endothermic event in the DTA curve, corresponding to the removal of all water molecules (Figure 3 and Figure S10 in the Supporting Information). On further heating, the TG curves look similar to that of **1**.

When the heating is stopped after water removal and the residue is investigated by XRPD, a mixture of compound **3/I** and an additional crystalline phase is formed, which does not correspond to compound **1** or **2** (Figure S12 in the Supporting Information). In the IR spectra of this mixture the asymmetric C−N-stretching vibration is observed at 2099.5 cm^{-1}, indicating that in both crystalline phases only μ-1,3-bridging thiocyanato anions are present (Figure S13 in the Supporting Information).[16] Elemental analysis of this mixture shows that the composition is still $Co(NCS)_2(4\text{-acetylpyridine})_2$. Consequently, the additional crystalline phase (**3/II**) must be a second modification of **3/I**.

To investigate whether the new form **3/II** can be prepared phase pure, heating rate dependent measurements were performed and the residues isolated after water removal were investigated by XRPD.[17] These investigations clearly show that with decreasing the heating rate the content of **3/II** increases, but even at very low heating rates of 1 K/min the residues still contain significant amounts of **3/I** (Figure S14 in the Supporting Information).

Similar results were also found when hydrate **2** was investigated by temperature dependent XRPD measurements, where no hints were found that **3/II** can be obtained as a pure phase (Figure S15 in the Supporting Information).

DOI: 10.1021/ic503029t
Inorg. Chem. 2015, 54, 2893−2901

All the results presented above strongly indicate that the 3/II phase is metastable and that on further heating it transforms into the more stable form 3/I. Therefore, the hydrate 2 was annealed at temperatures much below the decomposition temperature observed in the TG measurements at 1 K/min. To our surprise, annealing for some hours at 70 °C leads to the formation of form 3/II almost as a pure form, as no reflections of compounds 1, 2, and 3/I were visible in the XRPD pattern. IR spectroscopic investigations showed that the spectra of this new form are almost identical to that of 3/I (Figure S16 in the Supporting Information).

As stated above, the recrystallizations from different solvents always led to 3/I, and no (single crystal) sample of 3/II was obtained. Unfortunately, on thermal annealing only a microcrystalline powder is obtained that cannot be characterized by single crystal X-ray diffraction. However, a compound of composition $Cd(NCS)_2(4\text{-acetylpyridine})_2$ that crystallizes in two different modifications was already reported by our group, and its structures correspond to that what we expected for the Co compound.[18] Namely, in each of the two forms the Cd cations are octahedrally coordinated and are μ-1,3-bridged by pairs of thiocyanato anions into chains (Figure S17 in the Supporting Information). Obviously, for this metal cation the chain compounds are thermodynamically stable. Unfortunately, the Co compound 3/II seems to crystallize in a different modification, because none of the Cd forms are isotypic to it. Therefore, we tried to determine the structure of 3/II *ab initio* from XRPD data.

Crystal Structure of Compound 3/II. The XRPD pattern of 3/II can be indexed in a triclinic unit cell with $Z = 1$ molecules in the unit cell (Table 2). The structure was solved and refined in space group $P\bar{1}$ (Figure S1 in the Supporting Information). In the crystal structure each Co cation is octahedrally coordinated by two terminal N-bonded 4-acetylpyridine coligands and four thiocyanato anions; all of them are *trans* coordinated (Figure 4).

The Co cations are linked by pairs of μ-1,3-bridging thiocyanato ligands into chains, that elongate in the direction of the crystallographic *a*-axis (Figure 4). This structure corresponds to the chain structure expected at the beginning of our investigations, which is indeed frequently observed in this family of compounds. The intrachain Co···Co distance equals 5.6280 Å, whereas the shortest interchain Co···Co distance is 8.4717 Å. The chains are arranged in a way that all $N_{acetylpyridine}$–Co–$N_{acetylpyridine}$ vectors are parallel. The phenyl rings along the chain and of neighboring chains are rotated and shifted relative to each other, which means that even in this form no significant $\pi\cdots\pi$ interactions are involved.

Investigations on the Thermodynamic Stability of 3/I and 3/II. To investigate the relative thermodynamic stability of 3/I and 3/II, a solvent mediated conversion experiment was performed in which a mixture of both modifications was stirred in a saturated solution in ethanol for several hours, and afterward, the residue was investigated by XRPD. All crystals of 3/II disappeared within 3 h; afterward, only form 3/I was present (Figure 5). This observation clearly proves that form 3/I represents the thermodynamically stable form at room temperature, at which form 3/II is metastable.

To investigate whether the two modifications can be transformed into each other, experiments using DSC and XRPD were performed for both forms (Figures S18–S20 in the Supporting Information). On heating 3/I, decomposition is observed at a peak temperature T_p of 213 °C without any hint

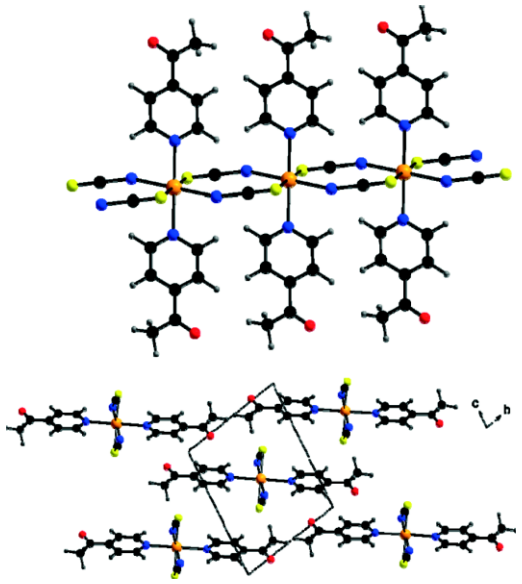

Figure 4. Crystal structure of form 3/II with view of the Co thiocyanato chains (top) and of the arrangement of the chains with view along the crystallographic *a*-axis (bottom).

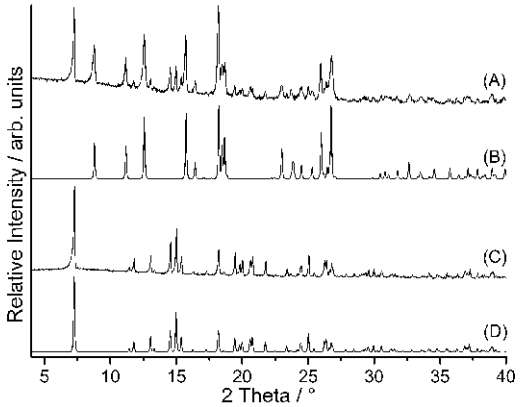

Figure 5. Experimental X-ray powder pattern of a mixture of 3/I and 3/II before (A), calculated powder pattern for 3/II (B), mixture after stirring for 3 h (C), and powder pattern for 3/I (D) calculated from single crystal data.

for a further transformation into (e.g.) 3/II (Figure S18 in the Supporting Information). On the contrary, for 3/II a small endothermic peak was observed at about 70 °C, but surprisingly, the XRPD pattern of a residue obtained at 80 °C corresponds to that of the pristine material 3/II. It should be noted that the reversibility of this event was not checked.

However, on further heating an additional endothermic signal is observed at T_p = 190 °C, followed by a second strong endothermic event at 200 °C that corresponds to the decomposition of the material (Figure S19 in the Supporting Information). If the residue is isolated at 190 °C and investigated by XRPD measurements, it is proven that 3/II has been transformed into 3/I. This is consistent with the temperature dependent XRPD measurements shown in

DOI: 10.1021/ic503029t
Inorg. Chem. 2015, 54, 2893–2901

Supporting Information Figure S15, where the same transition is observed. Because this transition is endothermic one can assume that both forms are related by enantiotropism with **3/II** being stable at lower temperatures.

Magnetic Investigations. Compounds **1**, **2**, **3/I**, and **3/II** were investigated for their magnetic properties. For all four compounds the effective magnetic moment at 300 K reaches 4.9–5.1 μ_B per Co ion. These values are within the typical range 4.7–5.2 μ_B for the room temperature magnetic moment of the Co(II) ion in an octahedral surrounding.[19] Below 300 K the decrease of $\chi T(T)$ with decreasing temperature is an effect of Co(II) single ion properties, which is illustrated by the magnetic moment dependence for discrete complexes **1** and **2** (Figures S21 and S22 in the Supporting Information). For **1** and **2** no magnetic anomaly is observed down to 2 K. For **3/I** an additional effect is observed: the increase of $\chi T(T)$ below 20 K. This is the effect of an exchange interaction mediated through the −NCS− bridges between Co centers that create *ab* layers (Figure S23 in the Supporting Information). However, no signs of a magnetic ordering were observed. On the basis of susceptibility data measured at 100 Oe, the $\chi T(T)$ dependence changes smoothly down to 2 K. For **3/II** the exchange interaction through the anionic ligands creates a 1D system of Co(II) spins, leading to interesting magnetic properties at low temperatures. For this reason, detailed investigations of magnetic properties of this compound were undertaken and are presented below.

The magnetic susceptibility of **3/II** measured at 1 kOe leads to χT = 3.1 cm^3 K/mol at 300 K, corresponding to an effective magnetic moment of 4.98 μ_B (see Figure 6). Below 50 K the

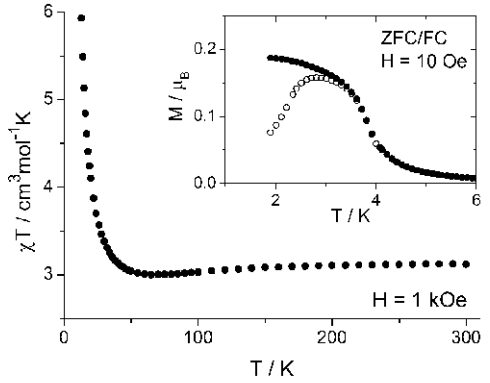

Figure 6. Temperature dependence of magnetic susceptibility of **3/II** measured at H_{DC} = 1 kOe. Figure is cut at t he top. Inset: zero-field cooled (○) and field cooled (●) magnetization at 10 Oe.

decrease expected due to single ion properties of Co(II) ions is overcome by a strong increase due to a ferromagnetic exchange interaction between Co magnetic moments. Very similar behavior was observed in a number of related Co chain compounds.[7,20] Below 10 K the susceptibility measured at the low magnetic field of 10 Oe increases significantly and saturates. The maximum slope of $\chi(T)$ is reached at 3.8 K. Zero-field cooled and field cooled magnetization curves measured at the same field bifurcate below 3.6 K (inset of Figure 6 and Figure S24 in the Supporting Information). These properties point to a kind of freezing of Co magnetic moments in **3/II** at low temperatures.

The magnetization of **3/II** measured at 1.8 K as a function of field is shown in Figure 7 with the low-field hysteresis loop

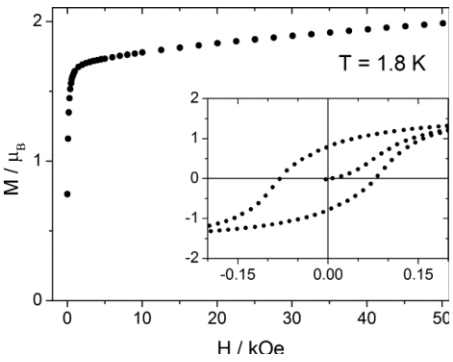

Figure 7. Field dependence of magnetization for **3/II** measured at 1.8 K. Inset: hysteresis loops measured at 1.8 K.

zoomed in the inset. The coercive field is of the order of 60 Oe, and depends slightly on the sweep rate of the magnetic field. At low fields a rapid increase is observed (up to 1.65 μ_B at 1 kOe). At higher fields the slower increase of the magnetization at higher fields (up to 2.0 μ_B at 50 kOe) is related to the strong single-ion anisotropy of Co(II).

The susceptibility data above the freezing temperature allows us to estimate the exchange interaction between Co ions. For Co^{II} in a distorted octahedral crystal field the ground 3d electron state is a Kramers doublet, and the first excited state usually has an energy higher by 100–200 cm^{-1}. In such a case, below 20 K the magnetic properties can be described assuming that each Co has the effective spin s = 1/2 with a high anisotropy. We used the model of a chain of s = 1/2 Ising spins with an exchange interaction between nearest neighbors, defined by the Hamiltonian

$$\hat{\mathcal{H}} = -J\sum_i \hat{s}_i^z \hat{s}_{i+1}^z + \mu_B \sum_i \vec{H} \cdot \hat{g} \cdot \vec{s}_i \qquad (1)$$

where $\hat{g}$ tensor includes g-factors parallel and perpendicular to the deformation axis. The solution given by Fisher leads to zero-field magnetic susceptibility[21]

$$\chi_{\parallel} = \frac{N g_{\parallel}^2 \mu_B^2}{4kT} \exp\left(\frac{J}{2kT}\right)$$

$$\chi_{\perp} = \frac{N g_{\perp}^2 \mu_B^2}{2J}\left[\tanh\left(\frac{J}{4kT}\right) + \frac{J}{4kT}\operatorname{sech}^2\left(\frac{J}{4kT}\right)\right] \qquad (2)$$

for the field parallel and perpendicular to the easy axis of Ising spins, respectively. For $J > 0$ at low temperatures the parallel susceptibility strongly dominates and is responsible for the exponential increase of χT.

The $\ln(\chi T)$ versus $1/T$ dependence calculated using the low field susceptibility of **3/II** is shown in Figure 8. The demagnetization correction was taken into account. The linear dependence observed in the 5–20 K temperature range is in agreement with eqs 2, but below 5 K χT increases faster. This effect can be accounted for by introducing a ferromagnetic interaction between chains, quantified by the zJ' parameter in the mean field model approximation

DOI: 10.1021/ic503029t
Inorg. Chem. 2015, 54, 2893−2901

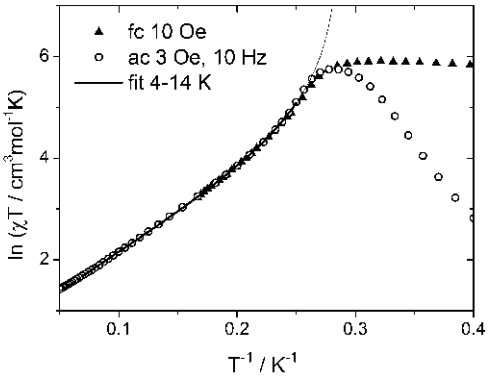

Figure 8. Low field magnetic susceptibility of **3/II**: field cooled dc data (▲) and ac data (○). The solid line is the fit and its extrapolation (see text).

$$\chi_i = \frac{\chi_i^{chain}}{1 - zJ'\chi_i^{chain}/N_A g_i^2 \mu_B^2} \quad (3)$$

For the polycrystalline sample the average susceptibility is

$$\chi = (\chi_{\parallel} + 2\chi_{\perp})/3$$

The parameters $g_{\parallel}$, J, and zJ' were fitted to reproduce the ac susceptibility data in the temperature range 4−14 K. The parameter $g_{\perp}$ was fixed to zero, which corresponds to neglecting the $\chi_{\perp}^{chain}$ term. We obtained $g_{\parallel} = 7.74(3)$, $J/k = 30.2(1)$ K, $zJ'/k = +0.18(1)$ K. The curve calculated using these parameters diverges to infinity at $T = 3.48$ K (see Figure 8). An attempt to fit the same data also including in the model $\chi_{\perp}^{chain}$ leads to $g_{\perp} = 0$, but with a huge uncertainty.

To investigate the relaxation properties of **3/II** ac susceptibility measurements were performed as a function of temperature. The ac susceptibility measured at zero dc field (shown in Figure 9) strongly depends on the driving field frequency. The peaks of in-phase susceptibility $\chi'(T)$ are accompanied by peaks of out-of-phase susceptibility χ''. All maxima significantly shift to lower temperatures with decreasing ac frequency, which is indicative for a slow relaxation of the magnetization as observed in, e.g., superparamagnets and spin glasses. The parameter φ, calculated here as the temperature shift of the χ'' peak on a decade of frequency

$$\phi = \Delta T_1 / [T_1 \Delta(\log f)]$$

equals 0.074, if the data at 0.1 and 1000 Hz are used to estimate the differences. This is just below the range typical for ideal superparamagnets and single chain magnets, where usually $\varphi >$ 0.1, but rather falls in the range typical for spin glasses (0.01−0.08).[22]

To get more precise information about magnetic relaxation in **3/II** we made isothermal, frequency dependent ac measurements (see Figure S25 in the Supporting Information). The Cole−Cole model was used for their analysis. The relaxation time τ was obtained for temperatures from 2.4 to 3.6 K. At lower and higher temperatures the relaxation time is beyond the available frequency window. It should be noted that the distribution of the relaxation times is broad, which is illustrated by the parameter α which varies from 0.4 to 0.52. The temperature dependence of the mean τ roughly follows the Arrhenius law $\tau = \tau_0 \exp(\Delta_\tau/kT)$, with the barrier energy Δ_τ/k

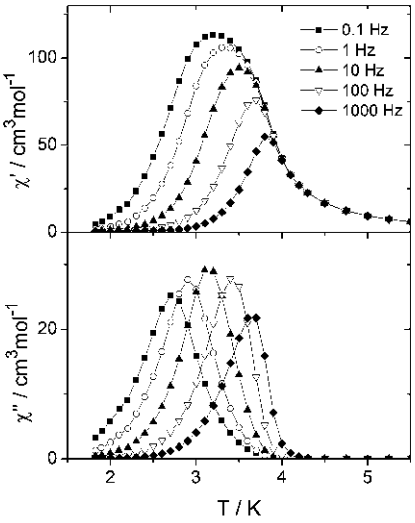

Figure 9. Temperature dependence of ac susceptibility for **3/II** measured at $H_{DC} = 0$ and $H_{AC} = 3$ Oe for different ac field frequencies from 0.1 to 1000 Hz.

= 74(3) K and $\tau_0 = 0.66$ ps (see Figure S26 in the Supporting Information). The magnetic properties of **3/II** show some features characteristic for single chain magnets (crystal structure with one-dimensional system of strongly interacting spins, weak interchain interaction, lack of obvious source of crystal disorder). Some features are characteristic for ordered ferromagnets (high magnetization at low field, nonzero interchain interaction creating a 3-dimensional magnetic network leading to a divergence of susceptibility at $T > 0$), and some features are characteristic of a cluster spin-glasses (distribution of relaxation times). To get additional insight and adjudicate if a long-range magnetic ordering transition takes place in **3/II** we measured its specific heat.

Specific Heat of 3/II. The specific heat C measured in zero magnetic field is presented in Supporting Information Figure S27, while the extracted magnetic contribution C_{magn} is shown in Figure 10. A peak present at $T_c = 3.8$ K in the $C_{magn}(T)$ dependence points to an ordering transition around this temperature.

A quantitative analysis of $C(T)$ data requires estimation of the phonon contribution and the magnetic contribution to the specific heat. The phonon contribution was included using the single mode Debye model, which is the appropriate approximation in the limit of low temperatures. For this reason only data below 15 K were taken into account in further analysis. The specific heat of the chain defined by Hamiltonian (eq 1) in zero magnetic field is equal[21b]

$$C_{chain} = R(J/kT)^2 \mathrm{sech}^2(J/kT)$$

where R is the gas constant. The total specific heat

$$C(T) = BC_{chain}(J, T) + A\, C_{Debye}(\theta_D, T)$$

used to model the experimental data of **3/II** did not include any interchain interactions, so it could not account for the ordering transition, and reproduce the peak at 3.8 K. For this reason the parameters B, J, A, and θ_D were fitted using the data in the range 4.3−15 K, i.e., above T_c. We obtained the

DOI: 10.1021/ic503029t
Inorg. Chem. 2015, 54, 2893−2901

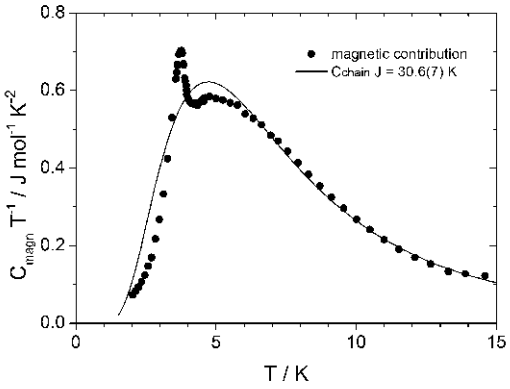

Figure 10. Magnetic contribution to the specific heat of **3/II** vs temperature. The dashed line is the fitted Ising chain contribution.

parameters J/k = 30.6(7) K, the effective Debye temperature θ_D = 82(4) K, and the factors A = 0.23(2) and B = 0.93(4). For the Ising chain, the zero field specific heat does not depend on the sign of J. The positive sign (ferromagnetic interaction) was assigned on the basis of the magnetic properties of **3/II**. The J value obtained here from specific heat data is almost identical to the value 30.2(1) K obtained from magnetic measurements.

The magnetic contribution, calculated as

$$C_{mag} = C - C_{Debye}(\theta_D, T)$$

is shown in Figure 10. Above 4 K the fitted curve follows experimental points, confirming that magnetic properties of **3/II** can be described above this temperature using a one-dimensional model. However, at lower temperatures, the fitted $C(T)$ deviates from measured data, which denotes a crossover from 1D to 3D system, due to magnetic interactions between chains. The critical entropy, i.e., the entropy change from 0 to T_c, quantifies how ideal a 1D magnetic system is. It is zero for the 1D system, about 0.805R ln2 for 1/2 Ising spins on a simple cubic 3D lattice,[21b,23] and reaches R ln2 for a mean-field model. For **3/II** the entropy change from 2 to 3.8 K (which is close to the critical entropy, see Figure 10) is only 0.10R ln2, close to the 1D case.

The parameter B should be equal to 1.0 in the ideal case. A slightly smaller value obtained for **3/II** may have two sources. The first is a possible error of the sample mass, which we estimate to 4% on the basis of mass uncertainty. The second possible explanation is an impurity in the sample, in this case a very small fraction of **3/I**, which is indicated by the Rietveld refinement. In zero magnetic field noninteracting Co(II) ions do not add any contribution to the specific heat. If any exchange interaction between spins is present, it produces a heat capacity with a maximum at a temperature proportional to this exchange interaction. The magnetic properties of **3/I** exclude any strong exchange interactions, and predict lack of significant specific heat contribution above 2 K. This second explanation is also supported by specific heat measurements in external field (Figure S28 in the Supporting Information), where a small upturn of $C(T)$ is visible below 3 K for 10 kOe data. The external field splits the lowest Kramers doublet of isolated Co(II) giving rise to a Schottky anomaly with a maximum below 2 K. No such effect is expected for the Ising chain. However, a very small impurity of **3/I** does not influence the fitted value of J, and most importantly, the deduced fact that **3/II** orders magnetically.

CONCLUSION

In the present contribution two new compounds of the same chemical composition were prepared that show completely different coordination networks. Surprisingly, the syntheses in solution always lead to the formation of the compound with the 2D network, that was proven to represent the thermodynamically stable phase at room temperature. However, the desired 1D compound was accessible by thermal annealing of the precursor hydrate complex, and it was shown that, compared to the 2D compound, it is thermodynamically metastable. These results once again show that the synthesis of relatively simple chemical compounds can be much more difficult to achieve than expected if more polymorphic modifications are involved. To prepare the metastable phases, alternative synthetic procedures such as thermal decomposition of suitable precursor compounds must be used, as otherwise these compounds can be easily overlooked, which is highly undesirable as from a magnetic point of view the metastable compound may be much more interesting.

The metastable compound **3/II** is a quasi-one-dimensional magnetic system. The intrachain exchange interaction between Co(II) ions is mediated through $(NCS)_2$ bridges, which leads to an exchange constant J = 30.5 K, as determined both from magnetic and specific heat data. The growing correlation length in such a chain leads to strong increase of χT at low temperatures. The much weaker interchain interaction is most probably of dipolar origin, because there is neither covalent nor hydrogen bond path between the chains. In such a case the phase transition to an ordered ferromagnetic state is possible if the magnetic moments have a pronounced component perpendicular to the chain. Due to a high anisotropy of Co(II) ions in the ground state, and the fact that all local anisotropy axes of the Co ions have the same orientation in the crystal structure, the magnetic structure is most probably collinear. In spite of the clear ordering transition at T_c = 3.8 K the relaxation of magnetization is present well below the T_c. The analysis of relaxation times leads to the energy barrier 74 K, which is much higher than the values from 33 to 39 K determined for related Co−$(NCS)_2$−Co chain compounds,[9a,20] in spite of the exchange J for all these compounds being very similar. This, together with the small τ_0 prefactor and the substantial distribution of relaxation times, suggests that the objects that relax in **3/II** are not single chains, but bigger objects having a higher energy barrier in the relaxation process. The presence of magnetic domains consisting of a bundle of chains (including parts of multiple chains) may lead to the observed relaxation behavior. Such a conviction is strengthened by the fact that previously reported compounds of this family have an antiferromagnetic ground state and show a metamagnetic transition, in contrast to **3/II**, which is a ferromagnet.

ASSOCIATED CONTENT

Supporting Information

X-ray crystallographic data in CIF format. XRPD pattern, IR spectra, DTA-TG curves, and additional magnetic measurements. This material is available free of charge via the Internet at http://pubs.acs.org.

DOI: 10.1021/ic503029t
Inorg. Chem. 2015, 54, 2893−2901

AUTHOR INFORMATION

Corresponding Author

*E-mail: cnaether@ac.uni-kiel.de.

Notes

The authors declare no competing financial interest.

ACKNOWLEDGMENTS

This project was supported by the Deutsche Forschungsgemeinschaft (Project No. NA 720/5-1) and the State of Schleswig-Holstein. We thank Professor Dr. Wolfgang Bensch for access to his experimental facility. Z.T. thanks National Science Centre Poland for financial support granted under decision DEC-2013/11/B/ST3/03799. The research was in part carried out with the equipment purchased with the support of European Regional Development Fund within the Polish Innovation Economy Operational Program (POIG.02.01.00-12-023/08).

REFERENCES

(1) (a) Desiraju, G. R. *Crystal Engineering—The Design of Organic Solids*; Elsevier: Amsterdam, 1989; p 54. (b) Desiraju, G. R. *Angew. Chem., Int. Ed.* **2007**, *46*, 8342−8356. (c) Aakeröy, C. B.; Beatty, A. M. *Aust. J. Chem.* **2001**, *54*, 409−421. (d) Braga, D.; Grepioni, F.; Desiraju, G. R. *Chem. Rev.* **1998**, *98*, 1375−1406. (e) Moulton, B.; Zaworotko, M. J. *Chem. Rev.* **2001**, *101*, 1629−1658. (f) Brammer, L. *Chem. Soc. Rev.* **2004**, *33*, 476−489. (g) Zaworotko, M. J. *Chem. Soc. Rev.* **1994**, *23*, 283−288. (h) Blake, A. J.; Champness, N. R.; Hubberstey, P.; Li, W.-S.; Withersby, M. A.; Schröder, M. *Coord. Chem. Rev.* **1999**, *183*, 117−138. (i) Sharma, C. V. K. *Cryst. Growth Des.* **2002**, *2*, 465−474. (j) Zaworotko, M. J. *Nat. Chem.* **2011**, *3*, 653−653. (k) Braga, D.; Maini, L.; Polito, M.; Scaccianoce, L.; Cojazzi, G.; Grepioni, F. *Coord. Chem. Rev.* **2001**, *216*, 225−248. (l) Khlobystov, A. N.; Blake, A. J.; Champness, N. R.; Lemenovskii, D. A.; Majouga, A. G.; Zyk, N. V.; Schröder, M. *Coord. Chem. Rev.* **2001**, *222*, 155−192.

(2) (a) Braga, D.; Grepioni, F. *Chem. Soc. Rev.* **2000**, *29*, 229−238. (b) Näther, C.; Bhosekar, G.; Jeß, I. *Inorg. Chem.* **2007**, *46*, 8079−8087. (c) Näther, C.; Jeß, I. *Inorg. Chem.* **2003**, *42*, 2968−2976. (d) Wöhlert, S.; Boeckmann, J.; Jess, I.; Näther, C. *CrystEngComm* **2012**, *14*, 5412−5420. (e) Wöhlert, S.; Jess, I.; Englert, U.; Näther, C. *CrystEngComm* **2013**, *15*, 5326−5336. (f) Blake, A. J.; Brooks, N. R.; Champness, N. R.; Crew, M.; Gregory, D. H.; Hubberstey, P.; Schröder, M.; Deveson, A.; Fenske, D.; Hanton, L. R. *Chem. Commun.* **2001**, 1432−1433. (g) Barnett, S. A.; Blake, A. J.; Champness, N. R.; Wilson, C. *Chem. Commun.* **2002**, 1640−1641. (h) Batten, S. R.; Murray, K. S. *Aust. J. Chem.* **2001**, *54*, 605−609.

(3) (a) Wöhlert, S.; Boeckmann, J.; Wriedt, M.; Näther, C. *Angew. Chem., Int. Ed.* **2011**, *50*, 6920−6923. (b) Wöhlert, S.; Ruschewitz, U.; Näther, C. *Cryst. Growth Des.* **2012**, *12*, 2715−2718. (c) Wöhlert, S.; Wriedt, M.; Fic, T.; Tomkowicz, Z.; Haase, W.; Näther, C. *Inorg. Chem.* **2013**, *52*, 1061−1068. (d) Wriedt, M.; Näther, C. *Chem. Commun.* **2010**, *46*, 4707−4709.

(4) (a) Sekiya, R.; Nishikiori, S.-i. *Cryst. Growth Des.* **2011**, *11*, 5574−5591. (b) Sekiya, R.; Nishikiori, S.-i. *CrystEngComm* **2011**, *13*, 6405−6414. (c) Shi, J. M.; Chen, J. N.; Wu, C. J.; Ma, J. P. *J. Coord. Chem.* **2007**, *60*, 2009−2013.

(5) (a) Wöhlert, S.; Peters, L.; Näther, C. *Dalton Trans.* **2013**, *42*, 10746−10758. (b) Wöhlert, S.; Fink, L.; Schmidt, M.; Näther, C. *CrystEngComm* **2013**, *15*, 945−957. (c) Wöhlert, S.; Näther, C. *Eur. J. Inorg. Chem.* **2013**, *2013*, 2528−2537.

(6) (a) Boeckmann, J.; Näther, C. *Polyhedron* **2012**, *31*, 587−595. (b) Foner, S.; Frankel, R. B.; Reiff, W. M.; Wong, H.; Long, G. J. *J. Chem. Phys.* **1978**, *68*, 4781−4783.

(7) Boeckmann, J.; Näther, C. *Dalton Trans.* **2010**, *39*, 11019−11026.

(8) (a) Zhang, W.-X.; Ishikawa, R.; Breedlovea, B.; Yamashita, M. *RSC Adv.* **2013**, *3*, 3772−3798. (b) Sun, H.-L.; Wang, Z.-M.; Gao, S. *Coord. Chem. Rev.* **2010**, *254*, 1081−1100. (c) Bogani, L.; Vindigni, A.; Sessoli, R.; Gatteschi, D. *J. Mater. Chem.* **2008**, *18*, 4733−4880. (d) Caneschi, A.; Gatteschi, D.; Lalioti, N.; Sangregorio, C.; Sessoli, R.; Venturi, G.; Vindigni, A.; Rettori, A.; Pini, M. G.; Novak, M. A. *Angew. Chem., Int. Ed.* **2001**, *40*, 1760−1763. (e) Palii, A. V.; Reu, O. S.; Ostrovsky, S. M.; Klokishner, S. I.; Tsukerblat, B. S.; Sun, Z.-M.; Mao, J.-G.; Prosvirin, A. V.; Zhao, H.-H.; Dunbar, K. R. *J. Am. Chem. Soc.* **2008**, *130*, 14729−14738. (f) Feng, X.; Liu, J.; Harris, T. D.; Hill, S.; Long, J. R. *J. Am. Chem. Soc.* **2012**, *134*, 7521−7529. (g) Zhang, S.-Y.; Shi, W.; Lan, Y.; Xu, N.; Zhao, X.-Q.; Powell, A. K.; Zhao, B.; Cheng, P.; Liao, D.-Z.; Yan, S.-P. *Chem. Commun.* **2011**, *47*, 2859−2861. (h) Miyasaka, H.; Madanbashi, T.; Saitoh, A.; Motokawa, N.; Ishikawa, R.; Yamashita, M.; Bahr, S.; Wernsdorfer, W.; Clérac, R. *Chem.—Eur. J.* **2012**, *18*, 3942−3954. (i) Yang, C.-I.; Chuang, P.-H.; Lu, K.-L. *Chem. Commun.* **2011**, *47*, 4445−4447. (j) Luo, F.; Liao, Z.-w.; Song, Y.-m.; Huang, H.-x.; Tian, X.-z.; Sun, G.-m.; Zhu, Y.; Yuan, Z.-Z.; Luo, M.-b.; Liu, S.-j.; Xu, W.-y.; Feng, X.-F. *Dalton Trans.* **2011**, *40*, 12651−12655. (k) Miyasaka, H.; Takayama, K.; Saitoh, A.; Furukawa, S.; Yamashita, M.; Clérac, R. *Chem.—Eur. J.* **2010**, *16*, 3656−3662. (l) Li, Z.-X.; Zeng, Y.-F.; Ma, H.; Bu, X.-H. *Chem. Commun.* **2010**, *46*, 8540−8542. (m) Coulon, C.; Clérac, R.; Wernsdorfer, W.; Colin, T.; Miyasaka, H. *Phys. Rev. Lett.* **2009**, *102*, 164204−164207. (n) Ishikawa, R.; Katoh, K.; Breedlove, B. K.; Yamashita, M. *Inorg. Chem.* **2012**, *51*, 9123−9131. (o) Coulon, C.; Miyasaka, H.; Clérac, R. In *Single-Chain Magnets:Theoretical Approach and Experimental Systems*; Winpenny, R., Ed.; Springer: Berlin, 2006; Vol. *122*, pp 163−206. (p) Tomkowicz, Z.; Rams, M.; Bałanda, M.; Foro, S.; Nojiri, H.; Krupskaya, Y.; Kataev, V.; Büchner, B.; Nayak, S. K.; Yakhmi, J. V.; Haase, W. *Inorg. Chem.* **2012**, *51*, 9983−9994. (q) Peresypkina, E. V.; Majcher, A. M.; Rams, M.; Vostrikova, K. E. *Chem. Commun.* **2014**, *50*, 7150−7153. (r) Rams, M.; Peresypkina, E. V.; Mironov, V. S.; Wernsdorfer, W.; Vostrikova, K. E. *Inorg. Chem.* **2014**, *53*, 10291−10300.

(9) (a) Wöhlert, S.; Fic, T.; Tomkowicz, Z.; Ebbinghaus, S. G.; Rams, M.; Haase, W.; Näther, C. *Inorg. Chem.* **2013**, *52*, 12947−12957. (b) Boeckmann, J.; Näther, C. *Chem. Commun.* **2011**, *47*, 7104−7106.

(10) Boeckmann, J.; Wriedt, M.; Näther, C. *Chem.—Eur. J.* **2012**, *18*, 5284−5289.

(11) (a) Patra, G. K.; Goldberg, I. *Acta Crystallogr., Sect. E* **2001**, *57*, m483−m484. (b) Drew, M. G. B.; Gray, N. I.; Cabral, M. F.; Cabral, J. d. O. *Acta Crystallogr., Sect. C* **1985**, *41*, 1434−1437.

(12) *Topas, Vol.*; Bruker AXS: Karlsruhe, Germany, 2007.

(13) Pawley, G. *J. Appl. Crystallogr.* **1981**, *14*, 357−361.

(14) Andreev, Y. G.; MacGlashan, G. S.; Bruce, P. G. *Phys. Rev. B* **1997**, *55*, 12011−12017.

(15) Rietveld, H. *J. Appl. Crystallogr.* **1969**, *2*, 65−71.

(16) Näther, C.; Wöhlert, S.; Boeckmann, J.; Wriedt, M.; Jeß, I. Z. *Anorg. Allg. Chem.* **2013**, *639*, 2696−2714.

(17) Näther, C.; Jeß, I. *J. Solid State Chem.* **2002**, *169*, 103−112.

(18) Werner, J.; Jeß, I.; Näther, C. *Z. Naturforsch.* **2013**, *68b*, 643−652.

(19) (a) Kahn, O. *Molecular Magnetism*; VCH: Weinheim, 1993. (b) Kurmoo, M. *Chem. Soc. Rev.* **2009**, *38*, 1353−1379.

(20) Wöhlert, S.; Tomkowicz, Z.; Rams, M.; Ebbinghaus, S. G.; Fink, L.; Schmidt, M. U.; Näther, C. *Inorg. Chem.* **2014**, *53*, 8298−8310.

(21) (a) Fisher, M. E. *J. Math. Phys.* **1963**, *4*, 124−135. (b) Carlin, R. L. *Magnetochemistry*; Springer-Verlag: New York, 1986; p 166.

(22) Mydosh, J. A. *Spin Glasses: An Experimental Introduction*; Taylor and Francis: London, 1993; p 67.

(23) de Jongh, L. J.; Miedema, A. R. *Adv. Phys.* **1974**, *23*, 1.

DOI: 10.1021/ic503029t
Inorg. Chem. 2015, 54, 2893−2901

4. Der Einfluss von neutralen Co-Liganden auf die Struktur, die thermischen und die magnetischen Eigenschaften von Thiocyanat-Koordinationsverbindungen mit Mn(II), Fe(II), Co(II) und Ni(II)

4.1. Synthesis, Structure and Properties of Coordination Polymers with Layered Transition Metal Thiocyanto Networks

Julia Werner, Zbigniew Tomkowicz, Thorben Reinert und Christian Näther, *Eur. J. Inorg. Chem.* **2015**, *19*, 3066-2075.

DOI: 10.1002/ejic.201500176

Motivation

Bislang wurde nur über die Untersuchungen von Koordinationspolymeren mit dem Übergangsmetall Kobalt berichtet, in denen jeweils eine langsame Relaxation der Magnetisierung beobachtet wird. Im Verlauf der hier vorgestellten systematischen Untersuchungen wurde jedoch auch der Einfluss des Metallkations auf die magnetischen Eigenschaften von Thiocyanat-Koordinationspolymeren untersucht. Wie aus den bislang vorgestellten Untersuchungen offensichtlich wird, wurden mit monodentaten Co-Liganden immer 1D-Strukturen erhalten, in denen die Metallkationen von Paaren aus µ-1,3-verbrückenden Thiocyanatanionen zu Ketten verbunden sind.

In der hier vorgestellten Arbeit wird nun über Verbindungen mit Mn(II), Fe(II), Co(II) und Ni(II) Thiocyanat sowie 4-tert-Butylpyridin als Co-Liganden berichtet. Dabei wurden Verbindungen erhalten, in deren Strukturen die Metallkationen durch einzelne µ-1,3-verbrückende anionische Liganden zu Schichten verknüpft sind. Die magnetischen Messungen ergaben, dass die Verbindung mit Mn(II) einen antiferromagnetischen Ordnungspunkt aufweist und dass die Verbindungen mit Co(II) und Ni(II) Ferromagnetismus zeigen. Eine analoge Verbindung mit Eisen konnte nicht erhalten werden.

Job/Unit: I50176 /KAP1 Date: 08-06-15 14:45:14 Pages: 11

EurJIC European Journal of Inorganic Chemistry

ChemPubSoc Europe

FULL PAPER

DOI:10.1002/ejic.201500176

Synthesis, Structure, and Properties of Coordination Polymers with Layered Transition-Metal Thiocyanato Networks

Julia Werner,[a] Zbigniew Tomkowicz,[b] Thorben Reinert,[a] and Christian N ther*[a]

Keywords: Layered compounds / Polymers / Thermal properties / Magnetic properties

Reaction of 4-*tert*-butylpyridine (*t*BP) with transition-metal thiocyanates leads to the formation of compounds of composition $[M(NCS)_2(tBP)_4]$ [M = Mn (**1-Mn**), Fe (**1-Fe**), Co (**1-Co**), Ni (**1-Ni**)] that consist of discrete complexes, in which the metal centers are octahedrally coordinated by two terminal thiocyanato anions and four *t*BP ligands. If less *t*BP is used in the synthesis, two compounds of composition $[M(NCS)_2(tBP)_2]_n$ with M = Co (**2-Co**) and Ni (**2-Ni**) are obtained, in which the metal centers are linked into a 2D network by single thiocyanato anions. Thermal decomposition of **1-Co** leads to the formation of an additional modification of $[Co(NCS)_2(tBP)_2]$ (**3-Co**). Magnetic measurements of **2-Ni** and **2-Co** reveal that **2-Ni** shows a ferromagnetic phase transition at T_c = (14.8 ± 0.1) K and **2-Co** shows a transition to the magnetic state with uncompensated magnetic moment at (3.15 ± 0.03) K.

Introduction

The thiocyanato anion is a versatile ligand because it adopts a large number of different coordination modes, for example, the terminal coordination as well as the μ-1,1- and μ-1,3-bridging mode. This is one of the reasons why an increasing number of new compounds with different structures containing this ligand have been recently reported.[1–13] A similar situation is also found for selenocyanato coordination compounds, but they have been less investigated.[14–20] In this context, compounds in which paramagnetic metal cations are linked by the anionic ligands into coordination polymers are of special interest, because they show a rich variety of magnetic properties. In most of these compounds the metal cations are linked by μ-1,3-bridging anionic ligands that, dependent on the neutral co-ligand, show a different dimensionality as well as a different connectivity of the thiocyanato coordination network. In one of the most common motifs, the metal cations are linked by pairs of μ-1,3-bridging anions into chains that can either be terminated by monodentate or linked into layers by bridging co-ligands (Figure 1).[2,8,21–30] However, in a few cases a different connectivity of the thiocyanato coordination network is observed (Figure 1). This includes, for example, chains in which alternating terminal and μ-1,3-bridging thiocyanato anions or more 1D structures with μ-1,3- and μ-1,1,3-bridging anions are present (Figure 1).[31–35]

However, in some cases 2D thiocyanato networks are observed, in which the metal cations are linked by single thiocyanato anions into layers, like in $[Ni(NCS)_2(2\text{-methylpyrazine})_2]_n$, and the analogous Co compound in which the metal cations are linked by alternating pairs of thiocyanato anions and single thiocyanato anions into a 2D network (Figure 1).[36,37]

In our ongoing project on the synthesis, structure, and properties of such thiocyanato coordination polymers we were especially interested in systematic investigations on the influence of a chemical and structural modification on the magnetic properties of such compounds.[3] For compounds in which the metal (M) cations are coordinated to, for example, pyridine and are linked by pairs of μ-1,3-bridging thiocyanato ligands into linear chains, we observed antiferromagnetic intrachain coupling for M = Mn, and ferromagnetic intrachain and antiferromagnetic interchain coupling leading to metamagnetic behavior for M = Fe, Ni, and for M = Co ferromagnetic intrachain interactions, and a slow relaxation of the magnetization is observed.[21,22] In this regard, it should be noted that this structure is commonly observed in thiocyanato coordination polymers with monodentate ligands.

To study the influence of the co-ligand on the magnetic properties in detail we reacted Mn, Fe, Co, and Ni thiocyanate with the monodentate ligand 4-*tert*-butylpyridine (*t*BP). Based on our previous work, the formation of a 1D

[a] Institut f r Anorganische Chemie, Christian-Albrechts-Universit t zu Kiel,
Max-Eyth-Strasse 2, 24118 Kiel, Germany
E-mail: cnaether@ac.uni-kiel.de
http://www.ac.uni-kiel.de/de/pd-dr.-christian-naether-1
[b] Institute of Physics, Jagiellonian University,
Łojasiewicza 11, 30-348 Krakow, Poland
Supporting information for this article is available on the WWW under http://dx.doi.org/10.1002/ejic.201500176.

Job/Unit: I50176 /KAP1 Date: 08-06-15 14:45:14 Pages: 11

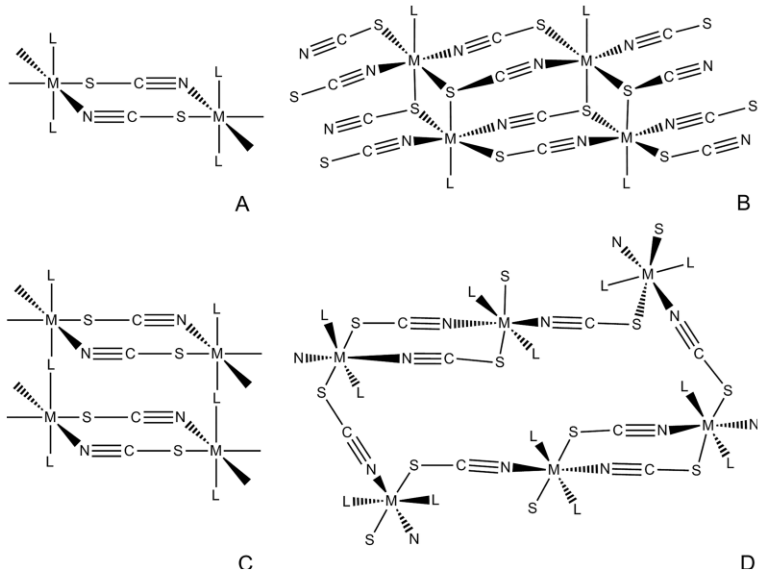

Figure 1. Different topologies of the coordination networks in chain and layered thiocyanato coordination polymers.

structure with linear metal thiocyanato chains was expected, but surprisingly, a special 2D network formed, which according to a search in the CSD database[38] was never observed before in this class of compounds. Here we report on our synthetic, structural, and magnetic investigations.

Results and Discussion

Synthetic Investigations

To investigate how many compounds based on $[M(NCS)_2]$ (M = Mn, Fe, Co, Ni) and *t*BP are available, various stoichiometric ratios of the reactants were used in the synthesis and the residues obtained were investigated by X-ray powder diffraction (XRPD), IR spectroscopy, and elemental analysis. For all of the metal salts, compounds of composition $[M(NCS)_2(tBP)_4]$ (**1-M**) were obtained. It should be noted that **1-Ni** is already known from the literature.[39] We also found that with Co and Ni a second crystalline phase of composition $[M(NCS)_2(tBP)_2]_n$ (**2-M** = **2-Co**, **2-Ni**) is available.

XRPD investigations indicate that compound **1-Mn** and **1-Fe** are isotypic, which is also the case for **1-Co** and **1-Ni** (Figures S1 and S2 in the Supporting Information). The fact that a pair of thiocyanato coordination compounds with Mn and Fe and a pair with Ni and Co have different structures is not uncommon and was recently reported.[40] The XRPD investigations indicate that compounds **2-M** are also isotypic (Figure S3 in the Supporting Information). IR spectroscopic investigations reveal that compounds **1-M** contains only terminally coordinated N-bonded thiocyanato anions, because the value of the CN-stretching vibration range from 2046 cm^{-1} for compound **1-Mn** to 2071 cm^{-1} for **1-Ni** (Table 1, Figures S4–S7 in the Supporting Information). In contrast, the CN-stretching vibrations for compounds **2-M** are shifted to higher values, which indicates that the metal cations are linked by μ-1,3-bridging thiocyanato anions (Table 1, Figures S8 and S9 in the Supporting Information).

Table 1. Energy value of the asymmetric CN stretching vibration ν_{as}(CN) for **1-Mn**, **1-Fe**, **1-Co**, **1-Ni**, **2-Co**, and **2-Ni**.

	1-Mn	**1-Fe**	**1-Co**	**1-Ni**	**2-Co**	**2-Ni**
ν_{as}(CN) [cm^{-1}]	2046	2051	2060	2071	2105	2118

To determine the crystal structures of these compounds, crystallization experiments were performed at room temperature, which lead to the formation of single crystals of **1-Mn**, **1-Fe**, **1-Co**, and **2-Ni**. Based on the crystallographic data, powder patterns were calculated and compared with the experimental pattern, which indicated that **1-Mn**, **1-Fe**, **1-Co**, and **2-Ni** were obtained as pure materials (Figures S10–S13 in the Supporting Information). For compound **2-Co** no single crystals could be obtained, but comparison of the experimental pattern with that calculated for the isotypic compound **2-Ni** also indicated that it was obtained as a pure phase (Figure S14 in the Supporting Information).

Job/Unit: I50176 /KAP1 Date: 08-06-15 14:45:14 Pages: 11

Crystal Structures

Compounds **1-Mn** and **1-Fe** are isotypic and crystallize in the monoclinic space group *C2/c* with four formula units in the unit cell. The asymmetric unit consists of a metal cation that is located on a center of inversion as well as of one thiocyanato anion and two crystallographically independent *t*BP ligands in general positions. Compound **1-Co** is isotypic to **1-Ni** reported recently[39] and crystallizes in the tetragonal space group $I4_1/a$ with eight formula units in the unit cell. The asymmetric unit consists of a cobalt cation that is located on a twofold rotation axis, and one thiocyanato anion and two *t*BP ligands that occupy general positions. Each metal cation is coordinated by two terminally N-bonded thiocyanato anions and four *t*BP ligands within slightly distorted octahedra (Figure 2 and Tables S1–S3 in the Supporting Information). The M–N_{tBP} distances are between 2.175(2) and 2.350(3) and the M–N distances to the thiocyanato anions range from 2.071(2) to 2.156(3) (Tables S1–S3 in the Supporting Information).

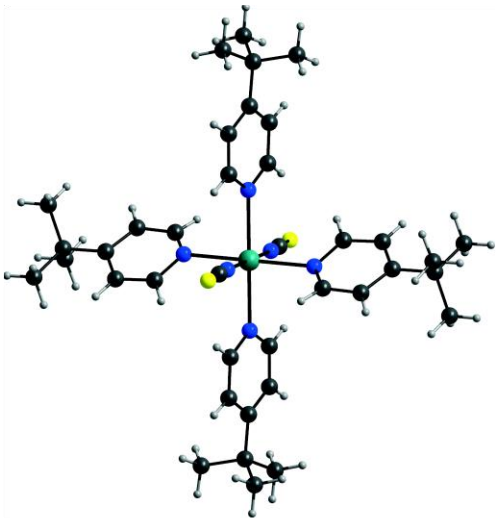

Figure 2. Crystal structure of **1-Mn** with a view of the coordination sphere of the Mn^{II} cation as a representative example (ORTEP plots of **1-Mn**, **1-Fe**, and **1-Co** are shown in Figures S15–S17 in the Supporting Information).

Compounds **2-Ni** and **2-Co** are isotypic and crystallize in the monoclinic space group $P2_1/c$ with two formula units in the unit cell. The asymmetric unit consists of one M cation, which is located on a center of inversion, as well as of one thiocyanato anion and one *t*BP ligand in general positions. The metal cations are coordinated by two *t*BP ligands and four μ-1,3-bridging thiocyanato anions in a slightly distorted-octahedral environment (Figure 3, top and Table S4 in the Supporting Information).

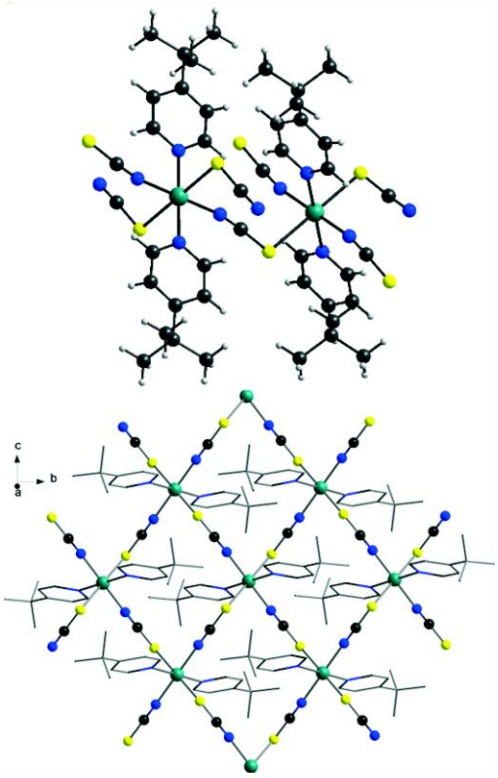

Figure 3. Crystal structure of **2-Ni** with view of the coordination sphere of the Ni^{II} cation (top) and view of the layered thiocyanato network approximately along the *a* axis (bottom). Hydrogen atoms and disorder is not shown for clarity (ORTEP plot of **2-Ni** is shown in Figure S18 in the Supporting Information).

Each metal cation is linked by one single μ-1,3-bridging thiocyanato anion to four different cations forming four-membered M–NCS rings, that are further connected into layers parallel to the *bc* plane (Figure 3, bottom). The shortest Ni–Ni distance within the layers is 6.30 and the shortest interlayer distance is 14.57 .

It should be noted that such a 2D thiocyanato network was never observed before. However, crystal structures with the same connectivity of the coordination network were recently reported for an azide compound with a different neutral co-ligand of composition $[M(N_3)_2(4\text{-acetylpyridine})_2]_n$ (M = Mn, Fe, Co, and Ni).[41–44]

Thermoanalytical Investigations

As mentioned above, with Mn and Fe no *t*BP-deficient compounds can be obtained. To investigate whether they are available by thermal decomposition of the precursor compounds **1-Mn** and **1-Fe**, measurements using simulta-

Job/Unit: I50176 /KAP1 Date: 08-06-15 14:45:14 Pages: 11

neous differential thermoanalysis and thermogravimetry (DTA-TG) were performed. Similar measurements were also performed for **1-Co** and **1-Ni** because we found that different modifications of coordination polymers can be obtained by this route.[45]

If these compounds are heated in a thermobalance to 300 °C, three well-separated mass steps are observed in the TG curve for **1-Mn**, **1-Fe**, and **1-Ni**, whereas for **1-Co** only one distinct mass step is observed (Figure 4 and Figures S19–S22 in the Supporting Information). The experimental mass loss in the first TG step for **1-Mn**, **1-Co**, and **1-Ni** is in reasonable agreement with that calculated for the removal of two *t*BP ligands (Table 2). Surprisingly, for **1-Fe** a much lower value is observed, which indicates a more complicated reaction (Table 2). However, these results suggest that the compounds **1-M** transform into compounds of composition $[M(NCS)_2(tBP)_2]$.

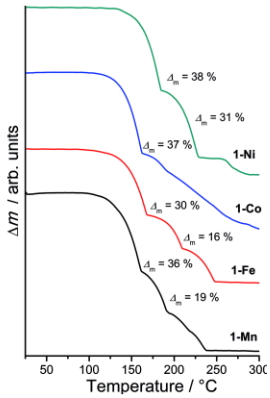

Figure 4. TG curves of compounds **1-Mn**, **1-Fe**, **1-Co**, and **1-Ni** at 1 °C min^{-1}. The experimental mass loss is given.

Table 2. Experimental and calculated mass loss for compounds **1-M**. $\Delta m_{calcd.}$ was calculated for the removal of two (*t*BP) ligands.

	1-Mn	1-Fe	1-Co	1-Ni
$\Delta m_{(exp)}$ [%]	36	30	37	38
$\Delta m_{(calcd.)}$ [%]	38	37	38	38

To identify the intermediates of the thermal reactions the TG measurements were repeated and stopped after the first step and the residues were investigated by XRPD, IR spectroscopy, and elemental analysis. The XRPD patterns of the residues show that compounds **1-Mn**, **1-Fe**, and **1-Ni** have been transformed into compounds **2-M**, which is also in agreement with IR spectroscopic investigations (Figure S23–25 in the Supporting Information). In contrast, the XRPD pattern of the residue of **1-Co** is completely different from that calculated for **2-Ni** and does not contain any reflections of precursor **1-Co**, which indicates that a pure phase (**3-Co**) was obtained (Figure S26 in the Supporting Information). The asymmetric C–N-stretching vibration is observed at 2041 cm^{-1}, which excludes the presence of μ-1,3-bridging thiocyanato anions in this compound (Figure S27 in the Supporting Information). Surprisingly, elemental analysis leads to the expected composition $[Co(NCS)_2(tBP)_2]$. Therefore, it is highly likely that the Co cations are only tetrahedrally coordinated in this compound.

To gain more information on this intermediate we prepared the analogous Zn compound (**3-Zn**) for which, based on our previous work, a tetrahedral coordination was expected. Crystal structure analysis shows that **3-Zn** crystallizes in the orthorhombic space group *Fdd*2 with eight formula units in the unit cell (Figure S28 and Table S5 in the Supporting Information). Comparison of the experimental XRPD pattern with that calculated shows that this compound is obtained as a pure phase (Figure S29 in the Supporting Information). As expected, the Zn cations are tetrahedrally coordinated by two *t*BP ligands as well as by two terminal N-bonded thiocyanato anions. Unfortunately, this compound is not isotypic to **3-Co**, which would allow the tetrahedral coordination in the Co compound to be unambiguously proven (Figure S30 in the Supporting Information). However, in previous studies the spectroscopic properties of tetrahedral thiocyanato complexes of Zn and Co were investigated and it was found that the C–N stretching vibration of the terminal N-bonded thiocyanato anions shifted from Co to Zn to higher values (Table 3). For **3-Co** a value for ν_{as}(CN) of 2046 cm^{-1} was found, which was shifted by about 23 wavenumbers to higher values in **3-Zn** (Table 3 and Figure S31 in the Supporting Information). Therefore, it is highly likely that in **3-Co** the cobalt cations are in a tetrahedral environment, coordinated by two terminally N-bonded thiocyanato anions and two *t*BP ligands.

Table 3. Energy values of the asymmetric CN stretching vibration ν_{as}(CN) for **3-Co** and **3-Zn** as well as of similar compounds with the same structure (values retrieved from the literature).

	ν_{as}(CN) [cm^{-1}]
3-Co	2046
3-Zn	2069
$[Co(NCS)_2$(2-bromopyridine)$_2]$	2058[46]
$[Zn(NCS)_2$(2-bromopyridine)$_2]$	2071[46]
$[Co(NCS)_2$(2-methylpyridine)$_2]$	2054[46]
$[Zn(NCS)_2$(2-methylpyridine)$_2]$	2065[46]

This is further supported by magnetic measurement of **3-Co**, because for a simple tetrahedral discrete complex only paramagnetic behavior is expected and this is exactly what we found in this case (Figure S32 in the Supporting Information).

Compound **3-Co**, which exhibits the same chemical composition as **2-Co**, seems to be more stable than the latter, because from the moment that we prepared **3-Co** for the first time it was more difficult to obtain pure samples of **2-Co**. This indicates that the environment is contaminated with the stable phase (**3-Co**), which always initiates crystallization of this form. Such phenomena are well known and were nicely described by Dunitz and Bernstein.[47]

Finally, compounds **1-Mn** and **1-Fe** show a second mass step that corresponds roughly to the removal of another

Job/Unit: I50176 /KAP1 Date: 08-06-15 14:45:14 Pages: 11

*t*BP ligand, which would lead to compounds of composition [M(NCS)$_2$(*t*BP)]. However, if the residues obtained after the second mass step are isolated and investigated by XRPD most of them consist of compounds **2-M**. There are some reflections of an additional crystalline phase that cannot be identified (Figure S33 in the Supporting Information).

Magnetic Investigations

Compounds **1-M** consist of discrete complexes for which only paramagnetic behavior is expected. Therefore, they are of minor interest. In contrast, in compounds **2-M** the metal centers are linked by the thiocyanato anions into layers, and thus cooperative magnetic properties are expected.

For **2-Mn**, the antiferromagnetic phase transition is inferred from the χT versus T curve that shows a maximum at 16 K but on further cooling a further increase of the susceptibility is observed, which indicates an impurity that cannot be observed by XRPD (Figure S34 in the Supporting Information). To prove this assumption a second batch was analyzed, because it is highly unlikely that the same amount of contamination is formed by thermal decomposition. As expected, in this case a different increase of the susceptibility was observed near the antiferromagnetic maximum, which confirmed the presence of an impurity (Figure S34 in the Supporting Information). It should be noted that antiferromagnetic transitions are usually observed in Mn thiocyanato coordination polymers. We also measured the DC susceptibility for **2-Fe** but very complicated behavior was observed, strongly indicating that this sample is contaminated with an unknown impurity. This is not surprising, because **2-Fe** can only be prepared by thermal decomposition of **1-Fe** and in this case a significant difference between the experimental and calculated mass loss was observed. Therefore, even if there is no indication of impurities from the XRPD patterns it is highly likely that no pure samples can be obtained.

In contrast, **2-Co** and **2-Ni** can be crystallized from solution as pure materials. For these compounds a series of temperature- and field-dependent magnetization measurements was performed. Temperature-dependent measurements were performed under field-cooling (FC) and zero-field-cooling (ZFC) conditions. First, the experimental data for **2-Ni** are presented. In Figure 5 the χT product (χ is defined as a magnetization to field ratio M/H) is plotted as a function of T for H = 10 Oe. The room-temperature value of this product is 1.45 K emu mol^{-1}, which is somewhat more than the value of 1.36 obtained for the analogous azide compound [Ni(N$_3$)$_2$(4-acetylpyridine)$_2$]$_n$.[44] χT, being nearly constant at higher temperatures, slowly increases upon cooling but below 16 K a sharp increase is observed, which suggests a ferromagnetic phase transition. χT obtains the greatest value of approximately 2000 K emu mol^{-1} at 12.5 K (530 K emu mol^{-1} in a higher field of 100 Oe) and upon further cooling it decreases because of M saturation. Above 25 K the Curie–Weiss law is obeyed with the paramagnetic Curie–Weiss temperature of +19.7 K, which indicates that ferromagnetic interactions dominate in the magnetic coupling between the Ni cations. To estimate the exchange constant we used the same procedure as Li et al.[48] based on the Lines equation for a square lattice of S = 1 spins and the following spin Hamiltonian[49]

$H = -J\Sigma_{i<I}S_iS_i + g\mu_BH\Sigma_iS_i$

The first sum is running over all pairs of nearest-neighbor spins. The corresponding fit was performed in the paramagnetic region 15–250 K. The parameters obtained are J = (+10.8 ± 0.3) cm^{-1}, g = 2.04 ± 0.1, zJ' = (0.2 ± 0.1) cm^{-1}, in which zJ' is the interlayer interaction. These values can be compared with the corresponding values of two Ni azide compounds:[44] J = 14.7 and 14.32 cm^{-1}, g = 2.18 and 2.12, zJ' = 1.37 and 1.68 cm^{-1}. Their T_c are equal to 25 and 23 K, respectively.

In Figure 6 the temperature dependence of magnetization is presented for H = 10 and 100 Oe. Strong FC versus ZFC bifurcation is observed, which is a manifestation of the domain behavior of a ferromagnet. By taking the derivative of the $M(T)$ curve of 10 Oe recorded in FC condition, the Curie temperature T_c may be determined to be (14.8 ± 0.1) K. This value is considerably lower than that for the two above-mentioned Ni azide compounds (see the inset in Figure 6). The thick curve in the inset is the fit to the power function $M \propto (1 - T/T_c)^\beta$, from which the critical exponent of the phase transition β = 0.36 ± 0.02 was ob-

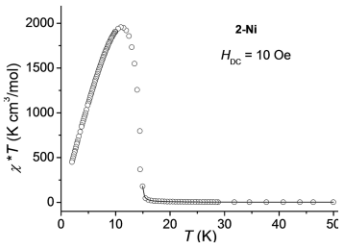

Figure 5. Temperature dependence of the χT product of **2-Ni** shown in the temperature range 2–50 K. Susceptibility was measured in a field of 10 Oe.

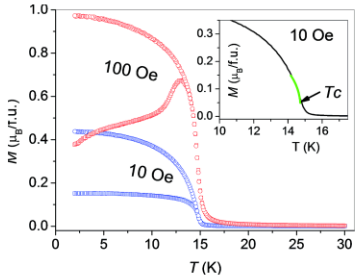

Figure 6. Temperature-dependent magnetization curves of **2-Ni** obtained in a field of 10 and 100 Oe under FC (upper curves, circles) and ZFC (bottom curves, squares) conditions. The inset presents a fragment of the magnetization curve for 10 Oe (FC). The thick green line is the power function fit used to estimate the critical exponent (see text).

Job/Unit: I50176 /KAP1 Date: 08-06-15 14:45:14 Pages: 11

tained. This β value is close to the theoretical value of the 3D Heisenberg model.[50]

The magnetization was also measured as a function of the field at T = 2.0 K. The corresponding $M(T)$ curve is presented in Figure 7. M initially increases sharply, then it changes slowly and saturates at the value of 2.22 μ_B. From this value the g factor, equal to 2.22, is obtained (with S = 1).

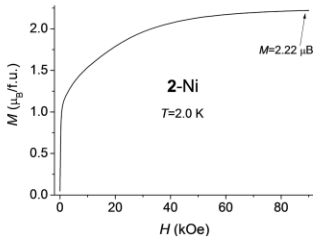

Figure 7. Magnetization versus field dependence of **2-Ni** obtained at 2.0 K.

In Figure 8, the hysteresis $M(H)$ recorded at a temperature of 2.0 K is presented. The full reversibility is observed at approximately 10 kOe. The coercive field equals 2.26 kOe.

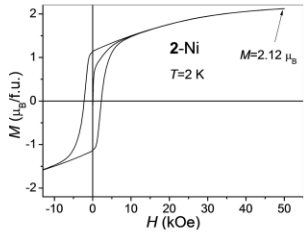

Figure 8. Hysteresis loop of **2-Ni** recorded at 2.0 K.

The AC susceptibility measured as a function of temperature at several frequencies is presented in Figure S35 in the Supporting Information. It can be seen that a frequency dispersion appears below T_c and slowly disappears with decreasing temperature. This behavior should result from the presence of domains.

As shown below, the analogous data for layered compound **2-Co** is distinctly different. In Figure 9, the temperature dependence of the χT product is presented. The measurement was recorded in a magnetic field of 50 Oe in the temperature range 2–300 K but only data below 60 K is presented here. The value of χT at 300 K equals 3.05 K cm^3 mol^{-1}, which is lower than that usually reported for Co^{II} ions but close to the value observed in the corresponding azide compound reported recently.[43] With decreasing temperature the product χT is nearly constant, but below 5 K a strong increase up to 100 K cm^3 mol^{-1} (at 2.6 K) is observed with the subsequent decrease. At higher magnetic field, for example, in a field of 5 kOe, similar behavior is observed at higher temperatures, but below 150 K a relatively strong decrease is observed with a minimum at approximately 25 K, then a subsequent maximum of 5 K cm^3 mol^{-1} at 3.75 K and a decrease upon further cooling. This decrease is due to spin–orbit coupling, which may be observed when the magnetic contribution is suppressed by a magnetic field. The Curie–Weiss law is obeyed above 50 K. The paramagnetic Curie–Weiss temperature equals approximately –3.2 K, however, the absolute value seems to be slightly enhanced due to the spin–orbit coupling. The strong increase of the χT product below 5 K may be due to an uncompensated magnetic moment in the canted antiferromagnetic structure, which is also confirmed by the observation of FC versus ZFC bifurcations (Figure 10). The critical temperature, T_c = (3.15 ± 0.03) K, was obtained by finding the derivative of the M/H versus T curve recorded in 10 Oe. A similar behavior was reported by Wang et al. for the analogous azide Co compound;[43,48] however, in their case the negative θ value was of much greater absolute value (–45 K) and T_c was equal to 11.2 K. To estimate the exchange interaction we fitted the Lines equation (with S = 3/2) for the data collected at 100 Oe in the paramagnetic region above T_c and the following Hamiltonian parameters were obtained: J = (–0.9 ± 0.2) cm^{-1}, g = 2.16 ± 0.1, zJ' = (0.03 ± 0.03) cm^{-1}. The J value may be compared with that recorded by Wang et al. (–2.64 cm^{-1}).

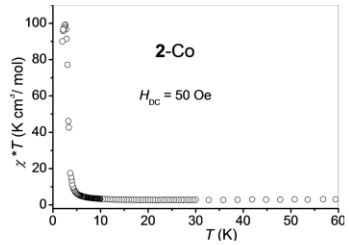

Figure 9. Temperature dependence of the χT product for **2-Co**. The magnetic susceptibility was measured in a field of 50 Oe.

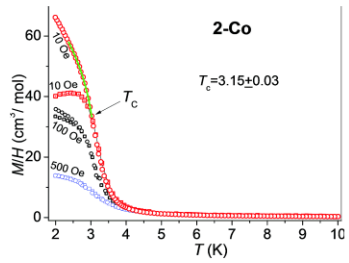

Figure 10. Temperature dependence of magnetization (normalized to susceptibility) measured for **2-Co** in several magnetic fields under FC (upper branches, circles) and ZFC (bottom branches, squares) conditions. No bifurcation was observed in 500 Oe. The thick green line is the power function that was fit to the data for 10 Oe to obtain the critical exponent; see text.

To know the universality class of the phase transition the critical exponent was determined by fitting the magnetiza-

Job/Unit: I50176 /KAP1 Date: 08-06-15 14:45:14 Pages: 11

tion to the power function in the temperature range near but below T_c. This thick green line in Figure 10 is the best fit with the exponent $\beta = 0.27 \pm 0.03$. This value is greater than the 2D value (0.125) and close to the 3D value (0.31) of the critical exponent in the Ising model.

Figure 11 shows the magnetization $M(H)$ curve that was recorded at 2.0 K in the field range 0–90 kOe. In Figure 12 the hysteresis loop, recorded in a small field range at the same temperature, is presented. The coercive field is very small, equal to 12 Oe. Measurements of the AC susceptibility showed that in **2-Co** magnetic relaxation is present, which appears as a domain effect (Figure S36 in the Supporting Information).

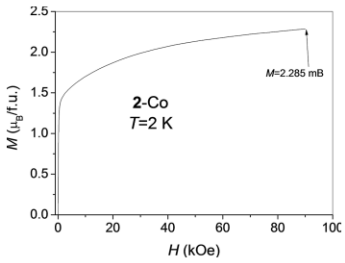

Figure 11. $M(H)$ dependence of **2-Co** recorded at 2.0 K.

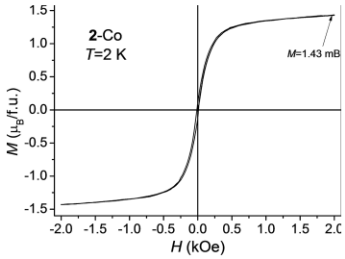

Figure 12. $M(H)$ hysteresis loop of **2** recorded at 2.0 K.

Conclusion

In the present contribution new thiocyanato coordination polymers of composition $[M(NCS)_2(tBP)_2]_n$ with Ni and Co were prepared in which the metal centers are linked by single μ-1,3-bridging thiocyanato anions into a 2D coordination network that, to the best of our knowledge, has never been observed before in this class of compounds. These results are surprising because in most cases 1D compounds are obtained in which the metal cations are linked by pairs of thio- or selenocyanato anions into chains. It is noted that several of the latter compounds with Co showed slow magnetic relaxations, which is indicative of single-chain magnetic behavior. In the present compounds ferromagnetic (**2-Ni**) or weak ferromagnetic (**2-Co**) behavior was also observed, but because the thiocyanato chains are linked into layers relaxation of single chains cannot occur. Even if this coordination network is unknown for the thiocyanato coordination polymers, it was observed in the corresponding azide compounds of composition $[M(N_3)_2(4\text{-acetylpyridine})_2]_n$ with M = Mn, Fe, Co, and Ni.[41–44] The corresponding Ni azide compound showed a similar ferromagnetic behavior but with higher Curie temperatures and stronger magnetic exchange. The reason why with *t*BP the layered instead of the common 1D coordination networks are observed is unknown and therefore, a rational access to such structures with different N-donor co-ligands is not available. In any case, it is highly likely that the chain compounds of composition $[M(NCS)_2(L)_2]_n$ (M = Mn, Fe, Co, Ni; L = co-ligand) are energetically preferred as they are frequently observed in this class of compounds.

Experimental Section

Syntheses: $MnSO_4 \cdot H_2O$, $FeCl_2 \cdot 4H_2O$, $NiSO_4 \cdot 6H_2O$, KNCS, $ZnSO_4 \cdot H_2O$, and 4-*tert*-butylpyridine were obtained from Merck; $Ba(NCS)_2 \cdot 3H_2O$ was obtained from Alfa Aesar. All solvents were used without further purification. Crystalline powders were synthesized by stirring the reactants in the respective solvents at room temperature. The residues were removed by filtration and washed with the used solvent and dried in air. The crystalline powders of the ligand-deficient compounds were prepared by stopping the thermal decomposition after the first TG step. The purity of all compounds was verified by X-ray powder diffraction and elemental analysis (Figures S in the Supporting Information).

Synthesis of 1-Mn: Single crystals were synthesized by using $Mn(NCS)_2 \cdot H_2O$ (0.15 mmol, 28.4 mg) and 4-*tert*-butylpyridine (0.60 mmol, 88.8 μL) in H_2O (1.5 mL). After 3 d suitable crystals for single-crystal analysis were obtained. Crystalline powder on a larger scale was synthesized by using $Mn(NCS)_2$ (1.00 mmol, 171.1 mg) and 4-*tert*-butylpyridine (4.00 mmol, 586 μL) in H_2O (4.0 mL). Yield: 88.2%. $C_{38}H_{52}MnN_6S_2$ (711.94 g mol^{-1}): calcd. C 64.11, H 7.36, N 11.80, S 9.01; found C 63.81, H 7.49, N 12.06, S 8.78. IR (ATR): $\tilde{\nu}_{max}$ = 3058 (w), 2966 (m), 2868 (w), 2046 (s), 1606 (s), 1544 (w), 1498 (m), 1416 (s), 1368 (m), 1226 (m), 1070 (m), 1011 (s), 831 (s), 720 (m), 570 (s) cm^{-1}.

Synthesis of 1-Fe: Single crystals were prepared by using $FeCl_2 \cdot 4H_2O$ (0.15 mmol, 29.8 mg), KNCS (0.30 mmol, 29.2 mg), and 4-*tert*-butylpyridine (0.30 mmol, 44.0 μL) in H_2O (1.5 mL). After a few days, suitable crystals for single-crystal analysis were obtained. Crystalline powder on a larger scale was synthesized by using $FeCl_2 \cdot 4H_2O$ (1.00 mmol, 198.8 mg), KNCS (2.00 mmol, 194.4 g), and 4-*tert*-butylpyridine (4.00 mmol, 586 μL) in H_2O (5.0 mL). Yield: 76.2%. $C_{38}H_{52}FeN_6S_2$ (712.85 g mol^{-1}): calcd. C 64.03, H 7.35, N 11.79, S 9.00; found C 64.37, H 7.03, N 11.54, S 8.65. IR (ATR): $\tilde{\nu}_{max}$ = 3059 (w), 2966 (m), 2869 (w), 2051 (s), 1606 (s), 1542 (w), 1497 (m), 1460 (m), 1415 (s), 1368 (m), 1272 (m), 1225 (m), 1070 (m), 1011 (s), 831 (s), 720 (m), 570 (s), 482 (m) cm^{-1}.

Synthesis of 1-Co: Single crystals were synthesized by using $Co(NCS)_2$ (0.15 mmol, 26.3 mg) and 4-*tert*-butylpyridine (0.60 mmol, 88.8 μL) in ethanol (1.5 mL). After 3 d, suitable crystals for single-crystal analysis were obtained. Crystalline powder on a larger scale was synthesized by using $Co(NCS)_2$ (1.00 mmol, 175.1 mg) and 4-*tert*-butylpyridine (4.00 mmol, 586 μL) in H_2O (5.0 mL). Yield: 85.6%. $C_{38}H_{52}CoN_6S_2$ (715.94 g mol^{-1}): calcd. C

Job/Unit: I50176 /KAP1 Date: 08-06-15 14:45:14 Pages: 11

63.75, H 7.32, N 11.74, S 8.96; found C 64.00, H 7.63, N 11.91, S 8.94. IR (ATR): $\tilde{\nu}_{max}$ = 2963 (m), 2865 (w), 2060 (s), 1609 (s), 1544 (w), 1499 (m), 1459 (m), 1418 (s), 1364 (m), 1273 (m), 1227 (m), 1072 (m), 1015 (s), 829 (s), 722 (m), 570 (s) cm^{-1}.

Synthesis of 1-Ni: The crystalline powder on a larger scale was synthesized by using $Ni(NCS)_2$ (1.00 mmol, 174.9 mg) and 4-*tert*-butylpyridine (3.40 mmol, 498 µL) in H_2O (5.0 mL). Yield: 78.3%. $C_{38}H_{52}N_6NiS_2$ (715.69 gmol^{-1}): calcd. C 63.77, H 7.32, N 11.74, S 8.96; found C 63.20, H 7.10, N 12.06, S 8.71. IR (ATR): $\tilde{\nu}_{max}$ = 2963 (m), 2867 (w), 2071 (s), 1611 (s), 1545 (w), 1500 (m), 1460 (m), 1418 (s), 1364 (m), 1273 (m), 1226 (m), 1072 (s), 1018 (s), 831 (s), 723 (m), 571 (s), 482 (m) cm^{-1}.

Synthesis of 2-Mn: The crystalline powder on a larger scale was obtained by thermal decomposition of **1-Mn** with a heating rate of 4 °Cmin^{-1}. $C_{20}H_{26}MnN_4S_2$ (441.52 gmol^{-1}): calcd. C 54.41, H 5.94, N 12.69, S 14.53; found C 54.31, H 5.94, N 12.16, S 14.43. IR (ATR): $\tilde{\nu}_{max}$ = 3072 (w), 3041 (w), 2954 (m), 2899 (w), 2862 (w), 2097 (s), 1610 (s), 1544 (w), 1501 (w), 1418 (m), 1367 (m), 1274 (m), 1231 (m), 1201 (w), 1070 (m), 1015 (s), 843 (m), 824 (s), 722 (m), 566 (s), 476 (m) cm^{-1}.

Synthesis of 2-Fe: The crystalline powder on a larger scale was obtained by thermal decomposition of **1-Fe** with a heating rate of 1 °Cmin^{-1}. $C_{20}H_{26}MnN_4S_2$ (441.52 gmol^{-1}): calcd. C 54.41, H 5.94, N 12.69, S 14.53; found C 53.64, H 6.12, N 12.30, S 12.65. IR (ATR): $\tilde{\nu}_{max}$ = 2954 (m), 2899 (w), 2864 (w), 2098 (s), 1612 (s), 1545 (w), 1500 (w), 1416 (m), 1367 (m), 1275 (m), 1229 (m), 1199 (w), 1069 (m), 1015 (m), 843 (m), 824 (s), 723 (m), 567 (s), 479 (m) cm^{-1}.

Synthesis of 2-Co: The crystalline powder on a larger scale was synthesized by using $Co(NCS)_2$ (2.40 mmol, 420 mg) and 4-*tert*-butylpyridine (0.90 mmol, 132 µL) in H_2O (1.5 mL). Yield: 45.1%. $C_{20}H_{26}CoN_4S_2$ (445.52 gmol^{-1}): calcd. C 53.92, H 5.88, N 12.58, S 14.39; found C 53.87, H 6.02, N 12.48, S 13.46. IR (ATR): $\tilde{\nu}_{max}$ = 3072 (w), 3041 (w), 2954 (m), 2899 (w), 2862 (w), 2097 (s), 1610 (s), 1544 (w), 1501 (w), 1418 (m), 1367 (m), 1274 (m), 1231 (m), 1201 (w), 1070 (m), 1015 (s), 843 (m), 824 (s), 722 (m), 566 (s), 476 (m) cm^{-1}.

Synthesis of 2-Ni: Single crystals were prepared by using $Ni(NCS)_2$ (0.60 mmol, 105 mg) and 4-*tert*-butylpyridine (0.15 mmol, 22.2 µL) in water (1.5 mL). After a few weeks, suitable crystals for single-crystal analysis were obtained. Crystalline powder on a larger scale was obtained by thermal decomposition of **1-Ni** with a heating rate of 1 °Cmin^{-1}. $C_{20}H_{26}N_4NiS_2$ (445.28 gmol^{-1}): calcd. C 53.95, H 5.89, N 12.58, S 14.40; found C 53.34, H 5.84, N 12.48, S 14.35. IR (ATR): $\tilde{\nu}_{max}$ = 3045 (w), 2956 (m), 2901 (w), 2864 (w), 2118 (s), 1613 (s), 1547 (w), 1501 (m), 1460 (w), 1418 (m), 1367 (m), 1276 (m), 1229 (m), 1202 (w), 1070 (m), 1019 (m), 825 (s), 778 (m), 724 (m), 567 (s), 481 (m) cm^{-1}.

Synthesis of 3-Co: The crystalline powder on a larger scale was obtained by thermal decomposition of **1-Co** with a heating rate of 1 °Cmin^{-1}. $C_{20}H_{26}CoN_4S_2$ (445.52 g/mol): calcd. C 53.92, H 5.88, N 12.58, S 14.39; found C 53.55, H 5.98, N 12.70, S 14.24. IR (ATR): $\tilde{\nu}_{max}$ = 3044 (w), 2966 (m), 2869 (w), 2041 (s), 1618 (s), 1545 (w), 1466 (m), 1425 (s), 1367 (m), 1275 (m), 1228 (m), 1204 (w), 1069 (s), 1032 (s), 965 (w), 835 (s), 730 (m), 570 (s), 481 (m) cm^{-1}.

Synthesis of 3-Zn: Single crystals were prepared by using $Zn(NCS)_2$ (0.15 mmol, 27.2 mg) and 4-*tert*-butylpyridine (0.60 mmol, 88.8 µL) in ethanol (1.5 mL) for 3 d. A crystalline powder on a larger scale was prepared by stirring $Zn(NCS)_2$ (0.25 mmol, 45.4 mg) and 4-*tert*-butylpyridine (0.50 mmol, 73.2 µL) in water (1.5 mL) for 3 d. $C_{20}H_{26}CoN_4S_2$ (451.97 gmol^{-1}): calcd. C 53.15, H 5.80, N 12.40, S 14.19; found C 53.33, H 5.86, N 12.52, S 14.10. IR (ATR): $\tilde{\nu}_{max}$ = 3045 (w), 2961 (m), 2868 (w), 2069 (s), 1618 (s), 1544 (w), 1504 (w), 1462 (m), 1426 (m), 1364 (m), 1272 (m), 1231 (m), 1204 (w), 1073 (s), 1033 (s), 961 (m), 829 (s), 730 (m), 568 (s), 478 (m) cm^{-1}.

Elemental Analysis: CHNS analysis was performed using an EURO EA elemental analyzer (EURO VECTOR Instruments and Software).

Spectroscopy: All IR data were obtained using an ATI Mattson Genesis Series FTIR spectrometer, control software: WINFIRST, from ATI Mattson.

X-ray Powder Diffraction (XRPD): The XRPD measurements were performed by using 1) a PANalytical X'Pert Pro MPD Reflection Powder Diffraction System with Cu-K_α radiation (λ = 154.0598 pm) equipped with a PIXcel semiconductor detector from PANanlytical and 2) a Stoe Transmission Powder Diffraction System (STADI P) with Cu-K_α radiation that was equipped with a linear position-sensitive MYTHEN detector from STOE & CIE.

Single-Crystal Structure Analyses: The investigations were performed with the imaging-plate diffraction system (IPDS-1 for **1-Mn**, **Fe-1**, **Co-1**; IPDS-2 for **2-Ni** and **3-Zn**) with Mo-K_α radiation from STOE & CIE. The structure solution was performed with direct methods using SHELXS-97, and structure refinements were performed against F^2 using SHELXL-97. All non-hydrogen atoms were refined with anisotropic displacement parameters.

Single-crystal data collections were carried out on an imaging-plate diffraction system: Stoe IPDS-1 for **1-Mn**, **1-Fe**, and **1-Co** as well as Stoe IPDS-2 for **2-Ni** and **3-Zn** with Mo-K_α radiation. The structures were solved with direct methods using SHELXS-97 and structure refinements were performed against F^2 using SHELXL-97.[51] A numerical absorption correction was applied using programs X-RED and X-SHAPE of the program package X-Area.[52–54] All non-hydrogen atoms, except some of the disordered methyl C atoms were refined with anisotropic displacement parameters. All hydrogen atoms were positioned with idealized geometry and were refined isotropically with $U_{iso}(H) = -1.2\,U_{eq}(C)$ (1.5 for methyl H atoms) using a riding model. In some compounds disorder of the *tert*-butyl groups occurred and therefore, they were refined using a split model partly with some restraints. Selected crystal data and details on the structure refinements are given in Table 4.

CCDC-1049997 (for **1-Mn**), -1049996 (for **1-Fe**), -1049995 (for **1-Co**), -1049998 (for **2-Ni**), and -1049999 (for **3-Zn**) contain the supplementary crystallographic data for this paper. These data can be obtained free charge from the Cambridge Crystallographic Data Centre via http://www.ccdc.cam.ac.uk/data_request/cif.

Differential Thermal Analysis and Thermogravimetry (DTA-TG): The thermal decomposition reactions were performed in a dynamic nitrogen atmosphere (purity: 5.0) in Al_2O_3 crucibles using a STA-409CD thermobalance from Netzsch. The instrument was calibrated using standard references materials. All measurements were performed with a flow rate of 75 mLmin^{-1} and were corrected for buoyancy.

Magnetic Measurements: All magnetic measurements were performed using a Physical Property Measuring System (PPMS) from Quantum Design, which was equipped with a 9 T magnet. The data were corrected for core diamagnetism.

Job/Unit: I50176 /KAP1 Date: 08-06-15 14:45:14 Pages: 11

Table 4. Selected crystal data and details on the structure refinements for compounds **1-Mn**, **1-Fe**, **1-Co**, **2-Ni**, and **3-Zn**.

	1-Mn	1-Fe	1-Co	2-Ni	3-Zn
Formula	$C_{38}H_{52}MnN_6S_2$	$C_{38}H_{52}FeN_6S_2$	$C_{38}H_{52}CoN_6S_2$	$C_{20}H_{26}N_4NiS_2$	$C_{20}H_{26}N_4S_2Zn$
M_r [gmol^{-1}]	711.92	712.83	715.91	445.28	451.94
Crystal system	monoclinic	monoclinic	tetragonal	monoclinic	orthorhombic
Space group	*C2/c*	*C2/c*	$I4_1/a$	$P2_1/c$	*Fdd2*
Z	4	4	8	2	8
$D_{calcd.}$ [mgcm^{-3}]	1.133	1.148	1.148	1.338	1.283
μ [mm^{-1}]	0.448	0.499	0.547	1.078	1.239
Min./max. transmission	–	–	–	–	0.6621/0.8469
a [ ]	23.4545(14)	23.3743(12)	21.4704(10)	14.5729(9)	20.6130(13)
b [ ]	11.3799(7)	11.3334(8)	21.4704(10)	7.7900(3)	38.7390(18)
c [ ]	16.6212(7)	16.5338(8)	17.9706(8)	9.8925(5)	5.8600(3)
α [°]	90	90	90	90	90
β [°]	109.814(6)	109.664(6)°	90	100.160(5)	90
γ [°]	90	90	90	90	90
V [^{3}]	4173.7(4)	4124.5(4)	8284.1(7)	1105.41(10)	4679.4(4)
T [K]	200(2)	200(2)	200(2)	293(2)	200(2)
θ_{max} [°]	2.56 to 26.00	2.57 to 27.00	2.40 to 25.98	2.98 to 26.09	2.24 to 27.96
Measured reflections	11613	16573	9594	9529	12619
R_{int}	0.1147	0.0743	0.0427	0.0458	0.0754
Unique reflections	3971	4454	4000	2178	2590
Reflections [$F_o > 4\sigma(F_o)$]	2582		2722	1902	2304
Parameters	213	214	213	160	123
R_1 [$F_o > 4\sigma(F_o)$]	0.0636	0.0573	0.0486	0.0473	0.0424
wR_2 [all data]	0.1549	0.1419	1315	0.1012	0.1085
GOF	1.016	1.026	1.033	1.154	1.116

Acknowledgments

This project was supported by the Deutsche Forschungsgemeinschaft (DFG) (project number Na 720/5-1) and the Federate State of Schleswig-Holstein, Germany. The authors thank Prof. Dr. Wolfgang Bensch for access to his experimental facilities. Special thanks go to Inke Jess for the single crystals and Maren Rasmussen as well as Henning L hmann for the magnetic measurements. Z. T. thanks the National Science Centre Poland for financial support granted under decision number DEC-2013/11/B/ST3/03799.

[1] S. S. Massoud, L. L. Quan, K. Gatterer, J. H. Albering, R. C. Fischer, F. A. Mautner, *Polyhedron* **2012**, *31*, 601–606.
[2] F. A. Mautner, M. Scherzer, C. Berger, R. C. Fischer, R. Vicente, S. S. Massoud, *Polyhedron* **2015**, *85*, 20–26.
[3] C. N ther, S. W hlert, J. Boeckmann, M. Wriedt, I. Jeß, *Z. Anorg. Allg. Chem.* **2013**, *639*, 2696–2714.
[4] F. Mautner, F. Louka, A. Gallo, J. Albering, M. Saber, N. Burham, S. Massoud, *Trans. Met. Chem.* **2010**, *35*, 613–619.
[5] C. J. Adams, J. A. Real, R. E. Waddington, *CrystEngComm* **2010**, *12*, 3547–3553.
[6] C. J. Adams, M. C. Mu oz, R. E. Waddington, J. A. Real, *Inorg. Chem.* **2011**, *50*, 10633–10642.
[7] E. Shurdha, S. H. Lapidus, P. W. Stephens, C. E. Moore, A. L. Rheingold, J. S. Miller, *Inorg. Chem.* **2012**, *51*, 9655–9665.
[8] E. Shurdha, C. E. Moore, A. L. Rheingold, S. H. Lapidus, P. W. Stephens, A. M. Arif, J. S. Miller, *Inorg. Chem.* **2013**, *52*, 10583–10594.
[9] B. Machura, J. Palion, M. Penkala, T. Groń, H. Duda, R. Kruszynski, *Polyhedron* **2013**, *56*, 189–199.
[10] B. Machura, A. Świtlicka, P. Zwoliński, J. Mroziński, B. Kaliń ska, R. Kruszynski, *J. Solid State Chem.* **2013**, *197*, 218–227.
[11] J. G. Małecki, T. Groń, H. Duda, *Polyhedron* **2012**, *36*, 56–68.
[12] J. G. Małecki, B. Machura, A. Świtlicka, T. Groń, M. Bałanda, *Polyhedron* **2011**, *30*, 746–753.
[13] R. Gonz lez, A. Acosta, R. Chiozzone, C. Kremer, D. Armentano, G. De Munno, M. Julve, F. Lloret, J. Faus, *Inorg. Chem.* **2012**, *51*, 5737–5747.
[14] C. J. Adams, M. F. Haddow, D. J. Harding, T. J. Podesta, R. E. Waddington, *CrystEngComm* **2011**, *13*, 4909–4914.
[15] M. Wriedt, C. N ther, *Chem. Commun.* **2010**, *46*, 4707–4709.
[16] J.-Q. Tao, Z.-G. Gu, T.-W. Wang, Q.-F. Yang, J.-L. Zuo, X.-Z. You, *Inorg. Chim. Acta* **2007**, *360*, 4125–4132.
[17] J. Boeckmann, M. Wriedt, C. N ther, *Chem. Eur. J.* **2012**, *18*, 5284–5289.
[18] J. Boeckmann, C. N ther, *Chem. Commun.* **2011**, *47*, 7104–7106.
[19] T. K. Maji, G. Mostafa, P. S. Mukherjee, A. Mondal, A. J. Welch, K. Okamoto, N. R. Chaudhuri, *Polyhedron* **2000**, *19*, 1903–1907.
[20] S. Gerber, H. Gr ger, J. Ensling, P. G tlich, H. Krautscheid, *Angew. Chem. Int. Ed.* **2005**, *44*, 7787–7790; *Angew. Chem.* **2005**, *117*, 7965.
[21] J. Boeckmann, C. N ther, *Dalton Trans.* **2010**, *39*, 11019–11026.
[22] J. Boeckmann, C. N ther, *Polyhedron* **2012**, *31*, 587–595.
[23] S. W hlert, Z. Tomkowicz, M. Rams, S. G. Ebbinghaus, L. Fink, M. U. Schmidt, C. N ther, *Inorg. Chem.* **2014**, *53*, 8298–8310.
[24] S. W hlert, J. Boeckmann, M. Wriedt, C. N ther, *Angew. Chem. Int. Ed.* **2011**, *50*, 6920–6923.
[25] S. W hlert, T. Fic, Z. Tomkowicz, S. G. Ebbinghaus, M. Rams, W. Haase, C. N ther, *Inorg. Chem.* **2013**, *52*, 12947–12957.
[26] S. W hlert, M. Wriedt, T. Fic, Z. Tomkowicz, W. Haase, C. N ther, *Inorg. Chem.* **2013**, *52*, 1061–1068.
[27] A. Tahli, J. K. Maclaren, I. Boldog, C. Janiak, *Inorg. Chim. Acta* **2011**, *374*, 506–513.
[28] F. A. Mautner, R. Vicente, S. S. Massoud, *Polyhedron* **2006**, *25*, 1673–1680.
[29] J. Werner, M. Rams, Z. Tomkowicz, C. Nather, *Dalton Trans.* **2014**, *43*, 17333–17342.
[30] M. R. J. Werner, Z. Tomkowicz, T. Runčevski, R. E. Dinnebier, S. Suckert, C. N ther, *Inorg. Chem.* **2015**, *54*, 2893.
[31] S. W hlert, I. Jess, C. N ther, *Z. Anorg. Allg. Chem.* **2013**, *639*, 385–391.
[32] M. Wriedt, C. N ther, *Eur. J. Inorg. Chem.* **2011**, 228–234.
[33] H.-L. Jia, M.-J. Jia, H. Ding, J.-H. Yu, J. Jin, J.-Q. Zhao, J.-Q. Xu, *CrystEngComm* **2012**, *14*, 8000–8009.

Job/Unit: I50176 /KAP1 Date: 08-06-15 14:45:14 Pages: 11

[34] Z. Jiang, P. Zhao, R. Li, L. An, Z. Zhang, J. Xu, *J. Chem. Crystallogr.* **2013**, *43*, 463–470.
[35] S. Das, K. Bhar, S. Chattopadhyay, P. Mitra, V. J. Smith, L. J. Barbour, B. K. Ghosh, *Polyhedron* **2012**, *38*, 26–35.
[36] S. W hlert, L. Fink, M. Schmidt, C. N ther, *CrystEngComm* **2013**, *15*, 945–957.
[37] S. W hlert, L. Peters, C. N ther, *Dalton Trans.* **2013**, *42*, 10746–10758.
[38] C. R. Groom, F. H. Allen, *Angew. Chem. Int. Ed.* **2014**, *53*, 662–671.
[39] L. R. Nassimbeni, M. L. Niven, M. W. Taylor, *Acta Crystallogr., Sect. B* **1990**, *46*, 354–361.
[40] S. W hlert, T. Runčevski, R. E. Dinnebier, S. G. Ebbinghaus, C. N ther, *Cryst. Growth Des.* **2014**, *14*, 1902–1913.
[41] A. Escuer, R. Vicente, M. A. S. Goher, F. A. Mautner, *Inorg. Chem.* **1995**, *34*, 5707–5708.
[42] M. A. M. Abu-Youssef, V. Langer, D. Luneau, E. Shams, M. A. S. Goher, L. hrstr m, *Eur. J. Inorg. Chem.* **2008**, 112–118.
[43] X.-Y. Wang, Z.-M. Wang, S. Gao, *Inorg. Chem.* **2008**, *47*, 5720–5726.
[44] R.-Y. Li, B.-W. Wang, X.-Y. Wang, X.-T. Wang, Z.-M. Wang, S. Gao, *Inorg. Chem.* **2009**, *48*, 7174–7180.
[45] C. N ther, G. Bhosekar, I. Jeß, *Inorg. Chem.* **2007**, *46*, 8079–8087.
[46] S. W hlert, I. Jess, U. Englert, C. N ther, *CrystEngComm* **2013**, *15*, 5326–5336.
[47] J. D. Dunitz, J. Bernstein, *Acc. Chem. Res.* **1995**, *28*, 193–200.
[48] R.-Y. Li, X.-Y. Wang, T. Liu, H.-B. Xu, F. Zhao, Z.-M. Wang, S. Gao, *Inorg. Chem.* **2008**, *47*, 8134–8142.
[49] M. E. Lines, *J. Phys. Chem. Solids* **1970**, *31*, 101–116.
[50] J. Zinn-Justin, *Quantum Field Theory and Critical Phenomena*, vol. 3, Clarendon Press, Oxford, **1996**.
[51] G. M. Sheldrick, *Acta Crystallogr., Sect. A* **2008**, *64*, 112–122.
[52] *X-Red*, version 1.11, *Program for Data Reduction and Absorption Correction*, STOE & CIE GmbH, Darmstadt, Germany, **1998**.
[53] *X-Shape*, version 1.03, *Program for the Crystal Optimization for Numerical Absorption Correction*, STOE & CIE GmbH, Darmstadt, Germany, **1998**.
[54] *X-Area*, version 1.44, *Program Package for Single Crystal Measurements*, STOE & CIE GmbH, Darmstadt, Germany, **2008**.

Received: February 18, 2015
Published Online: ■

Job/Unit: I50176 /KAP1 Date: 08-06-15 14:45:14 Pages: 11

EurJIC European Journal of Inorganic Chemistry www.eurjic.org FULL PAPER

Layered Metal-SCN Networks

Keywords: Layered compounds / Polymers / Thermal properties / Magnetic properties

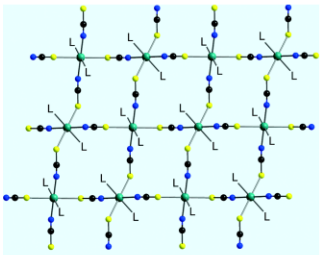

New layered thiocyanato coordination polymers of composition $[M(NCS)_2(4\text{-}tert\text{-}butylpyridine)_2]_n$ (M = Ni, Co) were prepared and investigated for their magnetic properties. The Ni compound shows a ferromagnetic transition whereas the Co compound shows a transition to a magnetic state with uncompensated magnetic moment.

4.2. Magnetic Properties of Isomeric and Polymorphic Coordination Polymers of Composition $[M(NCS)_2(4\text{-Acetylypridine})_2]_n$ (M = Fe, Ni)

Julia Werner, Tomče Runčevski, Robert Dinnebier, Stefan G. Ebbinghaus, Stefan Suckert, und Christian Näther, *Eur. J. Inorg. Chem.* **2015**, *20*, 3236-3245.

DOI: 10.1002/ejic.201500473

Motivation

In Kapitel 3.3 wurde über die Untersuchung von $Co(NCS)_2$ mit 4-Acetylpyridin berichtet. Es wurden zwei Isomere erhalten, von denen das 2D-Isomer thermodynamisch stabil, und das 1D-Isomer metastabil war. Aufbauend auf diesen Ergebnissen war es von Interesse zu untersuchen, ob auch mit anderen Metallkationen und 4-Acetylpyridin unterschiedliche Isomere auftreten und welchen Einfluss das Metallkation auf die Stabilität und die magnetischen Eigenschaften dieser Isomere ausübt.

Diese Untersuchungen ergaben, dass mit Fe(II) nur das 1D-Isomer erhalten werden konnte, welches Metamagnetismus aufweist. Für Mangan werden Gemenge unterschiedlicher kristalliner Phasen erhalten, die vermutlich ebenfalls Kettenstrukturen aufweisen. Im Gegensatz hierzu konnten für Nickel wieder beide Isomere isoliert werden, von denen das thermodynamisch stabile 2D-Isomer ferromagnetisches Verhalten zeigt, wohingegen es sich beim metastabilen 1D-Isomer um einen Paramagneten handelt.

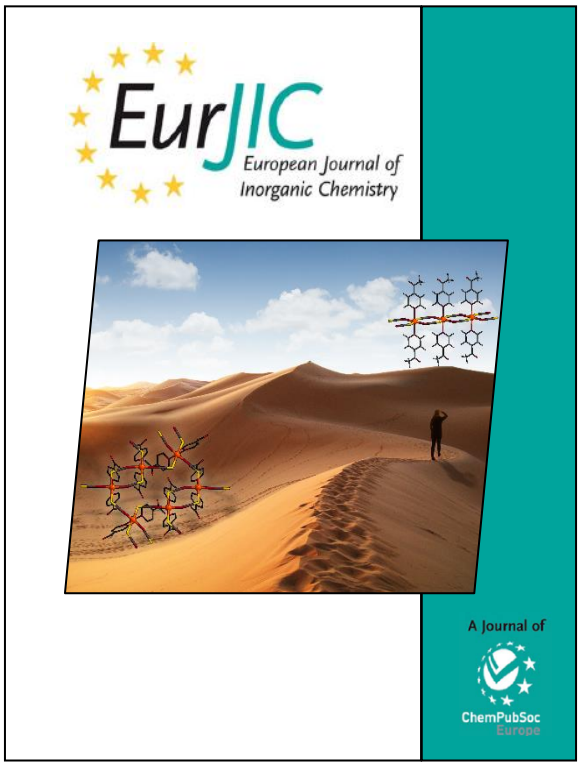

Job/Unit: I50473 /KAP1 Date: 10-06-15 18:02:55 Pages: 11

EurJIC European Journal of Inorganic Chemistry

ChemPubSoc Europe

FULL PAPER

DOI:10.1002/ejic.201500473

Thiocyanato Coordination Polymers with Isomeric Coordination Networks – Synthesis, Structures, and Magnetic Properties

Julia Werner,[a] Tomče Runčevski,[b] Robert Dinnebier,[b] Stefan G. Ebbinghaus,[c] Stefan Suckert,[a] and Christian N ther*[a]

Keywords: Coordination polymers / N ligands / Structure elucidation / Thermal properties / Magnetic properties

The reactions of $M(NCS)_2$ (M = Mn, Fe, and Ni) with 4-acetylpyridine (4-Acpy) in water lead to the formation of discrete complexes of composition $M(NCS)_2(4\text{-Acpy})_2(H_2O)_2$, in which the metal cations are coordinated only N-terminally to the thiocyanato anions. When heated, these precursors dehydrate, and some of them transform into compounds of composition $[M(NCS)_2(4\text{-Acpy})_2]_n$, in which the metal cations are linked by pairs of μ-1,3-bridging anionic ligands into chains (1D isomer). In contrast, the thermal decomposition of $Ni(NCS)_2(4\text{-Acpy})_4$ or crystallization from solution leads to the formation of an isomeric 2D network of the same composition, which is thermodynamically more stable than the 1D isomer. Temperature-dependent magnetic measurements of the 1D isomer $[Fe(NCS)_2(4\text{-Acpy})_2]_n$ at 200 Oe reveal antiferromagnetic ordering at T_N = 4.5 K. Field-dependent measurements show a metamagnetic transition into a saturated paramagnetic phase at a critical field of ca. 700 Oe. In contrast, magnetic measurements of the 2D isomer $[Ni(NCS)_2(4\text{-Acpy})_2]_n$ at 1000 Oe show a ferromagnetic transition at T_C = 8.6 K, whereas only paramagnetic behavior is observed for the Ni 1D isomer.

Introduction

Investigations on the crystal structures and properties of coordination polymers are an active field in chemical research. Coordination polymers based on metal cations with unpaired electrons are of increasing interest, because of their different magnetic properties, such as spin-crossover or low-dimensional magnetism.[1–16] In several cases, the metal cations are linked by small, two- or three-atom ligands (e.g., cyanide or azide anions) into coordination networks of different dimensionality, and some examples are given in refs.[17–29] In this regard, thiocyanato anions are also of interest because of their ambidentate nature and versatile coordination modes. Therefore, an increasing number of thiocyanato coordination compounds have been reported recently.[30–48] These compounds are similar to selenocyanato coordination polymers. Compared with the thiocyanato analogs, they are less stable; thus, only a relatively low number of compounds are known.[49–55]

Recently, we became interested in transition metal thiocyanato coordination polymers and focused on compounds of composition $[M(NCS)_2(L)_2]_n$ (M = Mn, Fe, Co, Ni; L = coligand), in which the metal centers are coordinated by simple N-donor coligands and are linked by μ-1,3-bridging anionic ligands into coordination networks.[56–66] In most cases, we crystallized structures in which the metal cations are linked by pairs of anionic ligands into chains.

Depending on the metal cation, these compounds show a variety of magnetic properties, including a slow relaxation of the magnetization that might originate from the relaxation of single chains.[56–64] In the course of our investigations, we studied the influence of the coligand on the structural and magnetic properties in detail. With cobalt(II) thiocyanate and 4-acetylpyridine (4-Acpy), surprisingly, we obtained a compound of composition $[Co(NCS)_2(4\text{-Acpy})_2]_n$ from solution; this compound consists of a 2D network instead of the 1D chains usually observed with monodentate ligands.[67] Further investigations showed that the 1D isomer can be synthetized by thermal annealing of the precursor hydrate $Co(NCS)_2(4\text{-Acpy})_2(H_2O)_2$. However, this 1D compound recrystallizes from solution at room temperature as the stable 2D isomer. The same transformation is observed on heating. Accordingly, the 2D network is, at least above room temperature, thermodynamically more stable than the 1D compound. The occurrence of different polymorphic modifications or isomeric compounds of this kind is not uncommon, and several examples have been reported.[60,64,68–76]

[a] Institut f r Anorganische Chemie, Christian-Albrechts-Universit t zu Kiel,
Max-Eyth-Straße 2, 24118 Kiel, Germany
E-mail: cnaether@ac.uni-kiel.de
http://www.ac.uni-kiel.de/de/pd-dr.-christian-naether-1
[b] Max Planck Institute for Solid State Research,
Heisenbergstraße 1, 70569 Stuttgart, Germany
[c] Martin-Luther-Universit t Halle-Wittenberg, Institut f r Chemie,
Kurt-Mothes-Straße 2, 06120 Halle/Saale, Germany
Supporting information for this article is available on the WWW under http://dx.doi.org/10.1002/ejic.201500473.

Job/Unit: I50473 /KAP1 Date: 10-06-15 18:02:55 Pages: 11

Interesting questions to answer are whether different isomers can be obtained by using other cations and whether 1D or 2D isomer formation is preferred depending on the metal cation. In this context, it is noted that the hydrate of composition $Fe(NCS)_2(4\text{-Acpy})_2(H_2O)_2$ has already been reported,[77] and two modifications of composition $[Cd(NCS)_2(4\text{-Acpy})_2]_n$ were recently reported (monoclinic $P2_1/c$ and $C2/c$); these Cd^{II} compounds consist of chains and are not isotypic to the Co^{II} analog.[78] We extended the study by preparing similar compounds with Mn^{II}, Fe^{II}, and Ni^{II} cations. These cations usually behave similarly to Co^{II}. In some cases, Co^{II} and Ni^{II} form isotypic structures that are structurally different from the isotypic Mn^{II} and Fe^{II} structures. Here, we report on these investigations.

Results and Discussion

Synthesis

The reactions of different ratios of $M(NCS)_2$ (M = Mn, Fe, and Ni) with 4-acetylpyridine in water or ethanol lead to the formation of the following compounds (see Exp. Sect.):

$Mn(NCS)_2(4\text{-Acpy})_2(H_2O)_2$ (**1**-Mn)

$Fe(NCS)_2(4\text{-Acpy})_2(H_2O)_2$ (**1**-Fe)

$Ni(NCS)_2(4\text{-Acpy})_2(H_2O)_2$ (**1**-Ni)

$Ni(NCS)_2(4\text{-Acpy})_2(H_2O)_2{\cdot}H_2O$ [**1**-Ni(H_2O)]

$Ni(NCS)_2(4\text{-Acpy})_4$ (**2**-Ni)

$[Ni(NCS)_2(4\text{-Acpy})_2]_n$ (**3**-Ni/I)

In the respective IR spectra, the asymmetric C–N stretching vibrations ν_{as}(CN) are observed at $\tilde{\nu}$ = 2075 (**1**-Mn), 2081 (**1**-Fe), 2098 (**1**-Ni), 2097 [**1**-Ni(H_2O)], and 2072 cm^{-1} (**2**-Ni), which indicates that the metal cations in all of these compounds are coordinated only by terminal N-bonded thiocyanato anions (Figures S1–S5 in the Supporting Information). On the contrary, for **3**-Ni/I, the CN stretching vibration is observed at $\tilde{\nu}$ = 2116 cm^{-1}, which indicates that the metal cations in this compound are linked by the anionic ligands into a coordination polymer (Figure S6). No other Mn and Fe compounds are available by this synthetic approach owing to the high stability of the hydrate complexes.

X-ray powder diffraction (XRPD) investigations showed that **1**-Mn, **1**-Fe, and **1**-Ni are isotypic to $Co(NCS)_2(4\text{-Acpy})_2(H_2O)_2$ and that **2**-Ni is isotypic to $Co(NCS)_2(4\text{-Acpy})_4$, both of which were reported recently (Figure S7 and S8).[67,77] The compound **3**-Ni/I seems to be isotypic to the more stable form of $Co(NCS)_2(4\text{-Acpy})_2$, in which the Co cations are linked by the anions into layers (Figure S9).[6] The **1**-Ni(H_2O) hydrate is very unstable; even at room temperature, it transforms into **1**-Ni and in some cases shows impurities of **3**-Ni/I (Figure S10).

Single crystals of **1**-Mn, **1**-Ni(H_2O), and **2**-Ni were obtained and investigated by single-crystal X-ray diffraction (see Exp. Sect.). For **1**-Ni and **3**-Ni/I, only very small and twinned crystals of low X-ray scattering ability were obtained and, thus, their structures were determined by Rietveld refinements (see Exp. Sect.).

Crystal Structures

Crystal Structure of $Mn(NCS)_2(4\text{-Acpy})_2(H_2O)_2$

Compound **1**-Mn crystallizes in the monoclinic space group $P2_1/n$ with two formula units in the unit cell and is isotypic to **1**-Ni as well as to **1**-Fe and $Co(NCS)_2(4\text{-Acpy})_2(H_2O)_2$, which were reported recently.[67,77] The crystal structure consists of discrete complexes located on centers of inversion. The metal cations are coordinated by two N atoms of terminal thiocyanato anions, two N atoms of the 4-Acpy ligands, and two water molecules within slightly distorted octahedra (Figure 1, top; Table S1). In the crystal structure, the complexes are linked into chains by intermolecular O–H···O hydrogen bonds between the O atom of the acetyl group and one water H atom (Table S2). These chains are further connected into layers by weak O–H···S interactions between the thiocyanato S atom and the water H atom that is not involved in O–H···O hydrogen bonding (Figure 1, bottom; Table S2).

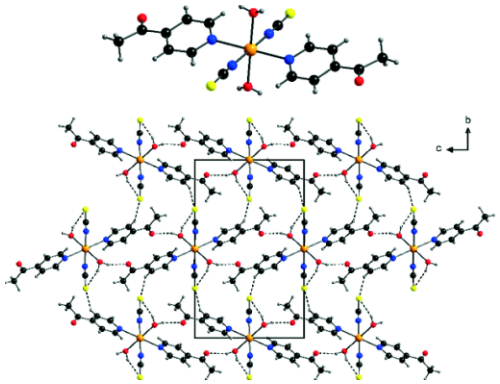

Figure 1. Coordination sphere (top) and crystal packing of **1**-Mn viewed along the crystallographic *a* axis (bottom). The intermolecular O–H···O and O–H···S hydrogen bonding is shown by dotted lines. An ORTEP plot of **1**-Mn is shown in Figure S11.

Crystal Structure of $Ni(NCS)_2(4\text{-Acpy})_2(H_2O)_2{\cdot}H_2O$

Compound **1**-Ni(H_2O) crystallizes in the monoclinic space group $P2_1/n$ with two formula units in the unit cell. The coordination sphere of the Ni cations is comparable to that observed in the compounds marked with **1**, and the Ni cations are octahedrally surrounded by two anionic ligands and four 4-Acpy ligands (Table S3 and Figure S12).

The discrete complexes are connected into chains by intermolecular O–H···O hydrogen bonding between one water H atom and the O atom of the acetyl group of a neighboring complex (Figure 2 and Table S4). Contrary to the other compounds marked with **1**, the second water H atom is hydrogen bonded to the uncoordinated water mo-

Job/Unit: I50473 /KAP1 Date: 10-06-15 18:02:55 Pages: 11

lecule. Additional hydrogen bonding between the H atoms of the uncoordinated water molecules and the acetyl O atom as well as the thiocyanate S atom link the building blocks into a three-dimensional network (Figure 2 and Table S4).

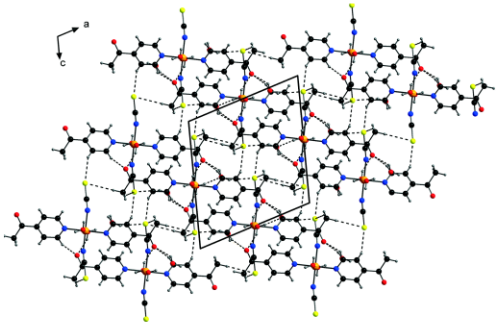

Figure 2. Crystal structure of **1**-Ni(H_2O) viewed along the crystallographic *b* axis. Intermolecular O–H···O and O–H···S hydrogen bonding is shown by dashed lines, and an ORTEP plot of **1**-Ni(H_2O) is shown in Figure S12.

Crystal Structure of Ni(NCS)$_2$(4-Acpy)$_4$

Compound **2**-Ni crystallizes in the orthorhombic space group *Pbca* with eight formula units in the unit cell and is isotypic to Co(NCS)$_2$(4-Acpy)$_4$ reported recently.[67] The asymmetric unit consists of one nickel(II) cation, two thiocyanato anions, and four 4-acetylpyridine anions, all in general positions. The Ni cation is coordinated by two terminal N-bonded thiocyanato anions and four 4-Acpy ligands within a slightly distorted octahedral geometry (Figure 3 and Table S5).

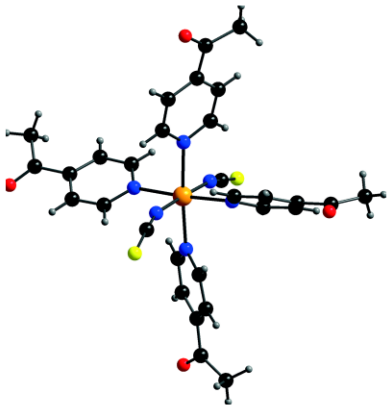

Figure 3. Coordination sphere of **2**-Ni. An ORTEP plot of **2**-Ni is shown in Figure S13.

Crystal Structure of [Ni(NCS)$_2$(4-Acpy)$_2$]$_n$

Compound **3**-Ni/I crystallizes in the orthorhombic space group *Pbca* with eight formula units in the unit cell and all atoms in general positions. This compound is isotypic to the thermodynamically stable isomer of [Co(NCS)$_2$(4-Acpy)$_2$]$_n$ reported recently.[67] In the crystal structure, each Ni cation is coordinated by two 4-Acpy ligands and four thiocyanato anions. The Co cations are linked by pairs of μ-1,3-bridging anions into dimers, which are further connected into layers by additional single μ-1,3-bridging anions (Figure 4).

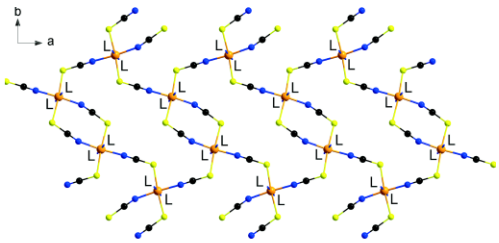

Figure 4. Crystal structure of **3**-Ni/I viewed along the crystallographic *c* axis; L = 4-Acpy.

On the basis of the available crystallographic data, XRPD patterns were calculated and compared with the experimental patterns, which show that **1**-Mn, **1**-Fe, **1**-Ni, **2**-Ni, and **3**-Ni/I were obtained as pure phases (Figure S14–S18). In the pattern of **1**-Ni(H_2O), traces of **3**-Ni/I are visible (as already mentioned, this compound is unstable; Figure S19).

Thermoanalytical Investigations

As mentioned before, crystallization from solution gives a phase of composition [Ni(NCS)$_2$(4-Acpy)$_2$]$_n$ (**3**-Ni/I), which is isotypic to the stable 2D isomer [Co(NCS)$_2$(4-Acpy)$_2$]$_n$. In this context, it is interesting to investigate whether a second, 1D isomer can be obtained by thermal decomposition of **1**-Ni or **2**-Ni, for example. Moreover, with Mn and Fe, no 4-Acpy-deficient phases were obtained; thus, there is a need to check if such compounds are available by thermal treatment of these precursors. Therefore, simultaneous differential thermoanalysis and thermogravimetry (DTA-TG) measurements were performed. As the outcomes of such investigations strongly depend on the kinetics of the reaction, heating-dependent measurements were also performed.[79]

The hydrate **1**-Mn was heated to 400 °C with a thermobalance and showed two mass-loss steps in the TG curve. The first step corresponds to the removal of the water molecules (Δm_{exp} = 6.6%; $\Delta m_{calcd.}$ = 8%; Figures 5, S20, and S21). The product formed was investigated by XRPD, which indicates that two modifications might have formed, which are isotypic to one form of [Cd(NCS)$_2$(4-Acpy)$_2$]$_n$ and to [Co(NCS)$_2$(4-Acpy)$_2$]$_n$ reported recently (Figure S22). The XRPD measurements of the products obtained at different heating rates show no changes to the product formed.

Job/Unit: I50473 /KAP1 Date: 10-06-15 18:02:55 Pages: 11

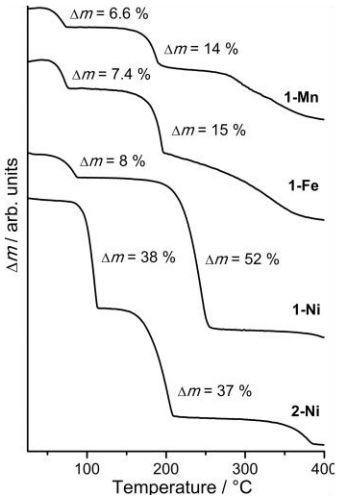

Figure 5. TG curves for **1-Mn**, **1-Fe**, **1-Ni**, and **2-Ni**. Heating rate 1 °C min^{-1}, N_2 atmosphere, Δm = mass loss [%].

The DTA-TG curve of **1-Fe** looks similar to that of **1-Mn**, and the experimental mass loss of the first step is also in reasonable agreement with that calculated for the removal of the coordinated water molecules (Figures 5, S23, and S24). The XRPD measurements of the residue obtained after water removal (**3-Fe/II**) looks different from that obtained from **1-Mn**, and the residue is isotypic to the 1D compound $[Co(NCS)_2(4\text{-Acpy})_2]_n$ (Figure S25). The same result is obtained if **1-Fe** is decomposed at different temperatures, and there are no indications that a 2D compound similar to **3-Ni/I** can be obtained.

The 1D compound **3-Fe/II** is isotypic to $[Co(NCS)_2(4\text{-Acpy})_2]_n$ reported recently and crystallizes in the triclinic space group $P\bar{1}$ with one molecule in the unit cell. In its crystal structure, the Fe cations are located on centers of inversion and are coordinated by two terminal N-bonded 4-acetylpyridine coligands and four thiocyanato anions within slightly distorted octahedra (Figure 6). The cations are linked into chains by pairs of μ-1,3-bridging thiocyanato anions (Figure 6). It is noted that the crystal structure of **3-Fe/II** exhibits severe strain, which is visible by the different shape and peak-broadening of the reflections in the XRPD pattern.

The DTA-TG measurements of **2-Ni** revealed two mass-loss steps in the thermogravimetric curve, which are accompanied by endothermic events in the DTA curve (Figures 5, S26, and S27). The experimental mass losses of Δm = 38% in the first step and Δm = 37% in the second step are in a good agreement with the calculated mass losses for the removal of two 4-Acpy ligands in each step ($\Delta m_{calcd.}$ = 37%). However, XRPD investigations of the product formed after the first step clearly prove that the 2D compound **3-Ni/I** is obtained as a pure phase, which does not

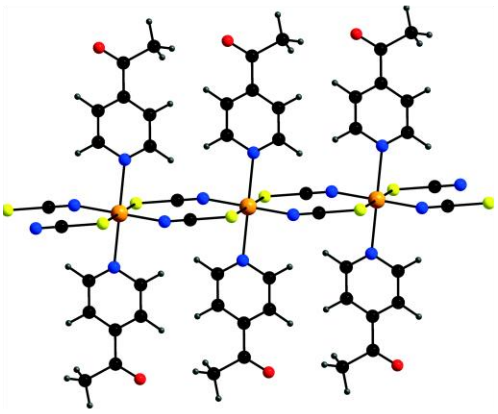

Figure 6. Crystal structure of **3-Fe/II** viewed along the chains.

change if **2-Ni** is decomposed at different heating rates (Figure S28).

In contrast, DTA-TG measurements of the hydrate **1-Ni** indicate the formation of different phases after water removal at different heating rates (Figures 5, 7, S29, and S30). If the water is removed at 16 °C min^{-1}, the powder pattern of the residue is very similar to that calculated for the 1D compound $[Co(NCS)_2(4\text{-Acpy})_2]_n$ reported recently. However, a closer look indicates that a very small amount of the 2D compound **3-Ni/I** is present, as is clear from the most intense peak of this form at $2\theta \approx 7°$ (compare Figure 7, A, E, and F).

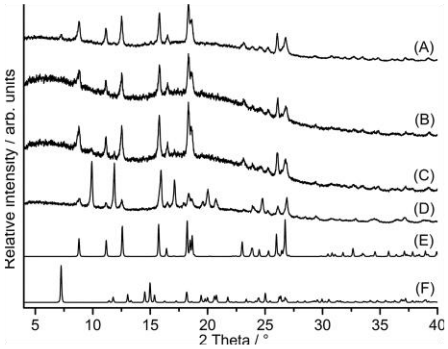

Figure 7. Experimental XRPD patterns of the residues obtained by thermal annealing of **1-Ni** at different heating rates: (A) 16, (B) 8, (C) 4, and (D) 1 °C min^{-1}; (E) calculated patterns of $[Co(NCS)_2(4\text{-Acpy})_2]_n$ (1D) and (F) $[Co(NCS)_2(4\text{-Acpy})_2]_n$ (2D).

At slower heating rates, additional peaks occur, and the residue obtained at 1 °C/min consists of a mixture of **3-Ni/II** and an additional phase that does not correspond to **3-Ni/I** or to one of the two 1D modifications of $[Cd(NCS)_2(4\text{-Acpy})_2]_n$ reported recently (Figure 7, D).[78] Unfortunately, this phase could not be obtained pure, even when **1-**

Job/Unit: I50473 /KAP1 Date: 10-06-15 18:02:55 Pages: 11

Ni was annealed for longer times. The IR spectra of the residue obtained at 1 °C min^{-1} shows only one value for the asymmetric CN stretching vibration at $\tilde{\nu}$ = 2115 cm^{-1}, which is close to the value measured for 3-Ni/I at $\tilde{\nu}$ = 2116 cm^{-1} (Figure S31). Therefore, it can be assumed that the Ni cations are also linked by bridging anionic ligands in the new phase.

These experiments indicate that the 1D compound 3-Ni/I is obtained by kinetic control. To obtain purer samples of 3-Ni/I, we used a different procedure in which samples of 1-Ni were placed in a drying oven preheated to 167 °C for ca. 5 min. The samples obtained by this procedure had no reflections of 3-Ni/I in the corresponding XRPD pattern; thus, they were used for magnetic measurements (Figure S32). Note that these samples were of poor crystallinity.

To unambiguously determine which of the two isomers 3-Ni/I and 3-Ni/II is thermodynamically more stable, a mixture of both forms was stirred in acetonitrile for several days; thereafter, the residue was investigated by XRPD. It could be clearly seen that all crystals of the chain compound 3-Ni/II had disappeared; therefore, the 2D isomer 3-Ni/I is more stable, as was already observed for $[Co(NCS)_2(4\text{-Acpy})_2]_n$ (Figure S33).[67]

Magnetic Investigations

The magnetic properties of the 1D compounds 3-Fe/II and 3-Ni/II, as well as those of the 2D compound 3-Ni/I were investigated by susceptibility measurements. Note that for the corresponding 2D Co compound, only paramagnetic behavior is observed, whereas the 1D compound $[Co(NCS)_2(4\text{-Acpy})_2]_n$ exhibits a ferromagnetic ground state and shows a slow relaxation of the magnetization.[67]

Temperature-dependent magnetic measurements on 3-Fe/II show a maximum at T_N = 4.5 K, which is indicative of antiferromagnetic ordering (Figure 8). The χT product slowly increases upon cooling, which indicates that ferromagnetic interactions are dominant; however, upon further cooling, a strong maximum is observed at the antiferromagnetic transition. Measurements at different fields show that T_N moves to lower temperatures with increasing direct-current (DC) field, as expected for an antiferromagnet.

Above 20 K, the Curie–Weiss law is obeyed with a Curie–Weiss temperature of 8.3 K, which indicates that ferromagnetic interactions between the Fe^{II} centers are dominant. The experimental magnetic moment of 5.40 μ_B is only slightly larger than that expected for an Fe^{II} cation in a high-spin configuration.

Additional measurements at 1000 Oe and higher fields show ferromagnetic behavior; therefore, a metamagnetic transition occurs at lower fields (Figure S34). This is in agreement with the field-dependent magnetization results at 2 K, which are typical for metamagnets and only show a small hysteresis above the critical field (Figure 9). The critical field H_c was determined to be 610 Oe from the first derivative of the magnetization curve, and the curve saturates at a value of 4 μ_B (Figure 9).

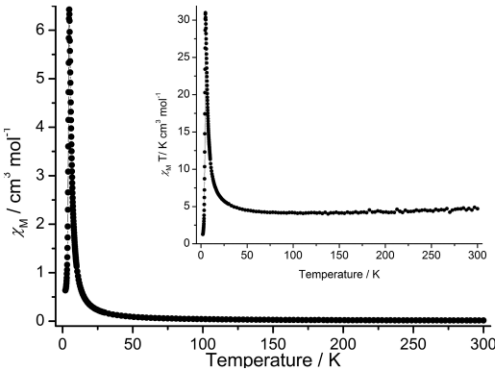

Figure 8. Temperature dependence of the susceptibility and the χT product (inset) of 3-Fe/II at 200 Oe in the temperature range 2–300 K.

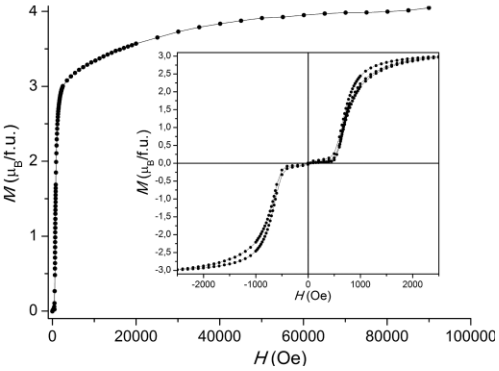

Figure 9. Magnetization versus field for 3-Fe/II at 2.0 K and full hysteresis curve at 2.0 K (inset).

The transition from the antiferromagnetic phase into the saturated paramagnetic phase is also clear from additional zero-field-cooled/field-cooled (ZFC-FC) measurements at different DC fields (Figure 10). Directly above H_c, only very small bifurcations are observed, which are completely suppressed at higher DC fields (Figure 10).

The observation of metamagnetic behavior for such a 1D Fe^{II} thiocyanato coordination polymer is not unusual. A similar behavior was observed for $[Fe(NCS)_2(pyridine)_2]_n$, which consists of the same Fe thiocyanato chains as those in 3-Fe/II.[57,80–82] In this compound, the antiferromagnetic ordering is observed at 5.6 K for a DC field of 1000 Oe, and the critical field was determined to be 1200 Oe.[57] A similar behavior is also found for the 2D compound $Fe(NCS)_2$[1,2-bis(4-pyridyl)ethylene], in which the thiocyanato chains are linked by the coligands into layers.[63] In this case, the N el temperature is 5.0 K at 1000 Oe, and an unusual two-step metamagnetic transition is observed at 1300 and 1775 Oe.[63]

Job/Unit: I50473 /KAP1 Date: 10-06-15 18:02:55 Pages: 11

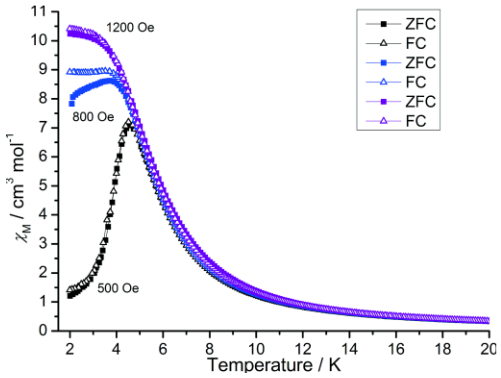

Figure 10. Susceptibility as a function of temperature at different DC fields [Oe] measured under FC (circles) and ZFC (squares) conditions.

Magnetic measurements for the 2D Ni compound **3-Ni/I** at 1000 Oe show a strong increase of the susceptibility on cooling until saturation, typical for ferromagnetic behavior. From the first derivative of the susceptibility curve, a Curie temperature T_C of 8.6 K is obtained (Figure 11). The data were analyzed according to the Curie–Weiss law, and the Curie–Weiss temperature of 17 K indicates dominant ferromagnetic interactions between the Ni centers. On cooling, the χT product passes a maximum, which indicates the ferromagnetic transition. The experimental magnetic moment of 3.10 μ_B is in reasonable agreement with that expected for a Ni^{II} cation in a high-spin configuration.

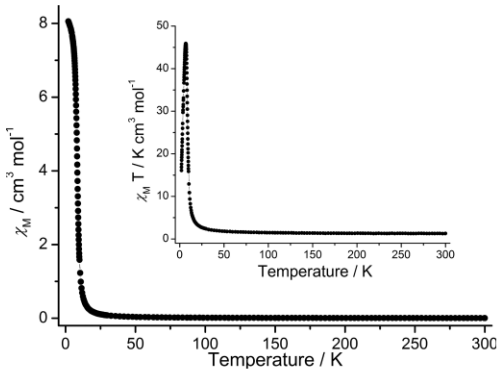

Figure 11. Temperature dependence of the susceptibility and the χT product (inset) of 3-Ni/I at 1000 Oe in the temperature range 2–300 K.

Note that the same topology of the coordination network is observed in $[Ni(NCS)_2(2\text{-methylpyrazine})_2]_n$ and that this compound shows a metamagnetic transition at 150 Oe.[66] A similar behavior is also observed for the corresponding compound with 2-chloropyrazine, but the metamagnetic transition occurs at very high fields in this case.[65] To exclude metamagnetic behavior for **3-Ni/I**, additional measurements at 10, 20, and 100 Oe were performed; as the results are similar to those at 1000 Oe, a metamagnetic transition at very low field can be excluded (Figure S35). From these measurements, it is clear that the transition temperature increases with increasing DC field, which is typical for a ferromagnetic transition.

The field-dependent magnetization measurements at 2 K are in agreement with the other findings and show that saturation is achieved at 2.2 μ_B (Figure 12). In the inset of Figure 12, the hysteresis $M(H)$ recorded at a temperature of 2.0 K is presented. It is clear that full reversibility can already be observed at ca. 500 Oe. The coercive field amounts to ca. 112 Oe, and the curves saturate at 2.1 μ_B.

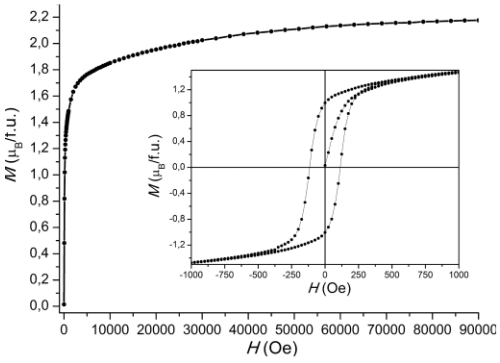

Figure 12. Magnetization versus field for 3-Ni/I at 2.0 K and full hysteresis curve at 2.0 K (inset).

ZFC/FC measurements at different DC fields show relatively strong bifurcations, which are manifestations of the domain behavior of a ferromagnet (Figure 13). At higher DC fields, these bifurcations are suppressed.

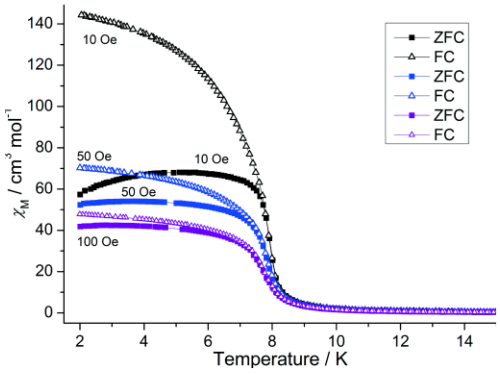

Figure 13. Susceptibility as a function of temperature at different DC fields measured in FC (circles) and ZFC (squares) conditions. For additional ZFC-FC measurements at other fields, see Figure S36.

Job/Unit: I50473 /KAP1 Date: 10-06-15 18:02:55 Pages: 11

Finally, we also performed measurements for the 1D compound **3-Ni/II**, which shows only paramagnetic behavior (Figure S37). However, in some batches, the increase in susceptibility starts at higher temperatures, as observed for **3-Ni/I**. This indicates that, depending on the reaction conditions, the 1D compound **3-Ni/II** might be contaminated with a very low amount of the more stable 2D compound **3-Ni/I** that is not detectable by XRPD (Figure S38). However, it does not influence the overall result that the chain compound shows only paramagnetic behavior without any magnetic anomalies; this is reasonable because similar compounds based on 1D $Ni(NCS)_2$ chains show either paramagnetic or metamagnetic behavior.[57,83]

Conclusions

In the present contribution, the synthesis, crystal structures, and properties of isomeric 1D and 2D thiocyanato coordination polymers with 4-acetylpyridine are reported. Through the thermal decomposition of appropriate precursor compounds, new coordination polymers that are not accessible from solution can be obtained. Moreover, depending on the precursors used, different stable and metastable isomers can be obtained. The 2D isomer with Ni is thermodynamically stable, whereas the 1D isomer is metastable. This is surprising, as most of the other compounds with a similar ratio between the metal thiocyanate and the coligand consist of 1D networks. With Fe and Mn, only the chain compounds were obtained; this does not necessarily mean that they are the stable isomers. However, there are some examples for this class of compound in which Mn and Fe as well as Co and Ni behave structurally similarly, and there are no reasons why this should be not valid for their solid-state reactivity. Note that there are only a few examples in which an identical layered structure has been observed. Interestingly, these compounds are metamagnets, whereas the 2D Ni compound presented here clearly shows ferromagnetism. The occurrence of metamagnetism for such $Fe(NCS)_2$ chains is reasonable, because the corresponding compound with pyridine as a coligand shows a similar magnetic behavior. Unfortunately, for the 1D Mn compound, no pure samples could be prepared and, thus, no magnetic measurements were performed. However, most such Mn compounds with different coligands show either paramagnetic behavior or antiferromagnetic ordering, and it can be assumed that this would also be the case for the compounds with 4-acetylpyridine.

Experimental Section

General: $MnSO_4·H_2O$ was purchased from Gr ssing, and $FeCl_2·4H_2O$ was purchased from Sigma–Aldrich. $NiSO_4·6H_2O$ was obtained from Merck, $Ba(NCS)_2·3H_2O$ and 4-actylpyridine were obtained from Alfa Aesar. $Ni(SCN)_2$ and $Mn(NCS)_2$ were prepared by the reaction of equimolar amounts of $NiSO_4·6H_2O$ with $MnSO_4·H_2O$ and $Ba(NCS)_2·3H_2O$, respectively, in water. The resulting white precipitate of $BaSO_4$ was removed by filtration, and the concentration of the filtrate to complete dryness resulted in a green residue of $Ni(SCN)_2$ and a beige residue of $Mn(NCS)_2$. The purity of the compounds was proved by XRPD and elemental analysis. Crystalline powders were prepared by stirring the reactants in solution for several days at room temperature. The residues were collected by filtration and air-dried. The crystalline powder of one ligand-deficient compound was prepared by annealing. The purity of all compounds was checked by X-ray powder diffraction and elemental analysis.

$Mn(NCS)_2$(4-acetylpyridine)$_2(H_2O)_2$ (1-Mn): Single crystals suitable for single-crystal X-ray diffraction were synthesized from $Mn(NCS)_2·4H_2O$ (0.50 mmol, 121.6 mg) and 4-acetylpyridine (1.00 mmol, 110.1 μL) in water (1.0 mL). After a few days, suitable crystals were obtained. A crystalline powder was prepared from $Mn(NCS)_2$ (1.00 mmol, 171.1 mg) and 4-acetylpyridine (2.00 mmol, 220.3 μL) in water (3 mL), yield 87.3%. $C_{16}H_{18}MnN_4O_4S_2$ (449.41): calcd. C 42.76, H 4.04, N 12.47, S 14.27; found C 42.79, H 4.00, N 12.85, S 14.09. IR (ATR): $\tilde{\nu}_{max}$ = 3324 (m), 3042 (w), 2075 (s), 1681 (s), 1625 (w), 1597 (w), 1557 (m), 1497 (w), 1412 (s), 1326 (w), 1274 (s), 1223 (m), 1090 (w), 1060 (m), 1009 (m), 964 (w), 829 (s), 795 (w), 751 (w), 595 (s), 528 (m), 468 (s), 430 (m) cm^{-1}.

$Fe(NCS)_2$(4-acetylpyridine)$_2(H_2O)_2$ (1-Fe): Crystalline powder was obtained on a large scale by stirring $FeCl_2·4H_2O$ (1.00 mmol, 199 mg), KNCS (2.00 mmol, 194 mg), and 4-acetylpyridine (2.50 mmol, 275 μL) in H_2O (4 mL) for 7 d, yield 85%. $C_{16}H_{18}FeN_4O_4S_2$ (450.32): calcd. C 42.68, H 4.03, N 12.44, S 14.24; found C 42.68, H 4.00, N 12.63, S 14.31. IR (ATR): $\tilde{\nu}_{max}$ = 3326 (b), 3222 (w), 3047 (w), 2081 (s), 1681 (s), 1630 (m), 1557 (m), 1497 (w), 1412 (s), 1362 (s), 1326 (w), 1274 (s), 1225 (m), 1092 (w), 1060 (m), 1011 (m), 964 (m), 831 (s), 595 (s), 471 (s), 432 (m) cm^{-1}.

$Ni(NCS)_2$(4-acetylpyridine)2$(H_2O)_2$ (1-Ni): A crystalline powder was prepared from $Ni(NCS)_2$ (1.00 mmol, 174.9 mg) and 4-acetylpyridine (1.00 mmol, 110.1 μL) in water (5 mL), yield 70.5%. $C_{16}H_{18}N_4NiO_4S_2$ (453.17): calcd. C 42.41, H 4.00, N 12.36, S 14.15; found C 42.48, H 4.03, N 12.73, S 14.15. IR (ATR): $\tilde{\nu}_{max}$ = 3590 (w), 3445 (b), 3326 (b), 2098 (s), 1683 (s), 1643 (w), 1597 (w), 1557 (m), 1498 (w), 1413 (s), 1362 (m), 1277 (s), 1227 (m), 1094 (w), 1060 (m), 1016 (m), 965 (w), 831 (s), 796 (w), 595 (s), 528 (m), 469 (m), 435 (m) cm^{-1}.

$Ni(NCS)_2$(4-acetylpyridine)2$(H_2O)_2·H_2O$ [1-Ni(H_2O)]: Single crystals suitable for single-crystal X-ray diffraction were synthesized from $Ni(NCS)_2$ (0.50 mmol, 87.4 mg) and 4-acetylpyridine (0.25 mmol, 27.5 μL) in water (1.5 mL). After one week, crystals were obtained. IR (ATR): $\tilde{\nu}_{max}$ = 3587 (m), 3445 (m), 3246 (b), 2889 (w), 2097 (s), 1684 (s), 1596 (m), 1557 (m), 1489 (w), 1418 (s), 1361 (m), 1277 (s), 1228 (m), 1094 (w), 1066 (m), 1016 (m), 827 (s), 787 (m), 668 (w), 591 (s), 486 (m) cm^{-1}.

$Ni(NCS)_2$(4-acetylpyridine)4 (2-Ni): Single crystals suitable for single-crystal X-ray diffraction were synthesized from $Ni(NCS)_2$ (0.25 mmol, 43.7 mg) and 4-acetylpyridine (1.00 mmol, 110.1 μL) in water (1.5 mL). After a few weeks, crystals were obtained. A crystalline powder was prepared from $Ni(NCS)_2$ (1.00 mmol, 174.9 mg) and 4-acetylpyridine (5.00 mmol, 605.7 μL) in water (5 mL), yield 75%. $C_{30}H_{28}N_6NiO_4S_2$ (659.41): calcd. C 54.64, H 4.28, N 12.74, S 9.73; found C 54.64, H 4.21, N 12.87, S 9.25. IR (ATR): $\tilde{\nu}_{max}$ = 3045 (w), 2900 (w), 2072 (s), 1694 (s), 1610 (w), 1557 (m), 1413 (m), 1362 (m), 1263 (s), 1225 (m), 1090 (w), 1059 (m), 1014 (m), 964 (m), 831 (s), 802 (m), 664 (w), 592 (s), 483 (m) cm^{-1}.

$[Ni(NCS)_2$(4-acetylpyridine)2$]_n$ (3-Ni/I): A crystalline powder was prepared from $Ni(NCS)_2$ (1.00 mmol, 174.9 mg) and 4-acetylpyr-

Job/Unit: I50473 /KAP1 Date: 10-06-15 18:02:55 Pages: 11

idine (2.00 mmol, 220.3 µL) in ethanol (5 mL), yield 81.1%. $C_{16}H_{14}N_4NiO_2S_2$ (417.14): calcd. C 46.07, H 3.38, N 13.43, S 15.37; found C 45.99, H 3.48, N 13.11, S 14.95. IR (ATR): $\tilde{\nu}_{max}$ = 3122 (w), 3083 (w), 3055 (w), 2116 (s), 1688 (s), 1643 (w), 1610 (w), 1557 (m), 1497 (w), 1413 (s), 1362 (s), 1270 (s), 1226 (m), 1059 (m), 1016 (m), 964 (m), 815 (s), 665 (w), 595 (s), 464 (m), 437 (m) cm^{-1}.

[Fe(NCS)$_2$(4-acetylpyridine)$_2$]$_n$ (3-Fe/II): A crystalline powder was prepared by thermal decomposition of **1**. $C_{16}H_{14}FeN_4O_2S_2$ (414.29): calcd. C 46.39, H 3.41, N 13.52, S 15.48; found C 46.31, H 3.36, N 13.82, S 15.61. IR (ATR): $\tilde{\nu}_{max}$ = 3074 (w), 2876 (w), 2090 (s), 1697 (s), 1610 (w), 1554 (m), 1412 (s), 1361 (s), 1321 (w), 1263 (s), 1216 (m), 1092 (w), 1060 (m), 1014 (m), 971 (w), 819 (s), 593 (s), 472 (s), 432 (m) cm^{-1}.

[Ni(NCS)$_2$(4-acetylpyridine)2]$_n$ (3-Ni/II): A crystalline powder was prepared by thermally annealing **3** for 5 min at 167 °C. $C_{16}H_{14}N_4NiO_2S_2$ (417.14): calcd. C 46.07, H 3.38, N 13.43, S 15.37; found C 45.82, H 3.28, N 13.79, S 14.70. IR (ATR): $\tilde{\nu}_{max}$ = 3104 (w), 3081 (w), 2899 (w), 2109 (s), 1697 (s), 1643 (w), 1609 (w), 1555 (m), 1410 (m), 1359 (m), 1322 (w), 1266 (s), 1215 (m), 1062 (m), 1015 (m), 971 (m), 817 (s), 785 (m), 665 (w), 593 (s), 478 (m), 434 (m) cm^{-1}.

Elemental Analysis: CHNS analysis was performed with a EURO EA elemental analyzer, fabricated by EURO VECTOR Instruments and Software.

Spectroscopy: All IR data were obtained with an ATI Mattson Genesis Series FTIR Spectrometer, and WINFIRST from ATI Mattson was used as the control software.

X-Ray Powder Diffraction (XRPD): The measurements were performed with (1) a PANalytical X'Pert Pro MPD Reflection Powder Diffraction System with Cu-K_α radiation equipped with a PIXcel semiconductor detector from PANalytical and (2) a Stoe Transmission Powder Diffraction System (STADI P) with Cu-K_α radiation equipped with a MYTHEN 1K detector.

For the refinement of the crystal structure of the 2D isomer of **3**-Ni/I X-ray powder patterns were collected at the European Synchrotron Radiation Facility (ESRF) at the ID31 High-Resolution Powder Diffraction Beamline with wavelength of 0.40000 by using a crystal analyzer detector at room temperature. Unfortunately, we did not have sufficient beamtime to analyze the samples of **1**-Ni and the 1D isomer of **3**-Fe/II. Therefore, the powder pattern for **1**-Ni was collected with a Stoe Stadi-P powder diffractometer [Mo-$K_{\alpha1}$ radiation from primary Ge(111) Johannson-type monochromator and a Mythen Dectris 1K detector]. For **3**-Fe/II, the powder pattern was collected with a Bruker D8 Advance powder diffractometer [Cu-$K_{\alpha1}$ radiation from primary Ge(111) Johannson-type monochromator, V ntag-1 position-sensitive detector (PSD) with an opening angle of 6° in Debye–Scherrer geometry]. All powdered samples were sealed in borosilicate glass capillaries (0.5 mm diameter Hilgenberg glass capillary No. 50), which were spun during the measurement for better data statistics. For the synchrotron measurements, the data collection time was 1 h, whereas it was 24 h for both laboratory measurements.

The Rietveld refinements[84] were performed with the program TOPAS 4.2.[85] During the refinements the lattice parameters, zero-error, and restrained atomic positions were refined. Chebyshev

Table 1. Selected crystal data and details on the structure refinements. Please note that the structures of **1**-Ni, **3**-Ni/I, and **3**-Fe/II were determined by Rietveld refinements.

	1-Mn	**1**-Ni(H_2O)	**2**-Ni	**1**-Ni	**3**-Ni/I	**3**-Fe/II
Formula	$C_{16}H_{18}MnN_4O_4S_2$	$C_{16}H_{22}N_4NiO_6S_2$	$C_{30}H_{28}N_6NiO_4S_2$	$C_{16}H_{18}NiN_4O_4S_2$	$C_{16}H_{14}NiN_4O_2S_2$	$C_{16}H_{14}FeN_4O_2S_2$
MW /gmol^{-1}	449.40	489.21	659.41	453.16	417.13	414.28
Crystal system	monoclinic	monoclinic	orthorhombic	monoclinic	orthorhombic	triclinic
Space group	$P2_1/n$	$P2_1/n$	$Pbca$	$P2_1/n$	$Pbca$	$P\bar{1}$
a /	6.3979(3)	11.8241(7)	11.883(2)	6.3513(3)	9.502(1)	5.677(3)
b /	16.3809(9)	7.3861(4)	16.005(3)	16.2750(9)	15.713(2)	8.406(4)
c /	10.5372(5)	12.7217(9)	34.104(7)	10.3864(5)	24.320(3)	10.442(8)
α /°	90	90	90	90	90	78.37(3)
β /°	107.700(4)	107.361(8)	90	108.939(3)	90	86.53(4)
γ /°	90	90	90	90	90	71.58(5)
V / ^{3}	1052.06(9)	1060.42(11)	6486(2)	1015.5(9)	3631.0(8)	463.1(5)
T /K	293(2)	200(2)	293(2)	293	293	293
Z	2	2	8	4	8	1
$D_{calcd.}$ /mgm^3	1.419	1.532	1.351	1.423	1.526	1.435
μ /mm^{-1}	0.853	1.151	0.770	–	–	–
Reflections collected	17597	8691	31063	–	–	–
Unique reflections	2515	2422	6058	–	–	–
R_{int}	0.0446	0.0677	0.0966	–	–	–
Reflections [$F_o > 4\sigma(F_o)$]	2515	1940	3557	–	–	–
Parameters	125	135	392	56	149	74
R_1 [$F_o > 4\sigma(F_o)$]	0.0456	0.0387	0.0769	–	–	–
R_{wp} /% [a]	–	–	–	7.91	22.94	7.92
R_p /% [a]	–	–	–	8.51	24.49	10.32
R_{exp} /% [a]	–	–	–	0.25	19.48	0.12
R_{Bragg} /%	–	–	–	1.79	5.66	0.30
wR_2	0.1104	0.0944	0.1311	–	–	–
GOF [a]	1.136	1.031	1.154	0.93	1.18	0.76
$\Delta\rho_{max./min.}$ /e $^{-3}$	0.197 //0.315	0.535 //0.881	0.223 //0.256	–	–	–

[a] Background-corrected values. The lower R_{wp} value compared to R_p is attributed to an inappropriate weighting scheme for data collected with position-sensitive detectors.

Job/Unit: I50473 /KAP1 Date: 10-06-15 18:02:55 Pages: 11

polynomials were used to model the background. The apparent microstrain in the structures (especially for **3**-Fe/II) caused strong anisotropy of width and asymmetry of the Bragg reflections, which was successfully modeled by applying symmetry-adapted spherical harmonics of eighth order to Gaussian, Lorentzian, and exponential distributions, which were then convoluted with geometrical and instrumental contributions to the final peak profiles. The final Rietveld plots of **1**-Ni, **3**-Fe/II, and **3**-Ni/I are given in Figures S39, S40, and S41, and the crystallographic details are given in Table 1. Data on the crystal structures solved from powder diffraction can be obtained free charge from the Cambridge Crystallographic Data Centre via http://www.ccdc.cam.ac.uk/data_request/cif.

Differential Thermal Analysis and Thermogravimetry (DTA-TG-MS): The heating-rate-dependent DTA-TG measurements were performed in a nitrogen atmosphere (purity: 5.0) in Al_2O_3 crucibles by using an STA-409CD instrument from Netzsch. All measurements were performed with a flow rate of 75 mL min^{-1} and were corrected for buoyancy and current effects. The instrument was calibrated by using standard reference materials.

Magnetic Measurements: All magnetic measurements were performed with a Physical Property Measurement System (PPMS) from Quantum Design, which was equipped with a 9 T magnet. The data were corrected for core diamagnetism.

Single-Crystal Structure Analyses: Single-crystal data collections were performed with imaging plate diffraction systems: Stoe IPDS-1 for **2** and Stoe IPDS-2 for **1** with Mo-K_α radiation (λ = 71.073 pm). The structures were solved by direct methods with SHELXS-97, and structure refinements were performed against F^2 with SHELXL-97.[86] Numerical absorption corrections were applied by using the programs X-RED and X-SHAPE of the program package X-Area.[87–89] All non-hydrogen atoms were refined with anisotropic displacement parameters. All hydrogen atoms were positioned with idealized geometries and refined isotropically with U_{iso}(H) = 1.2U_{eq}(C) (1.5 for methyl H atoms) by using a riding model. The O–H hydrogen atoms were located in a difference map, their bond lengths were set to ideal values, and finally they were refined by using a riding model with U_{iso}(H) = 1.5U_{eq}(O). Selected crystal data and details on the structure refinement are given in Table 1. CCDC-1062598 (for **1**-Mn), -1062599 [for **1**-Ni(H_2O)], and -1062597 (for **2**-Ni) contain the supplementary crystallographic data for this paper. These data can be obtained free of charge from The Cambridge Crystallographic Data Centre via www.ccdc.cam.ac.uk/data_request/cif.

Acknowledgments

This project was supported by the Deutsche Forschungsgemeinschaft (DFG) (project number Na 720/5-1) and the Federate State of Schleswig-Holstein, Germany. The authors thank Prof. Dr. Wolfgang Bensch for access to his experimental facilities. Special thanks to Inke Jess for the single crystal and to Maren Rasmussen and Henning L hmann for some magnetic measurements.

[1] J. Tao, R.-J. Wei, R.-B. Huang, L.-S. Zheng, *Chem. Soc. Rev.* **2012**, *41*, 703–737.
[2] G. S. Matouzenko, E. Jeanneau, A. Y. Verat, Y. de Gaetano, *Eur. J. Inorg. Chem.* **2012**, 969–977.
[3] C. Janiak, *Dalton Trans.* **2003**, 2781–2804.
[4] E. V. Peresypkina, A. M. Majcher, M. Rams, K. E. Vostrikova, *Chem. Commun.* **2014**, *50*, 7150–7153.
[5] W.-X. Zhang, R. Ishikawa, B. Breedlovea, M. Yamashita, *RSC Adv.* **2013**, *3*, 3772–3798.
[6] C. N ther, S. W hlert, J. Boeckmann, M. Wriedt, I. Jeß, *Z. Anorg. Allg. Chem.* **2013**, *639*, 2696–2714.
[7] D.-F. Weng, Z.-M. Wang, S. Gao, *Chem. Soc. Rev.* **2011**, *40*, 3157–3181.
[8] M. Murrie, *Chem. Soc. Rev.* **2010**, *39*, 1986–1995.
[9] P. Dechambenoit, J. R. Long, *Chem. Soc. Rev.* **2011**, *40*, 3249–3265.
[10] G. Aromi, D. Aguila, P. Gamez, F. Luis, O. Roubeau, *Chem. Soc. Rev.* **2012**, *41*, 537–546.
[11] M. Kurmoo, *Chem. Soc. Rev.* **2009**, *38*, 1353–1379.
[12] L. Bogani, A. Vindigni, R. Sessoli, D. Gatteschi, *J. Mater. Chem.* **2008**, *18*, 4750–4758.
[13] Z. Tomkowicz, M. Rams, M. Bałanda, S. Foro, H. Nojiri, Y. Krupskaya, V. Kataev, B. B chner, S. K. Nayak, J. V. Yakhmi, W. Haase, *Inorg. Chem.* **2012**, *51*, 9983–9994.
[14] M. Bałanda, Z. Tomkowicz, W. Haase, M. Rams, *J. Phys. Conf., Ser.* **2010**, *303*, 012036.
[15] J. Ferrando-Soria, R. Ruiz-Garc a, J. Cano, S.-E. Stiriba, J. Vallejo, I. Castro, M. Julve, F. Lloret, P. Amor s, J. Pas n, C. Ruiz-P rez, Y. Journaux, E. Pardo, *Chem. Eur. J.* **2012**, *18*, 1608–1617.
[16] R. Lescou zec, L. M. Toma, J. Vaissermann, M. Verdaguer, F. S. Delgado, C. Ruiz-P rez, F. Lloret, M. Julve, *Coord. Chem. Rev.* **2005**, *249*, 2691–2729.
[17] P. Bhowmik, S. Biswas, S. Chattopadhyay, C. Diaz, C. J. Gomez-Garcia, A. Ghosh, *Dalton Trans.* **2014**, *43*, 12414–12421.
[18] G. Bhargavi, M. V. Rajasekharan, J. P. Costes, J. P. Tuchagues, *Dalton Trans.* **2013**, *42*, 8113–8123.
[19] J.-P. Zhao, R. Zhao, Q. Yang, W.-C. Song, B.-W. Hu, X.-F. Zhang, X.-H. Bu, *Dalton Trans.* **2012**, *41*, 4852–4858.
[20] S. Naiya, S. Biswas, M. G. B. Drew, C. J. G mez-Garc a, A. Ghosh, *Inorg. Chem.* **2012**, *51*, 5332–5341.
[21] A. Escuer, G. Vlahopoulou, F. A. Mautner, *Inorg. Chem.* **2011**, *50*, 2717–2719.
[22] Z.-X. Li, Y.-F. Zeng, H. Ma, X.-H. Bu, *Chem. Commun.* **2010**, *46*, 8540–8542.
[23] D. Zhang, Y. Bian, J. Qin, P. Wang, X. Chen, *Dalton Trans.* **2014**, *43*, 945–949.
[24] D. Zhang, Z. Zhao, P. Wang, Z. Ni, *CrystEngComm* **2013**, *15*, 2504–2511.
[25] X. Chen, S.-Q. Wu, A.-L. Cui, H.-Z. Kou, *Chem. Commun.* **2014**, *50*, 2120–2122.
[26] Y.-F. Zeng, X. Hu, F.-C. Liu, X.-H. Bu, *Chem. Soc. Rev.* **2009**, *38*, 469–480.
[27] D. Maspoch, D. Ruiz-Molina, J. Veciana, *Chem. Soc. Rev.* **2007**, *36*, 770–818.
[28] T. Liu, H. Zheng, S. Kang, Y. Shiota, S. Hayami, M. Mito, O. Sato, K. Yoshizawa, S. Kanegawa, C. Duan, *Nat. Commun.* **2013**, *4*, 1–7.
[29] H. Miyasaka, T. Madanbashi, A. Saitoh, N. Motokawa, R. Ishikawa, M. Yamashita, S. Bahr, W. Wernsdorfer, R. Cl rac, *Chem. Eur. J.* **2012**, *18*, 3942–3954.
[30] S. Banerjee, B. Wu, P.-G. Lassahn, C. Janiak, A. Ghosh, *Inorg. Chim. Acta* **2005**, *358*, 535–544.
[31] A. Tahli, J. K. Maclaren, I. Boldog, C. Janiak, *Inorg. Chim. Acta* **2011**, *374*, 506–513.
[32] F. Mautner, F. Louka, A. Gallo, J. Albering, M. Saber, N. Burham, S. Massoud, *Transition Met. Chem.* **2010**, *35*, 613–619.
[33] S. S. Massoud, L. L. Quan, K. Gatterer, J. H. Albering, R. C. Fischer, F. A. Mautner, *Polyhedron* **2012**, *31*, 601–606.
[34] F. A. Mautner, M. Scherzer, C. Berger, R. C. Fischer, S. S. Massoud, *Inorg. Chim. Acta* **2015**, *425*, 46–51.
[35] E. Shurdha, C. E. Moore, A. L. Rheingold, S. H. Lapidus, P. W. Stephens, A. M. Arif, J. S. Miller, *Inorg. Chem.* **2013**, *52*, 10583–10594.
[36] E. Shurdha, S. H. Lapidus, P. W. Stephens, C. E. Moore, A. L. Rheingold, J. S. Miller, *Inorg. Chem.* **2012**, *51*, 9655–9665.

Job/Unit: I50473 /KAP1 Date: 10-06-15 18:02:55 Pages: 11

[37] I. N. B. Machura, K. Michalik, *Polyhedron* **2011**, *30*, 2619–2626.
[38] J. G. Małecki, T. Groń, H. Duda, *Polyhedron* **2012**, *36*, 56–68.
[39] R. Gonz lez, A. Acosta, R. Chiozzone, C. Kremer, D. Armentano, G. De Munno, M. Julve, F. Lloret, J. Faus, *Inorg. Chem.* **2012**, *51*, 5737–5747.
[40] B. Machura, A. Świtlicka, P. Zwoliński, J. Mroziński, B. Kalińska, R. Kruszynski, *J. Solid State Chem.* **2013**, *197*, 218–227.
[41] B. Machura, A. Świtlicka, J. Mroziński, B. Kalińska, R. Kruszynski, *Polyhedron* **2013**, *52*, 1276–1286.
[42] B. Machura, J. Palion, M. Penkala, T. Groń, H. Duda, R. Kruszynski, *Polyhedron* **2013**, *56*, 189–199.
[43] P. Bhowmik, S. Chattopadhyay, M. G. B. Drew, C. Diaz, A. Ghosh, *Polyhedron* **2010**, *29*, 2637–2642.
[44] M. Mousavi, V. Bereau, C. Duhayon, P. Guionneau, J.-P. Sutter, *Chem. Commun.* **2012**, *48*, 10028–10030.
[45] M. Wriedt, S. Sellmer, C. N ther, *Dalton Trans.* **2009**, 7975–7984.
[46] M. Wriedt, I. Jeß, C. N ther, *Eur. J. Inorg. Chem.* **2009**, 1406–1413.
[47] S. H. Lapidus, P. W. Stephens, E. Shurdha, J. G. DaSilva, J. S. Miller, *Polyhedron* **2013**, *52*, 713–718.
[48] J. G. Małecki, B. Machura, A. Świtlicka, T. Groń, M. Bałanda, *Polyhedron* **2011**, *30*, 746–753.
[49] R. Vicente, A. Escuer, J. Ribas, X. Solans, M. Font-Bardia, *Inorg. Chem.* **1993**, *32*, 6117–6118.
[50] J. Boeckmann, M. Wriedt, C. N ther, *Chem. Eur. J.* **2012**, *18*, 5284–5289.
[51] M. Wriedt, C. N ther, *Chem. Commun.* **2010**, *46*, 4707–4709.
[52] J.-Q. Tao, Z.-G. Gu, T.-W. Wang, Q.-F. Yang, J.-L. Zuo, X.-Z. You, *Inorg. Chim. Acta* **2007**, *360*, 4125–4132.
[53] S.-L. Li, J.-Y. Wu, Y.-P. Tian, H. Ming, P. Wang, M.-H. Jiang, H.-K. Fun, *Eur. J. Inorg. Chem.* **2006**, 2900–2907.
[54] T. K. Maji, G. Mostafa, P. S. Mukherjee, A. Mondal, A. J. Welch, K. Okamoto, N. R. Chaudhuri, *Polyhedron* **2000**, *19*, 1903–1907.
[55] C. J. Adams, M. F. Haddow, D. J. Harding, T. J. Podesta, R. E. Waddington, *CrystEngComm* **2011**, *13*, 4909–4914.
[56] J. Boeckmann, C. N ther, *Dalton Trans.* **2010**, *39*, 11019–11026.
[57] J. Boeckmann, C. N ther, *Polyhedron* **2012**, *31*, 587–595.
[58] S. W hlert, J. Boeckmann, M. Wriedt, C. N ther, *Angew. Chem. Int. Ed.* **2011**, *50*, 6920–6923; *Angew. Chem.* **2011**, *123*, 7053.
[59] S. W hlert, U. Ruschewitz, C. N ther, *Cryst. Growth Des.* **2012**, *12*, 2715–2718.
[60] S. W hlert, T. Runčevski, R. E. Dinnebier, S. G. Ebbinghaus, C. N ther, *Cryst. Growth Des.* **2014**, *14*, 1902–1913.
[61] S. W hlert, Z. Tomkowicz, M. Rams, S. G. Ebbinghaus, L. Fink, M. U. Schmidt, C. N ther, *Inorg. Chem.* **2014**, *53*, 8298–8310.
[62] J. Werner, M. Rams, Z. Tomkowicz, C. N ther, *Dalton Trans.* **2014**, *43*, 17333–17342.
[63] S. W hlert, M. Wriedt, T. Fic, Z. Tomkowicz, W. Haase, C. N ther, *Inorg. Chem.* **2013**, *52*, 1061–1068.
[64] S. W hlert, J. Boeckmann, I. Jess, C. N ther, *CrystEngComm* **2012**, *14*, 5412–5420.
[65] S. W hlert, C. N ther, *Eur. J. Inorg. Chem.* **2013**, 2528–2537.
[66] S. W hlert, L. Fink, M. Schmidt, C. N ther, *CrystEngComm* **2013**, *15*, 945–957.
[67] M. R. J. Werner, Z. Tomkowicz, T. Runčevski, R. E. Dinnebier, S. Suckert, C. N ther, *Inorg. Chem.* **2015**, *54*, 2893.
[68] D. Braga, F. Grepioni, *Chem. Soc. Rev.* **2000**, *29*, 229–238.
[69] T. L. Hennigar, D. C. MacQuarrie, P. Losier, R. D. Rogers, M. J. Zaworotko, *Angew. Chem. Int. Ed. Engl.* **1997**, *36*, 972–973; *Angew. Chem.* **1997**, *109*, 1044.
[70] S. A. Barnett, A. J. Blake, N. R. Champness, C. Wilson, *Chem. Commun.* **2002**, 1640–1641.
[71] D. Braga, M. Curzi, F. Grepioni, M. Polito, *Chem. Commun.* **2005**, 2915–2917.
[72] B. Moulton, M. J. Zaworotko, *Chem. Rev.* **2001**, *101*, 1629–1658.
[73] D. M. Shin, I. S. Lee, D. Cho, Y. K. Chung, *Inorg. Chem.* **2003**, *42*, 7722–7724.
[74] P. Jensen, S. R. Batten, B. Moubaraki, K. S. Murray, *J. Solid State Chem.* **2001**, *159*, 352–361.
[75] C. N ther, G. Bhosekar, I. Jeß, *Inorg. Chem.* **2007**, *46*, 8079–8087.
[76] C. N ther, I. Jeß, N. Lehnert, D. Hinz-H bner, *Solid State Sci.* **2003**, *5*, 1343–1357.
[77] G. J. Long, G. Galeazzi, U. Russo, G. Valle, S. Calogero, *Inorg. Chem.* **1983**, *22*, 507–510.
[78] J. Werner, I. Jeß, C. N ther, *Z. Naturforsch. B* **2013**, *68*, 643–652.
[79] C. N ther, I. Jeß, *J. Solid State Chem.* **2002**, *169*, 103–112.
[80] S. Foner, R. B. Frankel, J. E. J. McNiff, W. M. Reiff, B. F. Little, G. J. Long, *AIP Conf. Proc.* **1975**, *24*, 363–364.
[81] S. Foner, R. B. Frankel, W. M. Reiff, H. Wong, G. J. Long, *J. Chem. Phys.* **1978**, *68*, 4781–4783.
[82] S. Foner, R. B. Frankel, W. M. Reiff, B. F. Little, G. J. Long, *Solid State Commun.* **1975**, *16*, 159–161.
[83] S. W hlert, L. Fink, M. Schmidt, C. N ther, *Z. Anorg. Allg. Chem.* **2013**, *639*, 2186–2194.
[84] H. M. Rietveld, *J. Appl. Crystallogr.* **1969**, *2*, 65–71.
[85] *TOPAS*, v. 4.2, Bruker AXS, Karlsruhe, Germany, **2007**.
[86] G. M. Sheldrick, *Acta Crystallogr., Sect. A* **2008**, *64*, 112–122.
[87] *X-Red*, v. 1.11, *Program for Data Reduction and Absorption Correction*, STOE & CIE GmbH, Darmstadt, Germany, **1998**.
[88] *X-Shape*, v. 1.03, *Program for the Crystal Optimization for Numerical Absorption Correction*, STOE & CIE GmbH, Darmstadt, Germany, **1998**.
[89] *X-Area*, v. 1.44, *Program Package for Single Crystal Measurements*, STOE & CIE GmbH, Darmstadt, Germany, **2008**.

Received: April 30, 2015
Published Online: ■

Job/Unit: I50473 /KAP1 Date: 10-06-15 18:02:55 Pages: 11

Thiocyanato Coordination Polymers

Keywords: Coordination polymers / N ligands / Structure elucidation / Thermal properties / Magnetic properties

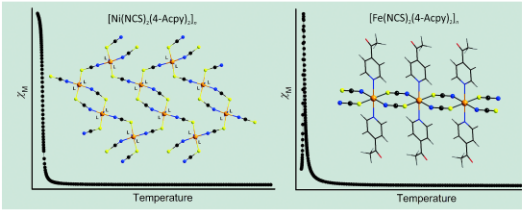

Thiocyanato coordination polymers of composition $M(NCS)_2(4\text{-acetylpyridine})_2$ (M = Mn, Fe, and Ni) are prepared, and their magnetic properties are investigated. Depending on the synthesis conditions and the nature of the metal cation, compounds with 1D or 2D coordination networks are obtained.

4.3. Bis(4-acetylpyridine-κ*N*)bis(ethanol-κ*O*)bis(thiocyanato-κ*N*)-manganese(II)

Julia Werner, Inke Jess und Christian Näther, *Acta Crystallogr. E* **2015**, *E71*, m81-m82.

DOI:10.1107/S2056989015004533

Motivation

Diese Arbeit entstand im Rahmen der systematischen Untersuchung von Übergangsmetallthiocyanaten mit dem Ligand 4-Acetylpyridin. Da es nicht möglich war diese Verbindung in größerem Maßstab herzustellen, eignete sie sich nicht für weitere analytische Untersuchungen und wurde aufgrund ihrer untergeordneten Bedeutung für diese Arbeit in Form einer Strukturmitteilung bei Acta Crystallographica E veröffentlicht.

CrossMark

data reports

Acta Cryst E CRYSTALLOGRAPHIC COMMUNICATIONS

OPEN ACCESS

ISSN 2056-9890

Crystal structure of bis(4-acetylpyridine-κN)bis(ethanol-κO)bis(thiocyanato-κN)-manganese(II)

Julia Werner,* Inke Jess and Christian Näther

Institut für Anorganische Chemie, Christian-Albrechts-Universität Kiel, Max-Eyth-Strasse 2, 24118 Kiel, Germany. *Correspondence e-mail: jwerner@ac.uni-kiel.de

Received 24 February 2015; accepted 4 March 2015

Edited by M. Weil, Vienna University of Technology, Austria

In the crystal structure of the title compound, $[Mn(NCS)_2(C_7H_7NO)_2(C_2H_5OH)_2]$, the Mn^{II} atom is coordinated by two *N*-bonded thiocyanate anions, two 4-acetylpyridine ligands, and two ethanol molecules within a slightly distorted octahedron. The asymmetric unit consits of one manganese cation, located on a centre of inversion, one thiocyanate anion, one 4-acetylpyridine ligand and one ethanol molecule in general positions. The discrete complexes are connected by intermolecular O—H···O hydrogen bonds between the alcohol OH group and the carbonyl O atom into chains parallel to [011].

Keywords: crystal structure; manganese(II); octahedral coordination; hydrogen bonding.

CCDC reference: 1052202

1. Related literature

For a similar structure with thiocyanato ligands in terminal coordination to a manganese(II) atom, see: Li *et al.* (2007).

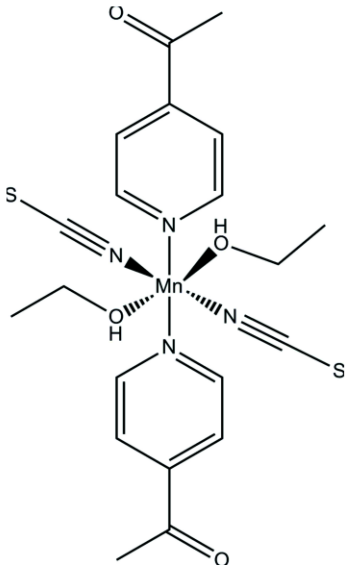

2. Experimental

2.1. Crystal data

$[Mn(NCS)_2(C_7H_7NO)_2(C_2H_6O)_2]$
M_r = 505.51
Triclinic, $P\overline{1}$
a = 6.9547 (7) Å
b = 9.7733 (9) Å
c = 10.1859 (9) Å
α = 117.449 (10)°
β = 94.978 (11)°
γ = 93.379 (11)°
V = 608.23 (11) Å^3
Z = 1
Mo $K\alpha$ radiation
μ = 0.75 mm^{-1}
T = 200 K
0.04 × 0.03 × 0.02 mm

2.2. Data collection

Stoe IPDS-1 diffractometer
Absorption correction: numerical (*X-SHAPE* and *X-RED32*; Stoe & Cie, 2008)
T_{min} = 0.966, T_{max} = 0.977
6535 measured reflections
2583 independent reflections
2163 reflections with $I > 2\sigma(I)$
R_{int} = 0.039

2.3. Refinement

$R[F^2 > 2\sigma(F^2)]$ = 0.033
$wR(F^2)$ = 0.088
S = 1.04
2583 reflections
144 parameters
H-atom parameters constrained
$\Delta\rho_{max}$ = 0.26 e Å^{-3}
$\Delta\rho_{min}$ = −0.35 e Å^{-3}

Table 1
Hydrogen-bond geometry (Å, °).

D—H···A	D—H	H···A	D···A	D—H···A
O21—H1*O*1···O11^{i}	0.84	1.95	2.7714 (17)	164

Symmetry code: (i) $x, y+1, z+1$.

Data collection: *X-AREA* (Stoe & Cie, 2008); cell refinement: *X-AREA*; data reduction: *X-AREA*; program(s) used to solve structure: *SHELXS97* (Sheldrick, 2008); program(s) used to refine structure:

SHELXL2013 (Sheldrick, 2015); molecular graphics: *XP* in *SHELXTL* (Sheldrick, 2008) and *DIAMOND* (Brandenburg, 1999); software used to prepare material for publication: *publCIF* (Westrip, 2010).

Acknowledgements

We gratefully acknowledge financial support by the State of Schleswig–Holstein. We thank Professor Dr Wolfgang Bensch for access to his experimental facilities.

Supporting information for this paper is available from the IUCr electronic archives (Reference: WM5131).

References

Brandenburg, K. (1999). *DIAMOND*. Crystal Impact GbR, Bonn, Germany.
Li, H., Li, C.-J. & Hu, Z.-Q. (2007). *Acta Cryst.* E**63**, m407–m408.
Sheldrick, G. M. (2008). *Acta Cryst.* A**64**, 112–122.
Sheldrick, G. M. (2015). *Acta Cryst.* C**71**, 3–8.
Stoe & Cie (2008). *X-AREA*, *X-RED32* and *X-SHAPE*. Stoe & Cie, Darmstadt, Germany.
Westrip, S. P. (2010). *J. Appl. Cryst.* **43**, 920–925.

supporting information

Acta Cryst. (2015). E**71**, m81–m82 [doi:10.1107/S2056989015004533]

Crystal structure of bis(4-acetylpyridine-κN)bis(ethanol-κO)bis(thiocyanato-κN)manganese(II)

Julia Werner, Inke Jess and Christian Näther

S1. Synthesis and crystallization

$MnSO_4 \cdot H_2O$ was purchased from Merck; 4-acetylpyridine and $Ba(NCS)_2 \cdot 3H_2O$ were purchased from Alfa Aesar. $Mn(NCS)_2$ was synthesized by stirring 17.97 g (58.44 mmol) $Ba(NCS)_2 \cdot 3H_2O$ and 9.88 g (58.44 mmol) $MnSO_4 \cdot H_2O$ in 400 ml water at room temperature for three hours. The white residue of $BaSO_4$ was filtered off and the solvent evaporated using a rotary evaporator. The homogeneity of the product was investigated by X-ray powder diffraction and elemental analysis. The title compound was prepared by the reaction of 42.8 mg (0.25 mmol) $Mn(NCS)_2$ and 55.1 μl (0.50 mmol) 4-acetylpyridine in 1.5 ml ethanol at room temperature. After several days, suitable crystals of the title compound were obtained.

S2. Refinement

The C-bound H atoms were positioned with idealized geometry (methyl H atoms allowed to rotate but not to tip) and were refined with U_{iso}(H) = 1.2U_{eq}(C) (1.5 for methyl H atoms) using a riding model with C—H = 0.95 Å for aromatic, C—H = 0.99 Å for methylene and C—H = 0.98 Å for methyl H atoms. The O-bound H atom was located in a difference map. Its bond length was set to a value of 0.84 Å and it was refined with U_{iso}(H) = 1.5U_{eq}(O) using a riding model.

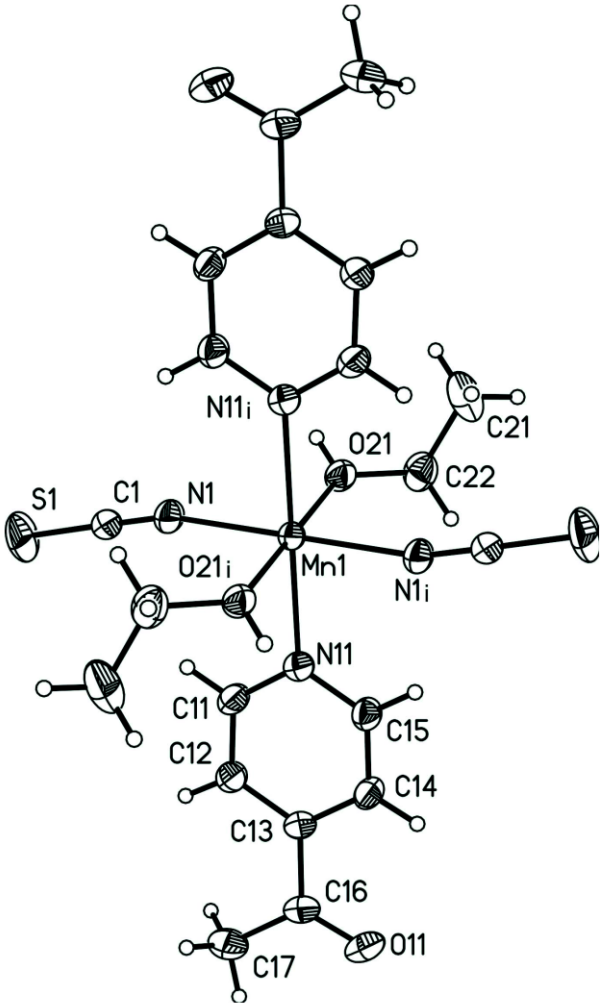

Figure 1

The coordination environment of the Mn^{II} atom in the title compound. Displacement ellipsoids are drawn at the 50% probability level. [Symmetry code: (i) $-x + 2, -y + 1, -z + 1$.]

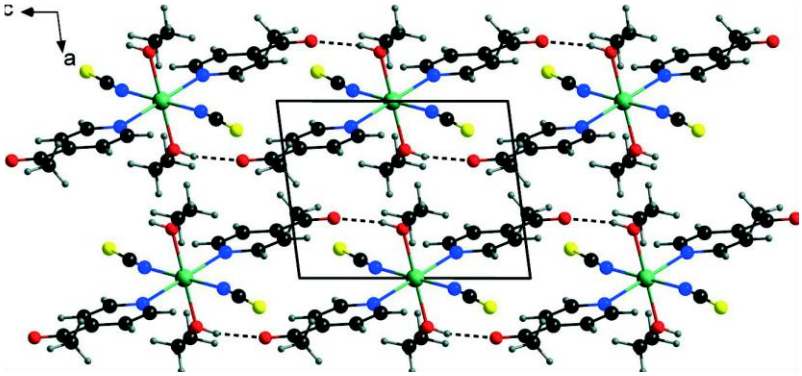

Figure 2

Crystal structure of the title compound in a view along [010]. Hydrogen bonds are indicated by dashed lines.

Bis(ethanol-κO)bis[1-(pyridin-4-yl)ethan-1-one-\ κN]bis(thiocyanato-κN)manganese(II)

Crystal data

$[Mn(NCS)_2(C_7H_7NO)_2(C_2H_6O)_2]$
$M_r = 505.51$
Triclinic, $P\overline{1}$
$a = 6.9547\ (7)$ Å
$b = 9.7733\ (9)$ Å
$c = 10.1859\ (9)$ Å
$\alpha = 117.449\ (10)°$
$\beta = 94.978\ (11)°$
$\gamma = 93.379\ (11)°$
$V = 608.23\ (11)$ Å^3
$Z = 1$
$F(000) = 263$
$D_x = 1.380$ Mg m^{-3}
Mo $K\alpha$ radiation, $\lambda = 0.71073$ Å
Cell parameters from 6535 reflections
$\theta = 2.4–27.0°$
$\mu = 0.75$ mm^{-1}
$T = 200$ K
Block, colorless
0.04 × 0.03 × 0.02 mm

Data collection

Stoe IPDS-1 diffractometer
phi scans
Absorption correction: numerical (*X-SHAPE* and *X-RED32*; Stoe & Cie, 2008)
$T_{min} = 0.966$, $T_{max} = 0.977$
6535 measured reflections
2583 independent reflections
2163 reflections with $I > 2\sigma(I)$
$R_{int} = 0.039$
$\theta_{max} = 27.0°$, $\theta_{min} = 2.4°$
$h = -8\rightarrow8$
$k = -12\rightarrow12$
$l = -13\rightarrow13$

Refinement

Refinement on F^2
Least-squares matrix: full
$R[F^2 > 2\sigma(F^2)] = 0.033$
$wR(F^2) = 0.088$
$S = 1.04$
2583 reflections
144 parameters
0 restraints
Hydrogen site location: mixed
H-atom parameters constrained
$w = 1/[\sigma^2(F_o^2) + (0.0565P)^2]$ where $P = (F_o^2 + 2F_c^2)/3$
$(\Delta/\sigma)_{max} < 0.001$
$\Delta\rho_{max} = 0.26$ e Å^{-3}
$\Delta\rho_{min} = -0.35$ e Å^{-3}
Extinction correction: *SHELXL2013* (Sheldrick, 2015), $Fc^*=kFc[1+0.001xFc^2\lambda^3/\sin(2\theta)]^{-1/4}$
Extinction coefficient: 0.069 (8)

supporting information

Special details

Geometry. All esds (except the esd in the dihedral angle between two l.s. planes) are estimated using the full covariance matrix. The cell esds are taken into account individually in the estimation of esds in distances, angles and torsion angles; correlations between esds in cell parameters are only used when they are defined by crystal symmetry. An approximate (isotropic) treatment of cell esds is used for estimating esds involving l.s. planes.

Fractional atomic coordinates and isotropic or equivalent isotropic displacement parameters (Å²)

	x	*y*	*z*	U_{iso}*/U_{eq}
Mn1	1.0000	0.5000	0.5000	0.02081 (14)
N1	0.9402 (2)	0.42929 (18)	0.66517 (15)	0.0300 (3)
C1	0.8976 (2)	0.35987 (19)	0.72660 (17)	0.0245 (3)
S1	0.83508 (10)	0.25963 (7)	0.80913 (7)	0.05345 (19)
N11	0.8542 (2)	0.25989 (15)	0.30663 (15)	0.0250 (3)
C11	0.8030 (3)	0.1414 (2)	0.33223 (19)	0.0339 (4)
H11	0.8081	0.1609	0.4329	0.041*
C12	0.7431 (3)	−0.0080 (2)	0.22080 (19)	0.0338 (4)
H12	0.7099	−0.0886	0.2451	0.041*
C13	0.7325 (2)	−0.03842 (18)	0.07316 (17)	0.0241 (3)
C14	0.7813 (3)	0.0837 (2)	0.04487 (18)	0.0276 (4)
H14	0.7738	0.0676	−0.0549	0.033*
C15	0.8413 (3)	0.2296 (2)	0.16300 (18)	0.0278 (4)
H15	0.8749	0.3123	0.1417	0.033*
C16	0.6741 (3)	−0.19848 (19)	−0.05499 (18)	0.0285 (4)
C17	0.6365 (3)	−0.3314 (2)	−0.0243 (2)	0.0417 (5)
H17A	0.6077	−0.4275	−0.1188	0.063*
H17B	0.5254	−0.3158	0.0322	0.063*
H17C	0.7515	−0.3384	0.0341	0.063*
O11	0.6621 (2)	−0.21465 (16)	−0.18155 (14)	0.0409 (3)
C21	0.6624 (4)	0.8271 (3)	0.4935 (3)	0.0549 (6)
H21A	0.5856	0.8597	0.4296	0.082*
H21B	0.6313	0.8831	0.5958	0.082*
H21C	0.8010	0.8504	0.4921	0.082*
C22	0.6154 (3)	0.6558 (2)	0.4366 (2)	0.0367 (4)
H22A	0.4748	0.6326	0.4363	0.044*
H22B	0.6445	0.5999	0.3325	0.044*
O21	0.72349 (18)	0.60072 (14)	0.52571 (12)	0.0291 (3)
H1O1	0.6854	0.6446	0.6101	0.044*

Atomic displacement parameters (Å²)

	U^{11}	U^{22}	U^{33}	U^{12}	U^{13}	U^{23}
Mn1	0.0266 (2)	0.01896 (19)	0.01844 (18)	0.00180 (12)	0.00503 (13)	0.00984 (14)
N1	0.0409 (9)	0.0290 (7)	0.0236 (7)	0.0005 (6)	0.0079 (6)	0.0150 (6)
C1	0.0280 (8)	0.0232 (7)	0.0217 (7)	0.0021 (6)	0.0039 (6)	0.0099 (6)
S1	0.0678 (4)	0.0535 (4)	0.0652 (4)	0.0037 (3)	0.0157 (3)	0.0489 (3)
N11	0.0295 (7)	0.0219 (7)	0.0220 (6)	0.0014 (5)	0.0027 (5)	0.0091 (6)
C11	0.0525 (12)	0.0266 (8)	0.0206 (7)	−0.0014 (8)	0.0051 (7)	0.0099 (7)

C12	0.0539 (12)	0.0225 (8)	0.0245 (8)	−0.0016 (8)	0.0056 (8)	0.0111 (7)
C13	0.0237 (8)	0.0241 (7)	0.0219 (7)	0.0041 (6)	0.0051 (6)	0.0080 (6)
C14	0.0323 (9)	0.0305 (8)	0.0194 (7)	0.0012 (7)	0.0039 (6)	0.0114 (7)
C15	0.0338 (9)	0.0267 (8)	0.0240 (7)	−0.0015 (7)	0.0026 (7)	0.0136 (7)
C16	0.0273 (8)	0.0258 (8)	0.0254 (8)	0.0060 (7)	0.0056 (7)	0.0053 (7)
C17	0.0550 (13)	0.0229 (9)	0.0374 (10)	−0.0008 (8)	0.0026 (9)	0.0069 (8)
O11	0.0527 (8)	0.0372 (7)	0.0221 (6)	0.0057 (6)	0.0073 (6)	0.0043 (5)
C21	0.0604 (15)	0.0522 (13)	0.0762 (16)	0.0160 (11)	0.0178 (13)	0.0477 (13)
C22	0.0325 (9)	0.0459 (11)	0.0341 (9)	0.0083 (8)	0.0003 (7)	0.0210 (9)
O21	0.0336 (6)	0.0315 (6)	0.0238 (5)	0.0115 (5)	0.0080 (5)	0.0128 (5)

Geometric parameters (Å, º)

Mn1—N1^{i}	2.1543 (15)	C14—C15	1.385 (2)
Mn1—N1	2.1543 (15)	C14—H14	0.9500
Mn1—O21^{i}	2.1928 (12)	C15—H15	0.9500
Mn1—O21	2.1929 (12)	C16—O11	1.219 (2)
Mn1—N11^{i}	2.3508 (14)	C16—C17	1.484 (3)
Mn1—N11	2.3508 (14)	C17—H17A	0.9800
N1—C1	1.157 (2)	C17—H17B	0.9800
C1—S1	1.6211 (18)	C17—H17C	0.9800
N11—C11	1.334 (2)	C21—C22	1.502 (3)
N11—C15	1.346 (2)	C21—H21A	0.9800
C11—C12	1.383 (2)	C21—H21B	0.9800
C11—H11	0.9500	C21—H21C	0.9800
C12—C13	1.386 (2)	C22—O21	1.435 (2)
C12—H12	0.9500	C22—H22A	0.9900
C13—C14	1.381 (3)	C22—H22B	0.9900
C13—C16	1.505 (2)	O21—H1O1	0.8400
N1^{i}—Mn1—N1	180.0	C13—C14—H14	120.2
N1^{i}—Mn1—O21^{i}	88.59 (5)	C15—C14—H14	120.2
N1—Mn1—O21^{i}	91.41 (5)	N11—C15—C14	123.05 (16)
N1^{i}—Mn1—O21	91.41 (5)	N11—C15—H15	118.5
N1—Mn1—O21	88.59 (5)	C14—C15—H15	118.5
O21^{i}—Mn1—O21	180.0	O11—C16—C17	122.10 (16)
N1^{i}—Mn1—N11^{i}	91.13 (5)	O11—C16—C13	118.40 (17)
N1—Mn1—N11^{i}	88.87 (5)	C17—C16—C13	119.49 (16)
O21^{i}—Mn1—N11^{i}	92.35 (5)	C16—C17—H17A	109.5
O21—Mn1—N11^{i}	87.65 (5)	C16—C17—H17B	109.5
N1^{i}—Mn1—N11	88.87 (5)	H17A—C17—H17B	109.5
N1—Mn1—N11	91.13 (5)	C16—C17—H17C	109.5
O21^{i}—Mn1—N11	87.65 (5)	H17A—C17—H17C	109.5
O21—Mn1—N11	92.35 (5)	H17B—C17—H17C	109.5
N11^{i}—Mn1—N11	180.0	C22—C21—H21A	109.5
C1—N1—Mn1	164.93 (13)	C22—C21—H21B	109.5
N1—C1—S1	178.67 (16)	H21A—C21—H21B	109.5
C11—N11—C15	116.73 (14)	C22—C21—H21C	109.5

C11—N11—Mn1	121.49 (11)	H21A—C21—H21C	109.5
C15—N11—Mn1	121.25 (11)	H21B—C21—H21C	109.5
N11—C11—C12	123.87 (16)	O21—C22—C21	112.19 (18)
N11—C11—H11	118.1	O21—C22—H22A	109.2
C12—C11—H11	118.1	C21—C22—H22A	109.2
C11—C12—C13	118.96 (17)	O21—C22—H22B	109.2
C11—C12—H12	120.5	C21—C22—H22B	109.2
C13—C12—H12	120.5	H22A—C22—H22B	107.9
C14—C13—C12	117.87 (15)	C22—O21—Mn1	130.79 (11)
C14—C13—C16	119.69 (15)	C22—O21—H1O1	105.5
C12—C13—C16	122.44 (16)	Mn1—O21—H1O1	120.2
C13—C14—C15	119.50 (15)		

Symmetry code: (i) −*x*+2, −*y*+1, −*z*+1.

Hydrogen-bond geometry (Å, º)

D—H···*A*	*D*—H	H···*A*	*D*···*A*	*D*—H···*A*
O21—H1*O*1···O11^{ii}	0.84	1.95	2.7714 (17)	164

Symmetry code: (ii) *x*, *y*+1, *z*+1.

4.4. Synthesis, Structures, and Magnetic Properties of New Thiocyanato Coordination Polymers with 4-(3-Phenylpropyl)pyridine as Ligand

Julia Werner, Inke Jess, und Christian Näther, *Z. Anorg. Allg. Chem.* **2014**, *640, (11),* 2161–2168.

DOI: 10.1002/zaac.201400261

Motivation

Im Kapitel 3.1 wurde über die Untersuchungen der eindimensionalen Verbindung $[Co(NCS)_2(4\text{-}(3\text{-}Phenylpropyl)pyridin)_2]_n$ berichtet. Um weitere Erkenntnis über die Struktur-Eigenschafts-Beziehungen derartiger Koordinationspolymere zu erhalten, wurde versucht, vergleichbare Verbindungen mit Mn, Fe und Ni darzustellen.
Die Untersuchungen ergaben, dass mit Mangan und Eisen lediglich diskrete Komplexe phasenrein erhalten werden, wohingegen mit Ni(II) als Übergangsmetall eine Verbindung erhalten wurde, die isotyp zu $[Co(NCS)_2(4\text{-}(3\text{-}Phenylpropyl)pyridin)_2]_n$ kristallisiert. Die magnetischen Untersuchungen ergaben, dass diese Verbindung ausschließlich Curie-Weiß Paramagnetismus zeigt.

ARTICLE

DOI: 10.1002/zaac.201400261

Synthesis, Structures, and Magnetic Properties of New Thiocyanato Coordination Polymers with 4-(3-Phenylpropyl)pyridine as Ligand

Julia Werner,[a] Inke Jess,[a] and Christian N ther*[a]

Keywords: Synthesis; Thiocyanates; Coordination polymers; Crystal Structure; Thermochemistry; Magnetochemistry

Abstract. The reaction of different metal salts with 4-(3-phenylpropyl)pyridine (ppp) lead to the formation of compounds of composition $M(NCS)_2(ppp)_4$ [M = Mn (**Mn-1**); Fe (**Fe-1**), Ni (**Ni-1**); Cd (**Cd-1**)], $M(NCS)_2(ppp)_2(H_2O)_2$ [M = Mn (**Mn-2**); Ni (**Ni-2**)] and $[M(NCS)_2(ppp)_2]_n$ [M = Mn (**Mn-3**); Ni (**Ni-3**); Cd (**Cd-3**)]. On heating compounds **M-1** decompose without the formation of any ppp deficient intermediate. In contrast, on heating, **Ni-2** transforms into a compound of composition $M(NCS)_2(ppp)_2$ that does not correspond to **Ni-3**. Unfortunately, this compound is of low crystallinity and therefore, its structure cannot be determined. The crystal structures of compounds **M-1** and **M-2** consist of discrete complexes, in which the metal cations are octahedrally coordinated. In compounds **M-3** the metal cations are linked by pairs of μ-1,3-bridging anions into chains. IR spectroscopic investigations show, that the value of the asymmetric CN stretching vibration depend on the coordination mode of the anionic ligand as well as on the nature of the metal cation. Magnetic measurements reveal that **Ni-3** shows only Curie-Weiss behavior without any magnetic anomaly. A similar behavior is also found for **Ni-3**. Comparison of the magnetic properties of **Ni-3** with those of similar compounds indicates that the magnetic properties are only minor influenced by the Co-ligand.

Introduction

Investigations on the syntheses, structures, and properties of new coordination compounds like e.g. coordination polymers, metal organic frameworks or inorganic-organic hybrid compounds are still a growing field in coordination chemistry.[1–19] One major advantage of such compounds is the fact, that based on the nature of the metal cations and the coordination properties of the ligands their structures can be influenced to some extent. This allows detailed investigations on their structure property relationships, which is needed for a more rational synthesis of compounds with desired physical properties.

In this context compounds with paramagnetic transition metal cations that show cooperative magnetic properties are of interest. This behavior can be observed if the spin centers are linked by ligands that can mediate strong magnetic exchange. Therefore, an increasing number of such compounds were recently reported.[14–27] This also includes compounds based on thio- or selenocyanates, especially in those cases where they act as bridging ligands.[28–37] In this regard we have reported on a number of compounds that shows different magnetic properties including metamagnetic behavior and a slow relaxation of the magnetization.[38–45]

However, thiocyanato compounds with bridging anions are frequently less stable than those with terminal bonded anions, which means that the former are frequently more difficult to prepare in solution. Therefore, we have developed an alternative route which is based on thermal decomposition of suitable precursor compounds.[46] In this context it is noted that different strategies for the synthesis of coordination compounds are reported that are not based on conventional synthesis in solution.[11,47–50] In the course of this project we have investigated several compounds of composition $M(NCS)_2(L)_2$ ($M = Mn^{II}$, Fe^{II}, Co^{II} and Ni^{II} and L = monodentate N-donor co-ligand), in which the metal cations are linked by centrosymmetric pairs of thiocyanato anions and are separated by the co-ligands. For the compounds with pyridine antiferromagnetic behavior is observed with Mn, the compounds with Fe and Ni show a metamagnetic transition and the Co compound shows a slow relaxation of the magnetization, which shows that interchain interactions must be of importance.[42,51] To study the influence of the co-ligand in more detail we decided to prepare compounds based on 4-(3-phenylpropylpyridine), which is much larger than pyridine and which should separate the chains more effectively. Within these investigations we obtain a large amount of compounds of different composition including the desired chain compounds with Mn and Ni. Unfortunately we have not found access to the corresponding Fe compound and that with Co shows a complicated magnetic behavior that cannot be explained without more detailed investigations. Within these investigations we also tried to prepare corresponding Cd compounds of same composition, which are

* Prof. Dr. C. N ther
Fax: +49-431-8801520
E-Mail: cnaether@ac.uni-kiel.de
[a] Institut f r Anorganische Chemie
Christian-Albrechts-Universit t zu Kiel
Max-Eyth-Straße 2
24118 Kiel, Germany

Supporting information for this article is available on the WWW under **http://dx.doi.org/10.1002/zaac.201400261** or from the author.

of interest for our project, because they can offer structural information on the paramagnetic counterparts in those cases, where the latter cannot be prepared as single crystalline materials.[52,53] Therefore, we are generally interested in their spectroscopic and structural properties.

Introduction

Synthetic Investigations

To investigate, which compounds are available, different stoichiometric ratios of the metal salts and 4-(3-phenylpropylpyridine) (ppp) were stirred in different solvents. The residues were investigated by elemental analysis, IR spectroscopy, and X-ray powder diffraction. These investigations reveal that with manganese and nickel three different compounds of composition $M(NCS)_2(ppp)_4$ (**Mn-1**, **Ni-1**), $M(NCS)_2(ppp)_2(H_2O)_2$ (**Mn-2**, **Ni-2**), and $[M(NCS)_2(ppp)_2]_n$ (**Mn-3**, **Ni-3**) are obtained. Iron shows only one crystalline phase of composition $Fe(NCS)_2(ppp)_4$ (**Fe-1**). In contrast, for most stoichiometric ratios between $Cd(NCS)_2$ and ppp only a compound of composition $[Cd(NCS)_2(ppp)_2]_n$ (**Cd-3**) could be synthesized but with a larger excess of the co-ligand a second crystalline phase of composition $Cd(NCS)_2(ppp)_4$ (**Cd-1**) could be obtained.

XRPD investigations indicate that all compounds **M-1** and **M-3** are isotypic, which seems to be also the case for compounds **M-2** (Figure 1 and Figure 2). However, **Mn-2** is contaminated with large amount of **Mn-3** (Figure S1, Supporting Information).

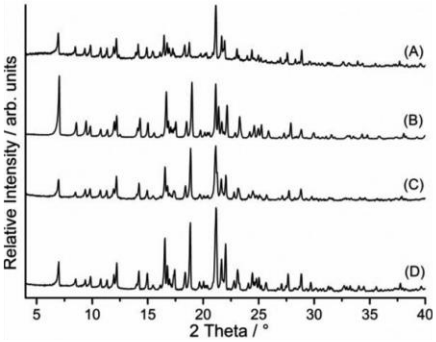

Figure 1. Experimental X-ray powder pattern of **Mn-1** (A), **Fe-1** (B), **Ni-1** (C), and **Cd-1** (D).

From the value of the asymmetric C–N stretching vibration it can be assumed that in compounds **1** and **2** the thiocyanato anions are only terminal *N*-bonded, whereas in compounds **3** they act as a bridging ligand (Figures S2–S10, Supporting Information).

In further work crystallization experiments were performed at room-temperature, which lead to single crystals of **Mn-1**, **Mn-2**, **Fe-1**, **Ni-1** as well as **Mn-3**, **Ni-3** and **Cd-3**. If the experimental powder pattern of compounds **M-1** and **M-3** are compared with those calculated from single crystal data it is proven that they are obtained as phase pure materials (Figures S11–S18, Supporting Information). For **Cd-1** no single crystals

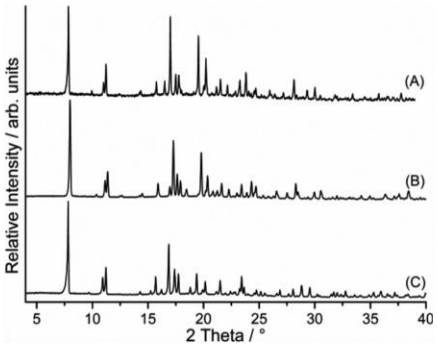

Figure 2. Experimental X-ray powder pattern of **Mn-3** (A), **Ni-3** (B), and **Cd-3** (C).

are available but comparison of its experimental pattern with that calculated for **Ni-1** proves that they are isotypic (Figure S14). Moreover, **Ni-2** is isotypic to **Mn-2** (Figure S15).

Crystal Structures

The compounds **Mn-1**, **Fe-1**, and **Ni-1** are isotypic and crystallize in the triclinic space group $P\bar{1}$ with one formula unit in the unit cell. The asymmetric unit consists of half a metal cation, one thiocyanato anion, and two crystallographically independent ppp ligands. The metal cations show a slightly distorted octahedrally environment. The metal cations are coordinated by six nitrogen atoms of two terminal *N*-bonded thiocyanato anions and four nitrogen atoms of terminal bonded ppp ligands into discrete complexes that are located on centers of inversion (Figure 3). The metal nitrogen distances range between 2.174(2) and 2.344(2) and the angles slightly deviate from ideal values (Tables S1–S3, Supporting Information).

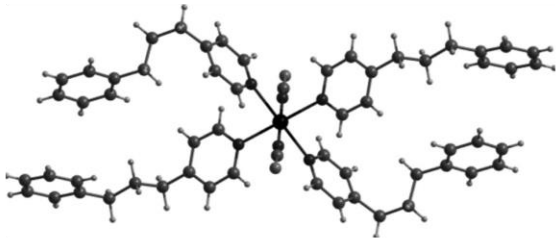

Figure 3. Coordination sphere of **Mn-1** as a representative (Ortep plots of **Mn-1**, **Fe-1**, and **Ni-1** are shown in Figures S19–S21 in the Supporting Information).

The hydrate **Mn-2** crystallizes triclinic in space group $P\bar{1}$ with two formula units in the unit cell. The asymmetric unit consists of two crystallographically independent manganese cations, which are located on centers of inversion. Two water molecules, two thiocyanato anions, and two ppp ligands are located in general positions. Each metal cation is coordinated by two terminally *N*-bonded thiocyanato anions, two water molecules, and two ppp ligands in a slightly distorted octahedral environment (Figure 4 and Table S4). The metal nitrogen

distances range between 2.1872(2) and 2.271(2) and are similar to those in compounds **1** (Tables S1–S3, Supporting Information).

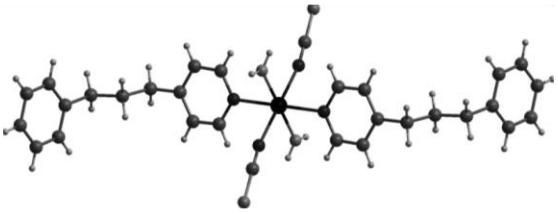

Figure 4. Coordination sphere of **Mn-2** (An Ortep plot of **Mn-2** is shown in Figure S22 in the Supporting Information).

Compounds **Mn-3**, **Ni-3**, and **Cd-3** are isotypic and crystallize in the monoclinic space group $P2_1/n$ with four formula units in the unit cell. The asymmetric unit consists of two crystallographically independent cations, which are located on centers of inversion. Two thiocyanato anions and two ppp ligands are in general positions. The metal cations are coordinated by two terminal ppp ligands and four μ-1,3-bridging thiocyanato anions within slightly distorted octahedra and are linked by pairs of μ-1,3-bridging thiocyanato anions into chains (Figure 5 and Tables S5–S7).

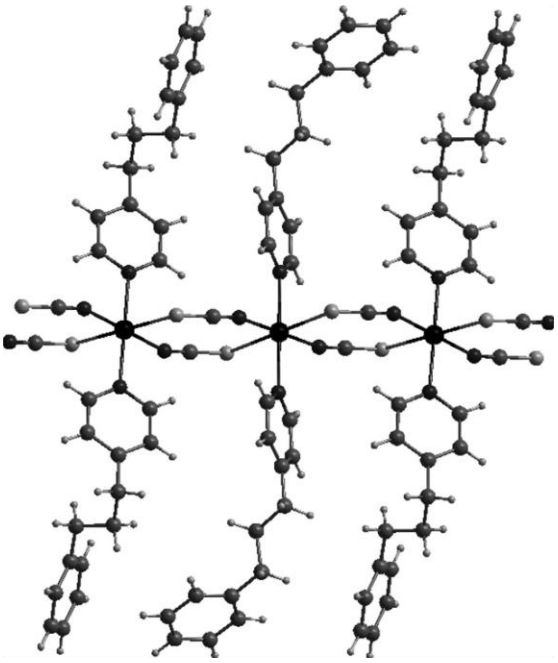

Figure 5. Coordination sphere of **Mn-3** as a representative (Ortep plots of **Mn-3**, **Ni-3**, and **Cd-3** are shown in Figures S23–S25 in the Supporting Information).

These chains elongate in the direction of the *a* axis and are arranged in a way that the N–M–N(ppp) vectors of neighboring chains are canted (Figure 6). The intrachain M–M distances are between 5.60 (**Ni-3**) and 5.81 (**Cd-3**) and the shortest interchain distance is found in **Mn-3** with 11.21 (Table 1). If these distances are compared with those of the corresponding pyridine compounds it is proven, that the intrachain distances are comparable, whereas the interchain distances are much larger than those in the pyridine compounds (Table 1).

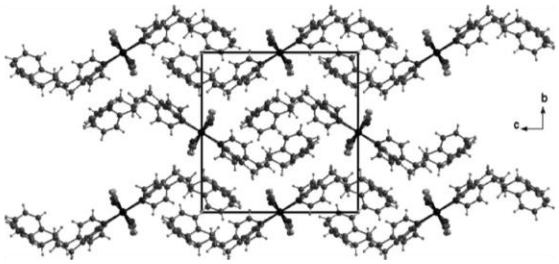

Figure 6. Crystal structure of **Mn-3** as a representative with view along the crystallographic *a* axis.

Table 1. The intrachain and interchain M–M distances / in **Mn-3**, **Ni-3**, and **Cd-3** as well as in the corresponding pyridine (Pyr) compounds retrieved from literature.

	Intrachain	Interchain	Reference
Mn-3	5.72	11.21	This work
Ni-3	5.60	12.15	This work
Cd-3	5.81	11.29	This work
$[Mn(NCS)_2(Pyr)_2]_n$	5.77	8.90	[51]
$[Ni(NCS)_2(Pyr)_2]_n$	5.57	8.38	[54]
$[Cd(NCS)_2(Pyr)_2]_n$	6.01/5.97	8.62	[55]

Thermoanalytical Investigations

To investigate if compounds **1** or **2** can be used as precursors for the preparation of additional compounds by thermal decomposition, measurements using differential thermoanalysis, and thermogravimetry (DTA-TG) were performed (Figure 7 and Figures S26–S30, Supporting Information). Because **Mn-2** is always contaminated with **Mn-3** it was not investigated but it can be assumed that it will transform completely into the latter compound.

On heating only one TG step is observed for compounds **1**, which proves that that all ligands are removed in one step without formation of any ppp deficient intermediate (Figure 7). If the hydrate **Ni-2** is investigated by DTA-TG measurements one mass loss is observed starting at about 100 °C that corresponds to the removal of the water molecules and on further heating the ppp ligands are emitted. From these investigations it can be assumed that in the first TG step a compound of composition $[Ni(NCS)_2(ppp)_2]_n$ has formed that must not necessarily be isotypic to **Ni-3** as shown previously.[56]

If the TG measurement is repeated and stopped after water removal and the residue is investigated by XRPD a pattern is obtained that is completely different from that of **Ni-3** and which does not contain any reflections of the precursor **Ni-2** (Figure 8). However, the crystallinity of this intermediate com-

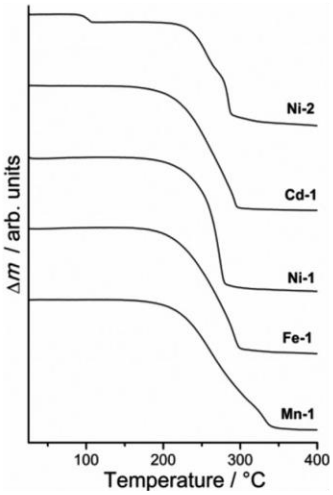

Figure 7. TG curves for **Mn-1**, **Fe-1**, **Ni-1**, **Cd-1**, and **Ni-2**.

pound is very poor with broad reflection profiles and all attempts to index its powder pattern failed. However, the asymmetric C–N stretching vibration is observed at 2170 cm^{-1} and 2112 cm^{-1} in the IR spectra and therefore, it can be assumed that also bridging thiocyanato anions are present.

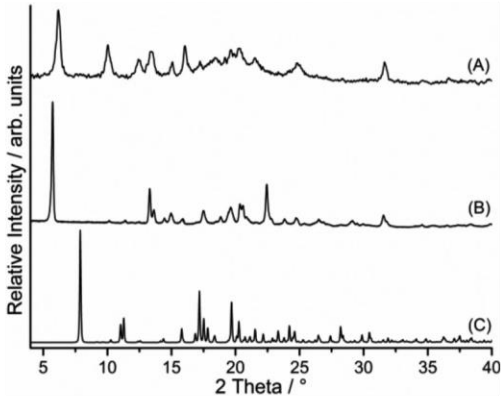

Figure 8. Experimental X-ray powder pattern of the residue obtained in a TG measurement of **Ni-2** after water removal (A), of **Ni-2** (B) and calculated XRPD pattern for **Ni-3** (C).

IR Spectroscopic Investigations

It is well known that the coordination mode of the thiocyanato anion can be estimated from the value of the CN stretching vibration. In the case of terminally *N*-bonded thiocyanato anions this vibration is observed at about 2050 cm^{-1}, whereas for the μ-1,3 bridging mode it is located around 2100 cm^{-1}.[57–59] However, it can be expected that the actual values depend on the nature of the metal cation and the organic co-ligand and therefore, in some cases no definite conclusions can be drawn. These correlations are of special importance for our project especially in those cases where no single crystals of a given compound are available and structural information must be retrieved from IR spectroscopic investigations. For compounds **1** and **3** these values slightly increase from Mn to Ni with larger differences for compounds **3** (Table 2). This general trend is also observed for compounds of similar structures retrieved from literature (Table 2). Even if they are small, differences are also found for compounds with different co-ligands. Finally, it is shown that dependent on the nature of the metal cation and the co-ligand the vibration are distributed over a relatively large range, but in any case no overlap between the terminal and the bridging coordination is observed. Therefore, in this case the coordination mode of the anionic ligand can easily be determined.

Table 2. Values of the asymmetric CN stretching vibration in cm^{-1} for compounds **M-1** and **M-3**, as well of similar compounds with same structure retrieved from literature (Pyr = pyridine).[51,56]

Compound	Cd	Mn	Fe	Ni
$M(NCS)_2(ppp)_4$	2064	2060	2063	2081
$M(NCS)_2(ppp)_2$	2091	2087	–	2109
$M(NCS)_2(Pyr)_4$	2050	2060	2066	2082
$M(NCS)_2(Pyr)_2$	2097	2090	2093	2110
$M(NCS)_2(Ethyl\text{-}Pyr)_4$	2037	2044	2050	2069
$M(NCS)_2(Ethyl\text{-}Pyr)_2$	2105	2092	–	2113

Magnetic Investigations

The magnetic properties of the paramagnetic compounds **M-1** were investigated by susceptibility measurements between room-temperature and 2 K. For the discrete complexes **1** and **2** only paramagnetic behavior without any magnetic anomaly is expected because the thiocyanato anions are only terminal bonded. In agreement the temperature dependence of the susceptibility follows the Curie (**Mn-1** and **Ni-1**) or Curie-Weiss (**Fe-1**) law, with significant antiferromagnetic interactions for **Fe-1** (Table 3 and Figures S31–S33, Supporting Information). The experimental magnetic moment for **Mn-1** is in good agreement with that calculated for a Mn^{II} ion in high-spin configuration, whereas the values for **Fe-1** and **Ni-1** are a slightly higher (Table 3).

Table 3. Selected experimental data of the magnetic measurements of **Mn-1**, **Fe-1**, **Ni-1**, and **Ni-3**.

	Mn-1	**Fe-1**	**Ni-1**	**Ni-3**
Θ /K	0.6	–21.5	1.6	8.0
C /cm^{-3}·K·mol^{-1}	4.43	4.30	1.13	1.21
μ_{eff} /μ_B	5.95	5.86	3.00	3.12
$\mu_{eff(HS)}$ /μ_B	5.92	4.89	2.82	2.82

For **Ni-3**, in which the metal cations are linked by μ-1,3-bridging anionic ligands also only Curie-Weiss behavior is observed (Figure S34, Supporting Information). The experimental magnetic moment of 3.12 μ_B is in good agreement with that calculated for Ni^{II} in a high-spin configuration. The Weiss constant of 8.0 K indicates dominant ferromagnetic interactions, which are also observed in similar compounds of this

Zeitschrift für anorganische und allgemeine Chemie ZAAC Journal of Inorganic and General Chemistry

Table 4. Selected magnetic data for compounds of composition $[Ni(NCS)_2(L)_2]_n$ (L = co-ligand). Please note the compound with 4-ethylpyridine exists in two polymorphic modifications.

Co-ligand	Θ /K	H_c /kOe	T_N /K	Interchain distance /	Reference
ppp	8.0	–	–	11.253	This work
Pyridine	14.8	6	3.9	8.380	[54]
4-Ethylpyridine I	4.6	–	–	8.308	[56]
4-ethylpyridine II	3.9	–	–	8.281	[56]

family. We also tried to measure **Mn-3** obtained from solution but we always obtained poor magnetic curves that indicates the presence of a contamination. If the material is investigated by XRPD measurements directly after the magnetic measurements always a mixture of **Mn-3** and the hydrate **Mn-2** is present, which shows that **Mn-3** is extremely hygroscopic. Several different batches were measured but all magnetic curves looks similar. A similar behavior is observed e.g. for $[Mn(NCS)_2(2\text{-methylpyrazine})_2]_n$, which shows antiferromagnetic ordering on cooling.[60] However, even this compound is hygroscopic, always contaminated with a very small amount and thus, it susceptibility curve shows a strong increases after the antiferromagnetic maximum. In contrast, **Mn-3** is always contaminated with large amounts of the hydrate **Mn-2** and therefore, the paramagnetic impurity seems to dominate. Therefore, one cannot decide if it **Mn-3** will also show antiferromagnetic ordering, which would be typical for this class of compounds.

Concerning the magnetic properties of **Ni-3** it is noted that in all compounds of composition $[Ni(NCS)_2(L)_2]_n$, in which the Nickel cations are connected by pairs of μ-1,3-bridging thiocyanato anions always ferromagnetic interactions with either Curie-Weiss behavior or metamagnetism is observed (Table 4). If these magnetic data are compared with that of **Ni-3** there is no simple correlation between the shortest interchain distances and the Weiss constant or the nature of the magnetic behavior observed (Table 4). Therefore, the packing of the chains in the crystal seems to be more important.

Conclusions

Several new coordination compounds based on transition metal thiocyanates with 4-(3-Phenylpropyl)-pyridine as co-ligand were synthesized. It was shown that the discrete complexes with terminal coordinated thiocyanato anions can easily be prepared for the paramagnetic compounds, whereas those, in which the metal cations are linked by the anionic ligands, are difficult to synthesize. This shows that the former compounds are energetically favored, which can be traced back to the low chalcophilicity of the paramagnetic compounds. It is noted that the opposite is the case for compounds based on Cd^{II}, which prefer coordination to sulfur. IR spectroscopic investigations reveal, that a continuous shift of the asymmetric stretching vibration is observed for the different metal cations and that in this case one can easily differ between a terminal and a bridging coordination. Unfortunately, only one compound with a bridging coordination of the anionic ligands can be prepared phase pure (**Ni-3**) that shows Curie-Weiss behavior and ferromagnetic interactions. This is in agreement with the results obtained for similar compounds and indicates that there is no simple correlation between the shortest interchain Ni–Ni distances and the strength of this interaction.

Experimental Section

Syntheses: $MnSO_4{\cdot}H_2O$, $NiSO_4{\cdot}6H_2O$ and $CdSO_4{\cdot}8/3H_2O$, KNCS, $FeCl_2{\cdot}4H_2O$ were obtained from Merck, $Ba(NCS)_2{\cdot}3H_2O$ and 4-(3-phenylpropyl)pyridine were obtained from Alfa Aesar. Solvents were used without further purification. Crystalline powders of all compounds were prepared by stirring the reactants in the respective solvents at room temperature. The residues were filtered off and washed with the used solvent and dried in air. The purity of all compounds was checked by X-ray powder diffraction and elemental analysis (Figures S11–S18, Supporting Information).

$Cd(NCS)_2$: $Ba(NCS)_2{\cdot}3H_2O$ (3.1 g, 10 mmol) and $CdSO_4{\cdot}8/3H_2O$ (2.6 g, 10 mmol) were stirred in water (100 mL). The white precipitate of $BaSO_4$ was filtered off and the water was removed from the filtrate by heating. The final product was dried by 80 °C. The homogeneity of the product was investigated by X-ray powder diffraction and elemental analysis.

$Mn(NCS)_2$: $Ba(NCS)_2{\cdot}3H_2O$ (17.9 g, 58.4 mmol) and $MnSO_4{\cdot}6H_2O$ (9.9 g, 58.4 mmol) were stirred in water (400 mL). The white precipitate of $BaSO_4$ was filtered off and the water evaporated using a rotary evaporator. The homogeneity of the product was investigated by X-ray powder diffraction and elemental analysis.

$Ni(NCS)_2$: $Ba(NCS)_2{\cdot}3H_2O$ (17.5 g, 57 mmol) and $NiSO_4{\cdot}6H_2O$ (15.0 g, 57 mmol) were stirred in water (400 mL). The white precipitate of $BaSO_4$ was filtered off and the water evaporated using a rotary evaporator. The homogeneity of the product was investigated by X-ray powder diffraction and elemental analysis.

Synthesis of Mn-1: Single crystals suitable for single-crystal X-ray diffraction were obtained by the reaction of $Mn(NCS)_2$ (0.25 mmol, 44.3 mg) and 4-(3-phenylpropyl)pyridine (0.50 mmol, 96.3 μL) in H_2O (1.5 mL). Colorless block-shaped crystals were obtained after two weeks. A white crystalline powder on a larger scale were obtained by stirring $Mn(NCS)_2$ (171.1 mg, 1.00 mmol), and 4-(3-phenylpropyl)-pyridine (770.6 μL, 4.00 mmol) in ethanol (5 mL) for 3 d. Yield: 97.1 %. $C_{58}H_{60}MnN_6S_2$ (960.22): calcd. C 72.55, H 6.30, N 8.75; S 6.68 %, found C 71.93, H 6.32, N 8.77, S 6.62 %. **IR** (ATR): $\tilde{\nu}_{max}$ = 3023 (w), 2942 (w), 2859 (w), 2060 (s), 1609 (m), 1419 (m), 1422 (m), 1222 (w), 1011 (m), 839 (m), 748 (s), 702 (s), 603 (m), 570 (m), 512 (s) cm^{-1}.

Synthesis of Fe-1: Single crystals suitable for single-crystal X-ray diffraction were obtained by the reaction of $FeCl_2{\cdot}4H_2O$ (0.25 mmol, 49.7 mg), KNCS (0.5 mmol, 48.6 mg) and 4-(3-phenylpropyl)pyridine (0.5 mmol, 93.3 μL) in water (1.5 mL). Orange colored crystals were

obtained after one month. A yellow crystalline powder on a larger scale were obtained by stirring $FeCl_2 \cdot 4H_2O$ (198.8 mg, 1.00 mmol), KNCS (194.4 mg, 2.00 mmol) and 4-(3-phenylpropyl)pyridine (770.6 µL, 4.00 mmol) in ethanol (5 mL) and H_2O (2 mL) and EtOH (3 mL) for 3 d. Yield: 90.1 %. $C_{58}H_{60}CoN_6S_2$ (964.22 g·mol^{-1}): calcd. C 72.25, H 6.27, N 8.72; S 6.65 %, found C 71.72, H 6.21, N 9.15, S 6.75 %. **IR** (ATR): $\tilde{\nu}_{max}$ = 3024 (w), 2942 (w), 2859 (w), 2063 (s), 2015 (m), 1609 (m), 1496 (m), 1419 (m), 1222 (m), 1011 (m), 841 (m), 749 (s), 702 (s), 603 (m), 570 (m), 513 (s) cm^{-1}.

Synthesis of Ni-1: Single crystals suitable for single-crystal X-ray diffraction were synthesized by $Ni(NCS)_2$ (0.25 mmol, 43.7 mg) and 4-(3-phenylpropyl)pyridine (0.5 mmol, 93.3 µL) in acetonitrile (1.5 mL). After few weeks, blue crystals were obtained. A blue colored crystalline powder on a larger scale was obtained by stirring $Ni(NCS)_2$ (87.4 mg, 0.50 mmol), and 4-(3-phenylpropyl)pyridine (385 µL, 2.00 mmol) in ethanol (4 mL) for 6 d. Yield: 93.8 %. $C_{58}H_{60}N_6NiS_2$ (963.98 g·mol^{-1}): calcd. C 72.27, H 6.27, N 8.72, S 6.65 %; found C 72.33, H 6.34, N 9.12, S 6.17 %. **IR** (ATR): $\tilde{\nu}_{max}$ = 3023 (w), 2942 (w), 2859 (w), 2081 (s), 1612 (m), 1496 (m), 1419 (s), 1423 (s), 1211 (m), 1014 (m), 824 (m), 750 (s), 703 (s), 570 (m), 515 (s) cm^{-1}.

Synthesis of Cd-1: A colorless crystalline powder was prepared by stirring $Cd(NCS)_2$ (114.3 mg, 0.50 mmol), and 4-(3-phenylpropyl)pyridine (577.8 µL, 3.00 mmol) in acetonitrile (5 mL) for 7 d. Yield: 89.2 %. $C_{58}H_{60}CdN_6S_2$ (1017.69 g·mol^{-1}): calcd. C 68.45, H 5.94, N 8.26, S 6.30 %; found C 68.38, H 6.20, N 8.36, S 5.94 %. **IR** (ATR): $\tilde{\nu}_{max}$ = 3024 (w), 2942 (w), 2861 (w), 2064 (s), 1609 (m), 1496 (m), 1422 (m), 1222 (m), 1014 (m), 839 (m), 749 (s), 702 (s), 602 (m), 788 (s), 571 (m), 513 (s) cm^{-1}.

Synthesis of Mn-2: $Mn(NCS)_2$ (0.25 mmol, 42.8 mg) and 4-(3-phenylpropyl)pyridine (0.50 mmol, 96.3 µL) were dissolved in acetonitrile (1.5 mL). The solvent was reduced by slow evaporation and after several months a few single crystals were obtained. **IR** (ATR): $\tilde{\nu}_{max}$ = 3424 (b), 3354 (w), 30198 (w), 3024 (w), 2944 (w), 2855 (w), 2095 (s), 1612 (s), 1558 (m), 1494 (m), 1452 (m), 1423 (m), 1225 (m), 1065 (m), 1015 (m), 822 (m), 754 (s), 697 (s), 602 (m), 516 (s), 496 (s), 454 (s) cm^{-1}.

Synthesis of Mn-3: A solution of $Mn(NCS)_2$ (0.50 mmol, 85.6 mg) and 4-(3-phenylpropyl)pyridine (0.25 mmol, 48.2 µL) in acetonitrile (1.5 mL) was heated at 80 °C for 3 d and cooled down. The resulting solution was reduced by slow evaporation. On slow evaporation of the solvent of the clear solution single crystals suitable for single-crystal X-ray diffraction was obtained. A beige crystalline powder was obtained. **IR** (ATR): $\tilde{\nu}_{max}$ = 3061 (w), 2942 (w), 2857 (w), 2087 (s), 1613 (m), 1558 (m), 1494 (m), 1423 (m), 1228 (m), 1069 (m), 1014 (m), 836 (m), 800 (m), 749 (s), 699 (s), 597 (m), 573 (m), 493 (s) cm^{-1}.

Synthesis of Ni-3: $Ni(NCS)_2$ (0.50 mmol, 87.4 mg) and 4-(3-phenylpropyl)pyridine (0.25 mmol, 48.2 µL) were dissolved in ethanol (1.5 mL) and heated at 80 °C for 3 d. The resulting solution was cooled down and single crystals suitable for single-crystal X-ray diffraction were obtained. A light green colored crystalline powder was synthesized by stirring $Ni(NCS)_2$ (174.9 mg, 1.00 mmol) and 4-(3-phenylpropyl)pyridine (192.6 µL, 1.00 mmol) in ethanol (5 mL) for 7 d. Yield: 80.2 %. $C_{30}H_{30}N_4NiS_2$ (569.42 g·mol^{-1}): calcd. C 63.28, H 5.31, N 9.84, S 11.26 %, found C 63.27, H 5.40, N 9.67, S 11.22 %. **IR** (ATR): $\tilde{\nu}_{max}$ = 3017 (w), 2942 (w), 2858 (w), 2109 (s), 1615 (m), 1422 (m), 1226 (m), 1018 (w), 804 (m), 750 (s), 699 (s), 598 (m), 514 (m) cm^{-1}.

Synthesis of Cd-3: $Cd(NCS)_2$ (0.30 mmol, 68.6 mg) and 4-(3-phenylpropyl)pyridine (0.15 mmol, 28.9 µL) were dissolved in ethanol (1.5 mL) and heated at 80 °C for 3 d. The resulting solution was cooled down and single crystals suitable for single-crystal X-ray diffraction were obtained. A colorless crystalline powder was synthesized by stirring $Cd(NCS)_2$ (229 mg, 1.00 mmol) and 4-(3-phenylpropyl)pyridine (192.6 µL, 1.00 mmol) in ethanol (5 mL) for 7 d. Yield: 75.8 %. $C_{58}H_{60}CdN_6S_2$ (1017.69 g·mol^{-1}): calcd. C 57.83, H 4.85, N 8.99, S 10.29 %, found C 57.42, H 4.70, N 8.97, S 10.51 %. **IR** (ATR): $\tilde{\nu}_{max}$ = 3018 (w), 2942 (w), 2858 (w), 2091 (s), 1612 (m), 1494 (w), 1425 (m), 1226 (w), 1015 (m), 799 (m), 749 (s), 699 (s), 597 (m), 493 (m) cm^{-1}.

Elemental Analysis: CHNS analysis was performed with an EURO EA elemental analyzer, fabricated by EURO VECTOR Instruments and Software.

Differential Thermal Analysis and Thermogravimetry: The DTA-TG measurements were performed in a dynamic nitrogen atmosphere (purity: 5.0) in Al_2O_3 crucibles with a STA-409CD thermobalance from Netzsch. All measurements were performed with a flow rate of 75 mL·min^{-1} and were corrected for buoyancy and current effects. The instrument was calibrated using standard reference materials.

Single-Crystal Structure Analysis: The investigations were performed with the imaging plate diffraction system (IPDS-1 for **Mn-1**, **Fe-1**, **Ni-1**, **Mn-2** and IPDS-2 for **Mn-3**, **Ni-3**, **Cd-3**) with Mo-K_α-radiation from STOE & CIE. The structure solution was performed with direct methods using SHELXS-97, and structure refinements were performed against F^2 using SHELXL-97.[61] All non-hydrogen atoms were refined with anisotropic displacement parameters. The hydrogen atoms were positioned with idealized geometry and were refined isotropic with $U_{iso}(H) = 1.2 \cdot U_{eq}(C)$ using a riding model. Selected crystal data and details of the structure refinements are listed in Table 5.

Crystallographic data (excluding structure factors) for the structures in this paper have been deposited with the Cambridge Crystallographic Data Centre, CCDC, 12 Union Road, Cambridge CB21EZ, UK. Copies of the data can be obtained free of charge on quoting the depository numbers CCDC-1015241 (**Mn-1**), CCDC-1015239 (**Fe-1**), CCDC-1015242 (**Ni-1**), CCDC-1015240 (**Mn-2**), CCDC-1015237 (**Mn-3**), CCDC-1015238 (**Ni-3**), and CCDC-1015236 (**Cd-3**) (Fax: +44-1223-336-033; E-Mail: deposit@ccdc.cam.ac.uk, http://www.ccdc.cam.ac.uk).

X-ray Powder Diffraction (XRPD): XRPD experiments were performed with a Stoe Transmission Powder Diffraction System (STADI P) with Cu-K_α-radiation (λ = 1.5406) that is equipped with a linear position-sensitive detector (Delta 2θ = 6.5–7° simultaneous; scan range overall = 2–130°) from STOE & CIE and an Image Plate Detector (scan range overall = 0–127°) and a PANalytical X'Pert Pro MPD reflection powder diffraction system with Cu-K_α radiation (λ = 154.0598 pm) equipped with a PIXcel semiconductor detector from PANanlytical.

Magnetic Measurements: All magnetic measurements were performed using a Physical Property Measuring System (PPMS) from Quantum Design, which is equipped with a 9 T magnet. The data were corrected for Core diamagnetism using Pascal constants.

IR Spectroscopy: IR spectroscopic investigations were performed with an ATI Mattson Genesis Series FTIR Spectrometer, control software: WINFIRST, from ATI Mattson.

Zeitschrift für anorganische und allgemeine Chemie ZAAC Journal of Inorganic and General Chemistry

Table 5. Selected crystal data and details on the structure determinations for compounds **Mn-1**, **Mn-2**, and **M-3**.

	Mn-1	**Fe-1**	**Ni-1**	**Mn-2**	**Mn-3**	**Ni-3**	**Cd-3**
Formula	$C_{58}H_{60}MnN_6S_2$	$C_{58}H_{60}FeN_6S_2$	$C_{58}H_{60}N_6NiS_2$	$C_{30}H_{34}MnN_4O_2S_2$	$C_{30}H_{30}MnN_4S_2$	$C_{30}H_{30}N_4NiS_2$	$C_{30}H_{30}CdN_4S_2$
MW /g·mol^{-1}	960.18	961.09	963.95	601.67	565.64	569.41	623.10
Crystal system	triclinic	triclinic	triclinic	triclinic	monoclinic	monoclinic	monoclinic
Space group	$P\bar{1}$	$P\bar{1}$	$P\bar{1}$	$P\bar{1}$	$P2_1/c$	$P2_1/n$	$P2_1/n$
Z	1	1	1	2	4	4	4
D_{calc} /mg·m^{-3}	1.237	1.257	1.263	1.300	1.309	1.343	1.399
μ /mm^{-1}	0.381	0.423	0.509	0.598	0.631	0.863	0.904
Min/max. transm.	–	0.8083, 0.9544	–	0.8401, 0.9423	0.6921, 0.9089	–	–
a /	9.4775(8)	9.4304(7)	9.4730(6)	8.0118(6)	11.4485(3)	11.2010(5)	11.6228(3)
b /	11.4676(10)	11.3925(9)	11.3573(9)	12.3995(10)	15.9460(4)	16.0326(6)	16.1656(6)
c /	13.2370(9)	13.1629(10)	13.1127(10)	15.8623(11)	15.7759(5)	15.7935(7)	15.7701(4)
α /°	72.275(9)	72.311(9)	72.416(9)	79.652(9)	90	90	90
β /°	82.587(9)	82.717(9)	83.004(8)	82.825(9)	94.624(2)	96.715(4)	93.387(2)
γ /°	70.243(9)	70.497(9)	70.540(8)	90.096(9)	90	90	90
V / ^{3}	1289.14(18)	1269.50(17)	1267.67(16)	1537.6(2)	2870.64(14)	2816.8(2)	2957.86(15)
T /K	200(2)	200(2)	200(2)	293(2)	200(2)	293(2)	293(2)
θ_{max} /°	2.50 to 25.00	2.52 to 27.00	2.51 to 25.00	2.31 to 26.01	2.12 to 28.00	1.82 to 25.00	2.12 to 27.97
Measured refl.	8547	14916	8049	12061	44573	19820	41660
R_{int}	0.0875	0.0512	0.0740	0.0484	0.0789	0.0679	0.0414
Unique reflns.	4402	5320	4372	5876	6898	4951	42407
Refl.[$F_o > 4\sigma(F_o)$]	2873	4021	3017	4582	5919	3535	5191
Parameters	304	305	301	359	337	337	337
R_1 [$F_o > 4\sigma(F_o)$]	0.0490	0.0400	0.0424	0.0417	0.0389	0.0569	0.0428
wR_2 [all data]	0.1243	0.1008	0.0885	0.1076	0.0933	0.1178	0.0923
GOF	0.950	0.953	0.936	1.001	1.089	1.141	1.101
$\Delta\rho$(max/min) /e· $^{-3}$	0.256 and –0.402	0.256 and –0.450	0.235 and –0.288	0.253 and –0.479	0.331 and –0.350	0.511 and –0.308	0.366 and –0.535

Supporting Information (see footnote on the first page of this article): Calculated XRPD patterns, Ortep plots of compounds **Mn-1**, **Fe-1**, **Ni-1**, **Cd-1**, **Mn-2** and **Ni-2**. TG curves for **Mn-1**, **Fe-1**, **Ni-1**, **Cd-1**. Experimental and calculated XRPD patterns for compounds **Mn-1**, **Fe-1**, **Ni-1**, **Cd-1**, **Mn-2** and **Ni-2**.

Acknowledgements

This project was supported by the Deutsche Forschungsgemeinschaft (DFG) (Project No. NA 720/5–1) and the State of Schleswig-Holstein. We thank *Professor Dr. Wolfgang Bensch* for access to his experimental facility and *Maren Rasmussen* as well as *Henning L hmann* for the magnetic measurements.

References

[1] A. J. Blake, N. R. Brooks, N. R. Champness, M. Crew, D. H. Gregory, P. Hubberstey, M. Schr der, A. Deveson, D. Fenske, L. R. Hanton, *Chem. Commun.* **2001**, 1432–1433.
[2] B. Moulton, M. J. Zaworotko, *Chem. Rev.* **2001**, *101*, 1629–1658.
[3] S. L. James, *Chem. Soc. Rev.* **2003**, *32*, 276–288.
[4] S. Kitagawa, K. Uemura, *Chem. Soc. Rev.* **2005**, *34*, 109–119.
[5] A. J. Blake, N. R. Champness, P. Hubberstey, W.-S. Li, M. A. Withersby, M. Schr der, *Coord. Chem. Rev.* **1999**, *183*, 117–138.
[6] S. Kitagawa, R. Matsuda, *Coord. Chem. Rev.* **2007**, *251*, 2490–2509.
[7] A. Y. Robin, K. M. Fromm, *Coord. Chem. Rev.* **2006**, *250*, 2127–2157.
[8] C. Janiak, J. K. Vieth, *New J. Chem.* **2010**, *34*, 2366–2388.
[9] C. N ther, G. Bhosekar, I. Jeß, *Inorg. Chem.* **2007**, *46*, 8079–8087.
[10] C. Janiak, *Dalton Trans.* **2003**, 2781–2804.
[11] K. M ller-Buschbaum, *Z. Anorg. Allg. Chem.* **2005**, *631*, 811–828.
[12] C. Janiak, L. Uehlin, H.-P. Wu, P. Kl fers, H. Piotrowski, T. G. Scharmann, *J. Chem. Soc., Dalton Trans.* **1999**, 3121–3131.
[13] D. Braga, L. Maini, M. Polito, L. Scaccianoce, G. Cojazzi, F. Grepioni, *Coord. Chem. Rev.* **2001**, *216*, 225–248.
[14] C. N ther, S. W hlert, J. Boeckmann, M. Wriedt, I. Jeß, Z. *Anorg. Allg. Chem.* **2013**, *639*, 2696–2714.
[15] D. Maspoch, D. Ruiz-Molina, J. Veciana, *Chem. Soc. Rev.* **2007**, *36*, 770–818.
[16] Y.-F. Zeng, X. Hu, F.-C. Liu, X.-H. Bu, *Chem. Soc. Rev.* **2009**, *38*, 469–480.
[17] W. L. Leong, J. J. Vittal, *Chem. Rev.* **2011**, *111*, 688–764.
[18] S. R. Batten, K. S. Murray, *Coord. Chem. Rev.* **2003**, *246*, 103–130.
[19] D. Maspoch, D. Ruiz-Molina, J. Veciana, *J. Mater. Chem.* **2004**, *14*, 2713–2723.
[20] D.-F. Weng, Z.-M. Wang, S. Gao, *Chem. Soc. Rev.* **2011**, *40*, 3157–3181.
[21] T. Liu, H. Zheng, S. Kang, Y. Shiota, S. Hayami, M. Mito, O. Sato, K. Yoshizawa, S. Kanegawa, C. Duan, *Nat. Commun.* **2013**, *4*.
[22] W.-X. Zhang, T. Shiga, H. Miyasaka, M. Yamashita, *J. Am. Chem. Soc.* **2012**, *134*, 6908–6911.
[23] C. Coulon, R. Cl rac, W. Wernsdorfer, T. Colin, H. Miyasaka, *Phys. Rev. Lett.* **2009**, *102*, 164204–164207.
[24] H. Miyasaka, R. Cl rac, *Bull. Chem. Soc. Jpn.* **2005**, *78*, 1725–1748.
[25] Y.-Z. Zhang, U. P. Mallik, R. Cl rac, N. P. Rath, S. M. Holmes, *Polyhedron* **2013**, *32*, 115–121.
[26] A. V. Prosvirin, H. Zhao, K. R. Dunbar, *Inorg. Chim. Acta* **2012**, *389*, 118–121.
[27] P. Dechambenoit, J. R. Long, *Chem. Sci. Rev.* **2011**, *40*, 3249–3265.
[28] E. Shurdha, S. H. Lapidus, P. W. Stephens, C. E. Moore, A. L. Rheingold, J. S. Miller, *Inorg. Chem.* **2012**, *51*, 9655–9665.
[29] C. J. Adams, M. C. Mu oz, R. E. Waddington, J. A. Real, *Inorg. Chem.* **2011**, *50*, 10633–10642.

[30] C. J. Adams, M. F. Haddow, D. J. Harding, T. J. Podesta, R. E. Waddington, *CrystEngComm* **2011**, *13*, 4909–4914.
[31] B. Machura, A. Świtlicka, I. Nawrot, J. Mroziński, R. Kruszynski, *Polyhedron* **2011**, *30*, 832–840.
[32] B. Machura, A. Świtlicka, P. Zwoliński, J. Mroziński, B. Kalińska, R. Kruszynski, *J. Solid State Chem.* **2013**, *197*, 218–227.
[33] M. Wriedt, I. Jeß, C. N ther, *Eur. J. Inorg. Chem.* **2009**, 1406–1413.
[34] M. Wriedt, C. N ther, *Chem. Commun.* **2010**, *46*, 4707–4709.
[35] R. Gonz lez, A. Acosta, R. Chiozzone, C. Kremer, D. Armentano, G. De Munno, M. Julve, F. Lloret, J. Faus, *Inorg. Chem.* **2012**, *51*, 5737–5747.
[36] J. G. Małecki, T. Groń, H. Duda, *Polyhedron* **2012**, *36*, 56–68.
[37] J. G. Małecki, B. Machura, A. Świtlicka, T. Groń, M. Bałanda, *Polyhedron* **2011**, *30*, 746–753.
[38] S. W hlert, M. Wriedt, T. Fic, Z. Tomkowicz, W. Haase, C. N ther, *Inorg. Chem.* **2013**, *52*, 1061–1068.
[39] S. W hlert, U. Ruschewitz, C. N ther, *Cryst. Growth Des.* **2012**, *12*, 2715–2718.
[40] J. Boeckmann, M. Wriedt, C. N ther, *Chem. Eur. J.* **2012**, *18*, 5284–5289.
[41] S. W hlert, J. Boeckmann, M. Wriedt, C. N ther, *Angew. Chem. Int. Ed.* **2011**, *50*, 6920–6923.
[42] J. Boeckmann, C. N ther, *Dalton Trans.* **2010**, *39*, 11019–11026.
[43] S. W hlert, T. Fic, Z. Tomkowicz, S. G. Ebbinghaus, M. Rams, W. Haase, C. N ther, *Inorg. Chem.* **2013**, *52*, 12947–12957.
[44] J. Boeckmann, C. N ther, *Chem. Commun.* **2011**, *47*, 7104–7106.
[45] S. W hlert, L. Fink, M. Schmidt, C. N ther, *CrystEngComm* **2013**, *15*, 945–957.
[46] C. N ther, J. Greve, *J. Solid State Chem.* **2003**, *176*, 259–265.
[47] S. L. James, C. J. Adams, C. Bolm, D. Braga, P. Collier, T. Friscic, F. Grepioni, K. D. M. Harris, G. Hyett, W. Jones, A. Krebs, J. Mack, L. Maini, A. G. Orpen, I. P. Parkin, W. C. Shearouse, J. W. Steed, D. C. Waddell, *Chem. Soc. Rev.* **2012**, *41*, 413–447.
[48] D. Braga, S. L. Giaffreda, F. Grepioni, A. Pettersen, L. Maini, M. Curzi, M. Polito, *Dalton Trans.* **2006**, 1249–1263.
[49] I. Kalf, P. Mathieu, U. Englert, *New J. Chem.* **2010**, *34*, 2491–2495.
[50] C. J. Adams, M. A. Kurawa, M. Lusi, A. G. Orpen, *CrystEngComm* **2008**, *10*, 1790–1795.
[51] J. Boeckmann, C. N ther, *Polyhedron* **2012**, *31*, 587–595.
[52] J. Boeckmann, I. Jeß, T. Reinert, C. N ther, *Eur. J. Inorg. Chem.* **2011**, 5502–5511.
[53] S. W hlert, L. Peters, C. N ther, *Dalton Trans.* **2013**, *42*, 10746–10758.
[54] T. Neumann, I. Jess, C. N ther, *Acta Crystallogr. Sect. E* **2014**, *70*, m196.
[55] S. W hlert, J. Boeckmann, I. Jess, C. N ther, *CrystEngComm* **2012**, *14*, 5412–5420.
[56] S. W hlert, T. Runčevski, R. E. Dinnebier, S. G. Ebbinghaus, C. N ther, *Cryst. Growth Des.* **2014**, *14*, 1902–1913.
[57] R. A. Bailey, S. L. Kozak, T. W. Michelsen, W. N. Mills, *Coord. Chem. Rev.* **1971**, *6*, 407–445.
[58] G. A. Van Albada, R. A. G. De Graaff, J. G. Haasnoot, J. Reedijk, *Inorg. Chem.* **1984**, *23*, 1404–1408.
[59] R. J. H. Clark, C. S. Williams, *Spectrochim. Acta* **1966**, *22*, 1081–1090.
[60] S. W hlert, T. Runčevski, R. E. Dinnebier, C. N ther, *Z. Anorg. Allg. Chem.* **2013**, *639*, 2648–2656.
[61] G. M. Sheldrick, *Acta Crystallogr., Sect. A* **2008**, *64*, 112–122.

Received: May 27, 2014
Published Online: July 25, 2014

4.5. Synthesis, Structures, and Properties of Transition Metal Thiocyanato Coordination Compounds with 4-(4-Chlorobenzyl)pyridine as Ligand

Julia Werner, Tristan Neumann, und Christian Näther, *Z. Anorg. Allg. Chem.* **2014**, *640, (14),* 2839–2846.

DOI: 10.1002/zaac.201400341

Motivation

In Kapitel 3.2 wurde bereits über die Verbindung $[Co(NCS)_2(4\text{-}(4\text{-chlorobenzyl})pyridin)_2]_n$ berichtet, welche metamagnetisches Verhalten aufweist. In Anlehnung an diese Arbeit wurde versucht entsprechende Verbindungen mit den Übergangsmetallen Mn(II), Fe(II) und Ni(II) darzustellen. Es konnten Vorläufer-Verbindungen dargestellt werden, die aus vier neutralen Co-Liganden und zwei N-terminalen Thiocyanatanionen bestehen. Eine ligandenarme Verbindung entsprechend zu dem bereits bekannten Kobalt Analogon konnte ausschließlich mit Ni(II) phasenrein synthetisiert werden. Diese Verbindung weißt Curie-Weiß Paramagnetismus auf.

ARTICLE

DOI: 10.1002/zaac.201400341

Synthesis, Structures, and Properties of Transition Metal Thiocyanato Coordination Compounds with 4-(4-Chlorobenzyl)pyridine as Ligand

Julia Werner,[a] Tristan Neumann,[a] and Christian N ther*[a]

Dedicated to Professor Martin Jansen on the Occasion of His 70th Birthday

Keywords: Crystal structure; Thiocyanato coordination polymers; Thermochemistry; IR spectroscopy; Magnetochemistry

Abstract. Reactions of transition metal thiocyanates with 4-(4-chlorobenzyl)pyridine (Clbp) lead to the formation of compounds of composition $M(NCS)_2$(4-(4-chlorobenzyl)pyridine)$_4$ (**Mn-1**, **Fe-1/I**, **Fe-1/II**, **Ni-1**, and **Cd-1**) and $M(NCS)_2$(4-(4-chlorobenzyl)pyridine)$_2$ (**Mn-2**, **Ni-2**, and **Cd-2**). In the crystal structures of compounds ***M*-1** the metal cations are octahedrally coordinated by two terminal N-bonded thiocyanato anions and four Clbp ligands, whereas in compounds ***M*-2** the metal cations are linked by μ-1,3-bridging anionic ligands. IR spectroscopic investigations show that the value of the asymmetric C–N stretching vibration depends on the coordination mode of the thiocyanato ligand and the nature of the metal cations. The thermal properties were investigated by simultaneous differential thermoanalysis and thermogravimetry as well as temperature dependent X-ray powder diffraction. On heating compound **Ni-1** looses half of the Clbp ligands and transforms into **Ni-2**. Clbp deficient intermediates were also detected on thermal decomposition of **Mn-1** and **Fe-1/I** but the samples are of low crystallinity and therefore, their structures cannot be determined. Magnetic investigations reveal that **Ni-2** show only Curie-Weiss paramagnetism without any magnetic anomaly.

Introduction

Investigations on the synthesis, structure, and properties of new coordination compounds are still an active field in coordination chemistry. The major goal in this area includes the development of strategies for a more rational synthesis of compounds with definite structures and desired physical properties.[1–11] This also includes investigations on compounds that show cooperative magnetic phenomena and therefore, a large number of compounds based on small ligands like e.g. azides, oxalates and others were recently reported.[12–18] In this context also coordination compounds based on thio- or selenocyanates are of interest and some representative examples are given in the reference list.[19–34]

In our own research, we are also interested in the magnetic properties of thio- and selenocyanato coordination polymers, with focus on compounds, in which the central metal atoms are linked by μ-1,3-bridging anionic ligands.[35] In the course of this project we have investigated several of such compounds, predominantly based on Mn^{II}, Fe^{II}, Co^{II}, and Ni^{II} that as function of the metal cations and the neutral N-donor co-ligand show different magnetic properties.[36–44] Within this project we are especially interested in compounds, in which the central metal atoms are coordinated only by monodentate ligands and are linked by pairs of thio- or selenocyanato anions into chains, which are not further connected into layers by the co-ligands. Unfortunately, the compounds with bridging ligands are sometimes difficult to prepare in solution and therefore, we use an alternative solid state route, in which suitable precursor compounds with terminal bonded anionic ligands are thermally decomposed.[45–47] The synthesis of coordination compounds via typical solid state methods is not uncommon and also other strategies were reported.[48–51] However, one disadvantage of thermal decomposition reactions is the fact that only crystalline powders and sometimes different modifications are obtained and therefore, structural information is difficult to retrieve.[52] In some cases the coordination mode of the anionic ligands might be determined by IR spectroscopy.[53,54] Moreover, structural information can also be extracted by preparing the corresponding compounds with cadmium or zinc, because in several cases they are isotypic to the paramagnetic analogs.[55,56] Therefore, systematic investigations on the synthesis, the crystal structures as well as the thermal and spectroscopic properties of thio- and selenocyanato coordination compounds are of extraordinary importance for our project.

In the course of our investigations we decided to study the influence of larger monodentate N-donor co-ligands on the thermal reactivity in more detail and for the present study Clbp was selected, for which no coordination compounds are reported in the Cambridge Structural Database.[57] Within these

* Prof. Dr. C. N ther
Fax: +49-431-8801520
E-Mail: cnaether@ac.uni-kiel.de
[a] Institut f r Anorganische Chemie
Christian-Albrechts-Universit t zu Kiel
Max-Eyth-Straße 2
24118 Kiel; Germany

Supporting information for this article is available on the WWW under **http://dx.doi.org/10.1002/zaac.201400341** or from the author.

investigations we prepared several new compounds based on Mn^{II}, Fe^{II}, Ni^{II}, and Cd^{II}, in which the central metal atoms are coordinated by terminal N-bonded anions and which might be useful as precursors for the preparation of the desired compounds with a bridging coordination. Herein we report on our results.

Results and Discussion

Synthetic Investigations

To investigate, which compounds are available in solution different ratios of $M(NCS)_2$ (M = Mn, Fe, Ni, Cd) and 4-(4-chlorobenzyl)pyridine) (Clbp) were reacted in different solvents at room temperature and the residues obtained were filtered of and investigated by elemental analysis and X-ray powder diffraction (XRPD). Elemental analyses showed that compounds of composition $M(NCS)_2(4\text{-}(4\text{-chlorobenzyl})pyridine)_4$ (**Mn-1**, **Fe-1/I**, **Ni-1**, and **Cd-1**) and of composition $M(NCS)_2(4\text{-}(4\text{-chlorobenzyl})pyridine)_2$ (**Mn-2**, **Ni-2**, and **Cd-2**) were formed (Table S1, Supporting Information). For **Mn-2** some deviations from the calculated values are found, indicating that this compound contains some contamination.

XRPD investigations indicate that **Mn-1**, **Fe-1/I**, and **Cd-1** are isotypic and that **Ni-1** crystallizes differently (Figure 1). Moreover, the residue obtained with iron at ratio 1:4 shows a different powder pattern, indicating that a second modification is obtained (**Fe-1/II**) that might be contaminated with **Fe-1/I** (Figure 1). It is noted, that the powder pattern of **Fe-1/II** is similar to that of **Ni-1** (Figure 1). IR spectroscopic investigations indicate that the C–N stretching vibrations of compounds **M-1** are in the range expected for terminally N-bonded thiocyanato anions (see below).

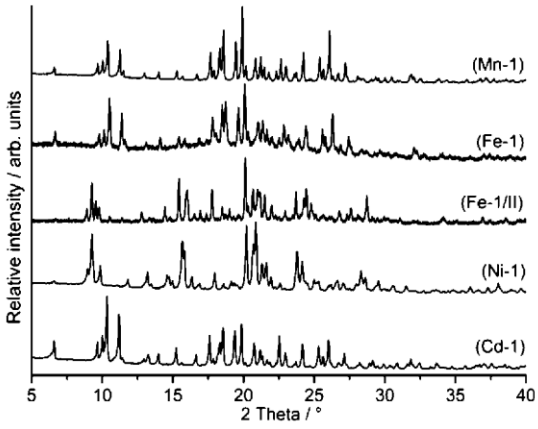

Figure 1. Experimental XRPD pattern of **Mn-1**, **Fe-1/I**, **Fe-1/II**, **Ni-1**, and **Cd-1**.

For the ***M*-2** compounds XRPD investigations indicate that **Mn-2** and **Ni-2** are isotypic, that **Cd-2** exhibits a different structure and that **Mn-2** is contaminated with large amounts of **Mn-1** (Figure 2). Based on the value of the asymmetric C–N stretching vibration it can be assumed that in compounds ***M*-2** bridging thiocyanato anions are present (see below).

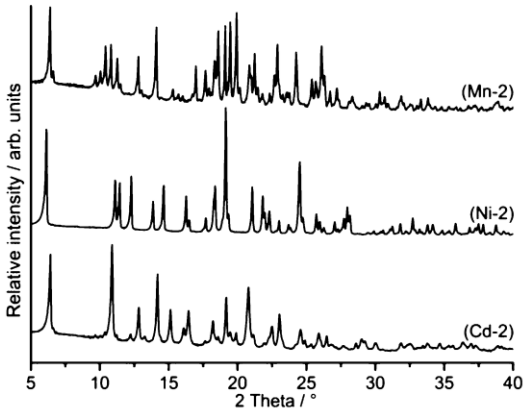

Figure 2. Experimental XRPD pattern of **Mn-2**, **Ni-2**, and **Cd-2**.

Solvent mediated conversion experiments of a mixture of **Fe-1/I** and **Fe-1/II** prove, that in water **Fe-1/II** transforms into **Fe-1/I** and therefore, that **Fe-1/I** represent the thermodynamic stable modification at room temperature (Figure S1 in the Supporting Information).

In further work crystallization experiments were performed at room temperature and under solvothermal conditions, which lead to the formation of single crystals of **Mn-1**, **Fe-1/I**, **Ni-1**, **Cd-1** as well as of **Mn-2**, **Ni-2** and **Cd-2**. Comparison of the experimental powder patterns of compounds ***M*-1** and ***M*-2** with that calculated from single crystal data proves that **Mn-1**, **Fe-1/I**, **Ni-1**, **Cd-1**, and **Ni-2** are obtained as pure phases, whereas **Mn-2** is contaminated with **Mn-1** and **Cd-2** with a small amount of an additional phase, that cannot be identified (Figures S2–S8, Supporting Information).

Crystal Structures

The compounds $M(NCS)_2(4\text{-}(4\text{-chlorobenzyl})pyridine)_4$ [M = Mn (**Mn-1**), Fe (**Fe-1/I**), and Cd (**Cd-1**)] are isotypic and crystallize in the monoclinic centrosymmetric space group *C2/c* with four formula units in the unit cell. The asymmetric unit consists of one crystallographically independent discrete complex, which is located on a center of inversion, as well as of one thiocyanato anion and two 4-(4-chlorobenzyl)pyridine ligands in general position (Figure 3). $Ni(NCS)_2(4\text{-}(4\text{-chlorobenzyl})pyridine)_4$ (**Ni-1**) crystallizes monoclinic in space group $P2_1$ with two formula units in the unit cell and all atoms in general positions.

In the crystal structures of compounds ***M*-1** the metal cations are coordinated by two nitrogen atoms of two terminal thiocyanato anions and four nitrogen atoms of terminal bonded 4-(4-chlorobenzyl)pyridine ligands within a slightly distorted octahedral coordination arrangement. The angles around the metal cations range between 88.33(17) and 91.39(8)° and the metal-

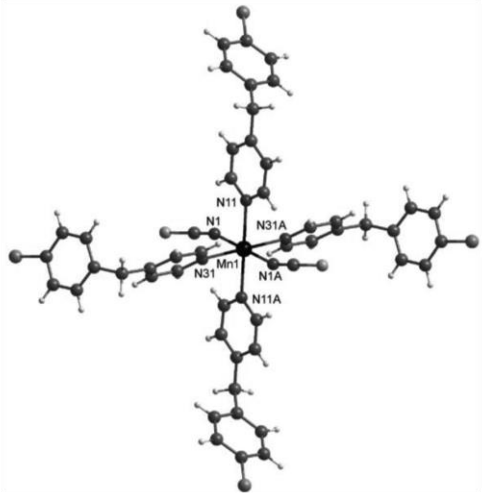

Figure 3. Crystal structure of **Mn-1** as a representative with atom labeling (Ortep plots of **Mn-1**, **Fe-1/I**, **Ni-1** and **Cd-1** are shown in Figures S9–S12 in the Supporting Information).

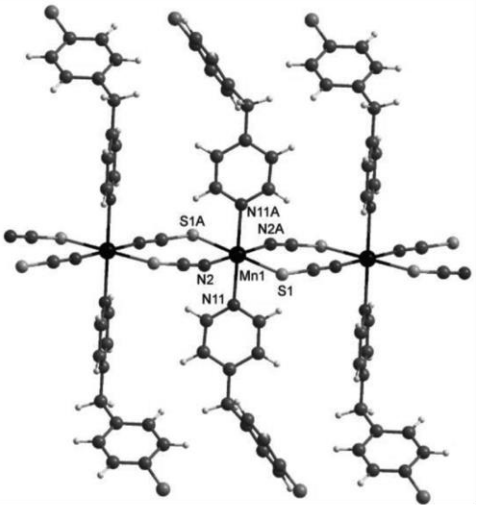

Figure 4. Crystal structure of compound **Mn-2** as a representative with atom labeling (Ortep plots of **Mn-2**, **Ni-2**, and **Cd-2** are shown in Figures S13–S15 in the Supporting Information).

nitrogen distances range between 2.040(3) and 2.381(2) . (Tables S2–S5, Supporting Information).

The compounds $[M(NCS)_2(4\text{-}(4\text{-chlorobenzyl})pyridine)_2]_n$ (M = Mn, Ni) crystallize in the triclinic centrosymmetric space group $P\bar{1}$ with two formula units in the unit cell. The asymmetric unit consists of two metal cations, which are situated on a center of inversion as well as two 4-(4-chlorobenzyl)pyridine and two thiocyanato ligands in general positions (Figure 4). $[Cd(NCS)_2(4\text{-}(4\text{-chlorobenzyl})pyridine)_2]_n$ crystallizes monoclinic in space group $P2_1/c$ with two formula unit in the unit cell. The asymmetric unit consists of two metal cations, three thiocyanato anions and three 4-(4-chlorobenzyl)pyridine ligands. One metal cation is located on center of inversion; all other atoms are located in general positions.

In their crystal structures the metal cations are coordinated by two N-bonded Clbp ligands and two N-bonded μ-1,3 bridging thiocyanato anions as well as two adjacent S-bonded μ-1,3 bridging thiocyanato anions. The cations are linked into chains by pairs of μ-1,3 bridging thiocyanato anions. The metal–nitrogen distances range between 2.027(2) and 2.335(3) as well as the metal–sulfur distances range between 2.5151(6) and 2.7438(10) (Tables S6–S8, Supporting Information).

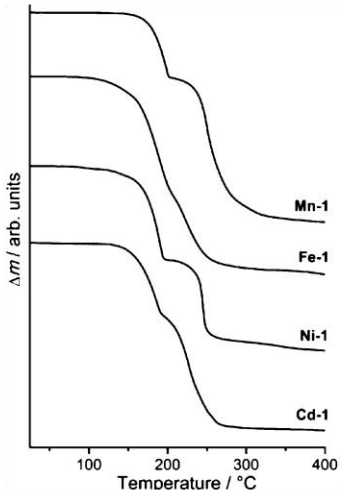

Figure 5. TG curves for the compounds **Mn-1**, **Fe-1/I**, **Ni-1**, and **Cd-1**. Heating rate = 1 °C·min^{-1}.

Thermoanalytical Investigations

To check if Clpb deficient compounds are accessible, the precursor compounds $M(NCS)_2(4\text{-}(4\text{-chlorobenzyl})$ pyridine)$_4$ (M = Mn, Fe, Ni, Cd) were investigated by simultaneous differential thermoanalysis and thermogravimetry (DTA-TG). On heating all ***M*-1** compounds show one mass step at about 200 °C, which, as function of the metal cation is differently resolved (Figure 5).

For **Mn-1** the mass loss of the first step does not correspond to that calculated for the removal of two Clbp ligands and if the residue formed in the first step is investigated by XRPD it is obvious that a mixture of **Mn-1** and **Mn-2** is obtained (Figure S20, Supporting Information). For **Fe-1/I** and **Cd-1** similar observations were made and there are no indications for additional intermediates. This does not change if all compounds are investigated by heating rate dependent measurements, which show that the best resolution is obtained with 1 °C·min^{-1} (Figures S16–19, Supporting Information). In contrast, **Ni-1** shows two good resolved mass steps and the experimental mass loss of 39.7 % in the first and 39.0 % in the second TG

step is in moderate agreement with the calculated mass loss for the removal of two 4-(4-chlorobenzyl)pyridine ligands ($\Delta m_{calcd.}$ = –41.2 %). If the residue formed after the first mass step is investigated by XRPD it is proven that **Ni-2** has formed as a pure phase (Figure 6).

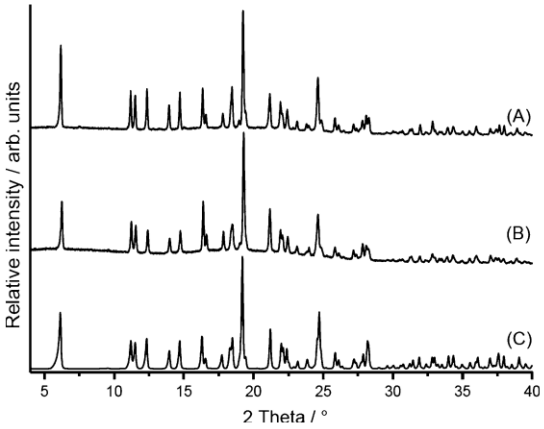

Figure 6. Experimental XRPD pattern of the residue obtained after the first mass step in thermal decomposition of compound **Ni-1** (A), experimental XRPD pattern for **Ni-2** obtained from solution (B) and calculated XRPD for compound **Ni-2** (C).

Further investigations using temperature dependent XRPD measurements on **Mn-1**, **Fe-1/I**, and **Cd-1** indicate that even for these compounds new Clbp deficient intermediates are formed, which are of low crystallinity (Figures S21–23, Supporting Information). The powder patterns of these samples do not correspond to that of compounds ***M*-2** or their mixtures with compounds **M-1** but indexing failed because of their poor quality. Summarizing, we have found no access to pure samples of **Mn-2**.

IR Spectroscopy

To investigate how the value of the C–N stretching vibration depends on the coordination mode of the ligand and the nature of the metal cation all compounds were measured by IR spectroscopy (Figures S24–31, Supporting Information). These investigations show that for all compounds with terminal N-bonded anions; ν_{as}(CN) is observed between 2051 and 2071 cm^{-1} and increases from Mn to Ni (Table 1). A similar trend is observed for the bridging compounds, for which values between 2094 and 2117 cm^{-1} are observed (Table 1). There is a clear gap between the ***M*-1** and ***M*-2** compounds, which in this case definitely allows differing between a terminal and a bridging coordination. If these values are compared with those for the corresponding compounds with pyridine as reference a small influence of the co-ligand becomes obvious, because most values are shifted by several wave numbers.[38,40]

Table 1. Values of the asymmetric C–N stretching vibration for compounds ***M*-1** and ***M*-2** as well as for the corresponding compounds with pyridine retrieved from literature.[38,40]

Compound	ν_{as}(CN) /cm^{-1}	Compound	ν_{as}(CN) /cm^{-1}
Cd-1	2054	**Cd-2**	2107
Mn-1	2051	**Mn-2**	2094
Fe-1/I	2056	**Fe-2**	–
Ni-1	2071	**Ni-2**	2117
$Cd(NCS)_2(Pyr)_4$	2050	$Mn(NCS)_2(Pyr)_2$	2097
$Mn(NCS)_2(Pyr)_4$	2060	$Mn(NCS)_2(Pyr)_2$	2090
$Fe(NCS)_2(Pyr)_4$	2066	$Mn(NCS)_2(Pyr)_2$	2093
$Ni(NCS)_2(Pyr)_4$	2082	$Mn(NCS)_2(Pyr)_2$	2110

This clearly shows that an assignment of the coordination mode for different compounds only on the basis of IR spectroscopic data might be sometimes difficult to achieve.

Magnetic Investigations

Compound **Ni-2**, in which the central metal atoms are linked by pairs of μ-1,3 bridging thiocyanato anions was investigated for its magnetic properties. It is noted that compounds ***M*-1** consist of discrete complexes and therefore, only Curie or Curie-Weiss behavior is expected as observed for related compounds reported recently.[38,40] As shown above, compound **Mn-2** is contaminated with **Mn-1** and therefore, were not investigated.

The temperature dependence of the susceptibility χ was measured as function of temperature for **Ni-2** and only paramagnetic behavior is observed. The experimental magnetic moment at room-temperature retrieved from the $(8\chi T)^{1/2}$ curve of about 2.8 μ_B is in perfect agreement with that calculated for Ni^{II} in high-spin configuration (2.82 μ_B). Analyzing the magnetic data using an Curie-Weiss fit, leads to an effective magnetic moment of 2.89 μ_B and a positive Weiss constant of 16.5 K On cooling the χT product increases indicating dominating ferromagnetic interactions between the Ni cations and afterwards the susceptibility curve passes a maximum (Figure 7).

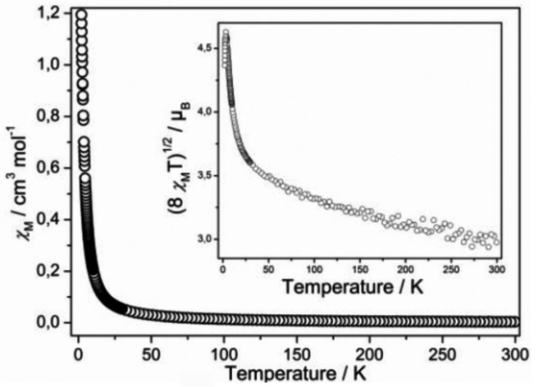

Figure 7. χ and $(8\chi T)^{1/2}$ as function of temperature for **Ni-2** measured at H_{dc} = 1 kOe.

Zeitschrift für anorganische und allgemeine Chemie ZAAC Journal of Inorganic and General Chemistry

This is in agreement with results for compounds with similar $Ni(NCS)_2$ chains like, e.g. in the two modifications of $Ni(NCS)_2$(4-ethylpyridine)$_2$, for which paramagnetic behavior dominating ferromagnetic interactions are observed and for which the χT vs. T curves looks similar.[52] It is noted, that the corresponding compound with pyridine is a metamagnet with an antiferromagnetic ground state.[40] Therefore, it cannot be excluded that antiferromagnetic ordering will occur at lower temperatures for **Ni-2**.

Conclusions

In the presented contribution new thiocyanato coordination compounds with 4 -(4-chlorobenzyl)pyridine as co-ligand were prepared and investigated for their properties. For the paramagnetic compounds it was found that the compounds with terminal bonded thiocyanato anions can easily be prepared in solution, whereas not all of the corresponding compounds with bridging anionic ligands are accessible from solution. The bridging compounds with Mn and Fe can also not be prepared by thermal decomposition and this might be traced back to the relatively large co-ligand because similar compounds with smaller co-ligands are easily accessible by this route. IR spectroscopic investigations reveal that one can easily differ between the different coordination modes and that only a small shift is observed for the different cations. Magnetic measurements on **Ni-2** reveal that only paramagnetic behavior without any magnetic anomaly is observed and this is in agreement with our findings for compounds of same composition but with slightly different co-ligands. If there is any correlation between the size of the co-ligand and the thermal reactivity of the corresponding coordination compounds will be the subject of further investigations.

Experimental Section

Synthesis: $MnSO_4 \cdot H_2O$, $NiSO_4 \cdot 6H_2O$, $CdSO_4 \cdot 8/3H_2O$, KNCS, and $FeCl_2 \cdot 4H_2O$ were obtained from Merck, $Ba(NCS)_2 \cdot 3H_2O$ and 4-(4-chlorobenzyl)pyridine were obtained from Alfa Aesar. Solvents were used without further purification. Crystalline powders of all compounds were prepared by stirring the reactants in open vessels in the respective solvents at room temperature. The residues were filtered off and washed with appropriate solvents and dried in air. The purity of all compounds was checked by X-ray powder diffraction and elemental analysis

$Cd(NCS)_2$: $Ba(NCS)_2 \cdot 3H_2O$ (3.076 g, 10 mmol) and $CdSO_4 \cdot 8/3H_2O$ (2.566 g, 10 mmol) were stirred in water (100 mL). The white precipitate of $BaSO_4$ was filtered off and the water was removed from the filtrate by heating. The final product was dried by 80 °C. The homogeneity of the product was investigated by Xray powder diffraction and elemental analysis.

$Mn(NCS)_2$: $Ba(NCS)_2 \cdot 3H_2O$ (17.9 g, 58.44 mmol) and $MnSO_4 \cdot 6H_2O$ (9.9 g, 58.44 mmol) were stirred in water (400 mL). The white precipitate of $BaSO_4$ was filtered off and the water evaporated using a rotary evaporator. The homogeneity of the product was investigated by Xray powder diffraction and elemental analysis.

$Ni(NCS)_2$: $Ba(NCS)_2 \cdot 3H_2O$ (17.5 g, 57 mmol) and $NiSO_4 \cdot 6H_2O$ (15.0 g, 57 mmol) were stirred in water (400 mL). The white precipitate of $BaSO_4$ was filtered off and the water evaporated using a rotary evaporator. The homogeneity of the product was investigated by Xray powder diffraction and elemental analysis

Synthesis of Cd-1: Single crystals suitable for single-crystal X-ray diffraction were prepared by the reaction of $Cd(NCS)_2$ (0.15 mmol, 34.3 mg) and 4-(4-chlorobenzyl)pyridine (0.15 mmol, 26.4 µL) in ethanol (1.5 mL). Colorless crystals were obtained after several days. A colorless crystalline powder on a larger scale was prepared by stirring $Cd(NCS)_2$ (114.3 mg, 0.50 mmol), and 4-(4-chlorobenzyl)pyridine (877.9 µL, 5.00 mmol) in ethanol (5 mL) for 3 d. Yield: 90.7 %. $C_{50}H_{40}N_6Cl_4S_2Cd$ (1043.25 g·mol^{-1}): calcd. C 57.57, H 3.86, N 8.06, S 6.15 %; found C 57.22, H 3.81, N 8.10, S 6.06 %. **IR** (ATR): $\tilde{\nu}_{max}$ = 3063 (w), 3038 (w), 2054 (s), 1614 (m), 1558 (w), 1490 (m), 1423 (m), 1222 (m), 1091 (m), 1069 (m), 1015 (s), 856 (m), 804 (s), 788 (s), 592 (s), 487 (s) cm^{-1}.

Synthesis of Mn-1: Single crystals suitable for single-crystal X-ray diffraction were obtained by a reaction of $Mn(NCS)_2$ (0.3 mmol, 51.3 mg) and 4-(4-chlorobenzyl)pyridine (0.15 mmol, 26.4 µL) in methanol (1.5 mL). Yellow colored block-shaped crystals were obtained after several days. A white crystalline powder on a larger scale was obtained by stirring $Mn(NCS)_2$ (171.1 mg, 1.00 mmol), and 4-(4-chlorobenzyl)pyridine (702.3 µL, 4.00 mmol) in ethanol (5 mL) for 3 d. Yield: 95.2 %. $C_{50}H_{40}N_6Cl_4S_2Mn$ (985.79): calcd. C 60.92, H 4.09, N 8.51; S 6.51 %; found C60.82, H 3.97, N 8.55, S 6.39 %. **IR** (ATR): $\tilde{\nu}_{max}$ = 3066 (w), 3036 (w), 2051 (s), 1615 (m), 1557 (w), 1488 (m), 1422 (m), 1348 (w), 1223 (m), 1014 (s), 855 (m), 804 (s), 788 (s), 591 (s), 488 (s) cm^{-1}.

Synthesis of Fe-1: Single crystals suitable for single-crystal X-ray diffraction were obtained by a reaction of $FeCl_2 \cdot 4H_2O$ (0.15 mmol, 29.8 mg), KNCS (0.3 mmol, 29.2 mg) and 4-(4-chlorobenzyl)pyridine (0.6 mmol, 105.4 µL) in acetonitrile (1.5 mL). Red colored block-shaped crystals were obtained after several days. A red-brown crystalline powder on a larger scale was obtained by stirring $FeCl_2 \cdot 4H_2O$ (198.8 mg, 1.00 mmol), KNCS (194.4 mg, 2.00 mmol) and 4-(4-chlorobenzyl)pyridine (1629.3 µL, 4.00 mmol) in H_2O (5 mL) and EtOH (3 mL) for 4 d. Yield: 92.7 %. $C_{50}H_{40}Cl_4FeN_6S_2$ (986.70): calcd. C 60.86, H 4.09, N 8.52; S 6.50 %, found C 60.84, H 4.04, N 8.36, S 5.68 %. **IR** (ATR): $\tilde{\nu}_{max}$ = 3070 (w), 3039 (w), 2915 (w), 2056 (s), 2015 (m), 1613 (s), 1557 (m), 1488 (s), 1422 (s), 1406 (m), 1222 (m), 1091 (m), 1013 (s), 855 (m), 804 (s), 788 (s), 591 (s), 489 (s) cm^{-1}.

Synthesis of Ni-1: Single crystals suitable for single-crystal X-ray diffraction were prepared by $Ni(NCS)_2$ (0.15 mmol, 26.3 mg) and 4-(4-chlorobenzyl)pyridine (0.6 mmol, 105.4 µL). After few days, light-blue well-shaped single crystals were obtained. A light-green crystalline powder on a larger scale was obtained by stirring $Ni(NCS)_2$ (174.9 mg, 0.50 mmol), and 4-(4-chlorobenzyl)pyridine (1222 µL, 6.00 mmol) in ethanol (5 mL) for 3 d. Yield: 97.6 %. $C_{50}H_{40}N_6Cl_4S_2Ni$ (989.54): calcd. C 60.69, H 4.07, N 8.49, S 6.48 %; found C 60.35, H 4.06, N 8.64, S 6.24 %. **IR** (ATR): $\tilde{\nu}_{max}$ = 3074 (w), 3031 (w), 2086 (m), 2069 (s), 1610 (m), 1558 (m), 1489 (s), 1423 (s), 1222 (m), 1090 (m), 1016, 917 (w), 788 (s), 650 (w), 592 (s), 485 (s) cm^{-1}.

Synthesis of Mn-2: Single crystals suitable for single-crystal X-ray diffraction were prepared by slow evaporation of the filtrate of the reaction of $Mn(NCS)_2$ (3.0 mmol, 511.0 mg), and 4-(4-chlorobenzyl) pyridine (0.75 mmol, 131.8 µL) in 4 mL acetonitrile.

Synthesis of Ni-2: Single crystals suitable for single-crystal X-ray diffraction were obtained by a reaction of $Ni(NCS)_2$ (0.15 mmol, 26.3 mg) and 4-(4-chlorobenzyl)pyridine (0.3 mmol, 52.7 µL) in water (1.5 mL) at 105 °C in a closed 10 mL glass culture tube. Light-blue colored crystals were obtained after several days. A light-blue crystalline powder on a larger scale was obtained by stirring $Ni(NCS)_2$ (349.7 mg, 4.00 mmol), and 4-(4-chlorobenzyl)pyridine (176 µL, 1.00 mmol) in ethanol (5 mL) for 10 d. Yield: 93.7 %. $C_{26}H_{20}N_4Cl_2S_2Ni$ (582.20): calcd. C 53.64, H 3.46, N 9.62, S 11.02 %; found C 53.45, H 3.42, N 9.88, S 11.03 %. **IR** (ATR): $\tilde{\nu}_{max}$ = 2910 (w), 2118 (s), 1613 (m), 1559 (w), 1489 (m), 1423 (m), 1223 (w), 1094 (m), 1067 (m), 1014 (m), 919 (w), 852 (m), 807 (m), 787 (s), 656 (w), 597 (s), 492 (s) cm^{-1}.

Synthesis of Cd-2: Single crystals suitable for single-crystal X-ray diffraction were obtained by a reaction of $Cd(NCS)_2$ (0.30 mmol, 68.6 mg) and 4-(4-chlorobenzyl)pyridine (0.15 mmol, 26.3 µL) in acetonitrile (1.5 mL) at room temperature. Colorless crystals were obtained after several days. A colorless crystalline powder on a larger scale was obtained by stirring $Cd(NCS)_2$ (114.3 mg, 0.50 mmol), and 4-(4-chlorobenzyl)pyridine (93.8 µL, 0.50 mmol) in ethanol (2 mL) and H_2O (1 mL) for 3 d. Yield: 75.2 %. $C_{26}H_{20}CdCl_2N_4S_2$ (635.91): calcd. C 49.11, H 3.17, N 8.81, S 10.09 %; found C 49.12, H 3.09, N 8.93, S 10.22 %. **IR** (ATR): $\tilde{\nu}_{max}$ = 2108 (s), 1665 (m), 1609 (m), 1558 (w), 1491 (m), 1425 (m), 1286 (w), 1225 (m), 1092 (m), 1070 (m), 1017 (s), 918 (w), 855 (m), 786 (s), 669 (w), 594 (s), 482 (s) cm^{-1}.

Elemental Analysis: CHNS analysis was performed with an EURO EA elemental analyzer, fabricated by EURO VECTOR Instruments and Software.

Elemental Analysis of the Residue Obtained in the Thermal Decomposition: Isolated in the first heating step (see thermoanalytical investigations) of compound **Ni-1**. Calculated for the ligand-deficient compound **Ni-2**: $C_{26}H_{20}N_4Cl_2S_2Ni$ (582.20): calcd. C 53.64, H 3.46, N 9.62; S 11.02 %; found C 53.53, H 3.39, N 9.50, S 11.03 %.

Differential Thermal Analysis and Thermogravimetry: The DTA-TG measurements were performed in a dynamic nitrogen atmosphere (purity: 5.0) in Al_2O_3 crucibles with a STA-409CD thermobalance from Netzsch. All measurements were performed with a flow rate of 75 mL min^{-1} and were corrected for buoyancy and current effects. The instrument was calibrated using standard reference materials.

Single-Crystal Structure Analysis: The investigations were performed with the imaging plate diffraction system (IPDS-1 for **Cd-1**; IPDS-2 for **Mn-1, Fe-1, Ni-1, Mn-2, Ni-2**) with Mo-K_α-radiation from STOE & CIE. The structure solution was performed with direct methods using SHELXS-97 and structure refinements were performed against F^2 using SHELXL-97. All non-hydrogen atoms were refined with anisotropic displacement parameters. The hydrogen atoms were positioned with idealized geometry and were refined with fixed isotropic displacement parameters [$U_{iso}(H) = 1.2 \cdot U_{eq}(C_{aromatic})$ using a riding model. For compounds **Mn-1**, **Fe-1**, and **Cd-1** the Cl atom is disordered over two sites and was refined using a split model. The crystal of compound **Ni-1** is racemically twinned and therefore, a twin refinement was performed (BASF parameter: 0.28401).

Crystallographic data (excluding structure factors) for the structures in this paper have been deposited with the Cambridge Crystallographic Data Centre, CCDC, 12 Union Road, Cambridge CB21EZ, UK. Copies of the data can be obtained free of charge on quoting the depository numbers CCDC-1021251 (**Mn-1**), CCDC-1021533 (**Fe-1**), CCDC-

Table 2. Selected crystal data and details on the structure determinations for compounds ***M*-1** (*M* = Cd, Mn, Fe, Ni) and ***M*-2** (*M* = Cd, Mn, Ni).

	Cd-1	**Mn-1**	**Fe-1**	**Ni-1**	**Cd-2**	**Mn-2**	**Ni-2**
Formula	$C_{50}H_{40}CdN_6Cl_4S_2$	$C_{50}H_{40}Cl_4MnN_6S_2$	$C_{50}H_{40}Cl_4FeN_6S_2$	$C_{50}H_{40}Cl_4N_6NiS_2$	$C_{78}H_{60}Cd_3Cl_6N_{12}S_6$	$C_{26}H_{20}Cl_2MnN_4S_2$	$C_{26}H_{20}Cl_2N_4NiS_2$
MW /g·mol^{-1}	1043.20	985.74	986.65	989.51	1907.64	578.42	582.19
Crystal system	monoclinic	monoclinic	monoclinic	monoclinic	monoclinic	triclinic	triclinic
Space group	*C*2/*c*	*C*2/*c*	*C*2/*c*	$P2_1$	$P2_1/c$	$P\bar{1}$	$P\bar{1}$
a /	18.9719(13)	19.0051(8)	18.8321(6)	13.199(3)	17.4730(6)	9.0790(10)	9.0222(4)
b /	9.7143(5)	9.6769(4)	9.5826(2)	13.613(3)	8.2738(4)	11.0140(15)	10.7966(5)
c /	27.6679(19)	27.8212(9)	27.6478(10)	13.454(3)	29.5128(13)	14.898(3)	14.9511(7)
α /°	90.000	90.00	90.00	90.000	90.000	73.854(13)	73.166(4)
β /°	106.855(8)	106.656(3)	106.794(3)	95.54(3)	107.970(3)°	82.870(13)	83.501(4)
γ /°	90.000	90.000	90.00	90.000	90.000	68.830(9)	67.963(4)
V / ^{3}	4880.1(5)	4901.9(3)	4776.5(3)	2406.1(8)	4058.5(3)	1333.9(3)	1292.11(10)
T /K	293	293	293	293	200	200	200
Z	4	4	4	2	2	2	2
D_{calc} /g·cm^{-3}	1.420	1.336	1.372	1.366	1.561	1.440	1.496
μ /mm^{-1}	0.793	0.613	0.669	0.753	1.181	0.874	1.142
θ_{max} /°	28.06	26.00	27.53	26.00	25.45	26.99	27.00
Measured refl.	20586	19496	29617	17043	36322	15000	18683
R_{int}	0.0768	0.0251	0.0338	0.0380	0.0460	0.0471	0.0413
Unique reflns.	5805	4793	5454	9281	7435	5789	5641
Refl. [$F_o > 4\sigma(F_o)$]	4223	3844	4575	6826	6148	4497	4398
Parameters	296	295	296	569	541	319	320
R_1 [$F_o > 4\sigma(F_o)$]	0.0438	0.0489	0.0491	0.0575	0.0417	0.0333	0.0421
wR_2 [all data]	0.1035	0.1232	0.1074	0.1140	0.0793	0.0870	0.0939
GOF	1.026	1.058	1.075	1.108	1.092	1.026	1.047
$\Delta\rho_{max/min}$ /e· $^{-3}$	0.500/ –0.526	0.418/ –0.366	0.417/ –0.337	0.270/ –0.177	0.706/ –0.654	0.310/ –0.375	0.349/ –0.427

Zeitschrift für anorganische und allgemeine Chemie ZAAC Journal of Inorganic and General Chemistry

1021252 (**Ni-1**), CCDC-1021250 (**Cd-1**), CCDC-1021248 (**Mn-2**), CCDC-1021249 (**Ni-2**) and CCDC-1021247 (**Cd-2**) (Fax: +44-1223-336-033; E-Mail: deposit@ccdc.cam.ac.uk, http://www.ccdc.cam.ac.uk).

X-ray Powder Diffraction (XRPD): XRPD experiments were performed with a Stoe Transmission Powder Diffraction System (STADI P) with Cu-K_α-radiation (λ = 1.5406) that is equipped with a linear position-sensitive detector (Delta 2 θ = 6.5–7° simultaneous; scan range overall = 2–130°) from STOE & CIE and an Image Plate Detector (scan range overall = 0–127°) and a PANalytical X'Pert Pro MPD reflection powder diffraction system with Cu-K_α radiation (λ = 154.0598 pm) equipped with a PIXcel semiconductor detector from PANanlytical. Crystallographic data and structure refinement results are summarized in Table 2.

Temperature dependent XRPD measurements were performed with a high temperature chamber HTK 1200N with He atmosphere from Anton Paar (heating rate 3 °C·min^{-1} in a temperature rate from 25–300 °C).

Magnetic Measurements: All magnetic measurements were performed with a Physical Property Measuring System (PPMS) from Quantum Design, which is equipped with a 9 T magnet. The data were corrected for Core diamagnetism using Pascal constants.[58]

Supporting Information (see footnote on the first page of this article): Calculated XRPD patterns, Ortep plots, tables with bond lengths and angles, TG curves, temperature dependent XRPD measurements, and selected magnetic curves.

Acknowledgements

This project was supported by the Deutsche Forschungsgemeinschaft (Project No. NA 720/5–1) and the State of Schleswig-Holstein. We thank *Professor Dr. Wolfgang Bensch* for access to his experimental facility. Special thanks to *Inke Jess* for the single crystal measurements.

References

[1] S. R. Batten, K. S. Murray, *Coord. Chem. Rev.* **2003**, *246*, 103–130.
[2] C. Janiak, *Dalton Trans.* **2003**, 2781–2804.
[3] C. Janiak, L. Uehlin, H.-P. Wu, P. Kl fers, H. Piotrowski, T. G. Scharmann, *J. Chem. Soc., Dalton Trans.* **1999**, 3121–3131.
[4] S. Kitagawa, R. Matsuda, *Coord. Chem. Rev.* **2007**, *251*, 2490–2509.
[5] D. Maspoch, D. Ruiz-Molina, J. Veciana, *J. Mater. Chem.* **2004**, *14*, 2713–2723.
[6] D. Maspoch, D. Ruiz-Molina, J. Veciana, *Chem. Soc. Rev.* **2007**, *36*, 770–818.
[7] B. Moulton, M. J. Zaworotko, *Chem. Rev.* **2001**, *101*, 1629–1658.
[8] A. Y. Robin, K. M. Fromm, *Coord. Chem. Rev.* **2006**, *250*, 2127–2157.
[9] D. Braga, L. Maini, M. Polito, L. Scaccianoce, G. Cojazzi, F. Grepioni, *Coord. Chem. Rev.* **2001**, *216*, 225–248.
[10] C. N ther, G. Bhosekar, I. Jeß, *Inorg. Chem.* **2007**, *46*, 8079–8087.
[11] C. Janiak, J. K. Vieth, *New J. Chem.* **2010**, *34*, 2366–2388.
[12] Y.-Q. Wang, Q. Sun, Q. Yue, A.-L. Cheng, Y. Song, E.-Q. Gao, *Dalton Trans.* **2011**, *40*, 10966–10974.
[13] Y.-F. Zeng, X. Hu, F.-C. Liu, X.-H. Bu, *Chem. Soc. Rev.* **2009**, *38*, 469–480.
[14] X.-M. Zhang, Y.-Q. Wang, X.-B. Li, E.-Q. Gao, *Dalton Trans.* **2012**, *41*, 2026–2033.
[15] X.-Y. Wang, Z.-M. Wang, S. Gao, *Chem. Commun.* **2008**, 281–294.
[16] B. Gil-Hernandez, J. K. Maclaren, H. A. Hoppe, J. Pasan, J. Sanchiz, C. Janiak, *CrystEngComm* **2012**, *14*, 2635–2644.
[17] X.-Y. Wang, L. Wang, Z.-M. Wang, G. Su, S. Gao, *Chem. Mater.* **2005**, *17*, 6369–6380.
[18] J. Carranza, J. Sletten, F. Lloret, M. Julve, *Inorg. Chim. Acta* **2011**, *371*, 13–19.
[19] E. Shurdha, S. H. Lapidus, P. W. Stephens, C. E. Moore, A. L. Rheingold, J. S. Miller, *Inorg. Chem.* **2012**, *51*, 9655–9665.
[20] C. J. Adams, M. F. Haddow, D. J. Harding, T. J. Podesta, R. E. Waddington, *CrystEngComm* **2011**, *13*, 4909–4914.
[21] C. J. Adams, M. C. Mu oz, R. E. Waddington, J. A. Real, *Inorg. Chem.* **2011**, *50*, 10633–10642.
[22] J. Tercero, C. Diaz, J. Ribas, J. Mahia, M. Maestro, X. Solans, *J. Chem. Soc., Dalton Trans.* **2002**, 2040–2046.
[23] J. M. Shi, J. N. Chen, C. J. Wu, J. P. Ma, *J. Coord. Chem.* **2007**, *60*, 2009–2013.
[24] B. Machura, J. Palion, M. Penkala, T. Groń, H. Duda, R. Kruszynski, *Polyhedron* **2013**, *56*, 189–199.
[25] B. Machura, A. Świtlicka, J. Mroziński, B. Kalińska, R. Kruszynski, *Polyhedron* **2013**, *52*, 1276–1286.
[26] E. Shurdha, C. E. Moore, A. L. Rheingold, S. H. Lapidus, P. W. Stephens, A. M. Arif, J. S. Miller, *Inorg. Chem.* **2013**, *52*, 10583–10594.
[27] M. Mousavi, V. Bereau, C. Duhayon, P. Guionneau, J.-P. Sutter, *Chem. Commun.* **2012**, *48*, 10028–10030.
[28] J.-F. L tard, S. Asthana, H. J. Shepherd, P. Guionneau, A. E. Goeta, N. Suemura, R. Ishikawa, S. Kaizaki, *Chem. Eur. J.* **2012**, *18*, 5924–5934.
[29] R. Gonz lez, A. Acosta, R. Chiozzone, C. Kremer, D. Armentano, G. De Munno, M. Julve, F. Lloret, J. Faus, *Inorg. Chem.* **2012**, *51*, 5737–5747.
[30] P. Bhowmik, S. Chattopadhyay, M. G. B. Drew, C. Diaz, A. Ghosh, *Polyhedron* **2010**, *29*, 2637–2642.
[31] Q. Ma, M. Zhu, L. Lu, S. Feng, J. Yan, *Inorg. Chim. Acta* **2011**, *370*, 102–107.
[32] S. S. Massoud, L. L. Quan, K. Gatterer, J. H. Albering, R. C. Fischer, F. A. Mautner, *Polyhedron* **2012**, *31*, 601–606.
[33] F. Mautner, F. Louka, A. Gallo, J. Albering, M. Saber, N. Burham, S. Massoud, *Transition Met. Chem.* **2010**, *35*, 613–619.
[34] F. A. Mautner, R. Vicente, S. S. Massoud, *Polyhedron* **2006**, *25*, 1673–1680.
[35] C. N ther, S. W hlert, J. Boeckmann, M. Wriedt, I. Jeß, Z. *Anorg. Allg. Chem.* **2013**, *639*, 2696–2714.
[36] S. W hlert, J. Boeckmann, M. Wriedt, C. N ther, *Angew. Chem. Int. Ed.* **2011**, *50*, 6920–6923.
[37] J. Boeckmann, M. Wriedt, C. N ther, *Chem. Eur. J.* **2012**, *18*, 5284–5289.
[38] J. Boeckmann, C. N ther, *Dalton Trans.* **2010**, *39*, 11019–11026.
[39] S. W hlert, U. Ruschewitz, C. N ther, *Cryst. Growth Des.* **2012**, *12*, 2715–2718.
[40] J. Boeckmann, C. N ther, *Polyhedron* **2012**, *31*, 587–595.
[41] S. W hlert, Z. Tomkowicz, M. Rams, S. G. Ebbinghaus, L. Fink, M. U. Schmidt, C. N ther, *Inorg. Chem.* **2014**, *53*, 8298–8310.
[42] S. W hlert, T. Fic, Z. Tomkowicz, S. G. Ebbinghaus, M. Rams, W. Haase, C. N ther, *Inorg. Chem.* **2013**, *52*, 12947–12957.
[43] S. W hlert, M. Wriedt, T. Fic, Z. Tomkowicz, W. Haase, C. N ther, *Inorg. Chem.* **2013**, *52*, 1061–1068.
[44] J. Boeckmann, C. N ther, *Chem. Commun.* **2011**, *47*, 7104–7106.
[45] M. Wriedt, I. Jeß, C. N ther, *Eur. J. Inorg. Chem.* **2009**, 1406–1413.
[46] M. Wriedt, S. Sellmer, C. N ther, *Dalton Trans.* **2009**, 7975–7984.
[47] M. Wriedt, C. N ther, *Chem. Commun.* **2010**, *46*, 4707–4709.
[48] C. J. Adams, M. A. Kurawa, M. Lusi, A. G. Orpen, *CrystEngComm* **2008**, *10*, 1790–1795.

[49] S. L. James, C. J. Adams, C. Bolm, D. Braga, P. Collier, T. Friscic, F. Grepioni, K. D. M. Harris, G. Hyett, W. Jones, A. Krebs, J. Mack, L. Maini, A. G. Orpen, I. P. Parkin, W. C. Shearouse, J. W. Steed, D. C. Waddell, *Chem. Soc. Rev.* **2012**, *41*, 413–447.
[50] D. Braga, S. L. Giaffreda, F. Grepioni, A. Pettersen, L. Maini, M. Curzi, M. Polito, *Dalton Trans.* **2006**, 1249–1263.
[51] K. M ller-Buschbaum, *Z. Anorg. Allg. Chem.* **2005**, *631*, 811–828.
[52] S. W hlert, T. Runčevski, R. E. Dinnebier, S. G. Ebbinghaus, C. N ther, *Cryst. Growth Des.* **2014**, *14*, 1902–1913.
[53] R. J. H. Clark, C. S. Williams, *Spectrochim. Acta* **1966**, *22*, 1081–1090.
[54] R. A. Bailey, S. L. Kozak, T. W. Michelsen, W. N. Mills, *Coord. Chem. Rev.* **1971**, *6*, 407–445.
[55] S. W hlert, L. Peters, C. N ther, *Dalton Trans.* **2013**, *42*, 10746–10758.
[56] I. Jeß, J. Boeckmann, C. N ther, *Dalton Trans.* **2012**, *41*, 228–236.
[57] F. Allen, *Acta Crystallogr., Sect. B* **2002**, *58*, 380–388.
[58] G. A. Bain, J. F. Berry, *J. Chem. Educ.* **2008**, *85*, 532–536.

Received: July 25, 2014
Published Online: October 6, 2014

4.6. Synthesis, Crystal Structures, and Thermal and Spectroscopic Properties of Thiocyanato Coordination Compounds with 3-Acetylpyridine as a Ligand

Julia Werner, Inke Jeß und Christian Näther, *Z. Naturforsch.* **2014**, *69b*, 1419-1428.

DOI: 10.5560/ZNB.2014-4148

Motivation

Im Rahmen systematischer Untersuchungen wurden $M(NCS)_2$ (M = Mn, Fe, Ni) mit 3-Acetylpyridin zur Reaktion gebracht. Es konnten zum einen diskrete Komplexe mit zwei N-terminal koordinierten Thiocyanatanionen und vier 3-Acetylpyridin Liganden und zum anderen diskrete Komplexe mit zwei N-terminal koordinierten Thiocyanatanionen, zwei Wassermolekülen und zwei 3-Acetylpyridin Liganden synthetisiert werden. Diese Komplexe eignen sich als Vorläufer Verbindungen für thermische Abbaureaktionen, welche sich als mögliche Route zur Herstellung von Koordinationspolymeren mit μ-1,3-verbrückenden Thiocyanatanionen bewährt hat. Dabei wurden Verbindungen der Zusammensetzung $[M(NCS)_2(3\text{-Acetylpyridin})_2]_n$ und $[M(NCS)_2(3\text{-Acetylpyridin})]_n$ erhalten, die jedoch nur über IR spektroskopische Untersuchungen charakterisiert werden konnten. Diese Untersuchungen legen nahe, dass die Metallkationen in diesen Verbindungen durch Thiocyanatanionen zu Koordinationsnetzwerken verbunden sind. Die Ergebnisse werden in der nachfolgenden Arbeit vorgestellt.

Synthesis, Crystal Structures, and Thermal and Spectroscopic Properties of Thiocyanato Coordination Compounds with 3-Acetylpyridine as a Ligand

Julia Werner, Inke Jeß and Christian N ther

Institut f r Anorganische Chemie, Christian-Albrechts-Universit t zu Kiel, Max-Eyth-Straße 2, 24118 Kiel, Germany

Reprint requests to Prof. Dr. Christian N ther. Fax: +49-431-8801520.
E-mail: cnaether@ac.uni-kiel.de

Z. Naturforsch. **2014**, *69b*, 1419 – 1428 / DOI: 10.5560/ZNB.2014-4148
Received July 8, 2014

Dedicated to Professor Hubert Schmidbaur on the occasion of his 80th birthday

The reaction of transition metal thiocyanates with 3-acetylpyridine (3-Acpy) leads to the formation of compounds of compositions $M(NCS)_2(3\text{-Acpy})_4$ (**M1**; M = Mn, Fe, Ni) and $M(NCS)_2(3\text{-Acpy})_2(H_2O)_2$ (**M2**; M = Mn, Fe, Ni). Thermogravimetric investigations show that in the first step some of these compounds transform into the new coordination polymers $M(NCS)_2(3\text{-Acpy})_2$ (**M3** with M = Mn, Fe and Ni), that decompose into the new compounds $M(NCS)_2(3\text{-Acpy})$ (**M4** with M = Mn and Ni) in the second step. Unfortunately, the powder patterns of compounds **M3** and **M4** cannot be indexed, and there are strong indications that these compounds are contaminated with a small amount of the precursor or unknown crystalline phases. IR spectroscopic investigations indicate that in compounds **M3** the metal cations are linked by μ-1,3-bridging thiocyanato anions into 1D or 2D coordination polymers that are further linked by the 3-Acpy ligands in compounds **M4**.

Key words: Synthesis, Thiocyanato Coordination Compounds, Crystal Structures, Thermoanalytical Measurements, IR Spectroscopy

Introduction

Investigations on the synthesis, structures and properties of transition metal coordination polymers is still an important field in inorganic chemistry [1 – 12]. One interesting aspect of this class of compounds is that their network dimensionality and their network topology can be influenced to some extend based on some basic knowledge on the coordination properties of the metal cations, the anionic ligands and the neutral co-ligands [1 – 8]. In most cases such compounds are prepared in solution, in which different species might exists in equillibria and therefore, on crystallization mixtures of different compounds are sometimes obtained [13]. In some cases, these problems can be overcome if typical solid-state methods are used, and some selected examples are given in the reference list [14 – 19].

In this context we have reported on thermal decomposition reactions for the preparation of new copper(I) halide coordination polymers [20 – 22]. Later on we became interested in the synthesis of magnetic materials based on transition metal thiocyanates. For such compounds interesting properties like, *e. g.*, spin crossover or cooperative magnetic phenomena have been reported [23 – 41]. The latter are especially observed in cases, where the metal cations are linked by μ-1,3-bridging ligands. However, in contrast to compounds in which the thiocyanato anions are only terminally bonded, the corresponding species with bridging anionic ligands are less stable and thus, sometimes more difficult to prepare. This is the reason why we have developed an alternative approach that is based on the thermal decomposition of precursors with terminally bonded thio- and selenocyanato anions [42 – 45]. Within this project we have reported a number of compounds that show different magnetic properties including a slow relaxation of the magnetization [46 – 55]. Unfortunately, upon thermal decomposition usually crystalline powders are obtained that hinder a struc-

ture determination. First information on the coordination mode of the anionic ligands can be retrieved from IR spectroscopy, but – because these values are based on relatively old work – in some cases no definite decision can be made [56–58]. This is one of the reasons why we are also interested in the spectroscopic properties of such compounds. However, structural information can also be obtained by preparing the corresponding cadmium compounds. In several cases they are isotypic to the paramagnetic compounds, which allows the determination of their structures using Rietveld refinements [59–61].

In the course of our project we have also investigated the influence of the neutral *N*-donor co-ligand on the thermal, spectroscopic and magnetic properties of such compounds, and in this contribution we report on new coordination compounds based on Mn, Fe and Ni thiocyanates with 3-acetylpyridine as a co-ligand.

Results and Discussion

Synthetic investigations

Different molar ratios of $M(NCS)_2$ (M = Mn, Fe, Ni) and 3-acetylpyridine (3-Acpy) were stirred in water, ethanol, methanol, and acetonitrile, and the resulting crystalline powders were investigated by powder X-ray diffraction. These experiments indicated the presence of three different crystalline phases, and elemental analyses revealed that the compositions of these phases are $M(NCS)_2(3\text{-Acpy})_4$ (M = Mn, Fe, Ni) (**M1**) and $M(NCS)_2(3\text{-Acpy})_2(H_2O)_2$ (M = Mn, Fe, Ni) (**M2**). IR-spectroscopic measurements suggested that the thiocyanato anions are terminally bonded. The compounds **Mn1** and **Fe1** are isotypic, whereas **Ni1** crystallizes in a different modification, and according to PXRD investigations all compounds **M2** are isotypic.

Crystallization experiments led to single crystals of **Mn1**, **Fe1**, **Mn2**, **Fe2**, and **Ni2**, which were investigated by single-crystal X-ray diffraction (see below). Based on these results the powder X-ray patterns were calculated and compared with the experimental patterns (Figs. 1 and 2). The results confirmed that the hydrates **M2** (M = Mn, Fe, Ni) are isotypic, **Mn1** and **Fe1** are also isotypic, whereas **Ni1** crystallizes in a different modification and that all compounds were obtained as pure phases (Figs. 1 and 2). The fact that the structures of such coordination compounds with Mn and Fe are isotypic, whereas those with Ni are different has also been found in related compounds with different co-ligands [55].

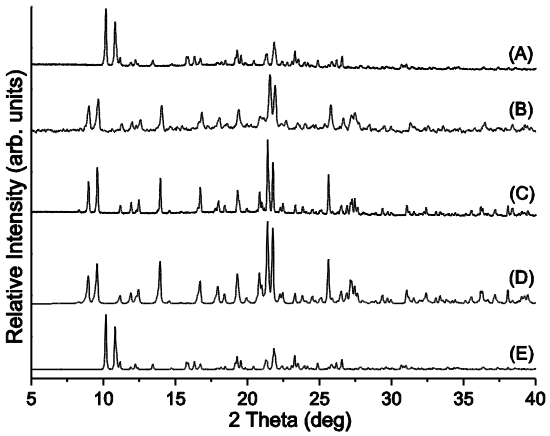

Fig. 1. Experimental powder X-ray patterns of **Ni1** (A), **Fe1** (B) and **Mn1** (C) together with the powder patterns of **Mn1** (D) and **Ni1** (E) calculated from single-crystal data. Please note that **Mn1** and **Fe1** are isotypic.

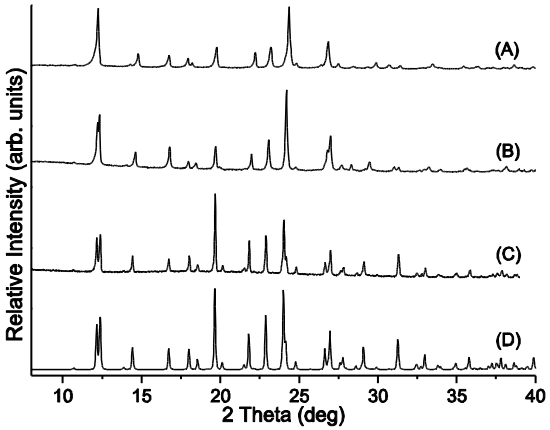

Fig. 2. Experimental powder X-ray patterns of **Ni2** (A), **Fe2** (B) and **Mn2** (C) together with the powder pattern of **Mn2** (D) as a representative calculated from single-crystal data.

Crystal structures of Fe1 and Ni1

$Fe(NCS)_2$(3-acetylpyridine)$_4$ (**Fe1**) and $Mn(NCS)_2$(3-acetylpyridine)$_4$ (**Mn1**) crystallize in the triclinic centrosymmetric space group $P\bar{1}$ with two formula

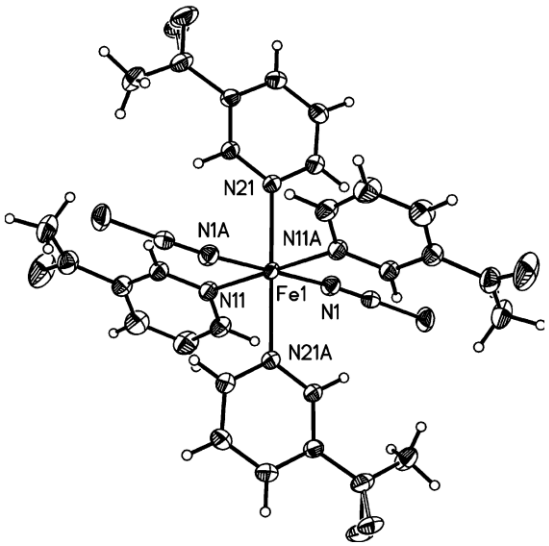

Fig. 3. View of one of the discrete complexes in the crystal structure of **Fe1** with atom labeling and displacement ellipsoids drawn at the 50 % probability level.

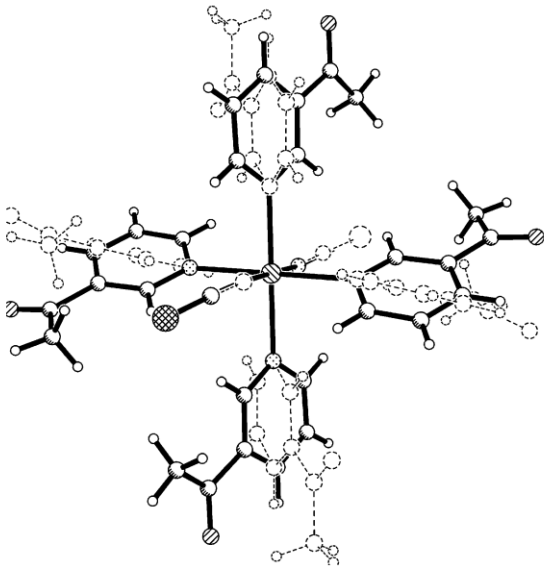

Fig. 4. Superposition of the two crystallographically independent complexes in the crystal structure of **Fe1**.

units in the unit cell. The asymmetric unit consists of two crystallographically independent metal cations which are located on centers of inversion and of two thiocyanato anions and four 3-Acpy ligands the atoms of which occupy general positions (Fig. 3).

$Ni(NCS)_2$(3-acetylpyridine)$_4$ (**Ni1**) crystallizes in the monoclinic space group $C2/c$ with 8 formula units in the unit cell. The asymmetric unit consists of two crystallographically independent nickel cations each of them located on a twofold ration axis, as well as of four thiocyanato anions and four 3-Acpy ligands with atoms on general positions. In the crystal structures of all compounds the metal cations are coordinated by two terminal *N*-bonded thiocyanato anions and four 3-Acpy ligands with a slightly distorted octahedral geometry.

Bond lengths and angles in the two independent complexes of **Fe1** are comparable but large differences are found in the conformation of the 3-Acpy ligands (Table 1, Fig. 4). As expected the *M*–N distances to the thiocyanato anions are shorter than those to the neutral co-ligands, and all these values are shorter for **Ni1** compared to **Mn1** (Table 1).

*Crystal structures of **Mn2**, **Fe2** and **Ni2***

The compounds $M(NCS)_2$(3-acetylpyridine)$_2$ $(H_2O)_2$ (**M2**; M = Mn, Fe, Ni) are isotypic and

Table 1. Selected bond lengths ( ) and angles (deg) for **Fe1** and **Ni1**. Symmetry codes: A: $-x, -y+1, -z+1$, B: $-x+1, -y, -z$.

	Fe1	**Ni1**		**Fe1**	**Ni1**
M(1)–N(1)	2.0849(14)	2.0452(17)	N(1)–*M*(1)–N(21A)	89.44(5)	90.30(7)
M(2)–N(2)	2.0697(14)	2.042(2)	N(2)–*M*(2)–N(31)	90.78(5)	90.08(8)
M(1)–N(11)	2.2372(14)	2.1292(16)	N(11)–*M*(1)–N(21)	93.54(5)	90.33(6)
M(1)–N(21)	2.2578(12)	2.1317(16)	N(11)–*M*(1)–N(21A)	86.46(5)	178.05(6)
M(2)–N(31)	2.2293(13)	2.1265(18)	N(2)–*M*(2)–N(31B)	89.22(5)	89.98(8)
M(2)–N(41)	2.3019(13)	2.1438(17)	N(2)–*M*(2)–N(41B)	91.18(5)	90.58(7)
N(1)–*M*(1)–N(11)	91.10(5)	91.52(7)	N(2)–*M*(2)–N(41)	88.82(5)	89.35(7)
N(1)–*M*(1)–N(11A)	88.90(5)	89.48(7)	N(31)–*M*(2)–N(41B)	87.31(5)	178.20(7)
N(1)–*M*(1)–N(21)	90.56(5)	88.69(7)	N(31)–*M*(2)–N(41)	92.69(5)	90.75(7)

Table 2. Selected bond lengths ( ) and angles (deg) for **Mn2**, **Fe2** and **Ni2**. Symmetry code: A: $-x, -y, -z$.

	Mn2	Fe2	Ni2
M(1)–N(1)	2.1753(15)	2.1222(13)	2.0456(14)
M(1)–N(11)	2.3135(14)	2.2403(13)	2.1293(15)
M(1)–O(1)	2.1922(13)	2.1217(11)	2.0845(12)
N(1)–*M*(1)–O(1)	92.11(6)	91.54(5)	90.91(6)
N(1)–*M*(1)–N(11)	91.46(6)	91.64(5)	91.05(6)
N(1)–*M*(1)–N(11A)	88.54(6)	88.36(5)	88.95(6)

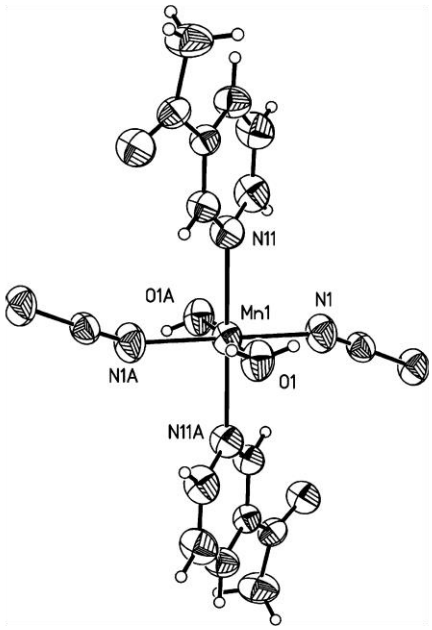

Fig. 5. Molecular structure of **Mn2** in the crystal with atom labeling and displacement ellipsoids drawn at the 50% probability level. For symmetry operations see caption to Table 2.

crystallize in the triclinic space group $P\bar{1}$ with one formula unit in the unit cell. The asymmetric unit consists of one metal cation, which is located on a center of inversion and one thiocyanato anion, one 3-Acpy ligand and one water molecule in general positions (Fig. 5). The metal cations are coordinated by two terminally bonded thiocyanato anions, two *N*-bonded 3-Acpy ligands and two water molecules within a slightly distorted octahedral geometry (Table 2). As expected, the *M*–N and *M*–O bond lengths decrease with decreasing cation radii, and the *M*–N bond lengths to the negatively charged 3-Acpy ligands are significantly shorter than those to the neutral 3-Acpy ligands.

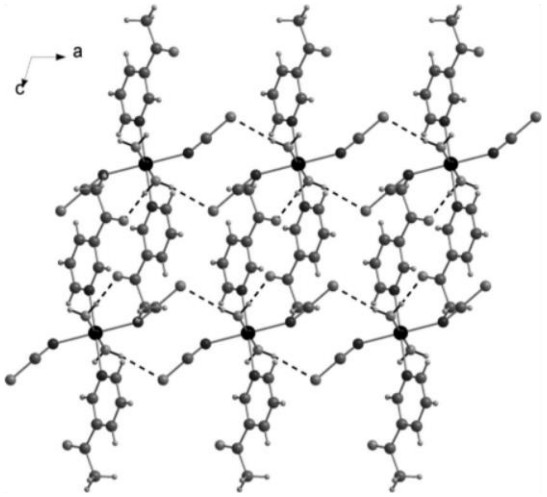

Fig. 6. Crystal structure of **Mn2** as a representative as viewed along the crystallographic *b* axis with intermolecular hydrogen bonding shown as dashed lines.

In the crystal structure the individual complexes are linked by intermolecular O–H···O hydrogen bonds into chains that elongate in the direction of the crystallographic *c* axis (Fig. 6). These chains are further linked by intermolecular O–H···S hydrogen bonds into layers that are located in the *a c* plane (Fig. 6). The intermolecular O···O and O···S distances of 2.740 and 3.226 and the O–H···O and O–H···S angles of 172.4 and 167.4°, respectively, indicate strong interactions.

*Thermoanalytical investigations on compounds **M1** and **M2***

To investigate if the 3-Acpy-rich compounds are suitable precursors for the preparation of new compounds with bridging thiocyanato anions the thermal properties were investigated using simultaneous differential thermoanalysis and thermogravimetry. Upon heating compounds **Mn1** and **Fe1** show a continuous mass loss up to 450 °C, which clearly proves that no intermediate compounds can be obtained. By contrast, **Ni1** shows three distinct mass losses, indicating that the 3-Acpy ligands are stepwise removed. The experimental mass loss of $\Delta m_{exp} = 36\,\%$ in the first and $\Delta m_{exp} = 35\,\%$ in the second TG step is in rough agreement with the loss of two 3-Acpy ligands in each step ($\Delta m_{calcd.} = 37\,\%$) (Fig. 7).

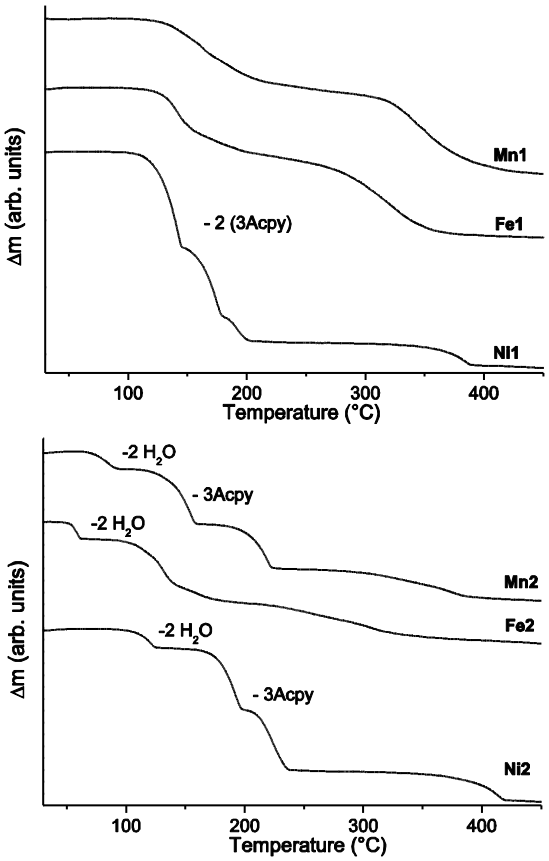

Fig. 7. TG curves for compounds **Mn1**, **Fe1** and **Ni1** (top), and for compounds **Mn2**, **Fe2** and **Ni2** (bottom).

Upon heating of compounds **M2** all compounds show three mass steps up to 450 °C, most of them are well resolved. The experimental mass loss of the first step is in good agreement with the one calculated for the removal of two water molecules (Table 3). On further heating compounds **Mn2** and **Ni2** show a second mass loss of $\Delta m_{exp} = 24\,\%$ for **Mn2** and $\Delta m_{exp} = 26\,\%$ for **Ni2**, which are in reasonable agreement with the removal of one 3-Acpy ligand (Table 3). For **Fe2** the second step is not well resolved. Finally, on further heating the remaining 3-Acpy ligands are removed, and the transition metal thiocyanates are formed.

To further characterize the intermediates formed upon thermal decomposition additional TG measurements were performed and stopped after the respective mass loss. Afterwards the residues were investigated by elemental analysis and powder X-ray diffraction.

Elemental analysis of the product formed in the first TG step of **Ni1** yields a composition of $Ni(NCS)_2(3\text{-}Acpy)_2$ (**Ni3**), and PXRD investigations show a completely different pattern, in which a small amount of the precursor seems to be present (Fig. 8 A). Similar investigations on **Mn2**, **Fe2** and **Ni2** always lead to the formation of intermediates of the composition $[M(NCS)_2(3\text{-}Acpy)_2]_n$ (**M3**) after the first TG step. Comparison of their experimental XRPD patterns indicates that **Ni3** and **Fe3** are isotypic but both of them contain reflections of an unknown crystalline phase (Fig. 8). Therefore, all attempts to index these powder patterns failed.

If the experimental pattern of **Mn3** is compared with that calculated for the corresponding Cd compound $Cd(NCS)_2(3\text{-}Acpy)_2$ reported recently, it becomes obvious that these compounds are isotypic (Fig. 8) [62]. However, an additional peak of an unknown phase proves that also this compound is not obtained as a pure crystalline phase. We carried out several different TG measurements using different heating rates and we also tried to obtain pure samples by isothermal annealing but all attempts remained unsuccessful. Therefore, the magnetic properties of these compounds were not investigated.

Additional TG measurements of compounds **Mn2** and **Ni2** were also performed and stopped after the second mass loss, in which compounds of the composition $M(NCS)_2(3\text{-}Acpy)$ (M = Mn and Ni) (**M4**) were obtained. The XRPD patterns of **Mn4** and **Ni4** are completely different, which proves that compounds with different structures are obtained (Fig. 9). Unfortunately, none of these patterns could be indexed, indicating the obtained samples are not phase-pure. Surprisingly, none of these PXRD patterns is similar to that of $[Cd(NCS)_2(3\text{-}Acpy)]_n$ reported recently [62].

Table 3. Experimental and calculated mass losses for compounds **M2**.

	First step:	Mn2	Fe2	Ni2	Second step:	Mn2	Ni2
Calculated (%)		8.0	8.0	8.0		27	27
Experimental (%)		7.0	7.3	8.0		24	26

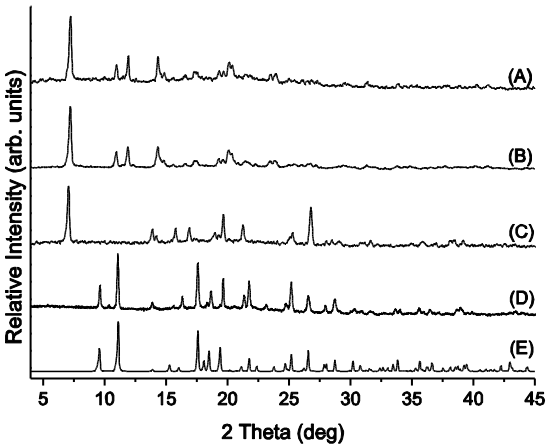

Fig. 8. Experimental powder X-ray patterns of the residues obtained after the first mass loss of **Ni1** (A), **Ni2** (B), **Fe2** (C), and **Mn2** (D) together with the powder pattern of $[Cd(NCS)_2(3\text{-Acpy})_2]_n$ (E) as calculated from single-crystal data.

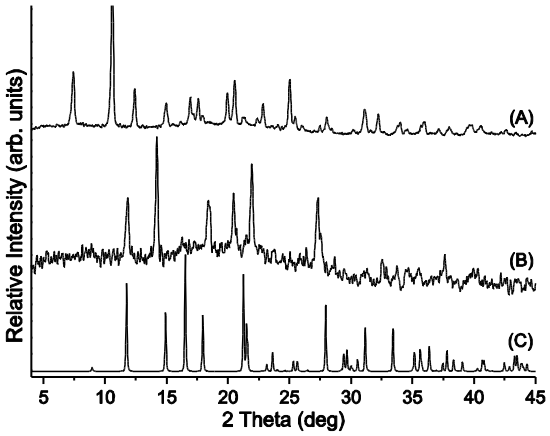

Fig. 9. Experimental powder X-ray patterns of the residues obtained after the second mass loss of **Ni2** (A) and **Mn2** (B) together with the powder pattern of $[Cd(NCS)_2(3\text{-Acpy})]_n$ (C) as calculated from single-crystal data.

IR spectroscopic investigations

In order to get information on the coordination mode in the 3-Acpy-deficient phases IR spectroscopic investigations were performed. For comparison the precursors **M1** and **M2** were also measured. For compounds in which the thiocyanato anions are terminally *N*-bonded the asymmetric CN stetching vibration is located at about 2050 cm^{-1}, whereas it is shifted to about 2100 cm^{-1} in compounds, in which they act as μ-1,3-bridging ligands [56, 58].

For compounds **M1** the CN stretching vibrations are detected between 2041 and 2078 cm^{-1}, which is in agreement with terminally *N*-bonded anions already found in the crystal structures (Table 4). In compounds **M2** this vibration is significantly shifted to values between 2067 and 2092 cm^{-1}. This shows that the coordinating water molecules lead to a shift of the CN vibration to higher values. However, in **Mn3** the CN stretching vibration is shifted above 2100 cm^{-1}, which clearly proves that the metal cations are linked by μ-1,3-bridging thiocyanato anions. This has already been found in $Cd(NCS)_2(3\text{-Acpy})_2$, which is isotypic to **Mn3**, and in which the metal cations are linked into chains by pairs of thiocyanato anions [62]. Similar values are also found for **Fe3** and **Ni3** and thus, these compounds should also contain bridging anionic ligands. Moreover, the CO stretching vibration of the acetyl O atom is similar to that in compounds **M1** and **M2**, which indicates that the 3-Acpy ligand is still terminally bonded.

For compounds **M4** the CN stretching vibrations are observed at about 2100 cm^{-1} and above, which again indicates the presence of μ-1,3-bridging thiocyanato anions (Table 4). In **Mn4** the CO stretching vibration is

Table 4. Values of the ν_{as}(CN) stretching vibration of the thiocyanato anion and of the ν_{as}(CO) stretching vibration of the acetyl group of the 3-Acpy ligand for compounds **M1**, **M2**, **M3**, and **M4** as well as for related Cd compounds taken from the literature [62].

Compound	ν_{as}CN	ν_{as}CO	Compound	ν_{as}CN	ν_{as}CO
Mn1	2041	1686	**Mn2**	2067	1678
Fe1	2044	1686	**Fe2**	2077	1678
Ni1	2078	1694	**Ni2**	2092	1678
Mn3	2086	1694	**Mn4**	2100/2082	1660
Fe3	2096	1694	**Ni4**	2142/2108	1688
Ni3	2114	1691	$Cd(NCS)_2(3\text{-Acpy})_4$	2043	1684
$Cd(NCS)_2(3\text{-Acpy})_2$	2092	1694	$Cd(NCS)_2(3\text{-Acpy})$	2096	1671

shifted to 1660 cm^{-1}, suggesting that this ligand also acts as a bridging ligand. This is supported by IR measurement on the corresponding Cd compound, which shows a similar value and in which the metal cations are linked by both, the thiocyanato anions and the 3-Acpy ligands (Table 4) [62].

The CO stretching vibration of **Ni4** is is similar to that in compounds **M3** and **M4**.

This strongly indicates that in this compound chains are present, in which μ-1,3(N,S) bridging thiocyanato anions and μ-1,5(N,O) bridging Acpy ligands are present as already observed in the crystal structure of $[Cd(NCS)_2(pyridine)]_n$ [63].

Conclusion

In the present study new coordination compounds obtained from transition metal thiocyanates and 3-acetylpyridine were prepared and investigated. In solution compounds with two different compositions were obtained, in which the metal cations are only coordinated by terminal *N*-bonded thiocyanato anions. Upon heating these compounds are transformed into 3-Acpy-deficient phases in the first step, in which the metal cations are linked by the 3-Acpy ligands into 1D or 2D coordination polymers. On further heating additional 3-Acpy ligands are removed leading to compounds with a more condensed coordination network. Unfortunately, none of these new compounds could be obtained in pure form and therefore, no magnetic measurements were performed. This is not unusual for this class of compounds, which upon thermal decomposition frequently form compounds of different stoichiometry including different polymorphic modifications.

Experimental Section

Materials

$MnSO_4 \cdot H_2O$, $Ni(SO_4)_2 \cdot 6H_2O$, KNCS and $FeCl_2 \cdot 4H_2O$ were obtained from Merck, $Ba(NCS)_2 \cdot 3H_2O$ and 3-acetylpyridine were obtained from Alfa Aesar. The chemicals were used without further purification. $Mn(NCS)_2$ was prepared by the reaction of $Ba(NCS)_2 \cdot 3H_2O$ (17.9 g, 58.44 mmol) and $MnSO_4 \cdot 6H_2O$ (9.9 g, 58.44 mmol) in water (400 mL). The colorless precipitate of $BaSO_4$ was filtered off, and the water was removed from the filtrate using a rotary evaporator. The homogeneity of the product was proven by powder X-ray diffraction and elemental analysis. $Ni(NCS)_2$ was prepared by the reaction of $Ba(NCS)_2 \cdot 3H_2O$ (17.5 g, 57 mmol) and $NiSO_4 \cdot 6H_2O$ (15.0 g, 57 mmol) in water (400 mL). The colorless precipitate of $BaSO_4$ was filtered off, and the water was removed from the filtrate using a rotary evaporator. The homogeneity of the product was proven by powder X-ray diffraction and elemental analysis

*Synthesis of $Mn(NCS)_2$(3-acetylpyridine)$_4$ (**Mn1**)*

A colorless crystalline powder was obtained by stirring 60.8 mg of $Mn(NCS)_2$ (0.25 mmol) in 436.5 μL of 3-Acpy (4.00 mmol) for 3 days. – $C_{30}H_{28}MnN_6O_4S_2$ (655.66 g mol^{-1}): calcd. C 55.0, H 4.3, N 12.8, S 9.8; found C 54.8, H 4.3, N 12.7, S 9.7. – IR (ATR): ν_{max} = 3100 (w), 3073 (w), 3007 (w), 2918 (w), 2041 (s), 1686 (s), 1593 (m), 1474 (w), 1420 (m), 1358 (m), 1267 (s), 1194 (m), 1033 (m), 1014 (w), 958 (m), 808 (m), 697 (s), 591 (m) cm^{-1}.

*Synthesis of $Fe(NCS)_2$(3-acetylpyridine)$_4$ (**Fe1**)*

A yellow crystalline powder was obtained by stirring 49.7 mg of $FeCl_2 \cdot 4\ H_2O$ (0.25 mmol), 48.6 mg of KNCS (0.50 mmol) and 272.8 μL of 3-Acpy (2.50 mmol) in 1.5 mL of H_2O. The precipitate was filtered off, and the volume of the filtrate was reduced by slow evaporation. After a few days single crystals suitable for X-ray diffraction were obtained. – $C_{30}H_{28}FeN_6O_4S_2$ (656.57 g mol^{-1}): calcd. C 54.9, H 4.3, N 12.8, S 9.8; found C 53.4, H 4.1, N 12.1, S 9.3. – IR (ATR): ν_{max} = 3103 (w), 3079 (w), 3007 (w), 2916 (w), 2044 (s), 1686 (s), 1593 (m), 1474 (w), 1419 (m), 1358 (m), 1267 (s), 1194 (m), 1034 (m), 1014 (m), 960 (m), 808 (m), 697 (s), 593 (m) cm^{-1}.

*Synthesis of $Ni(NCS)_2$(3-acetylpyridine)$_4$ (**Ni1**)*

A violet crystalline powder was obtained by stirring 43.7 mg of $Ni(NCS)_2$ (0.25 mmol) and 163.2 μL of 3-Acpy (1.50 mmol) in 1.5 mL of H_2O. The precipitate was filtered off, and the volume of the filtrate was reduced by slow evaporation. After three days single crystals suitable for X-ray diffraction were obtained. – $C_{30}H_{28}N_6NiO_4S_2$ (659.41 g mol^{-1}): calcd. C 54.6, H 4.3, N 12.7, S 9.7; found C 54.5, H 4.1, N 12.7, S 9.6. – IR (ATR): ν_{max} = 3106 (w), 3081 (w), 3007 (w), 2997 (w), 2916 (w), 2078 (s), 1694 (s), 1599 (m), 1576 (m), 1480 (w), 1426 (m), 1362 (m), 1272 (s), 1195 (m), 1100 (m), 1043 (m), 958 (m), 817 (m), 700 (s), 645 (m), 595 (s) cm^{-1}.

*Synthesis of $Mn(NCS)_2$(3-acetylpyridine)$_2$(H_2O)$_2$ (**Mn2**)*

A colorless crystalline powder was obtained by stirring 60.8 mg of $Mn(NCS)_2$ (0.25 mmol) and 54.6 μL of 3-Acpy (0.50 mmol) in 1.5 mL of H_2O. Single crystals suitable for single-crystal X-ray diffraction were prepared by slow evaporation of the solvent from the filtrate. – $C_{16}H_{18}MnN_4O_4S_2$ (449.41 g mol^{-1}): calcd. C 42.8, H 4.0, N 12.5, S 14.3; found C 42.7, H 4.0, N 12.5, S 14.5. –

Table 5. Selected crystal data and details on the structure determinations of **Fe1**, **Ni1**, **Mn2**, **Fe2** and **Ni2**.

Compound	**Fe1**	**Ni1**	**Mn2**	**Fe2**	**Ni2**
Empirical formula	$C_{30}H_{28}FeN_6OS_2$	$C_{30}H_{28}N_6NiO_4S_2$	$C_{16}H_{18}MnN_4O_4S_2$	$C_{16}H_{18}FeN_4O_4S_2$	$C_{16}H_{18}N_4NiO_4S_2$
M_r, g mol^{-1}	656.55	659.41	449.40	450.31	453.17
Crystal system	triclinic	monoclinic	triclinic	triclinic	triclinic
Space group	$P\bar{1}$	$C2/c$	$P\bar{1}$	$P\bar{1}$	$P\bar{1}$
a,	11.0109(8)	21.4818(9)	7.6466(6)	7.5944(6)	7.5507(5)
b,	11.3131(8)	25.1683(8)	8.2453(8)	8.1934(7)	8.1531(6)
c,	13.7326(10)	15.9547(7)	9.4017(7)	9.2989(6)	9.2004(6)
α, deg	68.790(8)	90	113.242(6)	113.495(6)	114.090(5)
β, deg	74.836(8)	131.138(3)	99.586(6)	98.945(6)	97.654(5)
γ, deg	79.967(9)	90	102.884(7)	102.127(6)	101.367(5)
V, ^{3}	1533.20(19)	6496.5(4)	509.06(7)	499.99(7)	492.27(6)
T, K	200(2)	293(2)	293(2)	293(2)	293(2)
Z	2	8	1	1	1
$D_{calcd.}$, mg cm^{-3}	1.42	1.35	1.47	1.50	1.53
μ, mm^{-1}	0.7	0.8	0.9	1.0	1.2
θ_{max}, deg	2.45–27.00	1.50–28.06	2.46–29.22	2.48–29.27	2.50–29.17
Measured refl.	17 362	39 880	7684	9521	9424
Unique refl./R_{int}	6513/0.0317	7779/0.0337	2734/0.0275	2679/0.0233	2646/0.0232
Min/max trans.	0.748, 0.933	0.713, 0.893	0.855, 0.979	0.761, 0.868	0.669, 0.825
Refl. [$F_0 > 4\,\sigma(F_0)$]	5524	6374	2186	2294	2223
Ref. parameters	416	410	125	125	125
R_1^a [$F_0 > 4\,\sigma(F_0)$]	0.0336	0.0428	0.0334	0.0282	0.0316
wR_2^b (all data)	0.0928	0.0999	0.0817	0.0735	0.0719
GoF^c	1.034	1.057	1.021	1.028	1.044
$\Delta\rho_{max/min}$, e $^{-3}$	0.40/−0.50	0.38/−0.47	0.30/−0.24	0.33/−0.33	0.33/−0.25

[a] $R_1 = \Sigma||F_o| - |F_c||/\Sigma|F_o|$; [b] $wR_2 = [\Sigma w(F_o^2 - F_c^2)^2/\Sigma w(F_o^2)^2]^{1/2}$, $w = [\sigma^2(F_o^2) + (AP)^2BP]^{-1}$, where $P = (\mathrm{Max}(F_o^2, 0) + 2F_c^2)/3$; [c] GoF = $[\Sigma w(F_o^2 - F_c^2)^2/(n_{obs} - n_{param})]^{1/2}$.

IR (ATR): ν_{max} = 3313 (b), 3220 (b), 2857 (w), 2067 (s), 1678 (s), 1591 (s), 1557 (m), 1472 (m), 1425 (m), 1357 (m), 1277 (s), 1194 (m), 1128 (m), 1039 (m), 960 (m), 811 (s), 695 (s), 639 (s), 600 (s), 469 (s) cm^{-1}.

Synthesis of Fe(NCS)$_2$(3-acetylpyridine)$_2$(H$_2$O)$_2$ (Fe2)

A yellow crystalline powder was obtained by stirring of 49.7 mg of $FeCl_2 \cdot 4H_2O$ (0.25 mmol), 48.6 mg of KNCS (0.50 mmol) and 54.6 µL of 3-Acpy (0.50 mmol) in 1.5 mL of H_2O. Single crystals suitable for single-crystal X-ray diffraction were prepared by slow evaporation of the solvent from the filtrate. – $C_{16}H_{18}FeN_4O_4S_2$ (450.32 g mol^{-1}): calcd. C 42.7, H 4.0, N 12.4, S 14.2; found C 42.7, H 4.0, N 12.3, S 14.4. – IR (ATR): ν_{max} = 3217 (b), 2861 (w), 2077 (s), 1678 (s), 1592 (s), 1473 (w), 1426 (m), 1357 (m), 1280 (s), 1194 (w), 1131 (w), 1097 (w), 1042 (m), 961 (m), 812 (s), 765 (m), 694 (s), 640 (s), 601 (m), 564 (m), 471 (m) cm^{-1}.

Synthesis of Ni(NCS)$_2$(3-acetylpyridine)$_2$(H$_2$O)$_2$ (Ni2)

A light-blue crystalline powder was obtained by stirring 43.7 mg of $Ni(NCS)_2$ (0.25 mmol) and 54.6 µL of 3-Acpy (0.50 mmol) in 1.5 mL of H_2O. Single crystals suitable for single-crystal X-ray diffraction were prepared under similar conditions without stirring. – $C_{16}H_{18}N_4NiO_4S_2$ (453.17 g mol^{-1}): calcd. C 42.4, H 4.0, N 12.4, S 14.2; found C 42.0, H 3.8, N 12.2, S 14.0. – IR (ATR): ν_{max} = 3295 (b), 3099 (w), 3062 (w), 2092 (s), 1678 (s), 1596 (s), 1474 (w), 1428 (m), 1357 (m), 1280 (s), 1197 (w), 1123 (w), 1046 (m), 960 (m), 815 (s), 774 (m), 696 (s), 645 (s), 601 (m), 553 (s), 471 (m) cm^{-1}.

Powder X-ray diffraction

The experiments were performed using a Stoe Transmission Powder Diffraction System (STADI P, Stoe & Cie, Darmstadt, Germany) with CuK_α radiation (λ = 154.0598 pm) equipped with a linear position-sensitive detector ($\delta 2\theta$ = 6.5–7° simultaneous; scan range overall = 2–130°).

Differential thermal analysis and thermogravimetry

The DTA-TG measurements were performed in nitrogen atmosphere (purity: 5.0) in Al_2O_3 crucibles using a STA-409CD thermobalance (Netzsch, Selb, Germany). All measurements were performed with a flow rate of 75 mL min^{-1}

and were corrected for buoyancy and current effects. The instrument was calibrated using standard reference materials.

Spectroscopy

IR spectra were recorded on a Bruker Alpha IR spectrometer equipped with a Platinum ATR QuickSnap™ sampling module between 4000 – 375 cm^{-1}.

Elemental analysis

CHNS analyses were performed using an EURO EA elemental analyzer (Euro Vector Instruments).

Single-crystal structure analyses

Data collection was performed with an imaging plate diffraction system (IPDS-2 for **Ni1**, **Mn2** and **Ni2**; IPDS-1 for **Fe1**) from Stoe & Cie with MoK_α radiation. The data were corrected for absorption using X-RED and X-SHAPE from Stoe [64, 65]. Structure solutions were performed with Direct Methods using SHELXS-97, and structure refinements were done against F^2 using SHELXL-97 [66]. All non-hydrogen atoms were refined with anisotropic displacement parameters. The hydrogen atoms were positioned with idealized geometry and were refined with fixed isotropic displacement parameters with $U_{iso}(H) = -1.2U_{eq}(C)$ (1.5 for methyl H atoms) using a riding model. The O–H H atoms were located in the Fourier difference map, their bond lengths were set to ideal values, and they were refined isotropically with $U_{eq}(H) = 1.5 \cdot U_{eq}(O)$ using a riding model. Details of the structure determination are given in Table 5.

CCDC 1021212 (**Fe-1**), 1021215 (**Ni1**), 1021213 (**Mn2**), 1021211 (**Fe2**) and 1021214 (**Ni2**) contain the supplementary crystallographic data for this paper. These data can be obtained free of charge from The Cambridge Crystallographic Data Centre *via* www.ccdc.cam.ac.uk/data_request/cif.

Acknowledgement

This project was supported by the Deutsche Forschungsgemeinschaft (project no. NA 720/5-1) and the State of Schleswig-Holstein. We thank Professor Dr. Wolfgang Bensch for access to his experimental facilities.

[1] B. Moulton, M. J. Zaworotko, *Chem. Rev.* **2001**, *101*, 1629 – 1658.
[2] S. L. James, *Chem. Soc. Rev.* **2003**, *32*, 276 – 288.
[3] A. J. Blake, N. R. Champness, P. Hubberstey, W.-S. Li, M. A. Withersby, M. Schr der, *Coord. Chem. Rev.* **1999**, *183*, 117 – 138.
[4] A. N. Khlobystov, A. J. Blake, N. R. Champness, D. A. Lemenovskii, A. G. Majouga, N. V. Zyk, M. Schr der, *Coord. Chem. Rev.* **2001**, *222*, 155 – 192.
[5] R. J. Puddephatt, *Coord. Chem. Rev.* **2001**, 216 – 217, 313 – 332.
[6] A. Y. Robin, K. M. Fromm, *Coord. Chem. Rev.* **2006**, *250*, 2127 – 2157.
[7] C. Janiak, *Dalton Trans.* **2003**, 2781 – 2804.
[8] C. Janiak, L. Uehlin, H.-P. Wu, P. Kl fers, H. Piotrowski, T. G. Scharmann, *J. Chem. Soc., Dalton Trans.* **1999**, 3121 – 3131.
[9] S. Kitagawa, K. Uemura, *Chem. Soc. Rev.* **2005**, *34*, 109 – 119.
[10] D. Maspoch, D. Ruiz-Molina, J. Veciana, *Chem. Soc. Rev.* **2007**, *36*, 770 – 818.
[11] S. R. Batten, K. S. Murray, *Coord. Chem. Rev.* **2003**, *246*, 103 – 130.
[12] D. Maspoch, D. Ruiz-Molina, J. Veciana, *J. Mater. Chem.* **2004**, *14*, 2713 – 2723.
[13] C. N ther, G. Bhosekar, I. Jeß, *Inorg. Chem.* **2007**, *46*, 8079 – 8087.
[14] S. L. James, C. J. Adams, C. Bolm, D. Braga, P. Collier, T. Friscic, F. Grepioni, K. D. M. Harris, G. Hyett, W. Jones, A. Krebs, J. Mack, L. Maini, A. G. Orpen, I. P. Parkin, W. C. Shearouse, J. W. Steed, D. C. Waddell, *Chem. Soc. Rev.* **2012**, *41*, 413 – 447.
[15] C. J. Adams, M. A. Kurawa, M. Lusi, A. G. Orpen, *CrystEngComm* **2008**, *10*, 1790 – 1795.
[16] M. Wriedt, S. Sellmer, C. N ther, *Dalton Trans.* **2009**, *38*, 7975 – 7984.
[17] D. Braga, S. L. Giaffreda, F. Grepioni, A. Pettersen, L. Maini, M. Curzi, M. Polito, *Dalton Trans.* **2006**, 1249 – 1263.
[18] K. M ller-Buschbaum, *Z. Anorg. Allg. Chem.* **2005**, *631*, 811 – 828.
[19] C. J. Adams, P. C. Crawford, A. G. Orpen, T. J. Podesta, B. Salt, *Chem. Commun.* **2005**, 2457 – 2458.
[20] C. N ther, I. Jeß, J. Greve, *Polyhedron* **2001**, *20*, 1017 – 1022.
[21] C. N ther, I. Jeß, *J. Solid State Chem.* **2002**, *169*, 103 – 112.
[22] C. N ther, J. Greve, I. Jeß, *Solid State Sci.* **2002**, *4*, 813 – 820.
[23] B. Machura, A. Świtlicka, P. Zwoliński, J. Mroziński, B. Kalińska, R. Kruszynski, *J. Solid State Chem.* **2013**, *197*, 218 – 227.
[24] B. Machura, A. Świtlicka, J. Mroziński, B. Kalińska, R. Kruszynski, *Polyhedron* **2013**, *52*, 1276 – 1286.

[25] J. G. Małecki, T. Groń, H. Duda, *Polyhedron* **2012**, *36*, 56–68.
[26] B. Machura, A. Świtlicka, I. Nawrot, J. Mroziński, R. Kruszynski, *Polyhedron* **2011**, *30*, 832–840.
[27] Q. Ma, M. Zhu, L. Lu, S. Feng, J. Yan, *Inorg. Chim. Acta* **2011**, *370*, 102–107.
[28] P. Bhowmik, S. Chattopadhyay, M. G. B. Drew, C. Diaz, A. Ghosh, *Polyhedron* **2010**, *29*, 2637–2642.
[29] C. J. Adams, M. C. Mu oz, R. E. Waddington, J. A. Real, *Inorg. Chem.* **2011**, *50*, 10633–10642.
[30] E. Shurdha, C. E. Moore, A. L. Rheingold, S. H. Lapidus, P. W. Stephens, A. M. Arif, J. S. Miller, *Inorg. Chem.* **2013**, *52*, 10583–10594.
[31] Y. Jin, Y.-X. Che, J.-M. Zheng, *J. Coord. Chem.* **2007**, *60*, 2067–2074.
[32] B. Zurowska, J. Mrozinski, M. Julve, F. Lloret, A. Maslejova, W. Sawka-Dobrowolska, *Inorg. Chem.* **2002**, *41*, 1771–1777.
[33] R. Gonz lez, A. Acosta, R. Chiozzone, C. Kremer, D. Armentano, G. De Munno, M. Julve, F. Lloret, J. Faus, *Inorg. Chem.* **2012**, *51*, 5737–5747.
[34] G. Bhargavi, M. V. Rajasekharan, J. P. Tuchagues, *Inorg. Chim. Acta* **2009**, *362*, 3247–3252.
[35] J. Mroziński, J. Kłak, R. Kruszyński, *Polyhedron* **2008**, *27*, 1401–1407.
[36] S. Banerjee, M. G. B. Drew, C.-Z. Lu, J. Tercero, C. Diaz, A. Ghosh, *Eur. J. Inorg. Chem.* **2005**, *2005*, 2376–2383.
[37] O. V. Nesterova, S. R. Petrusenko, V. N. Kokozay, B. W. Skelton, J. Jezierska, W. Linert, A. Ozarowski, *Dalton Trans.* **2008**, 1431–1436.
[38] A. Barasiński, P. Sobczak, A. Drzewiński, G. Kamieniarz, A. Bieńko, J. Mroziński, D. Gatteschi, *Polyhedron* **2010**, *29*, 1485–1491.
[39] J. M. Shi, J. N. Chen, C. J. Wu, J. P. Ma, *J. Coord. Chem.* **2007**, *60*, 2009–2013.
[40] M. G. Barandika, M. L. Hernandez-Pino, M. K. Urtiaga, R. Cortes, L. Lezama, M. I. Arriortua, T. Rojo, *J. Chem. Soc., Dalton Trans.* **2000**, 1469–1473.
[41] E. Shurdha, S. H. Lapidus, P. W. Stephens, C. E. Moore, A. L. Rheingold, J. S. Miller, *Inorg. Chem.* **2012**, *51*, 9655–9665.
[42] C. N ther, J. Greve, *J. Solid State Chem.* **2003**, *176*, 259–265.
[43] M. Wriedt, I. Jeß, C. N ther, *Eur. J. Inorg. Chem.* **2009**, 1406–1413.
[44] M. Wriedt, C. N ther, *Chem. Commun.* **2010**, *46*, 4707–4709.
[45] C. N ther, J. Greve, *J. Solid State Chem.* **2003**, *176*, 259–265.
[46] J. Boeckmann, C. N ther, *Chem. Commun.* **2011**, *47*, 7104–7106.
[47] J. Boeckmann, C. N ther, *Dalton Trans.* **2010**, *39*, 11019–11026.
[48] J. Boeckmann, C. N ther, *Polyhedron* **2012**, *31*, 587–595.
[49] J. Boeckmann, M. Wriedt, C. N ther, *Chem. Eur. J.* **2012**, *18*, 5284–5289.
[50] S. W hlert, J. Boeckmann, M. Wriedt, C. N ther, *Angew. Chem. Int. Ed.* **2011**, *50*, 6920–6923.
[51] S. W hlert, M. Wriedt, T. Fic, Z. Tomkowicz, W. Haase, C. N ther, *Inorg. Chem.* **2013**, *52*, 1061–1068.
[52] S. W hlert, T. Fic, Z. Tomkowicz, S. G. Ebbinghaus, M. Rams, W. Haase, C. N ther, *Inorg. Chem.* **2013**, *52*, 12947–12957.
[53] S. W hlert, U. Ruschewitz, C. N ther, *Cryst. Growth Des.* **2012**, *12*, 2715–2718.
[54] C. N ther, S. W hlert, J. Boeckmann, M. Wriedt, I. Jeß, *Z. Anorg. Allg. Chem.* **2013**, *639*, 2696–2714.
[55] S. W hlert, T. Runčevski, R. E. Dinnebier, S. G. Ebbinghaus, C. N ther, *Cryst. Growth Des.* **2014**, *14*, 1902–1913.
[56] R. J. H. Clark, C. S. Williams, *Spectrochim. Acta* **1966**, *22*, 1081–1090.
[57] C. W. Frank, L. B. Rogers, *Inorg. Chem.* **1966**, *5*, 615–622.
[58] R. A. Bailey, S. L. Kozak, T. W. Michelsen, W. N. Mills, *Coord. Chem. Rev.* **1971**, *6*, 407–445.
[59] I. Jeß, J. Boeckmann, C. N ther, *Dalton Trans.* **2012**, *41*, 228–236.
[60] J. Boeckmann, I. Jeß, T. Reinert, C. N ther, *Eur. J. Inorg. Chem.* **2011**, 5502–5511.
[61] S. W hlert, L. Peters, C. N ther, *Dalton Trans.* **2013**, *42*, 10746–10758.
[62] J. Werner, J. Boeckmann, C. N ther, *Z. Anorg. Allg. Chem.* **2012**, *638*, 2257–2264.
[63] S. W hlert, J. Boeckmann, I. Jess, C. N ther, *CrystEngComm* **2012**, *14*, 5412–5420.
[64] X-RED (version 1.11), Program for Data Reduction and Absorption Correction, Stoe & Cie GmbH, Darmstadt (Germany) **1998**.
[65] X-SHAPE (version 1.03), Program for the Crystal Optimization for Numerical Absorption Correction, Stoe & Cie GmbH, Darmstadt (Germany) **1998**.
[66] G. M. Sheldrick, *Acta Crystallogr.* **2008**, *A64*, 112–122.

4.7. Synthesis, Crystal Structures and Properties of $Ni(NCS)_2$-4-(hydroxymethyl)pyridine Coordination Compounds

Julia Werner und Christian Näther, *Polyhedron.* **2015**, *98*, 96-104.

Motivation

Im Verlauf weiterer systematischer Untersuchungen wurde 4-(Hydroxymethyl)pyridin als Co-Ligand verwendet. Hierbei stellte sich beispielsweise die Frage, ob die für vergleichbare Liganden typischen 1D-$Co(NCS)_2$-Ketten erhalten werden, oder ob auch die Hydroxylgruppe an der Metallkoordination beteiligt ist. In der folgenden Arbeit wurde über entsprechende Untersuchungen mit Ni(II) als Metallkation berichtet.

Dabei wurden eine Reihe von diskreten Komplexen mit der Zusammensetzung $Ni(NCS)_2$(4-(Hydroxymethyl)pyridin)$_4$, $Ni(NCS)_2$(4-(Hydroxymethyl)pyridin)$_2$(EtOH)$_2$ und $Ni(NCS)_2$(4-(Hydroxymethyl)pyridin)$_2$(H_2O)$_2$ erhalten. Darüber hinaus konnte eine Verbindung der Zusammensetzung $Ni(NCS)_2$(4-(Hydroxymethyl)pyridin)$_2$ erhalten werden, wobei IR-spektroskopische Untersuchungen nahe legten, dass neben µ-1,3-verbrückenden auch N-terminal koordinierende Thiocyanatanion enthalten sind. Eine Einkristallstrukturanalyse ergab, dass jeweils zwei Ni-Kationen über zwei µ-1,3-verbrückende Thiocyanatanionen zu Dimeren verknüpft sind, welche durch µ-1,6 verbrückende 4-(Hydroxymethyl)pyridin) Liganden zu Ketten verknüpft sind. Magnetische Messungen ergaben, dass diese Verbindung einen antiferromagnetischen Ordnungspunkt bei T_N =6.7 K hat.

Polyhedron 98 (2015) 96–104

Contents lists available at ScienceDirect

Polyhedron

journal homepage: www.elsevier.com/locate/poly

Synthesis, crystal structures and properties of $Ni(NCS)_2$-4-(hydroxymethyl)pyridine coordination compounds

Julia Werner, Christian Näther *

Institut für Anorganische Chemie, Universität Kiel, Max-Eyth.-Str. 2, 24118 Kiel, Germany

ARTICLE INFO

Article history:
Received 27 March 2015
Accepted 7 June 2015
Available online 15 June 2015

Keywords:
Coordination compounds
Thiocyanate
Crystal structures
IR spectroscopy
Thermal properties

ABSTRACT

Reaction of $Ni(NCS)_2$ with 4-(hydroxymethyl)pyridine leads to the formation of five new coordination compounds. The crystal structures of compounds **1-H_2O**, **1**, **2** and **3** consist of discrete complexes, in which the Ni cations are coordinated by two terminal N-bonded thiocyanato anions and four neutral co-ligands, within slightly distorted octahedra. In the structure of **4**, two Ni cations are linked into dimers by pairs of μ-1,3-bridging anions and are further connected into chains by the 4-(hydroxymethyl)pyridine ligand. Compound **4** shows an antiferromagnetic transition at $T_N = 6.7$ K. The compounds were additionally characterized by IR spectroscopy, thermoanalytical methods and X-ray powder diffraction.

1. Introduction

Thio- and selenocyanato anions are versatile three-atomic ligands that show a large variety of coordination modes and this might be one reason why an increasing number of such compounds were recently reported. The most common coordination is the terminal coordination of the N atom and the majority of these compounds consists of discrete complexes [1–27]. However, there are also several compounds reported in literature, in which the metal cations are linked by, e.g., μ-1,3-briding anions into coordination polymers. In this case the cations can be linked by pairs of anionic ligands into dimers or chains or can be connected by single anionic ligands into layers [8–12,28–46]. Even if for some compounds with terminal N-bonded ligands spin-crossover is observed [5–6,47–50], the coordination polymers with bridging anionic ligands show a more versatile magnetic behavior [32–40].

Our interest is focused on 1D thio- and selenocyanato compounds of composition $[M(NCS)_2(L)_2]_n$ (M = Mn, Fe, Co and Ni; L = neutral monodentate N-donor co-ligand), in which the paramagnetic transition metal cations Mn, Fe, Co and Ni are linked by pairs of μ-1,3-bridging anionic ligands into chains [51–59]. Such chain compounds are frequently observed and thus, it can be assumed that this is a very stable arrangement. However, in very few cases compounds of the same composition can be obtained that consist of an isomeric thiocyanato coordination network in which the metal cations form dimers by pairs of μ-1,3-bridging anions that are further linked into layers by single μ-1,3-bridging anionic ligands. It is noted that this arrangement is especially found with Ni(II) as it is the case, e.g. for $[Ni(NCS)_2(2\text{-methylpyrazine})_2]_n$ [46] and for $[Ni(NCS)_2(2\text{-chloropyrazine})_2]_n$ [60]. The reason for this unusual behavior is unclear but it is mentioned that for $[Co(NCS)_2(4\text{-acetylpyridine})_2]_n$ we have obtained both isomers [56]. Further investigations show that in this case the 1D isomer is thermodynamically metastable and transforms into the 2D stable isomer in solution or by heating. To investigate the influence of the co-ligand onto the structures and properties of such compounds in more detail, we tried to prepare compounds based on $Ni(NCS)_2$ and 4-(hydroxymethyl)pyridine, with special focus on compounds of composition $[Ni(NCS)_2(4\text{-(hydroxymethyl)pyridine})_2]_n$. This typical monodentate ligand should coordinate with the N atom to the metal centers to form compounds with thiocyanato networks mentioned above. However, in principle 4-(hydroxymethyl)pyridine can also act as a bridging ligand via the O atom of the hydroxyl group, but this should not be a favored coordination. In this context it is noted that no thiocyanato coordination compounds with this ligand are reported. Anyhow, a few coordination compounds with different anionic ligands are reported in the CCDC and some selected examples are given in the reference list [61–66]. In most of them this ligand does not act as bridging ligand and is coordinated only with the N atom to the metal center. There is only one Cu(II) compound with pyridine-2,6-dicarboxylate as anion, in which the metal cations are linked by the 4-(hydroxymethyl)pyridine ligands into chains [64]. One of these compounds based on cadmium azide is

* Corresponding author. Tel.: +49 431 880 2092; fax: +49 431 880 1520.
E-mail address: cnaether@ac.uni-kiel.de (C. Näther).

http://dx.doi.org/10.1016/j.poly.2015.06.004
0277-5387/

similar to that what is expected. In $[Cd(N_3)_2(4\text{-(hydroxymethyl)pyridine})_2]_n$ also 1D chains are found but in contrast to that usually observed in thiocyanato coordination polymers the metal cations are linked by alternating μ-1,3 and μ-1,1 anionic ligands [63]. Here we report our investigations.

2. Synthetic investigations

To investigate how many compounds of different stoichiometries are accessible different amounts of $Ni(NCS)_2$ and 4-(hydroxymethyl)pyridine were reacted at room temperature in water, ethanol and acetonitrile and all residues were analyzed by X-ray powder diffraction (XRPD), IR spectroscopy, and elemental analysis. XRPD investigations reveal that five different crystalline phases could be obtained (Table 1). The results of the elemental analysis indicate for two compounds a composition close to $Ni(NCS)_2(4\text{-(hydroxymethyl)pyridine})_4$ (**1-H_2O**, **1**). Two other might represent solvates of composition $Ni(NCS)_2(4\text{-(hydroxymethyl)pyridine})_2(EtOH)_2$ (**2**) and $Ni(NCS)_2(4\text{-(hydroxymethyl)pyridine})_2(H_2O)_2$ (**3**), whereas the last compound of composition $Ni(NCS)_2(4\text{-(hydroxymethyl)pyridine})_2$ (**4**) corresponds to that what is expected for the desired compound.

The asymmetric CN stretching vibration for **1-H_2O** and **1** is observed at 2081 and 2090 cm^{-1} indicating that the thiocyanato anions are only N-terminal coordinated (Figs. S1 and S2 in the Supplementary material). For compounds **2**, **3** this vibration is found at 2100 and 2120 cm^{-1}, whereas for compound **4** three different values of 2124, 2108 and 2100 cm^{-1} are observed (Figs. S3–S5 in the Supplementary material). These values are between an N-terminal and a bridging coordination of the thiocyanato anions and a definite decision cannot be made. Therefore, single crystals were grown and all compounds were characterized by single crystal X-ray analysis. Based on the crystallographic data XRPD pattern were calculated and compared with the experimental pattern, which show that **1-H_2O**, **1**, and **4** were obtained as pure phases, whereas **2** is contaminated with a small amount of **4** and **3** with a small amount of an unknown phase (Figs. S6–S10 in the Supplementary material).

3. Crystal structures

3.1. Crystal structures of *1* and *1-H_2O*

$Ni(NCS)_2(4\text{-(hydroxymethyl)pyridine})_4$ crystallizes in the orthorhombic space group $P2_12_12_1$ with four formula units in the unit cell. The asymmetric unit consists of one crystallographically independent complex in a general position. The nickel cation is coordinated by four 4-(hydroxymethyl)pyridine ligands and two terminally N-bonded thiocyanato anions within slightly distorted octahedra (Fig. 1 and Fig. S11 in the Supplementary material). The metal nitrogen distances to the thiocyanato anions of 2.071(2) and 2.075(2) Å are significantly shorter than those to the neutral N-donor co-ligands, which scatter between 2.121(2) and 2.139(2) Å (Table S1 in the Supplementary material).

Table 1
Products obtained by stirring $Ni(NCS)_2$ and 4-(hydroxymethyl)pyridine in different stoichiometric ratios in water, ethanol and acetonitrile.

Ratio	H_2O	EtOH	MeCN
1:7	**1-H_2O**	**2**, **1-H_2O**	**1**
1:4	**1-H_2O**	–	**1**
1:2	**1-H_2O**, **3**	**4**	**4**
1:1	**3**	**2**	–
2:1	**3**	**2**	–

In the crystal structure the molecules are linked by pairs of intermolecular O–H···S hydrogen bonding between the hydroxyl H atom and the thiocyanato S atom into chains that elongate in the direction of the crystallographic *a* axis (Fig. 1: bottom and Table S2 in the Supplementary material). From this arrangement hydrogen bonded centrosymmetric rings are formed between the metal centers that according to the Graph Set notation can be denoted as $R_2^2(22)$ [67]. The thiocyanato S atom is involved in a further O–H···S hydrogen bond to the hydroxyl H atom of a neighbored complex that connect the chains into layers parallel to the *a*/*b* plane (Fig. 1: bottom). Each of the S atoms act as acceptor for two S···H bonds to two symmetry related 4-(hydroxymethyl)pyridine ligands.

Compound **1-H_2O** crystallizes in the cubic space group *Pn*-3n with six formula units in the unit cell. The asymmetric unit consists of one nickel cation which is located on a 3-fold inversion axis, one thiocyanato anion that is located on a 4-fold rotation axis, and one 4-(hydroxymethyl)pyridine ligand that is located on a 2-fold axis. Due to symmetry, the hydroxyl group is disordered in two orientations (see Section 9). The crystal structure also consists of discrete complexes in which the Ni cations are coordinated by two terminal N-bonded anionic ligands and four 4-(hydroxymethyl)pyridine co-ligands within an octahedral geometry (Fig. S12 and Table S3 in the Supplementary material). The structure contains voids, in which additional water molecules are located that are disordered over two positions and their positions seems to be not fully occupied. Therefore, the data were corrected for disordered solvents using Squeeze in Platon (see Section 9). From TG measurements the water content was determined to be about 1.5 water per formula unit. In contrast to **1**, the hydroxyl H atom is not involved in O–H···S hydrogen bonding and thus, it can be assumed that it forms hydrogen bonding to the disordered water molecules.

3.2. Crystal structures of *2* and *3*

$Ni(NCS)_2(4\text{-(hydroxymethyl)pyridine})_2(EtOH)_2$ (**2**) and $Ni(NCS)_2(4\text{-(hydroxymethyl)-pyridine})_2(H_2O)_2$ (**3**) represent simple discrete solvato complexes (Fig. 2). **2** crystallizes in the centrosymmetric space group *C*2/*c* with *Z* = 4 and the Ni cation located on a 2-fold rotation axis. Compound **3** crystallizes in the centrosymmetric space group *P*bca with four formula units in the unit cell and the Ni cations located on centers of inversion.

In the crystal structure of **2** and **3** the Ni cations are coordinated by two terminal N-bonded thiocyanato anions, two 4-(hydroxymethyl)pyridine ligands, and two ethanol, respectively water molecules (Fig. 2). In contrast to compound **3**, where the neutral co-ligands are *trans*-coordinated, in compound **2** a *cis*-coordination is observed. In **2** the nickel nitrogen distances are 2.041(3) and 2.101(3) Å with the shorter to the thiocyanato N atom and the nickel oxygen distance amount to 2.100(2) Å (Tables S4 and S5 in the Supplementary material). For **3** similar distances are found (Ni–N: 2.0443(19)–2.1273(19) Å and Ni–O: 2.0896(17) Å, Tables S4 and S5 in the Supplementary material).

In the crystal structure of **2** a complex hydrogen bonding pattern is observed. The discrete complexes are linked by pairs of intermolekular O–H···S hydrogen bonding between the O–H H atom of 4-(hydroxymethyl)pyridine molecule of one complex and the S atom of the thiocyanato ligand of a second complex into $R_4^4(16)$ rings [67]. These rings are linked into chains that elongate in the direction of the crystallographic *b* axis (Fig. 3: top and Table S6). These chains are further connected by O–H···O hydrogen bonding between the hydroxyl H atom of the ethanol molecules of one complex and the hydroxyl O atom of a neighbored complex into layers. From this arrangement hydrogen bonded rings are formed that can be denoted as $R_2^2(18)$ (Fig. 3: top) [67].

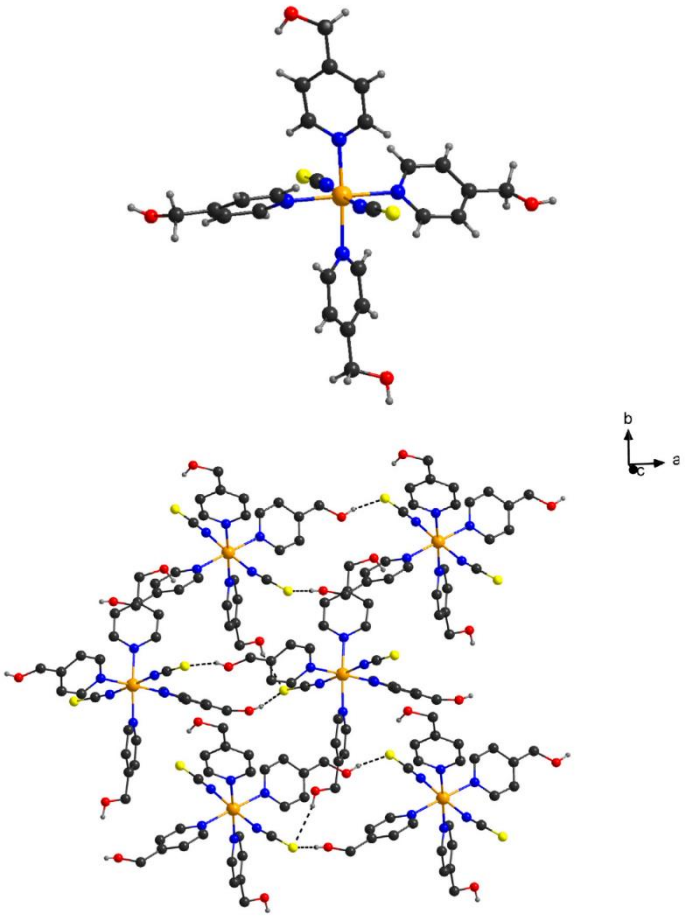

Fig. 1. Crystal structure of **1** with view of the coordination sphere of the Ni(II) cation (top) and approximately along the crystallographic *c*-axis (bottom). In Fig. 1: bottom intermolecular hydrogen bonding is shown as dashed lines and the C–H H atoms are omitted for clarity. An ORTEP plot is shown in Fig. S11 in the Supplementary material.

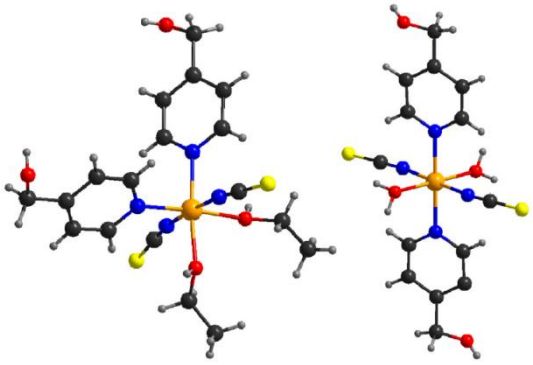

Fig. 2. Coordination sphere of the Ni cations in the crystal structure of **2** (left) and **3** (right). ORTEP plots of **2** and **3** are shown in Figs. S13 and S14 in the Supplementary material. The disordering of the ethanol molecule in **2** is omitted for clarity.

In the crystal structure of **3** four discrete complexes are linked by intermolecular O-H···O and O-H···S hydrogen bonding into R_4^3 (12) rings (Fig. 3: bottom and Table S7) [67]. These rings are built up by one O–H···O hydrogen bond between the O atom of the 4-(hydroxymethyl)pyridine ligand that acts as acceptor and one O–H hydrogen atom of the water molecule of a second complex (Fig. 3: bottom and Table S7). The second H atom of the water molecule of this complex is hydrogen bonded to one thiocyanato S anion of a third complex. The rings are completed by two O–H···S hydrogen bonds between a thiocyanato S atom of a fourth complex and one H atom of a water molecule as well as one H atom of the hydroxyl group that belongs to two different complexes (Fig. 3: bottom). Between two neighboring complexes an additional ring is formed denoted as R_2^2 (16), which is built up by two O–H···S hydrogen bonds between two thiocyanato S atoms of neighboring complexes and one water, respectively one hydroxyl H atom. From this arrangement layers are formed, that are parallel to the *a*-*b* plane (Fig. 3: bottom) [67].

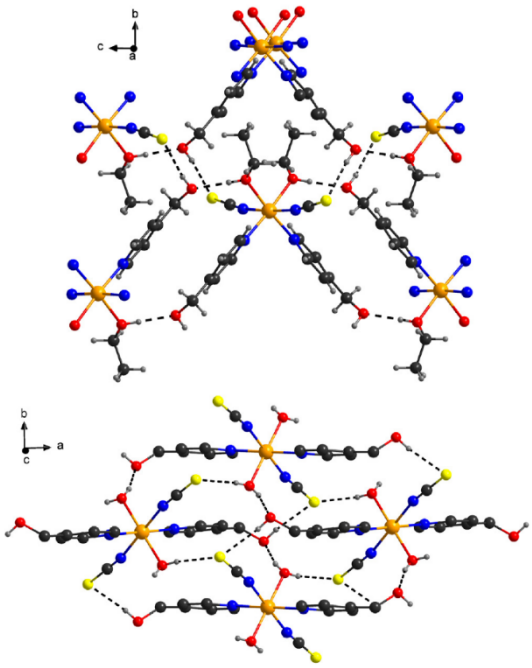

Fig. 3. Crystal structures of **2** (top) and **3** (bottom) with view along approximately the crystallographic *a* and *c* axis. Intermolecular hydrogen bonding is shown as dashed lines and the C-H H atoms for **3** as well as the disordered ethyl groups in **2** are omitted for clarity.

3.3. Crystal structure of **4**

$[Ni(NCS)_2(4\text{-(hydroxymethyl)pyridine})_2]_n$ crystallizes in the monoclinic centrosymmetric space group $P2_1/c$ with four formula units in the unit cell. The asymmetric unit consists of one nickel cation, two thiocyanato anions and two 4-hydroxymethylpyridine ligands in general positions. The Ni cations are coordinated by three thiocyanato anions, and three 4-(hydroxymethyl)pyridine ligands within a slightly distorted octahedral geometry (Table S8 in the Supplementary material). Each two cations are linked by pairs of μ-1,3-bridging thiocyanato anions into dimers, that are located on centers of inversion and are additional coordinated by one terminal N-bonded thiocyanato anion (Fig. 4). The dimers are linked into chains by μ-1,6 bridging 4-(hydroxymethyl)pyridine ligands *via* the pyridine N atom and the hydroxyl O atom (Fig. 4). Between the thiocyanato S atom and the hydroxyl H atom intermolecular O–H···S hydrogen bonding is found (Table S9 in the Supplementary material).

4. Spectroscopic properties

Single crystal structure analysis clearly showed that in compounds **1**, **1-H$_2$O**, **2** and **3** only terminal N-bonded thiocyanato anions are observed, whereas in compound **4** both, N-terminal and μ-1,3-bridging anions are found. This is somehow surprising, because in several cases the asymmetric CN stretching vibration can be used to differ between N-terminal and μ-1,3-bridiging anions, because for terminal N-bonded thiocyanato anions the CN stretch is usually observed below 2100 cm^{-1}, whereas for μ-1,3-bridging it is found above this value. In contrast, for compounds **2**, **3** and **4**, very similar values are observed. This is obvious from Table 2, where the values of the CN-stretching vibration are given together with same values retrieved from literature. However, for all discrete complexes in which the metal centers

Table 2
Values of the CN stretching vibrations of compounds **1**, **1-H$_2$O**, **2**, **3** and **4** and of selected pyridine derivatives retrieved from literature (Pyr = Pyridine, 4-Ethyl-Pyr = 4-ethylpyridine, 4-Acpy = 4-acetylpyridine, 4-Azpy = 4-azidopyrsidine, and dpt: bis(3-aminopropyl)amine).

	CN in cm^{-1}	NCS coordination	Reference
1-H$_2$O	2081	Terminal	This work
1	2090	Terminal	This work
2	2100	Terminal	This work
3	2120	Terminal	This work
4	2124/2108/2100	Terminal/μ-1,3	This work
$Ni(NCS)_2(Pyr)_4$	2082	Terminal	[68]
$[Ni(NCS)_2(Pyr)_2]_n$	2110	μ-1,3	[68]
$Ni(NCS)_2(4\text{-Ethyl-Pyr})_4$	2066	Terminal	[53]
$[Ni(NCS)_2(4\text{-Ethyl-Pyr})_2]_n$	2112	μ-1,3	[53]
$Ni(NCS)_2(4\text{-AcPy})_4$	2072	Terminal	[69]
$Ni(NCS)_2(4\text{-Acpy})_2(H_2O)_2$	2098	Terminal	[69]
$[Ni(NCS)_2(4\text{-Acpy})_2]_n$ 2D	2116	μ-1,3	[69]
$[Ni(NCS)_2(4\text{-Acpy})_2]_n$ 1D	2109	μ-1,3	[69]
$[Ni_2(NCS)_6(4\text{-Azpy})_4]$	2131/2078	Terminal/μ-1,3	[24]
$[Ni(NCS)_2(dpt)]$	2163/2112/2078	Terminal/μ-1,3	[70]

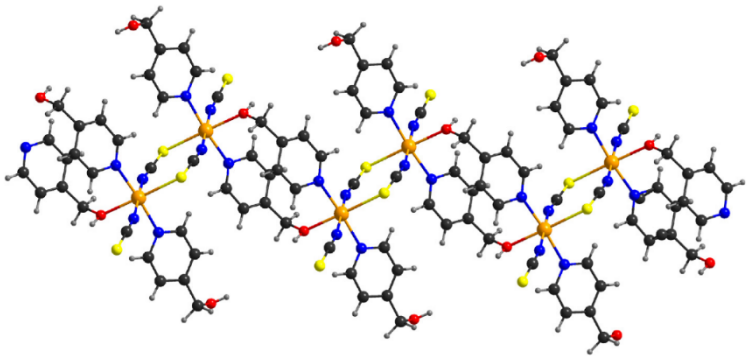

Fig. 4. Crystal structure of **4** with view of the chains. The disordering of one of the two 4-(hydroxymethyl)pyridine ligands is not shown for clarity. An ORTEP plot is shown in *Fig.* S15 in the Supplementary material.

are coordinated by four N-donor co-ligands and two terminal N-bonded anionic ligands the CN-stretching vibration is found clearly below 2100 cm^{-1} and this is also valid for most pyridine derivatives if two of the N-donor are exchanged by O-donor co-ligands like, e.g., H_2O. Surprisingly, the CN-stretching vibration for the hydrate complex **2** is found at 2120 cm^{-1}, which is higher than that observed in several compounds with μ-1,3 bridging thiocyanato anions.

It is also interesting to note, that in compound **4** where both, terminal and bridging anionic ligands are present similar values are observed. This is different in other compounds in which the metal cations are also linked by pairs of thiocyanato anions into dimers and are additionally coordinated by a terminal anionic ligand. In this case one can clearly distinguish between both coordination modes as it is the case for $[Ni_2(NCS)_6(4\text{-Azpy})_4]$ and $[Ni(NCS)_2(dpt)]$. The reason for this behavior is totally unclear but it shows, that an assignment of the coordination mode of thiocyanato anions only on the basis of IR spectroscopic data is not always possible.

5. Thermal properties

To investigate if the co-ligands can be stepwise removed measurements using simultaneously differential thermoanalysis and thermogravimetry were performed. In this context the question raises if by thermal treatment of the discrete complexes crystalline phases of composition $[Ni(NCS)_2(4\text{-(hydroxymethyl)pyridine})_2]_n$ can be observed and if they are different from that of **4** as frequently observed under these conditions [53,56,71].

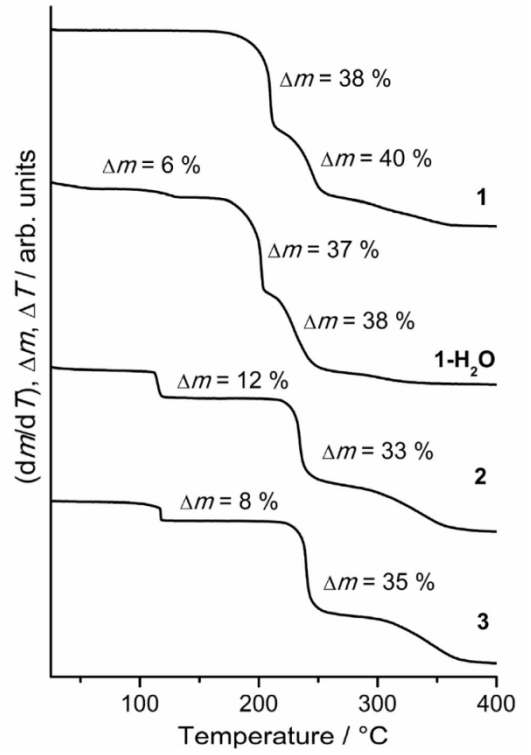

Fig. 5. Thermogravimetric curves for compound **1**, **1-H_2O**, **2** and **3**. Heating rate = 1 °C/min (**1**, **1-H_2O**), and heating rate = 4 °C/min (**2**, **3**), given is the mass change in %.

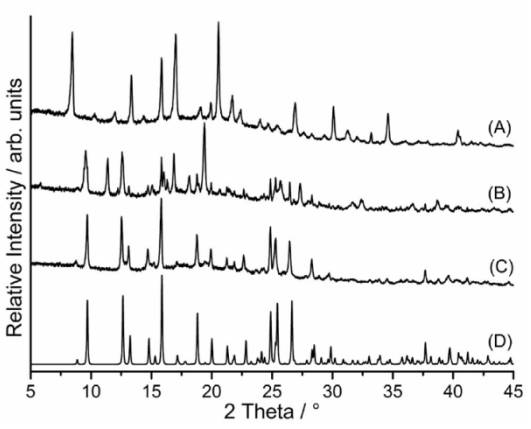

Fig. 6. Experimental XRPD pattern of the residues obtained after the first mass step of compound **1** (A), **2** (B), and **3** (C) and the calculated XRPD pattern of compound **4** (D).

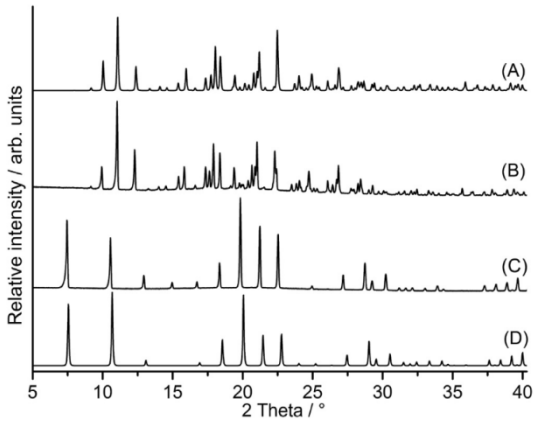

Fig. 7. Calculated XRPD pattern of **1** (A) and **1-H_2O** (D), as well as experimental XRPD pattern of **1** (B) and of the material obtained after stirring in water for 3 d (C).

If compound **1** is heated one mass step of Δm_{exp} = 38% is observed at 209 °C, which is in good agreement with that calculated for the removal of two of the 4-(hydroxymethyl)pyridine ligands (Δm_{calc} = 36%) (Figs. 5 and S16 in the Supplementary material). If compound **1-H_2O** is investigated several mass steps are observed in the thermogravimetric curve, of which the first step is consistent with the loss of about 2 water molecules and the second step correspond to the loss of two molecules of 4-(hydroxymethyl)pyridine (Fig. 5 and Fig. S17 in the Supplementary material). To prove if the water removal leads to the formation of **1**, the measurement was repeated and stopped after the first step. XRPD investigations prove, that compound **1** has formed as a pure phase (Fig. S18 in the Supplementary material).

Similar TG measurements for compounds **2** also show several good resolved mass steps in the TG curve of which the first step of Δm_{exp} = 12% is only in rough agreement with that calculated for the removal of two ethanol molecules (Δm_{calc} = 19%) (Figs. 5 and S19 in the Supplementary material). This deviation can be traced back to the fact, that **2** is always contaminated with very

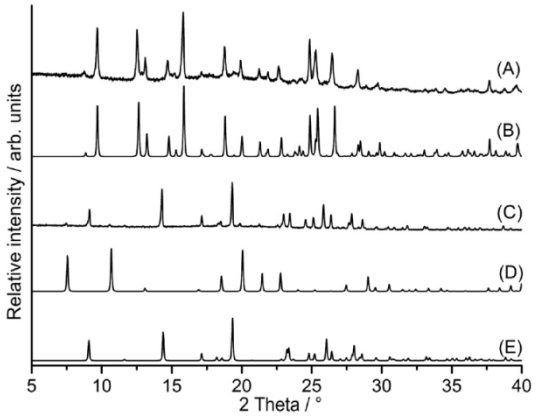

Fig. 8. Experimental XRPD pattern of the residue obtained after the first mass step of **3** (A) and if this residue is stirred in water for 3 d (C) as well as calculated XRPD pattern of **4** (B), **1-H$_2$O** (D) and of **3** (E).

Table 3
Selected experimental data of the magnetic measurements of **1-H$_2$O**, **1**, **3** and **4**. The data for compound **2** are not presented because this compound is contaminated with **4**.

	1-H$_2$O	**1**	**3**	**4**
Θ [K]	0.56	−0.21	0.46	−13.7
C [cm^3 K mol^{-1}]	1.10	1.10	1.60	1.40
μ_{eff} [μ_B]	2.90	3.00	3.50	3.40
$\mu_{eff(HS)}$ [μ_B]	2.82	2.82	2.82	2.82

small amounts of **4** (see Fig. S8 in the Supplementary material). For compound **3** the first mass loss of Δm_{exp} = 8% is in very good agreement with that calculated for the loss of two water molecules (Δm_{calc} = 8%) (Figs. 5 and S20 in the Supplementary material).

To identify the intermediates formed by the removal of 4-(hydroxymethyl)pyridine, ethanol or water the TG measurements were repeated, and stopped after the corresponding step, the isolated residues were investigated by XRPD (Fig. 6). For the residue of **1** a powder pattern is obtained, that is completely different from that of **4**. The elemental analysis reveals a composition of Ni(NCS)$_2$(4-(hydroxymethyl)pyridine)$_2$ but the CN stretching vibration is observed at 2075 cm^{-1} in the IR spectra, indicating that only terminal N-bonded thiocyanato anions are present (Fig. S21 in the Supplementary material). The residue obtained by thermal decomposition of **3** indicates that a mixture of compound **4** and an unknown crystalline phase has formed (Fig. 6). In contrast, water removal from **2** leads to the formation of pure samples of compound **4** (Fig. 6).

6. Investigations on the stability and rehydration behavior

The thermoanalytical investigations prove that **1-H$_2$O** transforms into **1** if the water is removed at elevated temperatures. To investigate the reversibility of this reaction and to definitely prove that water is embedded in the structure of **1-H$_2$O** a saturated solution with excess of solid of **1** was stirred in water and the residue obtained was investigated by XRPD (Fig. 7). This experiment clearly proves that **1** has been transformed into **1-H$_2$O** and that this reaction is fully reversible because a good crystalline material is observed. Thus, the residual electron density observed in the structure of **1-H$_2$O** corresponds to disordered water molecules.

Similar experiments were also performed for compound **4** prepared by solvent removal from **2** or **3**. If the residue obtained after the first TG step (**4**) is stirred in water, a transformation into the hydrate compound **3** is observed (Fig. 8). It is noted that this reaction does not take place if **4** is stored in a humid atmosphere for several days. In contrast, if **4** is reacted in ethanol, no transformation into the ethanol complex **2** is observed. However, a closer look into the powder pattern of the residue formed by rehydration reveal that a small amount of **1-H$_2$O** has been formed. Because not enough 4-(hydroxymethyl)pyridine is present, this transformation is incomplete.

7. Magnetic investigations

For Compounds **1-H$_2$O**, **1**, **2**, and **3** the temperature dependence of the susceptibility was measured as function of the temperature at H_{DC} = 1000 Oe. All these compounds consists of discrete complexes and therefore, as expected only paramagnetic behavior is observed (Figs. S22–S25). The magnetic data were analyzed using a Curie-Weiss fit, which shows that the Weiss constant for compound **1-H$_2$O**, **1**, and **3** is practically zero and therefore, no significant magnetic interactions occurs (Table 3). The experimental

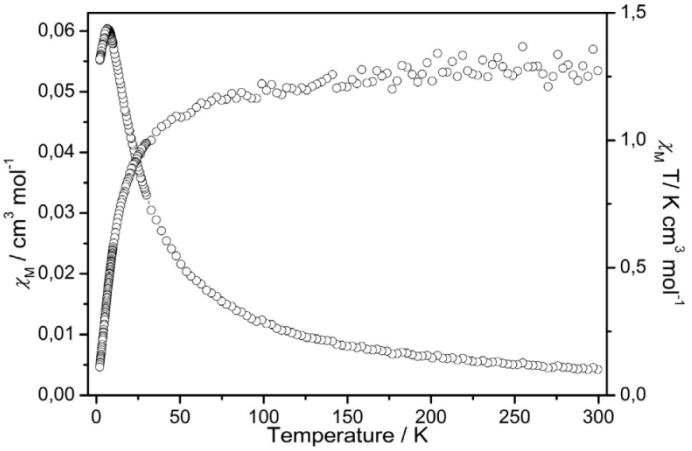

Fig. 9. χ_M and $\chi_M T$ as a function of the temperature for **4** at H_{DC} = 4 kOe.

magnetic moment for these compounds is in reasonable agreement with that calculated (Table 3). As mentioned before, compound **2** is always contaminated by compound **4** and this is obvious from the χ versus T curve, where the susceptibility increases after the antiferromagnetic maximum (see below and Fig. S24).

The temperature dependence of the susceptibility of **4** was measured at different DC fields in the range of 300–2 K. At H_{DC} = 4 kOe the susceptibility passes a maximum at T_N = 6.7 K which corresponds to an antiferromagnetic ordering (Fig. 9).

The χT product decreases with decreasing temperature indicating dominating antiferromagnetic interactions. Analyzing the magnetic data according to the Curie–Weiss law yields a negative Weiss-constant of θ = −13.7 K in agreement with the antiferromagnetic interactions and a Curie constant of C = 1.4 cm^3 K mol^{-1} (Table 3). The experimental effective moment of = 3.4 μ_B is slightly higher than that expected for Ni^{2+} in a high-spin configuration (2.82 μ_B) (Table 3). DC measurements at lower fields always lead to very noisy susceptibility curves (Figs. S26–S28 in the Supplementary material). Finally, the magnetization measured as a function of filed, shows a linear increase, as expected for an antiferromagnet (Fig. S29 in the Supplementary material).

8. Conclusions

In the present work new coordination compounds with 4-(hydroxymethyl)pyridine were prepared, with focus on compounds in which the metal cations are linked by μ-1,3 bridging anionic ligands into chains. One compound of composition $[Ni(NCS)_2(4\text{-(hydroxymethyl)pyridine})_2]_n$ was obtained, in which $Ni_2(NCS)_4$ dimers are linked by the 4-(hydroxymethyl)-pyridine ligands into chains. This is surprising, because in most coordination compounds with this ligand, it is only coordinated to the metal centers with the N atom of the pyridine ring. It might be the case that O-coordination to the relatively hard Ni(II) cations is energetically preferred over S-coordination of the anionic ligand needed for the generation of nickel thiocyanato chains. However, in this context it is noted, that in the corresponding compounds with 4-acetylpyridine, the co-ligand does not act as bridging ligand even if it is similar to 4-(hydroxymethyl)pyridine. Moreover, in the compounds with terminally N-bonded thiocyanato anions a strong shift of the CN stretching vibration to higher values is observed, and therefore, one cannot clearly distinguish between a terminal and a bridging coordination. Finally, our magnetic measurements indicate, that the 4-(hydroxymethyl)pyridine ligand mediate antiferromagnetic exchange.

9. Experimental

9.1. Synthesis

$NiSO_4 \cdot 6H_2O$ was obtained from Merck. $Ba(NCS)_2 \cdot 3H_2O$ and 4-(hydroxymethyl)pyridine were obtained from Alfa Aesar. Solvents were used without further purification. Crystalline powders of all compounds were prepared by stirring the reactants in the respective solvents at room temperature. The residues were filtered off and washed with appropriate solvent and dried in air. The purity of all compounds was checked by X-ray powder diffraction and elemental analysis.

9.2. $Ni(NCS)_2$

$Ba(NCS)_2 \cdot 3H_2O$ (17.5 g, 57 mmol) and $NiSO_4 \cdot 6H_2O$ (15.0 g, 57 mmol) were stirred in water (400 mL). The colorless precipitate of $BaSO_4$ was filtered off and the water evaporated using a rotary evaporator. The homogeneity of the product was investigated by X-ray powder diffraction and elemental analysis

9.3. Synthesis of compound ***1*-H_2O**

A crystalline light purple colored powder was synthesized by stirring $Ni(NCS)_2$ (87.4 mg, 0.50 mmol) and 4-(hydroxymethyl)pyridine (382 mg, 3.50 mmol) in 3 mL water for 1 d. Yield: 88% elemental analysis Calc. for $\mathbf{C_{26}H_{28}N_6NiO_4S_2}$: C, 51.08; H, 4.62; N, 13.75; S, 10.49. Found: C, 51.91; H, 4.91; N, 13.54; S, 8.93%. IR (ATR): ν_{max} = 3371 (b), 3068 (w), 2987 (w), 2875 (b), 2804 (w), 2081 (s), 2091 (s), 1942 (w), 1614 (s), 1561 (m), 1503 (m), 1453 (m), 1422 (s), 1337 (m), 1284 (w), 1221 (s), 1100 (m), 1049 (s), 1019 (s), 807 (s), 723 (m), 603 (m), 461 (b).

9.4. Synthesis of compound ***1***

Single crystals suitable for single crystal X-ray diffraction were prepared by reacting $Ni(NCS)_2$ (26.2 mg, 0.15 mmol) and 4-(hydroxymethyl)pyridine (65.5 mg, 0.60 mmol) in 1.5 mL methanol. A crystalline light purple colored powder was synthesized by stirring $Ni(NCS)_2$ (87.4 mg, 0.50 mmol) and 4-(hydroxymethyl)pyridine (382 mg, 3.50 mmol) in 3 mL acetonitrile for 5 d. Yield: 90% elemental analysis Calc. for $\mathbf{C_{26}H_{28}N_6NiO_4S_2}$: C, 51.08; H, 4.62; N, 13.75; S, 10.49. Found: C, 52.16; H, 4.79; N, 13.58; S, 9.10%. IR (ATR): ν_{max} = 3387 (b), 3062 (w), 2885 (b), 2823 (b), 2090 (s), 1946 (w), 1613 (s), 1561 (m), 1452 (m), 1419 (s), 1336 (m), 1281 (w), 1219 (s), 1100 (m), 1042 (s), 1019 (s), 805 (s), 723 (m), 666 (w), 603 (m), 483 (m).

9.5. Synthesis of compound ***2***

Single crystals suitable for single crystal X-ray diffraction were prepared by reacting $Ni(NCS)_2$ (52.5 mg, 0.30 mmol) and 4-(hydroxymethyl)pyridine (16.4 mg, 0.15 mmol) in 1.5 mL ethanol. A crystalline teal colored powder was synthesized by stirring $Ni(NCS)_2$ (87.4 mg, 0.50 mmol) and 4-(hydroxymethyl)pyridine (382 mg, 3.50 mmol) in 3 mL ethanol for 4 d. Yield: 62% elemental analysis Calc. for $\mathbf{C_{18}H_{26}N_4NiO_4S_2}$: C, 44.55; H, 5.40; N, 11.55; S, 13.22. Found: C, 45.85; H, 5.14; N, 11.90; S, 12.18%. IR (ATR): ν_{max} = 3242 (b), 2987 (w), 2891 (w), 2874 (w), 2100 (s), 1615 (s), 1561 (m), 1503 (w), 1422 (s), 1375 (w), 1320 (w), 1219 (s), 1093 (m), 1048 (s), 1021 (s), 984 (m), 886 (m), 799 (s), 720 (w), 666 (w), 605 (s), 483 (s).

9.6. Synthesis of compound ***3***

Single crystals suitable for single crystal X-ray diffraction were prepared by the reaction of $Ni(NCS)_2$ (26.2 mg, 0.15 mmol) and 4-(hydroxymethyl)pyridine (16.4 mg, 0.15 mmol) in 1.5 mL water at 105 °C in a closed glass culture tube. A crystalline light green colored powder was synthesized by stirring $Ni(NCS)_2$ (174.9 mg, 1.00 mmol) and 4-(hydroxymethyl)pyridine (54.6 mg, 0.50 mmol) in 3 mL water for 5 d. Yield: 80% elemental analysis Calc. for $\mathbf{C_{14}H_{18}N_4NiO_4S_2}$: C, 39.18; H, 4.23; N, 13.06; S, 14.94. Found: C, 38.74; H, 4.10; N, 13.58; S, 15.00%. IR (ATR): ν_{max} = 3377 (b), 3309 (b), 3242 (b), 2930 (w), 2905 (w), 2862 (w), 2120 (s), 1652 (m), 1616 (m), 1564 (m), 1504 (w), 1423 (s), 1398 (w), 1360 (w), 1214 (m), 1106 (m), 1036 (s), 1021 (s), 981 (m), 807 (s), 784 (w), 725 (m), 611 (s), 490 (s), 468 (s).

9.7. Synthesis of compound ***4***

Single crystals suitable for single crystal X-ray diffraction were prepared by the reaction of $Ni(NCS)_2$ (26.2 mg, 0.15 mmol) and 4-(hydroxymethyl)pyridine (32.7 mg, 0.30 mmol) in 1.5 mL ethanol.

A light blue colored crystalline powder was synthesized by stirring $Ni(NCS)_2$ (174.9 mg, 1.00 mmol) and 4-(hydroxymethyl)pyridine (218 mg, 2.00 mmol) in 3 mL acetonitril for 5 d. Yield: 91% elemental analysis Calc. for **$C_{14}H_{14}N_4NiO_2S_2$**: C, 42.78; H, 3.59; N, 14.93; S, 16.31. Found: C, 42.76; H, 3.58; N, 14.36; S, 15.78%. IR (ATR): ν_{max} = 3429 (b), 3234 (b), 2889 (w), 2850 (w), 2124 (s), 2108 (s), 2100 (s), 1616 (s), 1562 (m), 1506 (m), 1422 (s), 1392 (m), 1369 (m), 1325 (w), 1223 (m), 1102 (w), 1043 (s), 1009 (s), 968 (m), 802 (s), 723 (m), 606 (s), 472 (s).

9.8. Elemental analysis

CHNS analysis was performed using an EURO EA elemental analyzer, fabricated by EURO VECTOR Instruments and Software.

9.9. Spectroscopy

All IR data were obtained using an ATI Mattson Genesis Series FTIR Spectrometer, control software: WINFIRST, from ATI Mattson.

9.10. X-ray powder diffraction (XRPD)

The measurements were performed using (1) a PANalytical X'Pert Pro MPD Reflection Powder Diffraction System with Cu Kα radiation (λ = 154.0598 pm) equipped with a PIXcel semiconductor detector from PANanlytical and (2) a Stoe Transmission Powder Diffraction System (STADI P) with Cu Ka radiation (λ = 54.0598 pm) that was equipped with a MYTHEN K1000 detector from STOE & CIE.

9.11. Differential thermal analysis and thermogravimetry (DTA-TG-MS)

The heating-rate dependent DTA-TG measurements were performed in a nitrogen atmosphere (purity: 5.0) in Al_2O_3 crucibles using a STA-409CD instrument from Netzsch. All measurements were performed with a flow rate of 75 mL min^{-1} and were corrected for buoyancy and current effects. The instrument was calibrated using standard reference materials.

9.12. Magnetic measurements

All magnetic measurements were performed using a PPMS (Physical Property Measurement System) from Quantum Design, which was equipped with a 9 Tesla magnet. The data were corrected for core diamagnetism.

9.13. Single-crystal structure analyses

Single-crystal data collections were carried out on an imaging plate diffraction system: Stoe IPDS-1 for **1**, **1-H_2O** and **3** as well as Stoe IPDS-2 for **2** and **4** with Mo Kα radiation. The structures were solved with Direct Methods using SHELXS-97 and structure refinements were performed against F^2 using SHELXL-2013 [72]. Numerical absorption correction was applied using programs X-RED and X-SHAPE of the program package X-AREA. All non hydrogen atoms were refined with anisotropic displacement parameters. All hydrogen atoms were positioned with idealized geometry and were refined isotropic with $U_{iso}(H) = -1.2\ U_{eq}(C)$ (1.5 for methyl H atoms) using a riding model. The hydroxyl hydrogen atoms were located in a difference map, their bond lengths were set to ideal values and finally they were refined using a riding model. The hydroxymethyl group in **1-H_2O** is disordered in two orientations because of symmetry. If the structure is refined in space groups of lower symmetry the disordering remains constant. For **1-H_2O** there are some small residual electron density maxima in cavities of the structure that corresponds to disordered water molecules. Because no reasonable structure model was found the data were corrected for disordered solvent using SQUEEZE in Platon. In compound **2** the ethyl group of the ethanol molecule and in compound **4** one of the two 6-membered rings are disordered in two orientations and were refined using a split model. The crystal of **1** was racemically twinned and therefore, a twin refinement was performed (BASF parameter: 0.348 (16)).

Compound	**1-H_2O**	**1**	**2**	**3**	**4**
Formula	$C_{26}H_{28}N_6NiO_4S_2$	$C_{26}H_{28}N_6NiO_4S_2$	$C_{18}H_{26}N_4NiO_4S_2$	$C_{14}H_{18}N_4NiO_4S_2$	$C_{14}H_{14}N_4NiO_2S_2$
MW (g mol^{-1})	611.37	611.37	485.26	429.15	393.12
Crystal system	cubic	orthorhombic	monoclinic	orthorhombic	monoclinic
Space group	*Pn*-3n	$P2_12_12_1$	*C*2/c	*P*bca	$P2_1/c$
a (Å)	16.5526(7)	11.5025(5)	8.9402(3)	12.2019(8)	10.7120(3)
b (Å)	16.5526(7)	14.2859(8)	16.1754(8)	7.6528(5)	19.9594(6)
c (Å)	16.5526(7)	17.6171(8)	16.2783(6)	19.4727(14)	7.8088(3)
β (°)	90	90	95.507(3)	90	106.831(2)
V (Å^3)	4535.2(6)	2894.9(2)	2343.16(16)	1818.3(2)	1598.04(9)
T (K)	200(2)	200(2)	200(2)	200(2)	200(2)
Z	6	4	4	4	4
D_{calc} (mg cm^{-3})	1.343	1.403	1.376	1.568	1.634
μ (mm^{-1})	0.820	0.856	1.035	1.323	1.489
θ_{max} (°)	3.01 to 26.00	2.27 to 27.92	2.51 to 25.01	2.68 to 27.84°.	1.99 to 28.02
Measured reflections	25,450	21,315	13,493	17,099	24,270
Unique reflections	747	6876	2062	2134	3810
Reflections [$F_0 > 4\sigma(F_0)$]	697	5831	1861	1804	3520
Parameter	55	356	151	117	245
R_{int}	0.0572	0.0908	0.0577	0.0691	0.0441
R_1[a] [$F_0 > 4\sigma(F_0)$]	0.0612	0.0411	0.0492	0.0424	0.0373
wR_2[b] [all data]	0.1620	0.0870	0.1119	0.1169	0.0853
Goodness-of-fit (GOF)	1.177	1.015	1.133	1.062	1.151
$\Delta\rho_{max/min}$ (e Å^{-3})	0.566/−0.395	0.397/−0.414	0.700/−0.765	0.628/−0.826	0.637/−0.346

Acknowledgements

This project was supported by the Deutsche Forschungsgemeinschaft (Project No. NA 720/5-1) and by the State of Schleswig-Holstein. We thank Prof. Dr. Wolfgang Bensch for access to his experimental facilities. Special thanks to Inke

Jess for the single crystal measurements and to Maren Rasmussen and Henning Lühmann for the magnetic measurements.

Appendix A. Supplementary data

CCDC 1056273 (**1-H_2O**), 1056272 (**1**), 1056274 (**2**), 1056275 (**3**) and 1056276 (**4**) contain the supplementary crystallographic data for this paper. These data can be obtained free of charge via http://www.ccdc.cam.ac.uk/conts/retrieving.html, or from the Cambridge Crystallographic Data Centre, 12 Union Road, Cambridge CB2 1EZ, UK; fax: (+44) 1223 336 033; or e-mail: deposit@ccdc.cam.ac.uk. Supplementary data associated with this article can be found, in the online version, at http://dx.doi.org/10.1016/j.poly.2015.06.004.

References

[1] F.A. Mautner, M. Scherzer, C. Berger, R.C. Fischer, S.S. Massoud, Inorg. Chim. Acta 425 (2015) 46.
[2] F. Mautner, F. Louka, A. Gallo, J. Albering, M. Saber, N. Burham, S. Massoud, Transition Met. Chem. 35 (2010) 613.
[3] C.J. Adams, M.F. Haddow, D.J. Harding, T.J. Podesta, R.E. Waddington, CrystEngComm 13 (2011) 4909.
[4] S. Wöhlert, I. Jess, C. Näther, Polyhedron 63 (2013) 21.
[5] A. Lennartson, A.D. Bond, S. Piligkos, C.J. McKenzie, Angew. Chem. 124 (2012) 11211.
[6] C.J. Adams, M.C. Muñoz, R.E. Waddington, J.A. Real, Inorg. Chem. 50 (2011) 10633.
[7] C.J. Adams, J.A. Real, R.E. Waddington, CrystEngComm 12 (2010) 3547.
[8] E. Shurdha, C.E. Moore, A.L. Rheingold, S.H. Lapidus, P.W. Stephens, A.M. Arif, J.S. Miller, Inorg. Chem. 52 (2013) 10583.
[9] J. Boeckmann, C. Näther, Dalton Trans. 39 (2010) 11019.
[10] J. Boeckmann, C. Näther, Polyhedron 31 (2012) 587.
[11] C. Näther, J. Greve, J. Solid State Chem. 176 (2003) 259.
[12] M. Wriedt, I. Jeß, C. Näther, Eur. J. Inorg. Chem. (2009) 1406.
[13] G.D. Munno, M. Julve, J.A. Real, F. Lloret, R. Scopelliti, Inorg. Chim. Acta 250 (1996) 81.
[14] G.D. Munno, D. Armentano, T. Poerio, M. Julve, J.A. Real, J. Chem. Soc., Dalton Trans. (1999) 1813.
[15] G.D. Munno, F. Cipriani, D. Armentano, M. Julve, J.A. Real, New J. Chem. 25 (2001) 1031.
[16] J.G. Małecki, T. Groń, H. Duda, Polyhedron 36 (2012) 56.
[17] B. Machura, J. Palion, M. Penkala, T. Groń, H. Duda, R. Kruszynski, Polyhedron 56 (2013) 189.
[18] B. Machura, A. Świtlicka, I. Nawrot, J. Mroziński, R. Kruszynski, Polyhedron 30 (2011) 832.
[19] P. Bhowmik, S. Chattopadhyay, M.G.B. Drew, C. Diaz, A. Ghosh, Polyhedron 29 (2010) 2637.
[20] J.G. Małecki, B. Machura, A. Świtlicka, T. Groń, M. Bałanda, Polyhedron 30 (2011) 746.
[21] T.K. Maji, G. Mostafa, P.S. Mukherjee, A. Mondal, A.J. Welch, K. Okamoto, N.R. Chaudhuri, Polyhedron 19 (2000) 1903.
[22] A. Tahli, J.K. Maclaren, I. Boldog, C. Janiak, Inorg. Chim. Acta 374 (2011) 506.
[23] S. Banerjee, B. Wu, P.-G. Lassahn, C. Janiak, A. Ghosh, Inorg. Chim. Acta 358 (2005) 535.
[24] F.A. Mautner, M. Scherzer, C. Berger, R.C. Fischer, R. Vicente, S.S. Massoud, Polyhedron 85 (2015) 20.
[25] S.S. Massoud, M. Dubin, A.E. Guilbeau, M. Spell, R. Vicente, P. Wilfling, R.C. Fischer, F.A. Mautner, Polyhedron 78 (2014) 135.
[26] H. Xu, P.G. Williard, W.H. Bernskoetter, Dalton Trans. 43 (2014) 14696.
[27] R. Uhrecký, I. Ondrejkovičová, D. Lacková, Z. Fáberová, J. Mroziński, B. Kalińska, Z. Padělková, M. Koman, Inorg. Chim. Acta 414 (2014) 33.
[28] F.A. Mautner, R. Vicente, S.S. Massoud, Polyhedron 25 (2006) 1673.
[29] E. Shurdha, S.H. Lapidus, P.W. Stephens, C.E. Moore, A.L. Rheingold, J.S. Miller, Inorg. Chem. 51 (2012) 9655.
[30] J. Boeckmann, M. Wriedt, C. Näther, Chem. Eur. J. 18 (2012) 5284.
[31] M. Wriedt, C. Näther, Chem. Commun. 46 (2010) 4707.
[32] F. Lloret, G. De Munno, M. Julve, J. Cano, R. Ruiz, A. Caneschi, Angew. Chem., Int. Ed. 37 (1998) 135.
[33] R. González, A. Acosta, R. Chiozzone, C. Kremer, D. Armentano, G. De Munno, M. Julve, F. Lloret, J. Faus, Inorg. Chem. 51 (2012) 5737.
[34] J.A. Real, G. De Munno, M.C. Munoz, M. Julve, Inorg. Chem. 30 (1991) 2701.
[35] B. Zurowska, J. Mrozinski, M. Julve, F. Lloret, A. Maslejova, W. Sawka-Dobrowolska, Inorg. Chem. 41 (2002) 1771.
[36] B. Machura, A. Świtlicka, J. Mroziński, B. Kalińska, R. Kruszynski, Polyhedron 52 (2013) 1276.
[37] T.K. Maji, G. Mostafa, Juan M. Clemente-Juan, F. Lloret, K.-I. Okamoto, Nirmalendu R. Chaudhuri, Eur. J. Inorg. Chem. 1005 (2003).
[38] S. Wöhlert, L. Peters, C. Näther, Dalton Trans. 42 (2013) 10746.
[39] S. Wöhlert, C. Näther, Inorg. Chim. Acta 406 (2013) 196.
[40] M. Mousavi, V. Bereau, C. Duhayon, P. Guionneau, J.-P. Sutter, Chem. Commun. 48 (2012) 10028.
[41] B. Machura, A. Świtlicka, P. Zwoliński, J. Mroziński, B. Kalińska, R. Kruszynski, J. Solid State Chem. 197 (2013) 218.
[42] S. Banerjee, M.G.B. Drew, C.-Z. Lu, J. Tercero, C. Diaz, A. Ghosh, Eur. J. Inorg. Chem. 12 (2005) 2376.
[43] R. Kapoor, A. Kataria, A. Pathak, P. Venugopalan, G. Hundal, P. Kapoor, Polyhedron 24 (2005) 1221.
[44] J. Mroziński, J. Kłak, R. Kruszyński, Polyhedron 27 (2008) 1401.
[45] S. Wöhlert, J. Boeckmann, I. Jess, C. Näther, CrystEngComm 14 (2012) 5412.
[46] S. Wöhlert, L. Fink, M. Schmidt, C. Näther, CrystEngComm 15 (2013) 945.
[47] J. Tao, R.-J. Wei, R.-B. Huang, L.-S. Zheng, Chem. Soc. Rev. 41 (2012) 703.
[48] Z. Arcis-Castillo, S. Zheng, M.A. Siegler, O. Roubeau, S. Bedoui, S. Bonnet, Chem. Eur. J. 17 (2011) 14826.
[49] J. Cano, G. De Munno, F. Lloret, M. Julve, Inorg. Chem. 39 (2000) 1611.
[50] A. Barasiński, P. Sobczak, A. Drzewiński, G. Kamieniarz, A. Bieńko, J. Mroziński, D. Gatteschi, Polyhedron 29 (2010) 1485.
[51] C. Näther, S. Wöhlert, J. Boeckmann, M. Wriedt, I. Jeß, Z. Anorg. Allg. Chem. 639 (2013) 2696.
[52] S. Wöhlert, J. Boeckmann, M. Wriedt, C. Näther, Angew. Chem., Int. Ed. 50 (2011) 6920.
[53] S. Wöhlert, T. Runčevski, R.E. Dinnebier, S.G. Ebbinghaus, C. Näther, Cryst. Growth Des. 14 (2014) 1902.
[54] S. Wöhlert, U. Ruschewitz, C. Näther, Cryst. Growth Des. 12 (2012) 2715.
[55] J. Werner, M. Rams, Z. Tomkowicz, C. Nather, Dalton Trans. 43 (2014) 17333.
[56] M.R. Julia Werner, Zbigniew Tomkowicz, Tomče Runčevski, Robert E. Dinnebier, Stefan Suckert, Christian Näther, Inorg. Chem. 54 (2015) 2893.
[57] S. Wöhlert, T. Fic, Z. Tomkowicz, S.G. Ebbinghaus, M. Rams, W. Haase, C. Näther, Inorg. Chem. 52 (2013) 12947.
[58] S. Wöhlert, Z. Tomkowicz, M. Rams, S.G. Ebbinghaus, L. Fink, M.U. Schmidt, C. Näther, Inorg. Chem. 53 (2014) 8298.
[59] S. Wöhlert, M. Wriedt, T. Fic, Z. Tomkowicz, W. Haase, C. Näther, Inorg. Chem. 52 (2013) 1061.
[60] S. Wöhlert, C. Näther, Eur. J. Inorg. Chem. 2013 (2013) 2528.
[61] J. Maroszová, J. Moncol, Z. Padělková, R. Sillanpää, T. Lis, M. Koman, Cent. Eur. J. Chem. 9 (2011) 453.
[62] T.C. Stamatatos, D. Foguet-Albiol, S.P. Perlepes, C.P. Raptopoulou, A. Terzis, C.S. Patrickios, G. Christou, A.J. Tasiopoulos, Polyhedron 25 (2006) 1737.
[63] M.A.S. Goher, F.A. Mautner, K. Gatterer, M.A.M. Abu-Youssef, A.M.A. Badr, B. Sodin, C. Gspan, J. Mol. Struct. 876 (2008) 199.
[64] İ. Uçar, İ. Bulut, A. Bulut, A. Karadağ, Struct. Chem. 20 (2009) 825.
[65] J. Moncol, B. Kalinakova, J. Svorec, M. Kleinova, M. Koman, D. Hudecova, M. Melnik, M. Mazur, M. Valko, Inorg. Chim. Acta 357 (2004) 3211.
[66] J. Moncol, M. Mudra, P. Lonnecke, M. Koman, M. Melnik, J. Chem. Crystallogr. 34 (2004) 423.
[67] M.C. Etter, J.C. MacDonald, J. Bernstein, Acta Crystallogr., Sect. B 46 (1990) 256.
[68] F. Valach, P. Sivy, B. Koren, Acta Crystallogr. C40 (1984) 957.
[69] T.R. Julia Werner, Robert Dinnebier, Stefan G. Ebbinghaus, S.A.C. Näther, Eur. J. Inorg. Chem. (2015).
[70] J. Boeckmann, N. Evers, C. Näther, CrystEngComm 14 (2012) 1094.
[71] C. Näther, I. Jeß, J. Solid State Chem. 169 (2002) 103.
[72] G.M. Sheldrick, Acta Crystallogr. A64 (2008) 112.

5. Synthese, Kristallstrukturen und Eigenschaften von diamagnetischen Koordinationsverbindungen

5.1. Investigations on the Structure Diversity and Thermal Degradation Behavior of Cd^{II} and Zn^{II} Thiocyanato Coordination Compounds based on 3-Acetylpyridine as Neutral Co-Ligand

Julia Werner, Jan Boeckmann und Christian Näther, *Z. Anorg. Allg. Chem.* **2012**, *638*, *(14)*, 2257-2264.

DOI: 10.1002/zaac.201200268

Motivation

Wie bereits in Kapitel 4.6 gezeigt wurde, konnten mit den verwendeten paramagnetischen Metallkationen Verbindungen mit einer Zusammensetzung $M(NCS)_2$(3-Acetylpyridin)$_2$ und $M(NCS)_2$(3-Acetylpyridin) (Mn, Fe; Ni) durch thermischen Abbau hergestellt werden, jedoch war es nicht möglich, entsprechende Einkristalle zu synthetisieren.

Eine Möglichkeit, die entstandenen Verbindungen zu identifizieren, ist der Vergleich mit isotypen Strukturen. Das Übergangsmetall Cadmium weist eine höhere Chalkophilie als Mangan, Eisen, Kobalt und Nickel auf, weshalb die Bildung von μ-1,3 verbrückenden Thiocyantanionen begünstig ist, wohingegen Verbindungen mit Zink als Übergangsmetall häufig tetraedrisch koordinierte Komplexe bilden. Die folgende Arbeit stellt die Ergebnisse der Synthesen von $Cd(NCS)_2$ und $Zn(NCS)_2$ mit 3-Acetylpyridin dar.

ARTICLE

DOI: 10.1002/zaac.201200268

Investigations on the Structure Diversity and Thermal Degradation Behavior of Cd^{II} and Zn^{II} Thiocyanato Coordination Compounds based on 3-Acetylpyridine as Neutral Co-Ligand

Julia Werner,[a] Jan Boeckmann,[a] and Christian N ther*[a]

Keywords: Coordination chemistry; Zn^{II} and Cd^{II} coordination compounds; Crystal structures; Thermochemistry

Abstract. Reaction of Cd^{II} and Zn^{II} thiocyanate with 3-acetylpyridine leads to the formation of the new Cd^{II} and Zn^{II} coordination compounds $[Cd(NCS)_2(3\text{-acetylpyridine})_4]$ (**1A**), $[Cd(NCS)_2(3\text{-acetylpyridine})_2]_n$ (**1B**), $[Cd(NCS)_2(3\text{-acetylpyridine})]_n$ (**1C**) and $[Zn(NCS)_2(3\text{-acetylpyridine})_2]$ (**2A**). Compound **1A** consists of discrete complexes, in which the metal centers are octahedrally coordinated by four terminal bonded N-donor co-ligands and two terminal N-bonded thiocyanato anions. In compound **2A** the metal centers are only tetrahedrally coordinated by two terminal bonded N-donor co-ligands and two terminal N-bonded thiocyanato anions. In compound **1B** the Cd^{II} cations are octahedrally coordinated by two terminal bonded N-donor co-ligands and four thiocyanato anions. The metal centers are linked by μ-1,3 bridging thiocyanato anions into chains. In compound **1C** the metal cations are octahedrally coordinated by two μ-1,5 bridging 3-acetylpyridine ligands and four μ-1,3 bridging thiocyanato anions building up a three-dimensional coordination network. Investigations on the thermal degradation behavior of all compounds using simultaneous differential thermoanalysis and thermogravimetry as well as X-ray powder diffraction and IR spectroscopy prove that on heating compound **2A** decompose without the formation of 3-acetylpyridine-deficient intermediates. In contrast, for compound **1A** a stepwise decomposition is observed, leading to the formation of the 3-acetylpyridine-deficient compound $[Cd(NCS)_2(3\text{-acetylpyridine})_2]_n$ (**1B**) which decomposes on further heating

Introduction

The development of strategies for a rational synthesis of new coordination polymers that show cooperative magnetic phenomena is still an active field of chemical research.[1–14] For the preparation of such compounds paramagnetic metal cations must be connected by small-sized ligands that can mediate magnetic exchange interactions. In this context our interest has focused on the preparation of transition metal thio- and selenocyanates in which the metal cations are linked by bridging thiocyanato anions. However, because in these compounds the terminal coordination of the anionic ligand is usually preferred for hard metals like e.g. manganese, iron, cobalt, and nickel, bridging compounds are less reported and their synthesis is sometimes difficult to achieve or even impossible if the synthesis is performed in the liquid state.[15–23] Therefore, we reported on an alternative approach for the synthesis of such compounds which is based on thermal decomposition reactions.[24] Following our ideas octahedrally coordinated precursor compounds based on paramagnetic transition metals with terminally bonded thio- or selenocyanato anions and neutral N-donor co-ligands are thermally degraded, which enforces the formation of intermediates, in which the metal atoms are linked by μ-1,3 bridging anionic ligands.[25–29] Most of these compounds show cooperative magnetic phenomena and in some of them a slow relaxation of the magnetization is observed.[30–34]

Unfortunately, on thermal decomposition only microcrystalline powders of low crystallinity are obtained and therefore, the structural identity of these compounds is difficult to prove. In some cases the coordination mode of the anionic ligand – N-terminal or bridging – can be determined by IR spectroscopy analyzing the asymmetric CN stretching vibration but our previous investigations have shown that these values are strongly influenced by e.g. the nature of the co-ligand.[35–38] Moreover, using thermal decomposition as a synthetic tool intermediates with bridging anions can only be expected if the octahedral coordination is retained on ligand removal but one has to keep in mind that also a transformation into tetrahedral coordinated complexes might occur. In this context we reported on a very efficient approach which might help to overcome these problems. Using the chalcophilic metal cation Cd^{II} in the synthesis ligand-deficient intermediates with bridging anions can easily be crystallized in solution and identified by single crystal structure analysis.[39,40] In several cases they are isotypic to their paramagnetic counterparts, and the structures of the latter can be determined by Rietveld refinement. In contrast to cadmium, zinc prefers a tetrahedral coordination and therefore the preparation of such compounds can help in the identification of possible tetrahedral intermediates. Even in those cases,

* Prof. Dr. C. N ther
Fax: +49-431-8801520
E-Mail: cnaether@ac.uni-kiel.de
[a] Institut f r Anorganische Chemie
Christian-Albrechts-Universit t zu Kiel
Max-Eyth-Straße 2
24118 Kiel, Germany

Supporting information for this article is available on the WWW under http://dx.doi.org/10.1002/zaac.201200268 or from the author.

where these intermediates are not isotypic to their paramagnetic counterparts the comparison of their IR spectra can help to unambiguously determine the coordination mode of the paramagnetic intermediates. Finally, with cadmium thiocyanato different isomers including stable and metastable forms can be prepared as shown in our previous work.[41] This is the reason why we are generally interested in the synthesis, structures and thermal behavior of these diamagnetic compounds. In the course of systematic investigations we decided to investigate compounds based on Cd^{II} and Zn^{II} thiocyanate as well as 3-acetylpyridine (3-Acpy), because this ligand is of current interest for our project. According to a search in the CCDC database (conquest Ver. 1.14, 2012) no compounds built up of metal thiocyanates and this ligand are reported in literature.[42]

Synthetic Investigations

In order to investigate if different crystalline phases can be prepared in solution, different ratios of the corresponding metal salts and the N-donor co-ligand were reacted in water or pure co-ligand and the resulting precipitates were investigated by XRPD measurements (Table 1).

Table 1. Crystalline phases that can be obtained if different ratios of zinc and cadmium thiocyanate are reacted with 3-Acpy.

Ratio Metal salt	3-Acpy	Zn^{II}	Cd^{II}
1	pure	**2A**	**1A**
1	10	**2A**	**1A**
1	6	**2A**	**1A/1B**
1	4	**2A**	**1B**
1	2	**2A**	**1B**
2	1	**2A**	**1B**
4	1	**2A**	**1C**

These investigations clearly show that with Zn^{II} thiocyanate and 3-Acpy only one crystalline phase **2A** is formed. In contrast, with Cd^{II} thiocyanate three different crystalline phases **1A–1C** are obtained. Elemental analysis of these phases yielding compositions of $[Cd(NCS)_2(3\text{-Acpy})_4]$ for **1A**, $[Cd(NCS)_2(3\text{-Acpy})_2]$ for **1B**, $[Cd(NCS)_2(3\text{-Acpy})]$ for **1C** and $[Zn(NCS)_2(3\text{-Acpy})_2]$ for **2A** and X-ray powder diffraction proves that **2A** is not isotypic to **1B** (Figure S1 in the Supporting Information).

To get some preliminary information on the coordination mode of the thiocyanato anions and the 3-Acpy co-ligands, all compounds were investigated by IR spectroscopy (Figure S2–5 in the Supporting Information). In compounds with terminal N-bonded thiocyanato anions the asymmetric $\tilde{\nu}_{as}(CN)$ is expected at about 2050 cm^{-1}, whereas for bridging anions $\tilde{\nu}_{as}(CN)$ values of about 2100 cm^{-1} are expected.[35] For compound **1A** and **2A** values for $\tilde{\nu}_{as}(CN)$ are found, which are characteristic for terminal bonded thiocyanato anions (Table 2), whereas for **1B** and **1C** $\tilde{\nu}_{as}(CN)$ is about 2100 cm^{-1} (Table 2), consistent with bridging anions.

Table 2. Stretching vibration $\nu_{as}(CN)$ for the thiocyanato anions and $\nu_{as}(CO)$ for the acetyl group of the 3-acetylpyridine co-ligand in the infrared spectra of compounds **1A–1C** and **2A**.

Compound	$\nu_{as}(CN)$ /cm^{-1}	$\nu_{as}(CO)$ /cm^{-1}
1A	2043	1684
1B	2092	1694
1C	2096	1671
2A	2067	1688

Furthermore, in compound **1C** the $\tilde{\nu}_{as}(CO)$ band is shifted to lower wavenumbers, indicating that the acetyl group of the co-ligand is involved in metal coordination, which is not the case for the other compounds. Based on these results it can be assumed that the Cd compound **1A** consists of discrete complexes in which the metal cations are octahedrally coordinated by four 3-Acpy ligands and two terminal bonded thiocyanato anions, whereas in the zinc compound **2A** tetrahedral coordinated discrete complexes with terminal coordinated thiocyanato anions should be present. In **1B** the metal cations should be μ-1,3 bridged by the anionic ligands, whereas the coordination topology of **1C** should contain μ-1,3 bridging anions as well as bridging 3-Acpy ligands.

In further investigations crystallization experiments were performed in order to characterize all compounds by single crystal structure analysis.

Crystal Structures

The ligand-rich 1:4 (ratio metal salt to neutral co-ligand) compound $[Cd(NCS)_2(3\text{-Acpy})_4]$ (**1A**) crystallizes in the triclinic centrosymmetric space group $P\bar{1}$ with two formula units in the unit cell. The asymmetric unit consists of two crystallographically independent metal cations which are located on a center of inversion, two thiocyanato anions as well as four 3-Acpy ligands, all of them located in general position (Figure 1).

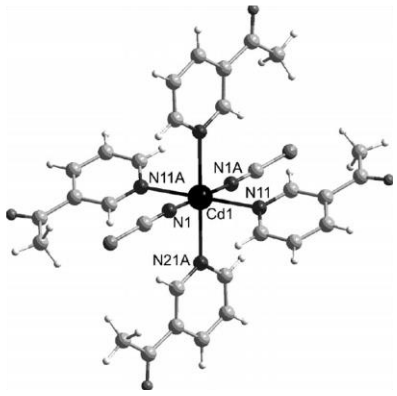

Figure 1. Coordination sphere in one of the two independent complexes of compound **1A** with atom labeling. Symmetry code used to generate equivalent atoms: A: –x, –y+1, –z+1. (an ORTEP plot of **1A** is shown in Figure S6 in the Supporting Information).

Each metal cation is coordinated by six nitrogen atoms of two terminal bonded thiocyanato anions and four nitrogen atoms of terminal bonded 3-Acpy ligands within a slightly distorted octahedral coordination geometry. The metal–nitrogen distances range between 2.258(2) and 2.4392(19) Å as well as the angles around the metal cations range between 86.62(7) and 93.38(7) ° (Table 3). The geometric parameters in both crystallographically independent metal complexes are similar (Table 3).

Table 3. Selected bond lengths / Å and angles /deg for both crystallographically independent metal complexes in compound **1A**. Symmetry code: A: –*x*, –*y*+1, –*z*+1.

Cd(1)–N(1)	2.262(2)
Cd(1)–N(11)	2.384(2)
Cd(1)–N(21)	2.378(2)
Cd(2)–N(2)	2.258(2)
Cd(2)–N(31)	2.360(2)
Cd(2)–N(41)	2.439(2)
N(1)–Cd(1)–N(11)	91.27(8)
N(1)–Cd(1)–N(11A)	88.73(8)
N(1)–Cd(1)–N(21)	90.20(8)
N(1)–Cd(1)–N(21A)	89.80(8)
N(11)–Cd(1)–N(21)	93.13(8)
N(11)–Cd(1)–N(21A)	86.87(8)
N(2)–Cd(2)–N(31)	90.39(8)
N(2)–Cd(2)–N(31B)	89.61(8)
N(2)–Cd(2)–N(41)	87.12(8)
N(2)–Cd(2)–N(41B)	92.88(8)
N(31)–Cd(2)–N(41)	93.38(7)
N(31)–Cd(2)–N(41B)	86.62(7)

The ligand-deficient 1:2 compound $[Cd(NCS)_2(3\text{-Acpy})_2]_n$ (**1B**) crystallizes in the monoclinic centrosymmetric space group $P2_1/c$ with two formula units in the unit cell. The asymmetric unit consists of one metal cation, which is situated on a center of inversion as well as of one 3-Acpy and one thiocyanato ligand in general positions (Figure 2).

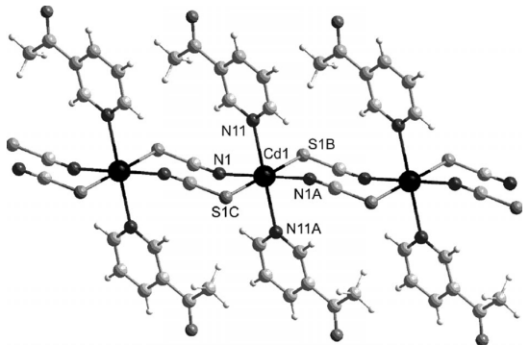

Figure 2. Molecular structure of compound **1B** with atom labeling. For clarity the disordered oxygen atom of the acetyl group is not shown. Symmetry transformations used to generate equivalent atoms: A: –*x*, –*y*+1, –*z*; B: *x*–1, *y*, *z*, C: –*x*+1, –*y*+1, –*z*. (an ORTEP plot of **1B** is shown in Figure S7 in the Supporting Information).

The metal cation is coordinated by four nitrogen atoms of two 3-Acpy ligands and two μ-1,3 bridging thiocyanato anions and two sulfur atoms of two adjacent μ-1,3 bridging thiocyanato anions in a mutually *trans* orientation in a slightly distorted octahedral coordination environment (Table 4).

Table 4. Selected bond lengths / Å and angles /deg for **1B**. Symmetry codes: A: –*x*, –*y*+1, –*z*; B: *x*–1, *y*, *z*, C: –*x*+1, –*y*+1, –*z*.

Cd(1)–N(1)	2.3056(15)
Cd(1)–N(11)	2.3856(15)
Cd(1)–S(1B)	2.7346(5)
N(1)–Cd(1)–N(11)	90.06(6)
N(1)–Cd(1)–N(11A)	89.94(6)
N(1)–Cd(1)–S(1B)	86.66(4)
N(1A)–Cd(1)–S(1B)	93.34(4)
N(11)–Cd(1)–S(1B)	93.19(4)
N(11)–Cd(1)–S(1C)	86.81(4)

The cadmium cations are μ-1,3 bridged via the thiocyanato anions into chains which elongate the crystallographic *a* axis. The Cd···Cd intrachain distance amounts to 5.7902(2) Å whereas the shortest interchain Cd···Cd distance amounts to 8.8051(3) Å. This structural motif is frequently observed in thiocyanato coordination polymers.[43] It must be noted that a similar topology is found in the related azide compounds of composition $[M(N_3)_2(3\text{-Acpy})_2]_n$ (M = Mn, Cd).[44–45] In contrast to **1B**, in the Cd azide compound the metal atoms are linked by pairs of μ-1,1 bridging anionic ligands, whereas in the manganese compound the metal centers are connected via pairs of alternating μ-1,1 and μ-1,3 bridging anionic ligands.

The most ligand-deficient 1:1 compound $[Cd(NCS)_2(3\text{-Acpy})]_n$ (**1C**) crystallizes in the monoclinic non-centrosymmetric space group *Pc* with two formula units in the unit cell. The asymmetric unit consists of one cadmium cation, two thiocyanato anions and one 3-Acpy ligand all of them located in general positions. The metal cations are coordinated by three nitrogen atoms of two μ-1,3 bridging thiocyanato anions and one μ-1,5 bridging 3-Acpy ligand, two sulfur atoms of two adjacent μ-1,3 bridging thiocyanato anions as well as one oxygen atom of one μ-1,5 bridging 3-Acpy ligand all in mutually *trans* orientation within a slightly distorted octahedral geometry (Figure 3).

The metal–nitrogen distances range between 2.288(4) and 2.349(4) Å and the angles around the metal cations range between 88.10(14) and 174.81(7) ° (Table 5). The metal cations are connected via μ-1,3 bridging thiocyanato anions into layers, that are located in the *bc* plane (Figure 4: top). These layers consist of 16-membered M-NCS rings, in which each metal cation is only linked by one single anionic ligand.

The layers are connected by μ-1,5 bridging 3-Acpy ligands into a three-dimensional network. Interestingly, all oxygen atoms of the acetyl substituent point in the direction of the *a* axis, which clearly shows the non-centrosymmetric arrangement of the building blocks (Figure 4: bottom).

It must be noted that a similar coordination topology was never observed before in a metal thiocyanato coordination polymer. However, a few examples of 12-membered respectively 16-membered M–NCS (M = Cd, Mn) rings can be found in the Cambridge Structural Database, but obviously exhibit a different coordination topology.[46–48] It must also be mentioned that a compound with a 24-membered Cd-NCS-membered rings was reported recently.[49]

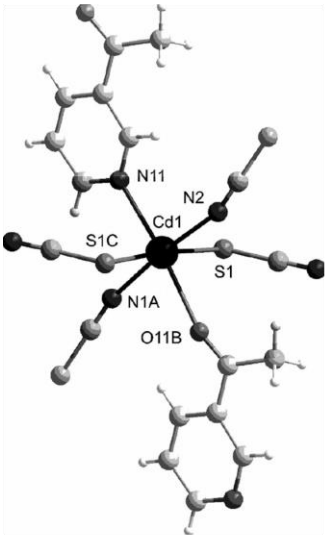

Figure 3. Molecular structure of compound **1C** with atom labeling. Symmetry transformations used to generate equivalent atoms: A: *x*, –*y*+1, *z*–1/2; B: *x*–1, *y*, *z*–1; C: *x*, –*y*, *z*–1/2. (an ORTEP plot of **1C** is shown in Figure S8 in the Supporting Information).

Table 5. Selected bond lengths / and angles /deg for **1C**. Symmetry codes: A: *x*, –*y*+1, *z*–1/2; B: *x*–1, *y*, *z*–1; C: *x*, –*y*, *z*–1/2.

Cd(1)–N(1A)	2.288(4)
Cd(1)–N(2)	2.299(4)
Cd(1)–N(11)	2.349(4)
Cd(1)–O(11B)	2.474(4)
Cd(1)–S(**1**)	2.6621(16)
Cd(1)–S(2C)	2.6870(17)
N(1A)–Cd(1)–N(2)	174.60(19)
N(1A)–Cd(1)–N(11)	90.92(14)
N(1A)–Cd(1)–O(11B)	85.67(15)
N(1A)–Cd(1)–S(1)	93.68(13)
S(1)–Cd(**1**)–S(2C)	174.81(7)
N(2)–Cd(1)–N(11)	94.17(15)
N(2)–Cd(1)–O(11B)	89.39(15)
N(2)–Cd(1)–S(1)	88.10(14)
N(2)–Cd(1)–S(2C)	91.71(13)

The ligand-deficient 1:2 compound $[Zn(NCS)_2(3\text{-Acpy})_2]$ (**2A**) crystallizes in the monoclinic centrosymmetric space group *C*2/*c* with four formula units in the unit cell. The asymmetric unit consists of one metal cation situated on a twofold rotation axis as well as one thiocyanato anion and one 3-Acpy co-ligand in general positions (Figure 5). The metal cations are coordinated by four nitrogen atoms of two terminal N-bonded thiocyanato anions and two terminal bonded 3-Acpy co-ligands in a slightly distorted tetrahedron (Figure 5). The metal-nitrogen distances are 1.9349(18) and 2.0421(16) and the angles around the metal cations range between 104.00(7) and 123.56(12) ° (Table 6).

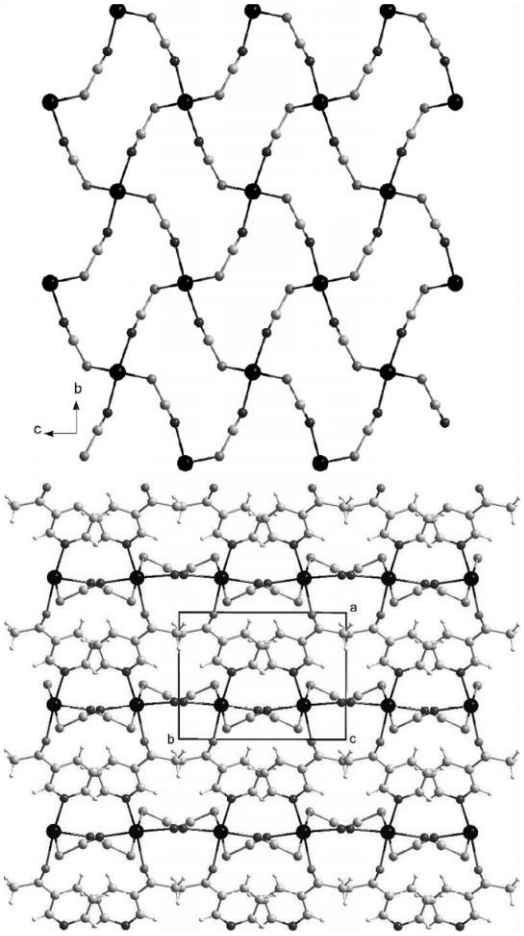

Figure 4. Crystal structure of compound **1C** with view of the layers along the *a* axis (top) and of the three-dimensional coordination network in the direction of the crystallographic *c* axis (bottom) (an ORTEP plot of **1C** is shown in Figure S5 in the Supporting Information).

Thermoanalytical Investigations

In order to prove if ligand-deficient compounds are also accessible by thermal decomposition, the ligand-rich 1:4 compound $[Cd(NCS)_2(3\text{-Acpy})_4]$ (**1A**) and the 1:2 compound $[Zn(NCS)_2(3\text{-Acpy})_2]$ (**2A**) were investigated for their thermal degradation behavior. On heating compound **1A** two mass steps are observed in the TG curve, which are accompanied with endothermic events in the DTA curve at 99 °C, 136 °C and 159 °C (Figure 6). The DTG curve for **1A** shows that the first mass step is well resolved whereas the second mass step is poorly resolved. The experimental mass loss in the first step of 35.6% is in good agreement with that calculated for the removal of two molecules 3-Acpy ($\Delta m_{calc.} = -34.0\,\%$) and giving evidence for the formation of a ligand-deficient compound of composition $[Cd(NCS)_2(3\text{-Acpy})_2]_n$ (Figure 6). The experimental mass loss in the second step of 27.6% is much lower

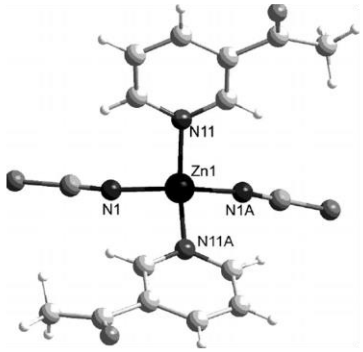

Figure 5. Molecular structure of compound **2A** with atom labeling. Symmetry transformations used to generate equivalent atoms: A: $-x+1$, y, $-z+1/2$. (an ORTEP plot of **2A** is shown in Figure S9 in the Supporting Information).

Table 6. Selected bond lengths / and angles /deg for **2A**. Symmetry code: A: $-x+1$, y, $-z+1/2$.

Zn(1)–N(1)	1.9349(18)
Zn(1)–N(11)	2.0421(16)
N(1)–Zn(1)–N(11)	104.00(7)
N(1)–Zn(1)–N(11A)	107.15(7)
N(1)–Zn(1)–N(1A)	123.56(12)
N(11)–Zn(1)–N(11A)	110.83(9)

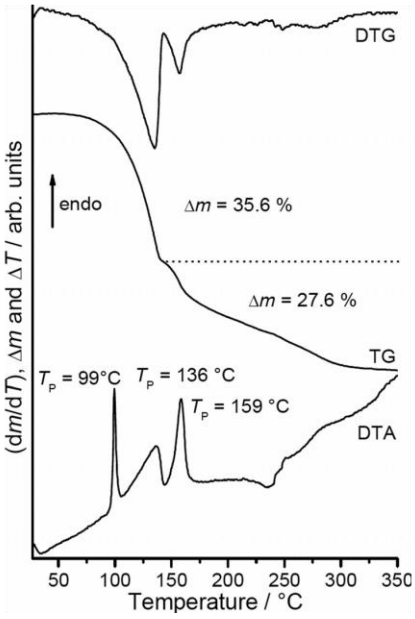

Figure 6. DTG, TG and DTA curves for compound **1A**. Heating rate = 1 $K \cdot min^{-1}$; given are the mass change /% and the peak temperature T_P /°C.

than expected for the removal of the remaining 3-Acpy ligands.

In order to verify the nature of the intermediate formed, additional TG measurements were performed and stopped after the first mass step. Elemental analysis of the residue obtained support the assumption of the formation of a ligand-deficient 1:2 compound of composition $[Cd(NCS)_2(3\text{-Acpy})_2]$ and XRPD investigations of this residue clearly prove that compound **1B** has formed in this reaction (Figure 7).

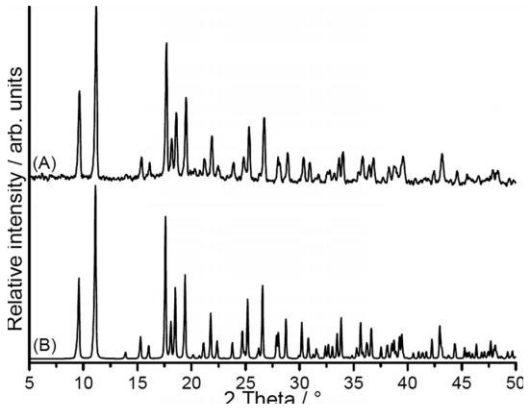

Figure 7. Experimental XRPD pattern of the residue obtained after the first mass step in thermal decomposition of compound **1A** (A), together with calculated XRPD for compound **1B** (B).

For compound **2A** two poor resolved mass steps are observed, which are accompanied with endothermic events in the DTA curve. The experimental mass loss is not in reasonable agreement for the loss of one or two 3-Acpy co-ligands and the overall reaction must be more complicated (Figure S10 in the Supporting Information).

Conclusions

In this contribution we investigated Zn^{II} and Cd^{II} thiocyanato coordination polymers based on 3-acetylpyridine as neutral N-donor co-ligand for their crystal structures and their thermal degradation behavior. Investigations using different ratios of the corresponding metal salts and the neutral N-donor co-ligand 3-Acpy resulted in the formation of two new coordination compounds of composition $[Cd(NCS)_2(3\text{-Acpy})_4]$ (**1A**) and $[Zn(NCS)_2(3\text{-Acpy})_2]$ (**2A**). If the 1:4 Cd^{II} compound **1A** is thermally decomposed, a ligand-deficient intermediate of composition $[Cd(NCS)_2(3\text{-Acpy})_2]_n$ (**1B**) can be isolated after the first mass step, which decomposed on heating. Moreover, from our synthetic work a further compound of composition $[Cd(NCS)_2(3\text{-Acpy})]_n$ (**1C**) was detected. In its crystal structure a 3D coordination network is found, which has never been observed before in such thiocyanato coordination polymers. Summarizing, we have shown that, with cadmium as counter cation, coordination polymers with μ-1,3-bridging thiocyanato anions can be easily prepared in solution, which for the paramagnetic metals manganese, iron, cobalt and nickel is frequently difficult to achieve.

Experimental Section

Synthesis: $ZnSO_4 \cdot H_2O$ and $CdSO_4 \cdot 8/3H_2O$ were obtained from Merck, $Ba(NCS)_2 \cdot 3H_2O$ and 3-acetylpyridine were obtained from Alfa Aesar. Solvents were used without further purification. Crystalline powders of compounds **1A–2B** were prepared by stirring the reactants in appropriate solvents at room temperature. The residues were filtered off and washed with mother liquor and dried in air. The purity of all compounds was checked by X-ray powder diffraction and elemental analysis (Figures S11–14 in the Supporting Information).

$Cd(NCS)_2$: $Ba(NCS)_2 \cdot 3H_2O$ (3.076 g, 10 mmol) and $CdSO_4 \cdot 8/3H_2O$ (2.566 g, 10 mmol) were stirred in water (100 mL). The white precipitate of $BaSO_4$ was filtered off and the water was removed from the filtrate by heating. The final product was dried by 80 °C. The homogeneity of the product was investigated by Xray powder diffraction and elemental analysis.

$Zn(NCS)_2$: $Ba(NCS)_2 \cdot 3H_2O$ (3.076 g, 10 mmol) and $ZnSO_4 \cdot H_2O$ (1.795 g, 10 mmol) were stirred in water (100 mL). The white precipitate of $BaSO_4$ was filtered off and the water was removed from the filtrate by heating. The final product was dried by 80 °C. The homogeneity of the product was investigated by Xray powder diffraction and elemental analysis.

Synthesis of Compound 1A: $Cd(NCS)_2$ (57.1 mg, 0.25 mmol) and 3-acetylpyridine (163.7 mg, 1.50 mmol) were stirred in water (1.5 mL) for 3 d. Yield: 88.7 %. Single crystals suitable for single crystal X-ray diffraction were prepared by slow evaporation of the filtrate. $C_{30}H_{28}N_6O_4S_2Cd$ (713.12): calcd. C 50.53, H 3.96, N 11.78, S 8.99; found C 49.96, H 3.96, N 11.45, S 8.42 %.

Synthesis of Compound 1B: $Cd(NCS)_2$ (57.1 mg, 0.25 mmol) and 3-acetylpyridine (54.6 mg, 0.50 mmol) were stirred in water (1.5 mL) for 3 d. Yield: 90.2 %. Single crystals suitable for single crystal X-ray diffraction were prepared by slow evaporation of the filtrate. $C_{16}H_{14}N_4O_2S_2Cd$ (470.84): calcd. C 40.82, H 3.00, N 11.90; S 13.62, found C 40.84, H 2.82, N 11.98, S 13.38 %.

Synthesis of Compound 1C: $Cd(NCS)_2$ (228.6 mg, 1.00 mmol) and 3-acetylpyridine (27.3 mg, 0.25 mmol) were stirred in water (1.5 mL) for 3 d. Yield: 87.6 %. Single crystals suitable for single crystal X-ray diffraction were prepared by the same method but without stirring. After 3 d, colorless well-shaped single crystals were obtained. $C_9H_7N_3OS_2Cd$ (349.71): calcd. C 30.91, H 2.02, N 12.02, S 18.34; found C 30.62, H 1.67, N 11.74, S 18.10 %.

Synthesis of Compound 2A: $Zn(NCS)_2$ (45.4 mg, 0.25 mmol), and 3-acetylpyridine (272.9 mg, 2.50 mmol) were stirred in water (1.5 mL) for 3 d. Yield: 85.2 %. Single crystals suitable for single crystal X-ray diffraction were prepared by slow evaporation of the filtrate. $C_{16}H_{14}N_4O_2S_2Zn$ (349.71): calcd. C 45.34, H 3.33, N 13.22, S 15.13; found C 44.72, H 3.13, N 13.22, S 14.08 %.

Elemental Analysis: CHNS analysis was performed using an EURO EA elemental analyzer, fabricated by EURO VECTOR Instruments and Software.

Elemental Analysis of the Residue Obtained in the Thermal Decomposition: Isolated in the first heating step (see thermoanalytical investigations) of compound **1A**. Calculated for the ligand-deficient compound **1B**: $C_{16}H_{14}N_4O_2S_2Cd$ (470.84): calcd. C 40.82, H 3.00, N 11.90; S 13.62, found C 40.78, H 2.92, N 11.86, S 13.42 %.

Differential Thermal Analysis and Thermogravimetry: The DTA-TG measurements were performed in a dynamic nitrogen atmosphere (purity: 5.0) in Al_2O_3 crucibles using a STA-409CD thermobalance from Netzsch. All measurements were performed with a flow rate of 75 $mL \cdot min^{-1}$ and were corrected for buoyancy and current effects. The instrument was calibrated using standard reference materials.

Single-Crystal Structure Analysis: The investigations were performed with the imaging plate diffraction system (IPDS-1 for **1A**, **2A** and IPDS-2 for **1B**, **1C**) with Mo-K_α-radiation from STOE & CIE. The structure solution was performed with direct methods using SHELXS-97,[50] and structure refinements were performed against F^2 using SHELXL-97.[50] All non-hydrogen atoms were refined with anisotropic displacement parameters. The hydrogen atoms were positioned with idealized geometry and were refined with fixed isotropic displacement parameters [$U_{iso}(H) = 1.2 \cdot U_{eq}(C_{aromatic})$ and $U_{iso}(H) = 1.5 \cdot U_{eq}(C_{aliphatic})$] using a riding model. For compound **1B** the oxygen atom of the acetyl group is disordered over two sites with occupancies of 60 and 40 % and was refined using a split model. The crystal of compound **1C** is racemically twinned and therefore, a twin refinement was performed (BASF parameter: 0.52 (4)). The structure can also be refined in the centrosymmetric space group $P2_1/c$ but in this case the 3-acetylpyridine ligand is disordered around a center of inversion, which clearly shows that space group Pc is correct.

Moreover, inspection of the crystal packing clearly shows that no center of inversion can be present. Details of the structure determination are given in Table 7.

CCDC-866924 (**1A**), CCDC- -866923 (**1B**), CCDC- -866922 (**1C**) and CCDC-866925 (**2A**) contain the supplementary crystallographic data for this paper. These data can be obtained free of charge from the Cambridge Crystallographic Data Centre via http://www.ccdc.cam.ac.uk/.

X-ray Powder Diffraction (XRPD): XRPD experiments were performed using a STOE Transmission Powder Diffraction System (STADI P) with Cu-K_α-radiation (λ = 1.5406) that is equipped with a linear position-sensitive detector ($\Delta 2\theta$ = 6.5–7° simultaneous; scan range overall = 2–130°) from STOE & CIE and an Image Plate Detector (scan range overall = 0–127°).

Spectroscopy: IR spectra were recorded with an Alpha IR spectrometer from Bruker equipped with a Platinum ATR QuickSnap™ sampling module between 4000–375 cm^{-1}.

Supporting Information (see footnote on the first page of this article): Calculated XRPD patterns, IR spectra and ORTEP plots of compounds **1A–1C** and **2A**. DTG, TG and DTA curves for **2A**. Experimental and calculated XRPD patterns for compounds **1A–1C** and **2A**.

Acknowledgment

This project was supported by the *Deutsche Forschungsgemeinschaft* (Project No. NA 720/3–1) and the *State of Schleswig-Holstein*. We thank *Professor Dr. Wolfgang Bensch* for access to his experimental facility. Special thanks to *Inke Jeß* for the single crystal measurements.

Zeitschrift für anorganische und allgemeine Chemie ZAAC Journal of Inorganic and General Chemistry

Table 7. Selected crystal data and details on the structure determinations for the compounds **1A–1C** and **2A**.

compound	**1A**	**1B**	**1C**	**2A**
formula	$C_{30}H_{28}CdN_6O_4S_2$	$C_{16}H_{14}CdN_4O_2S_2$	$C_9H_7CdN_3OS_2$	$C_{16}H_{14}N_4O_2S_2Zn$
MW /g·mol^{-1}	713.10	470.83	349.70	423.80
crystal system	triclinic	monoclinic	monoclinic	monoclinic
space group	$P\bar{1}$	$P2_1/c$	Pc	$C2/c$
a /	11.0640(9)	5.7902(2)	7.9268(5)	22.3035(19)
b /	11.5262(9)	18.3942(7)	9.8740(5)	4.9288(2)
c /	13.8111(12)	8.8051(3)	7.8131(5)	18.6395(15)
α /°	68.997(9)	90.00	90.000	90.000
β /°	74.361(10)	93.154(3)°.	108.318(5)	118.839(9)
γ /°	78.915(10)	90.000	90.000	90.000
V / ^{3}	1574.4(2)	936.38(6)	580.54(6)	1794.9(2)
T /K	200	293	293	180
Z	2	2	2	4
D_{calc} /g·cm^{-3}	1.504	1.670	2.001	1.568
μ /mm^{-1}	0.871	1.405	2.220	1.618
θ_{max} /deg	28.00	29.20	29.18	28.12
measured refl.	13982	17690	9575	7712
R_{int}	0.0450	0.0343	0.0268	0.0434
unique reflns.	7387	2517	2905	2157
refl.[$F_0 > 4\sigma(F_0)$]	6111	2156	2564	1695
parameters	396	126	147	115
R_1 [$F_0 > 4\sigma(F_0)$]	0.0405	0.0229	0.0220	0.0312
wR_2 [all data]	0.1146	0.0525	0.0427	0.0841
GOF	1.026	1.078	1.066	1.027
$\Delta\rho_{max/min}$/e· $^{-3}$	1.189/–1.836	0.427/–0.453	0.442/–0.400	0.401/–0.416

References

[1] D. Braga, L. Maini, M. Polito, L. Scaccianoce, G. Cojazzi, F. Grepioni, *Coord. Chem. Rev.* **2001**, *216*, 225–248.
[2] S. L. James, *Chem. Soc. Rev.* **2003**, *32*, 276–288.
[3] C. Janiak, *Dalton Trans.* **2003**, 2781–2804.
[4] D. Maspoch, D. Ruiz-Molina, J. Veciana, *J. Mater. Chem.* **2004**, *14*, 2713–2723.
[5] D. Maspoch, D. Ruiz-Molina, J. Veciana, *Chem. Soc. Rev.* **2007**, *36*, 770–818.
[6] D. Gatteschi, R. Sessoli, *Angew. Chem. Int. Ed.* **2003**, *42*, 268–297.
[7] X.-Y. Wang, Z.-M. Wang, S. Gao, *Chem. Commun.* **2008**, 281–294.
[8] S. R. Batten, K. S. Murray, *Coord. Chem. Rev.* **2003**, *246*, 103–130.
[9] L. Bogani, A. Vindigni, R. Sessoli, D. Gatteschi, *J. Mater. Chem.* **2008**, *18*, 4750–4758.
[10] H. L. Sun, Z. M. Wang, S. Gao, *Coord. Chem. Rev.* **2010**, *254*, 1081–1100.
[11] W. X. Zhang, W. Xue, J. B. Lin, Y. Z. Zheng, X. M. Chen, *CrystEngComm* **2008**, *10*, 1770–1776.
[12] B. Gil-Hern ndez, P. Gili, J. K. Vieth, C. Janiak, J. N. Sanchiz, *Inorg. Chem.* **2010**, *49*, 7478–7490.
[13] H. A. Habib, J. Sanchiz, C. Janiak, *Dalton Trans.* **2008**, 4877–4884.
[14] H. A. Habib, J. Sanchiz, C. Janiak, *Dalton Trans.* **2008**, 1734–1744.
[15] S. Gerber, H. Gr ger, J. Ensling, P. G tlich, H. Krautscheid, *Angew. Chem. Int. Ed.* **2005**, *44*, 7787–7790.
[16] J. Tercero, C. Diaz, J. Ribas, J. Mahia, M. Maestro, X. Solans, *J. Chem. Soc., Dalton Trans.* **2002**, 2040–2046.
[17] R. Vicente, A. Escuer, J. Ribas, X. Solans, M. Font-Bardia, *Inorg. Chem.* **1993**, *32*, 6117–6118.
[18] M. A. Porai-Koshits, G. N. Tishchenko, *Crystallogr. Rep.* **1960**, *4*, 239.
[19] H. Cai, Y. Guo, Y. Li, J.-G. Li, *Acta Crystallogr., Sect. A* **2007**, *63*, m936–m938.
[20] Y. Jin, Y.-X. Che, J.-M. Zheng, *J. Coord. Chem.* **2007**, *60*, 2067–2074.
[21] R. Sekiya, S.-i. Nishikiori, *CrystEngComm* **2011**, *13*, 6405–6414.
[22] J. M. Shi, J. N. Chen, C. J. Wu, J. P. Ma, *J. Coord. Chem.* **2007**, *60*, 2009–2013.
[23] D. Vujovic, H. G. Raubenheimer, L. R. Nassimbeni, *Dalton Trans.* **2003**, 631–637.
[24] C. N ther, J. Greve, *J. Solid State Chem.* **2003**, *176*, 259–265.
[25] M. Wriedt, I. Jeß, C. N ther, *Eur. J. Inorg. Chem.* **2009**, 1406–1413.
[26] M. Wriedt, C. N ther, *Dalton Trans.* **2009**, 10192–10198.
[27] M. Wriedt, C. N ther, *Eur. J. Inorg. Chem.* **2010**, 3201–3211.
[28] M. Wriedt, C. N ther, *Chem. Commun.* **2010**, *46*, 4707–4709.
[29] M. Wriedt, S. Sellmer, C. N ther, *Inorg. Chem.* **2009**, *48*, 6896–6903.
[30] J. Boeckmann, C. N ther, *Dalton Trans.* **2010**, *39*, 11019–11026.
[31] J. Boeckmann, C. N ther, *Chem. Commun.* **2011**, *47*, 7104–7106.
[32] J. Boeckmann, M. Wriedt, C. N ther, *Chem. Eur. J.* **2012**, *18*, 5284–5289.
[33] S. W hlert, J. Boeckmann, M. Wriedt, C. N ther, *Angew. Chem. Int. Ed.* **2011**, *50*, 6920–6923.
[34] S. W hlert, C. N ther, *Cryst. Growth Des.* **2012**, in press.
[35] R. A. Bailey, S. L. Kozak, T. W. Michelsen, W. N. Mills, *Coord. Chem. Rev.* **1971**, *6*, 407–445.
[36] R. J. H. Clark, C. S. Williams, *Spectrochim. Acta* **1966**, *22*, 1081–1090.
[37] P. O. Kinell, B. Strandberg, *Acta Chem. Scand.* **1959**, *13*, 1607–1622.
[38] L. Shen, Y.-Z. Xu, *J. Chem. Soc., Dalton Trans.* **2001**, 3414–3414.
[39] I. Jeß, J. Boeckmann, C. N ther, *Dalton Trans.* **2012**, *41*, 228–236.
[40] J. Boeckmann, I. Jeß, T. Reinert, C. N ther, *Eur. J. Inorg. Chem.* **2011**, 5502–5511.
[41] S. W hlert, J. Boeckmann, I. Jess, C. N ther, *Cryst. Eng. Comm.* **2012**, *accepted*.
[42] F. Allen, *Acta Crystallogr., Sect. B* **2002**, *58*, 380–388.
[43] S. Banerjee, B. Wu, P.-G. Lassahn, C. Janiak, A. Ghosh, *Inorg. Chim. Acta* **2005**, *358*, 535–544.
[44] A. Escuer, R. Vicente, M. A. S. Goher, F. A. Mautner, *Inorg. Chem.* **1997**, *36*, 3440–3446.

[45] M. A. S. Goher, F. A. Mautner, K. Gatterer, M. A. M. Abu-Youssef, A. M. A. Badr, B. Sodin, C. Gspan, *J. Mol. Struct.* **2008**, *876*, 199–205.
[46] J. N. McElearney, L. L. Balagot, J. A. Muir, R. D. Spence, *Phys. Rev. B* **1979**, *19*, 306–317.
[47] A. Ouchi, M. Taniguchi, *Bull. Chem. Soc. Jpn.* **1988**, *61*, 3347–3349.
[48] H.-L. Sun, B.-Q. Ma, S. Gao, S. R. Batten, *Cryst. Growth Des.* **2006**, *6*, 1261–1263.
[49] A. Tahli, J. K. Maclaren, I. Boldog, C. Janiak, *Inorg. Chim. Acta* **2011**, *374*, 506–513.
[50] G. M. Sheldrick, *Acta Crystallogr., Sect. A* **2008**, *64*, 112–122.

Received: June 08, 2012
Published Online: September 7, 2012

5.2. *Catena*-Poly[[bis(3-acetylpyridine-κ*N*)-cadmium]-di-μ-selenocyanato-$\kappa^2 N$:*Se*;$\kappa^2 Se$:*N*]

Julia Werner, Jan Boeckmann, Inke Jess und Christian Näther, *Acta Crystallogr. E* **2012**, *E68*, m704.

DOI: 10.1107/S1600536812018375

Motivation

Diese Verbindung wurde im Rahmen systematischer Untersuchungen von $Cd(NCSe)_2$ und 3-Acetylpyridin erhalten. Diese Verbindung konnte jedoch nicht zur Strukturaufklärung von entsprechenden paramagnetischen Verbindungen genutzt werden und wurde somit als Strukturmitteilung veröffentlicht.

metal-organic compounds

Acta Crystallographica Section E
Structure Reports Online
ISSN 1600-5368

catena-Poly[[bis(3-acetylpyridine-κN)-cadmium]-di-μ-selenocyanato-$\kappa^2 N$:Se;κ^2Se:N]

Julia Werner,* Jan Boeckmann, Inke Jess and Christian Näther

Institut für Anorganische Chemie, Christian-Albrechts-Universität Kiel, Max-Eyth-Strasse 2, 24118 Kiel, Germany
Correspondence e-mail: jwerner@ac.uni-kiel.de

Received 23 April 2012; accepted 24 April 2012

Key indicators: single-crystal X-ray study; T = 293 K; mean σ(C–C) = 0.005 Å; R factor = 0.031; wR factor = 0.061; data-to-parameter ratio = 21.0.

In the crystal structure of the title compound, $[Cd(NCSe)_2(C_7H_7NO)_2]_n$, the Cd^{2+} cation is coordinated by two 3-acetylpyridine ligands and four μ-1,3-bridging selenocyanate anions within a slightly distorted CdN_4Se_2 octahedron. The asymmetric units consists of one Cd^{2+} cation, which is situated on a center of inversion, as well as one selenocyanate anion and one 3-acetylpyridine ligand in general positions. The metal cations are μ-1,3-bridged *via* the selenocyanate anions into chains along the *a* axis.

Related literature

For general background information including details on thermal decomposition reactions and magnetic properties of the precursor and μ-1,3 bridging compounds, see: Näther & Greve (2003); Boeckmann & Näther (2010, 2011); Wöhlert *et al.* (2011). For a description of the Cambridge Structural Database, see: Allen (2002).

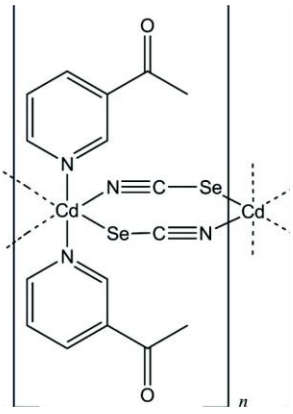

Experimental

Crystal data

$[Cd(NCSe)_2(C_7H_7NO)_2]$
M_r = 564.63
Monoclinic, $P2_1/c$
a = 5.9447 (3) Å
b = 18.7233 (10) Å
c = 8.7548 (5) Å
β = 94.020 (4)°
V = 972.05 (9) Å^3
Z = 2
Mo $K\alpha$ radiation
μ = 4.88 mm^{-1}
T = 293 K
0.16 × 0.07 × 0.02 mm

Data collection

Stoe IPDS-2 diffractometer
Absorption correction: numerical (*X-SHAPE* and *X-RED32*; Stoe & Cie, 2008)
T_{min} = 0.667, T_{max} = 0.902
17180 measured reflections
2458 independent reflections
2256 reflections with $I > 2\sigma(I)$
R_{int} = 0.045

Refinement

$R[F^2 > 2\sigma(F^2)]$ = 0.031
$wR(F^2)$ = 0.061
S = 1.13
2458 reflections
117 parameters
H-atom parameters constrained
$\Delta\rho_{max}$ = 0.47 e Å^{-3}
$\Delta\rho_{min}$ = −0.47 e Å^{-3}

Data collection: *X-AREA* (Stoe & Cie, 2008); cell refinement: *X-AREA*; data reduction: *X-AREA*; program(s) used to solve structure: *SHELXS97* (Sheldrick, 2008); program(s) used to refine structure: *SHELXL97* (Sheldrick, 2008); molecular graphics: *XP* (Sheldrick, 2008) and *DIAMOND* (Brandenburg, 2011); software used to prepare material for publication: *publCIF* (Westrip, 2010).

We gratefully acknowledge financial support by the DFG (project No. NA 720/3–1) and the State of Schleswig–Holstein. We thank Professor Dr Wolfgang Bensch for access to his experimental facilities.

Supplementary data and figures for this paper are available from the IUCr electronic archives (Reference: BT5897).

References

Allen, F. H. (2002). *Acta Cryst.* B**58**, 380–388.
Boeckmann, J. & Näther, C. (2010). *Dalton Trans.* **39**, 11019-11026.
Boeckmann, J. & Näther, C. (2011). *Chem. Commun.* **47**, 7104–7106.
Brandenburg, K. (2011). *DIAMOND*. Crystal Impact GbR, Bonn, Germany.
Näther, C. & Greve, J. (2003). *J. Solid State Chem.*, **176**, 259–265.
Sheldrick, G. M. (2008). *Acta Cryst.* A**64**, 112–122.
Stoe & Cie (2008). *X-AREA*, *X-RED32* and *X-SHAPE*. Stoe & Cie, Darmstadt, Germany.
Westrip, S. P. (2010). *J. Appl. Cryst.* **43**, 920–925.
Wöhlert, S., Boeckmann, J., Wriedt, M. & Näther, C. (2011). *Angew. Chem. Int. Ed.* **50**, 6920-6923.

supplementary materials

Acta Cryst. (2012). E**68**, m704 [doi:10.1107/S1600536812018375]

catena-Poly[[bis(3-acetylpyridine-κN)cadmium]-di-μ-selenocyanato-κ^2N:*Se*;κ^2*Se*:*N*]

Julia Werner, Jan Boeckmann, Inke Jess and Christian Näther

Comment

The title compound was prepared within a project on the synthesis and the magnetic properties of paramagnetic transition metal thio- and selenocyanato coordination polymers in which the metal cations are μ-1,3 bridged by the anionic ligands (Näther & Greve, 2003, Boeckmann & Näther, 2010, 2011 and Wöhlert *et al.*, 2011). In this context, also the corresponding compounds based on diamagnetic cadmium are of interest, because they are structural analogs of the paramagnetic compounds. In the course of systematic investigations crystals of the title compound were prepared and characterized by single crystal X-ray diffraction.

In the crystal structure of the title compound, the cadmium(II) cations each are coordinated by two nitrogen atoms of two terminal *N*-bonded 3-acetylpyridine and two nitrogen and two selenium atoms of μ-1,3 bridging selenocyanato anions (Fig. 1). The coordination polyhedron of the Cd cations can be described as a slightly distorted octahedra with the Cd cation located on a centre of inversion.

The Cd^{2+} cations are μ-1,3 bridged by selenocyanato anions into chains, which elongate in the direction of the crystallographic *a* axis (Fig. 2). The Cd···Cd intrachain distance amounts to 5.9447 (3) Å and the shortest interchain Cd···Cd distance amounts to 8.7548 (5) Å. It must be noted that according to a search in the CCDC database (ConQuest Ver.1.14.2012) (Allen, 2002) coordination compounds based on metal selenocyanates and 3-acetylpyridine are unknown.

Experimental

Potassium selenocyanate and 3-acetylpyridine were purchased from Alfa Aesar, $Cd(NO_3)_2.4H_2O$ were obtained from Merck. The title compound was prepared by the reaction of 77.1 mg $Cd(NO_3)_2.4H_2O$ (0.25 mmol), 64.8 mg KSeCN (0.45 mmol) and 109 μ*L* 3-acetylpyridine (1.00 mmol) in 1.5 mL H_2O at RT in a closed 3 ml snap cap vial. After several days colourless needles of the title compound were obtained.

Refinement

H atoms were positioned with idealized geometry (methyl H atoms allowed to rotate but not to tip) and were refined isotropically with U_{iso}(H) = 1.2 U_{eq}(C) for aromatic H atoms (1.5 for methyl H atoms) using a riding model with C—H = 0.93 Å (aromatic) and with C—H = 0.96 Å (methyl).

Computing details

Data collection: *X-AREA* (Stoe & Cie, 2008); cell refinement: *X-AREA* (Stoe & Cie, 2008); data reduction: *X-AREA* (Stoe & Cie, 2008); program(s) used to solve structure: *SHELXS97* (Sheldrick, 2008); program(s) used to refine structure: *SHELXL97* (Sheldrick, 2008); molecular graphics: *XP* (Sheldrick, 2008) and *DIAMOND* (Brandenburg, 2011); software used to prepare material for publication: *publCIF* (Westrip, 2010).

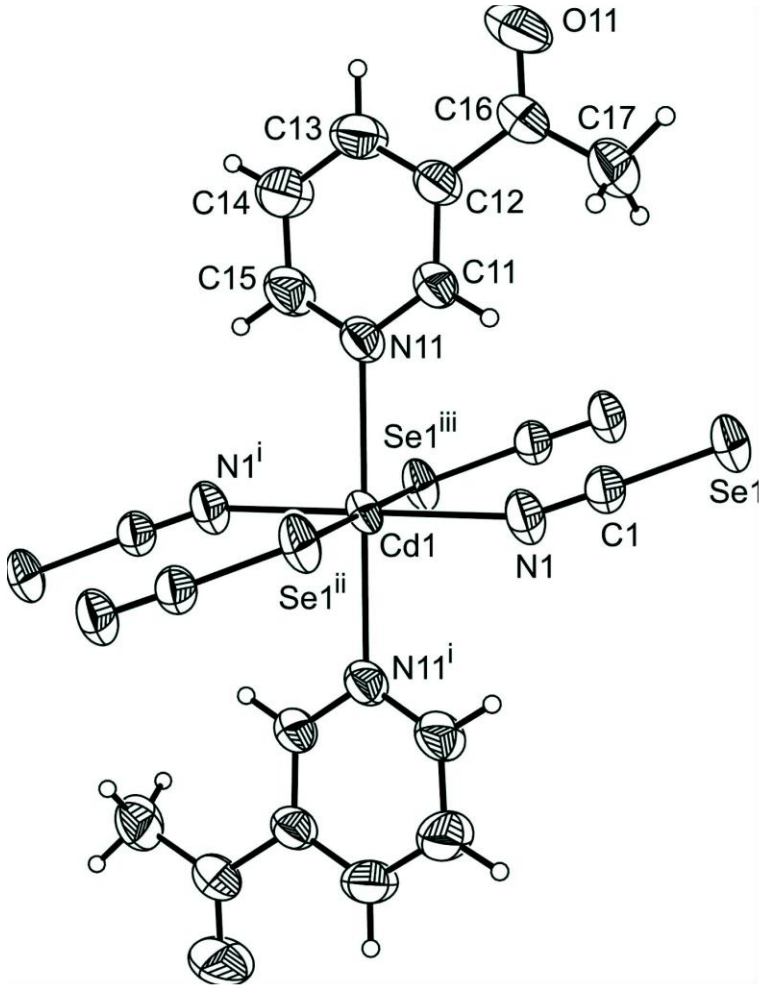

Figure 1

Crystal structure of the title compound with labelling and displacement ellipsoids drawn at the 50% probability level. Symmetry code: i = -x,-y+1,-z, ii = x-1, y, z, iii = -x+1, -y+1, -z

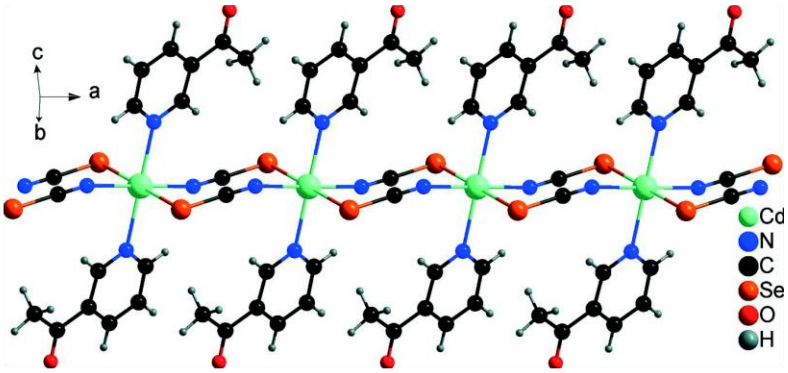

Figure 2

Crystal structure of the title compound with view of the chains that elongate in the direction of the crystallographic *a* axis.

catena-Poly[[bis(3-acetylpyridine-κN)cadmium]-di-μ- selenocyanato-κ²N:Se;κ²Se:N]

Crystal data

$[Cd(NCSe)_2(C_7H_7NO)_2]$	$F(000) = 540$
$M_r = 564.63$	$D_x = 1.929$ Mg m^{-3}
Monoclinic, $P2_1/c$	Mo $K\alpha$ radiation, $\lambda = 0.71073$ Å
Hall symbol: -P 2ybc	Cell parameters from 17180 reflections
$a = 5.9447$ (3) Å	$\theta = 2.2$–$28.6°$
$b = 18.7233$ (10) Å	$\mu = 4.88$ mm^{-1}
$c = 8.7548$ (5) Å	$T = 293$ K
$\beta = 94.020$ (4)°	Needle, colourless
$V = 972.05$ (9) Å^3	0.16 × 0.07 × 0.02 mm
$Z = 2$	

Data collection

Stoe IPDS-2 diffractometer	17180 measured reflections
Radiation source: fine-focus sealed tube	2458 independent reflections
Graphite monochromator	2256 reflections with $I > 2\sigma(I)$
ω scans	$R_{int} = 0.045$
Absorption correction: numerical (*X-SHAPE* and *X-RED32*; Stoe & Cie, 2008)	$\theta_{max} = 28.6°$, $\theta_{min} = 2.2°$
$T_{min} = 0.667$, $T_{max} = 0.902$	$h = -7 \rightarrow 7$
	$k = -25 \rightarrow 25$
	$l = -11 \rightarrow 11$

Refinement

Refinement on F^2	Secondary atom site location: difference Fourier map
Least-squares matrix: full	Hydrogen site location: inferred from neighbouring sites
$R[F^2 > 2\sigma(F^2)] = 0.031$	H-atom parameters constrained
$wR(F^2) = 0.061$	$w = 1/[\sigma^2(F_o^2) + (0.0164P)^2 + 1.1235P]$ where $P = (F_o^2 + 2F_c^2)/3$
$S = 1.13$	$(\Delta/\sigma)_{max} = 0.001$
2458 reflections	$\Delta\rho_{max} = 0.47$ e Å^{-3}
117 parameters	$\Delta\rho_{min} = -0.47$ e Å^{-3}
0 restraints	
Primary atom site location: structure-invariant direct methods	

Extinction correction: *SHELXL97* (Sheldrick, 2008), $Fc^*=kFc[1+0.001xFc^2\lambda^3/\sin(2\theta)]^{-1/4}$

Extinction coefficient: 0.0074 (5)

Special details

Geometry. All esds (except the esd in the dihedral angle between two l.s. planes) are estimated using the full covariance matrix. The cell esds are taken into account individually in the estimation of esds in distances, angles and torsion angles; correlations between esds in cell parameters are only used when they are defined by crystal symmetry. An approximate (isotropic) treatment of cell esds is used for estimating esds involving l.s. planes.

Refinement. Refinement of F^2 against ALL reflections. The weighted R-factor wR and goodness of fit S are based on F^2, conventional R-factors R are based on F, with F set to zero for negative F^2. The threshold expression of $F^2 > 2\text{sigma}(F^2)$ is used only for calculating R-factors(gt) etc. and is not relevant to the choice of reflections for refinement. R-factors based on F^2 are statistically about twice as large as those based on F, and R- factors based on ALL data will be even larger.

Fractional atomic coordinates and isotropic or equivalent isotropic displacement parameters (Å²)

	x	*y*	*z*	U_{iso}*/U_{eq}
Cd1	0.0000	0.5000	0.0000	0.03766 (9)
N1	0.3333 (4)	0.44388 (15)	0.0928 (3)	0.0478 (6)
C1	0.5139 (4)	0.43756 (15)	0.1480 (3)	0.0377 (6)
Se1	0.79466 (5)	0.429324 (18)	0.23721 (4)	0.04545 (11)
N11	0.0930 (4)	0.60142 (13)	0.1566 (3)	0.0422 (5)
O11	0.5790 (6)	0.72219 (18)	0.5227 (4)	0.1005 (13)
C11	0.2729 (5)	0.60423 (17)	0.2585 (3)	0.0430 (6)
H11	0.3604	0.5633	0.2736	0.052*
C12	0.3348 (5)	0.66449 (16)	0.3420 (4)	0.0442 (7)
C13	0.2032 (6)	0.72501 (18)	0.3206 (5)	0.0592 (9)
H13	0.2402	0.7666	0.3746	0.071*
C14	0.0168 (7)	0.72283 (19)	0.2183 (5)	0.0675 (11)
H14	−0.0757	0.7626	0.2034	0.081*
C15	−0.0302 (6)	0.66083 (17)	0.1387 (4)	0.0533 (8)
H15	−0.1548	0.6602	0.0683	0.064*
C16	0.5372 (6)	0.6672 (2)	0.4547 (4)	0.0570 (9)
C17	0.6815 (6)	0.6032 (2)	0.4794 (4)	0.0632 (10)
H17A	0.8070	0.6144	0.5503	0.095*
H17B	0.7360	0.5884	0.3837	0.095*
H17C	0.5951	0.5653	0.5202	0.095*

Atomic displacement parameters (Å²)

	U^{11}	U^{22}	U^{33}	U^{12}	U^{13}	U^{23}
Cd1	0.02405 (13)	0.04299 (16)	0.04447 (17)	−0.00160 (10)	−0.00794 (10)	−0.00268 (12)
N1	0.0285 (11)	0.0554 (15)	0.0583 (17)	0.0002 (10)	−0.0059 (11)	0.0068 (12)
C1	0.0305 (13)	0.0398 (14)	0.0425 (15)	0.0013 (10)	0.0002 (11)	0.0028 (11)
Se1	0.02761 (14)	0.0576 (2)	0.04962 (19)	0.00067 (12)	−0.00791 (11)	0.01084 (14)
N11	0.0365 (12)	0.0447 (13)	0.0439 (14)	−0.0023 (10)	−0.0074 (10)	0.0003 (10)
O11	0.088 (2)	0.082 (2)	0.123 (3)	0.0018 (18)	−0.053 (2)	−0.043 (2)
C11	0.0372 (14)	0.0447 (15)	0.0457 (16)	−0.0003 (12)	−0.0075 (12)	−0.0022 (12)
C12	0.0418 (15)	0.0442 (15)	0.0453 (16)	−0.0047 (12)	−0.0064 (12)	−0.0030 (12)
C13	0.067 (2)	0.0412 (17)	0.066 (2)	−0.0009 (15)	−0.0177 (18)	−0.0074 (15)
C14	0.074 (2)	0.0444 (18)	0.079 (3)	0.0125 (17)	−0.029 (2)	−0.0031 (17)
C15	0.0510 (18)	0.0498 (18)	0.056 (2)	−0.0003 (14)	−0.0182 (15)	0.0033 (14)

C16	0.0466 (18)	0.061 (2)	0.062 (2)	−0.0043 (15)	−0.0136 (15)	−0.0132 (16)
C17	0.0481 (19)	0.080 (3)	0.058 (2)	0.0041 (18)	−0.0163 (16)	−0.0063 (19)

Geometric parameters (Å, º)

Cd1—N1^{i}	2.337 (2)	C11—H11	0.9300
Cd1—N1	2.337 (2)	C12—C13	1.382 (5)
Cd1—N11	2.384 (2)	C12—C16	1.502 (4)
Cd1—N11^{i}	2.384 (2)	C13—C14	1.376 (5)
Cd1—Se1^{ii}	2.8124 (3)	C13—H13	0.9300
Cd1—Se1^{iii}	2.8124 (3)	C14—C15	1.373 (5)
N1—C1	1.152 (4)	C14—H14	0.9300
C1—Se1	1.799 (3)	C15—H15	0.9300
Se1—Cd1^{iv}	2.8124 (3)	C16—C17	1.481 (5)
N11—C15	1.335 (4)	C17—H17A	0.9600
N11—C11	1.345 (3)	C17—H17B	0.9600
O11—C16	1.206 (4)	C17—H17C	0.9600
C11—C12	1.380 (4)		
N1^{i}—Cd1—N1	180.00 (12)	C12—C11—H11	118.2
N1^{i}—Cd1—N11	89.92 (9)	C11—C12—C13	118.1 (3)
N1—Cd1—N11	90.08 (9)	C11—C12—C16	123.2 (3)
N1^{i}—Cd1—N11^{i}	90.08 (9)	C13—C12—C16	118.7 (3)
N1—Cd1—N11^{i}	89.92 (9)	C14—C13—C12	119.1 (3)
N11—Cd1—N11^{i}	180.0	C14—C13—H13	120.5
N1^{i}—Cd1—Se1^{ii}	86.16 (7)	C12—C13—H13	120.5
N1—Cd1—Se1^{ii}	93.84 (7)	C15—C14—C13	118.8 (3)
N11—Cd1—Se1^{ii}	87.41 (6)	C15—C14—H14	120.6
N11^{i}—Cd1—Se1^{ii}	92.59 (6)	C13—C14—H14	120.6
N1^{i}—Cd1—Se1^{iii}	93.84 (7)	N11—C15—C14	123.7 (3)
N1—Cd1—Se1^{iii}	86.16 (7)	N11—C15—H15	118.2
N11—Cd1—Se1^{iii}	92.59 (6)	C14—C15—H15	118.2
N11^{i}—Cd1—Se1^{iii}	87.41 (6)	O11—C16—C17	121.4 (3)
Se1^{ii}—Cd1—Se1^{iii}	180.0	O11—C16—C12	118.8 (3)
C1—N1—Cd1	159.1 (3)	C17—C16—C12	119.8 (3)
N1—C1—Se1	178.7 (3)	C16—C17—H17A	109.5
C1—Se1—Cd1^{iv}	94.39 (9)	C16—C17—H17B	109.5
C15—N11—C11	116.7 (3)	H17A—C17—H17B	109.5
C15—N11—Cd1	119.5 (2)	C16—C17—H17C	109.5
C11—N11—Cd1	123.7 (2)	H17A—C17—H17C	109.5
N11—C11—C12	123.6 (3)	H17B—C17—H17C	109.5
N11—C11—H11	118.2		

Symmetry codes: (i) −*x*, −*y*+1, −*z*; (ii) −*x*+1, −*y*+1, −*z*; (iii) *x*−1, *y*, *z*; (iv) *x*+1, *y*, *z*.

5.3. Synthesis, Crystal Structures and Polymorphism of New Cadmium and Zinc Thio- and Selenocyanato Coordination Compounds with 4-Acetylpyridine as N-Donor Ligand

Julia Werner, Inke Jess und Christian Näther, *Z. Naturforsch.* **2013**, *68b*, 643-652.

DOI: 10.5560/ZNB.2013-3046

Motivation

In der nachfolgenden Arbeit wird über die Synthesen von $Cd(NCS)_2$, $Cd(NCSe)_2$ und $Zn(NCS)_2$ mit dem Liganden 4-Acetylpyridin berichtet. Diese Synthesen dienten dazu Verbindungen herzustellen, welche ggf. isotyp zu ihren paramagnetischen Analoga kristallisieren. Es konnten unter anderem zwei Modifikationen der Zusammensetzung $[Cd(NCS)_2(4\text{-Acetylpyridin})_2]_n$ mit *trans* µ-1,3 verbrückenden Thiocyanatanionen erhalten werden, die zur Identifizierung analoger Manganverbindungen verwendet werden konnten (4.2).

Synthesis, Crystal Structures and Polymorphism of New Cadmium and Zinc Thio- and Selenocyanato Coordination Compounds with 4-Acetylpyridine as *N*-Donor Ligand

Julia Werner, Inke Jess and Christian Näther

Institut für Anorganische Chemie, Christian-Albrechts-Universität zu Kiel, Max-Eyth-Straße 2, 24118 Kiel, Germany

Reprint requests to Dr. Christian Näther. Fax: +49-431-8801520. E-mail: cnaether@ac.uni-kiel.de

Z. Naturforsch. **2013**, *68b*, 643 – 652 / DOI: 10.5560/ZNB.2013-3046
Received February 13, 2013

Dedicated to Professor Heinrich Nöth on the occasion of his 85th birthday

Reactions of cadmium(II) thio- and selenocyanate with 4-acetylpyridine in different molar ratios and in different solvents always lead to the formation of compounds of composition $Cd(NCS)_2$(4-acetylpyridine)$_2$ (**Cd1-I**) and $Cd(NCSe)_2$(4-acetylpyridine)$_2$ (**Cd2**). Both compounds are isotypic and crystallize in the monoclinic space group *C*2/*c*. In their crystal structures the Cd cations are coordinated by two *N*-bonded 4-acetylpyridine ligands as well as two *N*- and two *S*/*Se*-bonded thio- or selenocyanato anions within a slightly distorted octahedral geometry. The Cd cations are linked into chains by pairwise μ-1,3-coordinating thio- or selenocyanato anions. In one reaction single crystals of a second polymorphic modification of composition $Cd(NCS)_2$(4-acetylpyridine)$_2$ (**Cd1-II**) were obtained by accident. This modification crystallizes monoclinically in space group $P2_1/c$, exhibits the same topology of the coordination network as in **Cd1-I** and **Cd2** but a different arrangement of the chains in the crystal. Similar investigations with Zn(II) have revealed that only one compound of composition $Zn(NCS)_2$(4-acetylpyridine)$_2$ can be prepared that crystallizes in the triclinic space group $P\bar{1}$. Its structure consists of discrete complexes in which the Zn(II) cations are tetrahedrally coordinated. A corresponding selenocyanato coordination compound could not be prepared.

Key words: Synthesis, Thio- and Selenocyanato Coordination Compounds, Crystal Structures, Thermoanalytical Measurements

Introduction

Investigations on the synthesis, structures and properties of new coordination polymers are still an active field of chemical research [1 – 7]. In this context compounds that show cooperative magnetic properties are of importance, which can be prepared if paramagnetic transition metal cations are linked by, *e. g.*, small-sized anionic ligands that can mediate magnetic exchange interactions [8 – 12]. Consequently, a large number of such compounds were prepared in recent years based on oxalates, azides, formates and other ligands, and some selected examples are given in the reference list [13 – 19]. In contrast, transition metal thio- and selenocyanates in which the metal cations are linked by the anionic ligands are less well known, and most of the reported compounds have structures in which the anions are only terminally *N*-bonded [20 – 28]. This might be traced back to the fact that hard metal cations like *e. g.* Mn, Fe, Co and Ni are less chalcophilic and therefore, the synthesis of compounds with μ-1,3-bridging thio- or selenocyanato anions is sometimes difficult to achieve.

To overcome this problem we have established an alternative procedure in which coordination compounds with *N*-terminally bonded thio- and selenocyanato anions and additional neutral *N*-donor co-ligands are thermally decomposed leading to the formation of new coordination polymers in which the cations are octahedrally coordinated and linked by μ-1,3-bridging anions [29 – 31]. Within this project we have prepared several compounds that show different magnetic properties including single-chain magnetic behavior [32 – 39]. Unfortunately, on thermal decomposition only microcrystalline compounds are obtained that are not suitable for single-crystal structure determination. However, in some cases this problem can be solved if similar compounds based on the more chal-

cophilic cadmium(II) are prepared, which can easily be crystallized, and for which several compounds are reported in which the Cd cations are linked into different coordination networks by the thio- and selenocyanato anions [40–44]. In several cases these compounds are isotypic to the paramagnetic analogs and therefore, the latter can be identified by powder X-ray diffraction. In this context it should be noted that on thermal decomposition of Co compounds sometimes tetrahedrally coordinated intermediates are observed that can be identified with a similar procedure using the corresponding Zn(II) compounds as structural analogs because this diamagnetic metal cation frequently favors a tetrahedral coordination [45–49]. This is the reason why we have started systematic investigations on the synthesis, the structures and the properties of thio- and selenocyanato coordination compounds based on Cd(II) and Zn(II) [43, 50–52].

In the course of our project we also tried to prepare paramagnetic coordination polymers based on the monodentate ligand 4-acetylpyridine. Unfortunately, on thermal decomposition of compounds of composition $M(NCS)_2$(4-acetylpyridine)$_4$ (M = Mn, Fe, Co, Ni) several different crystalline phases of composition $M(NCS)_2$(4-acetylpyridine)$_2$ are obtained that so far could not be identified. These investigations have also shown that different polymorphic modifications or isomers might be formed on thermal decomposition, as also reported in the literature [53–60]. In order to check if compounds can be obtained that might be isotypic to the paramagnetic analogs we prepared coordination compounds based on $Cd(NCS)_2$ and $Zn(NCS)_2$ using 4-acetylpyridine as a co-ligand. Here we report on our investigations.

Results and Discussion

Synthetic investigations

To provide a broader basis for our study, $Cd(NCS)_2$, $Cd(NO_3)_2 \cdot 4H_2O$ and KNCSe were reacted in different molar ratios with 4-acetylpyridine in water, ethanol, methanol and acetonitrile, and the resulting precipitates were investigated by XRPD measurements. These investigations have shown that always one crystalline phase is found with $Cd(NCS)_2$ and $Cd(NCSe)_2$ that might be isotypic. Elemental analyses suggested that the composition of these compounds is $Cd(NCS)_2$(4-acetylpyridine)$_2$ (**Cd1**) and $Cd(NCSe)_2$(4-acetylpyridine)$_2$ (**Cd2**) and IR-spectroscopic investigations showed the asymmetric CN stretching vibration for **Cd1** at 2091 cm^{-1} and for **Cd2** at 2098 cm^{-1} indicating that μ-1,3-bridging thiocyanato anions are present [61–64].

Similar investigations have revealed that the reaction of $Zn(NCS)_2$with 4-acetylpyridine always leads to the formation of a compound of composition $Zn(NCS)_2$(4-acetylpyridine)$_2$ (**Zn1**). The asymmetric CN stretching vibration band appears at 2063 cm^{-1} indicating that in contrast to the Cd compounds **Cd1-I** and **Cd-2** only terminally N-bonded thiocyanato anions are present [61–64]. Therefore, it is highly likely that this compound consists of discrete complexes in which the Zn cations are tetrahedrally coordinated by two N-bonded thiocyanato anions and two 4-acetylpyridine ligands. In contrast, coordination compounds based on zinc selenocyanate could not be prepared. All precipitates obtained were unstable and decomposed immediately into elemental selenium and some crystalline phases that could not be identified.

To investigate the Cd compounds in more detail, single crystals were grown and investigated by X-ray diffraction. In the course of these investigations a few single crystals of a second modification of $Cd(NCS)_2$(4-acetylpyridine)$_2$ (**Cd1-II**) were obtained by accident.

Crystal structures of the Cd(II) compounds

$[Cd(NCS)_2$(4-acetylpyridine)$_2]_n$ (**Cd1-I**) and $[Cd(NCSe)_2$(4-acetylpyridine)$_2]_n$(**Cd2**) are isotypic and crystallize in the monoclinic centrosymmetric space group $C2/c$ with four formula units in the unit cell. The asymmetric units consist of one Cd(II) cation that is located on a center of inversion as well as of one 4-acetylpyridine ligand and one thiocyanato anion in general positions. The cadmium cations are each coordinated by two N atoms of two symmetry-related 4-acetylpyridine ligands as well as by two N- and two S- respectively Se- bonded anionic ligands in a slightly distorted octahedral geometry (Fig. 1: left and Table 1). As expected, the Cd–N and Cd–S/Se bond lengths to the anionic ligands are longer in the selenium compound, but surprisingly the Cd–N bond lengths to the 4-acetylpyridine ligand is not affected (Table 1). Bond lengths and angels are in good agreement with values reported in the literature [43, 44, 51, 52].

Table 1. Selected bond lengths (Å) and angles (deg) for **Cd1-I**, **Cd1-II** and **Cd2**. For symmetry codes see caption to Fig. 1.

	Cd1-I	**Cd1-II**		**Cd2**
Cd(1)–N(1)	2.301(4)	2.274(3)	Cd(1)–N(1)	2.328(4)
Cd(1)–N(11)	2.362(5)	2.396(3)	Cd(1)–N(11)	2.362(5)
Cd(1)–S(1B)	2.7424(16)	2.7472(10)	Cd(1)–Se(1B)	2.8129(6)
N(1)–Cd(1)–N(11)	89.81(16)	87.68(12)	N(1)–Cd(1)–N(11)	89.74(17)
N(1)–Cd(1)–N(11A)	90.19(16)	92.32(12)	N(1)–Cd(1)–N(11A)	90.26(17)
N(1)–Cd(1)–S(1B)	86.24(12)	87.20(8)	N(1)–Cd(1)–Se(1B)	85.79(11)
N(1)–Cd(1)–S(1C)	93.76(12)	92.80(8)	N(1)–Cd(1)–Se(1C)	94.21(11)
N(11)–Cd(1)–S(1C)	90.74(12)	91.29(8)	N(11)–Cd(1)–Se(1C)	90.15(11)
N(11A)–Cd(1)–S(1C)	89.26(12)	88.71(8)	N(11A)–Cd(1)–Se(1C)	89.85(11)

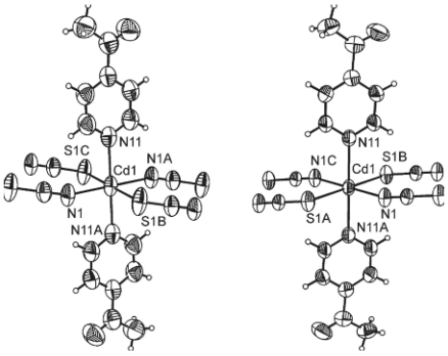

Fig. 1. Crystal structures of **Cd1-I** (left) and **Cd1-II** (right) with labeling and displacement ellipsoids drawn at the 50% probability level. Symmetry codes: A: $-x, -y, -z$; B: $x, y+1, z$; C: $-x, y-1, -z$ (**Cd1-I**) and A: $-x+1, -y+1, -z$; B: $x+1, y, z$; C: $-x, -y+1, -z$ (**Cd1-II**).

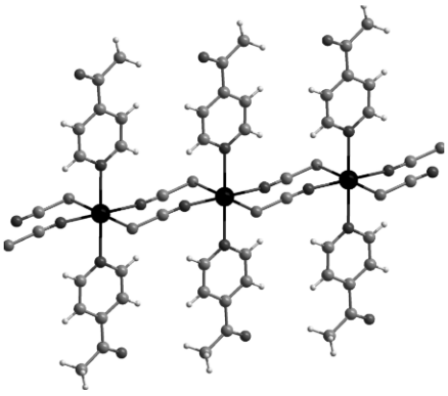

Fig. 2. Crystal structure of compound **Cd1-I**. View of the chains running in the direction of the crystallographic *b* axis.

The second modification of $[Cd(NCS)_2(4\text{-acetylpyridine})_2]_n$ (**Cd1-II**) crystallizes in the monoclinic centrosymmetric space group $P2_1/c$ with two formula units per cell. The asymmetric unit consists of a Cd(II) cation that is located on a center of inversion as well as one 4-acetylpyridine ligand and one thiocyanato anion in general positions. The Cd coordination is identical to that in **Cd1-I** in that the cations are coordinated by two *trans*-oriented 4-acetylpyridine ligands and two S as well as two N atoms of μ-1,3-bridging thiocyanato anions. Bond lengths and angles in both modifications are similar, but the Cd–N bond lengths to the anion are shortened, whereas that to the co-ligand are slightly elongated (Table 1).

The Cd cations are linked into chains by pairs of centrosymmetric μ-1,3-bridging anionic ligands (Fig. 2). Within these chains all ligands are *trans*-oriented. This is a well known structural motif for thio- or selenocyanato coordination compounds with monodentate ligands and has been observed in a number of related compounds [43, 44, 51, 52].

Structural differences between the modifications **Cd1-I** and **Cd1-II** are found predominantly in the coordination environment of the Cd cations, which is

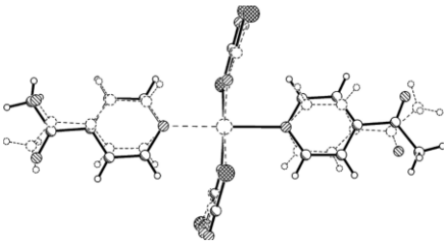

Fig. 3. Structural overlay plot for **Cd1-I** and **Cd1-II**.

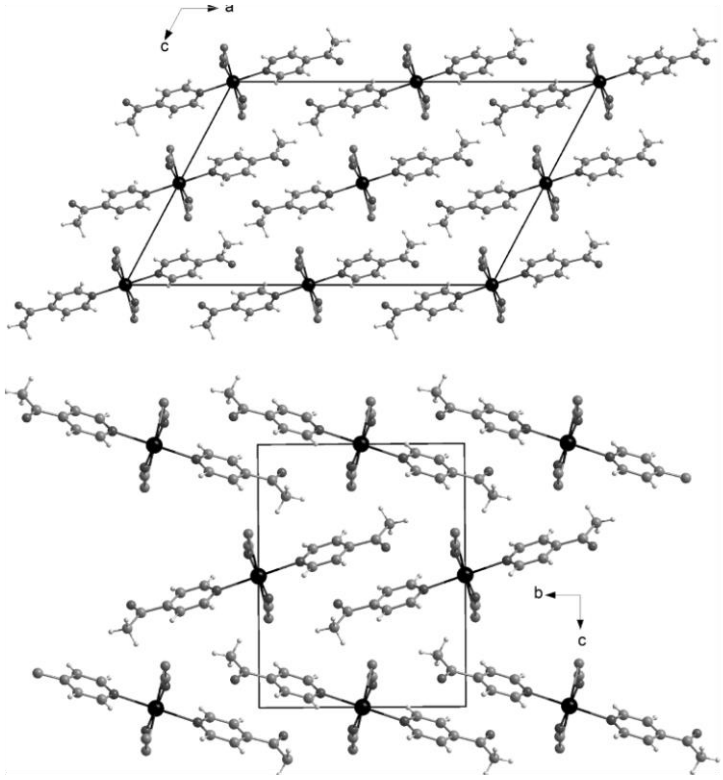

Fig. 4. Crystal structure of **Cd1-I**, viewed along the crystallographic *b* axis (top), and of **Cd1-II** as viewed along the crystallographic *a* axis (bottom).

obvious if their structures are fitted onto each other (Fig. 3). In each polymorph the 4-acetylpyridine oxygen atoms point in opposite directions as required by symmetry.

Structural differences are also found in the packing of the cadmium thiocyanato chains. In **Cd1-I** the thiocyanato chains extend in the direction of the crystallographic *b* axis (Fig. 4, top), whereas in form **Cd1-II** the chains point in the direction of the crystallographic *a* axis (Fig. 4, bottom). Moreover, in form **Cd1-I** the Cd(4-acetylpyridine)$_2$ units are parallel to each other, whereas in form **Cd1-II** they shows a herringbone-like arrangement (Fig. 4).

Based on the results of the single-crystal structure determinations, powder X-ray patters for the thiocyanato compound **Cd1-I** and the selenocyanato compound **Cd2** were calculated and compared with those measured. The results prove that both compounds are obtained as single-crystalline phases (Fig. 5).

*Thermoanalytical investigations and crystallization experiments on **Cd1-I***

In order to check if form **I** of **Cd-1** transforms into form **II** on heating, experiments using simultaneous differential thermoanalysis and thermogravime-

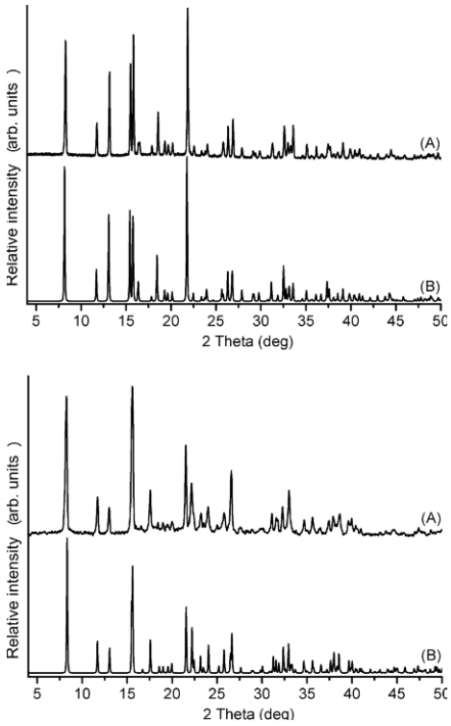

Fig. 5. Experimental powder X-ray patters of **Cd1-I** (top: A) and of **Cd-2** (bottom: A) together with the powder patters calculated from single-crystal data (bottom: B).

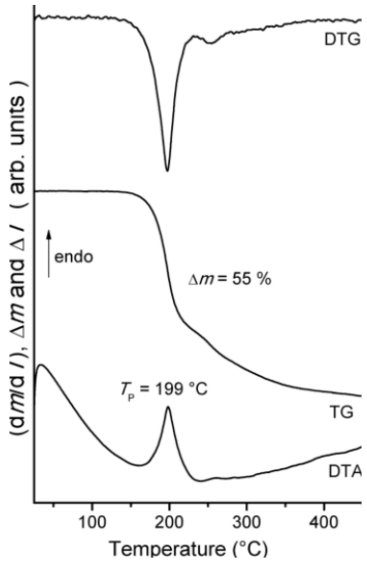

Fig. 6. DTG, TG and DTA curves for **Cd1-I** (heating rate = 4 °C min^{-1}; given are the mass changes (%) and the peak temperature T_P in °C).

try (DTA-TG) were performed. On heating compound **Cd1-I** in a thermobalance a continuous mass loss is observed, which is accompanied by an endothermic event at about 200 °C observed in the DTA curve. This mass step is not completely finished up to 450 °C (Fig. 6). If the experimental mass loss is compared with that calculated for the removal of all 4-acetylpyridine ligands it is obvious that the removal of all ligands ($\Delta m_{calcd.} = -51.4\,\%$) and the decomposition of $Cd(NCS)_2$ occur simultaneously. There is no hint for a polymorphic transformation prior to decomposition.

However, because the energies of polymorphic transformations are usually low, additional measurements using differential scanning calorimetry were performed on **Cd-1** (Fig. 7). On heating decomposition starts at an onset temperature of about 203 °C, which is in good agreement with the result of the DTA-TG measurements but even here, no indications for a transition from form **I** into form **II** were observed.

To investigate if form **II** of **Cd1** can be obtained by kinetic control, $Cd(NCS)_2$ and 4-acetylpyridine were mixed in water, ethanol, methanol, and acetonitrile, and the product was immediately filtered off after formation of a precipitate. When the experimental pattern was compared with those calculated for both forms, it was obvious that **Cd1-I** had formed as a pure crystalline phase. Therefore, we have found no access to form **II**, and it can be assumed that it is metastable at room temperature. Based on the crystallographic density of both forms, which is higher for form **II**, it might be possible that this modification is more stable at lower temperatures, but several exceptions are known from the so-called density rule [65, 66].

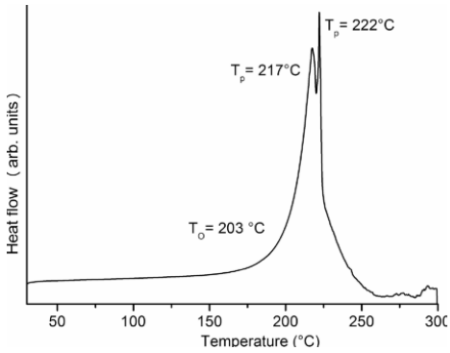

Fig. 7. DSC curve for **Cd1-I** (heating rate = 10 °C min^{-1}; given is the peak temperature in °C).

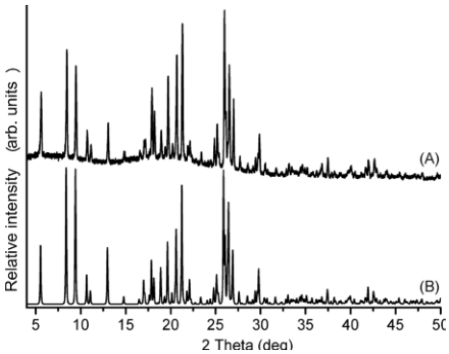

Fig. 9. Experimental powder X-ray pattern of **Zn1** (A) together with the powder pattern calculated from single-crystal data (B).

Crystal structure of ***Zn1***

The 1 : 2 compound [Zn(NCS)$_2$(4-acetylpyridine)$_2$] (**Zn1**) crystallizes in the centrosymmetric triclinic space group $P\bar{1}$ with two formula units in the unit cell and all atoms in general positions. The zinc(II) cations are coordinated by four nitrogen atoms of two terminally *N*-bonded thiocyanato anions and two *N*-bonded 4-acetylpyridine co-ligands in a slightly distorted tetrahedral coordination geometry. The Zn(II)–N distances are 1.929(3) and 2.031(2) Å, while the angles around the Zn(II) cations are between 105.37(9) and 116.40(12)° (Fig. 8, Table 2). These values are in agreement with those retrieved from the literature [46, 47, 49].

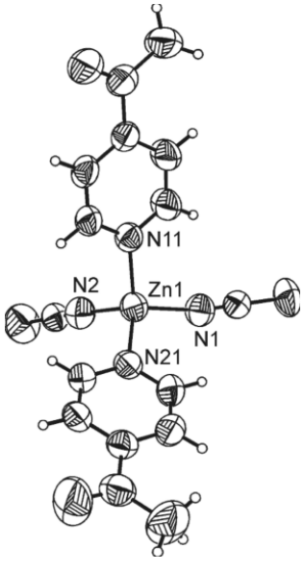

Fig. 8. Crystal structure of compound **Zn1** with atom labeling and displacement ellipsoids drawn at the 50 % probability level.

Comparison of the experimental powder X-ray pattern for **Zn1** with that calculated from single-crystal data proves that the compound is obtained as a single-crystalline phase (Fig. 9).

Conclusion

In this contribution investigations on the synthesis and structures of new Cd(II) and Zn(II) thio- and selenocyanato coordination compounds are described. In the course of these investigations two compounds of composition Cd(NCX)$_2$(4-acetylpyridine)$_2$ (X = S, Se) were prepared, with the thiocyanato compound crystallizing in two different modifications. Form **II** was obtained by accident, whereas form **I** can be prepared as a phase-pure material and does not transform into form **II** on heating. Additionally, one compound of composition Zn(NCS)$_2$(4-acetylpyridine)$_2$ was obtained that in contrast to the Cd compounds forms discrete tetrahedral complexes.

Table 2. Selected bond lengths (Å) and angles (deg) for **Zn1**.

Zn(1)–N(1)	1.939(2)	Zn(1)–N(11)	1.929(3)
Zn(1)–N(2)	2.031(2)	Zn(1)–N(21)	2.024(2)
N(1)–Zn(1)–N(2)	116.40(12)	N(2)–Zn(1)–N(11)	107.32(10)
N(1)–Zn(1)–N(11)	105.37(9)	N(2)–Zn(1)–N(21)	108.17(10)
N(1)–Zn(1)–N(21)	107.33(10)	N(11)–Zn(1)–N(21)	112.36(9)

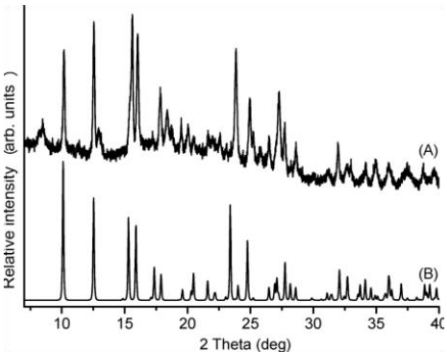

Fig. 10. Experimental powder X-ray pattern of the residue of the composition $Mn(NCS)_2(4\text{-acetylpyridine})_2(H_2O)_2$ together with the powder pattern calculated from single-crystal data of **Cd1-I** (B).

These investigations are part of our current work on the corresponding compounds of composition $M(NCS)_2(4\text{-acetylpyridine})_2$ with M = Mn(II), Fe(II), Co(II) and Ni(II) for which different polymorphic modifications or isomers may be obtained. We have already obtained one compound of composition $Mn(NCS)_2(4\text{-acetylpyridine})_2$ by thermal decomposition of $Mn(NCS)_2(4\text{-acetylpyridine})_2(H_2O)_2$, but this product could not be structurally identified. When the experimental powder X-ray pattern of the Mn compound was compared with that calculated for **Cd1-I**, it became obvious that this modification had been formed with manganese but was contaminated with a second crystalline phase of the same composition, which is different from **Cd1-II** (Fig. 10). This clearly shows that the preparation of corresponding diamagnetic compounds can help in the identification of the paramagnetic counterparts. The preparation of the paramagnetic compounds as single-crystalline phases will be the subject of further investigations.

Experimental Section

Materials

$Cd(NO_3)_2 \cdot 4H_2O$, KNCSe, $ZnSO_4 \cdot H_2O$, and $CdSO_4 \cdot 8/3H_2O$ were obtained from Merck, $Ba(NCS)_2 \cdot 3H_2O$ and 4-acetylpyridine were obtained from Alfa Aesar. The chemicals were used without further purification.

Synthesis of $Cd(NCS)_2$

$Ba(NCS)_2 \cdot 3H_2O$ (3.076 g, 10 mmol) and $CdSO_4 \cdot 8/3H_2O$ (2.566 g, 10 mmol) were stirred in water (100 mL). The colorless precipitate of $BaSO_4$ was filtered off, and the water was removed from the filtrate by heating. The final product was dried at 80 °C. The homogeneity of the product was investigated by powder Xray diffraction and elemental analysis.

Synthesis of $Zn(NCS)_2$

$Ba(NCS)_2 \cdot 3H_2O$ (3.076 g, 10 mmol) and $ZnSO_4 \cdot H_2O$ (1.795 g, 10 mmol) were stirred in water (100 mL). The colorless precipitate of $BaSO_4$ was filtered off, and the water was removed from the filtrate by heating. The final product was dried at 80 °C. The homogeneity of the product was investigated by powder Xray diffraction and elemental analysis.

Synthesis of $[Cd(NCS)_2(4\text{-acetylpyridine})_2]_n$ (Cd1-I)

57.1 mg $Cd(NCS)_2$ (1.50 mmol) and 55.1 µL 4-acetylpyridine (0.25 mmol) were stirred in 1.5 mL of methanol. The colorless precipitate was filtered off and dried. After slow evaporation of the solvent from the filtrate colorless single crystals suitable for X-ray diffraction were obtained. – $C_{16}H_{14}CdN_4O_2S_2$ (470.84 g mol^{-1}): calcd. C 40.8, H 3.0, N 11.9, S 13.6; found C 41.0, H 2.9, N 11.9, S 13.6. – IR (ATR): ν_{max} = 2089 (s), 1695 (s), 1413 (m), 1361 (m), 1263 (s), 1216 (w), 1060 (w), 1014 (w), 963 (w), 822 (s), 594 (s) cm^{-1}.

Synthesis of $[Cd(NCS)_2(4\text{-acetylpyridine})_2]_n$ (Cd1-II)

Single crystals were accidently obtained by the reaction of 342.9 mg $Cd(NCS)_2$ (1.50 mmol) and 27.5 µL 4-acetylpyridine (0.25 mmol) in 1.5 mL H_2O. The precipitate obtained was filtered off and after slow evaporation of the

filtrate colorless single crystals suitable for X-ray diffraction were obtained.

*Synthesis of [Cd(NCSe)$_2$(4-acetylpyridine)$_2$]$_n$ (**Cd2**)*

154.2 mg $Cd(NO_3)_2 \cdot 4H_2O$ (0.50 mmol), 136.9 mg KNCSe (0.95 mmol) and 27.5 µL 4-acetylpyridine (0.25 mmol) were stirred in 1.5 mL of H_2O. Single crystals suitable for X-ray diffraction were prepared under identical reaction conditions without stirring. After 5 d colorless single crystals were obtained. – IR (ATR): ν_{max} = 2098 (s), 1697 (s), 1609 (w), 1575 (w), 1413(m), 1361 (m), 1323 (w), 1266 (s), 1216 (m), 1059 (m), 1012 (m), 963 (w), 821 (s), 593 (s) cm^{-1}.

*Synthesis of Zn(NCS)$_2$(4-acetylpyridine)$_2$(**Zn1**)*

45.4 mg $Zn(NCS)_2$ (0.25 mmol) and 110.15 µL 4-acetylpyridine (1.00 mmol) were stirred in 1.5 mL H_2O for 2 d. Single crystals suitable for X-ray diffraction were prepared by slow evaporation of the solvent from the filtrate. – $C_{16}H_{14}N_4O_2S_2Zn$ (423.82 g mol^{-1}): calcd. C 45.3, H 3.3, N 13.2, S 15.4; found C 45.6, H 3.3, N 13.4, S 15.4. – IR (ATR): ν_{max} = 2063 (s), 1698 (s), 1618 (m), 1557 (m), 1503 (w), 1422 (s), 1360 (s), 1259 (s), 1232 (s), 1065 (s), 1031 (m), 965 (m), 882 (w), 824 (s), 594 (s) cm^{-1}.

Powder X-ray diffraction

The experiments were performed using a Stoe Transmission Powder Diffraction System (STADI P) with CuK_α radiation (λ = 154.0598 pm) that is equipped with a linear position-sensitive detector ($\delta - 2\theta = 6.5 - 7°$ simultaneous; scan range overall = 2 – 130°) from Stoe & Cie.

Elemental analysis

CHNS analysis was performed using an EURO EA elemental analyzer, fabricated by Euro Vector Instruments and Software.

Differential scanning calorimetry (DSC)

The DSC experiments were performed using a DSC 1 Star System with STARe Excellence Software from Mettler-Toledo AG.

Table 3. Selected crystal data and details on the structure determination for **Cd1-I**, **Cd1-II**, **Cd2**, and **Zn1**.

Compound	**Cd1-I**	**Cd1-II**	**Cd2**	**Zn1**
Formula	$C_{16}H_{14}CdN_4O_2S_2$	$C_{16}H_{14}CdN_4O_2S_2$	$C_{16}H_{14}CdN_4O_2Se_2$	$C_{16}H_{14}N_4O_2S_2Zn$
M_r	470.83	470.83	564.63	423.80
Crystal system	monoclinic	monoclinic	monoclinic	triclinic
Space group	$C2/c$	$P2_1/c$	$C2/c$	$P\bar{1}$
a, Å	24.508(4)	5.8899(3)	24.027(2)	5.5720(4)
b, Å	5.8069(6)	11.1429(7)	5.9301(3)	10.9241(8)
c, Å	15.322(2)	14.3704(7)	15.3667(14)	16.2121(13)
α, deg	90	90	90	95.927(6)°
β, deg	118.030(10)	100.837(4)	118.131(10)	96.322(6)
γ, deg	90	90	90	103.353(6)
V, Å^3	1924.9(4)	926.32(9)	1930.9(3)	945.81(12)
T, K	293 (2)	293 (2)	−103 (2)	293 (2)
Z	4	2	4	2
$D_{calcd.}$, mg cm^{-3}	1.63	1.69	1.94	1.49
μ(MoK_α), mm^{-1}	1.4	1.4	4.9	1.5
Min./max. trans.	0.5610/0.7381	0.6795/0.8779	0.3714/0.5581	0.6598/0.8377
θ_{max}, deg	26.00	29.22	27.97	27.92
Measured refins.	7954	13 104	7520	9507
Unique refins.	1892	2498	2306	4487
R_{int}	0.0615	0.0443	0.0951	0.0292
Refl. $F_0 > 4\,\sigma(F_0)$	1426	1905	1773	2985
Parameters	115	116	115	226
$R_1^a[F_0 > 4\,\sigma(F_0)]$	0.0522	0.0434	0.0496	0.0431
wR_2^b (all data)	0.1100	0.0997	0.1371	0.0949
GoF^c	1.171	1.109	1.048	0.975
$\Delta\rho_{max/min}$, e Å^{-3}	0.70/−0.43	0.55/−0.86	1.11/−1.70	0.31/−0.18

[a] $R_1 = \Sigma||F_o| - |F_c||/\Sigma|F_o|$; [b] $wR_2 = [\Sigma w(F_o^2 - F_c^2)^2/\Sigma w(F_o^2)^2]^{1/2}$, $w = [\sigma^2(F_o^2) + (AP)^2 + BP]^{-1}$, where $P = (\mathrm{Max}(F_o^2, 0) + 2F_c^2)/3$; [c] GoF = $[\Sigma w(F_o^2 - F_c^2)^2/(n_{obs} - n_{param})]^{1/2}$.

Single-crystal structure determinations

Data collection was performed with an imaging plate diffraction system (IPDS-2 for **Cd1-I**, **Cd1-II** and **Zn1**; IPDS-1 for **Cd2**) from Stoe & Cie with MoK_α radiation. The data were corrected for absorption using X-RED and X-SHAPE from Stoe [67, 68]. The structure solution was performed with Direct Methods using SHELXS-97, and structure refinements were performed against F^2 using SHELXL-97 [69]. All non-hydrogen atoms were refined with anisotropic displacement parameters. The hydrogen atoms were positioned with idealized geometry and were refined with fixed isotropic displacement parameters with $U_{iso}(H) = -1.2\ U_{eq}(C)$ (1.5 for methyl H atoms) using a riding model. Details of the structure determination are given in Table 3.

CCDC 927933 (**Cd1-I**), CCDC 927934 (**Cd1-II**), CCDC 927935 (**Cd2**) and CCDC 927932 (**Zn1**) contain the supplementary crystallographic data for this paper. These data can be obtained free of charge from The Cambridge Crystallographic Data Center *via* www.ccdc.cam.ac.uk/data_request/cif.

Differential thermal analysis and thermogravimetry

The DTA-TG measurements were performed in nitrogen atmosphere (purity: 5.0) in Al_2O_3 crucibles using a STA-409CD thermobalance from Netzsch. All measurements were performed with a flow rate of 75 mL min^{-1} and were corrected for buoyancy and current effects. The instrument was calibrated using standard reference materials.

Spectroscopy

IR spectra were recorded on an Alpha IR spectrometer from Bruker equipped with a Platinum ATR QuickSnap™ sampling module between 4000 – 375 cm^{-1}.

Acknowledgement

This project was supported by the Deutsche Forschungsgemeinschaft (project no. NA 720/3-1) and the State of Schleswig-Holstein. We thank Professor Dr. W. Bensch for access to his experimental facility.

[1] U. Englert, *Coord. Chem. Rev.* **2010**, *254*, 537 – 554.
[2] B. Moulton, M. J. Zaworotko, *Chem. Rev.* **2001**, *101*, 1629 – 1658.
[3] S. Kitagawa, R. Matsuda, *Coord. Chem. Rev.* **2007**, *251*, 2490 – 2509.
[4] R. J. Puddephatt, *Coord. Chem. Rev.* **2001**, *216 – 217*, 313 – 332.
[5] A. Y. Robin, K. M. Fromm, *Coord. Chem. Rev.* **2006**, *250*, 2127 – 2157.
[6] R. Diaz-Torres, S. Alvarez, *Dalton Trans.* **2011**, *40*, 10742 – 10750.
[7] C. Janiak, *Dalton Trans.* **2003**, 2781 – 2804.
[8] D. Maspoch, D. Ruiz-Molina, J. Veciana, *J. Mater. Chem.* **2004**, *14*, 2713 – 2723.
[9] D. Maspoch, D. Ruiz-Molina, J. Veciana, *Chem. Soc. Rev.* **2007**, *36*, 770 – 818.
[10] D.-F. Weng, Z.-M. Wang, S. Gao, *Chem. Soc. Rev.* **2011**, *40*, 3157 – 3181.
[11] D. Braga, L. Maini, M. Polito, L. Scaccianoce, G. Cojazzi, F. Grepioni, *Coord. Chem. Rev.* **2001**, *216*, 225 – 248.
[12] A. N. Khlobystov, A. J. Blake, N. R. Champness, D. A. Lemenovskii, A. G. Majouga, N. V. Zyk, M. Schröder, *Coord. Chem. Rev.* **2001**, *222*, 155 – 192.
[13] J. L. Manson, A. M. Arif, J. S. Miller, *Chem. Commun.* **1999**, 1479 – 1480.
[14] Y.-Q. Wang, Q. Sun, Q. Yue, A.-L. Cheng, Y. Song, E.-Q. Gao, *Dalton Trans.* **2011**, *40*, 10966 – 10974.
[15] X.-B. Li, Y. Ma, X.-M. Zhang, J.-Y. Zhang, E.-Q. Gao, *Eur. J. Inorg. Chem.* **2011**, *2011*, 4738 – 4744.
[16] S. Youngme, J. Phatchimkun, N. Wannarit, N. Chaichit, S. Meejoo, G. A. van Albada, J. Reedijk, *Polyhedron* **2008**, *27*, 304 – 318.
[17] X.-Y. Wang, H.-Y. Wei, Z.-M. Wang, Z.-D. Chen, S. Gao, *Inorg. Chem.* **2005**, *44*, 572 – 583.
[18] B. Gil-Hernandez, P. Gili, J. K. Vieth, C. Janiak, J. n. Sanchiz, *Inorg. Chem.* **2010**, *49*, 7478 – 7490.
[19] M. A. M. Abu-Youssef, V. Langer, D. Luneau, E. Shams, M. A. S. Goher, L. Öhrström, *Eur. J. Inorg. Chem.* **2008**, *2008*, 112 – 118.
[20] C.-F. Wang, Z.-Y. Zhu, X.-G. Zhou, L.-H. Weng, Q.-S. Shen, Y.-G. Yan, *Inorg. Chem. Commun.* **2006**, *9*, 1326 – 1330.
[21] L. Zhu, D. Xu, X. Wang, G. Yu, *J. Chem. Crystallogr.* **2008**, *38*, 609 – 612.
[22] J.-Q. Tao, Z.-G. Gu, T.-W. Wang, Q.-F. Yang, J.-L. Zuo, X.-Z. You, *Inorg. Chim. Acta* **2007**, *360*, 4125 – 4132.
[23] M. Wriedt, S. Sellmer, C. Näther, *Dalton Trans.* **2009**, 7975 – 7984.
[24] M. Wriedt, I. Jeß, C. Näther, *Eur. J. Inorg. Chem.* **2009**, 1406 – 1413.
[25] M. Wriedt, S. Sellmer, C. Näther, *Inorg. Chem.* **2009**, *48*, 6896 – 6903.
[26] H. A. Habib, A. Hoffmann, H. A. Höppe, G. Steinfeld, C. Janiak, *Inorg. Chem.* **2009**, *48*, 2166 – 2180.

[27] C. J. Adams, M. F. Haddow, D. J. Harding, T. J. Podesta, R. E. Waddington, *CrystEngComm* **2011**, *13*, 4909 – 4914.
[28] C. J. Adams, M. C. Muñoz, R. E. Waddington, J. A. Real, *Inorg. Chem.* **2011**, *50*, 10633 – 10642.
[29] C. Näther, J. Greve, *J. Solid State Chem.* **2003**, *176*, 259 – 265.
[30] M. Wriedt, C. Näther, *Chem. Commun.* **2010**, *46*, 4707 – 4709.
[31] C. Näther, I. Jeß, *J. Solid State Chem.* **2002**, *169*, 103 – 112.
[32] J. Boeckmann, C. Näther, *Dalton Trans.* **2010**, *39*, 11019 – 11026.
[33] J. Boeckmann, C. Näther, *Chem. Commun.* **2011**, *47*, 7104 – 7106.
[34] S. Wöhlert, J. Boeckmann, M. Wriedt, C. Näther, *Angew. Chem. Int. Ed.* **2011**, *50*, 6920 – 6923.
[35] J. Boeckmann, M. Wriedt, C. Näther, *Chem. Eur. J.* **2012**, *18*, 5284 – 5289.
[36] S. Wöhlert, U. Ruschewitz, C. Näther, *Crys. Growth Des.* **2012**, *12*, 2715 – 2718.
[37] S. Wöhlert, L. Fink, M. Schmidt, C. Näther, *CrystEngComm* **2013**, *15*, 945 – 957.
[38] S. Wöhlert, M. Wriedt, T. Fic, Z. Tomkowicz, W. Haase, C. Näther, *Inorg. Chem.* **2013**, *52*, 1061 – 1068.
[39] S. Wöhlert, C. Näther, *Eur. J. Inorg. Chem.* **2013**, doi:10.1002/ejic.201201486.
[40] H.-L. Sun, B.-Q. Ma, S. Gao, S. R. Batten, *Cryst. Growth Des.* **2006**, *6*, 1261 – 1263.
[41] I. N. B. Machura, K. Michalik *Polyhedron* **2011**, *30*, 2619 – 2626.
[42] Q. I. Ma, M. Zhu, C. Yuan, S. Feng, L. Lu, Q. Wang, *Cryst. Growth Des.* **2009**, *10*, 1706 – 1714.
[43] I. Jeß, J. Boeckmann, C. Näther, *Dalton Trans.* **2012**, *41*, 228 – 236.
[44] J. Boeckmann, I. Jeß, T. Reinert, C. Näther, *Eur. J. Inorg. Chem.* **2011**, 5502 – 5511.
[45] Q.-H. Jin, J.-J. Sun, J.-Q. Wu, Y.-C. Dai, C.-L. Zhang, *J. Chem. Crystallogr.* **2009**, *40* 310 – 315.
[46] J. Boeckmann, T. Reinert, C. Näther, *Z. Anorg. Allg. Chem.* **2011**, *637*, 940 – 946.
[47] J. Boeckmann, T. Reinert, I. Jeß, C. Näther, *Z. Anorg. Allg. Chem.* **2011**, *637*, 1137 – 1144.
[48] J. Boeckmann, B. Reimer, C. Näther, *Z. Naturforsch.* **2011**, *66b*, 819 – 827.
[49] L. Kong, W.-J. Li, X.-L. Li, W.-Q. Geng, F.-Y. Hao, J.-Y. Wu, H.-P. Zhou, J.-X. Yang, Y.-P. Tian, B.-K. Jin, *Polyhedron* **2010**, *29*, 1575 – 1582.
[50] S. Wöhlert, I. Jess, C. Näther, *Z. Anorg. Allg. Chem.* **2013**, *639*, 385 – 391.
[51] S. Wöhlert, J. Boeckmann, I. Jess, C. Näther, *CrystEngComm* **2012**, *14*, 5412 – 5420.
[52] J. Werner, J. Boeckmann, C. Näther, *Z. Anorg. Allg. Chem.* **2012**, *638*, 2257 – 2264.
[53] D. Braga, F. Grepioni, *Chem. Soc. Rev.* **2000**, *29*, 229 – 238.
[54] S. Galli, N. Masciocchi, G. Tagliabue, A. Sironi, J. A. R. Navarro, J. M. Salas, L. Mendez-Linan, M. Domingo, M. Perez-Mendoza, E. Barea, *Chem. Eur. J.* **2008**, *14*, 9890 – 9901.
[55] J. Tao, R.-J. Wei, R.-B. Huang, L.-S. Zheng, *Chem. Soc. Rev.* **2012**, *41*, 703 – 737.
[56] A. J. Blake, N. R. Brooks, N. R. Champness, M. Crew, D. H. Gregory, P. Hubberstey, M. Schröder, A. Deveson, D. Fenske, L. R. Hanton, *Chem. Commun.* **2001**, 1432 – 1433.
[57] T. L. Hennigar, D. C. MacQuarrie, P. Losier, R. D. Rogers, M. J. Zaworotko, *Angew. Chem., Int. Ed. Engl.* **1997**, *36*, 972 – 973.
[58] C. Näther, M. Wriedt, I. Jeß, *Inorg. Chem.* **2003**, *42*, 2391 – 2397.
[59] C. Näther, I. Jeß, *Inorg. Chem.* **2003**, *42*, 2968 – 2976.
[60] C. Näther, G. Bhosekar, I. Jeß, *Inorg. Chem.* **2007**, *46*, 8079 – 8087.
[61] P. O. Kinell, B. Strandberg, *Acta Chem. Scand.* **1959**, *13*, 1607 – 1622.
[62] R. J. H. Clark, C. S. Williams, *Spectrochim. Acta* **1966**, *22*, 1081 – 1090.
[63] R. A. Bailey, S. L. Kozak, T. W. Michelsen, W. N. Mills, *Coord. Chem. Rev.* **1971**, *6*, 407 – 445.
[64] G. A. Van Albada, R. A. G. De Graaff, J. G. Haasnoot, J. Reedijk, *Inorg. Chem.* **1984**, *23*, 1404 – 1408.
[65] A. I. Kitaigorodski, *Organic Chemical Crystallography*, Consultants Bureau, New York, **1961**.
[66] A. Burger, R. Ramberger, *Mikrochim. Acta* **1979**, 259 – 271.
[67] X-RED (version 1.11), Program for Data Reduction and Absorption Correction, Stoe & Cie GmbH, Darmstadt (Germany) **1998**.
[68] X-SHAPE (version 1.03), Crystal Optimization for Numerical Absorption Correction, Stoe & Cie GmbH, Darmstadt (Germany) **1998**.
[69] G. M. Sheldrick, *Acta Crystallogr.* **2008**, *A64*, 112 – 122.

5.4. Crystal Structure of Bis[4-(4-chlorobenzyl)pyridine-κN]bis(thiocyanato-κN)zinc

Julia Werner, Tristan Neumann, Inke Jess und Christian Näther, *Acta Crystallogr. E* **2014**, E70, m355-356.

DOI: 10.1107/S160053681402039X

Motivation

Die folgenden drei Strukturen wurden im Rahmen systematischer Untersuchungen von $Cd(NCS)_2$ und den Liganden 4-(4-Chlorbenzyl)pyridin, 4-*tert*-Butylpyridin und 4-(Hydroxymethyl)pyridin erhalten. Da diese jedoch nicht isotyp zu den entsprechenden paramagnetischen Verbindungen kristallisierten, waren diese von untergeordneter Bedeutung und wurden somit als Strukturmitteilungen veröffentlicht.

CrossMark

data reports

Acta Cryst E STRUCTURE REPORTS

OPEN ACCESS

ISSN 1600-5368

Crystal structure of bis[4-(4-chlorobenzyl)pyridine-κN]bis(thiocyanato-κN)zinc

Julia Werner,* Tristan Neumann, Inke Jess and Christian Näther

Institut für Anorganische Chemie, Christian-Albrechts-Universität Kiel, Max-Eyth-Strasse 2, 24118 Kiel, Germany. *Correspondence e-mail: jwerner@ac.uni-kiel.de

Received 30 August 2014; accepted 11 September 2014

Edited by M. Weil, Vienna University of Technology, Austria

In the crystal structure of the title compound, $[Zn(NCS)_2(C_{12}H_{10}ClN)_2]$, the Zn^{2+} cation is *N*-coordinated by two terminally bonded thiocyante anions and by two 4-(4-chlorobenzyl)pyridine ligands within a slightly distorted tetrahedron. The asymmetric unit consists of half of the discrete complex, the central Zn^{2+} cation of which is located on a twofold rotation axis. The discrete complexes are linked into layers *via* a weak intermolecular hydrogen-bonding interaction, with a H···Cl distance of 2.85 Å and a C—H···Cl angle of 151°. These layers extend parallel to the *ab* plane and are held together by dispersion forces only.

Keywords: crystal structure; zinc complex; thiocyanate; tetrahedral coordination; hydrogen bonding.

CCDC reference: 1021253

1. Related literature

For related crystal structures with thiocyanate ligands and Zn^{2+} in a tetrahedral coordination sphere, see: Fettouhi *et al.* (2002); Kong *et al.* (2010); Zhu *et al.* (2008).

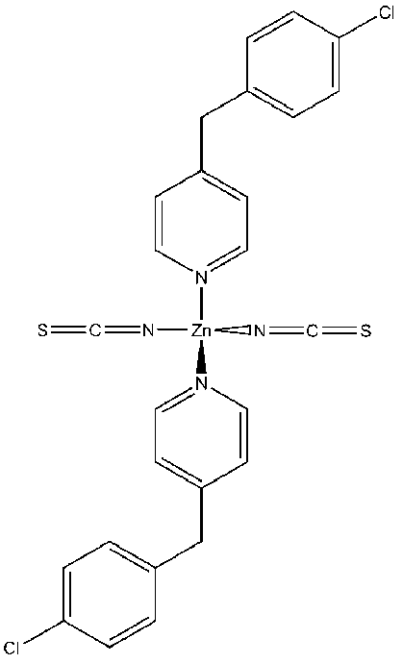

2. Experimental

2.1. Crystal data

$[Zn(NCS)_2(C_{12}H_{10}ClN)_2]$
M_r = 588.85
Monoclinic, $C2/c$
a = 29.094 (3) Å
b = 4.9911 (3) Å
c = 18.312 (2) Å
β = 98.867 (8)°
V = 2627.3 (4) Å^3
Z = 4
Mo $K\alpha$ radiation
μ = 1.32 mm^{-1}
T = 150 K
0.12 × 0.08 × 0.07 mm

2.2. Data collection

Stoe IPDS-2 diffractometer
Absorption correction: numerical (*X-SHAPE* and *X-RED32*; Stoe, 2008)
T_{min} = 0.879, T_{max} = 0.906
8309 measured reflections
2570 independent reflections
1773 reflections with $I > 2\sigma(I)$
R_{int} = 0.077

2.3. Refinement

$R[F^2 > 2\sigma(F^2)]$ = 0.063
$wR(F^2)$ = 0.148
S = 1.08
2570 reflections
159 parameters
H-atom parameters constrained
$\Delta\rho_{max}$ = 0.68 e Å^{-3}
$\Delta\rho_{min}$ = −0.46 e Å^{-3}

Data collection: *X-AREA* (Stoe, 2008); cell refinement: *X-AREA*; data reduction: *X-AREA*; program(s) used to solve structure: *SHELXS97* (Sheldrick, 2008); program(s) used to refine structure: *SHELXL97* (Sheldrick, 2008); molecular graphics: *XP* in *SHELXTL* (Sheldrick, 2008) and *DIAMOND* (Brandenburg, 2011); software used to prepare material for publication: *publCIF* (Westrip, 2010).

Acknowledgements

We gratefully acknowledge financial support by the DFG (project No. NA 720/5–1) and the State of Schleswig–Holstein. We thank Professor Dr Wolfgang Bensch for access to his experimental facilities.

Supporting information for this paper is available from the IUCr electronic archives (Reference: WM5054).

References

Brandenburg, K. (2011). *DIAMOND*. Crystal Impact GbR, Bonn, Germany.
Fettouhi, M., El Ali, B., El-Ghanam, A., Golhen, S., Ouahab, L., Daro, N. & Sutter, J.-P. (2002). *Inorg. Chem.* **41**, 3705–3712.
Kong, L., Li, W.-J., Li, X.-L., Geng, W.-Q., Hao, F.-Y., Wu, J.-Y., Zhou, H.-P., Yang, J.-X., Tian, Y.-P. & Jin, B.-K. (2010). *Polyhedron*, **29**, 1575–1582.
Sheldrick, G. M. (2008). *Acta Cryst.* A**64**, 112–122.
Stoe (2008). *X-AREA*, *X-RED32* and *X-SHAPE*. Stoe & Cie, Darmstadt, Germany.
Westrip, S. P. (2010). *J. Appl. Cryst.* **43**, 920–925.
Zhu, L. Y., Xu, D., Wang, X. Q. & Yu, G. (2008). *J. Chem. Crystallogr.* **38**, 609–612.

supporting information

Acta Cryst. (2014). E**70**, m355–m356 [doi:10.1107/S160053681402039X]

Crystal structure of bis[4-(4-chlorobenzyl)pyridine-κN]bis(thiocyanato-κN)zinc

Julia Werner, Tristan Neumann, Inke Jess and Christian Näther

S1. Synthesis and crystallization

$ZnSO_4 \cdot H_2O$ was purchased from Merck and 4-(4-chlorobenzyl)pyridine and $Ba(NCS)_2 \cdot 3H_2O$ were purchased from Alfa Aesar. $Zn(NCS)_2$ was synthesized by stirring 17.5 g (57.00 mmol) $Ba(NCS)_2 \cdot 3H_2O$ and 10.23 g (57.00 mmol) $ZnSO_4 \cdot H_2O$ in 300 mL water at RT for three hours. The white residue of $BaSO_4$ was filtered off, and the solution was evaporated by heating. The homogeneity of the product was investigated by X-ray powder diffraction and elemental analysis. The title compound was prepared by the reaction of (0.6 mmol) 108.9 mg $Zn(NCS)_2$ and (0.15 mmol) 105.5 μL 4-(4-chloro-benzyl)pyridine in 1.5 mL acetonitrile at RT. After few days, colorless needle-like crystals of the title compound were obtained.

S2. Refinement

Hydrogen atoms were positioned with idealized geometry and were refined with $U_{iso}(H) = 1.2\ U_{eq}(C)$ using a riding model with C—H = 0.95 Å for aromatic and C—H = 0.99 Å for methylene H atoms.

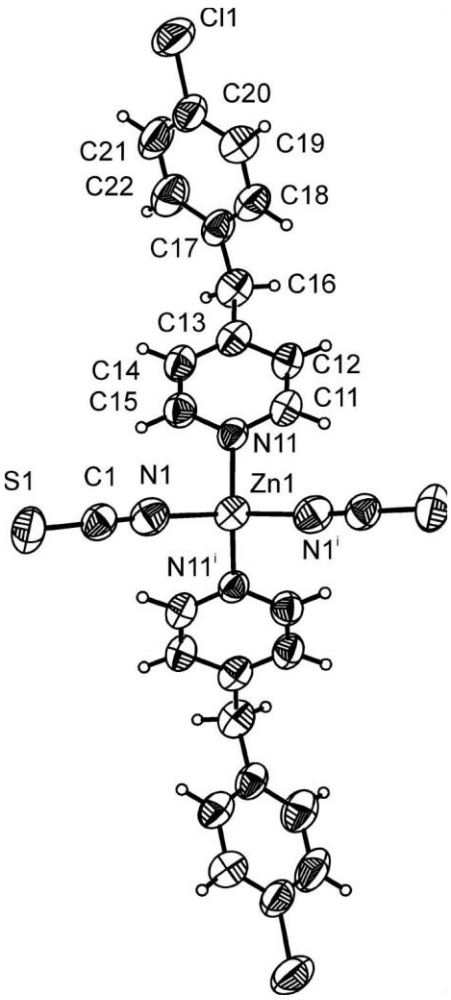

Figure 1

Molecular structure of the title compound with atom labelling and displacement ellipsoids drawn at the 50% probability level. [Symmetry code: i) -x, y, -z+1/2.]

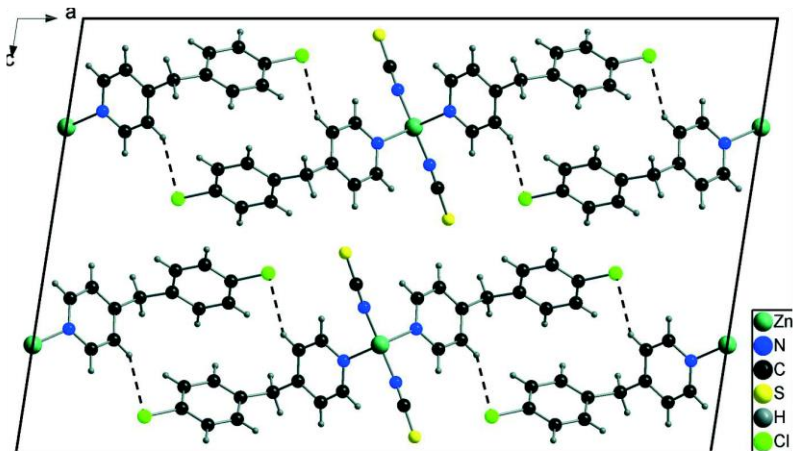

Figure 2

Crystal structure of the title compound in a projection along the *b* axis.

Bis[4-(4-chlorobenzyl)pyridine-κ*N*]bis(thiocyanato-κ*N*)zinc

Crystal data

$[Zn(NCS)_2(C_{12}H_{10}ClN)_2]$
$M_r = 588.85$
Monoclinic, *C*2/*c*
Hall symbol: -C 2yc
$a = 29.094$ (3) Å
$b = 4.9911$ (3) Å
$c = 18.312$ (2) Å
$\beta = 98.867$ (8)°
$V = 2627.3$ (4) Å^3
$Z = 4$
$F(000) = 1200$
$D_x = 1.489$ Mg m^{-3}
Mo *Kα* radiation, $\lambda = 0.71073$ Å
$\theta = 1.4$–26.0°
$\mu = 1.32$ mm^{-1}
$T = 150$ K
Needle, colourless
0.12 × 0.08 × 0.07 mm

Data collection

Stoe IPDS-2 diffractometer
Radiation source: fine-focus sealed tube
Graphite monochromator
ω scans
Absorption correction: numerical (*X-SHAPE* and *X-RED32*; Stoe, 2008)
$T_{min} = 0.879$, $T_{max} = 0.906$
8309 measured reflections
2570 independent reflections
1773 reflections with $I > 2\sigma(I)$
$R_{int} = 0.077$
$\theta_{max} = 26.0°$, $\theta_{min} = 1.4°$
$h = -35 \rightarrow 35$
$k = -6 \rightarrow 6$
$l = -22 \rightarrow 21$

Refinement

Refinement on F^2
Least-squares matrix: full
$R[F^2 > 2\sigma(F^2)] = 0.063$
$wR(F^2) = 0.148$
$S = 1.08$
2570 reflections
159 parameters
0 restraints
Primary atom site location: structure-invariant direct methods
Secondary atom site location: difference Fourier map
Hydrogen site location: inferred from neighbouring sites
H-atom parameters constrained
$w = 1/[\sigma^2(F_o^2) + (0.0577P)^2 + 3.849P]$ where $P = (F_o^2 + 2F_c^2)/3$
$(\Delta/\sigma)_{max} < 0.001$
$\Delta\rho_{max} = 0.68$ e Å^{-3}
$\Delta\rho_{min} = -0.46$ e Å^{-3}

Special details

Geometry. All esds (except the esd in the dihedral angle between two l.s. planes) are estimated using the full covariance matrix. The cell esds are taken into account individually in the estimation of esds in distances, angles and torsion angles; correlations between esds in cell parameters are only used when they are defined by crystal symmetry. An approximate (isotropic) treatment of cell esds is used for estimating esds involving l.s. planes.

Refinement. Refinement of F^2 against ALL reflections. The weighted R-factor wR and goodness of fit S are based on F^2, conventional R-factors R are based on F, with F set to zero for negative F^2. The threshold expression of $F^2 > 2\text{sigma}(F^2)$ is used only for calculating R-factors(gt) etc. and is not relevant to the choice of reflections for refinement. R-factors based on F^2 are statistically about twice as large as those based on F, and R- factors based on ALL data will be even larger.

Fractional atomic coordinates and isotropic or equivalent isotropic displacement parameters (Å²)

	x	*y*	*z*	U_{iso}*/U_{eq}
Zn1	0.0000	−0.30960 (18)	0.2500	0.0536 (3)
N1	0.03121 (14)	−0.4936 (9)	0.3362 (3)	0.0632 (11)
C1	0.04787 (16)	−0.6043 (11)	0.3893 (3)	0.0564 (12)
S1	0.07036 (5)	−0.7701 (3)	0.46152 (9)	0.0767 (5)
N11	0.04855 (12)	−0.0763 (8)	0.2133 (2)	0.0482 (9)
C11	0.04345 (16)	0.0091 (10)	0.1431 (3)	0.0547 (12)
H11	0.0185	−0.0612	0.1088	0.066*
C12	0.07260 (16)	0.1938 (10)	0.1181 (3)	0.0552 (11)
H12	0.0671	0.2525	0.0682	0.066*
C13	0.11000 (16)	0.2929 (10)	0.1667 (3)	0.0551 (12)
C14	0.11577 (16)	0.2014 (12)	0.2384 (3)	0.0591 (13)
H14	0.1411	0.2640	0.2731	0.071*
C15	0.08515 (16)	0.0205 (10)	0.2597 (3)	0.0561 (12)
H15	0.0899	−0.0395	0.3096	0.067*
C16	0.14365 (18)	0.4920 (11)	0.1412 (3)	0.0654 (14)
H16A	0.1505	0.6354	0.1786	0.078*
H16B	0.1289	0.5759	0.0944	0.078*
C17	0.18905 (16)	0.3592 (11)	0.1292 (3)	0.0600 (14)
C18	0.18905 (17)	0.1565 (13)	0.0792 (3)	0.0688 (15)
H18	0.1603	0.0952	0.0529	0.083*
C19	0.22994 (19)	0.0380 (15)	0.0660 (4)	0.0815 (18)
H19	0.2292	−0.1021	0.0307	0.098*
C20	0.27132 (18)	0.1235 (16)	0.1039 (4)	0.0776 (18)
C21	0.2727 (2)	0.3210 (18)	0.1536 (4)	0.093 (2)
H21	0.3017	0.3783	0.1800	0.112*
C22	0.2313 (2)	0.4443 (15)	0.1669 (4)	0.0854 (19)
H22	0.2324	0.5859	0.2018	0.103*
Cl1	0.32321 (5)	−0.0187 (5)	0.08551 (11)	0.1091 (8)

Atomic displacement parameters (Å²)

	U^{11}	U^{22}	U^{33}	U^{12}	U^{13}	U^{23}
Zn1	0.0483 (4)	0.0500 (5)	0.0615 (5)	0.000	0.0050 (3)	0.000
N1	0.058 (2)	0.057 (3)	0.074 (3)	0.006 (2)	0.008 (2)	0.004 (2)
C1	0.051 (2)	0.055 (3)	0.061 (3)	−0.003 (2)	0.003 (2)	−0.007 (3)
S1	0.0709 (8)	0.0855 (12)	0.0657 (9)	−0.0042 (7)	−0.0148 (7)	0.0094 (8)

N11	0.0429 (18)	0.050 (2)	0.050 (2)	0.0061 (17)	0.0016 (16)	−0.0037 (19)
C11	0.048 (2)	0.053 (3)	0.059 (3)	0.001 (2)	−0.004 (2)	−0.002 (2)
C12	0.053 (2)	0.051 (3)	0.058 (3)	−0.001 (2)	−0.004 (2)	0.004 (3)
C13	0.051 (2)	0.041 (3)	0.071 (3)	0.005 (2)	0.001 (2)	−0.006 (3)
C14	0.052 (2)	0.063 (3)	0.059 (3)	−0.002 (2)	−0.004 (2)	−0.007 (3)
C15	0.055 (3)	0.058 (3)	0.053 (3)	0.001 (2)	0.004 (2)	−0.005 (2)
C16	0.064 (3)	0.048 (3)	0.081 (4)	−0.007 (2)	0.003 (3)	−0.002 (3)
C17	0.050 (3)	0.061 (4)	0.066 (3)	−0.011 (2)	−0.003 (2)	0.014 (3)
C18	0.049 (3)	0.076 (4)	0.078 (4)	−0.008 (3)	−0.001 (2)	0.001 (3)
C19	0.061 (3)	0.103 (5)	0.080 (4)	0.009 (3)	0.008 (3)	0.000 (4)
C20	0.050 (3)	0.110 (5)	0.069 (4)	0.004 (3)	−0.001 (3)	0.027 (4)
C21	0.051 (3)	0.132 (6)	0.089 (5)	−0.024 (4)	−0.012 (3)	0.034 (5)
C22	0.066 (3)	0.091 (5)	0.093 (5)	−0.017 (3)	−0.006 (3)	−0.003 (4)
Cl1	0.0565 (8)	0.168 (2)	0.1023 (13)	0.0255 (10)	0.0118 (8)	0.0551 (14)

Geometric parameters (Å, º)

Zn1—N1^{i}	1.928 (5)	C15—H15	0.9500
Zn1—N1	1.928 (5)	C16—C17	1.524 (7)
Zn1—N11	2.024 (4)	C16—H16A	0.9900
Zn1—N11^{i}	2.024 (4)	C16—H16B	0.9900
N1—C1	1.157 (6)	C17—C18	1.363 (8)
C1—S1	1.611 (6)	C17—C22	1.380 (7)
N11—C11	1.342 (6)	C18—C19	1.383 (8)
N11—C15	1.346 (6)	C18—H18	0.9500
C11—C12	1.377 (7)	C19—C20	1.363 (8)
C11—H11	0.9500	C19—H19	0.9500
C12—C13	1.386 (7)	C20—C21	1.338 (10)
C12—H12	0.9500	C20—Cl1	1.747 (6)
C13—C14	1.375 (7)	C21—C22	1.408 (10)
C13—C16	1.518 (7)	C21—H21	0.9500
C14—C15	1.367 (7)	C22—H22	0.9500
C14—H14	0.9500		
N1^{i}—Zn1—N1	123.1 (3)	C14—C15—H15	118.6
N1^{i}—Zn1—N11	105.49 (17)	C13—C16—C17	112.0 (4)
N1—Zn1—N11	106.33 (16)	C13—C16—H16A	109.2
N1^{i}—Zn1—N11^{i}	106.32 (16)	C17—C16—H16A	109.2
N1—Zn1—N11^{i}	105.49 (17)	C13—C16—H16B	109.2
N11—Zn1—N11^{i}	109.7 (2)	C17—C16—H16B	109.2
C1—N1—Zn1	176.6 (4)	H16A—C16—H16B	107.9
N1—C1—S1	177.6 (5)	C18—C17—C22	118.2 (5)
C11—N11—C15	116.9 (4)	C18—C17—C16	120.6 (4)
C11—N11—Zn1	121.4 (3)	C22—C17—C16	121.2 (6)
C15—N11—Zn1	121.4 (3)	C17—C18—C19	121.6 (5)
N11—C11—C12	123.2 (4)	C17—C18—H18	119.2
N11—C11—H11	118.4	C19—C18—H18	119.2
C12—C11—H11	118.4	C20—C19—C18	119.5 (7)

C11—C12—C13	119.3 (5)	C20—C19—H19	120.2
C11—C12—H12	120.4	C18—C19—H19	120.2
C13—C12—H12	120.4	C21—C20—C19	120.6 (6)
C14—C13—C12	117.5 (5)	C21—C20—Cl1	119.6 (5)
C14—C13—C16	121.5 (5)	C19—C20—Cl1	119.7 (6)
C12—C13—C16	121.0 (5)	C20—C21—C22	120.2 (6)
C15—C14—C13	120.3 (5)	C20—C21—H21	119.9
C15—C14—H14	119.9	C22—C21—H21	119.9
C13—C14—H14	119.9	C17—C22—C21	119.9 (7)
N11—C15—C14	122.9 (5)	C17—C22—H22	120.1
N11—C15—H15	118.6	C21—C22—H22	120.1

Symmetry code: (i) $-x, y, -z+1/2$.

5.5. Crystal Structure of Catena-poly[[(3-tertbutylpyridine-κN)(4-tert-butylpyridineκN)cadmium]-di-μ-thiocyanato-κ2N:S;κ2S:N]

Julia Werner, Thorben Reinert, Inke Jess und Christian Näther, *Acta Crystallogr. E* **2014**, *E70*, m403-404.

DOI: 10.1107/S1600536814024647

CrossMark

data reports

Acta Cryst E STRUCTURE REPORTS

OPEN ACCESS

ISSN 1600-5368

Crystal structure of *catena*-poly[[(3-*tert*-butylpyridine-κN)(4-*tert*-butylpyridine-κN)cadmium]-di-μ-thiocyanato-$\kappa^2 N{:}S;\kappa^2 S{:}N$]

Julia Werner,[a]* Thorben Reinert,[b] Inke Jess[a] and Christian Näther[a]

[a]Institut für Anorganische Chemie, Christian-Albrechts-Universität Kiel, Max-Eyth-Strasse 2, 24118 Kiel, Germany, and [b]Institut für Physikalische Chemie, Christian-Albrechts-Universität Kiel, Max-Eyth-Strasse 1, 24118 Kiel, Germany. *Correspondence e-mail: jwerner@ac.uni-kiel.de

Received 25 October 2014; accepted 10 November 2014

Edited by S. Parkin, University of Kentucky, USA

In the crystal structure of the title compound, $[Cd(NCS)_2(C_9H_{13}N)_2]_n$, the Cd^{II} cations are coordinated in a slightly distorted octahedral geometry by one 3-*tert*-butylpyridine ligand, one 4-*tert*-butylpyridine ligand and two pairs of translationally-equivalent μ-1,3-bridging thiocyanate ligands, all of which are in general positions. These μ-1,3-bridging thiocyante anions bridge the Cd^{II} cations, forming chains that propagate parallel to the *b* axis.

Keywords: crystal structure; cadmium coordination polymer; μ-1,3-thiocyanate anions.

CCDC reference: 1033510

1. Related literature

For related crystal structures with μ-1,3-bridging thiocyanate anions, see: Banerjee *et al.* (2005); Reinert *et al.* (2012*a*,*b*); Tahli *et al.* (2011).

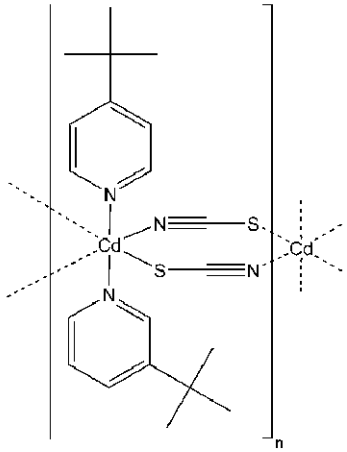

2. Experimental

2.1. Crystal data

$[Cd(NCS)_2(C_9H_{13}N)_2]$
M_r = 498.97
Monoclinic, $P2_1/c$
a = 20.0917 (8) Å
b = 5.9503 (2) Å
c = 21.0198 (9) Å
β = 115.902 (3)°
V = 2260.51 (15) Å^3
Z = 4
Mo $K\alpha$ radiation
μ = 1.16 mm^{-1}
T = 293 K
0.16 × 0.12 × 0.09 mm

2.2. Data collection

STOE IPDS-2 diffractometer
Absorption correction: numerical (*X-SHAPE* and *X-RED32*; Stoe & Cie, 2008)
T_{min} = 0.760, T_{max} = 0.895
25365 measured reflections
5407 independent reflections
4159 reflections with $I > 2\sigma(I)$
R_{int} = 0.044

2.3. Refinement

$R[F^2 > 2\sigma(F^2)]$ = 0.046
$wR(F^2)$ = 0.084
S = 1.14
5407 reflections
244 parameters
H-atom parameters constrained
$\Delta\rho_{max}$ = 0.41 e Å^{-3}
$\Delta\rho_{min}$ = −0.50 e Å^{-3}

Data collection: *X-AREA* (Stoe & Cie, 2008); cell refinement: *X-AREA*; data reduction: *X-AREA*; program(s) used to solve structure: *SHELXS97* (Sheldrick, 2008); program(s) used to refine structure: *SHELXL97* (Sheldrick, 2008); molecular graphics: *XP* in *SHELXTL* (Sheldrick, 2008) and *DIAMOND* (Brandenburg, 2011); software used to prepare material for publication: *publCIF* (Westrip, 2010).

Acknowledgements

We gratefully acknowledge financial support by the DFG (project No. NA 720/5–1) and the State of Schleswig–Holstein. We thank Professor Dr Wolfgang Bensch for access to his experimental facilities.

data reports

Supporting information for this paper is available from the IUCr electronic archives (Reference: PK2535).

References

Banerjee, S., Wu, B., Lassahn, P.-G., Janiak, C. & Ghosh, A. (2005). *Inorg. Chim. Acta*, **358**, 535–544.

Brandenburg, K. (2011). *DIAMOND*. Crystal Impact GbR, Bonn, Germany.

Reinert, T., Jess, I. & Näther, C. (2012*a*). *Acta Cryst.* E**68**, m1372.

Reinert, T., Jess, I. & Näther, C. (2012*b*). *Acta Cryst.* E**68**, m1333.

Sheldrick, G. M. (2008). *Acta Cryst.* A**64**, 112–122.

Stoe & Cie (2008). *X-AREA*, *X-RED32* and *X-SHAPE*. Stoe & Cie, Darmstadt, Germany.

Tahli, A., Maclaren, J. K., Boldog, I. & Janiak, C. (2011). *Inorg. Chim. Acta*, **374**, 506–513.

Westrip, S. P. (2010). *J. Appl. Cryst.* **43**, 920–925.

supporting information

Acta Cryst. (2014). E**70**, m403–m404 [doi:10.1107/S1600536814024647]

Crystal structure of *catena*-poly[[(3-*tert*-butylpyridine-κN)(4-*tert*-butylpyridine-κN)cadmium]-di-μ-thiocyanato-$\kappa^2 N$:S;$\kappa^2 S$:N]

Julia Werner, Thorben Reinert, Inke Jess and Christian Näther

S1. Structural commentary

S2. Synthesis and crystallization

$CdSO_4 \cdot 8/3H_2O$ was purchased from Merck, and 4-*tert*-butylpyridine and $Ba(NCS)_2 \cdot 3H_2O$ were purchased from Alfa Aesar. The 4-*tert*-butylpyridine has a purity of only 97% and is contaminated with 3-*tert*-butylpyridine, which cannot be separated. $Cd(NCS)_2$ was synthesized by stirring 17.5 g (57.00 mmol) $Ba(NCS)_2 \cdot 3H_2O$ and 14.6 g (57.00 mmol) $CdSO_4 \cdot 8/3H_2O$ in 300 mL H_2O at RT for three hours. The white residue of $BaSO_4$ was filtered off and the solvent was evaporated by heating. The homogeneity of the product was investigated by X-ray powder diffraction and elemental analysis. The title compound was prepared by the reaction of (0.15 mmol) 34.3 mg $Cd(NCS)_2$ and (0.15 mmol) 22.2 μL 4-tert-butylpyridine in 1.0 mL H_2O at 80 °C in a closed 10 mL glass culture tube. After several days, colorless crystalline blocks were obtained.

S3. Refinement

Carbon-bound H atoms were positioned with idealized geometry and refined with $U_{iso}(H) = 1.2\ U_{eq}(C)$ using a riding model with C—H = 0.95 Å for aromatic and C—H = 0.99 Å for methyl H atoms.

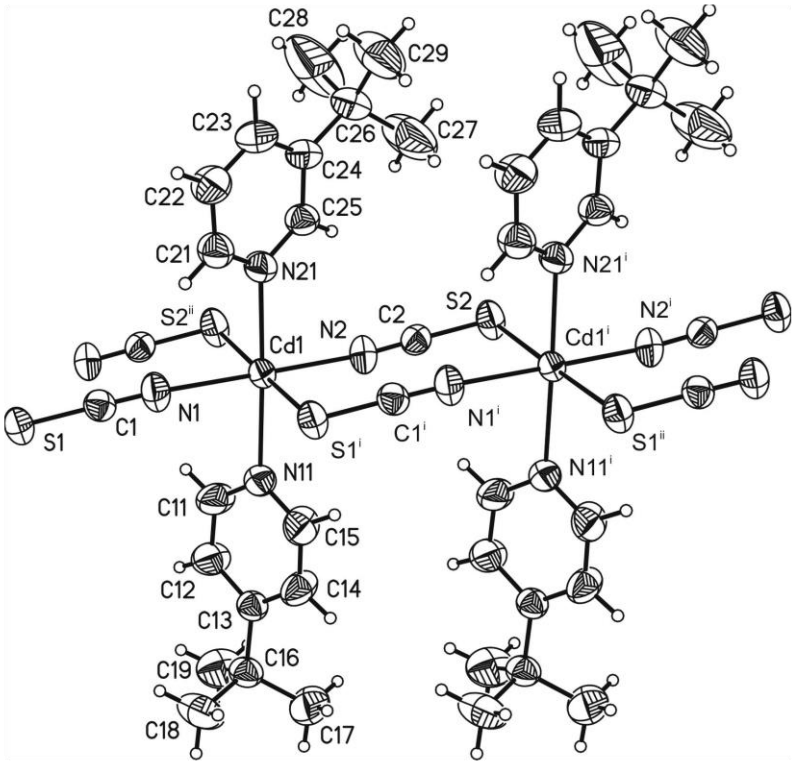

Figure 1

Crystal structure of the title compound. Displacement ellipsoids are drawn at the 50% probability level. Symmetry code: i: (x, y+1, z); ii: (x, y-1, z).

catena-Poly[[(3-*tert*-butylpyridine-κN)(4-*tert*-butylpyridine-κN)cadmium]-di-μ-thiocyanato-$\kappa^2 N$:S;$\kappa^2 S$:N]

Crystal data

$[Cd(NCS)_2(C_9H_{13}N)_2]$
$M_r = 498.97$
Monoclinic, $P2_1/c$
Hall symbol: -P 2ybc
$a = 20.0917\ (8)$ Å
$b = 5.9503\ (2)$ Å
$c = 21.0198\ (9)$ Å
$\beta = 115.902\ (3)°$
$V = 2260.51\ (15)$ Å^3
$Z = 4$
$F(000) = 1016$
$D_x = 1.466$ Mg m^{-3}
Mo $K\alpha$ radiation, $\lambda = 0.71073$ Å
Cell parameters from 25365 reflections
$\theta = 2.0–28.0°$
$\mu = 1.16$ mm^{-1}
$T = 293$ K
Block, colourless
0.16 × 0.12 × 0.09 mm

Data collection

STOE IPDS-2 diffractometer
Radiation source: fine-focus sealed tube
Graphite monochromator
ω scans
Absorption correction: numerical (*X-SHAPE* and *X-RED32*; Stoe & Cie, 2008)
$T_{min} = 0.760$, $T_{max} = 0.895$
25365 measured reflections
5407 independent reflections

4159 reflections with $I > 2\sigma(I)$
$R_{int} = 0.044$
$\theta_{max} = 28.0°$, $\theta_{min} = 2.0°$
$h = -26 \rightarrow 26$
$k = -7 \rightarrow 7$
$l = -27 \rightarrow 27$

Refinement

Refinement on F^2
Least-squares matrix: full
$R[F^2 > 2\sigma(F^2)] = 0.046$
$wR(F^2) = 0.084$
$S = 1.14$
5407 reflections
244 parameters
0 restraints
Primary atom site location: structure-invariant direct methods
Secondary atom site location: difference Fourier map
Hydrogen site location: inferred from neighbouring sites
H-atom parameters constrained
$w = 1/[\sigma^2(F_o^2) + (0.0326P)^2 + 0.8678P]$ where $P = (F_o^2 + 2F_c^2)/3$
$(\Delta/\sigma)_{max} = 0.001$
$\Delta\rho_{max} = 0.41$ e Å^{-3}
$\Delta\rho_{min} = -0.50$ e Å^{-3}

Special details

Geometry. All esds (except the esd in the dihedral angle between two l.s. planes) are estimated using the full covariance matrix. The cell esds are taken into account individually in the estimation of esds in distances, angles and torsion angles; correlations between esds in cell parameters are only used when they are defined by crystal symmetry. An approximate (isotropic) treatment of cell esds is used for estimating esds involving l.s. planes.

Refinement. Refinement of F^2 against ALL reflections. The weighted R-factor wR and goodness of fit S are based on F^2, conventional R-factors R are based on F, with F set to zero for negative F^2. The threshold expression of $F^2 > 2$sigma(F^2) is used only for calculating R-factors(gt) etc. and is not relevant to the choice of reflections for refinement. R-factors based on F^2 are statistically about twice as large as those based on F, and R- factors based on ALL data will be even larger.

Fractional atomic coordinates and isotropic or equivalent isotropic displacement parameters (Å^2)

	x	*y*	*z*	U_{iso}*/U_{eq}
Cd1	0.732991 (14)	0.24172 (4)	0.269228 (13)	0.04067 (8)
N1	0.67220 (19)	0.5638 (5)	0.20986 (17)	0.0535 (7)
C1	0.65872 (17)	0.7440 (6)	0.18809 (16)	0.0415 (6)
S1	0.63714 (5)	0.99805 (14)	0.15449 (5)	0.0484 (2)
N2	0.79392 (17)	−0.0756 (5)	0.32949 (17)	0.0514 (7)
C2	0.80555 (17)	−0.2557 (6)	0.35212 (16)	0.0421 (6)
S2	0.82427 (6)	−0.51157 (15)	0.38460 (5)	0.0554 (2)
N11	0.81232 (17)	0.2863 (5)	0.21360 (15)	0.0482 (7)
C11	0.8505 (3)	0.4716 (7)	0.2206 (2)	0.0724 (13)
H11	0.8473	0.5835	0.2501	0.087*
C12	0.8948 (3)	0.5105 (7)	0.1870 (2)	0.0713 (13)
H12	0.9209	0.6449	0.1950	0.086*
C13	0.9014 (2)	0.3547 (6)	0.14183 (19)	0.0443 (7)
C14	0.8606 (2)	0.1617 (7)	0.1342 (3)	0.0638 (11)
H14	0.8622	0.0474	0.1047	0.077*
C15	0.8174 (2)	0.1363 (7)	0.1698 (2)	0.0638 (11)
H15	0.7901	0.0047	0.1623	0.077*
C16	0.9479 (2)	0.3988 (7)	0.1019 (2)	0.0509 (8)
C17	0.9747 (3)	0.1778 (9)	0.0830 (3)	0.0847 (15)
H17A	1.0038	0.2105	0.0580	0.127*
H17B	0.9328	0.0882	0.0536	0.127*
H17C	1.0043	0.0967	0.1255	0.127*

C18	0.8990 (3)	0.5207 (10)	0.0334 (3)	0.0867 (16)
H18A	0.9269	0.5508	0.0072	0.130*
H18B	0.8821	0.6598	0.0444	0.130*
H18C	0.8571	0.4282	0.0056	0.130*
C19	1.0150 (3)	0.5424 (10)	0.1453 (3)	0.0862 (16)
H19A	1.0432	0.5674	0.1191	0.129*
H19B	1.0452	0.4664	0.1888	0.129*
H19C	0.9990	0.6840	0.1557	0.129*
N21	0.64660 (16)	0.2045 (5)	0.31532 (16)	0.0470 (7)
C21	0.5826 (2)	0.3142 (7)	0.2852 (2)	0.0546 (9)
H21	0.5733	0.4039	0.2459	0.066*
C22	0.5296 (2)	0.2999 (7)	0.3098 (2)	0.0629 (11)
H22	0.4855	0.3795	0.2879	0.076*
C23	0.5429 (2)	0.1660 (7)	0.3673 (2)	0.0573 (10)
H23	0.5075	0.1554	0.3846	0.069*
C24	0.60838 (19)	0.0467 (6)	0.39999 (18)	0.0454 (8)
C25	0.6582 (2)	0.0755 (6)	0.37141 (19)	0.0473 (8)
H25	0.7030	−0.0005	0.3928	0.057*
C26	0.6255 (2)	−0.0980 (7)	0.4648 (2)	0.0587 (10)
C27	0.6837 (4)	−0.2738 (12)	0.4745 (4)	0.133 (3)
H27A	0.6662	−0.3706	0.4339	0.200*
H27B	0.6933	−0.3611	0.5160	0.200*
H27C	0.7285	−0.2011	0.4797	0.200*
C28	0.6512 (6)	0.0518 (13)	0.5280 (3)	0.171 (4)
H28A	0.6627	−0.0373	0.5696	0.257*
H28B	0.6127	0.1569	0.5223	0.257*
H28C	0.6945	0.1319	0.5327	0.257*
C29	0.5577 (3)	−0.2282 (11)	0.4579 (4)	0.1055 (19)
H29A	0.5416	−0.3255	0.4175	0.158*
H29B	0.5188	−0.1249	0.4521	0.158*
H29C	0.5699	−0.3165	0.4997	0.158*

Atomic displacement parameters (Å²)

	U^{11}	U^{22}	U^{33}	U^{12}	U^{13}	U^{23}
Cd1	0.04773 (12)	0.03305 (11)	0.04745 (12)	0.00141 (12)	0.02654 (10)	0.00495 (11)
N1	0.064 (2)	0.0352 (15)	0.0566 (18)	0.0003 (14)	0.0216 (16)	0.0037 (14)
C1	0.0434 (15)	0.0405 (15)	0.0407 (15)	−0.0062 (17)	0.0185 (13)	−0.0032 (17)
S1	0.0550 (5)	0.0374 (4)	0.0470 (5)	0.0007 (4)	0.0167 (4)	0.0063 (4)
N2	0.0536 (18)	0.0355 (14)	0.0603 (19)	0.0036 (13)	0.0204 (15)	0.0053 (14)
C2	0.0422 (15)	0.0421 (16)	0.0425 (15)	−0.0014 (17)	0.0190 (13)	−0.0044 (17)
S2	0.0675 (6)	0.0385 (4)	0.0481 (5)	−0.0007 (4)	0.0141 (5)	0.0058 (4)
N11	0.0579 (17)	0.0447 (16)	0.0456 (15)	−0.0034 (14)	0.0260 (14)	−0.0023 (13)
C11	0.108 (4)	0.055 (2)	0.084 (3)	−0.028 (2)	0.070 (3)	−0.024 (2)
C12	0.097 (3)	0.057 (2)	0.086 (3)	−0.032 (2)	0.065 (3)	−0.021 (2)
C13	0.0418 (18)	0.0475 (18)	0.0463 (19)	0.0013 (15)	0.0218 (16)	0.0042 (15)
C14	0.069 (3)	0.055 (2)	0.090 (3)	−0.017 (2)	0.055 (3)	−0.023 (2)
C15	0.063 (2)	0.052 (2)	0.088 (3)	−0.017 (2)	0.044 (2)	−0.011 (2)

C16	0.048 (2)	0.059 (2)	0.053 (2)	0.0025 (17)	0.0279 (17)	0.0068 (17)
C17	0.087 (3)	0.081 (3)	0.115 (4)	0.013 (3)	0.071 (3)	0.004 (3)
C18	0.082 (3)	0.117 (4)	0.074 (3)	0.019 (3)	0.047 (3)	0.038 (3)
C19	0.064 (3)	0.111 (4)	0.097 (4)	−0.026 (3)	0.047 (3)	−0.013 (3)
N21	0.0460 (15)	0.0488 (17)	0.0530 (16)	0.0030 (13)	0.0278 (14)	0.0065 (13)
C21	0.052 (2)	0.060 (2)	0.054 (2)	0.0076 (17)	0.0246 (18)	0.0103 (17)
C22	0.046 (2)	0.074 (3)	0.071 (3)	0.0149 (19)	0.0288 (19)	0.013 (2)
C23	0.048 (2)	0.075 (2)	0.058 (2)	−0.0019 (19)	0.0309 (19)	−0.0028 (19)
C24	0.0450 (18)	0.055 (2)	0.0395 (17)	−0.0068 (16)	0.0220 (15)	−0.0049 (15)
C25	0.0436 (18)	0.054 (2)	0.0477 (19)	0.0038 (16)	0.0230 (16)	0.0046 (16)
C26	0.063 (2)	0.071 (3)	0.049 (2)	−0.007 (2)	0.0303 (19)	0.0052 (19)
C27	0.118 (5)	0.159 (7)	0.151 (6)	0.059 (5)	0.084 (5)	0.103 (5)
C28	0.323 (12)	0.124 (6)	0.047 (3)	−0.086 (7)	0.063 (5)	−0.013 (3)
C29	0.094 (4)	0.110 (5)	0.124 (5)	−0.012 (4)	0.058 (4)	0.038 (4)

Geometric parameters (Å, º)

Cd1—N2	2.305 (3)	C18—H18A	0.9600
Cd1—N1	2.322 (3)	C18—H18B	0.9600
Cd1—N21	2.339 (3)	C18—H18C	0.9600
Cd1—N11	2.368 (3)	C19—H19A	0.9600
Cd1—S2^{i}	2.7412 (10)	C19—H19B	0.9600
Cd1—S1^{ii}	2.7513 (10)	C19—H19C	0.9600
N1—C1	1.151 (4)	N21—C21	1.330 (5)
C1—S1	1.644 (4)	N21—C25	1.339 (4)
S1—Cd1^{i}	2.7513 (10)	C21—C22	1.375 (5)
N2—C2	1.154 (4)	C21—H21	0.9300
C2—S2	1.644 (4)	C22—C23	1.374 (6)
S2—Cd1^{ii}	2.7412 (10)	C22—H22	0.9300
N11—C11	1.314 (5)	C23—C24	1.385 (5)
N11—C15	1.319 (5)	C23—H23	0.9300
C11—C12	1.378 (5)	C24—C25	1.384 (4)
C11—H11	0.9300	C24—C26	1.518 (5)
C12—C13	1.373 (5)	C25—H25	0.9300
C12—H12	0.9300	C26—C28	1.492 (7)
C13—C14	1.379 (5)	C26—C27	1.514 (7)
C13—C16	1.527 (5)	C26—C29	1.518 (6)
C14—C15	1.379 (5)	C27—H27A	0.9600
C14—H14	0.9300	C27—H27B	0.9600
C15—H15	0.9300	C27—H27C	0.9600
C16—C19	1.519 (6)	C28—H28A	0.9600
C16—C18	1.525 (6)	C28—H28B	0.9600
C16—C17	1.537 (6)	C28—H28C	0.9600
C17—H17A	0.9600	C29—H29A	0.9600
C17—H17B	0.9600	C29—H29B	0.9600
C17—H17C	0.9600	C29—H29C	0.9600
N2—Cd1—N1	179.28 (11)	H18A—C18—H18B	109.5

N2—Cd1—N21	90.40 (11)	C16—C18—H18C	109.5
N1—Cd1—N21	89.39 (11)	H18A—C18—H18C	109.5
N2—Cd1—N11	93.03 (11)	H18B—C18—H18C	109.5
N1—Cd1—N11	87.23 (11)	C16—C19—H19A	109.5
N21—Cd1—N11	175.34 (11)	C16—C19—H19B	109.5
N2—Cd1—S2^{i}	87.88 (8)	H19A—C19—H19B	109.5
N1—Cd1—S2^{i}	91.43 (8)	C16—C19—H19C	109.5
N21—Cd1—S2^{i}	90.86 (8)	H19A—C19—H19C	109.5
N11—Cd1—S2^{i}	92.42 (8)	H19B—C19—H19C	109.5
N2—Cd1—S1^{ii}	92.89 (8)	C21—N21—C25	117.4 (3)
N1—Cd1—S1^{ii}	87.79 (8)	C21—N21—Cd1	119.6 (2)
N21—Cd1—S1^{ii}	87.21 (8)	C25—N21—Cd1	123.0 (2)
N11—Cd1—S1^{ii}	89.46 (8)	N21—C21—C22	122.5 (4)
S2^{i}—Cd1—S1^{ii}	177.92 (3)	N21—C21—H21	118.8
C1—N1—Cd1	163.7 (3)	C22—C21—H21	118.8
N1—C1—S1	178.0 (3)	C23—C22—C21	118.8 (4)
C1—S1—Cd1^{i}	98.96 (11)	C23—C22—H22	120.6
C2—N2—Cd1	161.9 (3)	C21—C22—H22	120.6
N2—C2—S2	178.6 (3)	C22—C23—C24	120.7 (3)
C2—S2—Cd1^{ii}	100.68 (11)	C22—C23—H23	119.6
C11—N11—C15	115.2 (3)	C24—C23—H23	119.6
C11—N11—Cd1	121.6 (2)	C25—C24—C23	115.6 (3)
C15—N11—Cd1	122.9 (2)	C25—C24—C26	122.4 (3)
N11—C11—C12	124.1 (4)	C23—C24—C26	122.0 (3)
N11—C11—H11	118.0	N21—C25—C24	124.9 (3)
C12—C11—H11	118.0	N21—C25—H25	117.5
C13—C12—C11	121.3 (4)	C24—C25—H25	117.5
C13—C12—H12	119.3	C28—C26—C27	110.3 (6)
C11—C12—H12	119.3	C28—C26—C24	108.3 (4)
C12—C13—C14	114.3 (3)	C27—C26—C24	111.8 (3)
C12—C13—C16	122.0 (3)	C28—C26—C29	109.6 (5)
C14—C13—C16	123.6 (3)	C27—C26—C29	105.6 (5)
C13—C14—C15	120.7 (4)	C24—C26—C29	111.2 (4)
C13—C14—H14	119.6	C26—C27—H27A	109.5
C15—C14—H14	119.6	C26—C27—H27B	109.5
N11—C15—C14	124.3 (4)	H27A—C27—H27B	109.5
N11—C15—H15	117.8	C26—C27—H27C	109.5
C14—C15—H15	117.8	H27A—C27—H27C	109.5
C19—C16—C18	109.7 (4)	H27B—C27—H27C	109.5
C19—C16—C13	111.2 (3)	C26—C28—H28A	109.5
C18—C16—C13	107.7 (3)	C26—C28—H28B	109.5
C19—C16—C17	108.5 (4)	H28A—C28—H28B	109.5
C18—C16—C17	108.5 (4)	C26—C28—H28C	109.5
C13—C16—C17	111.3 (3)	H28A—C28—H28C	109.5
C16—C17—H17A	109.5	H28B—C28—H28C	109.5
C16—C17—H17B	109.5	C26—C29—H29A	109.5
H17A—C17—H17B	109.5	C26—C29—H29B	109.5
C16—C17—H17C	109.5	H29A—C29—H29B	109.5

H17A—C17—H17C	109.5	C26—C29—H29C	109.5
H17B—C17—H17C	109.5	H29A—C29—H29C	109.5
C16—C18—H18A	109.5	H29B—C29—H29C	109.5
C16—C18—H18B	109.5		

Symmetry codes: (i) *x*, *y*+1, *z*; (ii) *x*, *y*−1, *z*.

5.6. Crystal Structure of Poly[[μ-4-(hydroxymethyl)pyridine-κ^2N:O][4-(hydroxymethyl)pyridine-κN](μ-thiocyanato-κ^2N:S)(thiocyanatoκN)cadmium][$Cd(NCS)_2(C_6H_7NO)_2$]

Julia Werner, Inke Jess und Christian Näther, *Acta Crystallogr. E* **2015**, *E71*, m129-m130.

DOI: 10.1107/S2056989015008890

CrossMark

data reports

Acta Cryst E CRYSTALLOGRAPHIC COMMUNICATIONS

OPEN ACCESS

ISSN 2056-9890

Crystal structure of poly[[μ-4-(hydroxymethyl)pyridine-κ^2N:O][4-(hydroxymethyl)pyridine-κN](μ-thiocyanato-κ^2N:S)(thiocyanato-κN)cadmium]

Julia Werner,* Inke Jess and Christian Näther

Institut für Anorganische Chemie, Christian-Albrechts-Universität Kiel, Max-Eyth-Strasse 2, 24118 Kiel, Germany. *Correspondence e-mail: jwerner@ac.uni-kiel.de

Received 4 May 2015; accepted 7 May 2015

Edited by M. Weil, Vienna University of Technology, Austria

The crystal structure of the title compound, $[Cd(NCS)_2(C_6H_7NO)_2]_n$ is made up of Cd^{2+} cations that are coordinated by three thiocyanate ligands and three 4-(hydroxymethyl)pyridine ligands within distorted N_4OS octahedra. The asymmetric unit consists of one Cd^{2+} cation, two thiocyanate anions and two 4-(hydroxymethyl)pyridine ligands in general positions. Two Cd^{2+} cations are linked by two μ-1,3 *N*- and *S*-bonding thiocyanate anions into dimers which are further linked into branched chains along [100] by two μ-1,6 *N*- and *O*-bonding 4-(hydroxymethyl)pyridine ligands. One additional *N*-bonded 4-(hydroxymethyl)pyridine ligand and one additional *N*-bonded thiocyanate anion are only terminally bonded to the metal cation. Interchain O—H···S hydrogen bonds between the hydroxy H atoms and one of the thiocyanate S atoms connect the chains into a three-dimensional network.

Keywords: crystal structure; coordination polymer; cadmium; octahedral coordination; hydrogen bonding.

CCDC reference: 1063786

1. Related literature

For similar structures with thiocyanate anions in bridging coordination to cadmium, see: Banerjee *et al.* (2005); Tahli *et al.* (2011).

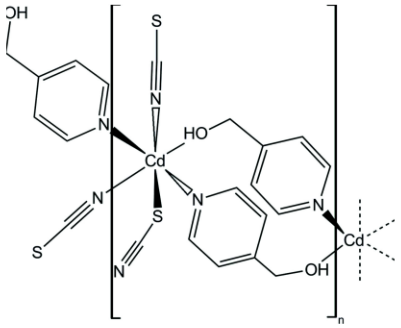

2. Experimental

2.1. Crystal data

$[Cd(NCS)_2(C_6H_7NO)_2]$
M_r = 446.81
Monoclinic, $P2_1/c$
a = 10.9124 (3) Å
b = 20.3261 (6) Å
c = 7.9722 (2) Å
β = 105.965 (2)°
V = 1700.08 (8) Å^3
Z = 4
Mo $K\alpha$ radiation
μ = 1.54 mm^{-1}
T = 200 K
0.47 × 0.33 × 0.20 mm

2.2. Data collection

Stoe IPDS-2 diffractometer
Absorption correction: numerical (*X-SHAPE* and *X-RED 32*; Stoe, 2008)
T_{min} = 0.526, T_{max} = 0.672
25370 measured reflections
3597 independent reflections
3259 reflections with $I > 2\sigma(I)$
R_{int} = 0.063

2.3. Refinement

$R[F^2 > 2\sigma(F^2)]$ = 0.025
$wR(F^2)$ = 0.058
S = 1.12
3597 reflections
245 parameters
H-atom parameters constrained
$\Delta\rho_{max}$ = 0.39 e Å^{-3}
$\Delta\rho_{min}$ = −0.44 e Å^{-3}

Table 1
Hydrogen-bond geometry (Å, °).

D—H···A	D—H	H···A	D···A	D—H···A
O11—H11O···S1^{i}	0.84	2.49	3.330 (2)	174
O21—H21O···S1^{ii}	0.84	2.42	3.2410 (18)	164

Symmetry codes: (i) $x-1, -y+\frac{3}{2}, z-\frac{1}{2}$; (ii) $-x+2, y-\frac{1}{2}, -z+\frac{3}{2}$.

Data collection: *X-AREA* (Stoe, 2008); cell refinement: *X-AREA*; data reduction: *X-AREA*; program(s) used to solve structure: *SHELXS97* (Sheldrick, 2008); program(s) used to refine structure: *SHELXL2013* (Sheldrick, 2015); molecular graphics: *XP* in *SHELXTL* (Sheldrick, 2008) and *DIAMOND* (Brandenburg, 1999); software used to prepare material for publication: *publCIF* (Westrip, 2010).

Acknowledgements

We gratefully acknowledge financial support by the State of Schleswig–Holstein. We thank Professor Dr Wolfgang Bensch for access to his experimental facilities.

Supporting information for this paper is available from the IUCr electronic archives (Reference: WM5156).

References

Banerjee, S., Wu, B., Lassahn, P.-G., Janiak, C. & Ghosh, A. (2005). *Inorg. Chim. Acta*, **358**, 535–544.
Brandenburg, K. (1999). *DIAMOND*. Crystal Impact GbR, Bonn, Germany.
Sheldrick, G. M. (2008). *Acta Cryst.* **A64**, 112–122.
Sheldrick, G. M. (2015). *Acta Cryst.* **C71**, 3–8.
Stoe (2008). *X-AREA*, *X-RED32* and *X-SHAPE*. Stoe & Cie, Darmstadt, Germany.
Tahli, A., Maclaren, J. K., Boldog, I. & Janiak, C. (2011). *Inorg. Chim. Acta*, **374**, 506–513.
Westrip, S. P. (2010). *J. Appl. Cryst.* **43**, 920–925.

supporting information

Acta Cryst. (2015). E**71**, m129–m130 [doi:10.1107/S2056989015008890]

Crystal structure of poly[[μ-4-(hydroxymethyl)pyridine-κ^2N:O][4-(hydroxymethyl)pyridine-κN](μ-thiocyanato-κ^2N:S)(thiocyanato-κN)cadmium]

Julia Werner, Inke Jess and Christian Näther

S1. Synthesis and crystallization

$CdSO_4 \cdot 3/8H_2O$ was purchased from Merck and 4-(hydroxymethyl)pyridine and $Ba(NCS)_2 \cdot 3H_2O$ were purchased from Alfa Aesar. $Cd(NCS)_2$ was synthesized by stirring 17.5 g (57.0 mmol) $Ba(NCS)_2 \cdot 3H_2O$ and 14.6 g (57.0 mmol) $CdSO_4 \cdot 3/8H_2O$ in 300 ml water at RT for three hours. The white residue of $BaSO_4$ was filtered off and dried at 353 K. The homogeneity of the product was checked by X-ray powder diffraction and elemental analysis. The title compound was prepared by the reaction of 34.3 mg (0.15 mmol) $Cd(NCS)_2$ and 32.7 mg (0.30 mmol) 4-(hydroxymethyl)pyridine in 1.5 ml methanol at RT. After one week suitable crystals of the title compound were obtained.

S2. Refinement

The carbon-bound hydrogen atoms were positioned with idealized geometry and were refined with $U_{iso}(H) = 1.2U_{eq}(C)$ using a riding model with C—H = 0.95 Å for aromatic and C—H = 0.99 Å for methylene H atoms. The oxygen-bound hydrogen atoms were located in a difference map. For the non-coordinating hydroxyl group the H atom was positioned with idealized geometry allowed to rotate but not to tip, and for the coordinating hydroxyl group its bond length was set to an ideal value of 0.84 Å. Finally, these H atoms were refined with $U_{iso}(H) = 1.5U_{eq}(O)$ using a riding model. The pyridine ring of one of the 4-(hydroxymethyl)pyridine ligands is disordered and was refined using a split model in two orientations with an occupancy ratio of 0.46:0.54.

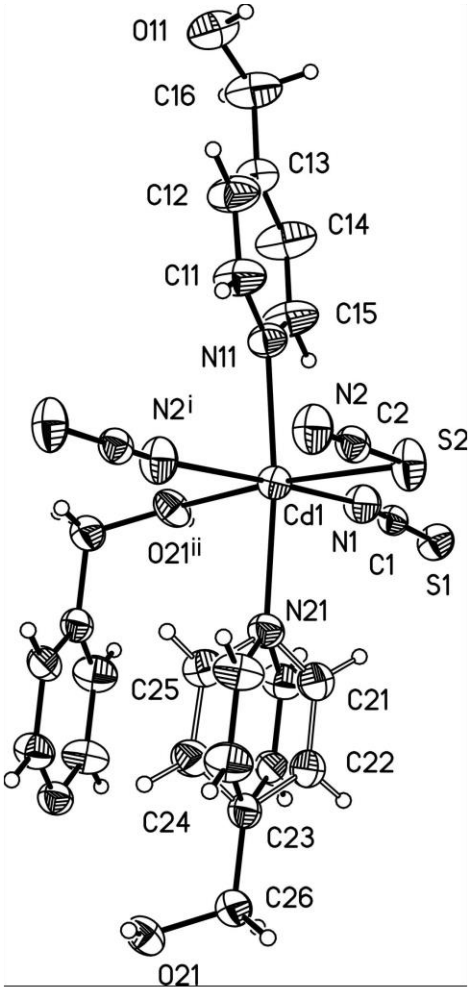

Figure 1

Part of the crystal structure of the title compound with labelling and displacement ellipsoids drawn at the 50% probability level. [Symmetry codes: (i) $-x+1, -y+1, -z+1$; (ii) $-x+2, -y+1, -z+1$.]

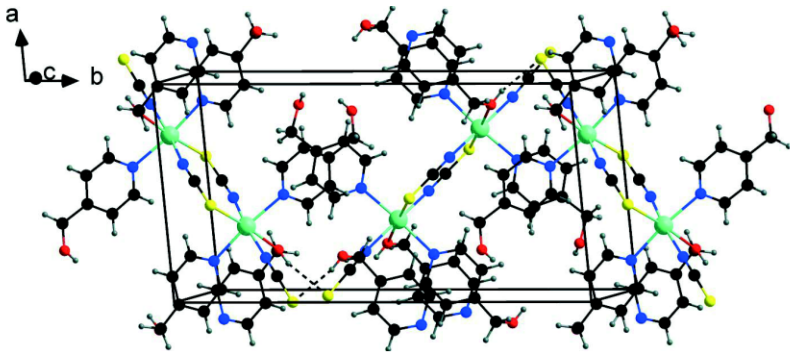

Figure 2

Crystal structure of the title compound in a view approximately along [001]. Intermolecular O—H···S hydrogen bonding is shown as dashed lines; the disordered pyridine rings are omitted for clarity.

Poly[[μ-4-(hydroxymethyl)pyridine-κ^2N:O][4-\ (hydroxymethyl)pyridine-κN](μ-thiocyanato-κ^2N:S)\ (thiocyanato-κN)cadmium]

Crystal data

$[Cd(NCS)_2(C_6H_7NO)_2]$
$M_r = 446.81$
Monoclinic, $P2_1/c$
$a = 10.9124$ (3) Å
$b = 20.3261$ (6) Å
$c = 7.9722$ (2) Å
$\beta = 105.965$ (2)°
$V = 1700.08$ (8) Å^3
$Z = 4$
$F(000) = 888$
$D_x = 1.746$ Mg m^{-3}
Mo $K\alpha$ radiation, $\lambda = 0.71073$ Å
$\theta = 1.9$–$26.7°$
$\mu = 1.54$ mm^{-1}
$T = 200$ K
Block, colorless
0.47 × 0.33 × 0.20 mm

Data collection

Stoe IPDS-2 diffractometer
ω scans
Absorption correction: numerical (*X-SHAPE* and *X-RED 32*; Stoe, 2008)
$T_{min} = 0.526$, $T_{max} = 0.672$
25370 measured reflections
3597 independent reflections
3259 reflections with $I > 2\sigma(I)$
$R_{int} = 0.063$
$\theta_{max} = 26.7°$, $\theta_{min} = 1.9°$
$h = -13 \rightarrow 13$
$k = -25 \rightarrow 25$
$l = -10 \rightarrow 10$

Refinement

Refinement on F^2
Least-squares matrix: full
$R[F^2 > 2\sigma(F^2)] = 0.025$
$wR(F^2) = 0.058$
$S = 1.12$
3597 reflections
245 parameters
0 restraints
Hydrogen site location: mixed
H-atom parameters constrained
$w = 1/[\sigma^2(F_o^2) + (0.0217P)^2 + 1.0598P]$ where $P = (F_o^2 + 2F_c^2)/3$
$(\Delta/\sigma)_{max} = 0.003$
$\Delta\rho_{max} = 0.39$ e Å^{-3}
$\Delta\rho_{min} = -0.44$ e Å^{-3}

Special details

Geometry. All esds (except the esd in the dihedral angle between two l.s. planes) are estimated using the full covariance matrix. The cell esds are taken into account individually in the estimation of esds in distances, angles and torsion angles; correlations between esds in cell parameters are only used when they are defined by crystal symmetry. An approximate (isotropic) treatment of cell esds is used for estimating esds involving l.s. planes.

Fractional atomic coordinates and isotropic or equivalent isotropic displacement parameters (Å²)

	x	*y*	*z*	U_{iso}*/U_{eq}	Occ. (<1)
Cd1	0.70099 (2)	0.59480 (2)	0.62587 (2)	0.02720 (6)	
N1	0.8330 (2)	0.65716 (10)	0.8375 (3)	0.0371 (5)	
C1	0.9127 (2)	0.68944 (11)	0.9253 (3)	0.0274 (5)	
S1	1.02442 (6)	0.73463 (3)	1.05226 (9)	0.03659 (15)	
N2	0.4160 (2)	0.45729 (11)	0.6240 (3)	0.0390 (5)	
C2	0.4891 (2)	0.49106 (11)	0.7172 (3)	0.0291 (5)	
S2	0.59224 (7)	0.53855 (3)	0.85273 (8)	0.04034 (16)	
N11	0.5601 (2)	0.68370 (10)	0.5577 (3)	0.0338 (5)	
C11	0.4387 (3)	0.67718 (14)	0.4676 (4)	0.0477 (7)	
H11	0.4082	0.6342	0.4318	0.057*	
C12	0.3544 (3)	0.72883 (15)	0.4229 (4)	0.0515 (8)	
H12	0.2685	0.7212	0.3582	0.062*	
C13	0.3958 (3)	0.79188 (13)	0.4729 (4)	0.0396 (6)	
C14	0.5211 (3)	0.79861 (14)	0.5691 (5)	0.0587 (9)	
H14	0.5536	0.8409	0.6090	0.070*	
C15	0.5992 (3)	0.74464 (13)	0.6074 (5)	0.0521 (8)	
H15	0.6855	0.7509	0.6726	0.062*	
C16	0.3100 (3)	0.85176 (15)	0.4315 (5)	0.0578 (9)	
H16A	0.2975	0.8690	0.5418	0.069*	
H16B	0.3538	0.8863	0.3821	0.069*	
O11	0.1919 (2)	0.84038 (11)	0.3164 (3)	0.0560 (6)	
H11O	0.1440	0.8225	0.3695	0.084*	
N21	0.8576 (2)	0.51330 (10)	0.6674 (3)	0.0331 (5)	
C21	0.9847 (8)	0.5311 (4)	0.7358 (11)	0.0369 (17)	0.46
H21	1.0044	0.5753	0.7720	0.044*	0.46
C22	1.0837 (8)	0.4867 (4)	0.7529 (10)	0.0371 (17)	0.46
H22	1.1695	0.5001	0.8019	0.045*	0.46
C23	1.0562 (2)	0.42284 (12)	0.6982 (3)	0.0315 (5)	
C24	0.9315 (9)	0.4061 (4)	0.6329 (12)	0.0421 (19)	0.46
H24	0.9090	0.3620	0.5981	0.050*	0.46
C25	0.8377 (10)	0.4528 (5)	0.6170 (13)	0.040 (2)	0.46
H25	0.7521	0.4396	0.5653	0.048*	0.46
C21′	0.9611 (8)	0.5162 (4)	0.7970 (9)	0.0456 (18)	0.54
H21′	0.9666	0.5494	0.8825	0.055*	0.54
C22′	1.0627 (8)	0.4740 (4)	0.8169 (9)	0.0435 (17)	0.54
H22′	1.1371	0.4797	0.9113	0.052*	0.54
C24′	0.9438 (7)	0.4180 (3)	0.5626 (9)	0.0372 (15)	0.54
H24′	0.9342	0.3840	0.4781	0.045*	0.54
C25′	0.8466 (9)	0.4627 (4)	0.5515 (10)	0.0365 (17)	0.54

H25′	0.7697	0.4581	0.4606	0.044*	0.54
C26	1.1645 (3)	0.37527 (14)	0.7161 (4)	0.0394 (6)	
H26A	1.2445	0.3965	0.7837	0.047*	
H26B	1.1497	0.3364	0.7828	0.047*	
O21	1.17960 (17)	0.35385 (8)	0.5527 (2)	0.0352 (4)	
H21O	1.1185	0.3283	0.5100	0.053*	

Atomic displacement parameters (Å²)

	U^{11}	U^{22}	U^{33}	U^{12}	U^{13}	U^{23}
Cd1	0.02612 (10)	0.02547 (9)	0.02941 (10)	−0.00284 (6)	0.00661 (7)	−0.00213 (6)
N1	0.0362 (12)	0.0363 (11)	0.0353 (11)	−0.0040 (10)	0.0041 (10)	−0.0081 (9)
C1	0.0310 (12)	0.0257 (10)	0.0268 (11)	0.0038 (9)	0.0101 (10)	0.0012 (9)
S1	0.0352 (3)	0.0342 (3)	0.0357 (3)	−0.0051 (3)	0.0018 (3)	−0.0052 (3)
N2	0.0413 (13)	0.0408 (11)	0.0337 (11)	−0.0132 (10)	0.0081 (10)	−0.0055 (9)
C2	0.0319 (13)	0.0285 (11)	0.0298 (12)	0.0006 (10)	0.0135 (10)	0.0028 (9)
S2	0.0436 (4)	0.0491 (4)	0.0293 (3)	−0.0211 (3)	0.0117 (3)	−0.0072 (3)
N11	0.0285 (11)	0.0324 (10)	0.0381 (11)	−0.0011 (8)	0.0052 (9)	−0.0008 (9)
C11	0.0339 (15)	0.0357 (14)	0.0641 (19)	0.0000 (11)	−0.0025 (13)	−0.0130 (13)
C12	0.0317 (15)	0.0474 (16)	0.064 (2)	0.0022 (12)	−0.0054 (14)	−0.0131 (14)
C13	0.0342 (14)	0.0353 (13)	0.0474 (15)	0.0020 (11)	0.0083 (12)	0.0023 (11)
C14	0.0390 (17)	0.0307 (13)	0.093 (3)	−0.0030 (12)	−0.0039 (17)	−0.0012 (15)
C15	0.0320 (15)	0.0327 (13)	0.080 (2)	−0.0039 (11)	−0.0046 (15)	−0.0001 (14)
C16	0.0403 (17)	0.0426 (16)	0.082 (2)	0.0062 (13)	0.0033 (16)	0.0040 (16)
O11	0.0403 (12)	0.0575 (13)	0.0648 (14)	0.0061 (10)	0.0053 (10)	0.0117 (11)
N21	0.0369 (12)	0.0297 (10)	0.0348 (11)	0.0041 (9)	0.0132 (9)	0.0021 (8)
C21	0.032 (4)	0.033 (3)	0.043 (5)	−0.002 (3)	0.005 (3)	−0.012 (3)
C22	0.031 (3)	0.048 (4)	0.032 (5)	0.006 (3)	0.008 (3)	−0.009 (3)
C23	0.0361 (13)	0.0318 (11)	0.0301 (12)	0.0034 (10)	0.0150 (10)	0.0053 (9)
C24	0.044 (4)	0.026 (3)	0.057 (6)	−0.002 (3)	0.014 (4)	−0.003 (4)
C25	0.029 (4)	0.029 (4)	0.063 (7)	−0.004 (3)	0.016 (5)	0.000 (4)
C21′	0.051 (5)	0.050 (4)	0.032 (4)	0.014 (3)	0.005 (3)	−0.009 (3)
C22′	0.044 (4)	0.052 (4)	0.028 (4)	0.012 (3)	0.001 (3)	−0.009 (3)
C24′	0.041 (3)	0.031 (3)	0.038 (4)	0.004 (2)	0.009 (3)	−0.005 (3)
C25′	0.035 (4)	0.031 (3)	0.041 (4)	−0.001 (3)	0.005 (3)	−0.003 (3)
C26	0.0435 (15)	0.0432 (14)	0.0353 (14)	0.0099 (12)	0.0170 (12)	0.0054 (11)
O21	0.0388 (10)	0.0305 (8)	0.0427 (10)	−0.0039 (7)	0.0217 (8)	−0.0027 (7)

Geometric parameters (Å, º)

Cd1—N1	2.279 (2)	N21—C25	1.294 (11)
Cd1—N2^{i}	2.306 (2)	N21—C21′	1.305 (8)
Cd1—N11	2.337 (2)	N21—C25′	1.366 (9)
Cd1—N21	2.337 (2)	N21—C21	1.392 (9)
Cd1—O21^{ii}	2.4153 (17)	C21—C22	1.385 (12)
Cd1—S2	2.6771 (7)	C21—H21	0.9500
N1—C1	1.158 (3)	C22—C23	1.376 (9)
C1—S1	1.636 (2)	C22—H22	0.9500

N2—C2	1.155 (3)	C23—C24	1.360 (9)
N2—Cd1^{i}	2.306 (2)	C23—C22′	1.395 (8)
C2—S2	1.643 (2)	C23—C24′	1.398 (8)
N11—C11	1.329 (3)	C23—C26	1.503 (4)
N11—C15	1.334 (3)	C24—C25	1.376 (14)
C11—C12	1.376 (4)	C24—H24	0.9500
C11—H11	0.9500	C25—H25	0.9500
C12—C13	1.381 (4)	C21′—C22′	1.376 (11)
C12—H12	0.9500	C21′—H21′	0.9500
C13—C14	1.379 (4)	C22′—H22′	0.9500
C13—C16	1.516 (4)	C24′—C25′	1.381 (12)
C14—C15	1.371 (4)	C24′—H24′	0.9500
C14—H14	0.9500	C25′—H25′	0.9500
C15—H15	0.9500	C26—O21	1.426 (3)
C16—O11	1.380 (4)	C26—H26A	0.9900
C16—H16A	0.9900	C26—H26B	0.9900
C16—H16B	0.9900	O21—Cd1^{ii}	2.4152 (17)
O11—H11O	0.8400	O21—H21O	0.8400
N1—Cd1—N2^{i}	169.07 (8)	C21′—N21—C25′	117.8 (5)
N1—Cd1—N11	89.06 (7)	C25—N21—C21	115.7 (6)
N2^{i}—Cd1—N11	88.96 (8)	C25—N21—Cd1	125.2 (5)
N1—Cd1—N21	90.03 (8)	C21′—N21—Cd1	121.3 (4)
N2^{i}—Cd1—N21	90.36 (8)	C25′—N21—Cd1	120.8 (4)
N11—Cd1—N21	171.60 (7)	C21—N21—Cd1	118.8 (4)
N1—Cd1—O21^{ii}	82.07 (7)	C22—C21—N21	122.3 (7)
N2^{i}—Cd1—O21^{ii}	87.11 (7)	C22—C21—H21	118.8
N11—Cd1—O21^{ii}	87.47 (7)	N21—C21—H21	118.8
N21—Cd1—O21^{ii}	84.13 (7)	C23—C22—C21	119.2 (7)
N1—Cd1—S2	92.58 (6)	C23—C22—H22	120.4
N2^{i}—Cd1—S2	98.31 (6)	C21—C22—H22	120.4
N11—Cd1—S2	95.85 (6)	C24—C23—C22	117.8 (5)
N21—Cd1—S2	92.54 (5)	C22′—C23—C24′	116.6 (5)
O21^{ii}—Cd1—S2	173.68 (5)	C24—C23—C26	123.6 (4)
C1—N1—Cd1	168.3 (2)	C22—C23—C26	118.7 (4)
N1—C1—S1	179.0 (2)	C22′—C23—C26	121.5 (4)
C2—N2—Cd1^{i}	161.6 (2)	C24′—C23—C26	121.9 (4)
N2—C2—S2	179.0 (2)	C23—C24—C25	120.2 (8)
C2—S2—Cd1	99.07 (9)	C23—C24—H24	119.9
C11—N11—C15	116.3 (2)	C25—C24—H24	119.9
C11—N11—Cd1	122.87 (17)	N21—C25—C24	124.8 (9)
C15—N11—Cd1	120.82 (17)	N21—C25—H25	117.6
N11—C11—C12	124.0 (3)	C24—C25—H25	117.6
N11—C11—H11	118.0	N21—C21′—C22′	123.9 (7)
C12—C11—H11	118.0	N21—C21′—H21′	118.1
C11—C12—C13	119.4 (3)	C22′—C21′—H21′	118.1
C11—C12—H12	120.3	C21′—C22′—C23	119.8 (6)
C13—C12—H12	120.3	C21′—C22′—H22′	120.1

C14—C13—C12	116.6 (3)	C23—C22′—H22′	120.1
C14—C13—C16	120.0 (3)	C25′—C24′—C23	119.9 (6)
C12—C13—C16	123.3 (3)	C25′—C24′—H24′	120.0
C15—C14—C13	120.4 (3)	C23—C24′—H24′	120.0
C15—C14—H14	119.8	N21—C25′—C24′	121.9 (7)
C13—C14—H14	119.8	N21—C25′—H25′	119.0
N11—C15—C14	123.2 (3)	C24′—C25′—H25′	119.0
N11—C15—H15	118.4	O21—C26—C23	113.3 (2)
C14—C15—H15	118.4	O21—C26—H26A	108.9
O11—C16—C13	114.7 (3)	C23—C26—H26A	108.9
O11—C16—H16A	108.6	O21—C26—H26B	108.9
C13—C16—H16A	108.6	C23—C26—H26B	108.9
O11—C16—H16B	108.6	H26A—C26—H26B	107.7
C13—C16—H16B	108.6	C26—O21—Cd1^{ii}	128.55 (16)
H16A—C16—H16B	107.6	C26—O21—H21O	106.3
C16—O11—H11O	109.5	Cd1^{ii}—O21—H21O	121.7

Symmetry codes: (i) −*x*+1, −*y*+1, −*z*+1; (ii) −*x*+2, −*y*+1, −*z*+1.

Hydrogen-bond geometry (Å, °)

D—H···*A*	*D*—H	H···*A*	*D*···*A*	*D*—H···*A*
O11—H11*O*···S1^{iii}	0.84	2.49	3.330 (2)	174
O21—H21*O*···S1^{iv}	0.84	2.42	3.2410 (18)	164

Symmetry codes: (iii) *x*−1, −*y*+3/2, *z*−1/2; (iv) −*x*+2, *y*−1/2, −*z*+3/2.

6. Weitere Arbeiten

6.1. Poly[(*μ*-1,3-thiocyanato-κ*N*,*S*)(isonicotinato-κ*N*,*O*)(ethanol-κ*O*)-cadmium(II)]

Tristan Neumann, Julia Werner, Inke Jess und Christian Näther, *Acta Crystallogr. E* **2012**, *E68*, m1338.

DOI: 10.1107/S1600536812040913

Motivation

Die folgenden drei Verbindungen entstanden im Zuge systematischer Untersuchungen, konnten jedoch nicht im größeren Maßstab hergestellt werden oder wurden nur als Nebenprodukt erhalten. Da diese Verbindungen keinen direkten Bezug zu der Fragestellung dieser Arbeit haben, wurden die erhaltenen Kristalle mittels Einkristallstrukturanalyse charakterisiert und als Strukturmitteilung veröffentlicht.

metal-organic compounds

Acta Crystallographica Section E
Structure Reports Online
ISSN 1600-5368

Poly[(μ-1,3-thiocyanato-κN,S)(isonicotinato-κN,O)(ethanol-κO)-cadmium(II)]

Tristan Neumann, Julia Werner, Inke Jess and Christian Näther*

Institut für Anorganische Chemie, Christian-Albrechts-Universität Kiel, Max-Eyth-Strasse 2, 24118 Kiel, Germany
Correspondence e-mail: cnaether@ac.uni-kiel.de

Received 12 September 2012; accepted 28 September 2012

Key indicators: single-crystal X-ray study; T = 293 K; mean σ(C–C) = 0.004 Å; R factor = 0.026; wR factor = 0.061; data-to-parameter ratio = 20.1.

In the crystal structure of the title compound, $[Cd(NCS)(C_6H_4NO_2)(C_2H_5OH)]_n$, the Cd^{2+} cation is coordinated by one N and two O atoms of two symmetry-related isonicotinate anions, one ethanol molecule and two μ-1,3-bridging thiocyanate anions in a distorted octahedral N_2O_3S geometry. The metal cations are μ-1,3-bridged *via* thiocyanate anions into chains that are further connected into layers parallel to the *ab* plane by bridging isonicotinate anions. The layers are stacked along the *c* axis. The crystal structure is stabilized by O—H···O hydrogen bonds.

Related literature

For general background information, including details of thermal decomposition reactions and magnetic properties, see: Näther & Greve (2003); Boeckmann & Näther (2010, 2011); Wöhlert *et al.* (2011). For related structures, see: Yang *et al.* (2001). For a description of the Cambridge Structural Database, see: Allen (2002).

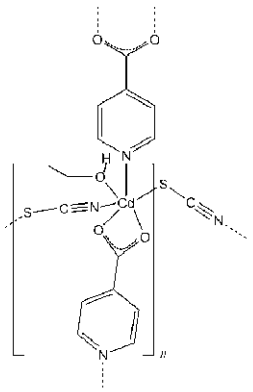

Experimental

Crystal data

$[Cd(NCS)(C_6H_4NO_2)(C_2H_6O)]$
M_r = 338.65
Monoclinic, $P2_1/c$
a = 5.7778 (2) Å
b = 16.1804 (6) Å
c = 13.0855 (6) Å
β = 94.685 (3)°
V = 1219.24 (8) Å^3
Z = 4
Mo $K\alpha$ radiation
μ = 1.96 mm^{-1}
T = 293 K
0.28 × 0.10 × 0.04 mm

Data collection

Stoe IPDS-1 diffractometer
Absorption correction: numerical (*X-SHAPE* and *X-RED32*; Stoe, 2008)
T_{min} = 0.803, T_{max} = 0.931
17537 measured reflections
2920 independent reflections
2545 reflections with $I > 2\sigma(I)$
R_{int} = 0.032

Refinement

$R[F^2 > 2\sigma(F^2)]$ = 0.026
$wR(F^2)$ = 0.061
S = 1.06
2920 reflections
145 parameters
H-atom parameters constrained
$\Delta\rho_{max}$ = 0.38 e Å^{-3}
$\Delta\rho_{min}$ = −0.44 e Å^{-3}

Table 1
Hydrogen-bond geometry (Å, °).

D—H···A	D—H	H···A	D···A	D—H···A
O21—H1*O*1···O12^{i}	0.82	1.89	2.703 (3)	172

Symmetry code: (i) $x-1, y, z$.

Data collection: *X-AREA* (Stoe, 2008); cell refinement: *X-AREA*; data reduction: *X-AREA*; program(s) used to solve structure: *SHELXS97* (Sheldrick, 2008); program(s) used to refine structure: *SHELXL97* (Sheldrick, 2008); molecular graphics: *XP* in *SHELXTL* (Sheldrick, 2008) and *DIAMOND* (Brandenburg, 2011); software used to prepare material for publication: *publCIF* (Westrip, 2010).

The authors gratefully acknowledge financial support from the DFG (project No. NA720/3-1) and the State of Schleswig–Holstein. We thank Professor Dr Wolfgang Bensch for access to his experimental facilities.

Supplementary data and figures for this paper are available from the IUCr electronic archives (Reference: BT6838).

References

Allen, F. H. (2002). *Acta Cryst.* B**58**, 380–388.
Boeckmann, J. & Näther, C. (2010). *Dalton Trans.* **39**, 11019–11026.
Boeckmann, J. & Näther, C. (2011). *Chem. Commun.* **47**, 7104–7106.
Brandenburg, K. (2011). *DIAMOND*. Crystal Impact GbR, Bonn, Germany.
Näther, C. & Greve, J. (2003). *J. Solid State Chem.*, **176**, 259–265.
Sheldrick, G. M. (2008). *Acta Cryst.* A**64**, 112–122.
Stoe (2008). *X-AREA*, *X-RED32* and *X-SHAPE*. Stoe & Cie, Darmstadt, Germany.
Westrip, S. P. (2010). *J. Appl. Cryst.* **43**, 920–925.
Wöhlert, S., Boeckmann, J., Wriedt, M. & Näther, C. (2011). *Angew. Chem. Int. Ed.* **50**, 6920–6923.
Yang, G., Zhu, H. G., Liang, B.-H. & Chen, X. M. (2001). *Dalton Trans.* pp. 580–585.

supplementary materials

Acta Cryst. (2012). E**68**, m1338 [doi:10.1107/S1600536812040913]

Poly[(*μ*-1,3-thiocyanato-*κN*,*S*)(isonicotinato-*κN*,*O*)(ethanol-*κO*)cadmium(II)]

Tristan Neumann, Julia Werner, Inke Jess and Christian Näther

Comment

The structure of the title compound was prepared within a project on the synthesis of transition metal thiocyanato coordination polymers in which the metal cations are *μ*-1,3 bridged by the anionic ligands (Näther & Greve, 2003; Boeckmann & Näther, 2010, 2011; Wöhlert *et al.*, 2011). In the course of our investigations crystals of the title compound were obtained and characterized by single-crystal X-ray diffraction.

In the crystal structure the cadmium(II) cations are coordinated by one N and two O atoms of two *μ*-1,3,6 bridging isonicotinato anions which are related by symmetry, one N and one S atom of two symmetry-related *μ*-1,3 bridging thiocyanato anions and one O atom of an ethanol molecule (Fig. 1). The coordination polyhedron of the cadmium cations can be described as a slightly distorted octahedron (Table 1).

The Cd^{2+} cations are *μ*-1,3 bridged by thiocyanato anions into chains, which elongate in the direction of the crystallographic *a* axis. These chains are bridged by *μ*-1,3,6 bridging isonicotinato anions into layers in the direction of the crystallographic *b* axis and the layers are stacked along the crystallographic *c* axis (Fig. 2).

The shortest Cd···Cd distances within the layers amounts to 5.7778 (3) Å and to 9.2393 (4) Å. It must be noted that according to research in the CCDC database (ConQuest Ver.1.14; Allen, 2002) one coordination compound based on $Cd(NCS)_2$, isonicotinato anions and thiocyanato anions is known, in which ethanol is exchanged by water. The overall coordination topology is similar but this compound is not isotypic to the title compound (Yang *et al.*, 2001).

The crystal structure is stabilized by an O—H···O hydrogen bond.

Experimental

Potassium thiocyanate and isonicotinic acid were purchased from Alfa Aesar, $Cd(SO_4)_2.4H_2O$ was obtained from Merck. The $Cd(NCS)_2$ was prepared by stirring $Ba(NCS)_2.3H_2O$ (3.076 g, 10 mmol) and $CdSO_4.8/3H_2O$ (2.566 g, 10 mmol) in water (100 ml). The white precipitate of $BaSO_4$ was filtered off and the water was removed from the filtrate by heating. The final product was dried at 80°C. The homogeneity of the product was investigated by X-ray powder diffraction. The title compound was prepared by the reaction of 34.3 mg $Cd(NCS)_2$(0.15 mmol) and 36.9 mg isonicotinic acid (0.30 mmol) in 2 ml ethanol at 80°C in a closed 10 ml glass culture tube. After several days colourless needles of the title compound were obtained.

Refinement

The C—H H atoms were positioned with idealized geometry (methyl H atoms allowed to rotate but not to tip) and were refined isotropically with U_{iso}(H) = 1.2U_{eq}(C) for aromatic H atoms (1.5 for methyl H atoms) using a riding model with C—H = 0.93 Å (aromatic H atoms) and with C—H = 0.96 Å (methyl H atoms). The O—H H atom was located in difference map, its bond length set to ideal value of 0.82 Å and finally it was refined using a riding model with U_{iso}(H) = 1.2U_{eq}(O).

Computing details

Data collection: *X-AREA* (Stoe, 2008); cell refinement: *X-AREA* (Stoe, 2008); data reduction: *X-AREA* (Stoe, 2008); program(s) used to solve structure: *SHELXS97* (Sheldrick, 2008); program(s) used to refine structure: *SHELXL97* (Sheldrick, 2008); molecular graphics: *XP* in *SHELXTL* (Sheldrick, 2008) and *DIAMOND* (Brandenburg, 2011); software used to prepare material for publication: *publCIF* (Westrip, 2010).

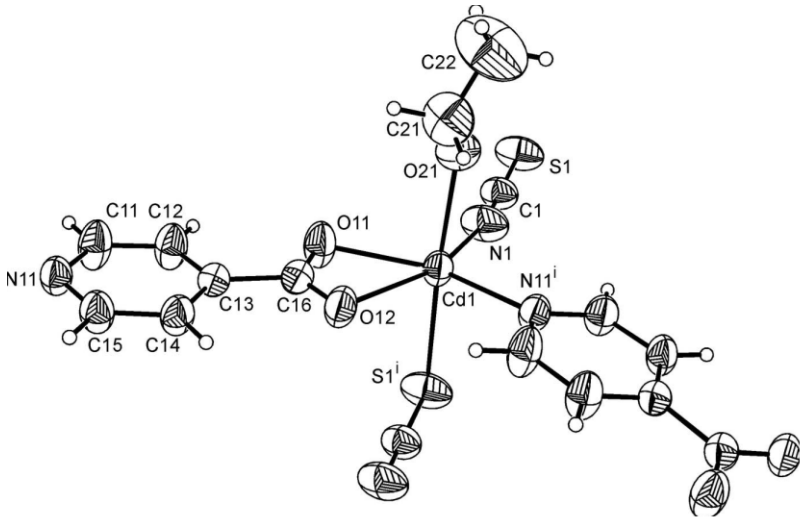

Figure 1

Crystal structure of the title compound with labelling and displacement ellipsoids drawn at the 50% probability level. Symmetry code: i = -x + 1, y + 1/2, -z + 3/2.

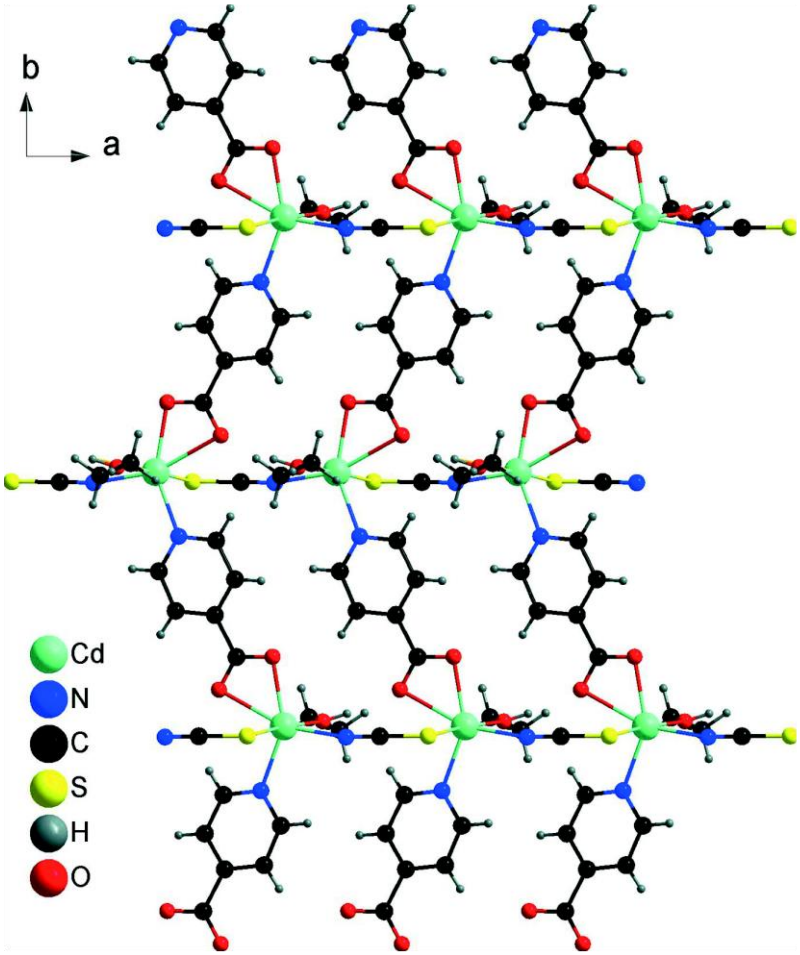

Figure 2

Crystal structure of the title compound with view in the direction of the crystallographic *c* axis.

Poly[(μ-1,3-thiocyanato-κ*N*,*S*)(isonicotinato- κ*N*,*O*)(ethanol-κ*O*)cadmium(II)]

Crystal data

[Cd(NCS)($C_6H_4NO_2$)(C_2H_6O)]	$F(000) = 664$
$M_r = 338.65$	$D_x = 1.845$ Mg m^{-3}
Monoclinic, $P2_1/c$	Mo $K\alpha$ radiation, $\lambda = 0.71073$ Å
$a = 5.7778$ (2) Å	Cell parameters from 17537 reflections
$b = 16.1804$ (6) Å	$\theta = 2.0$–$28.0°$
$c = 13.0855$ (6) Å	$\mu = 1.96$ mm^{-1}
$\beta = 94.685$ (3)°	$T = 293$ K
$V = 1219.24$ (8) Å^3	Needle, colourless
$Z = 4$	0.28 × 0.10 × 0.04 mm

Data collection

Stoe IPDS-1 diffractometer
Radiation source: fine-focus sealed tube
Graphite monochromator
φ scans
Absorption correction: numerical (*X-SHAPE* and *X-RED32*; Stoe, 2008)
T_{min} = 0.803, T_{max} = 0.931

17537 measured reflections
2920 independent reflections
2545 reflections with $I > 2\sigma(I)$
R_{int} = 0.032
θ_{max} = 28.0°, θ_{min} = 2.0°
h = −7→7
k = −21→21
l = −17→17

Refinement

Refinement on F^2
Least-squares matrix: full
$R[F^2 > 2\sigma(F^2)]$ = 0.026
$wR(F^2)$ = 0.061
S = 1.06
2920 reflections
145 parameters
0 restraints
Primary atom site location: structure-invariant direct methods

Secondary atom site location: difference Fourier map
Hydrogen site location: inferred from neighbouring sites
H-atom parameters constrained
$w = 1/[\sigma^2(F_o^2) + (0.0288P)^2 + 0.6822P]$ where $P = (F_o^2 + 2F_c^2)/3$
$(\Delta/\sigma)_{max}$ = 0.001
$\Delta\rho_{max}$ = 0.38 e Å^{-3}
$\Delta\rho_{min}$ = −0.44 e Å^{-3}

Special details

Geometry. All esds (except the esd in the dihedral angle between two l.s. planes) are estimated using the full covariance matrix. The cell esds are taken into account individually in the estimation of esds in distances, angles and torsion angles; correlations between esds in cell parameters are only used when they are defined by crystal symmetry. An approximate (isotropic) treatment of cell esds is used for estimating esds involving l.s. planes.

Refinement. Refinement of F^2 against ALL reflections. The weighted R-factor wR and goodness of fit S are based on F^2, conventional R-factors R are based on F, with F set to zero for negative F^2. The threshold expression of $F^2 > 2\text{sigma}(F^2)$ is used only for calculating R-factors(gt) etc. and is not relevant to the choice of reflections for refinement. R-factors based on F^2 are statistically about twice as large as those based on F, and R- factors based on ALL data will be even larger.

Fractional atomic coordinates and isotropic or equivalent isotropic displacement parameters (Å²)

	x	*y*	*z*	U_{iso}*/U_{eq}
Cd1	0.14587 (3)	0.856111 (10)	0.668028 (15)	0.04089 (7)
N1	−0.1966 (4)	0.8771 (2)	0.5822 (2)	0.0667 (8)
C1	−0.3839 (5)	0.87582 (19)	0.5463 (2)	0.0492 (6)
S1	−0.65079 (13)	0.87510 (7)	0.49397 (6)	0.0662 (2)
N11	0.7272 (4)	0.48256 (13)	0.77586 (18)	0.0432 (5)
C11	0.5200 (6)	0.49095 (17)	0.7245 (3)	0.0578 (8)
H11	0.4417	0.4437	0.7005	0.069*
C12	0.4168 (5)	0.56691 (17)	0.7052 (2)	0.0540 (7)
H12	0.2722	0.5702	0.6687	0.065*
C13	0.5275 (4)	0.63720 (15)	0.7401 (2)	0.0396 (5)
C14	0.7445 (5)	0.62913 (15)	0.7913 (2)	0.0480 (6)
H14	0.8275	0.6757	0.8145	0.058*
C15	0.8372 (5)	0.55133 (16)	0.8077 (2)	0.0490 (6)
H15	0.9834	0.5466	0.8426	0.059*
C16	0.4083 (5)	0.71974 (15)	0.7252 (2)	0.0426 (5)
O11	0.2091 (4)	0.71926 (12)	0.67857 (18)	0.0592 (5)
O12	0.5052 (3)	0.78408 (11)	0.75867 (17)	0.0510 (5)

O21	−0.0682 (4)	0.84635 (14)	0.81279 (16)	0.0572 (5)
H1O1	−0.2025	0.8310	0.7996	0.086*
C21	0.0069 (7)	0.8386 (3)	0.9186 (3)	0.0778 (11)
H21A	0.1454	0.8720	0.9327	0.093*
H21B	0.0497	0.7815	0.9324	0.093*
C22	−0.1619 (11)	0.8630 (4)	0.9880 (4)	0.129 (2)
H22A	−0.0982	0.8552	1.0574	0.193*
H22B	−0.2990	0.8298	0.9757	0.193*
H22C	−0.2010	0.9201	0.9771	0.193*

Atomic displacement parameters (Å²)

	U^{11}	U^{22}	U^{33}	U^{12}	U^{13}	U^{23}
Cd1	0.03291 (10)	0.03170 (10)	0.05680 (12)	−0.00051 (7)	−0.00408 (7)	0.00070 (8)
N1	0.0336 (12)	0.098 (2)	0.0675 (16)	0.0051 (13)	−0.0028 (11)	0.0164 (15)
C1	0.0382 (14)	0.0617 (17)	0.0476 (14)	0.0037 (12)	0.0028 (11)	0.0077 (12)
S1	0.0357 (3)	0.1101 (7)	0.0514 (4)	−0.0010 (4)	−0.0046 (3)	0.0062 (4)
N11	0.0401 (11)	0.0317 (10)	0.0569 (13)	0.0011 (8)	−0.0020 (10)	−0.0014 (9)
C11	0.0541 (17)	0.0349 (13)	0.080 (2)	−0.0018 (12)	−0.0226 (16)	−0.0042 (13)
C12	0.0452 (15)	0.0390 (13)	0.0739 (19)	0.0016 (12)	−0.0192 (14)	0.0019 (13)
C13	0.0386 (12)	0.0341 (11)	0.0466 (13)	0.0009 (10)	0.0053 (10)	0.0031 (10)
C14	0.0381 (13)	0.0320 (12)	0.0724 (18)	−0.0039 (10)	−0.0043 (12)	−0.0003 (11)
C15	0.0381 (13)	0.0376 (13)	0.0692 (18)	0.0013 (10)	−0.0074 (13)	−0.0007 (12)
C16	0.0408 (13)	0.0357 (12)	0.0517 (14)	0.0007 (10)	0.0052 (11)	0.0057 (11)
O11	0.0486 (11)	0.0379 (10)	0.0880 (15)	0.0055 (9)	−0.0130 (11)	0.0024 (10)
O12	0.0483 (11)	0.0317 (9)	0.0721 (13)	0.0001 (8)	−0.0004 (9)	0.0024 (8)
O21	0.0479 (11)	0.0665 (14)	0.0564 (12)	−0.0085 (10)	−0.0011 (9)	0.0004 (10)
C21	0.072 (2)	0.092 (3)	0.066 (2)	0.011 (2)	−0.0128 (18)	0.0078 (19)
C22	0.125 (5)	0.201 (7)	0.059 (2)	0.049 (4)	−0.002 (3)	0.000 (3)

Geometric parameters (Å, º)

Cd1—N1	2.220 (3)	C12—H12	0.9300
Cd1—O11	2.247 (2)	C13—C14	1.379 (4)
Cd1—N11^{i}	2.275 (2)	C13—C16	1.508 (3)
Cd1—O21	2.351 (2)	C14—C15	1.378 (4)
Cd1—O12	2.583 (2)	C14—H14	0.9300
Cd1—S1^{ii}	2.6644 (9)	C15—H15	0.9300
Cd1—C16	2.746 (3)	C16—O12	1.245 (3)
N1—C1	1.144 (4)	C16—O11	1.258 (3)
C1—S1	1.635 (3)	O21—C21	1.422 (4)
S1—Cd1^{iii}	2.6644 (9)	O21—H1O1	0.8199
N11—C11	1.331 (4)	C21—C22	1.441 (7)
N11—C15	1.331 (3)	C21—H21A	0.9700
N11—Cd1^{iv}	2.275 (2)	C21—H21B	0.9700
C11—C12	1.380 (4)	C22—H22A	0.9600
C11—H11	0.9300	C22—H22B	0.9600
C12—C13	1.365 (4)	C22—H22C	0.9600
N1—Cd1—O11	108.39 (10)	C12—C13—C14	117.8 (2)

N1—Cd1—N11^{i}	106.05 (11)	C12—C13—C16	119.9 (2)
O11—Cd1—N11^{i}	145.09 (8)	C14—C13—C16	122.3 (2)
N1—Cd1—O21	84.95 (9)	C15—C14—C13	119.2 (2)
O11—Cd1—O21	88.73 (8)	C15—C14—H14	120.4
N11^{i}—Cd1—O21	88.70 (8)	C13—C14—H14	120.4
N1—Cd1—O12	161.97 (10)	N11—C15—C14	123.0 (2)
O11—Cd1—O12	53.60 (7)	N11—C15—H15	118.5
N11^{i}—Cd1—O12	91.82 (7)	C14—C15—H15	118.5
O21—Cd1—O12	93.19 (7)	O12—C16—O11	122.9 (2)
N1—Cd1—S1^{ii}	89.26 (8)	O12—C16—C13	120.5 (2)
O11—Cd1—S1^{ii}	94.89 (7)	O11—C16—C13	116.6 (2)
N11^{i}—Cd1—S1^{ii}	91.09 (6)	O12—C16—Cd1	69.29 (14)
O21—Cd1—S1^{ii}	173.91 (6)	O11—C16—Cd1	53.83 (13)
O12—Cd1—S1^{ii}	92.90 (5)	C13—C16—Cd1	169.39 (19)
N1—Cd1—C16	135.24 (11)	C16—O11—Cd1	99.30 (16)
O11—Cd1—C16	26.87 (8)	C16—O12—Cd1	83.93 (15)
N11^{i}—Cd1—C16	118.58 (8)	C21—O21—Cd1	130.7 (2)
O21—Cd1—C16	92.37 (8)	C21—O21—H1O1	112.8
O12—Cd1—C16	26.78 (7)	Cd1—O21—H1O1	113.7
S1^{ii}—Cd1—C16	93.06 (6)	O21—C21—C22	114.9 (3)
C1—N1—Cd1	168.3 (3)	O21—C21—H21A	108.5
N1—C1—S1	179.2 (3)	C22—C21—H21A	108.5
C1—S1—Cd1^{iii}	96.29 (10)	O21—C21—H21B	108.5
C11—N11—C15	117.4 (2)	C22—C21—H21B	108.5
C11—N11—Cd1^{iv}	120.52 (17)	H21A—C21—H21B	107.5
C15—N11—Cd1^{iv}	121.17 (18)	C21—C22—H22A	109.5
N11—C11—C12	122.7 (3)	C21—C22—H22B	109.5
N11—C11—H11	118.7	H22A—C22—H22B	109.5
C12—C11—H11	118.7	C21—C22—H22C	109.5
C13—C12—C11	119.8 (3)	H22A—C22—H22C	109.5
C13—C12—H12	120.1	H22B—C22—H22C	109.5
C11—C12—H12	120.1		

Symmetry codes: (i) −*x*+1, *y*+1/2, −*z*+3/2; (ii) *x*+1, *y*, *z*; (iii) *x*−1, *y*, *z*; (iv) −*x*+1, *y*−1/2, −*z*+3/2.

Hydrogen-bond geometry (Å, º)

D—H···*A*	*D*—H	H···*A*	*D*···*A*	*D*—H···*A*
O21—H1*O*1···O12^{iii}	0.82	1.89	2.703 (3)	172

Symmetry code: (iii) *x*−1, *y*, *z*.

6.2. Poly[(μ_3-pyridine-4-carboxylato-κ^3O:O':N)(pyridin-1-ium-4-carboxylatoκO)(thiocyanato-κN)cobalt(II)]

Tristan Neumann, Julia Werner, Inke Jess und Christian Näther, *Acta Crystallogr. E* **2012**, *E68*, m1435.

DOI: 10.1107/S1600536812044431

metal-organic compounds

Acta Crystallographica Section E
Structure Reports Online
ISSN 1600-5368

Poly[(μ_3-pyridine-4-carboxylato-$\kappa^3O:O':N$)(pyridin-1-ium-4-carboxylato-κO)(thiocyanato-κN)cobalt(II)]

Tristan Neumann, Julia Werner, Inke Jess and Christian Näther*

Institut für Anorganische Chemie, Christian-Albrechts-Universität Kiel, Max-Eyth-Strasse 2, 24118 Kiel, Germany
Correspondence e-mail: cnaether@ac.uni-kiel.de

Received 12 September 2012; accepted 26 October 2012

Key indicators: single-crystal X-ray study; T = 293 K; mean σ(C–C) = 0.005 Å; R factor = 0.045; wR factor = 0.098; data-to-parameter ratio = 14.3.

In the title compound, $[Co(C_6H_5NO_2)(NCS)(C_6H_4NO_2)]_n$, the Co^{2+} cation is coordinated by one N and two O atoms of three bridging pyridine-4-carboxylate anions, one O atom of one zwitterionic pyridinium-4-carboxylate ligand and one terminal N-bonding thiocyanate anion within a distorted N_2O_3 trigonal bipyramid. The bridging coordination mode of the ligands leads to the formation of layers parallel to $(\bar{1}01)$. N—H···O hydrogen-bonding interactions within the layers and S···S contacts of 3.257 (3) Å between the layers lead to the cohesion of the structure.

Related literature

For general background information on the synthesis and properties of transition metal–thiocyanate coordination polymers, see: Boeckmann & Näther (2010, 2011); Wöhlert *et al.* (2011).

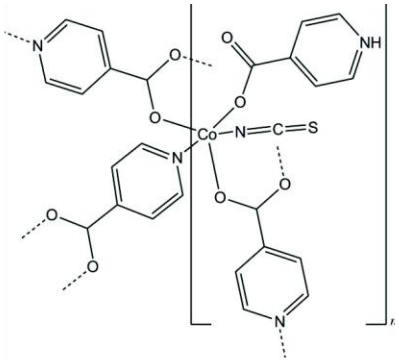

Experimental

Crystal data

$[Co(C_6H_5NO_2)(NCS)(C_6H_4NO_2)]$
M_r = 362.22
Monoclinic, $P2_1/n$
a = 8.7857 (7) Å
b = 13.5401 (8) Å
c = 12.2054 (9) Å
β = 95.740 (6)°
V = 1444.67 (18) Å^3
Z = 4
Mo $K\alpha$ radiation
μ = 1.35 mm^{-1}
T = 293 K
0.18 × 0.13 × 0.04 mm

Data collection

Stoe IPDS-2 diffractometer
Absorption correction: numerical (*X-SHAPE* and *X-RED32*; Stoe & Cie, 2008)
T_{min} = 0.808, T_{max} = 0.954
12489 measured reflections
2844 independent reflections
2353 reflections with $I > 2\sigma(I)$
R_{int} = 0.041

Refinement

$R[F^2 > 2\sigma(F^2)]$ = 0.045
$wR(F^2)$ = 0.098
S = 1.13
2844 reflections
199 parameters
H-atom parameters constrained
$\Delta\rho_{max}$ = 0.46 e Å^{-3}
$\Delta\rho_{min}$ = −0.39 e Å^{-3}

Table 1
Selected bond lengths (Å).

Co1—O22	2.004 (2)	Co1—O12	2.097 (2)
Co1—O21^{i}	2.004 (2)	Co1—N21^{ii}	2.146 (2)
Co1—N1	2.010 (4)		

Symmetry codes: (i) $-x+1, -y+1, -z+1$; (ii) $-x+\frac{1}{2}, y+\frac{1}{2}, -z+\frac{1}{2}$.

Table 2
Hydrogen-bond geometry (Å, °).

D—H···A	D—H	H···A	D···A	D—H···A
N11—H1*N*···O11^{iii}	0.86	1.80	2.561 (4)	147

Symmetry code: (iii) $x+\frac{1}{2}, -y+\frac{1}{2}, z+\frac{1}{2}$.

Data collection: *X-AREA* (Stoe & Cie, 2008); cell refinement: *X-AREA*; data reduction: *X-AREA*; program(s) used to solve structure: *SHELXS97* (Sheldrick, 2008); program(s) used to refine structure: *SHELXL97* (Sheldrick, 2008); molecular graphics: *XP* in *SHELXTL* (Sheldrick, 2008) and *DIAMOND* (Brandenburg, 2011); software used to prepare material for publication: *publCIF* (Westrip, 2010).

We gratefully acknowledge financial support by the DFG (project No. NA 720/3–1) and the State of Schleswig–Holstein. We thank Professor Dr Wolfgang Bensch for access to his experimental facilities.

Supplementary data and figures for this paper are available from the IUCr electronic archives (Reference: WM2684).

References

Boeckmann, J. & Näther, C. (2010). *Dalton Trans.* **39**, 11019–11026.
Boeckmann, J. & Näther, C. (2011). *Chem. Commun.* **47**, 7104–7106.
Brandenburg, K. (2011). *DIAMOND*. Crystal Impact GbR, Bonn, Germany.
Sheldrick, G. M. (2008). *Acta Cryst.* A**64**, 112–122.
Stoe & Cie (2008). *X-AREA*, *X-RED32* and *X-SHAPE*. Stoe & Cie, Darmstadt, Germany.
Westrip, S. P. (2010). *J. Appl. Cryst.* **43**, 920–925.
Wöhlert, S., Boeckmann, J., Wriedt, M. & Näther, C. (2011). *Angew. Chem. Int. Ed.* **50**, 6920–6923.

supplementary materials

Acta Cryst. (2012). E**68**, m1435 [doi:10.1107/S1600536812044431]

Poly[(μ_3-pyridine-4-carboxylato-κ^3O:O':N)(pyridin-1-ium-4-carboxylato-κO)(thiocyanato-κN)cobalt(II)]

Tristan Neumann, Julia Werner, Inke Jess and Christian Näther

Comment

The title compound was prepared within a project on the synthesis and properties of transition metal thiocyanato coordination polymers (Boeckmann & Näther, 2010, 2011; Wöhlert *et al.*, 2011). During our attempts to prepare a one-dimensional coordination polymer based on pyridine-4-carboxylic acid as a co-ligand, crystals of the title compound, [Co(NCS)($C_6H_4NO_2$)($C_6H_5NO_2$)], (I), were obtained serendipitously and characterized by single crystal X-ray diffraction.

In the crystal structure of (I), the cobalt(II) cation is coordinated by one terminally *O*-bonded pyridinium-4-carboxylate ligand, one terminally *N*-bonded thiocyanate anion, one *N*-bonded μ-1,3,6-bridging pyridine-4-carboxylate and two *O*-bonded μ-1,3,6-bridging pyridine-4-carboxylate anions (Fig. 1). The coordination polyhedron of the Co^{2+} cations can be described as a distorted trigonal bipyramid (Fig. 1, Table 1).

The Co^{2+} cations are μ-1,3 bridged *via* pyridine-4-carboxylato anions into dimers, which are further connected into layers parallel to ($\bar{1}$01) (Fig. 2). The Co···Co distance within the dimer amounts to 3.4951 (6) Å. Within the layers N—H···O hydrogen bonding between the bridging pyridine-4-carboxylate anions and the non-bridging pyridinium carboxylate ligands (Fig. 3 and Table 2) is present. A short S···S contact of 3.257 (3) Å between the layers is also observed.

Experimental

Cobalt thiocyanate and pyridine-4-carboxylic acid were purchased from Alfa Aesar. The title compound was prepared by the reaction of 43.8 mg $Co(NCS)_2$ (0.25 mmol), and 61.6 mg pyridine-4-carboxylic acid (0.50 mmol) in 1.5 mL ethanol at 354 K in a closed 10 ml glas culture tube. After several days pink block-shaped crystals of the title compound were obtained.

Refinement

The C-H and N-H H atoms were localized in a difference map but were positioned with idealized geometry and were refined isotropically with U_{iso}(H) = 1.2 U_{eq}(C,N) using a riding model with C—H = 0.93 Å and N—H = 0.86 Å.

Computing details

Data collection: *X-AREA* (Stoe & Cie, 2008); cell refinement: *X-AREA* (Stoe & Cie, 2008); data reduction: *X-AREA* (Stoe & Cie, 2008); program(s) used to solve structure: *SHELXS97* (Sheldrick, 2008); program(s) used to refine structure: *SHELXL97* (Sheldrick, 2008); molecular graphics: *XP* in *SHELXTL* (Sheldrick, 2008) and *DIAMOND* (Brandenburg, 2011); software used to prepare material for publication: *publCIF* (Westrip, 2010).

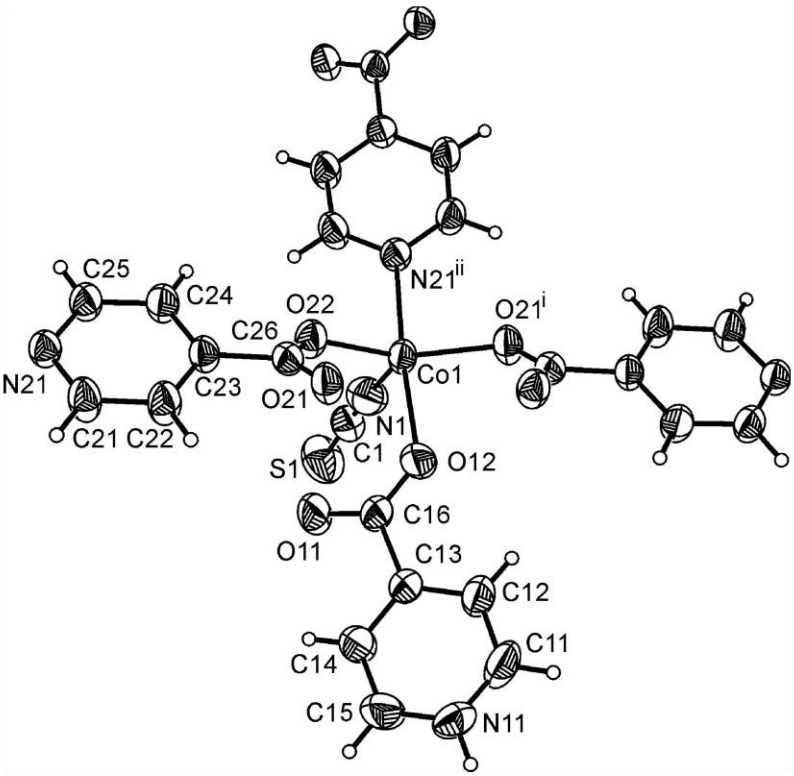

Figure 1

The coordination environment of the Co^{2+} cation in the title compound with labelling and displacement ellipsoids drawn at the 50% probability level. [Symmetry codes: i = -x+1,-y+1,-z+1, ii = -x+1/2, y+1/2, -z+1/2.]

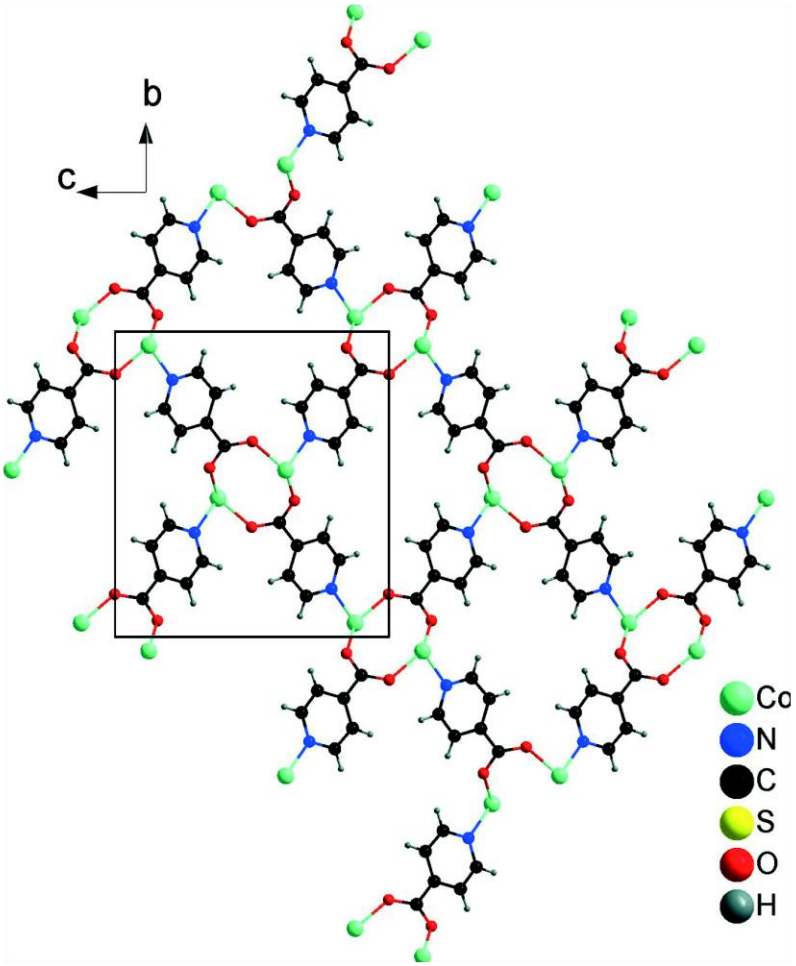

Figure 2

The layers parallel to $(\bar{1}01)$ in the title compound in a projection along the *a* axis. For clarity, the non-bridging ligands and the thiocyanato anions are not shown.

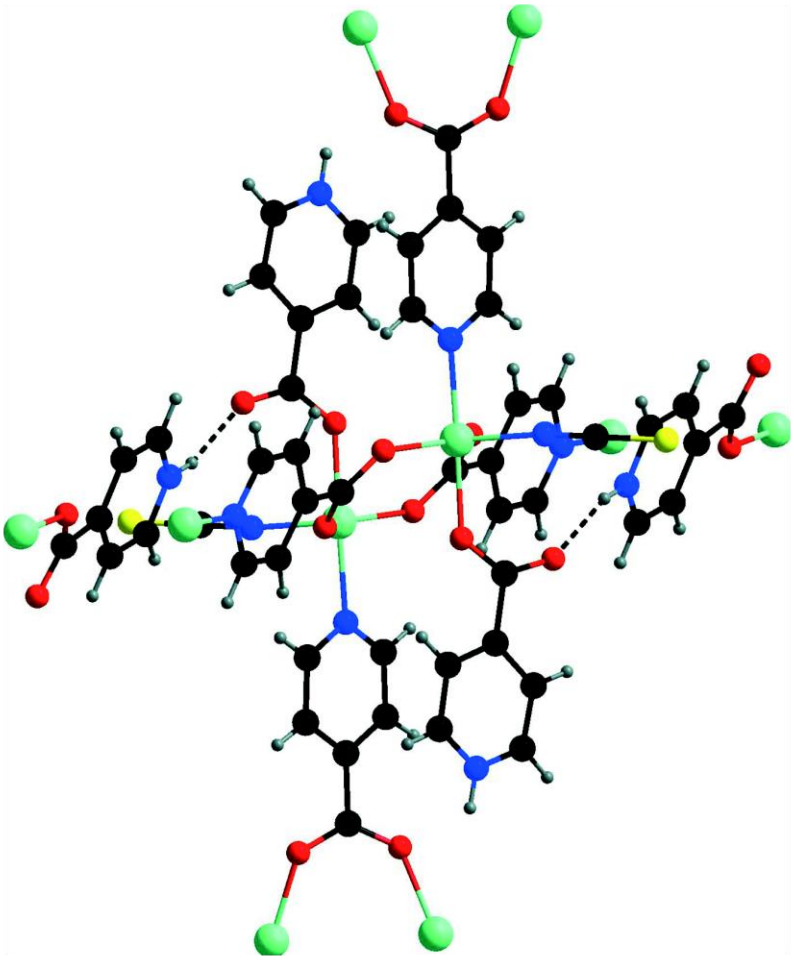

Figure 3

The N—H···O hydrogen bonding interactions (dashed lines) within the layers in the crystal structure of the title compound.

Poly[(μ_3-pyridine-4-carboxylato-κ^3O:O':N)(pyridin- 1-ium-4-carboxylato-κO)(thiocyanato-κN)cobalt(II)]

Crystal data

$[Co(C_6H_5NO_2)(NCS)(C_6H_4NO_2)]$
$M_r = 362.22$
Monoclinic, $P2_1/n$
Hall symbol: -P 2yn
$a = 8.7857$ (7) Å
$b = 13.5401$ (8) Å
$c = 12.2054$ (9) Å
$\beta = 95.740$ (6)°
$V = 1444.67$ (18) Å^3
$Z = 4$

$F(000) = 732$
$D_x = 1.665$ Mg m^{-3}
Mo $K\alpha$ radiation, $\lambda = 0.71073$ Å
Cell parameters from 12489 reflections
$\theta = 2.3$–26.0°
$\mu = 1.35$ mm^{-1}
$T = 293$ K
Block, pink
0.18 × 0.13 × 0.04 mm

Data collection

Stoe IPDS-2 diffractometer
Radiation source: fine-focus sealed tube
Graphite monochromator
ω scans
Absorption correction: numerical (*X-SHAPE* and *X-RED32*; Stoe & Cie, 2008)
T_{min} = 0.808, T_{max} = 0.954

12489 measured reflections
2844 independent reflections
2353 reflections with $I > 2\sigma(I)$
R_{int} = 0.041
θ_{max} = 26.0°, θ_{min} = 2.3°
h = −9→10
k = −16→16
l = −15→15

Refinement

Refinement on F^2
Least-squares matrix: full
$R[F^2 > 2\sigma(F^2)]$ = 0.045
$wR(F^2)$ = 0.098
S = 1.13
2844 reflections
199 parameters
0 restraints
Primary atom site location: structure-invariant direct methods
Secondary atom site location: difference Fourier map
Hydrogen site location: inferred from neighbouring sites
H-atom parameters constrained
$w = 1/[\sigma^2(F_o^2) + (0.0434P)^2 + 0.689P]$ where $P = (F_o^2 + 2F_c^2)/3$
$(\Delta/\sigma)_{max} < 0.001$
$\Delta\rho_{max}$ = 0.46 e Å^{-3}
$\Delta\rho_{min}$ = −0.39 e Å^{-3}

Special details

Geometry. All esds (except the esd in the dihedral angle between two l.s. planes) are estimated using the full covariance matrix. The cell esds are taken into account individually in the estimation of esds in distances, angles and torsion angles; correlations between esds in cell parameters are only used when they are defined by crystal symmetry. An approximate (isotropic) treatment of cell esds is used for estimating esds involving l.s. planes.

Refinement. Refinement of F^2 against ALL reflections. The weighted R-factor wR and goodness of fit S are based on F^2, conventional R-factors R are based on F, with F set to zero for negative F^2. The threshold expression of $F^2 > 2\text{sigma}(F^2)$ is used only for calculating R-factors(gt) etc. and is not relevant to the choice of reflections for refinement. R-factors based on F^2 are statistically about twice as large as those based on F, and R- factors based on ALL data will be even larger.

Fractional atomic coordinates and isotropic or equivalent isotropic displacement parameters (Å^2)

	x	*y*	*z*	U_{iso}*/U_{eq}
Co1	0.55767 (5)	0.54579 (3)	0.37683 (3)	0.04212 (15)
N1	0.6768 (4)	0.5335 (2)	0.2453 (3)	0.0650 (8)
C1	0.7529 (4)	0.5189 (3)	0.1751 (3)	0.0569 (9)
S1	0.85857 (16)	0.50015 (10)	0.07668 (11)	0.0870 (4)
O11	0.7180 (4)	0.3217 (2)	0.3482 (2)	0.0961 (12)
N11	1.0561 (4)	0.2118 (2)	0.6656 (2)	0.0602 (8)
H1N	1.1155	0.1797	0.7133	0.072*
C11	1.0285 (5)	0.3058 (3)	0.6833 (3)	0.0691 (11)
H11	1.0737	0.3363	0.7467	0.083*
O12	0.7060 (4)	0.44642 (18)	0.4654 (2)	0.0746 (9)
C12	0.9336 (5)	0.3592 (3)	0.6092 (3)	0.0626 (10)
H12	0.9141	0.4255	0.6219	0.075*
C13	0.8682 (4)	0.3134 (2)	0.5164 (3)	0.0472 (8)
C14	0.9021 (6)	0.2159 (3)	0.4995 (3)	0.0731 (13)
H14	0.8619	0.1840	0.4356	0.088*
C15	0.9951 (6)	0.1659 (3)	0.5768 (3)	0.0797 (14)
H15	1.0155	0.0993	0.5667	0.096*

C16	0.7540 (5)	0.3656 (3)	0.4352 (3)	0.0585 (10)
N21	0.0790 (3)	0.15794 (17)	0.20950 (19)	0.0409 (6)
C21	0.1656 (4)	0.1340 (2)	0.3023 (3)	0.0541 (9)
H21	0.1687	0.0682	0.3243	0.065*
O21	0.3758 (3)	0.35997 (15)	0.50108 (16)	0.0480 (5)
O22	0.3902 (3)	0.44629 (15)	0.34512 (17)	0.0468 (5)
C22	0.2501 (4)	0.2017 (2)	0.3666 (3)	0.0525 (9)
H22	0.3069	0.1817	0.4311	0.063*
C23	0.2502 (4)	0.2995 (2)	0.3350 (2)	0.0392 (7)
C24	0.1599 (4)	0.3245 (2)	0.2392 (3)	0.0520 (8)
H24	0.1560	0.3896	0.2146	0.062*
C25	0.0765 (4)	0.2528 (2)	0.1808 (3)	0.0503 (8)
H25	0.0149	0.2714	0.1177	0.060*
C26	0.3462 (4)	0.3749 (2)	0.3992 (2)	0.0397 (7)

Atomic displacement parameters (Å²)

	U^{11}	U^{22}	U^{33}	U^{12}	U^{13}	U^{23}
Co1	0.0532 (3)	0.0318 (2)	0.0380 (2)	−0.00216 (19)	−0.01220 (16)	−0.00046 (16)
N1	0.061 (2)	0.0587 (18)	0.076 (2)	0.0046 (16)	0.0107 (17)	−0.0018 (16)
C1	0.055 (2)	0.0454 (18)	0.070 (2)	−0.0019 (16)	0.0022 (19)	−0.0096 (16)
S1	0.0904 (9)	0.0886 (8)	0.0864 (8)	−0.0032 (7)	0.0312 (7)	−0.0235 (7)
O11	0.144 (3)	0.0572 (16)	0.0716 (18)	0.0320 (18)	−0.066 (2)	−0.0231 (14)
N11	0.0593 (19)	0.0640 (19)	0.0532 (17)	0.0088 (15)	−0.0147 (14)	0.0118 (14)
C11	0.078 (3)	0.066 (2)	0.056 (2)	−0.016 (2)	−0.031 (2)	0.0079 (18)
O12	0.100 (2)	0.0499 (14)	0.0645 (15)	0.0289 (14)	−0.0373 (15)	−0.0134 (12)
C12	0.077 (3)	0.0465 (18)	0.058 (2)	−0.0028 (18)	−0.0265 (19)	−0.0022 (15)
C13	0.0520 (19)	0.0437 (16)	0.0430 (16)	0.0054 (14)	−0.0095 (14)	−0.0023 (13)
C14	0.105 (3)	0.057 (2)	0.049 (2)	0.030 (2)	−0.031 (2)	−0.0147 (17)
C15	0.109 (4)	0.063 (2)	0.061 (2)	0.037 (2)	−0.023 (2)	−0.0084 (19)
C16	0.072 (2)	0.0440 (18)	0.0532 (19)	0.0084 (17)	−0.0277 (17)	−0.0045 (15)
N21	0.0492 (15)	0.0369 (13)	0.0350 (12)	−0.0022 (11)	−0.0040 (11)	−0.0004 (10)
C21	0.080 (2)	0.0332 (15)	0.0446 (17)	−0.0082 (15)	−0.0168 (16)	0.0043 (13)
O21	0.0702 (15)	0.0338 (10)	0.0367 (11)	−0.0032 (10)	−0.0108 (10)	−0.0008 (8)
O22	0.0565 (13)	0.0368 (11)	0.0444 (11)	−0.0065 (10)	−0.0086 (10)	0.0029 (9)
C22	0.076 (2)	0.0396 (16)	0.0373 (15)	−0.0055 (16)	−0.0168 (15)	0.0026 (12)
C23	0.0497 (18)	0.0340 (14)	0.0324 (14)	−0.0022 (13)	−0.0037 (13)	−0.0027 (11)
C24	0.066 (2)	0.0332 (15)	0.0518 (18)	−0.0011 (14)	−0.0194 (16)	0.0025 (13)
C25	0.063 (2)	0.0376 (16)	0.0458 (17)	0.0009 (15)	−0.0183 (15)	−0.0002 (13)
C26	0.0462 (17)	0.0309 (14)	0.0402 (15)	0.0021 (12)	−0.0054 (13)	−0.0014 (11)

Geometric parameters (Å, º)

Co1—O22	2.004 (2)	C14—C15	1.364 (5)
Co1—O21^{i}	2.004 (2)	C14—H14	0.9300
Co1—N1	2.010 (4)	C15—H15	0.9300
Co1—O12	2.097 (2)	N21—C25	1.331 (4)
Co1—N21^{ii}	2.146 (2)	N21—C21	1.339 (4)
N1—C1	1.155 (5)	N21—Co1^{iii}	2.146 (2)
C1—S1	1.610 (4)	C21—C22	1.376 (4)

O11—C16	1.230 (4)	C21—H21	0.9300
N11—C15	1.316 (5)	O21—C26	1.261 (3)
N11—C11	1.318 (5)	O21—Co1^{i}	2.004 (2)
N11—H1N	0.8600	O22—C26	1.253 (3)
C11—C12	1.373 (5)	C22—C23	1.379 (4)
C11—H11	0.9300	C22—H22	0.9300
O12—C16	1.242 (4)	C23—C24	1.388 (4)
C12—C13	1.366 (4)	C23—C26	1.495 (4)
C12—H12	0.9300	C24—C25	1.373 (4)
C13—C14	1.374 (5)	C24—H24	0.9300
C13—C16	1.514 (4)	C25—H25	0.9300
O22—Co1—O21^{i}	136.53 (10)	N11—C15—H15	119.9
O22—Co1—N1	102.78 (12)	C14—C15—H15	119.9
O21^{i}—Co1—N1	120.67 (12)	O11—C16—O12	128.1 (3)
O22—Co1—O12	94.28 (10)	O11—C16—C13	115.8 (3)
O21^{i}—Co1—O12	84.54 (9)	O12—C16—C13	116.0 (3)
N1—Co1—O12	90.72 (13)	C25—N21—C21	116.7 (3)
O22—Co1—N21^{ii}	90.97 (9)	C25—N21—Co1^{iii}	124.0 (2)
O21^{i}—Co1—N21^{ii}	91.26 (9)	C21—N21—Co1^{iii}	119.1 (2)
N1—Co1—N21^{ii}	88.66 (12)	N21—C21—C22	123.3 (3)
O12—Co1—N21^{ii}	174.71 (11)	N21—C21—H21	118.3
C1—N1—Co1	173.2 (3)	C22—C21—H21	118.3
N1—C1—S1	179.2 (4)	C26—O21—Co1^{i}	130.33 (18)
C15—N11—C11	121.6 (3)	C26—O22—Co1	132.53 (19)
C15—N11—H1N	119.2	C21—C22—C23	119.7 (3)
C11—N11—H1N	119.2	C21—C22—H22	120.1
N11—C11—C12	120.6 (3)	C23—C22—H22	120.1
N11—C11—H11	119.7	C22—C23—C24	117.0 (3)
C12—C11—H11	119.7	C22—C23—C26	121.7 (3)
C16—O12—Co1	128.6 (2)	C24—C23—C26	121.4 (3)
C13—C12—C11	119.0 (3)	C25—C24—C23	119.7 (3)
C13—C12—H12	120.5	C25—C24—H24	120.2
C11—C12—H12	120.5	C23—C24—H24	120.2
C12—C13—C14	118.7 (3)	N21—C25—C24	123.5 (3)
C12—C13—C16	121.8 (3)	N21—C25—H25	118.2
C14—C13—C16	119.4 (3)	C24—C25—H25	118.2
C15—C14—C13	119.8 (3)	O22—C26—O21	126.8 (3)
C15—C14—H14	120.1	O22—C26—C23	116.0 (2)
C13—C14—H14	120.1	O21—C26—C23	117.2 (3)
N11—C15—C14	120.1 (4)		

Symmetry codes: (i) −*x*+1, −*y*+1, −*z*+1; (ii) −*x*+1/2, *y*+1/2, −*z*+1/2; (iii) −*x*+1/2, *y*−1/2, −*z*+1/2.

Hydrogen-bond geometry (Å, º)

D—H···*A*	*D*—H	H···*A*	*D*···*A*	*D*—H···*A*
N11—H1*N*···O11^{iv}	0.86	1.80	2.561 (4)	147

Symmetry code: (iv) *x*+1/2, −*y*+1/2, *z*+1/2.

6.3. Bis(4,4‘-sulfanediyldipyridinium) tetrachloridonickelate(II) dichloride

Julia Werner, Inke Jess und Christian Näther, *Acta Crystallogr. E* **2012**, *E69*, m59.

DOI: 10.1107/S1600536812050623

metal-organic compounds

Acta Crystallographica Section E
Structure Reports Online
ISSN 1600-5368

Bis(4,4′-sulfanediyldipyridinium) tetrachloridonickelate(II) dichloride

Julia Werner,* Inke Jess and Christian Näther

Institut für Anorganische Chemie, Christian-Albrechts-Universität Kiel, Max-Eyth-Strasse 2, 24118 Kiel, Germany
Correspondence e-mail: jwerner@ac.uni-kiel.de

Received 14 November 2012; accepted 12 December 2012

Key indicators: single-crystal X-ray study; T = 200 K; mean σ(C–C) = 0.004 Å; R factor = 0.037; wR factor = 0.084; data-to-parameter ratio = 20.9.

In the title compound, $(C_{10}H_{10}N_2S)_2[NiCl_4]Cl_2$, the Ni^{2+} cation is tetrahedrally coordinated by four chloride anions. Two 4,4′-sulfanediyldipyridinium cations and two non-coordinating chloride anions are connected *via* N—H···Cl hydrogen-bonding interactions into 20-membered rings, in the middle of which are situated the $[NiCl_4]^{2-}$ complex anions. These rings are stacked in the *b*-axis direction. The Ni^{2+} cation is located on a twofold rotation axis, whereas the chloride anions and the 4,4′-sulfanediyldipyridinium cations occupy general positions.

Related literature

For background information on this project, see: Boeckmann & Näther (2010, 2011); Wöhlert *et al.* (2011). For the crystal structure of 4,4′-thiodipyridine, see: Vaganova *et al.* (2004).

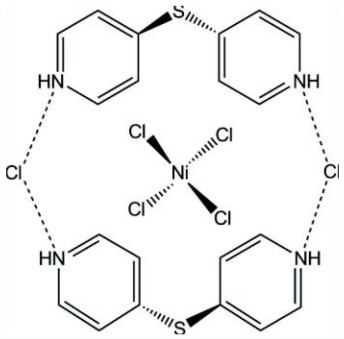

Experimental

Crystal data

$(C_{10}H_{10}N_2S)_2[NiCl_4]Cl_2$
M_r = 651.93
Monoclinic, $C2/c$
a = 19.0497 (9) Å
b = 8.0534 (5) Å
c = 17.7883 (11) Å
β = 92.368 (6)°
V = 2726.7 (3) Å^3
Z = 4
Mo $K\alpha$ radiation
μ = 1.47 mm^{-1}
T = 200 K
0.32 × 0.13 × 0.07 mm

Data collection

Stoe IPDS-1 diffractometer
Absorption correction: numerical (*X-SHAPE* and *X-RED32*; Stoe & Cie, 2008)
T_{min} = 0.789, T_{max} = 0.899
10707 measured reflections
3162 independent reflections
2308 reflections with $I > 2\sigma(I)$
R_{int} = 0.062

Refinement

$R[F^2 > 2\sigma(F^2)]$ = 0.037
$wR(F^2)$ = 0.084
S = 0.99
3162 reflections
151 parameters
H-atom parameters constrained
$\Delta\rho_{max}$ = 0.47 e Å^{-3}
$\Delta\rho_{min}$ = −0.43 e Å^{-3}

Table 1
Selected bond lengths (Å).

Ni1—Cl1	2.2569 (7)	Ni1—Cl2	2.2706 (6)

Table 2
Hydrogen-bond geometry (Å, °).

D—H···*A*	*D*—H	H···*A*	*D*···*A*	*D*—H···*A*
N2—H1*N*2···Cl3^{i}	0.88	2.12	2.987 (3)	168
N1—H1*N*1···Cl3	0.88	2.32	3.078 (3)	144

Symmetry code: (i) $-x+1, y, -z+\frac{3}{2}$.

Data collection: *X-AREA* (Stoe & Cie, 2008); cell refinement: *X-AREA*; data reduction: *X-AREA*; program(s) used to solve structure: *SHELXS97* (Sheldrick, 2008); program(s) used to refine structure: *SHELXL97* (Sheldrick, 2008); molecular graphics: *XP* in *SHELXTL* (Sheldrick, 2008) and *DIAMOND* (Brandenburg, 2011); software used to prepare material for publication: *publCIF* (Westrip, 2010).

We gratefully acknowledge financial support by the DFG (project No. NA 720/3–1) and the State of Schleswig–Holstein. We thank Professor Dr Wolfgang Bensch for access to his experimental facilities.

Supplementary data and figures for this paper are available from the IUCr electronic archives (Reference: WM2703).

References

Boeckmann, J. & Näther, C. (2010). *Dalton Trans.* **39**, 11019–11026.
Boeckmann, J. & Näther, C. (2011). *Chem. Commun.* **47**, 7104–7106.
Brandenburg, K. (2011). *DIAMOND*. Crystal Impact GbR, Bonn, Germany.
Sheldrick, G. M. (2008). *Acta Cryst.* A**64**, 112–122.
Stoe & Cie (2008). *X-AREA*, *X-RED32* and *X-SHAPE*. Stoe & Cie, Darmstadt, Germany.
Vaganova, E., Wachtel, E., Rozenberg, H., Khodorkovsky, V., Leitus, V., Shimon, L., Reich, S. & Yitzchaik, S. (2004). *Chem. Mater.* **16**, 3976–3979.
Westrip, S. P. (2010). *J. Appl. Cryst.* **43**, 920–925.
Wöhlert, S., Boeckmann, J., Wriedt, M. & Näther, C. (2011). *Angew. Chem. Int. Ed.* **50**, 6920–6923.

supplementary materials

Acta Cryst. (2013). E**69**, m59 [doi:10.1107/S1600536812050623]

Bis(4,4′-sulfanediyldipyridinium) tetrachloridonickelate(II) dichloride

Julia Werner, Inke Jess and Christian Näther

Comment

The title compound was prepared within a project on the synthesis and properties of transition metal thiocyanato coordination polymers (Boeckmann & Näther, 2010, 2011; Wöhlert *et al.*, 2011). During our attempts to prepare a one-dimensional coordination polymer based on 4-chloropyridine as a co-ligand, crystals of the title compound, $(C_{10}H_{10}N_2S^+)_2[NiCl_4]Cl_2$ (I), have been obtained accidentally and were characterized by single crystal X-ray diffraction.

In the crystal structure of (I) the Ni^{2+} cation is coordinated by four chloride anions within a slightly distorted tetrahedral coordination environment. The complex $[NiCl_4]^{2-}$ anions are surrounded by two 4,4′-sulfanediyldipyridinium cations and two chloride counter-anions (Fig. 1 and Table 1). Intermolecular N—H···Cl hydrogen bonding is found between the 4,4′-sulfanediyldipyridinium cations and the non-coordinating chloride anions, which leads to the formation of 20-membered rings (Fig. 2 and Table 2). These rings are stacked in the direction of the *b* axis.

The dihedral angle between the pyridine rings in the cations amounts to 52.57 (7) °. The corresponding bond lengths and angles are comparable to those in the neutral 4,4′-thiodipyridine molecule. Slight differences are found with respect to the dihedral angle between the pyridine rings which amounts to 65.4° in the neutral molecule (Vaganova *et al.*, 2004).

Experimental

Barium thiocyanate trihydrate and 4-chloropyridine hydrochloride were purchased from Alfa Aesar, $Ni(SO_4)_2{\cdot}6H_2O$ was obtained from Merck. $Ni(NCS)_2$ was prepared by stirring $Ba(NCS)_2{\cdot}3H_2O$ (17.5 g, 56.9 mmol) and $NiSO_4{\cdot}6H_2O$ (15.0 g, 57 mmol) in water (500 mL). The white residue of $BaSO_4$ was filtered off and the solution evaporated using a rotary evaporator. The homogeneity of the product was investigated by X-ray powder diffraction. The title compound was prepared by the reaction of 26.2 mg $Ni(NCS)_2$ (0.15 mmol) and 97.5 mg 4-chloropyridine hydrochloride (0.60 mmol) in 1.5 mL ethanol at 354 K in a closed 10 mL glas culture tube. After one day blue needles of the title compound were obtained. The formation of 4,4′-thiodipyridine starting from 4-chloropyridine in an SCN^--containing environment and the presence of free Cl^- and complex $[NiCl_4]^{2-}$ anions seem to be a result of cleavage reactions of both the 4-chloropyridine and SCN^- anions. However, the exact mechanism is unclear.

Refinement

The aromatic H atoms (C- and N-bound) were located in a difference map but were positioned with idealized geometries and were refined isotropically with $U_{iso}(H) = 1.2{\cdot}U_{eq}(C,N)$ using a riding model approximation with C—H = 0.95 Å and N—H = 0.88 Å.

Computing details

Data collection: *X-AREA* (Stoe & Cie, 2008); cell refinement: *X-AREA* (Stoe & Cie, 2008); data reduction: *X-AREA* (Stoe & Cie, 2008); program(s) used to solve structure: *SHELXS97* (Sheldrick, 2008); program(s) used to refine structure: *SHELXL97* (Sheldrick, 2008); molecular graphics: *XP* in *SHELXTL* (Sheldrick, 2008) and *DIAMOND* (Brandenburg,

2011); software used to prepare material for publication: *publCIF* (Westrip, 2010).

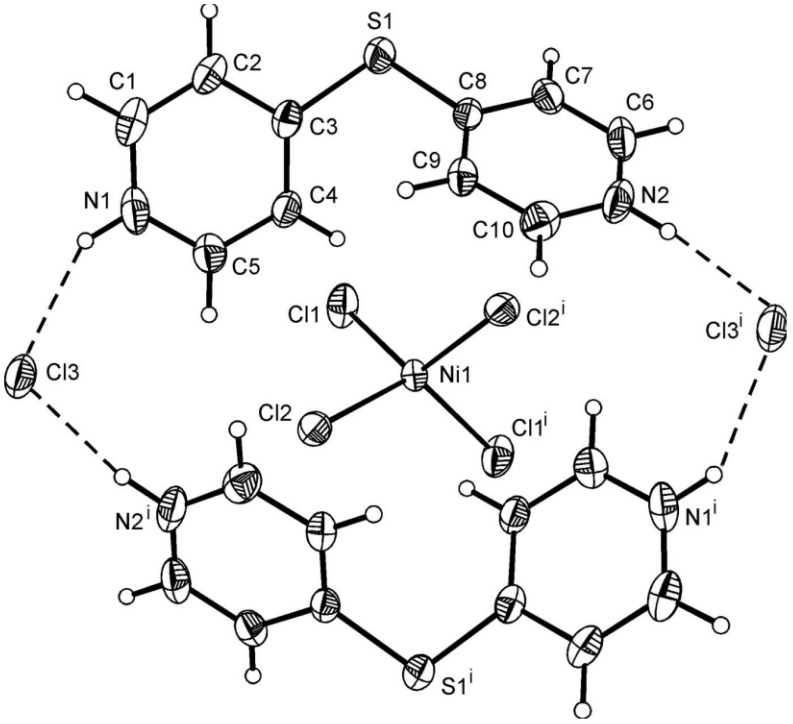

Figure 1

Crystal structure of the title compound with labelling and displacement ellipsoids drawn at the 50% probability level. [Symmetry code: i = -x+1, y, -z+3/2.]

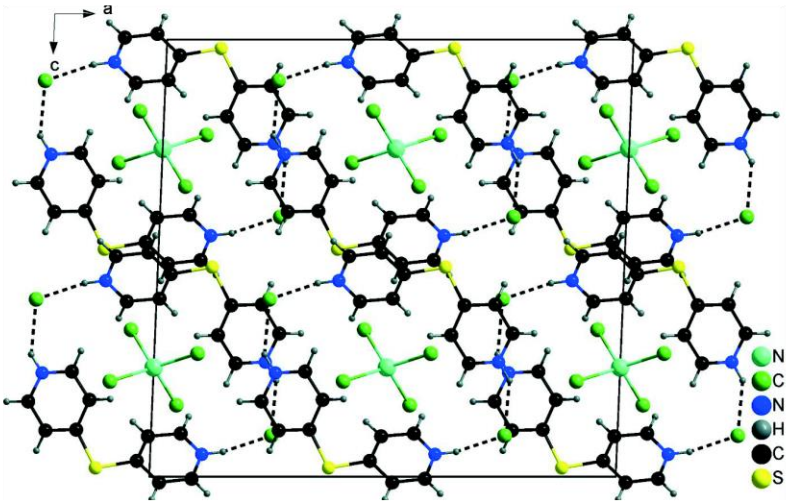

Figure 2

Crystal structure of the title compound in a view along the *b*-axis. N—H···Cl hydrogen bonding is shown as dashed lines.

Bis(4,4′-sulfanediyldipyridinium) tetrachloridonickelate(II) dichloride

Crystal data

$(C_{10}H_{10}N_2S)_2[NiCl_4]Cl_2$
$M_r = 651.93$
Monoclinic, *C*2/*c*
Hall symbol: -C 2yc
$a = 19.0497$ (9) Å
$b = 8.0534$ (5) Å
$c = 17.7883$ (11) Å
$\beta = 92.368$ (6)°
$V = 2726.7$ (3) Å^3
$Z = 4$
$F(000) = 1320$
$D_x = 1.588$ Mg m^{-3}
Mo $K\alpha$ radiation, $\lambda = 0.71073$ Å
Cell parameters from 10707 reflections
$\theta = 2.3$–$27.9°$
$\mu = 1.47$ mm^{-1}
$T = 200$ K
Needle, blue
0.32 × 0.13 × 0.07 mm

Data collection

Stoe IPDS-1 diffractometer
Radiation source: fine-focus sealed tube
Graphite monochromator
Phi scans
Absorption correction: numerical (*X-SHAPE* and *X-RED32*; Stoe & Cie, 2008)
$T_{min} = 0.789$, $T_{max} = 0.899$
10707 measured reflections
3162 independent reflections
2308 reflections with $I > 2\sigma(I)$
$R_{int} = 0.062$
$\theta_{max} = 27.9°$, $\theta_{min} = 2.3°$
$h = -23 \rightarrow 22$
$k = -10 \rightarrow 10$
$l = -23 \rightarrow 23$

Refinement

Refinement on F^2
Least-squares matrix: full
$R[F^2 > 2\sigma(F^2)] = 0.037$
$wR(F^2) = 0.084$
$S = 0.99$
3162 reflections
151 parameters
0 restraints
Primary atom site location: structure-invariant direct methods
Secondary atom site location: difference Fourier map
Hydrogen site location: inferred from neighbouring sites

H-atom parameters constrained
$w = 1/[\sigma^2(F_o^2) + (0.0463P)^2]$
where $P = (F_o^2 + 2F_c^2)/3$
$(\Delta/\sigma)_{max} = 0.001$
$\Delta\rho_{max} = 0.47$ e Å^{-3}
$\Delta\rho_{min} = -0.43$ e Å^{-3}
Extinction correction: *SHELXL*,
$Fc^* = kFc[1+0.001xFc^2\lambda^3/\sin(2\theta)]^{-1/4}$
Extinction coefficient: 0.0013 (3)

Special details

Geometry. All esds (except the esd in the dihedral angle between two l.s. planes) are estimated using the full covariance matrix. The cell esds are taken into account individually in the estimation of esds in distances, angles and torsion angles; correlations between esds in cell parameters are only used when they are defined by crystal symmetry. An approximate (isotropic) treatment of cell esds is used for estimating esds involving l.s. planes.

Refinement. Refinement of F^2 against ALL reflections. The weighted R-factor wR and goodness of fit S are based on F^2, conventional R-factors R are based on F, with F set to zero for negative F^2. The threshold expression of $F^2 > 2\text{sigma}(F^2)$ is used only for calculating R-factors(gt) etc. and is not relevant to the choice of reflections for refinement. R-factors based on F^2 are statistically about twice as large as those based on F, and R- factors based on ALL data will be even larger.

Fractional atomic coordinates and isotropic or equivalent isotropic displacement parameters (Å²)

	x	*y*	*z*	U_{iso}*/U_{eq}
Ni1	0.5000	0.66427 (5)	0.7500	0.02527 (13)
Cl1	0.59273 (4)	0.81985 (9)	0.71816 (4)	0.0465 (2)
Cl2	0.55194 (4)	0.49082 (8)	0.83619 (3)	0.03563 (17)
Cl3	0.75812 (4)	0.08791 (10)	0.90585 (4)	0.04236 (19)
N1	0.73877 (13)	0.1738 (3)	0.73764 (14)	0.0425 (6)
H1N1	0.7637	0.1582	0.7798	0.051*
C1	0.76591 (16)	0.1281 (4)	0.67229 (18)	0.0424 (7)
H1	0.8121	0.0839	0.6718	0.051*
C2	0.72674 (14)	0.1451 (3)	0.60598 (16)	0.0366 (6)
H2	0.7444	0.1073	0.5598	0.044*
C3	0.66077 (14)	0.2189 (3)	0.60792 (14)	0.0305 (5)
C4	0.63496 (14)	0.2699 (3)	0.67604 (14)	0.0319 (5)
H4	0.5905	0.3227	0.6779	0.038*
C5	0.67510 (14)	0.2424 (3)	0.74071 (15)	0.0351 (6)
H5	0.6575	0.2724	0.7880	0.042*
S1	0.61640 (4)	0.26112 (10)	0.52047 (4)	0.03808 (18)
N2	0.38935 (13)	0.1530 (3)	0.55137 (14)	0.0394 (5)
H1N2	0.3443	0.1351	0.5570	0.047*
C6	0.40903 (15)	0.2520 (4)	0.49540 (15)	0.0383 (6)
H6	0.3746	0.2986	0.4615	0.046*
C7	0.47845 (14)	0.2859 (3)	0.48701 (14)	0.0313 (5)
H7	0.4926	0.3573	0.4479	0.038*
C8	0.52829 (13)	0.2148 (3)	0.53643 (13)	0.0262 (5)
C9	0.50641 (14)	0.1074 (3)	0.59261 (14)	0.0284 (5)
H9	0.5398	0.0541	0.6257	0.034*
C10	0.43635 (15)	0.0807 (3)	0.59898 (15)	0.0357 (6)
H10	0.4206	0.0100	0.6376	0.043*

Atomic displacement parameters (Å²)

	U^{11}	U^{22}	U^{33}	U^{12}	U^{13}	U^{23}
Ni1	0.0281 (3)	0.0202 (2)	0.0271 (2)	0.000	−0.00296 (16)	0.000

Cl1	0.0355 (4)	0.0461 (4)	0.0574 (4)	−0.0070 (3)	−0.0039 (3)	0.0256 (3)
Cl2	0.0370 (4)	0.0359 (3)	0.0341 (3)	0.0052 (3)	0.0038 (2)	0.0137 (3)
Cl3	0.0275 (4)	0.0549 (4)	0.0440 (4)	0.0065 (3)	−0.0057 (3)	−0.0111 (3)
N1	0.0347 (15)	0.0451 (13)	0.0462 (14)	0.0034 (11)	−0.0153 (10)	−0.0021 (11)
C1	0.0290 (17)	0.0392 (16)	0.0586 (19)	0.0058 (11)	−0.0034 (12)	0.0004 (13)
C2	0.0266 (15)	0.0371 (15)	0.0462 (15)	0.0021 (11)	0.0050 (10)	−0.0019 (12)
C3	0.0248 (14)	0.0302 (12)	0.0365 (13)	−0.0030 (9)	−0.0002 (9)	0.0021 (10)
C4	0.0256 (14)	0.0339 (13)	0.0359 (13)	0.0016 (10)	−0.0006 (9)	−0.0040 (10)
C5	0.0351 (16)	0.0326 (13)	0.0372 (14)	0.0001 (11)	−0.0035 (10)	−0.0023 (11)
S1	0.0278 (4)	0.0548 (4)	0.0316 (3)	−0.0045 (3)	0.0014 (2)	0.0041 (3)
N2	0.0240 (13)	0.0422 (13)	0.0520 (14)	−0.0035 (10)	−0.0005 (9)	−0.0154 (11)
C6	0.0339 (16)	0.0375 (14)	0.0421 (15)	0.0076 (12)	−0.0139 (11)	−0.0110 (12)
C7	0.0360 (16)	0.0305 (13)	0.0269 (12)	0.0033 (10)	−0.0051 (9)	−0.0018 (9)
C8	0.0265 (13)	0.0239 (11)	0.0280 (11)	0.0017 (9)	−0.0005 (9)	−0.0082 (9)
C9	0.0282 (14)	0.0236 (11)	0.0330 (12)	0.0000 (9)	−0.0039 (9)	−0.0021 (9)
C10	0.0384 (17)	0.0292 (13)	0.0397 (14)	−0.0060 (11)	0.0038 (11)	−0.0047 (11)

Geometric parameters (Å, º)

Ni1—Cl1	2.2569 (7)	C4—H4	0.9500
Ni1—Cl1^{i}	2.2569 (7)	C5—H5	0.9500
Ni1—Cl2^{i}	2.2706 (7)	S1—C8	1.754 (3)
Ni1—Cl2	2.2706 (6)	N2—C10	1.340 (4)
N1—C5	1.336 (4)	N2—C6	1.341 (4)
N1—C1	1.343 (4)	N2—H1N2	0.8800
N1—H1N1	0.8800	C6—C7	1.365 (4)
C1—C2	1.376 (4)	C6—H6	0.9500
C1—H1	0.9500	C7—C8	1.391 (3)
C2—C3	1.392 (4)	C7—H7	0.9500
C2—H2	0.9500	C8—C9	1.398 (3)
C3—C4	1.389 (4)	C9—C10	1.361 (4)
C3—S1	1.772 (3)	C9—H9	0.9500
C4—C5	1.373 (4)	C10—H10	0.9500
Cl1—Ni1—Cl1^{i}	112.56 (5)	N1—C5—H5	119.7
Cl1—Ni1—Cl2^{i}	119.73 (3)	C4—C5—H5	119.7
Cl1^{i}—Ni1—Cl2^{i}	100.79 (2)	C8—S1—C3	104.00 (12)
Cl1—Ni1—Cl2	100.79 (2)	C10—N2—C6	121.9 (3)
Cl1^{i}—Ni1—Cl2	119.73 (3)	C10—N2—H1N2	119.1
Cl2^{i}—Ni1—Cl2	104.07 (4)	C6—N2—H1N2	119.1
C5—N1—C1	122.1 (2)	N2—C6—C7	120.1 (2)
C5—N1—H1N1	119.0	N2—C6—H6	119.9
C1—N1—H1N1	119.0	C7—C6—H6	119.9
N1—C1—C2	120.0 (3)	C6—C7—C8	119.2 (3)
N1—C1—H1	120.0	C6—C7—H7	120.4
C2—C1—H1	120.0	C8—C7—H7	120.4
C1—C2—C3	118.7 (3)	C7—C8—C9	119.4 (2)
C1—C2—H2	120.7	C7—C8—S1	116.3 (2)
C3—C2—H2	120.7	C9—C8—S1	124.26 (19)
C4—C3—C2	120.0 (2)	C10—C9—C8	118.6 (2)

C4—C3—S1	122.4 (2)	C10—C9—H9	120.7
C2—C3—S1	117.3 (2)	C8—C9—H9	120.7
C5—C4—C3	118.6 (3)	N2—C10—C9	120.7 (3)
C5—C4—H4	120.7	N2—C10—H10	119.7
C3—C4—H4	120.7	C9—C10—H10	119.7
N1—C5—C4	120.5 (3)		

Symmetry code: (i) −*x*+1, *y*, −*z*+3/2.

Hydrogen-bond geometry (Å, º)

D—H···*A*	*D*—H	H···*A*	*D*···*A*	*D*—H···*A*
N2—H1*N*2···Cl3^{i}	0.88	2.12	2.987 (3)	168
N1—H1*N*1···Cl3	0.88	2.32	3.078 (3)	144

Symmetry code: (i) −*x*+1, *y*, −*z*+3/2.

7. Zusammenfassung und Ausblick

Ausgangspunkt dieser Arbeit bildeten frühere Untersuchungen der Struktur-Eigenschaftsbeziehungen in Übergangsmetall-Thiocyanat-Koordinationspolymeren mit Mn(II)-, Fe(II)-, Co(II)- und Ni(II)-Kationen, sowie unterschiedlichen neutralen Co-Liganden. Im Verlauf dieser Untersuchungen wurden eine Vielzahl von Verbindungen dargestellt und der Einfluss des Metallkations sowie des Co-Liganden auf die Strukturen dieser Verbindungen und deren magnetischen Eigenschaften systematisch untersucht. Von besonderem Interesse sind hier vor Allem die Verbindungen mit Kobalt, von denen einige eine langsame Relaxation der Magnetisierung aufweisen, die vermutlich auf die Relaxation von Einzelketten zurückzuführen ist. In der hier vorliegenden Arbeit sollten diese systematischen Untersuchungen vervollständigt werden und insbesondere der Einfluss des Co-Liganden auf die Strukturen und die magnetischen Eigenschaften derartiger Verbindungen studiert werden.

Im Verlauf dieser Arbeit konnten eine Vielzahl neuer Verbindungen mit zum Teil für Thiocyanat-Koordinationspolymere noch unbekannten Strukturmotiven synthetisiert werden.

Die mit Abstand wichtigsten Ergebnisse wurden jedoch für Verbindungen mit Kobalt erhalten, die eine langsame Relaxation der Magnetisierung zeigen und deren magnetisches Verhalten die bekannten Verbindungen in einem völlig neuen Licht erscheinen lassen. Hierüber wurde in Kapitel 3 berichtet. Hier wurde zunächst über Untersuchungen mit dem Liganden 4-(3-Phenylpropyl)pyridin (PPP) berichtet. Es wurde ein vergleichsweise großer monodentater Ligand gewählt, da untersucht werden sollte, welchen Einfluss die Struktur auf die magnetischen Eigenschaften und insbesondere auf die Interkettenwechselwirkungen hat. Die Intrakettenabstände zwischen den Kobaltkationen sollten konstant bleiben, da nach wie vor Thiocyanatanionen die Metallzentren verbrücken, jedoch sollte sich der Abstand zwischen den Ketten durch die Größe des Liganden verändern. Die Synthese einer entsprechenden Verbindung mit der typischen eindimensionalen Struktur mit μ-1,3 verbrückenden Thiocyanatanionen verlief erfolgreich und es zeigte sich, dass die Interkettenabstände durch die Wahl des Liganden im Vergleich zu denen in bekannten Verbindungen tatsächlich vergrößert werden konnten.

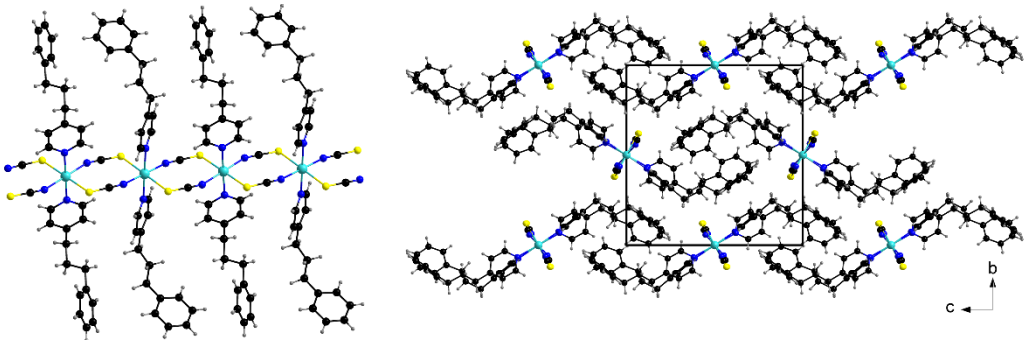

Abbildung 11. Ausschnitt aus der Kristallstruktur von $[Co(NCS)_2(PPP)_2]_n$ mit Blick auf die Kobalt-Thiocyanatketten (links) und das Packungsbild (rechts).

Die nachfolgenden Magnetmessungen ergaben, dass diese Verbindung im Gegensatz zu den vorherigen Verbindungen einen ferromagnetischen Grundzustand aufweist. In diesem Zusammenhang sei erwähnt, dass die entsprechende Stammverbindung mit Pyridin vermutlich ebenfalls einen ferromagnetischen Grundzustand aufweist, deren magnetisches Verhalten jedoch noch nicht abschließend aufgeklärt worden ist. Wie in den anderen Verbindungen auch, wird ein frequenzabhängiger Versatz der Peakmaxima in der AC Suszeptibilitätsmessungen beobachtet,

welcher auf eine langsame Relaxation der Magnetisierung hindeutet. Der Mydosh Parameter, welcher aus dem Versatz der Peakmaxima der AC Suszeptibilitätsmessungen errechnet wird, zeigte jedoch kleine Werte, welche untypisch für Einzelkettenmagneten sind. Die weiteren Analysen ergaben deutliche Hinweise darauf, dass die in dieser Verbindung beobachteten Relaxationen vermutlich nicht auf die Relaxation von Einzelketten zurückzuführen sind, sondern dass es sich bei dieser Verbindung eher um einen 3D-Ferromagneten handelt.

Eine Verbindung mit vergleichbarer Struktur wurde auch mit 4-(4-Chlorbenzyl)pyridin als Co-Liganden erhalten. Auch wenn es sich hierbei ebenfalls um einen relativ großen monodentaten Liganden handelt, sind die Interkettenabstände nicht wie erwartet größer als bei anderen vergleichbaren Verbindungen. Die magnetischen Messungen ergaben, dass die Verbindung $[Co(NCS)_2(4\text{-}(4\text{-Chlorbenzyl})pyridin)_2]_n$ einen metamagnetischen Übergang bei $H_C = 260$ Oe besitzt, und sie somit einen antiferromagnetischen Grundzustand aufweist. Die AC Suszeptibilitätsmessungen zeigen einen frequenzabhängigen Versatz und die Auswertung der Daten bestätigte, dass es sich bei dieser Verbindung um einen Einzelkettenmagneten handelt (Abbildung 12).

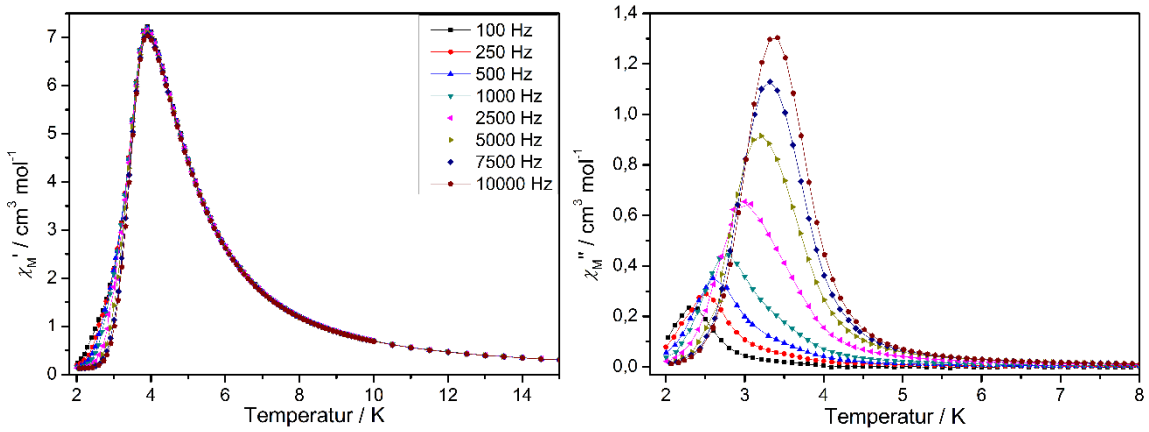

Abbildung 12. AC-Suszeptibilitätsmessungen der Verbindung $[Co(NCS)_2(4\text{-}(4\text{-Chlorbenzyl})pyridin)_2]_n$. Verlauf des Realteils (links) und des Imaginärteils (rechts).

In weiteren Untersuchungen wurde versucht eine entsprechende Verbindung mit 4-Acetylpyridin zu erhalten. Die Synthese der eindimensionalen Verbindung $[Co(NCS)_2(4\text{-Acetylpyridin})_2]_n$ gestaltete sich jedoch weitaus schwieriger, da zwar problemlos eine Verbindung mit der Stöchiometrie von 1:2 (Metall:Ligand) synthetisiert werden konnte, diese Verbindung jedoch entgegen der Erwartungen eine Schichtstruktur aufweist. Dieser Koordinationsmodus ist zwar nicht unbekannt gewesen, jedoch für Verbindungen mit $Co(NCS)_2$ ungewöhnlich (Abbildung 13).

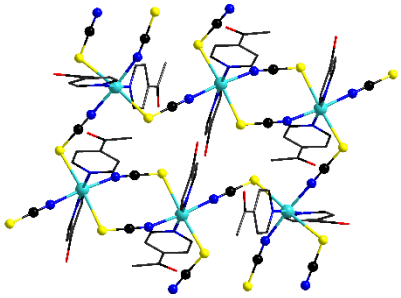

Abbildung 13. Ausschnitt aus der Kristallstruktur der Verbindung $[Co(NCS)_2(4\text{-Acetylpyridin})_2]_n$.

Es konnten im Zuge der systematischen Untersuchungen auch eine Reihe von 4-acetylpyridinreichen Vorläuferverbindungen wie $Co(NCS)_2(4\text{-Acetylpyridin})_4$ und $Co(NCS)_2(4\text{-Acetylpyridin})_2(H_2O)_2$ erhalten werden. Beim thermischen Abbau von $Co(NCS)_2(4\text{-Acetylpyridin})_4$ wurde jedoch auch nur das 2D-Isomer erhalten. Im Gegensatz hierzu konnte durch Tempern von $Co(NCS)_2(4\text{-Acetylpyridin})_2(H_2O)_2$ eine weitere kristalline Phase erhalten werden, deren Struktur *ab-initio* aus Röntgen-Pulverdaten bestimmt wurde und bei der es sich um das gewünschte 1D-Isomer handelte. Weitere Untersuchungen belegten, dass das 1D-Isomer zwischen Raumtemperatur und dem Zersetzungspunkt metastabil ist, wohingegen das 2D-Isomer die thermodynamisch stabile Phase darstellt.

Die durchgeführten magnetischen Messungen an der 2D Verbindung ergaben, dass diese paramagnetisches Verhalten zeigt. Im Gegensatz hierzu werden für das 1D-Isomer wiederum Relaxationen beobachtet, die jedoch wie die bei $[Co(NCS)_2(PPP)_2]_n$ nicht auf die Relaxation von Einzelketten zurückgeführt werden können. Überraschenderweise weist auch diese Verbindung einen ferromagnetischen Grundzustand auf.

In weiteren Untersuchungen wurden zwei weitere Verbindungen der Zusammensetzung $[Co(NCS)_2(4\text{-Vinylpyridin})_2]_n$ und $[Co(NCS)_2(4\text{-Benzoylpyridin})_2]_n$ dargestellt, welche ebenfalls eindimensionale Strukturen mit μ-1,3 verbrückenden Thiocyanatanionen ausbilden, wobei in der Struktur von $[Co(NCS)_2(4\text{-Benzoylpyridin})_2]_n$ die Anionen *cis*- und nicht wie sonst üblich *trans*-koordiniert sind (Abbildung 14).

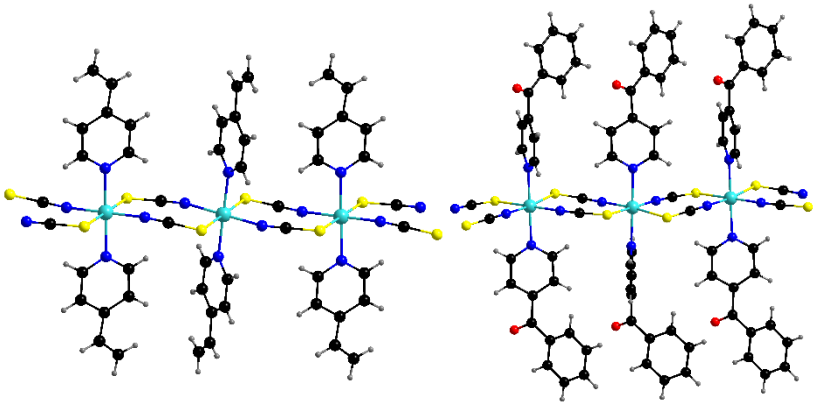

Abbildung 14. Ausschnitt aus der Kristallstruktur von $[Co(NCS)_2(4\text{-Vinylpyridin})_2]_n$ (links) und $[Co(NCS)_2(4\text{-Benzoylpyridin})_2]_n$ (rechts).

Die magnetischen Messungen der beiden Verbindungen zeigen, dass es sich in beiden Fällen um Metamagneten handelt. Die kritischen Feldstärken liegen bei 575 Oe ($[Co(NCS)_2(4\text{-Vinylpyridin})_2]_n$) und 300 Oe ($[Co(NCS)_2(4\text{-Benzoylpyridin})_2]_n$). AC Suszeptibilitätsmessungen unterhalb der kritischen Feldstärke zeigen zwei deutliche Maxima im Imaginärteil. Das Maximum im Bereich von 2-3.5 K zeigt einen frequenzabhängigen Versatz, wohingegen das Maximum bei höheren Temperaturen frequenzunabhängig ist. Das Auftreten von zwei Maxima könnte auf einen zweiten Relaxationsprozess zurückzuführen sein, jedoch steht eine abschließende Interpretation der Ergebnisse noch aus, um den Sachverhalt eindeutig zu klären, weswegen die Ergebnisse dieser Untersuchungen noch nicht publiziert worden sind (Abbildung 15).

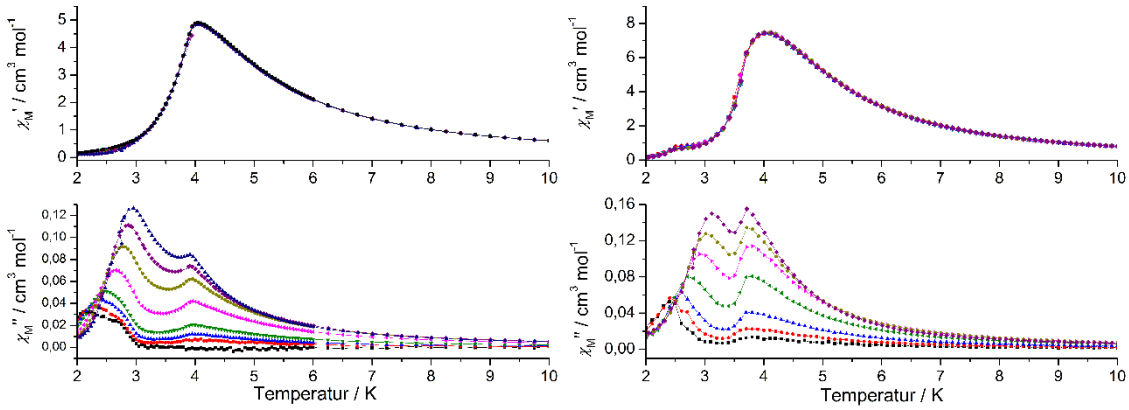

Abbildung 15. AC-Suszeptibilitätsmessungen der Verbindungen $[Co(NCS)_2(4\text{-Vinylpyridin})_2]_n$ (links) und der Verbindung $[Co(NCS)_2(4\text{-Benzoylpyridin})_2]_n$ (rechts). Verlauf des Realteils (oben) und des Imaginärteils (unten) bei verschiedenen Frequenzen.

Werden nun die Ergebnisse der magnetischen Messungen der in dieser Arbeit vorgestellten Verbindungen mit denen vorangegangener Untersuchungen verglichen, wird offensichtlich, dass sich all diese Verbindungen gemäß Ihrer magnetischen Eigenschaften in zwei Gruppen aufteilen, von denen die Verbindungen der einen Gruppe einen antiferromagnetischen, die der anderen Gruppe einen ferromagnetischen Grundzustand aufweisen (Tabelle 2). All diese Verbindungen zeigen eine langsame Relaxation der Magnetisierung, wobei die Analysen ergaben, dass diese Relaxationen nur in den Verbindungen mit einem antiferromagnetischen Grundzustand auf die Relaxation von Einzelketten zurückgeführt werden können, wohingegen die in den Verbindungen mit einem ferromagnetischen Grundzustand vermutlich auf die Relaxation der Wände von 3D-Domänen zurückgeführt werden können. Wie sich die Stammverbindung mit Pyridin als Co-Ligand hier einordnet, ist bislang noch nicht eindeutig geklärt. Da diese Verbindung gemäß der damaligen Befunde einen ferromagnetischen Grundzustand aufweist, sollten die in den AC-Messungen beobachteten Relaxationen auf 3D-Domänen und nicht auf Einzelkettenmagnetismus zurückgeführt werden können. Andererseits wurde ein Mydosh-Parameter bestimmt, der dem entspricht, welcher für superparamagnetisches Verhalten erwartet wird. Erwartungsgemäß wird auch eine relative geringe Verteilung der Relaxationszeiten bestimmt und die Analyse der Relaxationszeiten gemäß dem Arrheniusgesetz führt zu relativ vernünftigen Werten für die Energiebarriere sowie dem präexponentiellen Faktor. Die Art der damaligen Analysen unterscheidet sich jedoch von denen folgender Arbeiten, sodass die magnetischen Eigenschaften dieser Verbindungen erneut untersucht werden müssen.

In diesem Zusammenhang sei auch erwähnt, dass für all diese Verbindungen nur zwei unterschiedliche Strukturmotive gefunden wurden. In den einen verlaufen benachbarte Kobaltthiocyanat-Ketten parallel, wohingegen diese in den anderen Verbindungen gegeneinander verkantet sind. Leider korreliert dies nicht mit dem magnetischen Grundzustand, weswegen noch weitere Untersuchungen vonnöten sind.

Tabelle 2. Ausgewählte Parameter für die Verbindungen $[Co(NCS)_2(4\text{-}(4\text{-Chlorbenzyl})pyridin)_2]_n$ (ClBP), $[Co(NCS)_2(4\text{-Ethylpyridin})_2]_n$ (Etpy), $[Co(NCS)_2(1,2\text{-bis}(4\text{-pyridiyl})ethylen)]_n$ (bpe), $[Co(NCS)_2(1,2\text{-bis}(4\text{-pyridiyl})ethan)]_n$ (bpa), $[Co(NCS)_2(4\text{-Acetylpyridin})_2]_n$ (4-Acpy) und $([Co(NCS)_2(4\text{-}(3\text{-Phenylpropyl})pyridin)_2]_n$ (PPP). AF: Antiferromagnetischer Grundzustand, FM: Ferromagnetischer Grundzustand, H_C: Kritische Feldstärke, T_C: kritische Temperatur, J: Intrakettenwechselwirkungen, zJ': Interkettenwechselwirkungen, ΔE: Energiebarriere, τ_0: präexponentieller Faktor, Δa: Maß für die Anisotropie, α: Verteilung der Relaxationszeiten, φ: Mydosh Parameter.

	ClBP	Etpy	bpe	bpa	4-Acpy	PPP
Grundzustand	AF	AF	AF	AF	FM	FM
H_c (Oe)	~260 (2 K)	~175 (1.5 K)	~400 (2 K)	~40 (2K)	-	-
T_c (K)	3.9	3.4	4.0	3.1	3.8	3.3
J/k_B (K)	29.8	27.0	26.8	27.8	30.2	28.4
zJ'/k_B (K)	−0.43	−0.42	−0.66	−0.22	+0.17	+0.15
$\Delta E/k_B$ (K)	37.1	45.3	33.3	39.2	74	116
τ_0 (s)	9.5×10^{-11}	2×10^{-12}	1.2×10^{-11}	1.2×10^{-11}	6×10^{-13}	10^{-19}
Δ_A/k_B (K)	22.2 (k=1)	31.8 (k=1)	19.9 (k=1)	25.3 (k=1)	-	-
α	0.09 - 0.37	0.1 - 0.4	0.10 - 0.46	0.06 - 0.41	0.4 - 0.52	-
φ	0.14	0.14	0.16	0.11	0.074	0.059

In weiteren systematischen Untersuchungen wurde auch 4-*tert*-Butylpyridin als Co-Ligand verwendet. Mit den Übergangsmetallen Mn(II), Fe(II), Co(II) und Ni(II) konnten sowohl ligandenreiche 1:4 Verbindungen als auch ligandenarme 1:2 Verbindungen erhalten werden, jedoch werden in den Kristallstrukturen der Verbindungen mit verbrückenden Anionen bislang unbekannte Thiocyanat-Koordinationsnetzwerke beobachtet. Jedes Metallkation ist von vier µ-1,3-verbrückenden Thiocyanatanionen koordiniert, welche jeweils zu einem anderen weiteren Metallkation verbrücken. Diese Art von Netzwerk war bis dahin nur für Azidanionen bekannt (Abbildung 16).

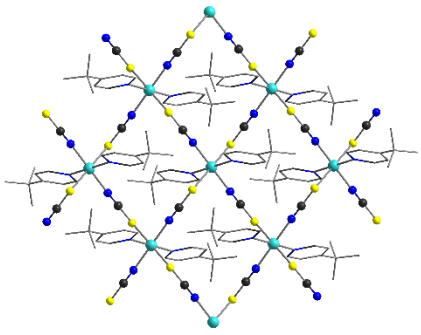

Abbildung 16. Ausschnitt aus der Kristallstruktur $[Ni(NCS)_2(4\text{-}tert\text{-Butylpyridin})_2]_n$.

Die Untersuchungen der magnetischen Eigenschaften dieser Schichtverbindungen ergaben, dass sowohl die Verbindung $[Ni(NCS)_2(4\text{-}tert\text{-Butylpyridin})_2]_n$ als auch die Verbindung $[Co(NCS)_2(4\text{-}tert\text{-Butylpyridin})_2]_n$ Ferromagneten sind. Die Verbindungen mit $Mn(NCS)_2$ und $Fe(NCS)_2$ waren deutlich schwieriger zugänglich und nicht phasenrein zu erhalten, jedoch zeigten die magnetischen Messungen, dass $[Mn(NCS)_2(4\text{-}tert\text{-Butylpyridin})_2]_n$ einen antiferromagnetischen Grundzustand hat.

Aufbauend auf den Ergebnissen für $[Co(NCS)_2(4\text{-Acetylpyridin})_2]_n$, wurde auch untersucht, ob mit anderen Metallkationen unterschiedliche Isomere dargestellt werden können und welchen Einfluss das Metallkation auf deren Stabilität und deren magnetische Eigenschaften ausübt. Für $[Ni(NCS)_2(4\text{-Acetylpyridin})_2]_n$ konnten ebenfalls beide Isomere dargestellt werden, wobei wie bei der Verbindung mit $Co(NCS)_2$ die Schichtstruktur gegenüber der Kettenstruktur thermodynamisch stabil ist. Im

Gegensatz hierzu konnten für Eisen und Mangan nur 1D-Isomere dargestellt werden, wobei für Mangan ein Gemenge unterschiedlicher Modifikationen erhalten wurde.

Die magnetischen Messungen ergaben, dass die zweidimensionale Struktur $[Ni(NCS)_2(4\text{-Acetylpyridin})_2]_n$ (2D) ferromagnetisches Verhalten aufweist, wohingegen die eindimensionale Struktur paramagnetisches Verhalten zeigt. Die Verbindung $[Fe(NCS)_2(4\text{-Acetylpyridin})_2]_n$ ist ein Metamagnet mit einer kritischen Feldstärke von 700 Oe (Abbildung 17).

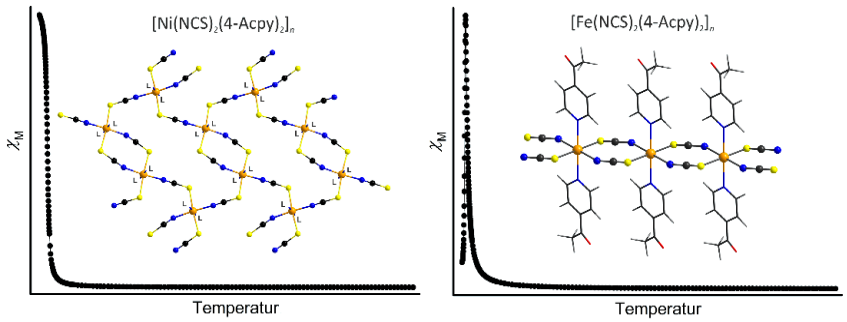

Abbildung 17. DC-Suszeptibilitätsmessung und Ausschnitt aus der Kristallstruktur von $[Ni(NCS)_2(4\text{-Acetylpyridin})_2]_n$ (links); DC-Suszeptibilitätsmessung und Ausschnitt aus der Kristallstruktur von $[Fe(NCS)_2(4\text{-Acetylpyridin})_2]_n$ (rechts).

Des Weiteren wurde eine Verbindung mit dem bereits bekannten zweidimensionalen Strukturtyp aus $Ni(NCS)_2$ und 4-Ethylisonicotinat synthetisiert. Die magnetischen Messungen an dieser Verbindung zeigten, dass diese Verbindung einen ferromagnetischen Ordnungspunkt aufweist, wie bereits die Verbindung $[Ni(NCS)_2(4\text{-Acetylpyridin})_2]_n$ (2D). Jedoch steht die abschließende Auswertung der erhaltenen Daten noch aus, sodass diese Ergebnisse bislang nicht publiziert sind (Abbildung 18).

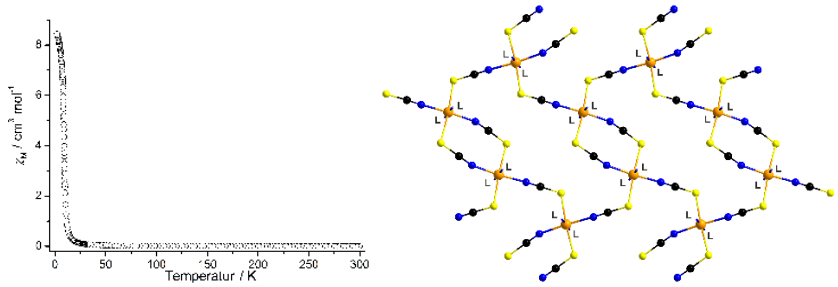

Abbildung 18. DC-Suszeptibilitätsmessungen von $[Ni(NCS)_2(Ethylisonicotinat)_2]_n$ (links) und Ausschnitt aus der Kristallstruktur (rechts); L = Ethylisonicotinat.

In weiteren Untersuchungen wurde auch versucht Verbindungen mit $Ni(NCS)_2$ und 4-(hydroxymethyl)pyridin herzustellen. Hier stellte sich die Frage, ob wieder die typischen 1D-Kettenstrukturen erhalten werden, oder ob auch die Hydroxylgruppe des Co-Liganden an der Metallkoordination beteiligt ist. Neben einer Reihe von diskreten Komplexen konnte auch eine Verbindung der Zusammensetzung $Ni(NCS)_2(4\text{-(hydroxymethyl)pyridin})_2$ kristallisiert werden, die eine eindimensionale Struktur aufweist. Eine Einkristallstrukturanalyse ergab, dass jeweils zwei Ni-Kationen über zwei μ-1,3-verbrückende Thiocyanatanionen zu Dimeren verknüpft sind, welche durch μ-1,6 verbrückende 4-(Hydroxymethyl)pyridin) Liganden zu Ketten verbrückt sind (Abbildung 19).

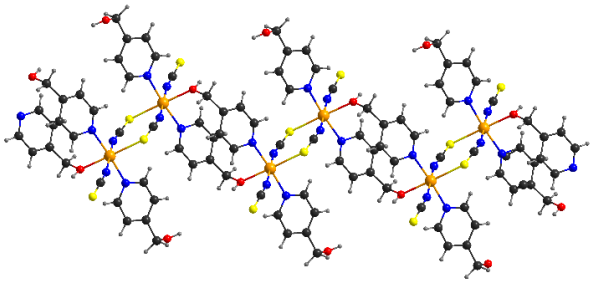

Abbildung 19. Ausschnitt aus der Kristallstruktur $[Ni(NCS)_2(4\text{-(hydroxymethyl)pyridin})_2]_n$.

Die Auswertung der magnetischen Messungen zeigte, dass die diese Verbindung einen antiferromagnetischen Ordnungspunkt bei T_N = 6.7 K aufweist.
Auch die systematischen Untersuchungen zu $Ni(NCS)_2$, 4-(3-Phenylpropyl)pyridin und 4-(4-Chlorbenzyl)pyridin zeigten, dass eine eindimensionale Struktur zugänglich ist, jedoch weisen die erhaltenen Verbindungen paramagnetisches Verhalten mit ferromagnetischen Wechselwirkungen auf; dieses Verhalten wurde zuvor auch schon bei vergleichbaren Verbindungen festgestellt. Die Untersuchungen zu Mn(II), Fe(II), Ni(II) und 3-Acetylpyridin zeigten, dass diskrete Komplexe gegenüber Koordinationspolymeren bevorzugt gebildet werden, und ligandenarme Verbindungen nur mittels thermischen Abbaus zugänglich sind.
Weitere Untersuchungen wurden zu den diamagnetischen Übergangsmetallkationen Cd(II) und Zn(II) unternommen, da diese eine höhere Chalkophilie als ihre paramagnetischen Analoga aufweisen und ein verbrückender Koordinationsmodus der Thiocyanatanionen begünstigt ist. Außerdem weisen diese Verbindungen häufig Polymorphe auf, so konnten für $[Cd(NCS)_2(4\text{-Acetylpyridin})_2]_n$ zwei Polymorphe identifiziert werden, die sich ausschließlich durch die Stellung der Acetylgruppe in der Kristallstruktur unterscheiden. Die Verbindung $[Cd(NCS)_2(3\text{-Acetylpyridin})]_n$ hingegen weist eine bis dahin unbekannte Koordinationstopologie auf, in der sowohl die Thiocyanatanionen als auch die 3-Acetylpyridin-Liganden an der einer dreidimensionalen Koordination beteiligt sind.
Zusammenfassend konnten die systematischen Untersuchungen an Übergangsmetall-Thiocyanaten und verschiedenen Pyridinderivaten weitere Erkenntnisse bezüglich der Struktur-Eigenschaftsbeziehungen derartiger Koordinationspolymere liefern. Dennoch bleibt auch hier eine Reihe von Fragen offen, die vor allem die Verbindungen mit einer langsamen Relaxation der Magnetisierung betreffen. Hier wäre vor allem von Interesse, was für den unterschiedlichen magnetischen Grundzustand verantwortlich ist und ob überhaupt ein einfacher Zusammenhang zwischen diesem Grundzustand und strukturellen Paramatern hergestellt werden kann. Hierzu muss zunächst die Richtung der „easy axis“ bestimmt werden, wozu größere Einkristalle hergestellt und magnetisch untersucht werden müssen. Da viele dieser Verbindung jedoch bislang nur über den thermischen Abbau zugänglich sind, gestaltet sich die Synthese größerer Einkristalle als schwierig.
Es konnten zwei Verbindungen synthetisiert werden, die einen ferromagnetischen Grundzustand aufweisen und eine langsame Relaxation der Magnetisierung zeigen und deren magnetisches Verhalten weit komplizierter als das anderer ist. Diese Verbindungen tragen dazu bei, die Ursachen des Auftretens von langsamer Relaxation der Magnetisierung weiter zu ergründen, da Einzelkettenmagnetismus nicht der alleinige Grund für das Auftreten dieses Phänomens ist. Es gibt noch eine Reihe weiterer Phänomene, die die langsame Relaxation der Magnetisierung hervorrufen können. Außerdem konnte gezeigt werden, dass die Wahl des neutralen Co-Liganden einen großen Einfluss auf die Topologie der jeweiligen Verbindungen hat und so konnten neben eindimensionalen auch zweidimensionale Strukturen synthetisiert werden. Auch die magnetischen Untersuchungen an diesen Verbindungen geben weitere Aufschlüsse über die Zusammenhänge von Struktur und Eigenschaften. So konnte gezeigt werden, dass die chemische Modifikation sowohl einen großen Einfluss auf die Struktur als auch auf die magnetischen Eigenschaften hat.

8. Anhang

8.1. Supporting Information: A Co(II) Thiocyanato Coordination Polymer with 4-(3-phenylpropyl)pyridine: The Influence of the Co-Ligand on the Magnetic Properties

Suppprting Information

A New Co(II) Thiocyanato Coordination Polymer with 4-(3-Phenyl-propyl)pyridine: Influence of the Co-Ligand on the Magnetic Properties

Julia Werner, Michał Rams, Zbigniew Tomkowicz, and Christian Näther

`1

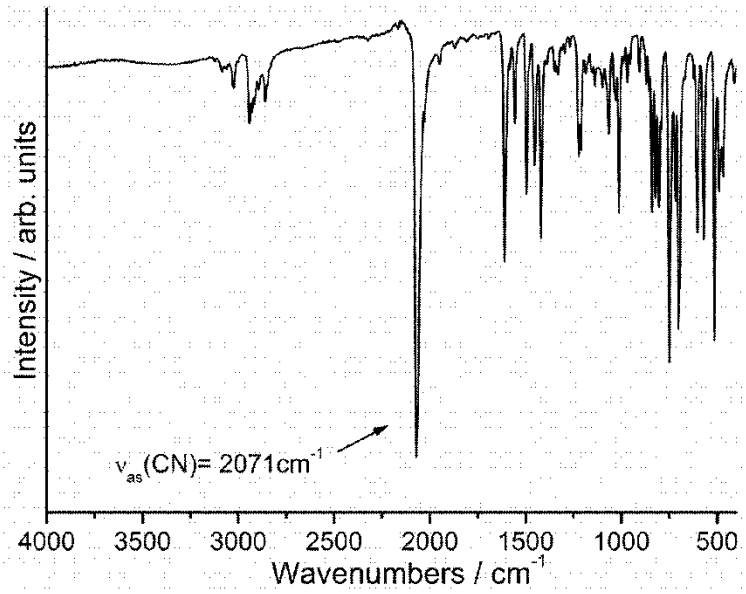

Figure S1. IR spectra of compound **1**.

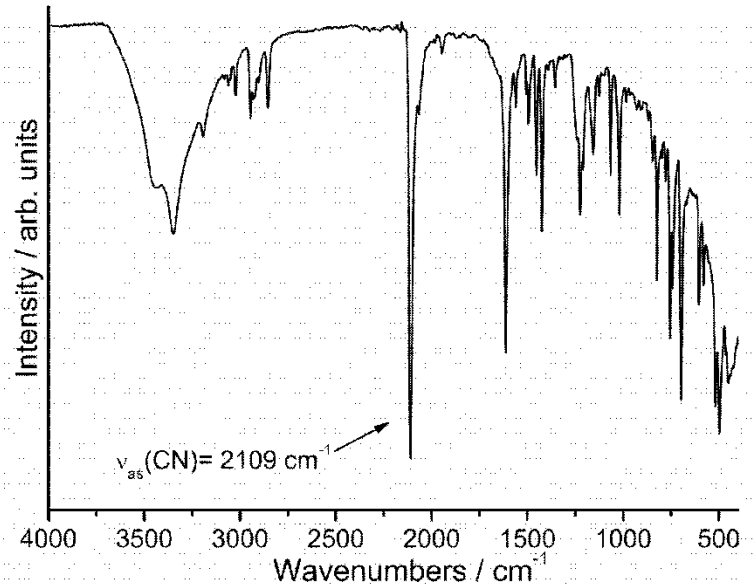

Figure S2. IR spectra of compound **2**.

`2

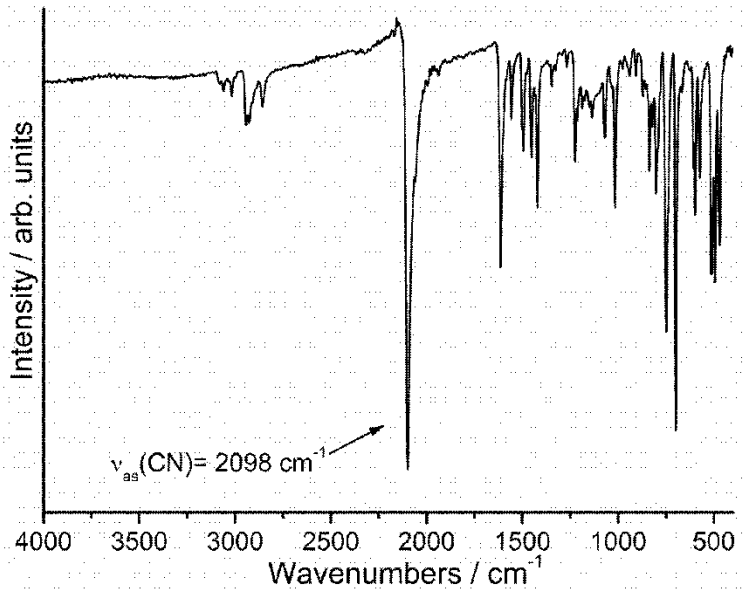

Figure S3. IR spectra of compound **3**.

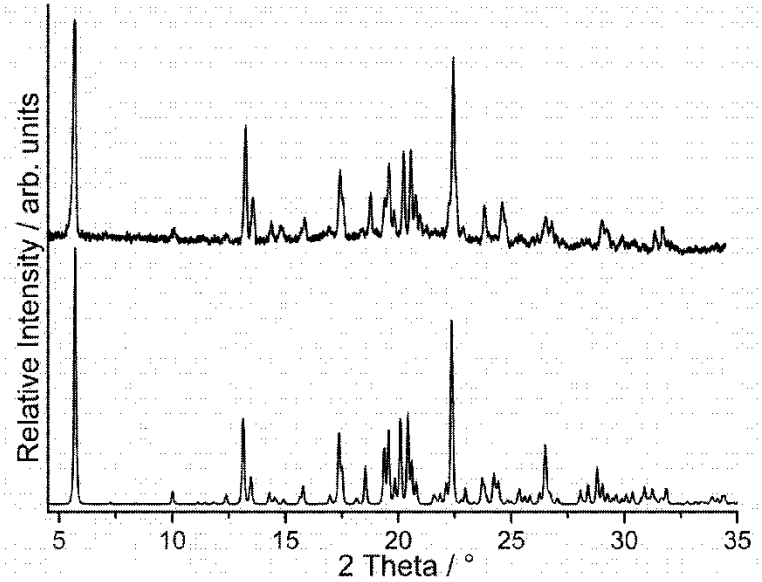

Figure S4. Experimental (top) X-ray powder pattern of compound **2** measured in transmission geometry and calculated X-ray powder pattern of $Mn(NCS)_2$(4-(3-Phenylpropyl)pyridine)$_2$(H_2O)$_2$ retrieved from literature (bottom).

`3

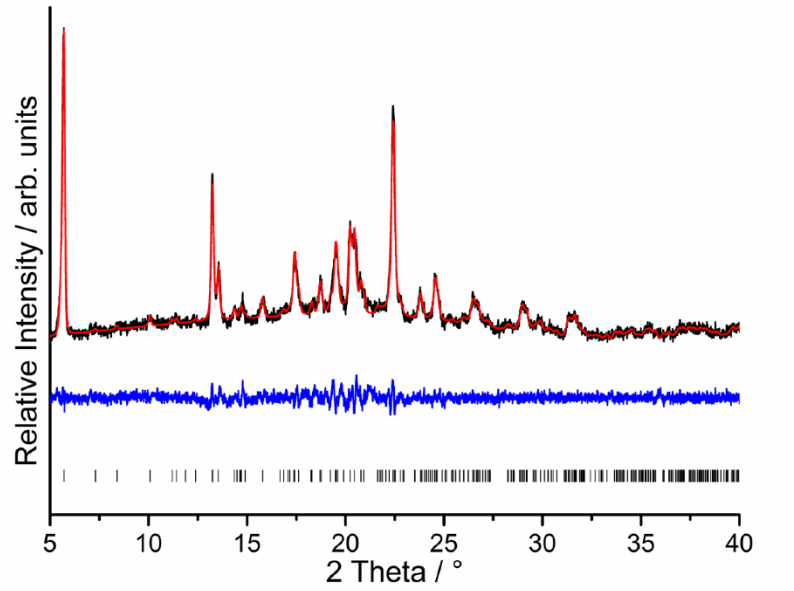

Figure S5. Pawley fit of a pattern of compound **2** measured in transmission geometry.

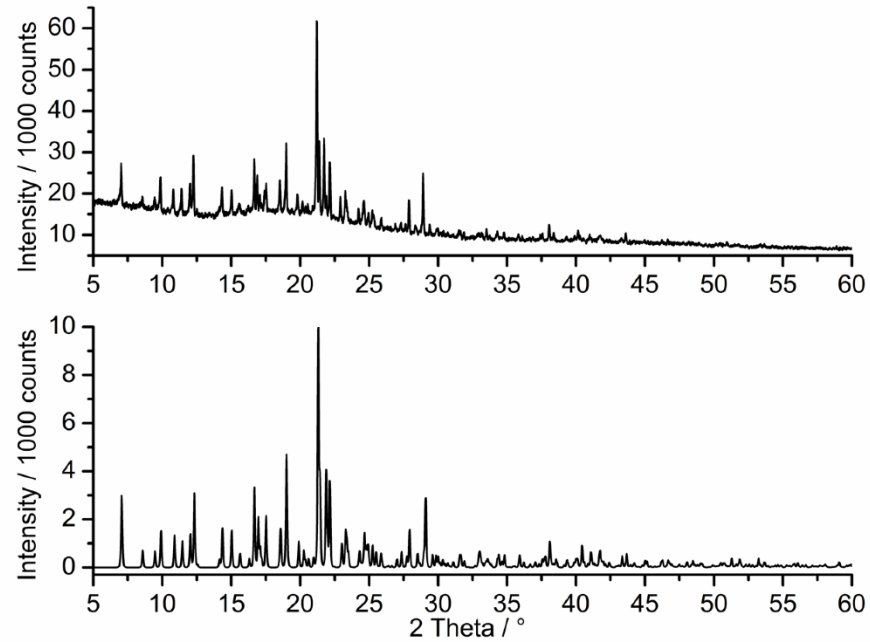

Figure S6. Experimental (top) and calculated (bottom) X-ray powder pattern of compound **1** measured in refelction geometry.

`4

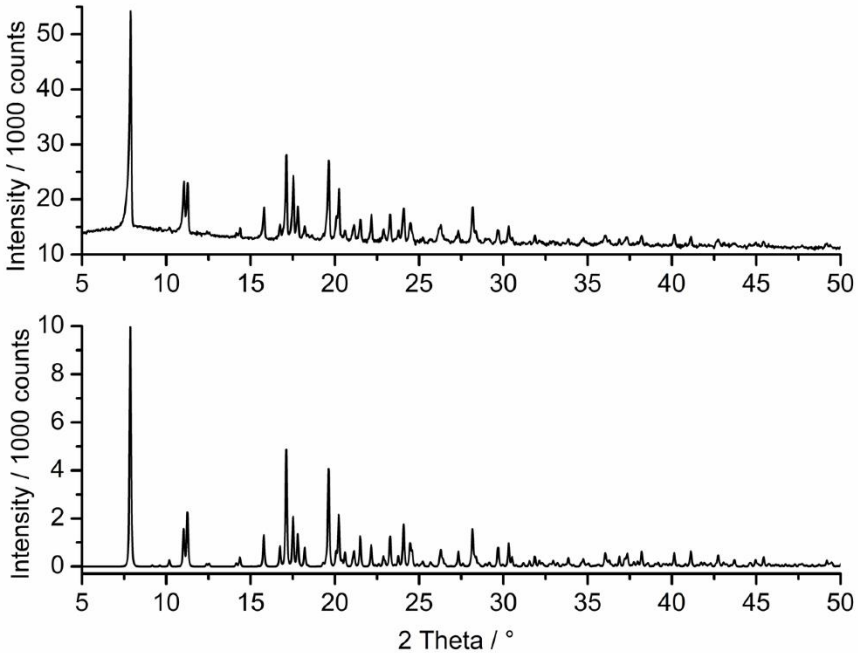

Figure S7. Experimental (top) and calculated (bottom) X-ray powder pattern of compound **3** measured in reflection geometry.

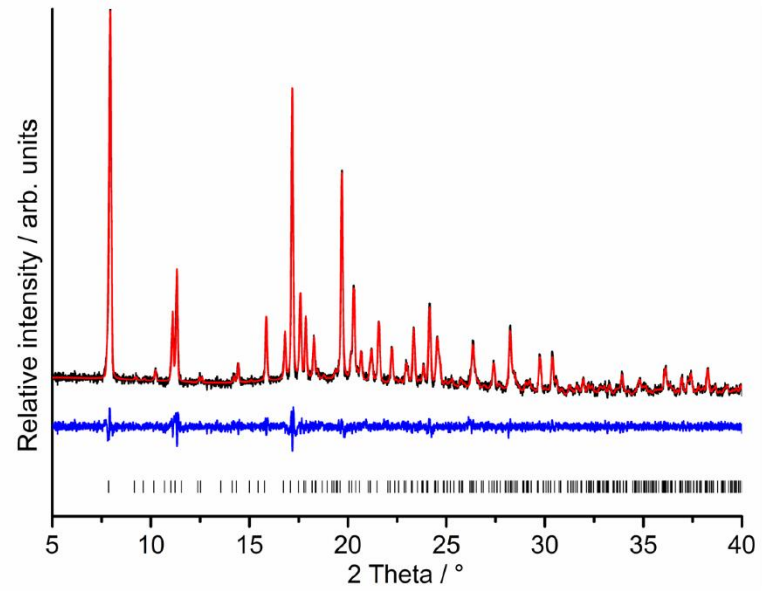

Figure S8. Pawley fit of a pattern of compound **3** measured in reflection geometry.

`5

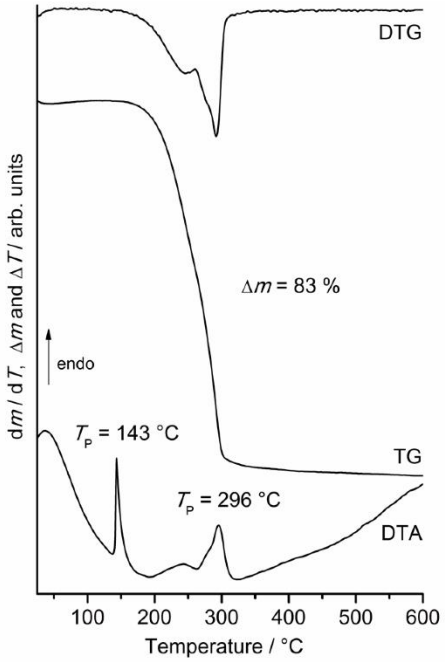

Figure S9. DTA-, TG- and DTG-curve of compound **1**. Heating rate = 4 °C/min.

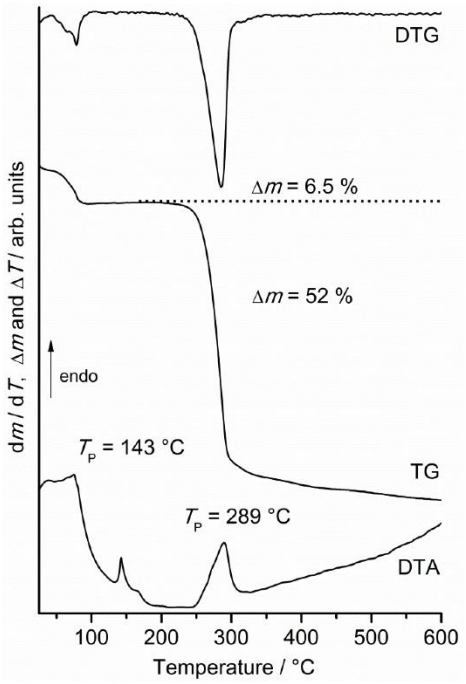

Figure S10. DTA-, TG- and DTG-curve of compound **2**. Heating rate = 4 °C/min.

`6

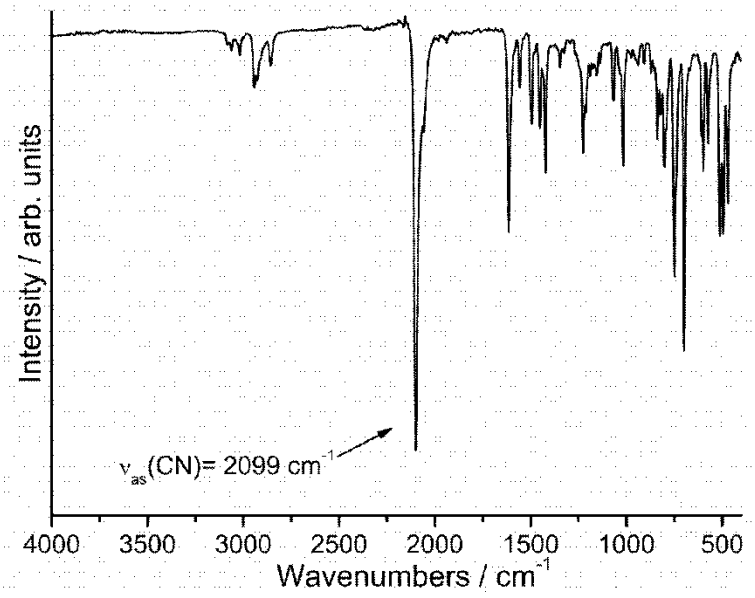

Figure S11. IR spectra of the residue of obtained by thermal decomposition of **2**.

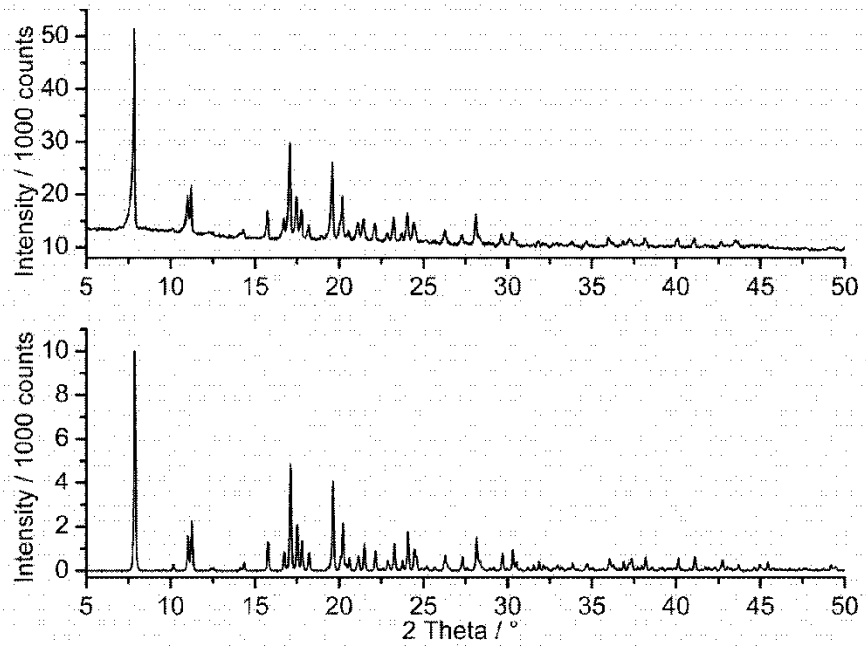

Figure S12. Experimental X-ray powder pattern of the residue obtained by thermal decomposition of **2** (top) and calculated pattern for **3** (bottom).

`7

Table S1. Selected bond lengths (Å) and angles (°) for **1**.

Co(1)-N(1)	2.0809(16)	Co(1)-N(31)	2.1922(14)
Co(1)-N(11)	2.2466(15)		
N(1A)-Co(1)-N(1)	180.000(1)	N(1)-Co(1)-N(11)	88.36(6)
N(1)-Co(1)-N(31A)	89.16(6)	N(31)-Co(1)-N(11A)	88.12(5)
N(1)-Co(1)-N(31)	90.84(6)	N(31)-Co(1)-N(11)	91.88(5)
N(1)-Co(1)-N(11A)	91.64(6)		

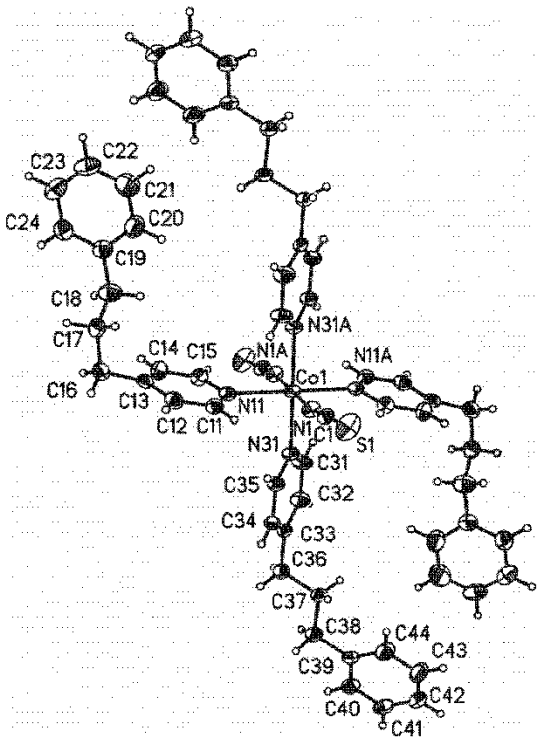

Figure S13. ORTEP plot of **1** with labelling and displacement ellipsoids drawn at the 50 % probability level. Symmetry transformation used to generate equivalent atoms: A: -x+1,-y+1,-z+1.

`8

Table S2. Selected bond lengths (Å) and angles (°) for **3**.

Co(1)-N(1)	2.077(4)	Co(2)-N(2)	2.055(4)
Co(1)-N(11)	2.161(4)	Co(2)-N(31)	2.169(5)
Co(1)-S(2)	2.5801(13)	Co(2)-S(1)	2.6232(14)
N(1)-Co(1)-N(1A)	180.0(2)	N(31B)-Co(2)-N(31)	180.0(2)
N(1)-Co(1)-N(11)	89.69(16)	N(2)-Co(2)-N(31)	90.13(18)
N(1)-Co(1)-N(11A)	90.31(16)	N(2)-Co(2)-N(31B)	89.87(18)
N(1)-Co(1)-S(2)	93.46(12)	N(2)-Co(2)-S(1)	93.69(12)
N(1)-Co(1)-S(2A)	86.54(12)	N(2)-Co(2)-S(1B)	86.31(12)
N(11)-Co(1)-S(2)	92.03(12)	N(31)-Co(2)-S(1)	91.46(12)
N(11)-Co(1)-S(2A)	87.97(12)	N(31)-Co(2)-S(1B)	88.54(12)

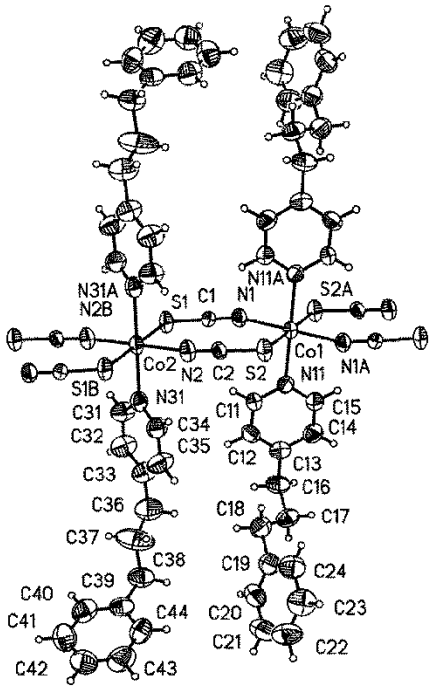

Figure S14. ORTEP plot of **3** with labelling and displacement ellipsoids drawn at the 50 % probability level. Symmetry transformation used to generate equivalent atoms: A: -x,-y+1,-z, B: -x+1,-y+1,-z.

`9

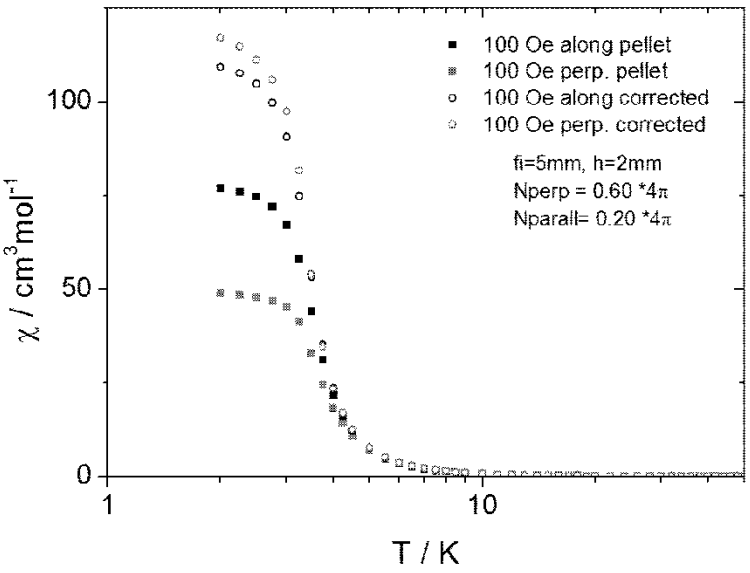

Fig. S15. The influence of demagnetization on the measured low temperature susceptibility of compound **3**. The two curves were measured using the same pellet sample, once oriented perpendicular to the field (red), and once with the flat parallel to the field (black). The open symbols denote the values corrected for the demagnetization effect. The demagnetization factors used in the two cases fulfill relation $N_{\perp} + 2N_{\parallel} = 4\pi$.

`10

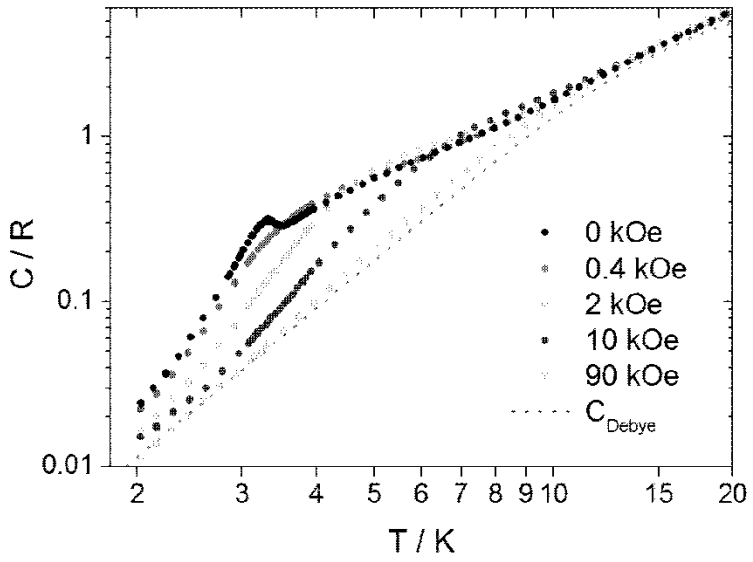

Fig. S16. Specific heat of compound **3** measured at different applied fields, using a powder sample. The dotted line represents the phonon contribution C_{Debye} to the specific heat, fitted as described in the main text. C_{Debye} is close to the experimental points measured at 90 kOe. This is expected, because high magnetic field aligns magnetic moments and the entropy change related to spins is shifted to higher temperatures. In the case of **3**, even a higher field would be necessary to obtain precisely the phonon contribution directly from the specific heat measurements. This is due to the high anisotropy of Co^{II} ions and random orientations of crystallites in the powder sample. For this reason we have chosen to fit the phonon contribution together with the magnetic contribution, and not to assume that 90 kOe data represents the phonon contribution only. The field of 0.4 kOe is enough to conceal the peak observed at zero magnetic field. The internal field is much smaller due to the demagnetization field. The demagnetization factor is close to $N = 4\pi$ for the thin, flat sample oriented perpendicular to the external field. The demagnetization field $H_{demag} = -NM/V$, where M/V is the magnetic moment per volume, is strongly dependent on temperature, due to strong $M(T)$ dependence. At T_c =3.3 K and below we estimate H_{demag} = -0.35(5) kOe basing on the magnetic measurements. At 0.4 kOe the $M(H)$ curve (measured for such a sample geometry) is already saturated above $1.5\mu_B$, which corresponds to lack of the peak in specific heat, already at 0.4 kOe.

`11

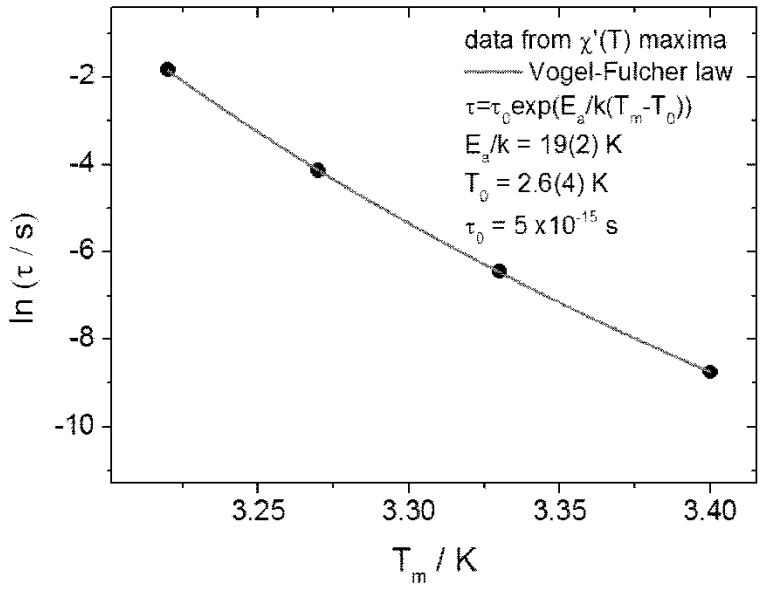

Fig. S17. Analysis of the temperature dependence of the relaxation time for **3.** T_m is the position of the $\chi'(T)$ maximum from ac measurement made using different frequency f. The relaxation time $\tau = 1/(2\pi f)$. The fit using the Vogel-Fulcher law is shown by solid line.

`12

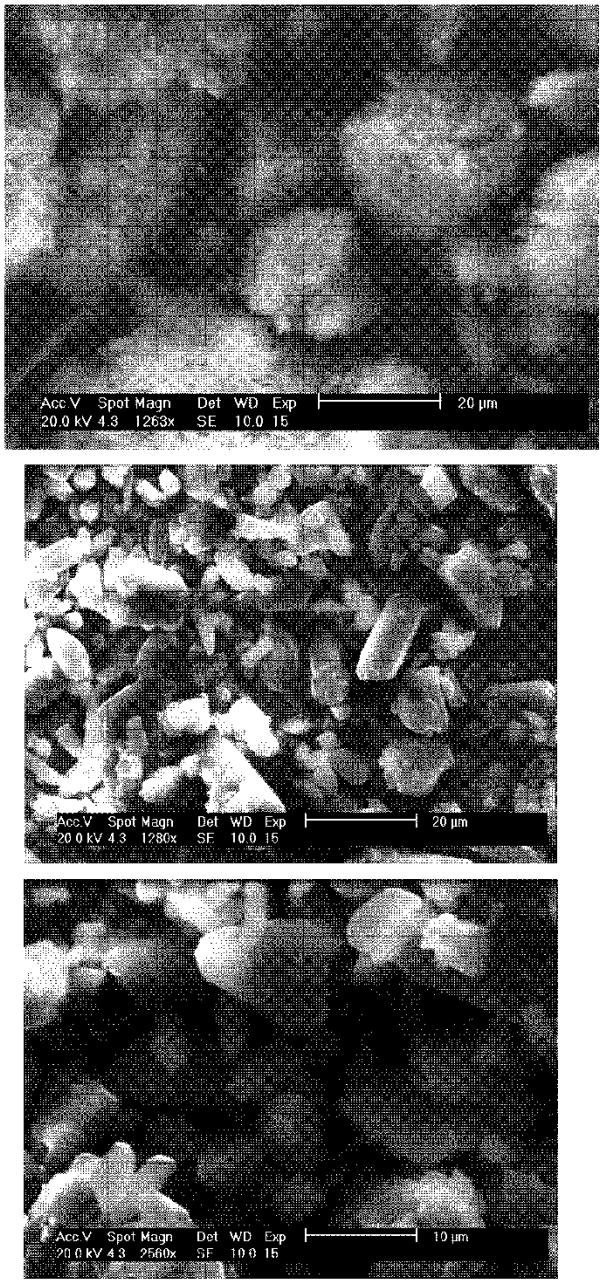

Fig. S18. SEM images of compound **3** obtained after thermal annealing (top) and obtained by synthesis at RT (mid and bottom).

`13

8.2. Supporting Information: Synthesis, Structure and Properties of $[Co(NCS)_2(4\text{-}(4\text{-Chlorobenzyl})pyridine)_2]_n$, that shows Slow Relaxations of the Magnetization and a Metamagnetic Transition

Synthesis, Structure and Properties of $[Co(NCS)_2(4\text{-}(4\text{-Chlorobenzyl})pyridine)_2]_n$, that shows Slow Magnetic Relaxations and a Metamagnetic Transition

Julia Werner, Zbigniew Tomkowicz, Michal Rams, Stefan G. Ebbinghaus, Tristan Neumann and Christian Näther

Content

`1

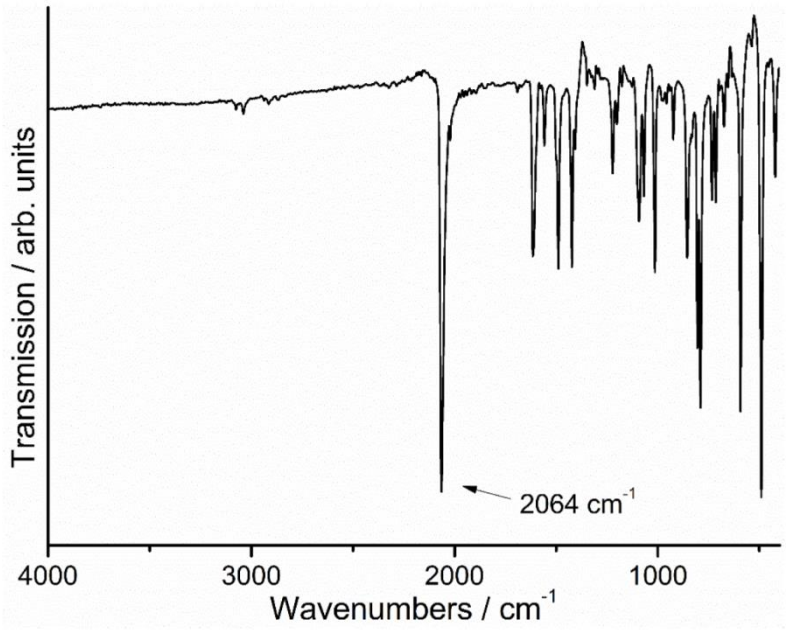

Figure S1: IR spectra of **1**. The CN stretching vibration is given.

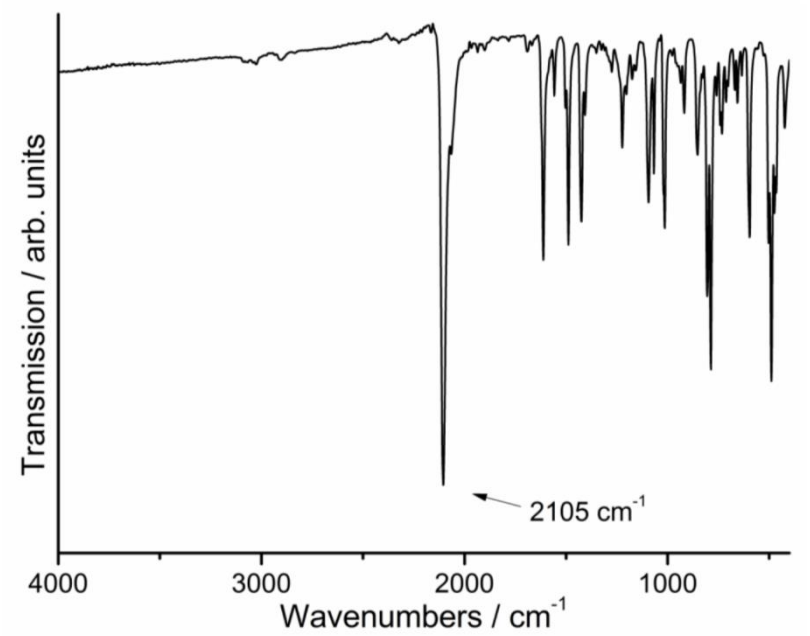

Figure S2: IR spectra of **2**. The CN stretching vibration is given.

`2

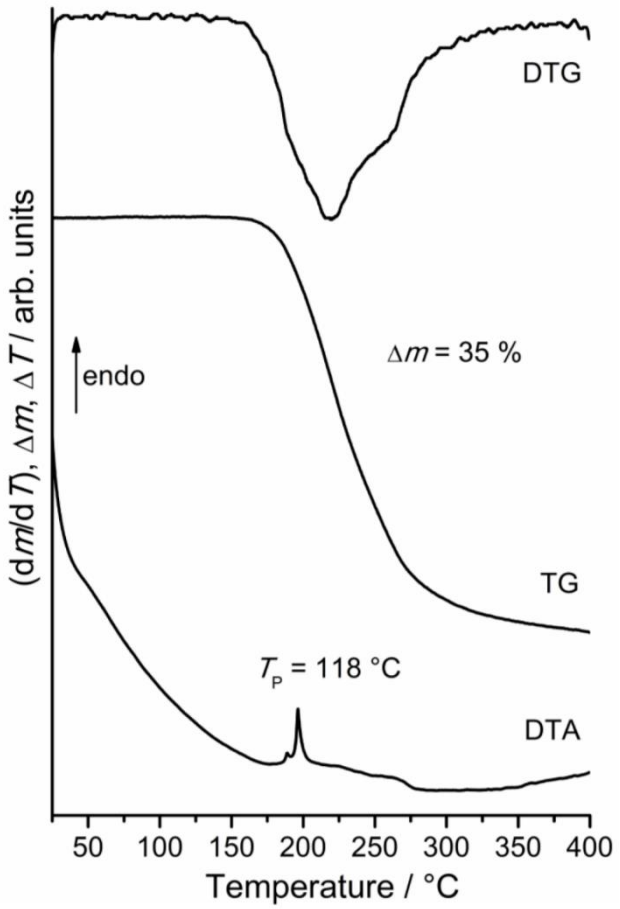

Figure S3. DTG, TG and DTA curves for **1**. Heating rate = 2 °C/min. Given are the mass change in % and the peak temperature in T_P in °C.

`3

Table S 1: Selected bond length (Å) and angles (°) for **1**.

Co(1)-N(1)	2.0943(15)	Co(1)-N(31)	2.2412(15)
Co(1)-N(11)	2.1641(15)		
N(1)-Co(1)-N(1A)	180.00(8)	N(11)-Co(1)-N(11A)	180.00(5)
N(1)-Co(1)-N(11)	89.21(6)	N(1)-Co(1)-N(31A)	88.66(6)
N(1)-Co(1)-N(11A)	90.79(6)	N(11)-Co(1)-N(31)	90.35(6)
N(1)-Co(1)-N(31)	91.34(6)	N(11)-Co(1)-N(31A)	89.65(6)

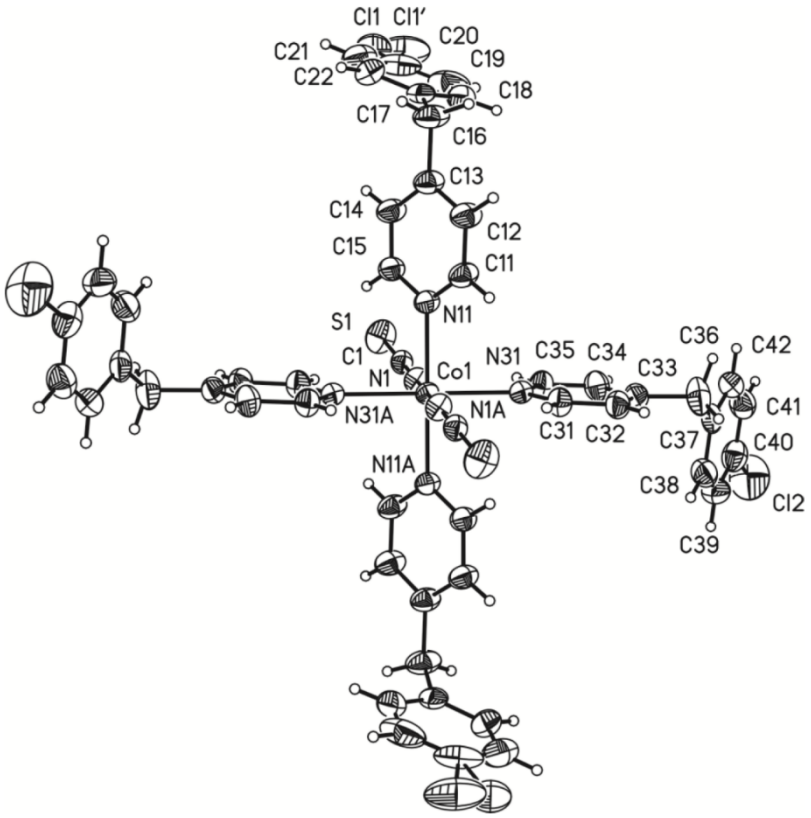

Figure S4: ORTEP plot of **1** with labelling and displacement ellipsoids drawn at 50 % probability level. Symmetry transformation used to generate equivalent atoms: A: -x+3/2,-y+1/2,-z+1.

`4

Table S2: Selected bond length (Å) and angles (°) for **2**.

Co(1)-N(2)	2.060(2)	Co(2)-N(1A)	2.066(2)
Co(1)-S(1)	2.5694(10)	Co(2)-S(2)	2.6066(10)
Co(1)-N(11)	2.165(2)	Co(2)-N(31)	2.145(2)
N(2)-Co(1)-N(2A)	180.00(9)	N(1B)-Co(2)-N(1A)	180.00(9)
N(2)-Co(1)-N(11)	89.93(8)	N(1A)-Co(2)-N(31)	89.83(8)
N(2)-Co(1)-N(11A)	90.07(8)	N(1A)-Co(2)-N(31C)	90.17(8)
N(2)-Co(1)-S(1)	86.73(6)	N(1A)-Co(2)-S(2)	94.23(6)
N(2)-Co(1)-S(1A)	93.27(6)	N(1A)-Co(2)-S(2C)	85.77(6)

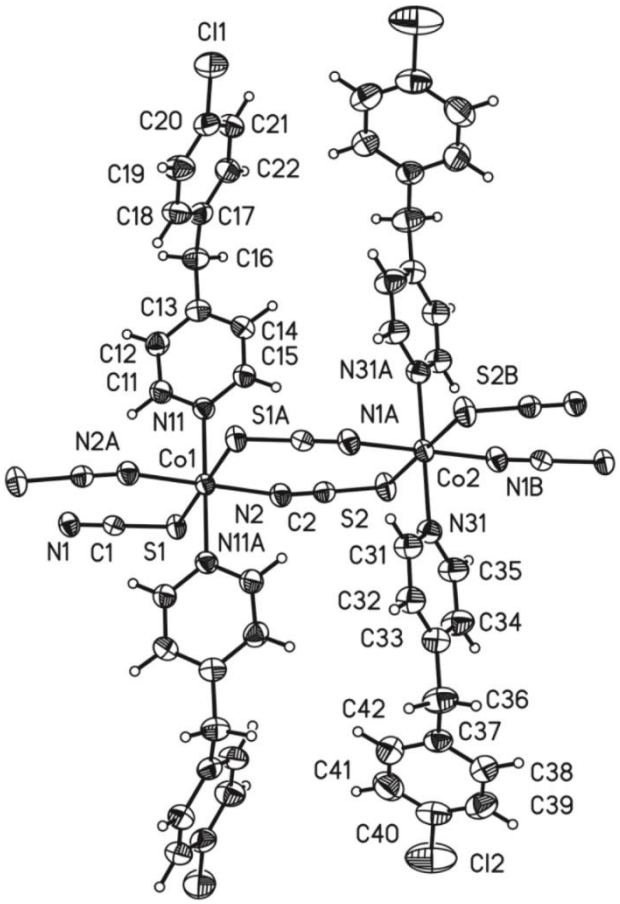

Figure S5: ORTEP plot of **2** with labelling and displacement ellipsoids drawn at 50 % probability level. Symmetry transformation used to generate equivalent atoms: A: -x+1,-y+1,-z+1, B: x-1,y+1,z, C: -x,-y+2,-z+1, D: x+1,y-1,z.

`5

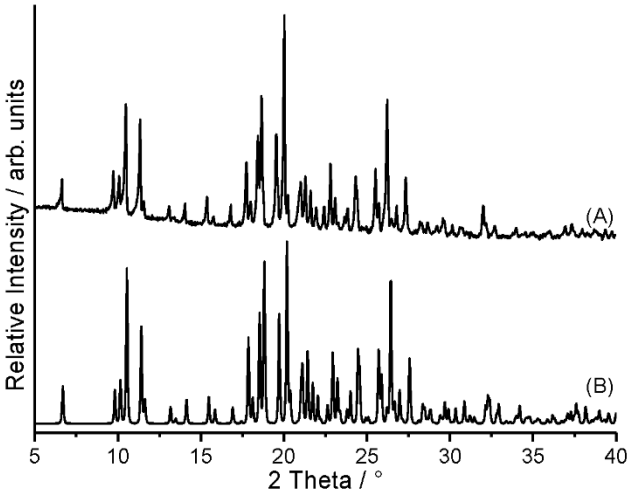

Figure S6: Experimental (top) and calculated (bottom) x-ray powder pattern for compound **1**.

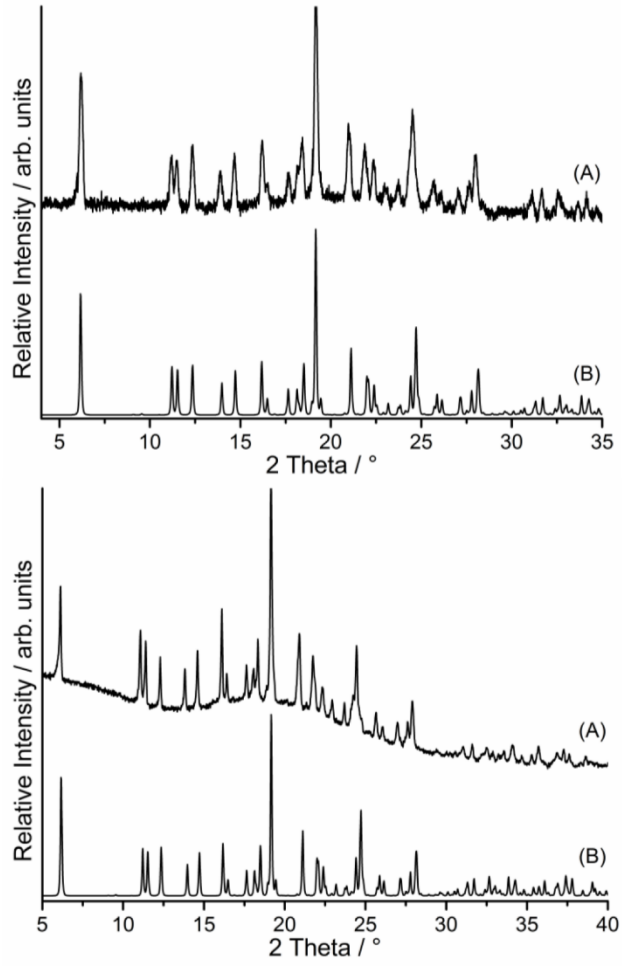

Figure S7: Experimental (top) and calculated (bottom) x-ray powder patterns for two samples of compound **2**.

`6

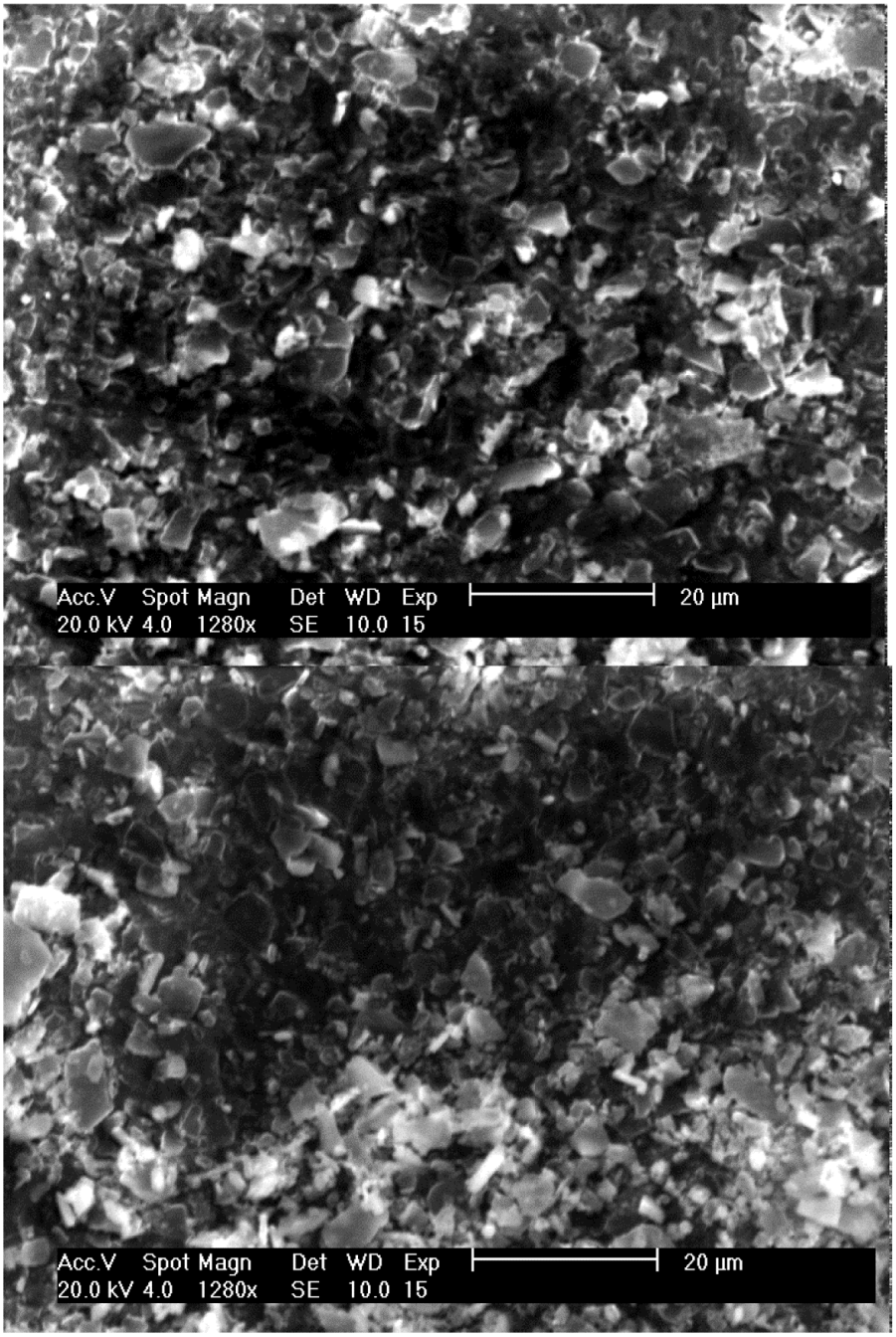

Figure S8: Selected SEM images of the crystals of compound **2**.

`7

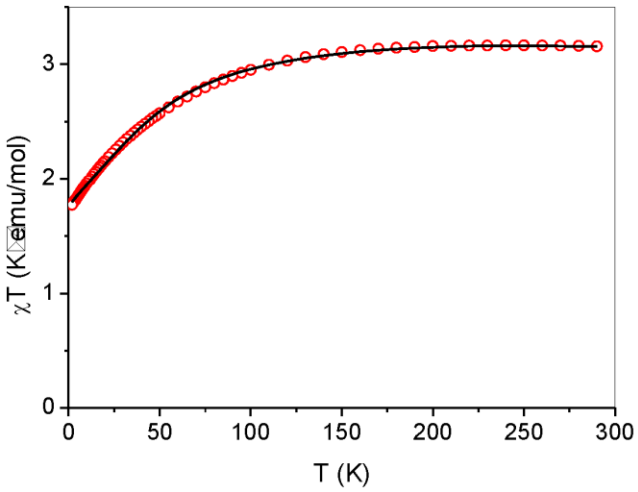

Figure S9. Temperature dependence of χ vs. *T* (top) and χ*T* vs. *T* (bottom) for **1**. The solid line is a fit done by an assumption of the axially distorted octahedral coordination of the Co(II) ion (spin orbit coupling λ=-100 ±3 cm^{-1}, orbital reduction factor κ=1.0 ± 0.02).

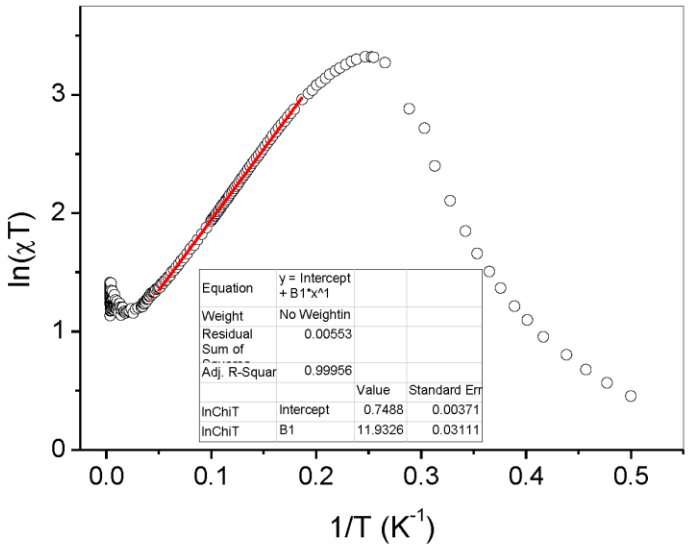

Figure S10: ln(χ*T*) vs. 1/*T* dependence for compound **2**.

`8

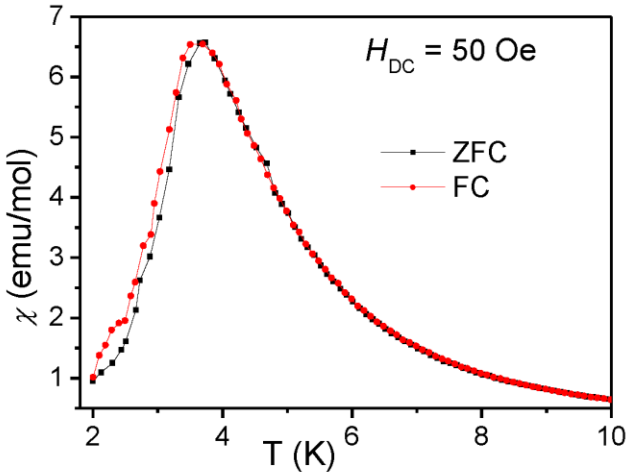

Figure S11. Comparison of $\chi(T)$ curves registered in FC and ZFC regimes for compound **2**.

Table S3: Fitting results of the AC data for compound **2**.

T (K)	χ_0	χ_∞	τ (s)	α	Reduced chi_{sqr}
3.4	4.300	0.0	5.205E-6	0.087	5.713E-4
3.3	3.590	0.0	7.102E-6	0.108	3.873E-4
3.2	2.983	0.0	9.800E-6	0.125	3.112E-4
3.1	2.484	0.0	1.405E-5	0.153	2.185E-4
3.0	2.091	0.110	2.300E-5	0.164	2.859E-4
2.9	1.753	0.129	3.581E-5	0.169	9.762E-5
2.8	1.495	0.122	5.715E-5	0.189	6.379E-5
2.7	1.296	0.109	8.516E-5	0.206	2.891E-4
2.6	1.134	0.095	1.508E-4	0.250	1.472E-4
2.5	1.007	0.104	2.868E-4	0.265	5.969E-5
2.4	0.913	0.106	5.533E-4	0.286	1.172E-5
2.3	0.821	0.112	1.02E-3	0.294	1.690E-5
2.2	0.792	0.105	2.19E-3	0.36	2.596E-5
2.1	0.770	0.110	5.28E-3	0.38	5.864E-6
2.0	0.679	0.117	8.08E-3	0.37	2.3893E-5

`9

8.3. Supporting Information: A Thermodynamically Metastable Thiocyanato Coordination Polymer that shows Slow Relaxations of the Magnetization

-Supporting Information-

A Thermodynamically Metastable Thiocyanato Coordination Polymer that shows Slow Relaxations of the Magnetization

Julia Werner, Michal Rams, Zbigniew Tomkowicz, Tomče Runčevski, Robert Dinnebier, Stefan Suckert, and Christian Näther

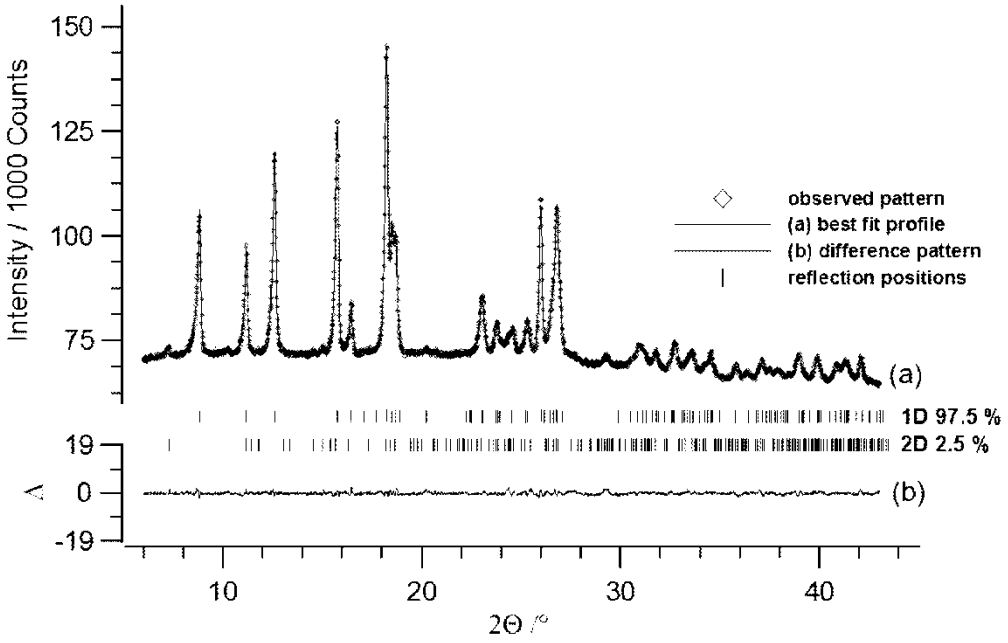

Figure S1. Difference plot from the Rietveld refinement of **3/II**.

Table S1. Products that are obtained if different ratios of $Co(NCS)_2$ and 4-acetylpyridine are stirred in different solvents at room-temperature for 3 days.

Ratio	H_2O	EtOH	MeOH	MeCN
1:6	**1**	**1**	**3/I**	**1**
1:4	**2**	**3/I**	**3/I**	**3/I**
1:2	**2**	**3/I**	**3/I**	**3/I**
1:1	**2**	**3/I**	**3/I**	**amorphous**
2:1	**2**	**3/I**	**amorphous**	**amorphous**
4:1	**2**	**amorphous**	**amorphous**	**amorphous**

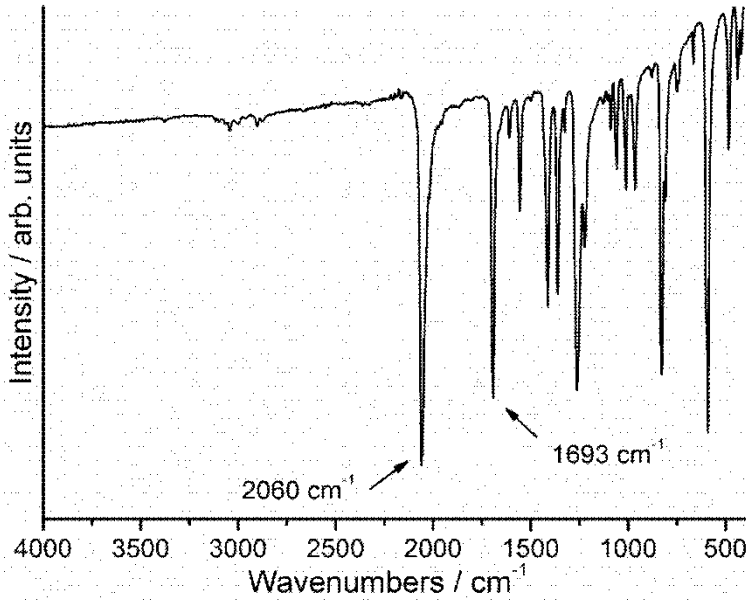

Figure S2. IR spectra of **1**. Given is the value for the CN stretching vibration of the thiocyanato anion and the C-O stretching vibration of the acetyl group.

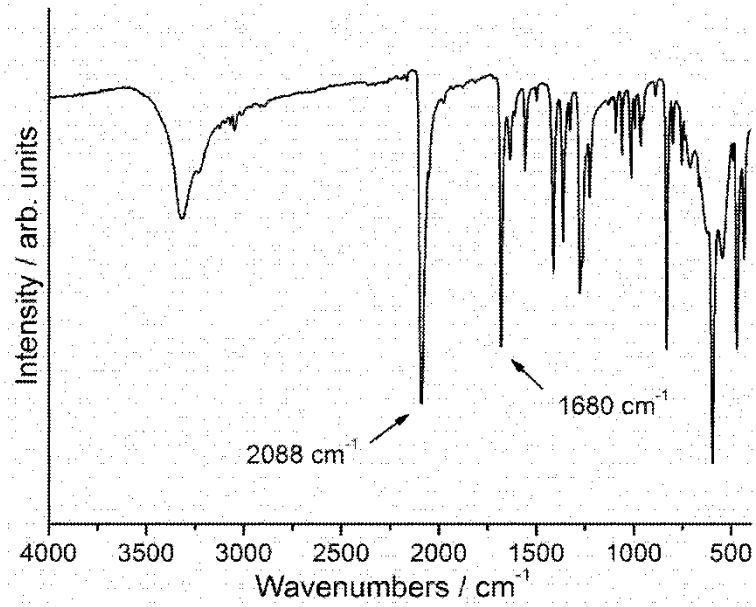

Figure S3. IR spectra of **2**. Given is the value for the CN stretching vibration of the thiocyanato anion and the C-O stretching vibration of the acetyl group.

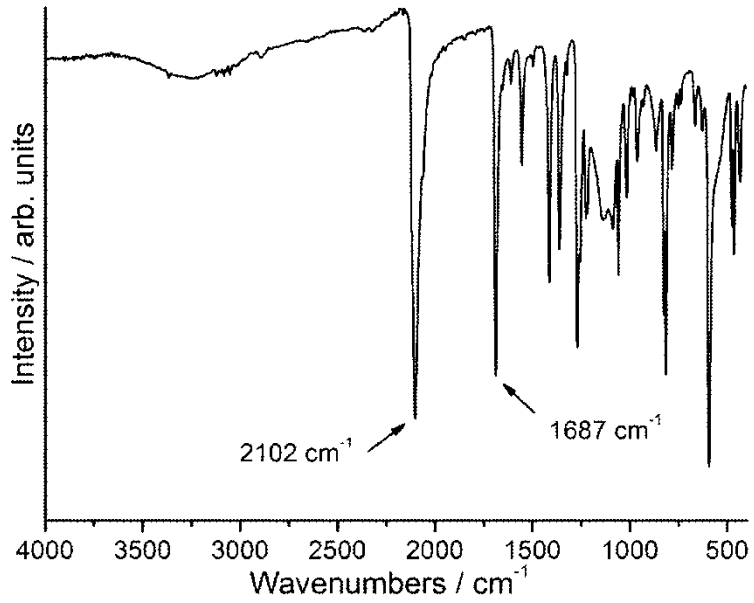

Figure S4. IR spectra of **3/I**. Given is the value for the CN stretching vibration of the thiocyanato anion and the C-O stretching vibration of the acetyl group.

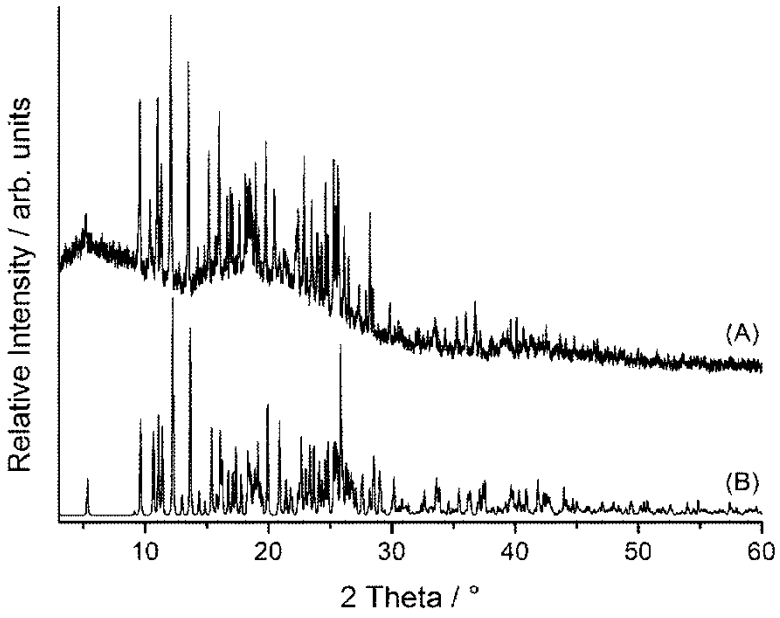

Figure S5. Experimental (A) and calculated (B) XRPD pattern for **1**.

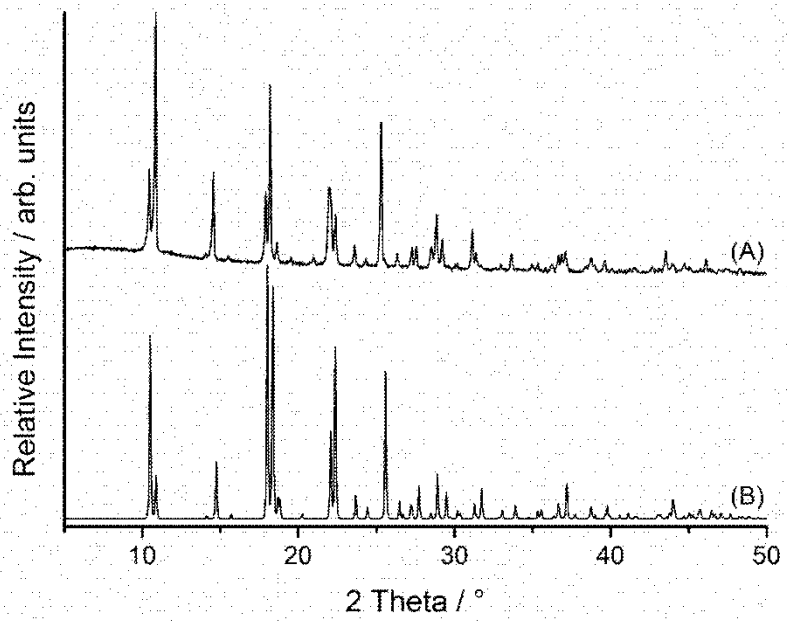

Figure S6. Experimental (A) and calculated (B) XRPD pattern for **2**.

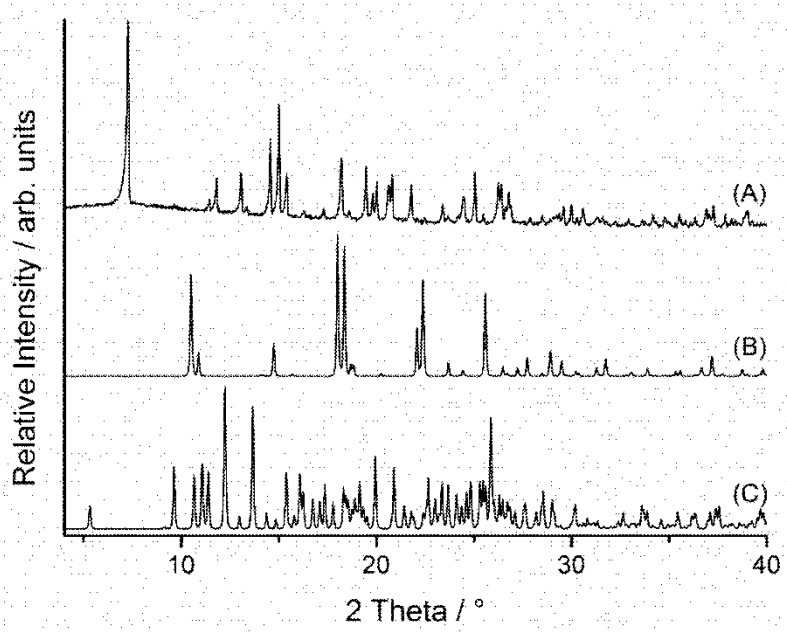

Figure S7. Comparison of the experimental XRPD pattern for **3/I** (A) with that calculated for **2** (B) and **1** (C).

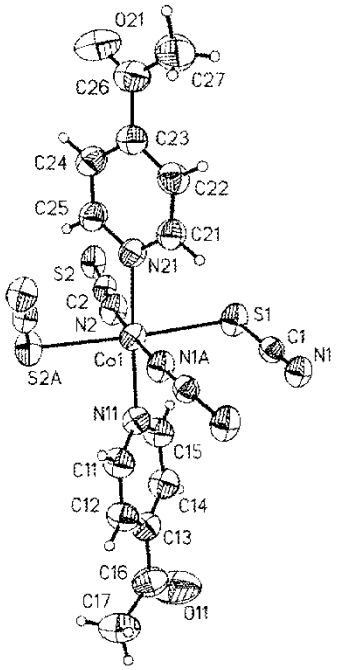

Figure S8. ORTEP plot of **3/I** with labeling and displacement ellipsoids drawn at 50 % probability level. Symmetry codes: A = -x + 1, -y + 1, -z + 1; B = x-1/2, -y + 3/2, -z + 1 C = x + 1/2, -y + 3/2, -z + 1.

Table S2. Selected distances (Å) and angles (°) for **3/I**.

[Co(NCS)$_2$(4-acetylpyridine)$_2$]$_n$ (**3/I**)			
Co(1)-N(1A)	2.064(2)	Co(1)-S(2B)	2.5717(9)
Co(1)-N(2)	2.065(2)	Co(1)-N(11)	2.174(2)
Co(1)-S(1)	2.6472(9)	Co(1)-N(21)	2.147(2)
N(1A)-Co(1)-N(2)	175.48(10)	S(2B)-Co(1)-S(1)	174.95(3)
N(1A)-Co(1)-N(11)	87.27(10)	N(2)-Co(1)-S(2B)	91.86(8)
N(1A)-Co(1)-N(21)	89.02(9)	N(11)-Co(1)-S(2B	90.69(7)
N(1A)-Co(1)-S(1)	92.22(7)	N(11)-Co(1)-S(1)	90.93(7)
N(1A)-Co(1)-S(2B)	92.63(7)	N(21)-Co(1)-S(1)	88.32(7)
N(2)-Co(1)-N(11)	92.15(10)	N(21)-Co(1)-S(2B)	90.37(7)
N(2)-Co(1)-N(21)	91.48(10)	N(21)-Co(1)-N(11)	176.18(9)
N(2)-Co(1)-S(1)	83.30(7)		

7

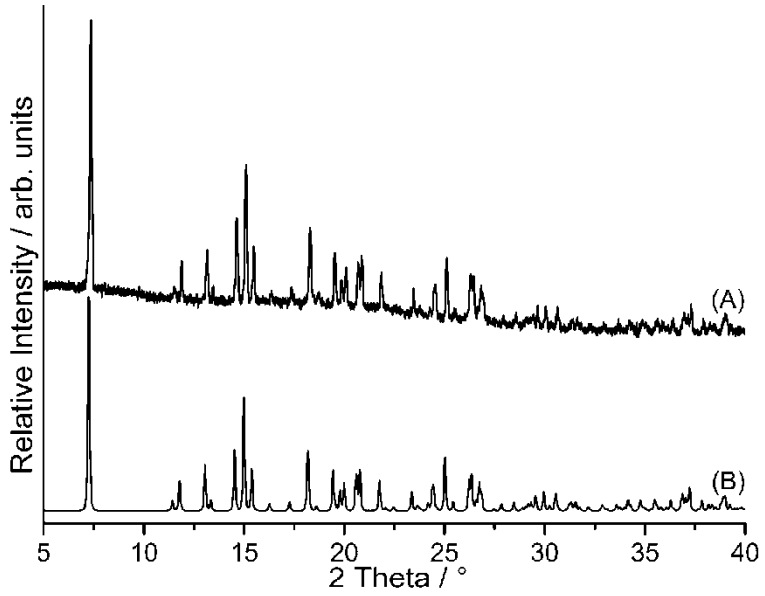

Figure S9. Experimental (A) and calculated (B) XRPD pattern for **3/I**.

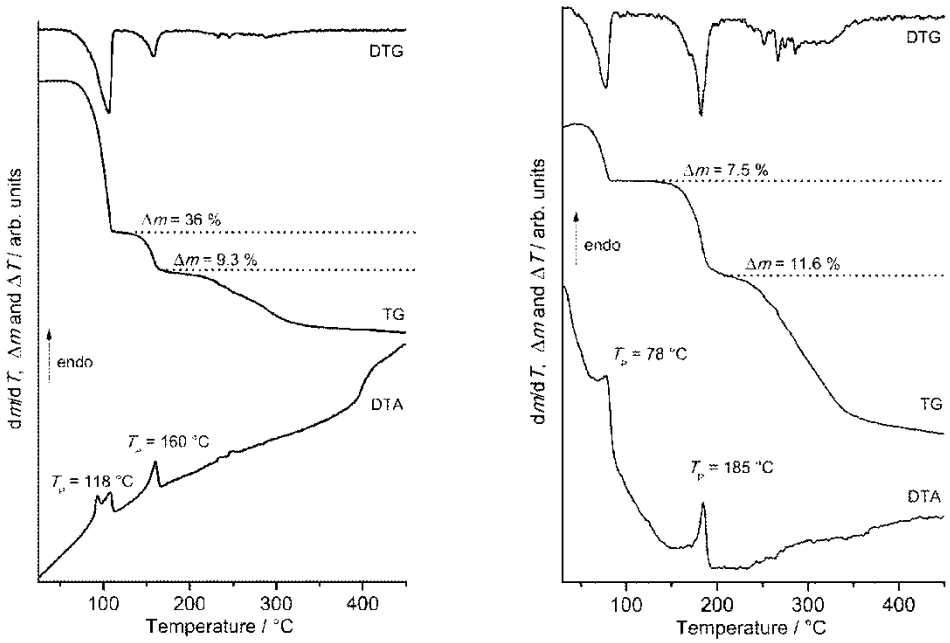

Figure S10. DTA-, TG- and DTG curve for **1** (left) and **2** (right) at 1°C/min.

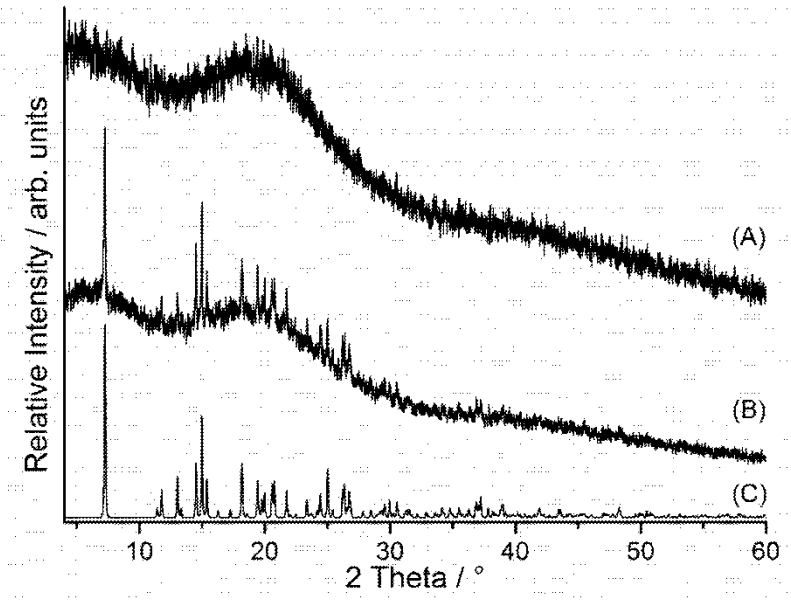

Figure S11. Experimental XRPD pattern of the residue obtained after the first TG step of **1** at 4°C/min. (A) and at 1°C/min (B) as well as XRPD pattern calculated for **3/1** from single crystal data (C).

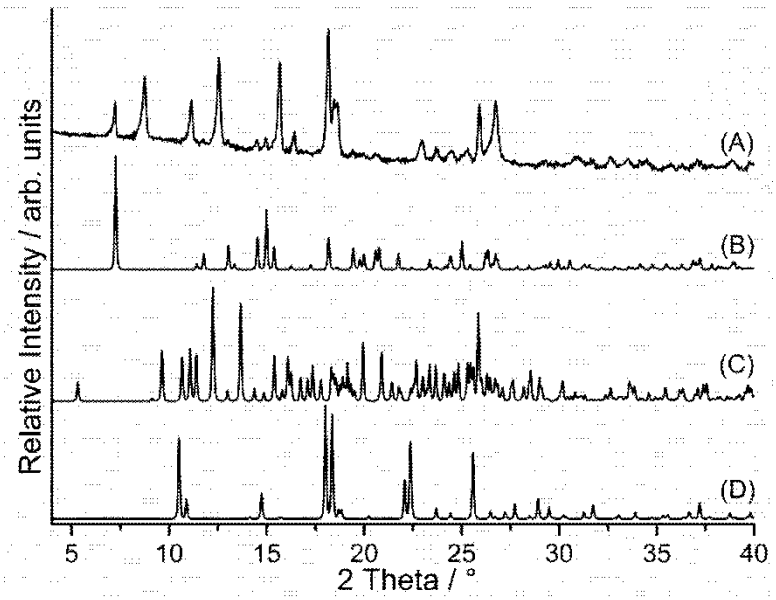

Figure S12. Experimental XRPD pattern of the residue obtained after the first TG step of **2** (A) and XRPD pattern for **3** (B), **1** (C) and **2** (D) calculated from single crystal data.

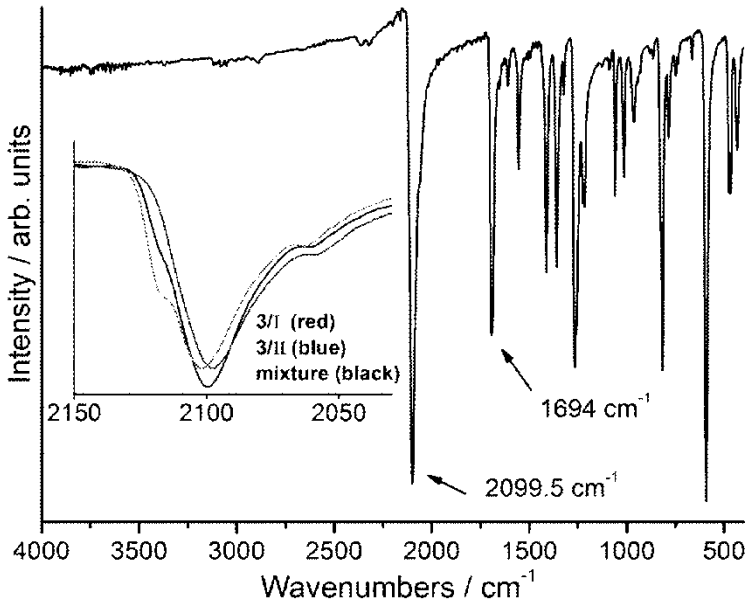

Figure S13. IR spectra of the mixture of **3/I** and **3/II** obtained in the TG measurement of **2**.

10

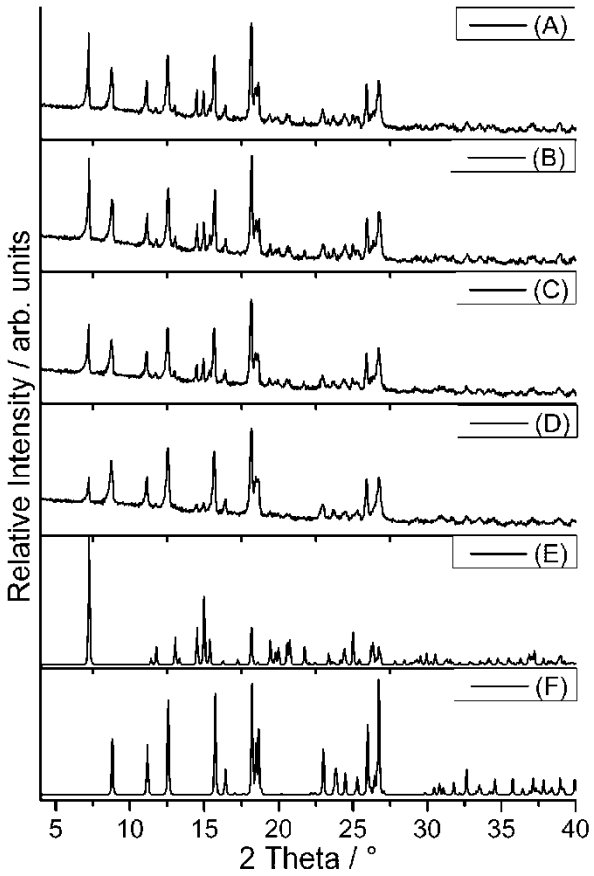

Figure S14. Experimental XRPD pattern of the residue obtained after the first TG step of **2** with a heating rate of 16 K/min (A), 8 K/min (B), 4 K/min (C), 1 K/min (D). XRPD pattern for **3/I** (E) calculated from single crystal data and XRPD pattern for **3/II** (F) calculated from the results of the Rietveld refinement.

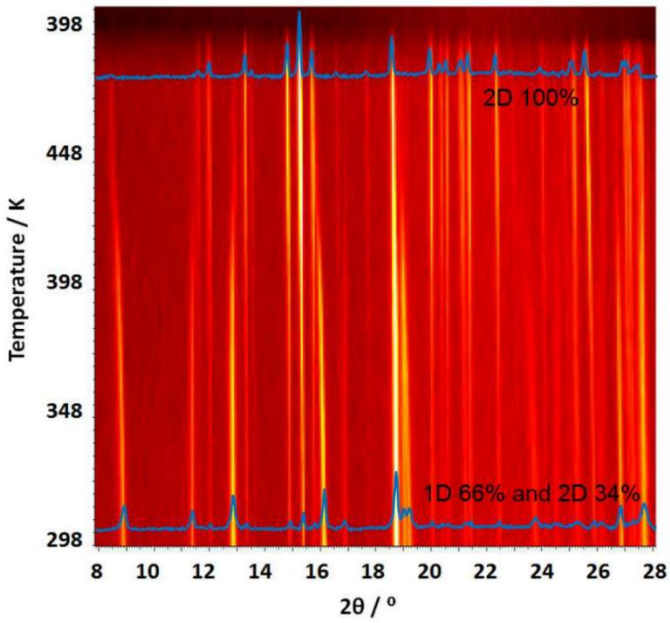

Figure S15. Temperature dependent XRPD pattern of **2**.

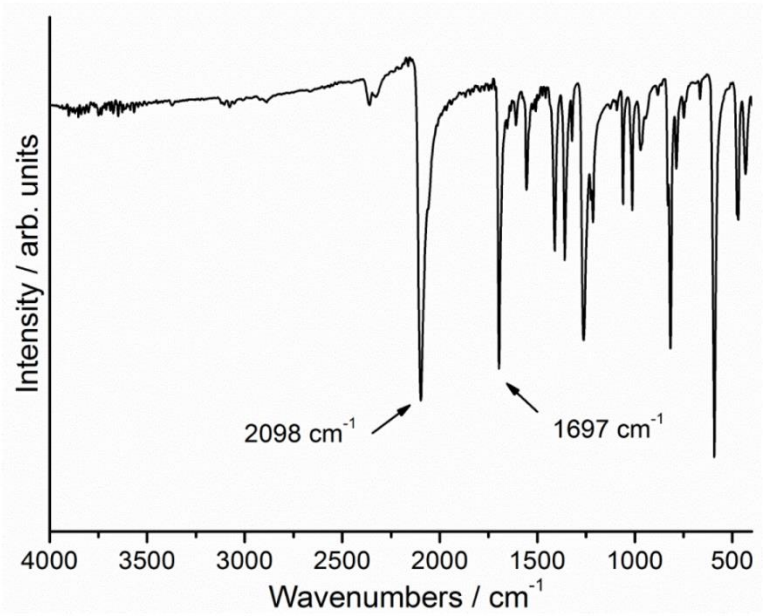

Figure S16. IR spectra of the residue obtained by thermal annealing of **2** at 70°C.

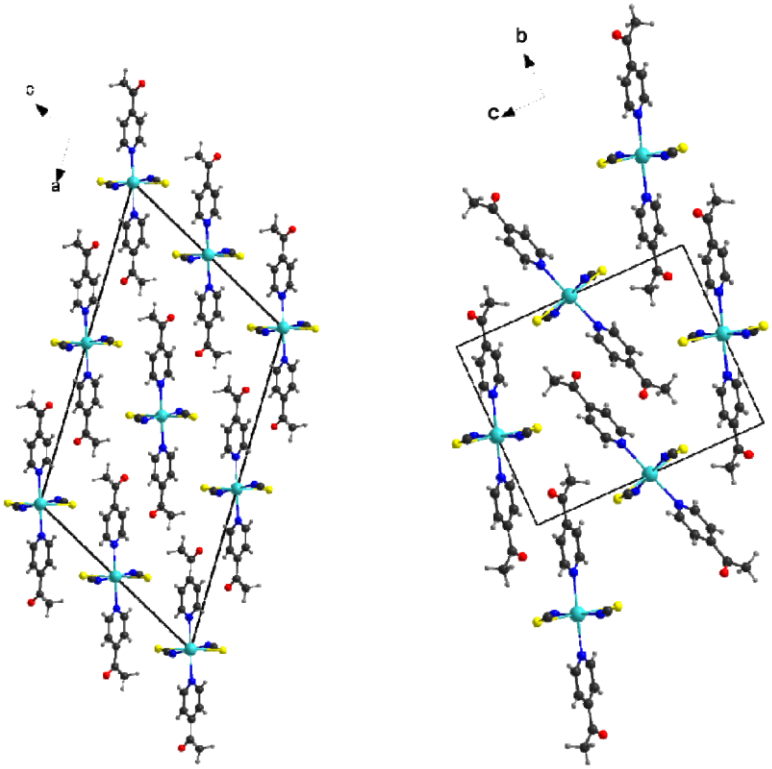

Figure S17. View of the chains in the *C*2/c and the *P*21/c form of $[Cd(NCS)_2(4\text{-acetylpyridine})_2]_n$ retrieved from literature.

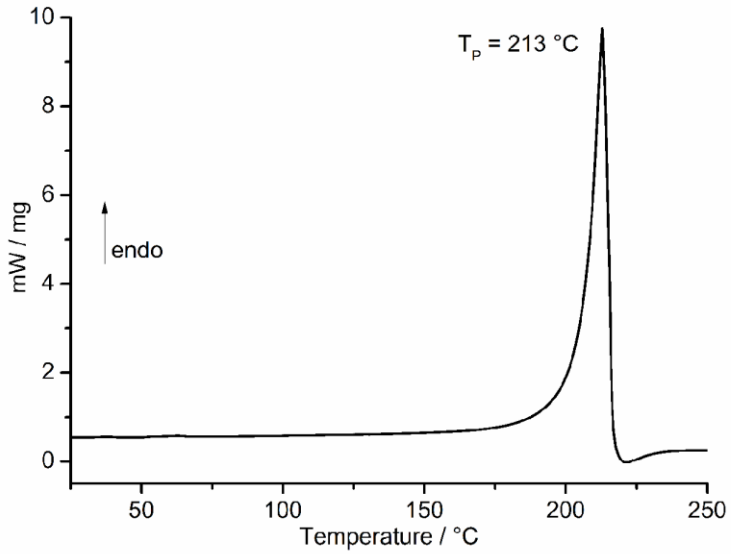

Figure S18. DSC curve at 5 °C/min for **3/I**.

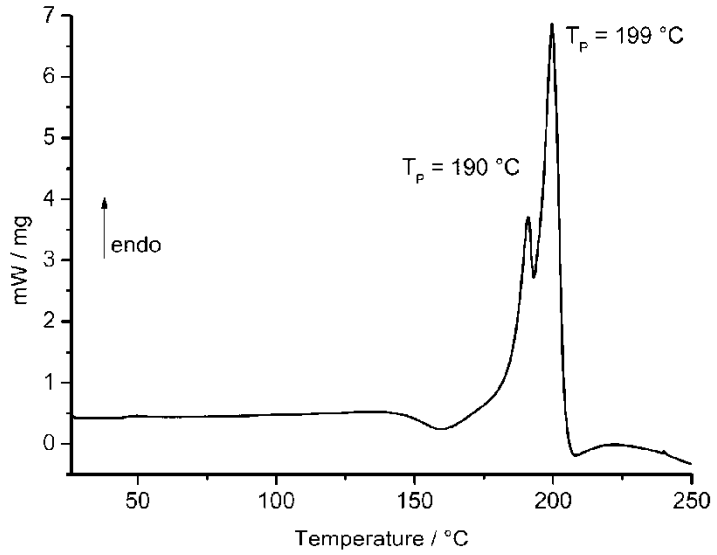

Figure S19. DSC curve at 5 °C/min for **3/II**.

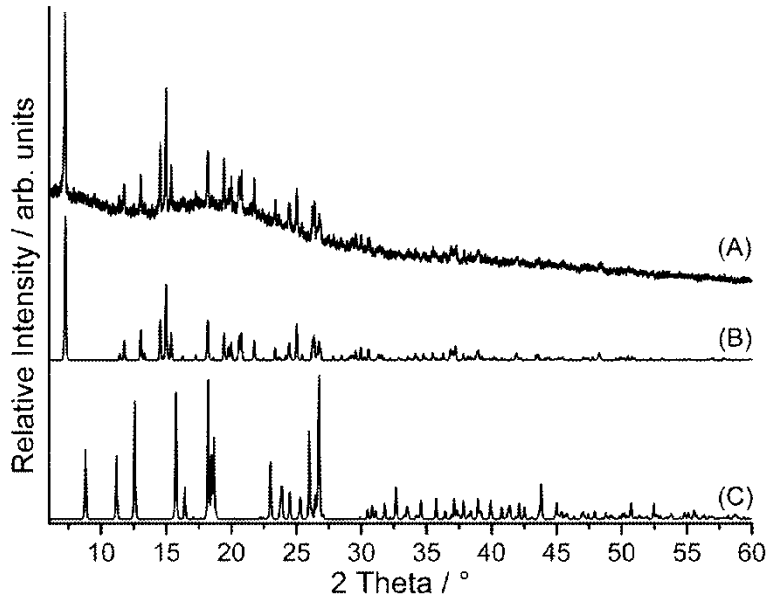

Figure S20. Experimental XRPD pattern of the residue obtained after the second DSC peak of **3/II** (A) and calculated XRPD pattern for **3/I** (B) and **3/II** (C).

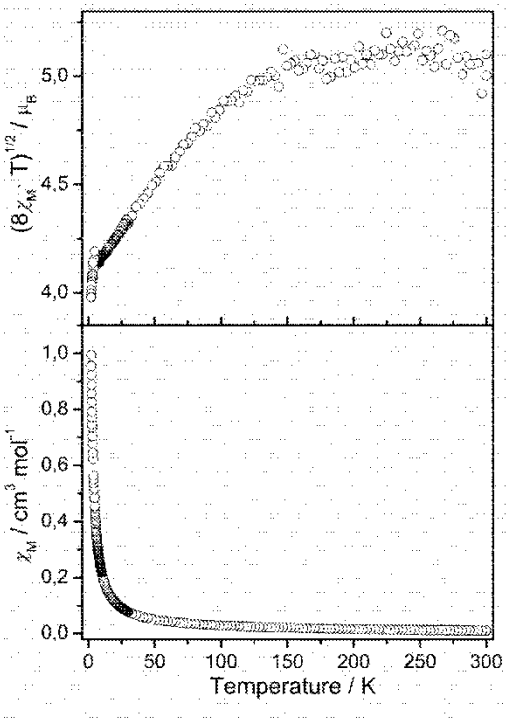

Figure S21. $(8\chi T)^{1/2}$ (top) and χ (bottom) versus T curve at H_{DC} = 1000 Oe for **1**. Please note: At lower DC fields the susceptibility curve is very noisy in the high temperature region.

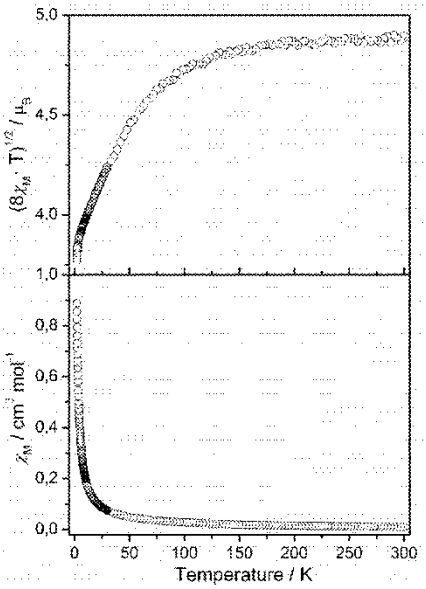

Figure S22. $(8\chi T)^{1/2}$ (top) and χ (bottom) versus T curve at H_{DC} = 1000 Oe for **2**.

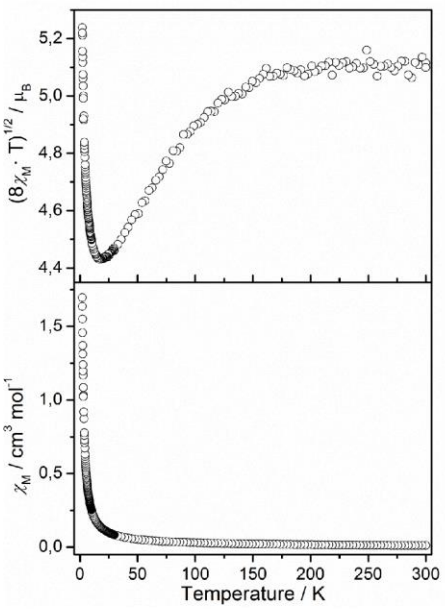

Figure S23. $(8\chi T)^{1/2}$ (top) and χ (bottom) versus T curve at $H_{DC} = 1000$ Oe for **3/I**.

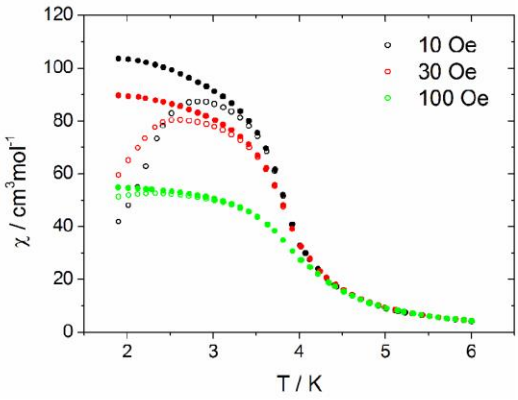

Figure S24. Zero-field cooled and field cooled susceptibility of **3/II** measured at fields 10, 30 and 100 Oe. The demagnetization was not taken into account, which is the reason why values at 10 Oe, 2 K are slightly smaller as those shown in figure 8, figure 9 and figure S25.

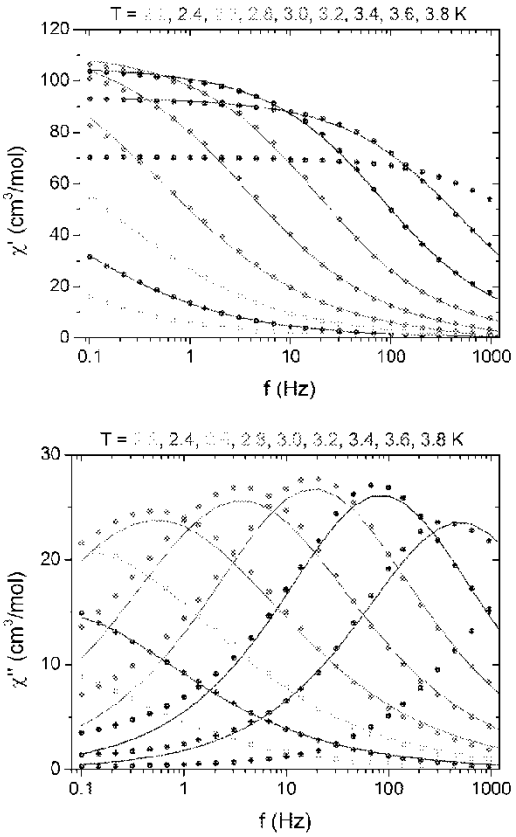

Figure S25. Frequency dependence of ac susceptibility for **3/II** measured at different temperatures using H_{ac} = 3 Oe in zero dc field. The solid lines were fitted using the Cole-Cole model to obtain mean relaxation time τ at each temperature. The obtained α parameter, describing the distribution of relaxation times, was in the range from 0.4 to 0.52.

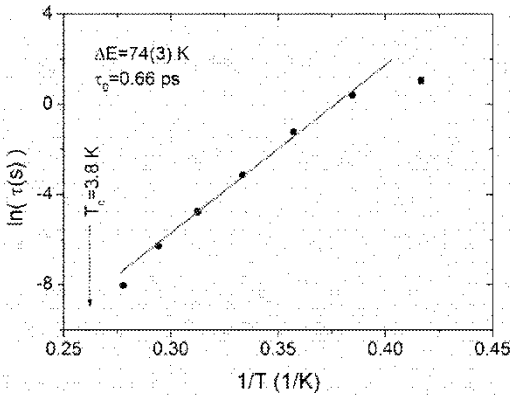

Figure S26. Temperature dependence of the mean relaxation time for **3/II** obtained from ac measurements. The straight line was fitted to five middle data points.

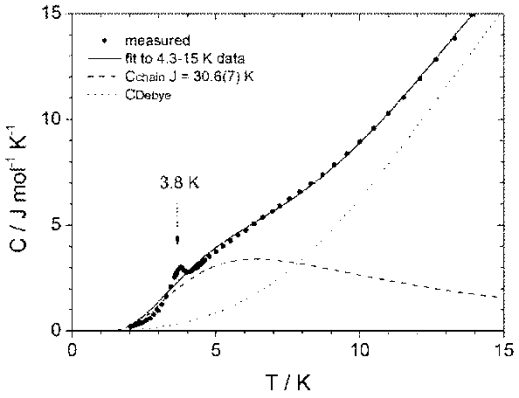

Figure S27. Specific heat of **3/II** in units of the gas constant R. Lines denote the fit (solid line) and its decomposition on the Ising chain contribution (dashed line) and the phonon contribution (dotted line).

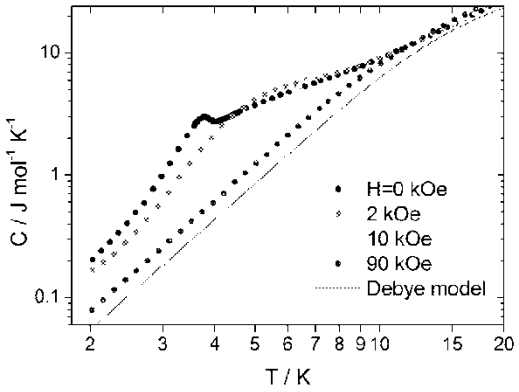

Figure S28. Specific heat of **3/II** measured in different applied fields. The line is the phonon contribution to specific heat, as determine from the fit (see main text).

8.4. Supporting Information: Synthesis, Structure and Properties of Coordination Polymers with Layered Transition Metal Thiocyanto Networks

Electronic Supplementary Information

Content

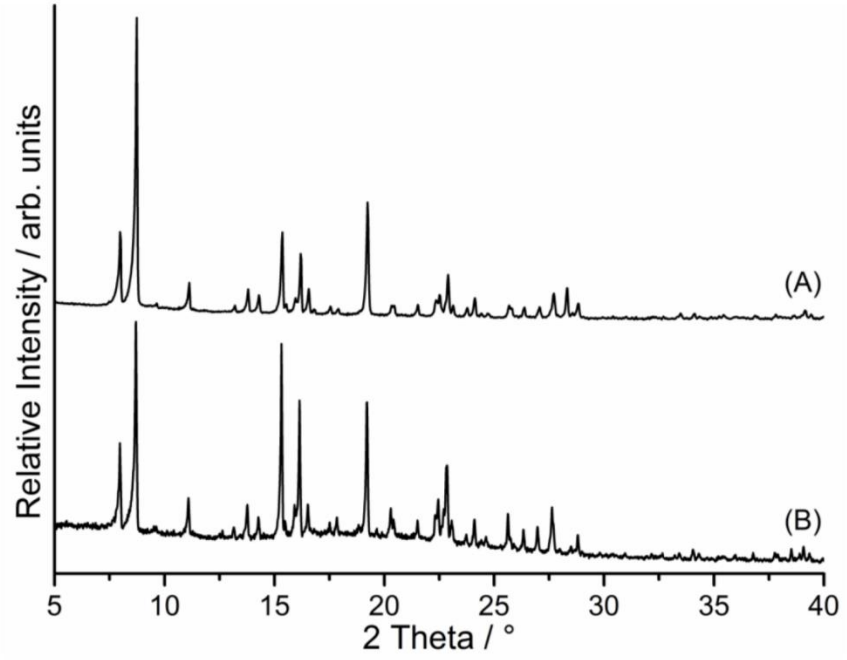

Figure S1. Experimental X-ray powder pattern of **1-Fe** (A) **1-Mn** (B).

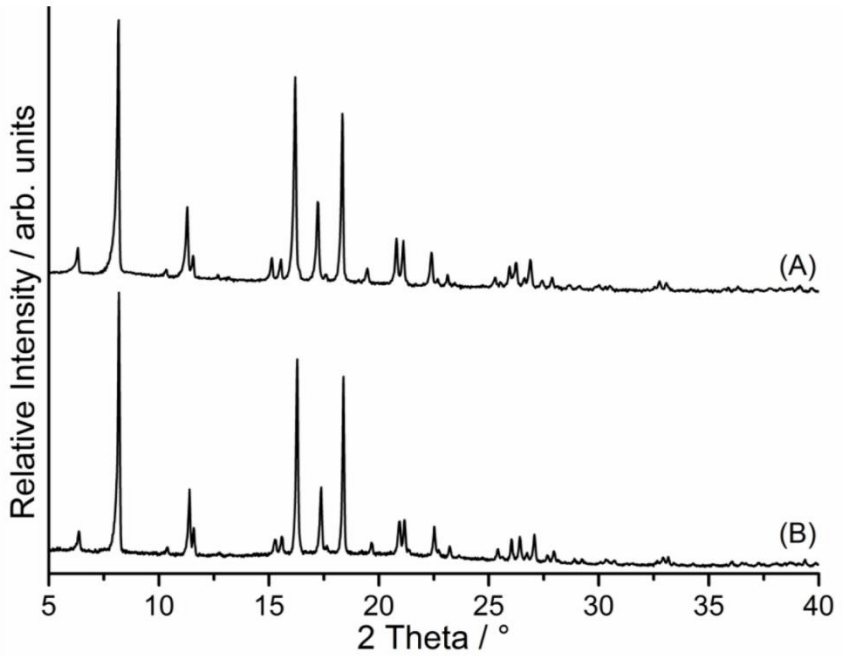

Figure S2. Experimental X-ray powder pattern of **1-Co** (A) **1-Ni** (B).

3

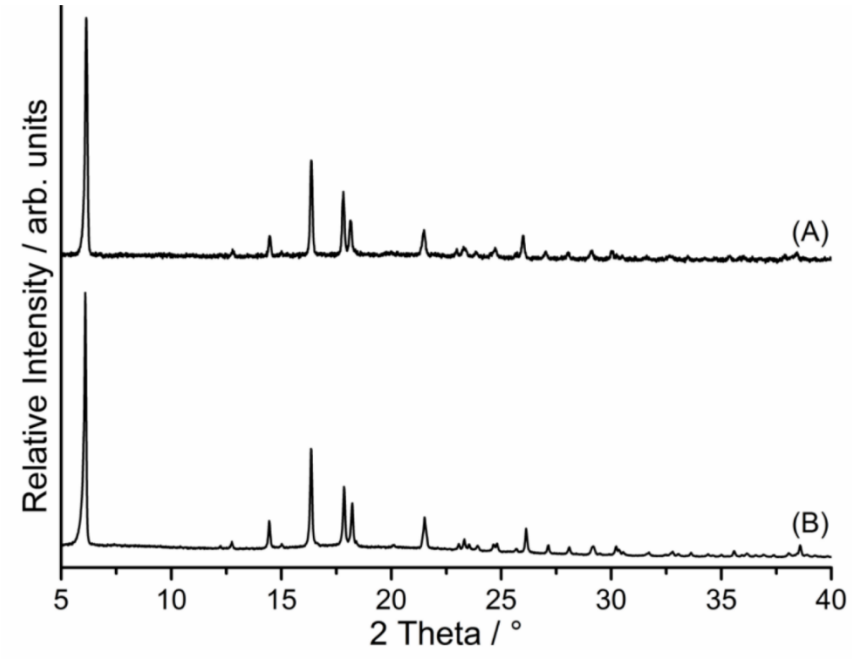

Figure S3. Experimental X-ray powder pattern of **2-Co** (A) **2-Ni** (B).

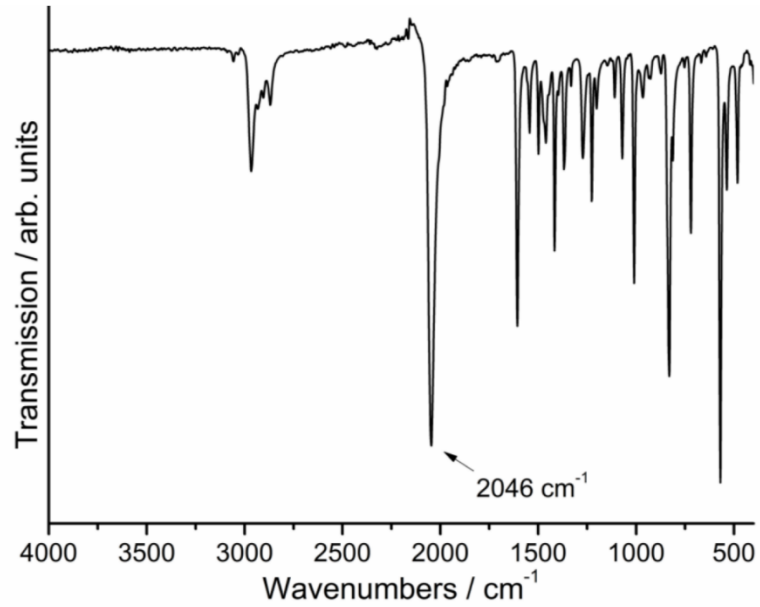

Figure S4. IR spectra of **1-Mn**. The CN stretching vibration is given.

4

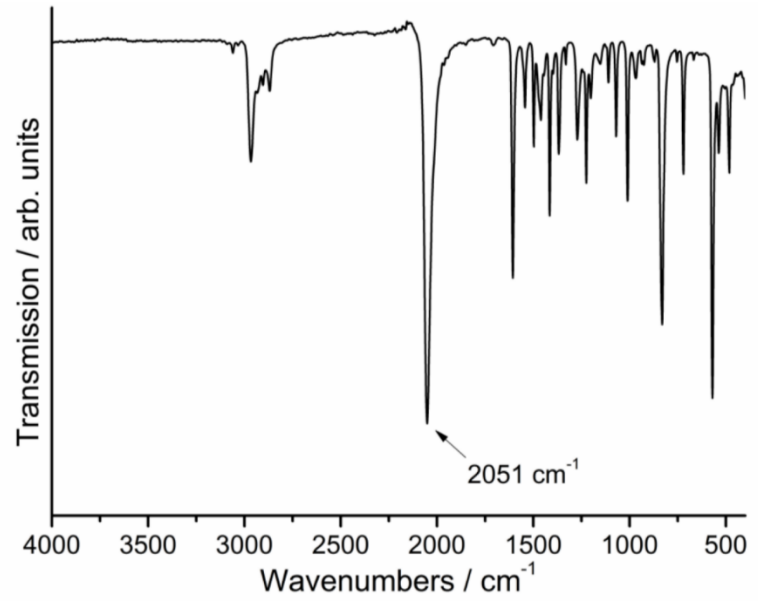

Figure S5. IR spectra of **1-Fe**. The CN stretching vibration is given.

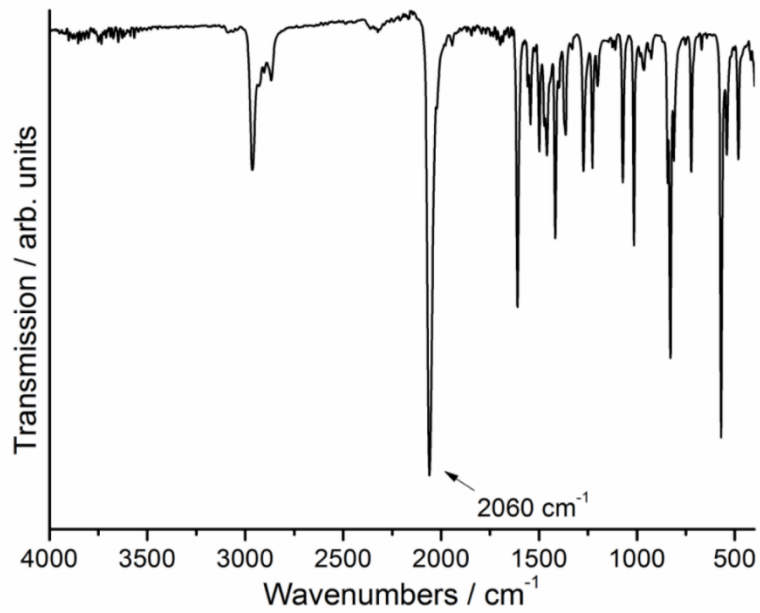

Figure S6. IR spectra of **1-Co**. The CN stretching vibration is given.

5

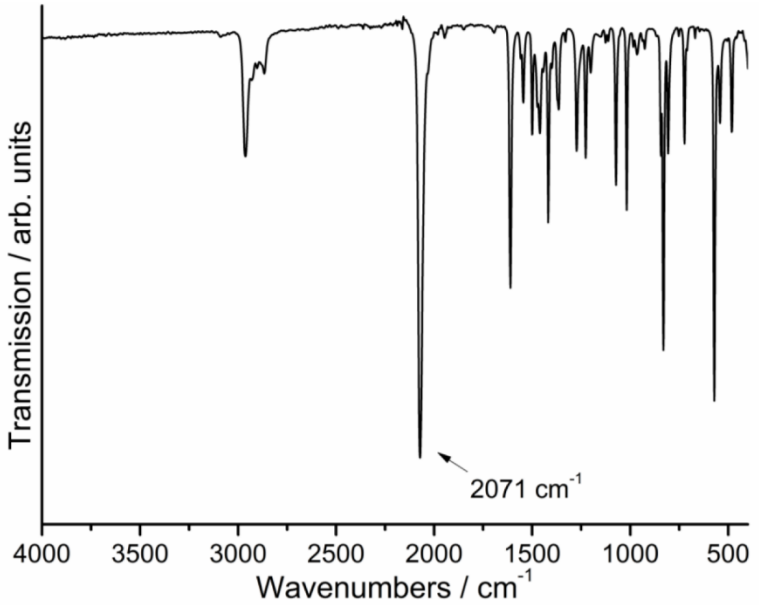

Figure S7. IR spectra of **1-Ni**. The CN stretching vibration is given.

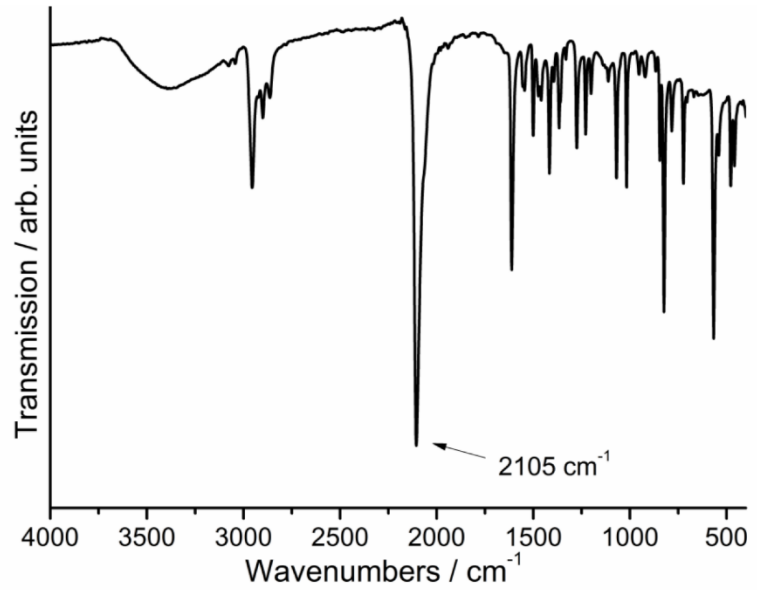

Figure S8. IR spectra of **2-Co**. The CN stretching vibration is given.

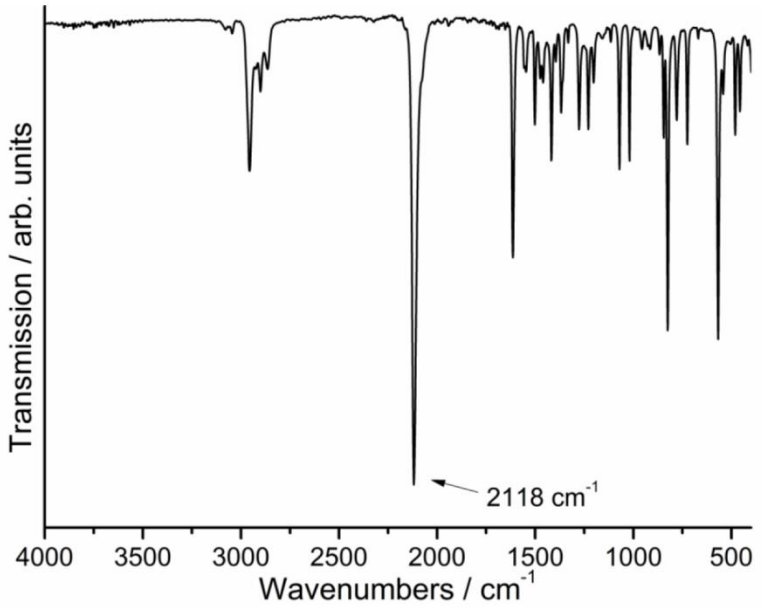

Figure S9. IR spectra of **2-Ni**. The CN stretching vibration is given.

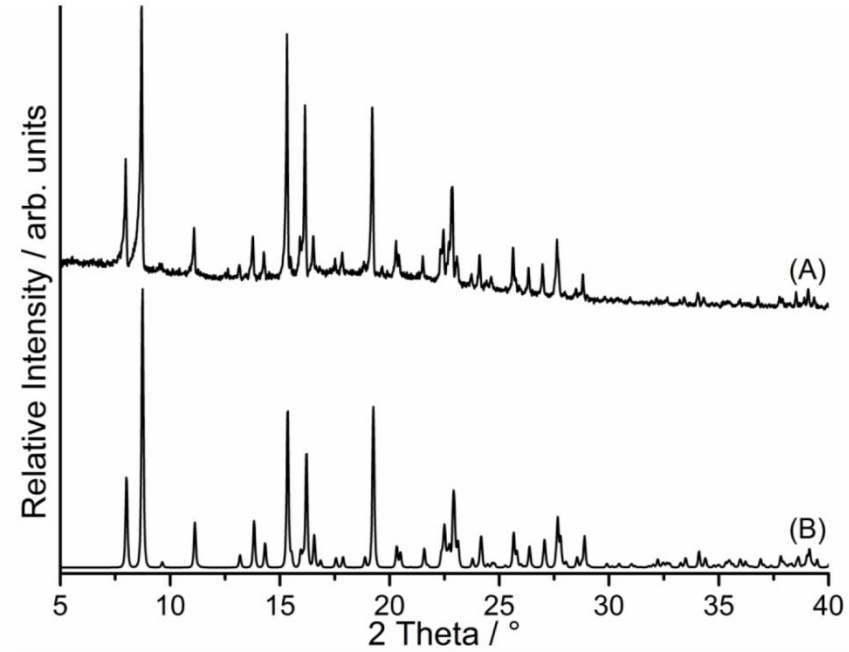

Figure S10. Experimental (A) and calculated (B) XRPD pattern for compound **1-Mn**.

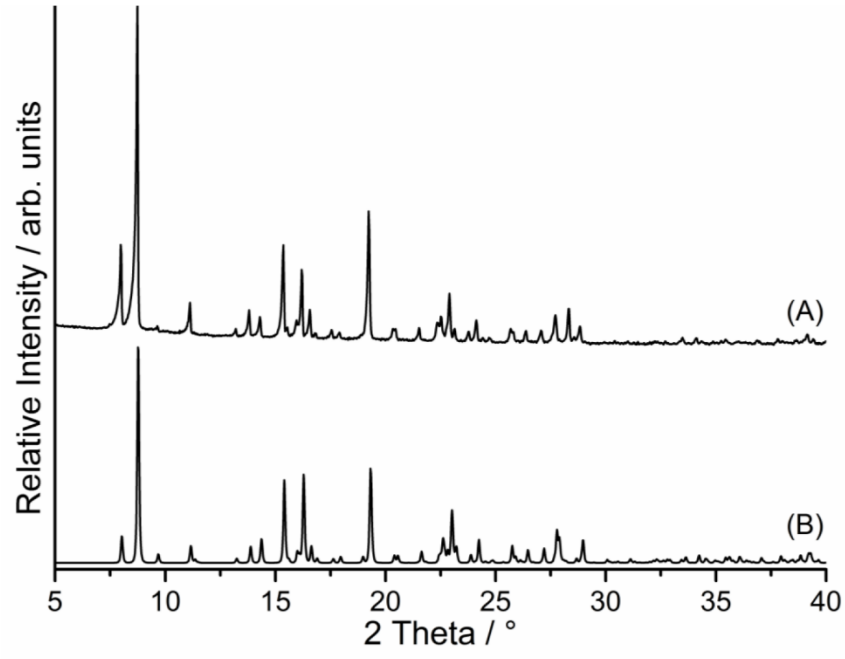

Figure S11. Experimental (A) and calculated (B) XRPD pattern for compound **1-Fe**.

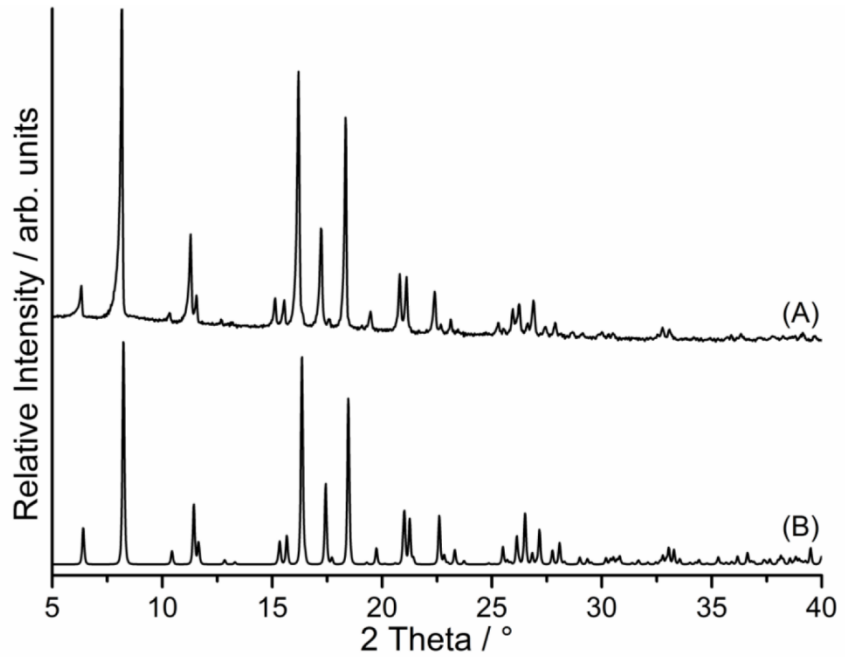

Figure S12. Experimental (A) and calculated (B) XRPD pattern for compound **1-Co**.

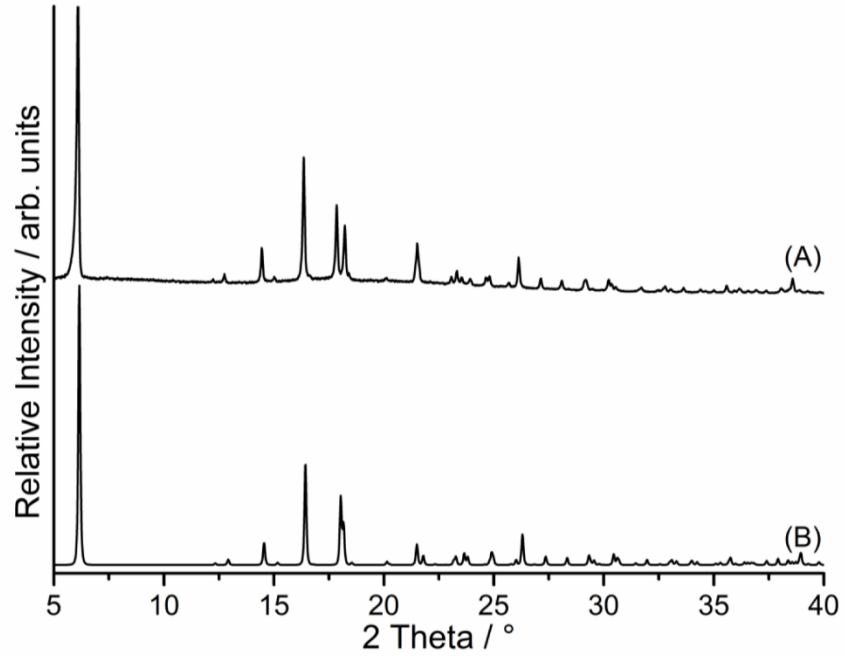

Figure S13. Experimental (A) and calculated (B) XRPD pattern for compound **2-Ni**.

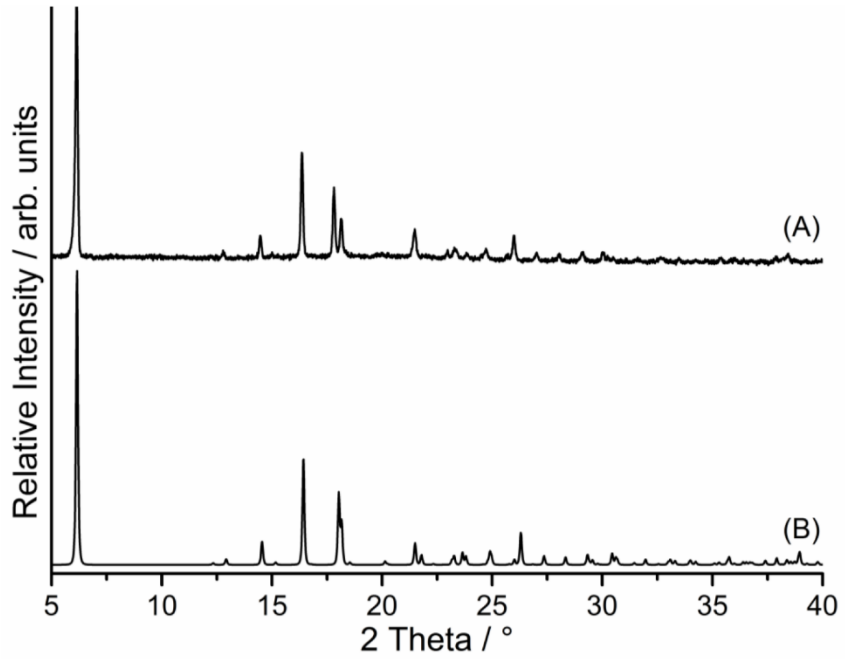

Figure S14. Experimental (A) for compound **2-Co** and calculated (B) XRPD pattern for compound **2-Ni**.

Tab S 1. Selected bond lengths (Å) and angles (°) for **1-Mn**. Symmetry code: A: -x+1, -y+1, -z+1.

$Mn(NCS)_2$(*tert*-Butylpyridine)$_4$ (1-Mn)			
Mn(1)-N(1)	2.156(3)	Mn(1)-N(21)	2.310(2)
Mn(1)-N(11)	2.350(3)		
N(1)-Mn(1)-N(1A)	180.0	N(1)-Mn(1)-N(21A)	90.08(10)
N(1)-Mn(1)-N(11)	88.53(10)	N(21)-Mn(1)-N(11)	93.24(9)
N(1)-Mn(1)-N(11A)	91.47(10)	N(21)-Mn(1)-N(11A)	86.76(9)
N(1)-Mn(1)-N(21)	89.92(10)		

Tab S 2. Selected bond lengths (Å) and angles (°) for **1-Fe**. Symmetry code: A: -x+1, -y+1, -z+1.

$Fe(NCS)_2$(*tert*-Butylpyridine)$_4$ (1-Fe)			
Fe(1)-N(1)	2.086(2)	Fe(1)-N(21)	2.2431(19)
Fe(1)-N(11)	2.287(2)		
N(1)-Fe(1)-N(1A)	180.000(1)	N(1)-Fe(1)-N(21A)	89.67(8)
N(1)-Fe(1)-N(11)	88.76(7)	N(21)-Fe(1)-N(11)	93.61(7)
N(1)-Fe(1)-N(11A)	91.24(7)	N(21)-Fe(1)-N(11A)	86.39(7)
N(1)-Fe(1)-N(21)	90.33(8)		

Tab S 3. Selected bond lengths (Å) and angles (°) for **1-Co**. Symmetry code: A: -x+1, -y+1/2, z+0.

$Co(NCS)_2$(*tert*-Butylpyridine)$_4$ (1-Co)			
Co(1)-N(1)	2.071(2)	Co(1)-N(21)	2.175(2)
Co(1)-N(11)	2.193(2)		
N(1)-Co(1)-N(1A)	176.48(14)	N(1)-Co(1)-N(21A)	89.75(9)
N(1)-Co(1)-N(11)	88.00(9)	N(21)-Co(1)-N(11)	90.03(8)
N(1)-Co(1)-N(11A)	89.51(9)	N(21)-Co(1)-N(11A)	177.74(8)
N(1)-Co(1)-N(21)	92.73(9)	N(21A)-Co(1)-N(11A)	90.03(8)

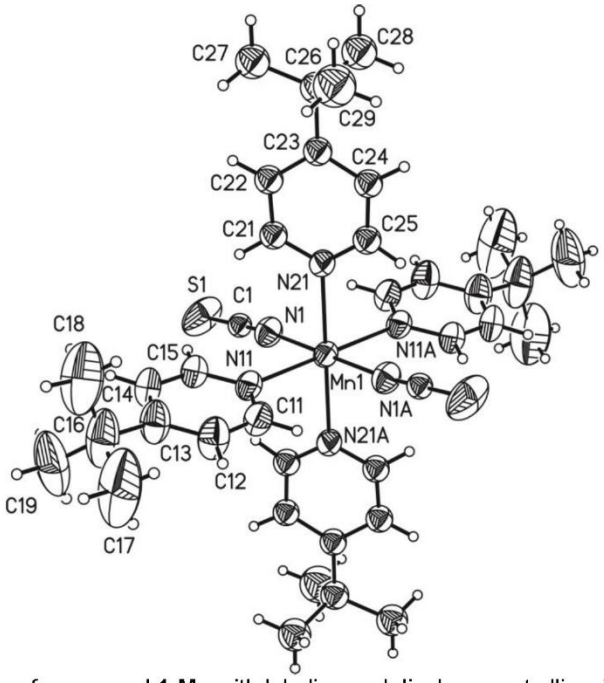

Figure S15 Crystal structure of compound **1-Mn** with labeling and displacement ellipsoids drawn at the 50 % probability level. Symmetry transformation used to generate equivalent atoms: A: -x+1, -y+1, -z+1.

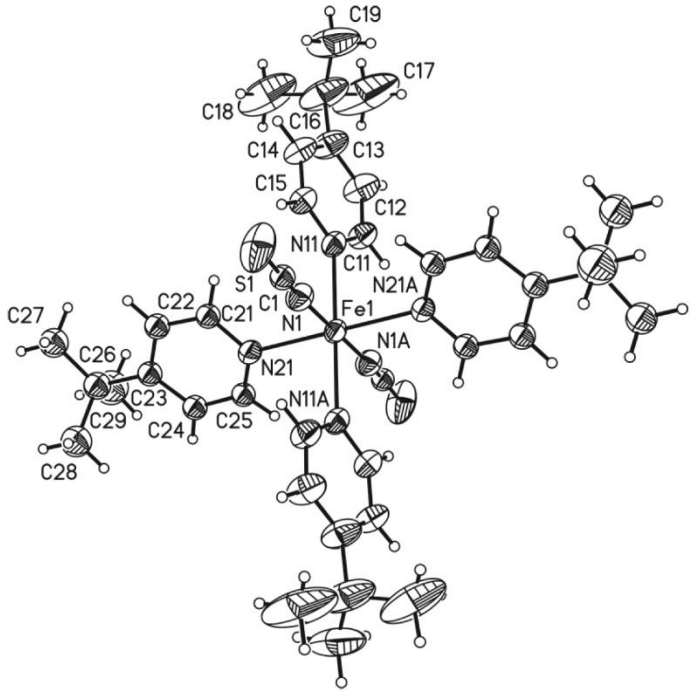

Figure S16 Crystal structure of compound **1-Fe** with labeling and displacement ellipsoids drawn at the 50 % probability level. Symmetry transformation used to generate equivalent atoms: A: -x+1, -y+1, -z+1.

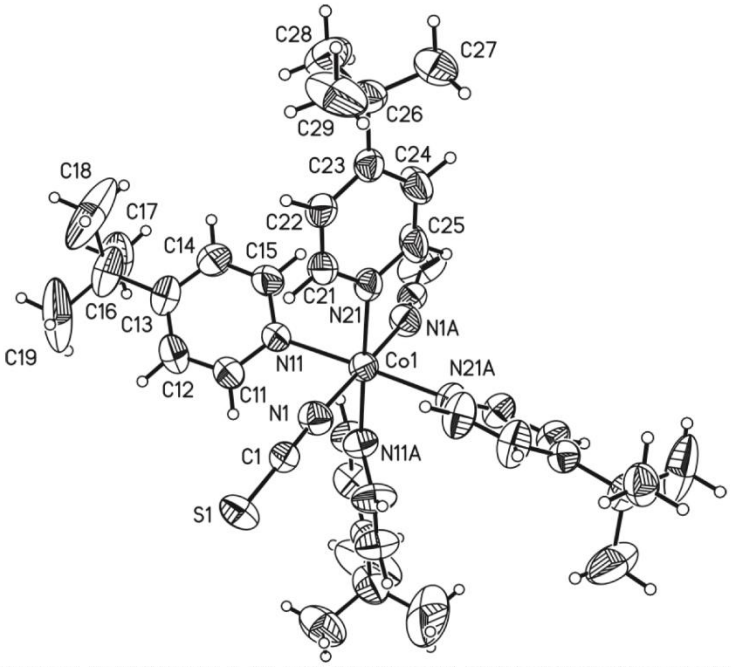

Figure S17. Crystal structure of compound **1-Co** with labeling and displacement ellipsoids drawn at the 50 % probability level. Symmetry transformation used to generate equivalent atoms: A: -x+1, -y+1/2, z+0.

Table S4. Selected bond lengths (Å) and angles (°) for **2-Ni**. Symmetry code: A: -x+1, -y+1/2, z+0.

$[Ni(NCS)_2(tert\text{-Butylpyridine})_2]_n$ (2-Ni)			
Ni(1)-N(1)	2.036(3)	Ni(1)-S(1B)	2.4948(9)
Ni(1)-N(11)	2.119(3)		
N(1A)-Ni(1)-N(1)	180.0	N(1)-Ni(1)-S(1B)	91.27(9)
N(1)-Ni(1)-N(11)	90.36(11)	N(11)-Ni(1)-S(1B)	84.54(7)
N(1)-Ni(1)-N(11A)	89.64(11)	N(11A)-Ni(1)-S(1B)	95.46(7)
N(1A)-Ni(1)-S(1B)	88.73(9)		

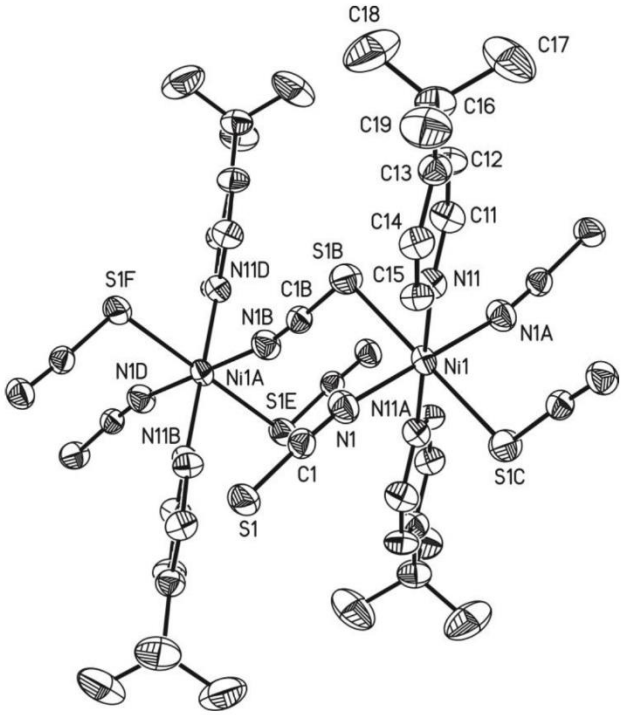

Figure S18. Crystal structure of compound **2-Ni** with labeling and displacement ellipsoids drawn at the 50 % probability level. H-atoms and disordering were left out for clarity. Symmetry transformation used to generate equivalent atoms: A: -x+1, -y, -z+1; B: -x+1, y-1/2, -z+1/2; C: x, -y+1/2, z+1/2; D: -x+1, y+1/2, -z+1/2.

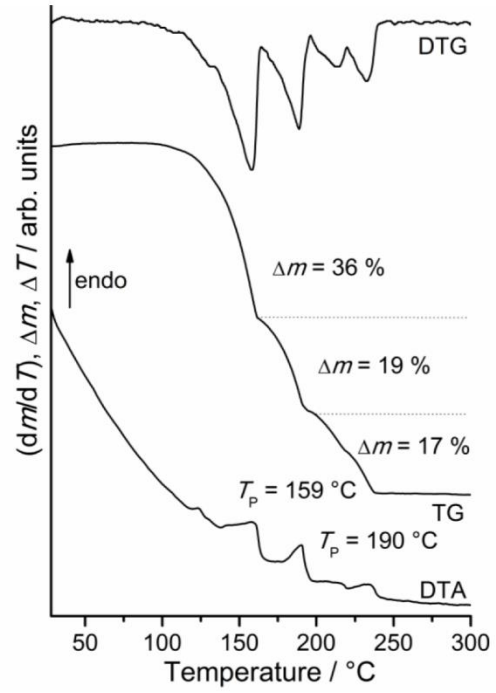

Figure S19. DTG, TG and DTA curves for **1-Mn**. Heating rate = 1 °C/min. Given are the mass change in % and the peak temperature in T_P in °C.

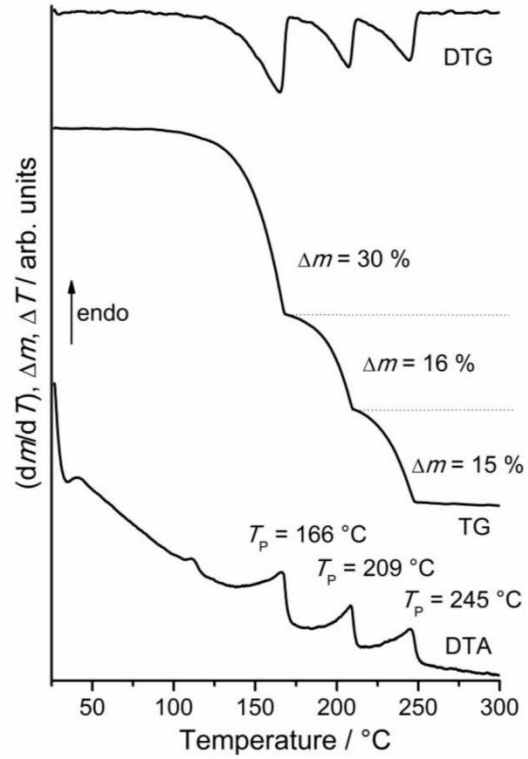

Figure S20. DTG, TG and DTA curves for **1-Fe**. Heating rate = 1 °C/min. Given are the mass change in % and the peak temperature in T_P in °C.

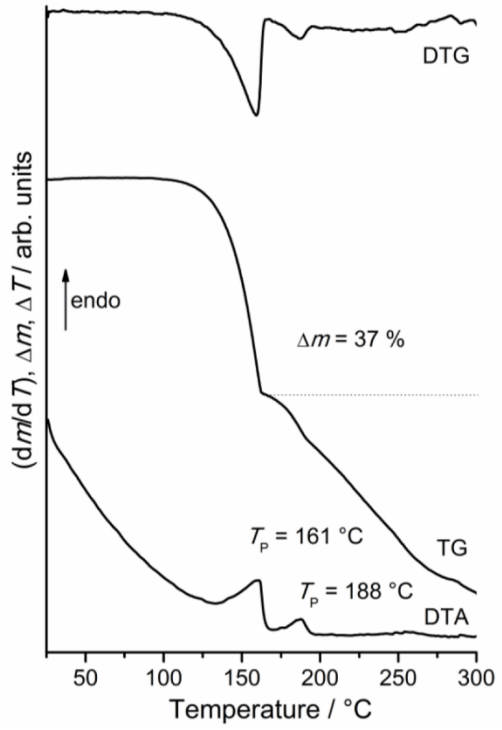

Figure S21. DTG, TG and DTA curves for **1-Co**. Heating rate = 1 °C/min. Given are the mass change in % and the peak temperature in T_P in °C.

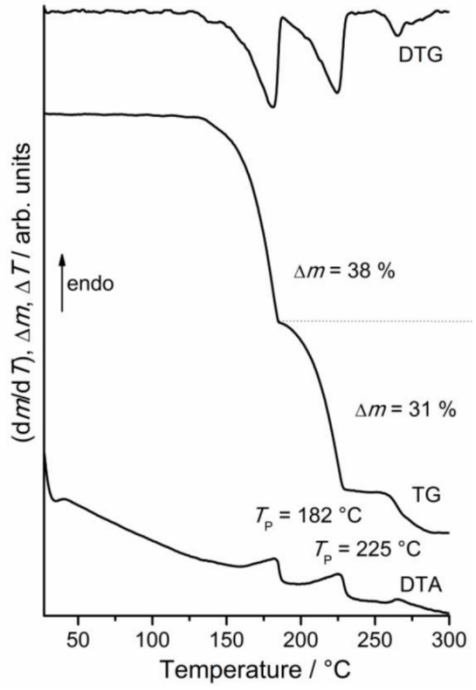

Figure S22. DTG, TG and DTA curves for **1-Ni**. Heating rate = 1 °C/min. Given are the mass change in % and the peak temperature in T_P in °C.

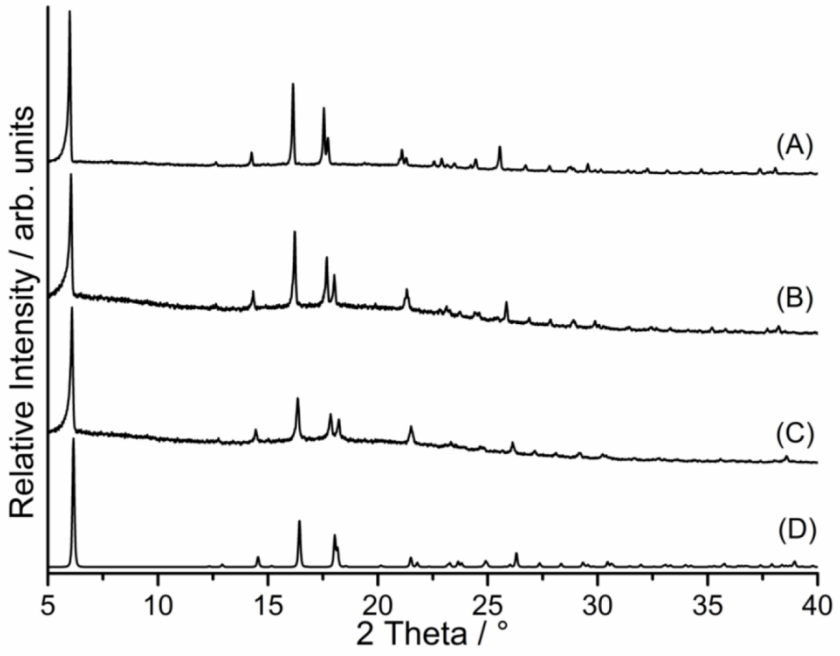

Figure S23. Experimental XRPD pattern for **2-Mn** (A), **2-Fe** (B), **2-Ni** (C) obtained by thermal decomposition and calculated XRPD pattern for compound **2-Ni** (D).

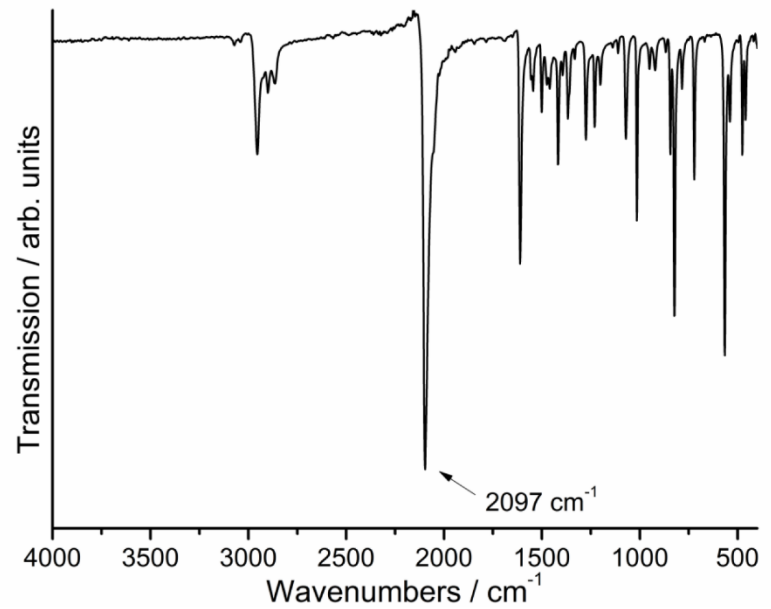

Figure S24. IR spectra of **2-Mn**. The CN stretching vibration is given.

15

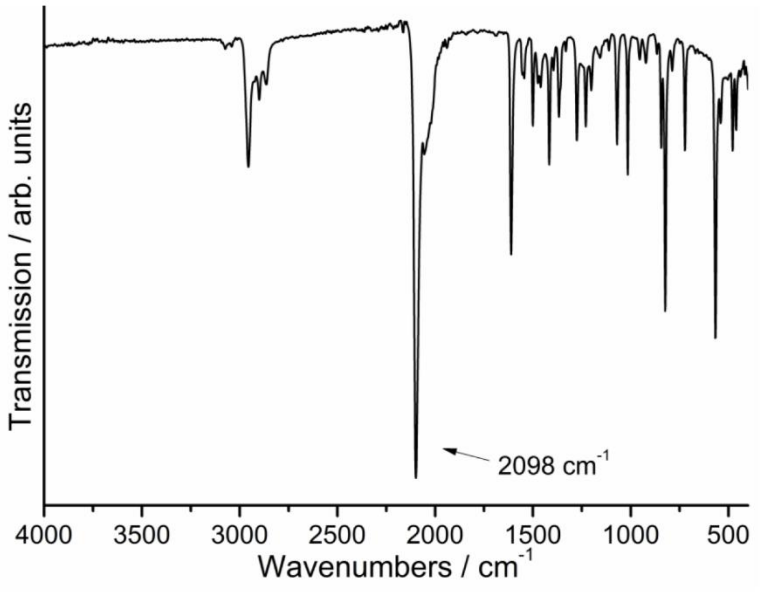

Figure S25. IR spectra of **2-Fe**. The CN stretching vibration is given.

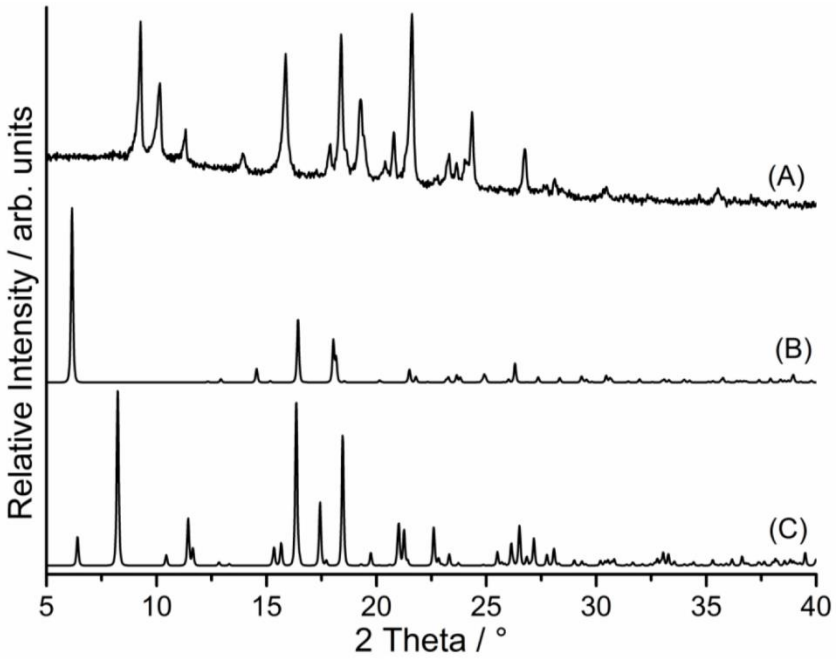

Figure S26. Experimental for compound **3-Co** (A) and calculated X-ray powder pattern of compound **2-Ni** (B) and **1-Co** (C).

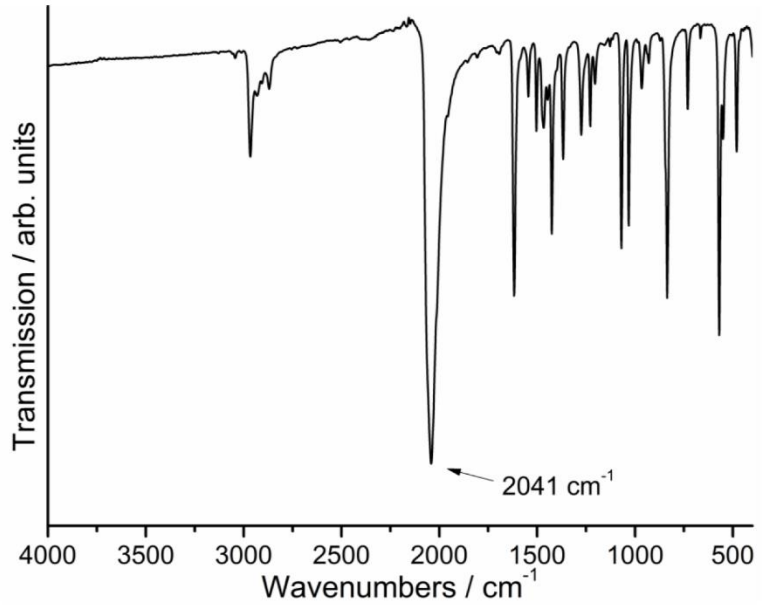

Figure S27. IR spectra of **3-Co**. The CN stretching vibration is given.

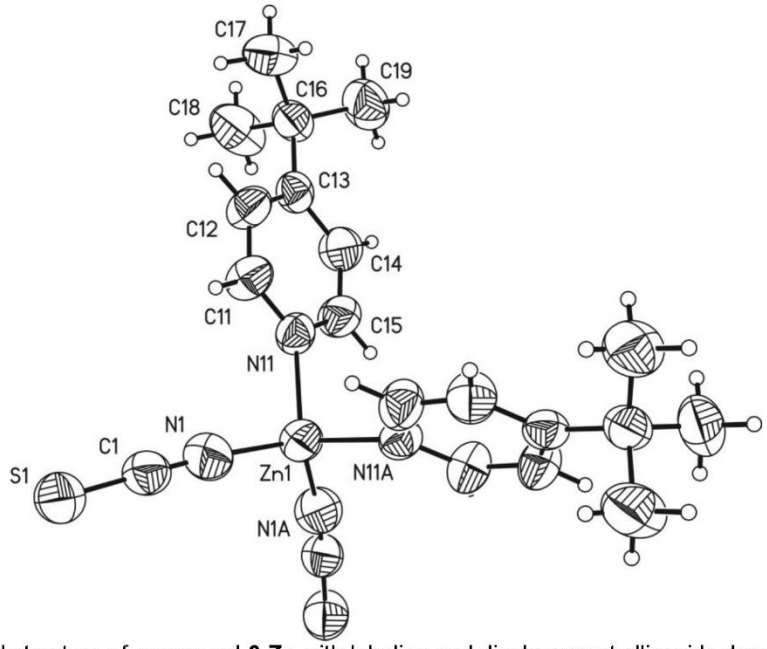

Figure S28. Crystal structure of compound **3-Zn** with labeling and displacement ellipsoids drawn at the 50 % probability level. Symmetry transformation used to generate equivalent atoms: A: -x+3/2, -y+1/2, z.

Tab S5. Selected bond lengths (Å) and angles (°) for **3-Zn**. Symmetry code: A: -x+3/2, -y+1/2, z.

$Zn(NCS)_2$(*tert*-Butylpyridine)$_2$ (3-Zn)			
Zn(1)-N(1)	1.935(4)	Zn(1)-N(11)	2.027(3)
N(1)-Zn(1)-N(11)	107.17(13)	N(11A)-Zn(1)-N(11)	103.62(15)
N(1)-Zn(1)-N(1A)	118.1(2)	C(1)-N(1)-Zn(1)	172.4(3)
N(1)-Zn(1)-N(11A)	109.91(12)		

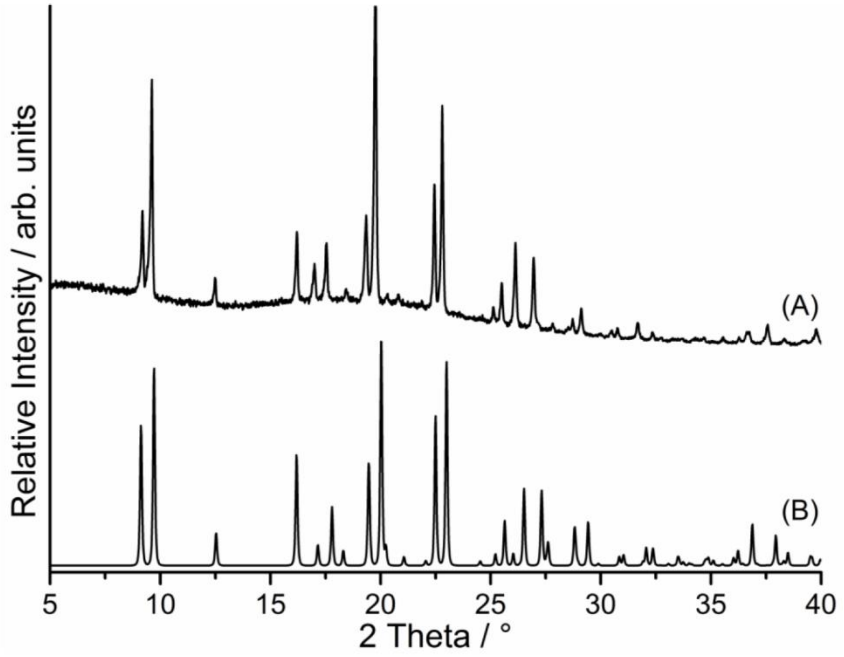

Figure S29. Experimental (A) and calculated (B) XRPD pattern for compound **3-Zn**.

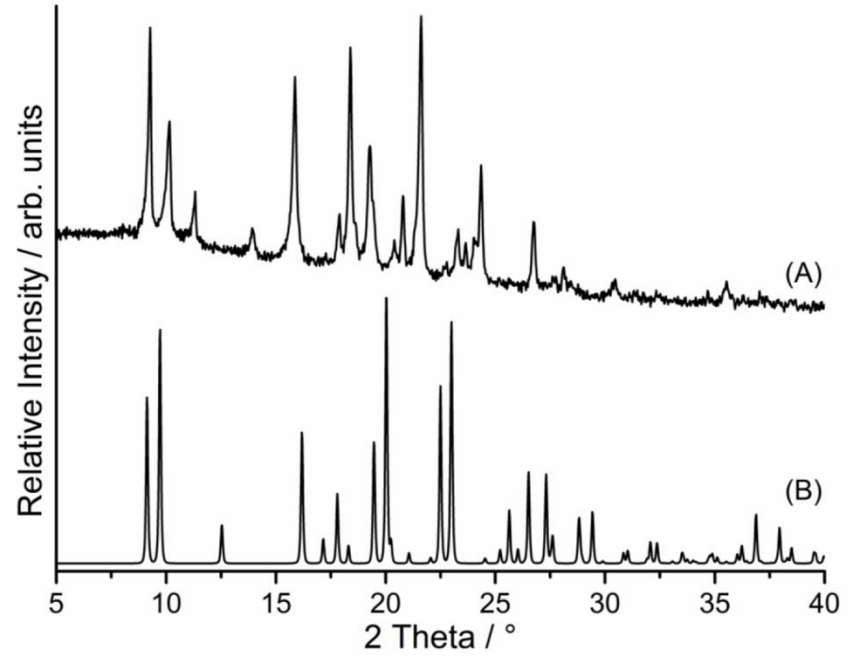

Figure S30. Experimental (A) for compound **3-Co** and calculated X-ray powder pattern of compound **3-Zn** (B).

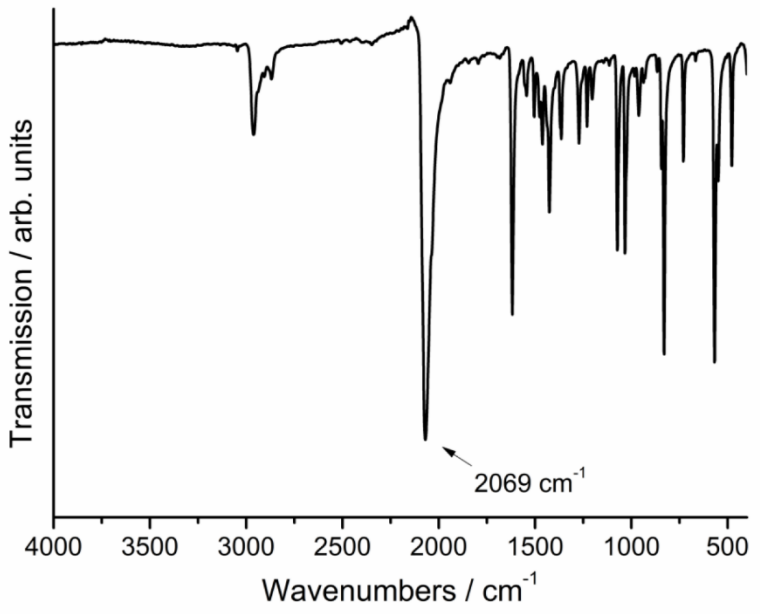

Figure S31. IR spectra of **3-Zn**. The CN stretching vibration is given.

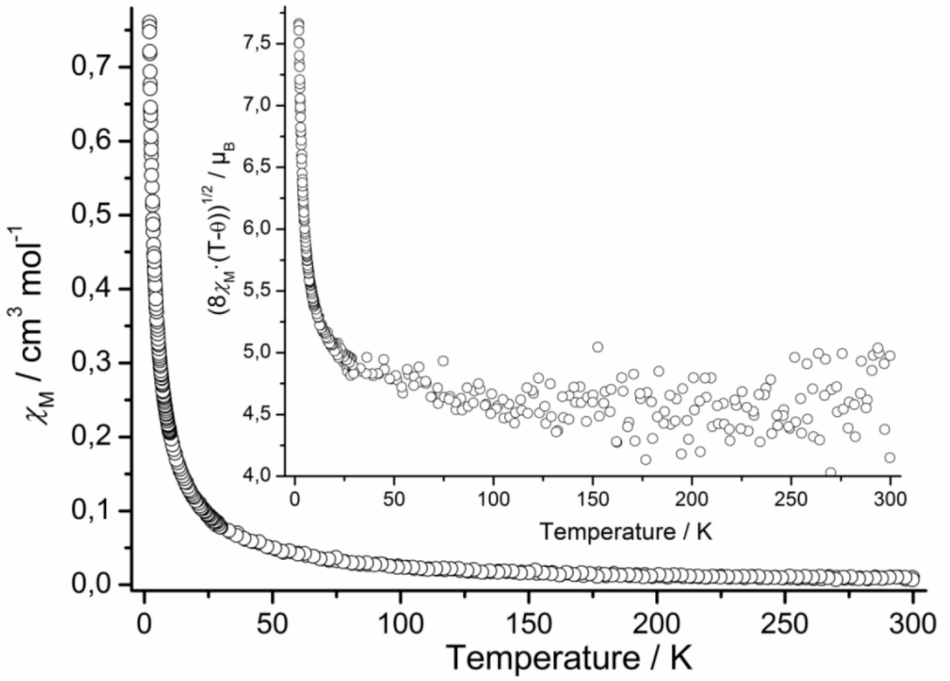

Figure S32. χ and (8*χ (T-θ)) $^{1/2}$ as function of temperature for **3-Co** measured at H_{DC} = 0.1 kOe.

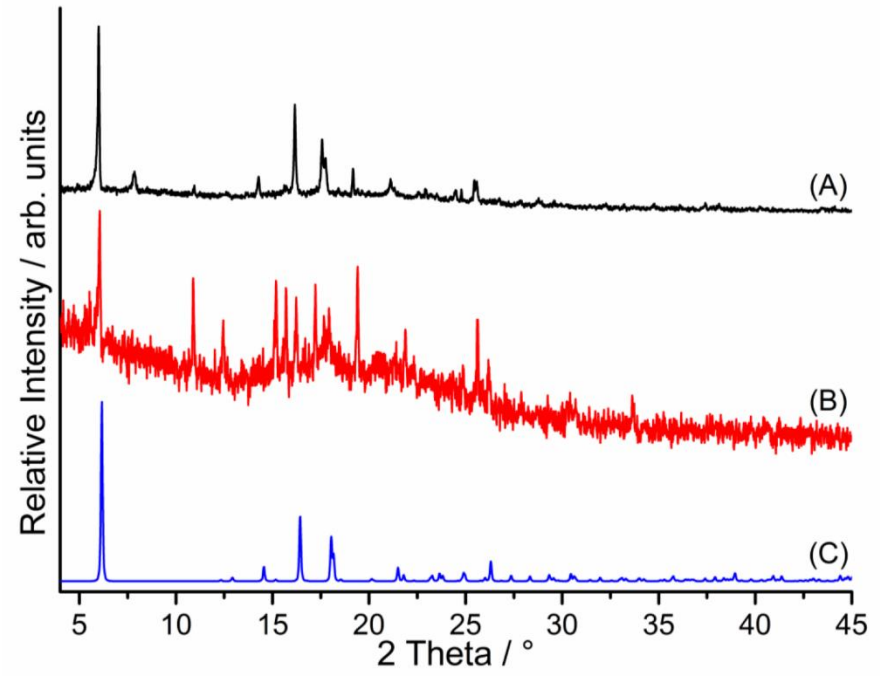

Figure S33. Experimental X-ray powder pattern of the residue obtained after the second mass step of **1-Mn** (A), **1-Fe** (B) and calculated X-ray powder pattern of compound **2-Ni** (C).

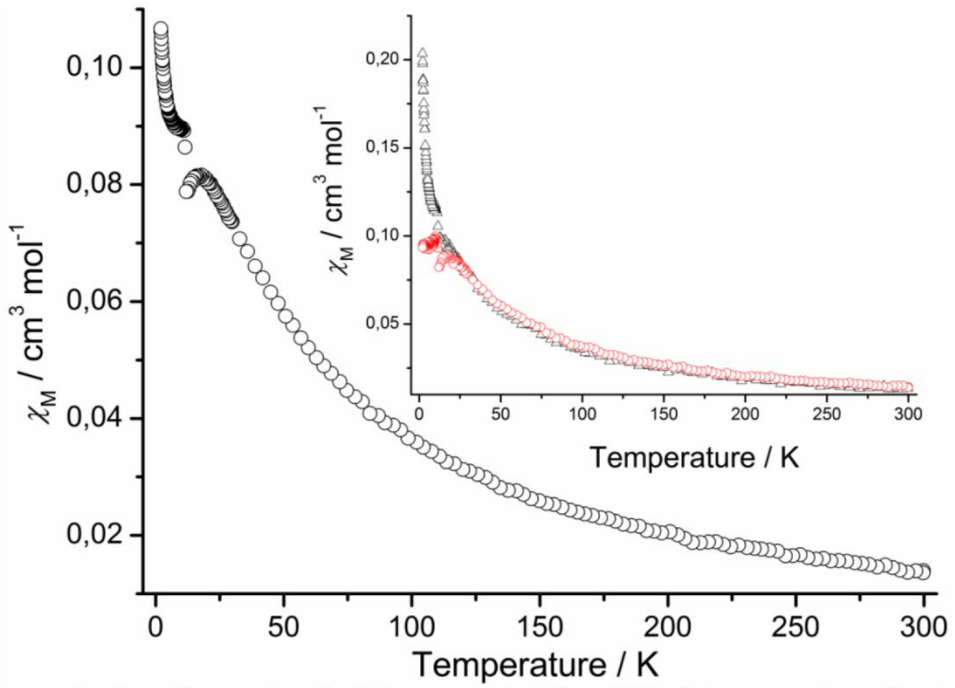

Figure S34. χ as function of temperature for **2-Mn** measured at H_{DC} = 1 kOe. Inlay: comparison of two batches of **2-Mn**.

20

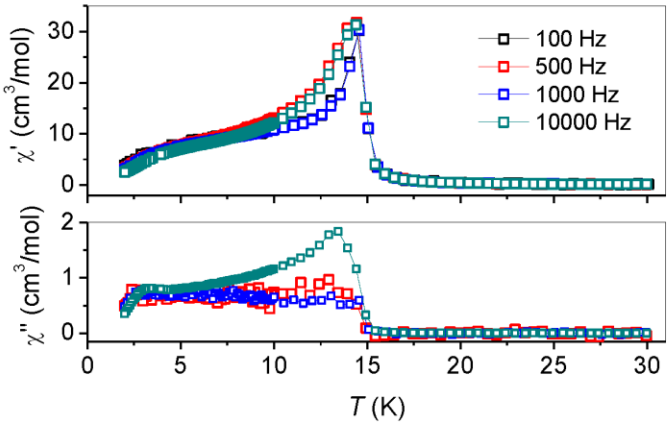

Figure S35. AC susceptibility of **2-Ni** measured as a function of temperature in zero DC field for several frequencies. In the bottom panel the curve for 100 Hz is not shown because it was very noisy.

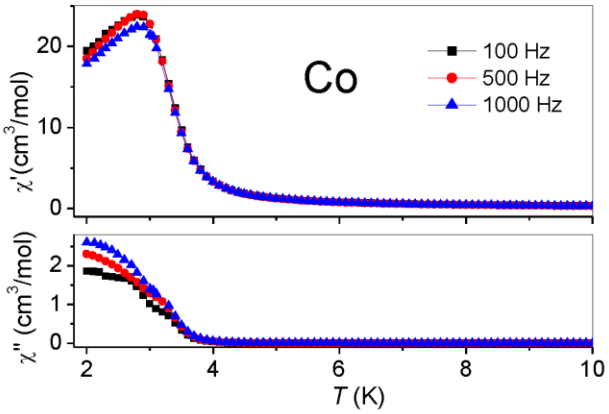

Figure S36. AC susceptibility vs. temperature of **2-Co** recorded for three frequencies.

8.5. Cover: Magnetic Properties of Isomeric and Polymorphic Coordination Polymers of Composition $[M(NCS)_2(4\text{-Acetylypridine})_2]_n$ (M = Fe, Ni)

EurJIC European Journal of Inorganic Chemistry
ChemPubSoc Europe
COVER PROFILE

Thiocyanato Coordination Polymers with Isomeric Coordination Networks: Synthesis, Structures and Magnetic Properties

DFG Deutsche Forschungsgemeinschaft

C A U
Institut für Anorganische Chemie
Christian-Albrechts-Universität zu Kiel
Max-Eyth-Straße 2,
24118 Kiel, Germany.

Max Planck Institute for Solid State Research,
Heisenbergstraße 1,
70569 Stuttgart
Germany.

Martin-Luther-Universität
Halle-Wittenberg
Institut für Chemie
Kurt-Mothes-Straße 2
06120 Halle / Saale
Germany.

Invited for the cover of this issue is the group of Christian Näther at the University of Kiel, Germany. The cover image shows the structures of two isomeric coordination polymers that are located somewhere in an energy hypersurface indicated by a desert landscape.

In one word, how would you describe your research?

Systematic! There is nothing I can add.

Did serendipity play a part in this work?

I have the feeling that I should say that this is never the case and that everything is planned and designed, but of course it plays a role in most of my investigations and I am sure that this problem is not limited to only my research. The important question is simply to what extent it plays a role in a project and I strongly believe that this can be influenced by detailed and systematic investigations, even if this is a long and sometimes an exhausting way. Miracles are usually very rare in chemistry.

What prompted you to investigate this topic/problem?

This topic is only a small part of a supervised project and it would be inappropriate to focus on only one paper. Within this project, we accidently obtained a compound with a chain structure that shows a slow relaxation of the magnetization, which is indicative of single chain magnet behavior. Based on this observation we started to investigate the influence of a chemical modification on those parameters that describe the performance of such materials. Therefore, compounds with always the same chain structures were needed, which in the beginning were frequently obtained. However, for one special ligand we obtained a compound with a layered network instead of the chain that did not show the desired magnetic behavior. Systematic investigations have shown that the layered compound is thermodynamically stable and that the desired chain compound, even if it is metastable, can be prepared by a different route. The present work was performed to investigate if similar isomers can also be prepared with different metal cations and if the order of stability depends on the nature of these metal cations. Even if this work is only a small piece of a much larger puzzle it is important, because usually, a puzzle cannot be completed if one piece is missing.

How did the collaboration on this project start?

In the beginning of my career I believed that I could investigate and might solve any problem by myself. Over the years I became more experienced and I have learned that science is frequently more complicated than expected or desired and that there is always someone who can do something better than me. This was the reason why I looked for and fortunately found some competent partners, not only for this work, and I am particularly pleased with this. Without such partners, one cannot reach a higher level and sooner or later one will make mistakes.

What was the inspiration for this cover design?

A major part not only for this work but also several of my recent investigations deals with investigations on stable and metastable crystalline compounds that are located somewhere on the energy hypersurface. This is indicated in the cover by this desert landscape where the metastable structure is located upon the mountain and the stable one is located in the valley. The woman walking through this endless desert might symbolize a chemist who would like to have one particular compound, one modification or one isomer that is located somewhere in this landscape. It appears to be hopeless but in this case she was able to climb up the "metastable" mountain, even if this needed some time.

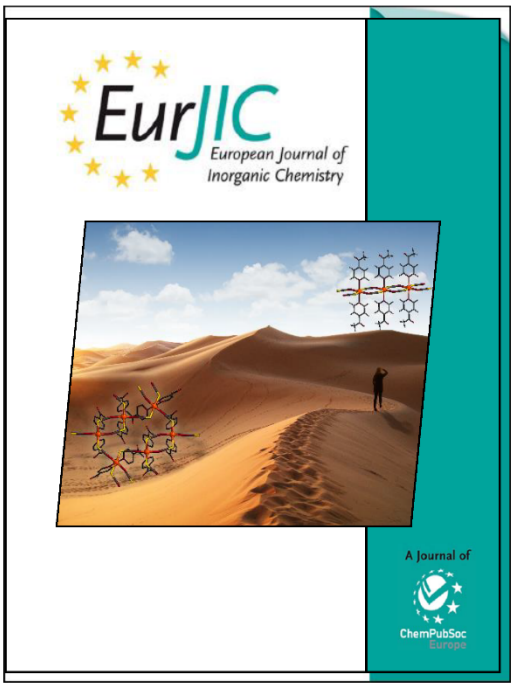

8.6. Supporting Information: Magnetic Properties of Isomeric and Polymorphic Coordination Polymers of Composition $[M(NCS)_2(4\text{-Acetylypridine})_2]_n$ (M = Fe, Ni)

Content

1

2

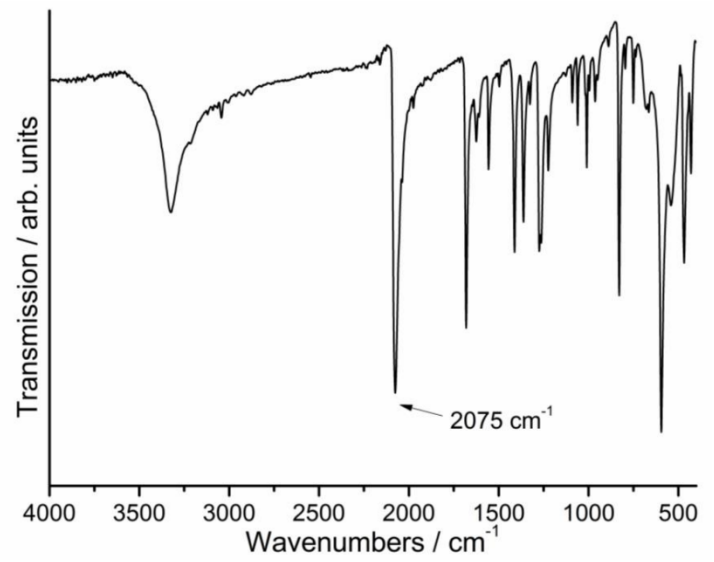

Figure S1. IR spectra of compound **1-Mn**. The value of the CN stretching vibration is given.

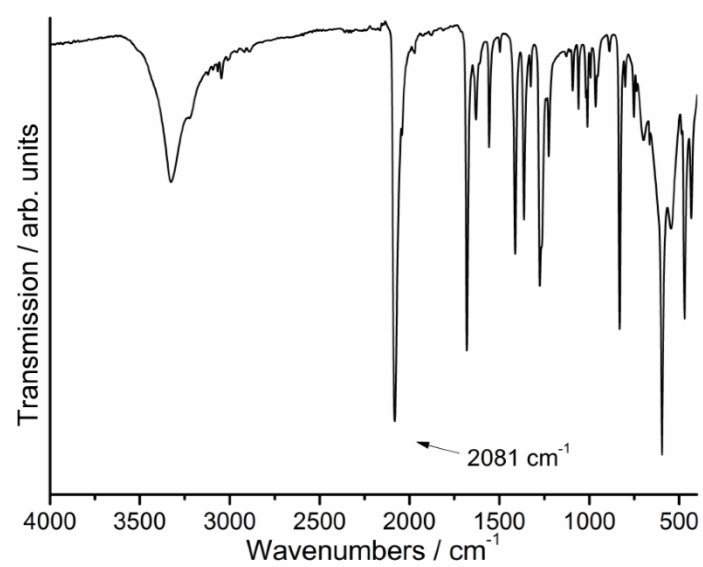

Figure S2. IR spectra of compound **1-Fe**. The value of the CN stretching vibration is given.

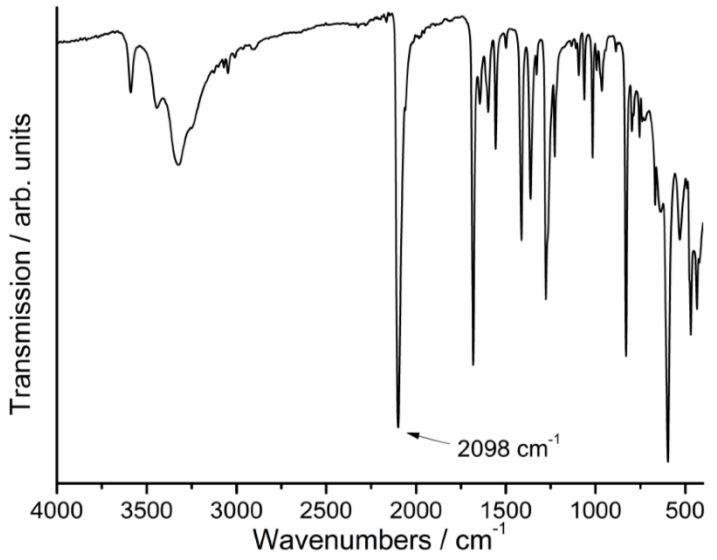

Figure S3. IR spectra of compound **1-Ni**. The value of the CN stretching vibration is given.

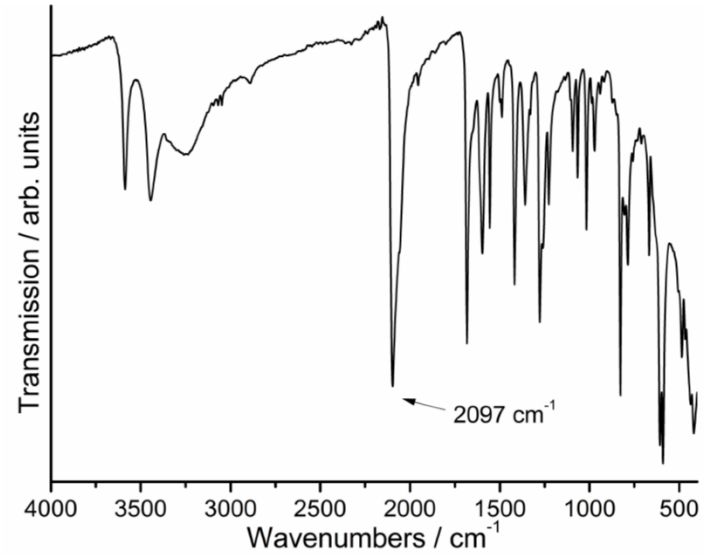

Figure S4. IR spectra of compound **1-Ni(H_2O)**. The value of the CN stretching vibration is given.

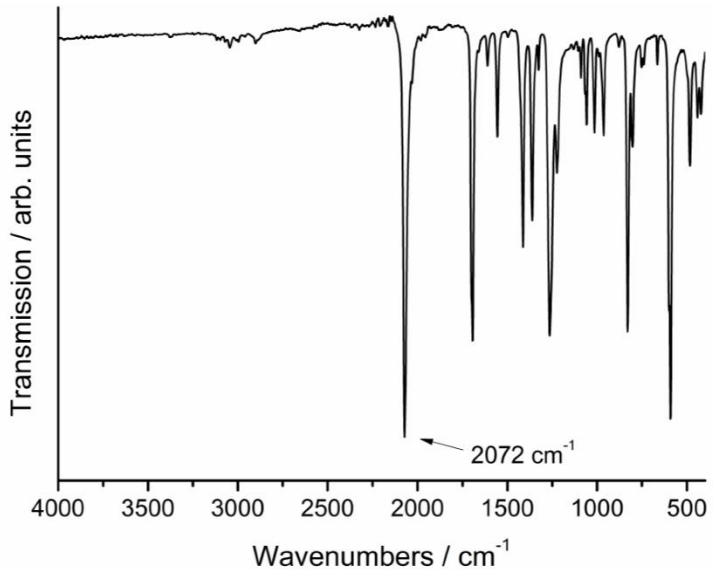

Figure S5. IR spectra of compound **2-Ni**. The value of the CN stretching vibration is given.

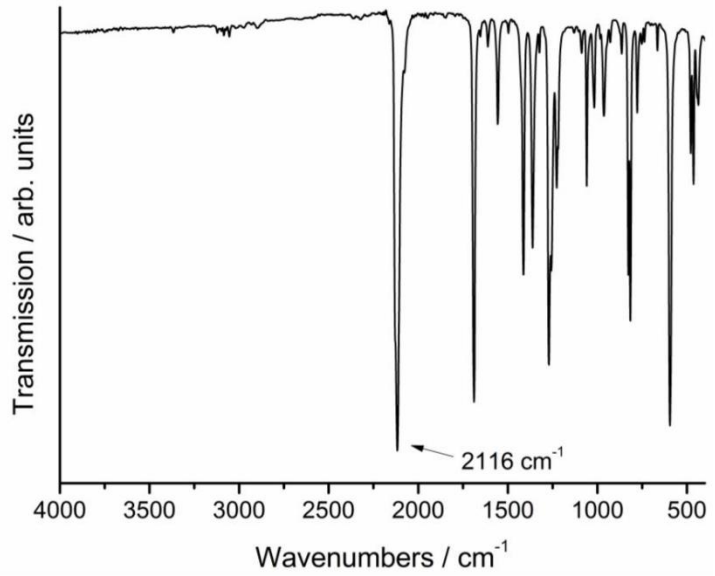

Figure S6. IR spectra of compound **3-Ni/I**. The value of the CN stretching vibration is given.

5

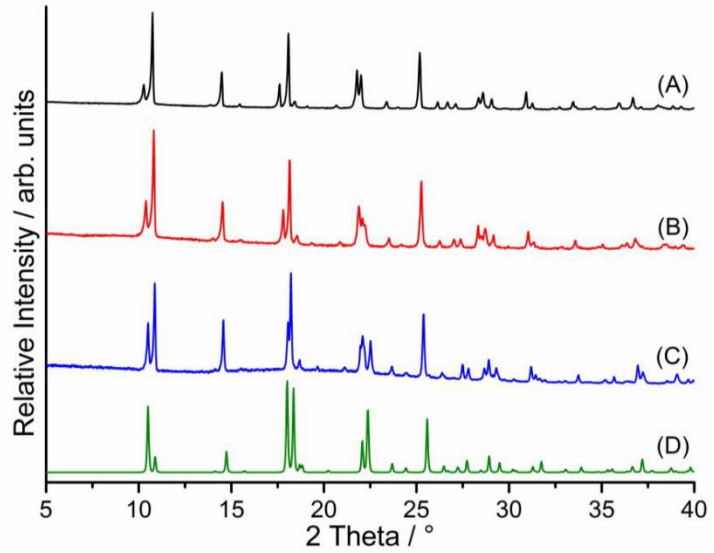

Figure S7. Experimental XRPD pattern of **1-Mn** (A), **1-Fe** (B) and **1-Ni** (C) together with the calculated pattern of **1-Co** (D).

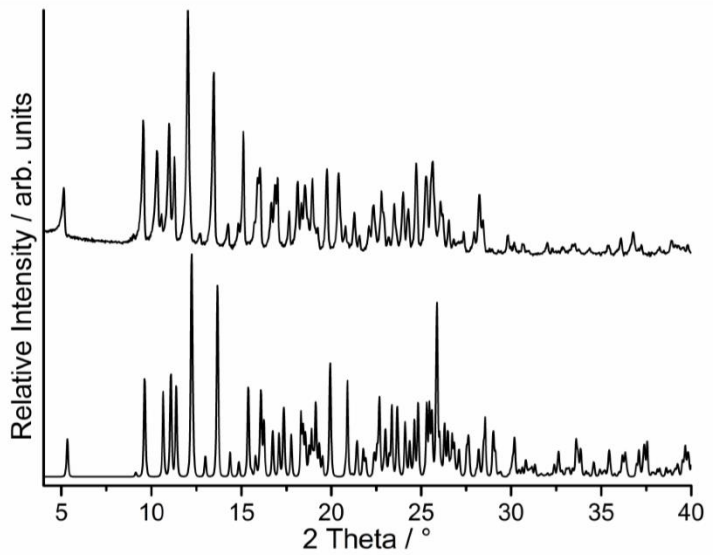

Figure S8. Experimental XRPD pattern of **2-Ni** (top) and calculated pattern of $Co(NCS)_2(4\text{-Acetylpyridine})_4$ (bottom).

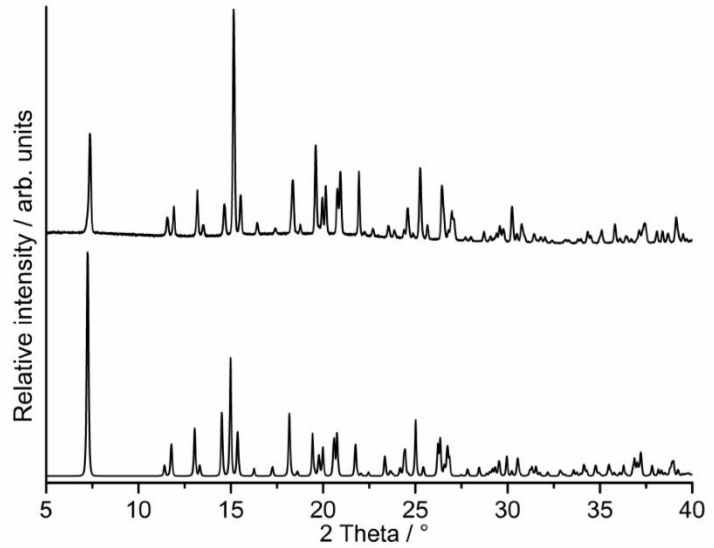

Figure S9. Experimental XRPD pattern of **3-Ni/I** (top) and calculated pattern of $[Co(NCS)_2(4\text{-Acetylpyridine})_2]_n$ 2D (bottom).

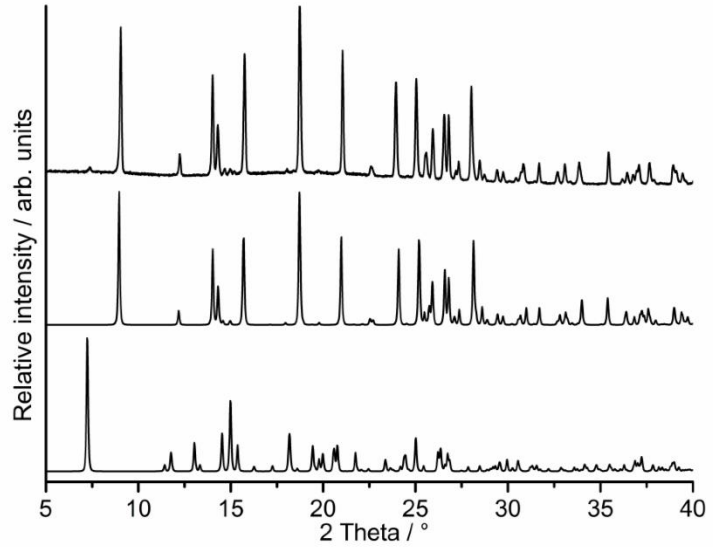

Figure S10. Experimental XRPD pattern of **1-Ni(H_2O)** stored for several hours at room-temperature (top), calculated pattern of **1-Ni(H_2O)** (mid) and of $[Co(NCS)_2(4\text{-Acetylpyridine})_2]_n$ 2D (bottom).

Table S1. Selected bond lengths (Å) and angles (°) for **1-Mn.**

Mn(1)-N(1A)	2.164(2)	Mn(1)-O(1)	2.2191(18)
Mn(1)-N(1)	2.164(2)	Mn(1)-N(11A)	2.3043(19)
Mn(1)-O(1A)	2.2191(18)	Mn(1)-N(11)	2.3044(19)
N(1A)-Mn(1)-N(1)	180.0	N(1)-Mn(1)-O(1)	90.33(8)
N(1A)-Mn(1)-O(1A)	90.33(8)	O(1A)-Mn(1)-O(1)	180.0
N(1)-Mn(1)-O(1A)	89.67(8)	N(1A)-Mn(1)-N(11A)	89.59(8)
N(1A)-Mn(1)-O(1)	89.67(8)	N(1)-Mn(1)-N(11A)	90.41(8)
O(1A)-Mn(1)-N(11)A	92.00(7)	O(1A)-Mn(1)-N(11)	88.00(7)
O(1)-Mn(1)-N(11A)	88.00(7)	O(1)-Mn(1)-N(11)	92.00(7)
N(1A)-Mn(1)-N(11)	90.41(8)	N(11A)-Mn(1)-N(11)	180.0

Table S2. Hydrogen bonding for **1-Mn**. Symmetry transformations used to generate equivalent atoms: A: -x,-y,-z+1, B: x+1,y,z, C: x-1,y,z-1, D: x+1/2,-y+1/2,z+1/2.

D-H…A	d(D-H)	d(H...A)	d(D...A)	<(DHA)
O(1)-H(1O1)...S(1B)	0.82	2.54	3.262(2)	147.9
O(1)-H(2O1)...O(11C)	0.82	1.99	2.781(2)	162.6
C(12)-H(12)...S(1D)	0.93	2.88	3.732	153.6

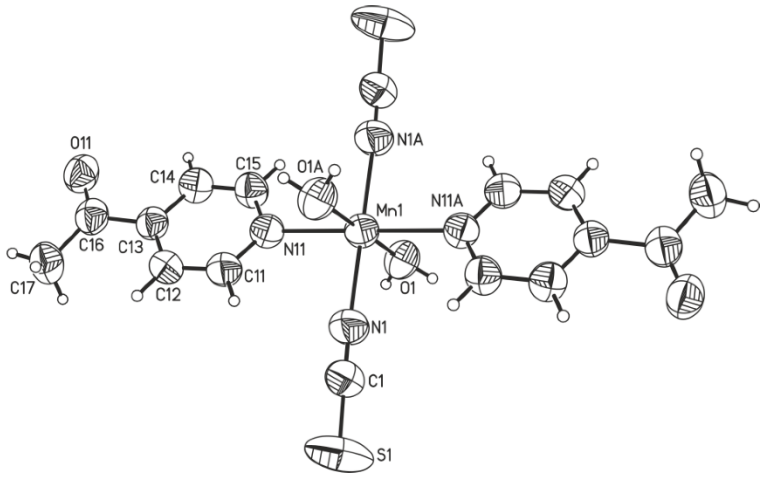

Figure S11. ORTEP plot of **1-Mn** with view of the coordination sphere of the Mn(II) cation with labeling and displacement ellipsoids drawn at 50 % probability level. Symmetry transformation used to generate equivalent atoms: A: -x,-y,-z+1.

Table S3. Selected bond lengths (Å) and angles (°) for **1-Ni(H_2O).**

Ni(1)-N(1A)	2.0532(19)	Ni(1)-O(1A)	2.0866(16)
Ni(1)-N(1)	2.0532(19)	Ni(1)-N(11)	2.1162(18)
Ni(1)-O(1)	2.0865(16)	Ni(1)-N(11A)	2.1162(18)
N(1A)-Ni(1)-N(1)	180.00(10)	N(1A)-Ni(1)-O(1A)	87.47(7)
N(1A)-Ni(1)-O(1)	92.53(7)	N(1)-Ni(1)-O(1A)	92.53(7)
N(1)-Ni(1)-O(1)	87.47(7)	O(1)-Ni(1)-O(1A)	180.0
N(1A)-Ni(1)-N(11)	91.02(7)	N(1A)-Ni(1)-N(11A)	88.98(7)
N(1)-Ni(1)-N(11)	88.98(7)	N(1)-Ni(1)-N(11A)	91.02(7)
O(1)-Ni(1)-N(11)	89.93(6)	O(1)-Ni(1)-N(11A)	90.07(6)
O(1A)-Ni(1)-N(11)	90.07(6)	O(1A)-Ni(1)-N(11A)	89.93(6)
N(11)-Ni(1)-N(11A)	180.0		

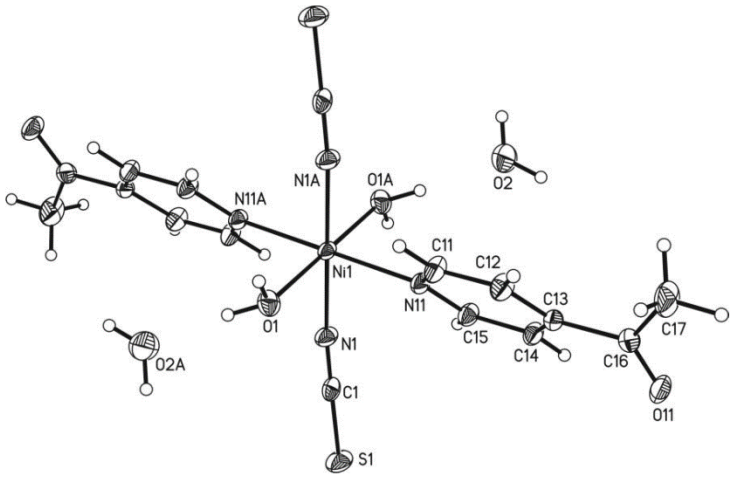

Figure S12. ORTEP plot of **1-Ni(H_2O)** with view of the coordination sphere of the Ni(II) cation with labeling and displacement ellipsoids drawn at 50 % probability level. Symmetry transformation used to generate equivalent atoms: A: -x,-y,-z+1.

Table S4. Hydrogen bonding for **1-Ni(H_2O)**. Symmetry transformations used to generate equivalent atoms: A: -x,-y,-z+1, B: x-1/2,-y-1/2,z-1/2, C: x-1/2,-y+1/2,z-1/2, D: -x+1/2,-y-1/2,-z+3/2.

D-H…A	d(D-H)	d(H...A)	d(D...A)	<(DHA)
O(1)-H(1O1)...O(2A)	0.84	1.90	2.733(3)	170.9
O(2)-H(1O2)...O(11B)	0.84	2.10	2.794(3)	139.3
O(1)-H(2O1)...O(11C)	0.84	2.03	2.829(2)	157.0
O(2)-H(2O2)...S(1D)	0.84	2.55	3.332(2)	155.8
C(11)-H(11)...O(11C)	0.95	2.57	3.456(3)	155.2

Table S5. Selected bond lengths (Å) and angles (°) for **2-Ni.**

Ni(1)-N(2)	2.032(4)	Ni(1)-N(41)	2.129(4)
Ni(1)-N(1)	2.035(4)	Ni(1)-N(11)	2.158(5)
Ni(1)-N(31)	2.109(4)	Ni(1)-N(21)	2.168(4)
N(2)-Ni(1)-N(1)	177.61(19)	N(1)-Ni(1)-N(41)	89.74(16)
N(2)-Ni(1)-N(31)	90.24(17)	N(31)-Ni(1)-N(41)	91.74(16)
N(1)-Ni(1)-N(31)	87.54(17)	N(2)-Ni(1)-N(11)	91.42(17)
N(2)-Ni(1)-N(41)	91.20(15)	N(1)-Ni(1)-N(11)	90.74(17)
N(31)-Ni(1)-N(11)	175.72(16)	N(31)-Ni(1)-N(21)	92.00(16)
N(41)-Ni(1)-N(11)	92.16(16)	N(41)-Ni(1)-N(21)	176.22(16)
N(2)-Ni(1)-N(21)	89.26(16)	N(11)-Ni(1)-N(21)	84.08(16)
N(1)-Ni(1)-N(21)	89.95(16)	N(1)-Ni(1)-N(41)	89.74(16)

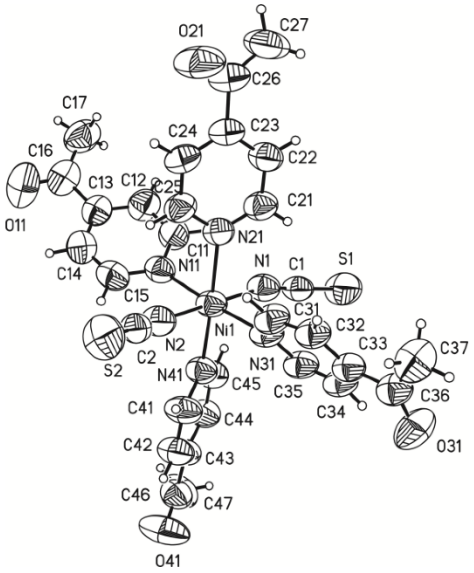

Figure S13. ORTEP plot of **2-Ni** with view of the coordination sphere of the Ni(II) cation with labeling and displacement ellipsoids drawn at 50 % probability level.

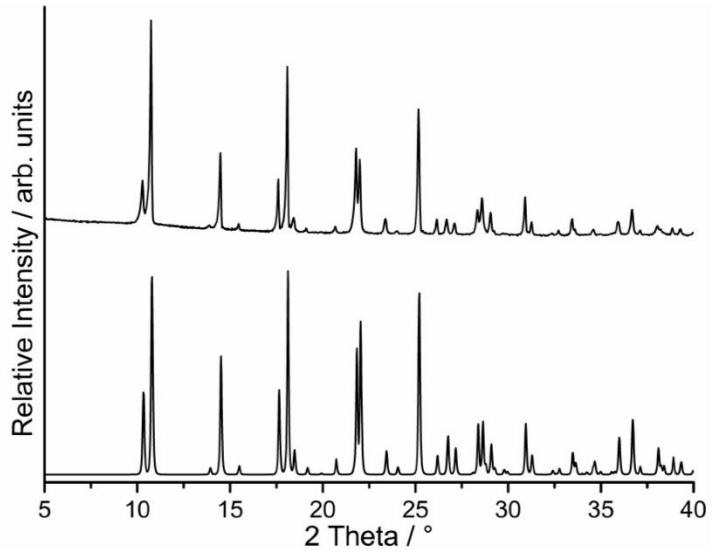

Figure S14. Experimental (top) and calculated XRPD pattern (bottom) of **1-Mn**.

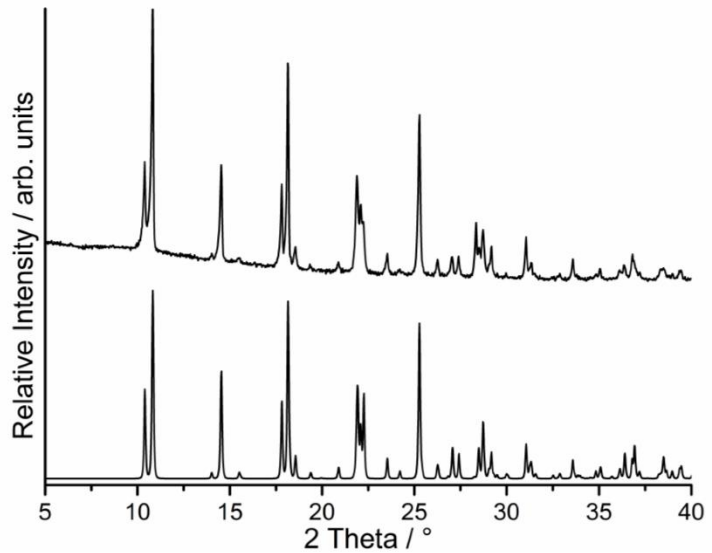

Figure S15. Experimental (top) and calculated XRPD pattern (bottom) of **1-Fe**.

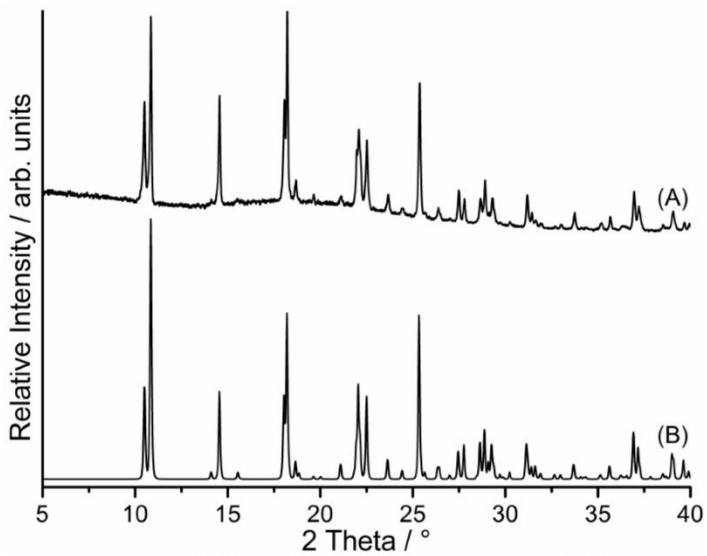

Figure S16. Experimental (top) and calculated XRPD pattern (bottom) of **1-Ni**.

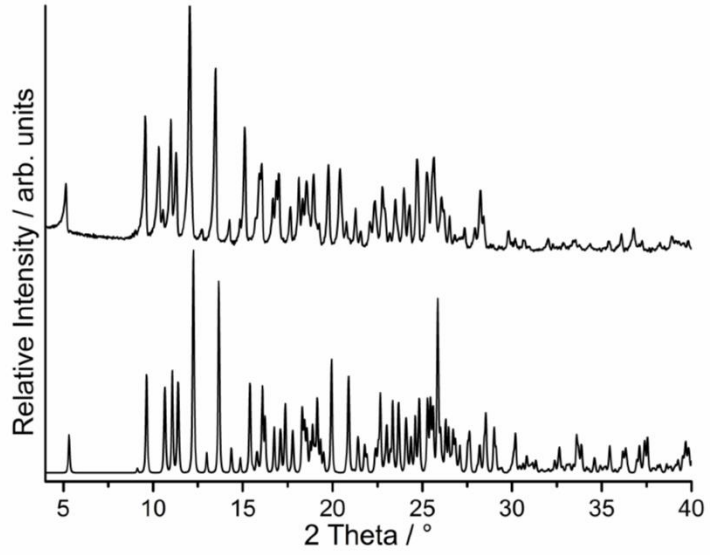

Figure S17. Experimental (top) and calculated XRPD pattern (bottom) of **2-Ni**.

12

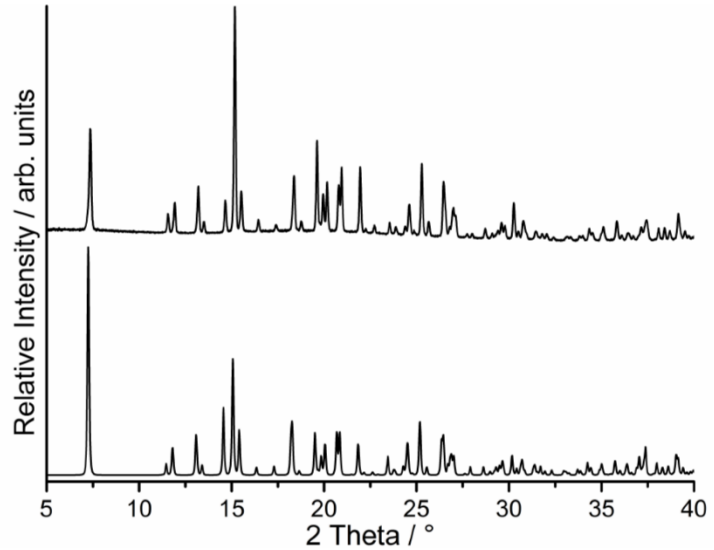

Figure S18. Experimental (top) and calculated (bottom) XRPD pattern of **3-Ni/I**.

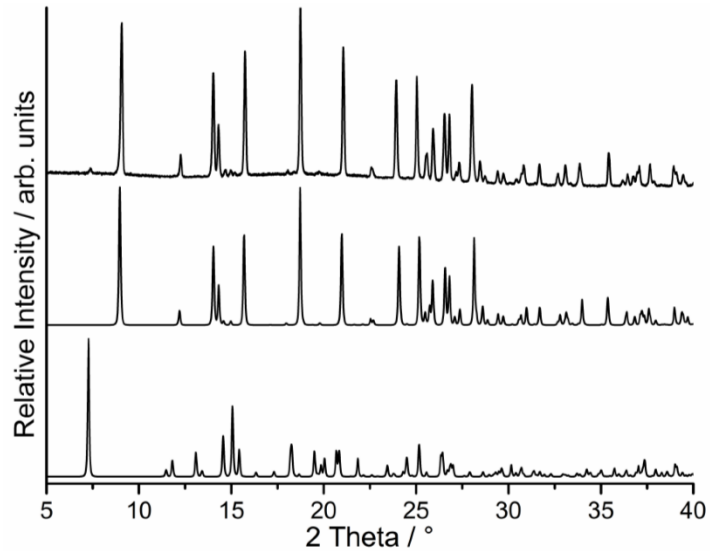

Figure S19. Experimental XRPD pattern of **1-Ni(H_2O)** (top) and calculated pattern for **1-Ni(H_2O)** (mid), and **3-Ni/I** (bottom).

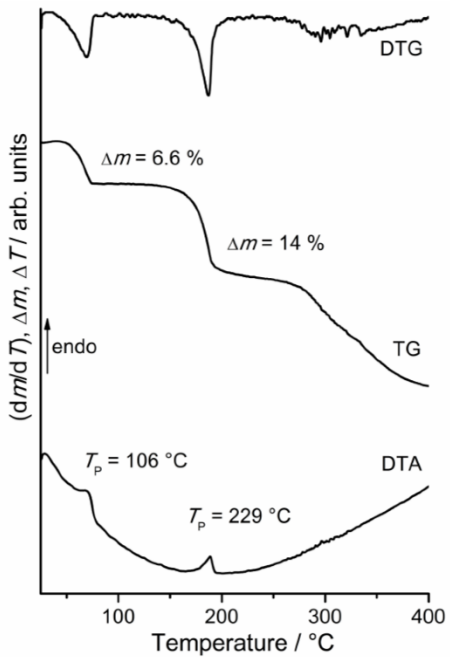

Figure S20. DTG, TG and DTA curves of compound **1-Mn**. Heating rate 1 °C / min; given are the mass change / % and the peak temperature T_P / °C.

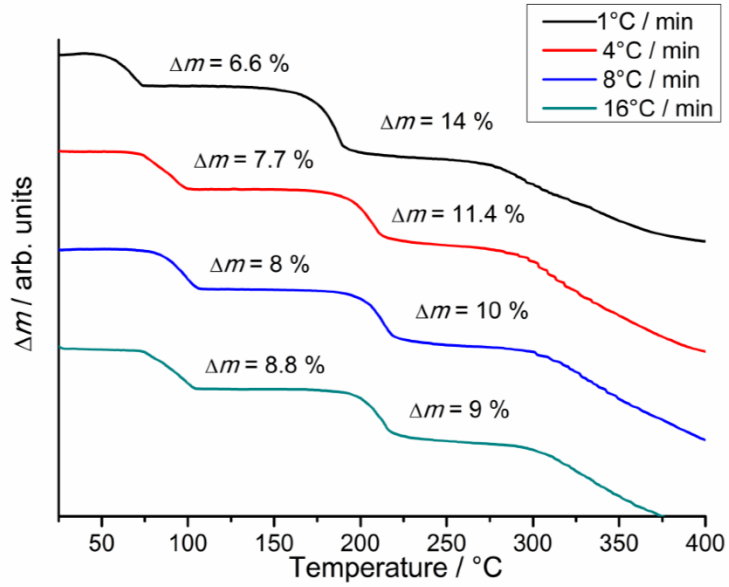

Figure S21. TG curves of **1-Mn** at different heating rates (1, 4, 8, 16 °C/min).

14

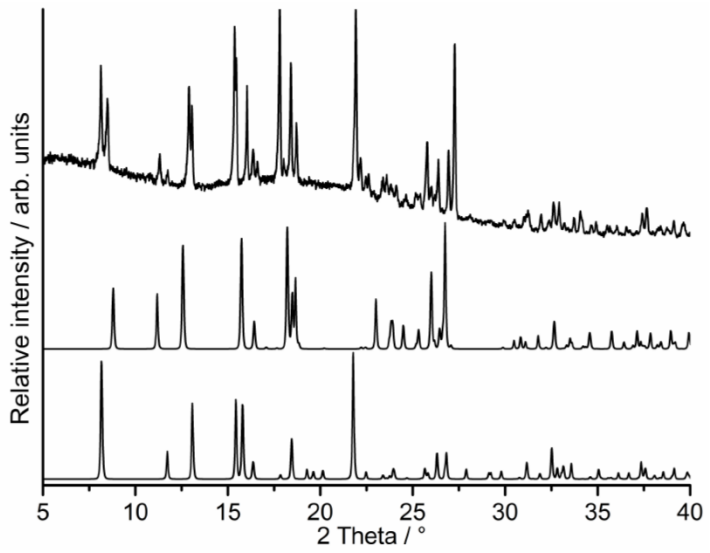

Figure S22. Experimental XRPD pattern of the residue obtained after the first TG step in the thermogravimetric measurement of **1-Mn** (top) and calculated XRPD pattern of the 1D modifications of $[Co(NCS)_2(4\text{-Acpy})_2]_n$ and $[Cd(NCS)_2(4\text{-Acpy})_2]_n$ (*C*2/c) reported recently (mid and bottom).

15

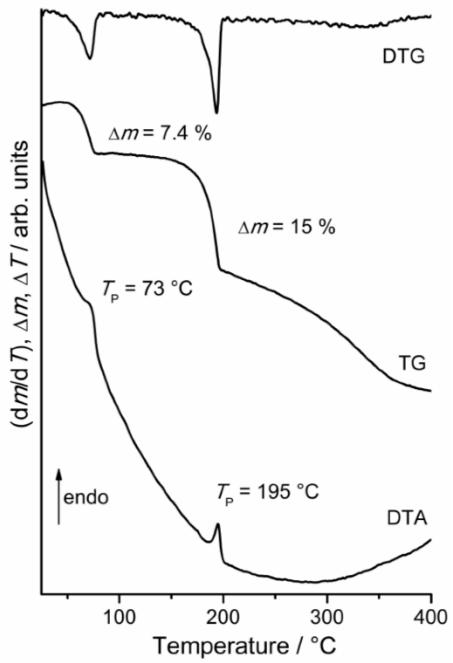

Figure S23. DTG, TG and DTA curves of compound **1-Fe**. Heating rate 1 °C / min; given are the mass change / % and the peak temperature T_P / °C.

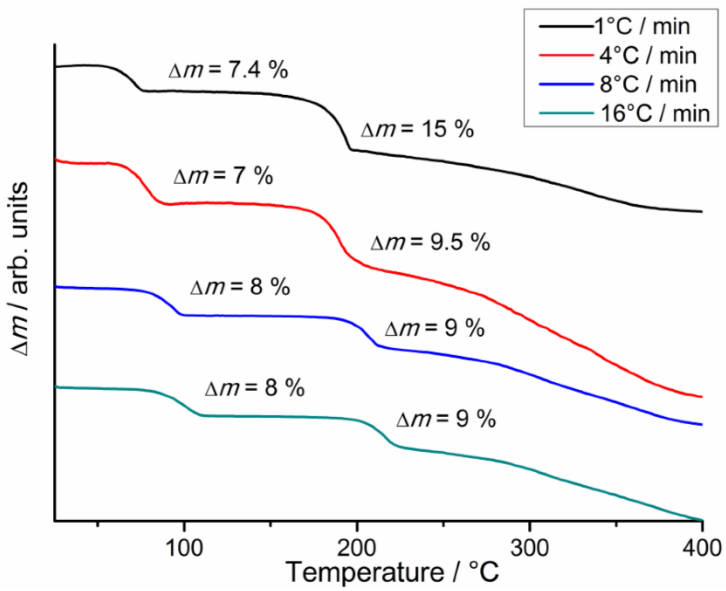

Figure S24. TG curves of **1-Fe** at different heating rates (1, 4, 8, 16 °C/min).

16

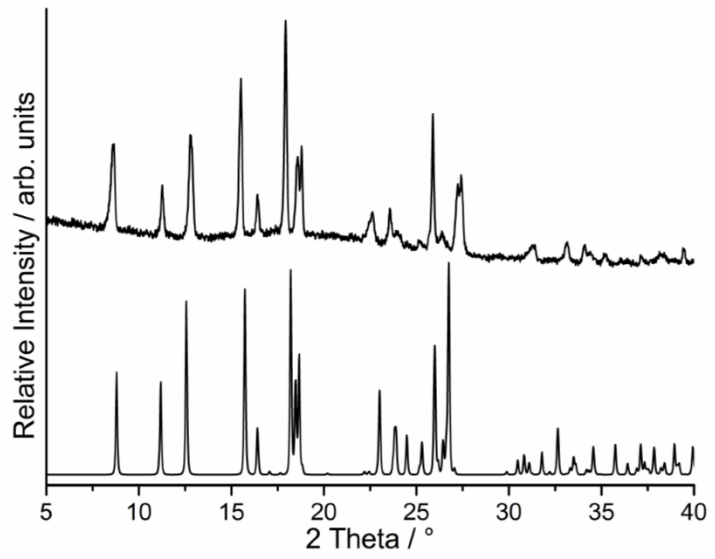

Figure S25. Experimental XRPD pattern of the residue obtained after the first TG step in the thermogravimetric measurement of **1-Fe** (top) and calculated XRPD pattern of the chain compound $[Co(NCS)_2(4\text{-Acpy})_2]_n$ reported recently (bottom).

17

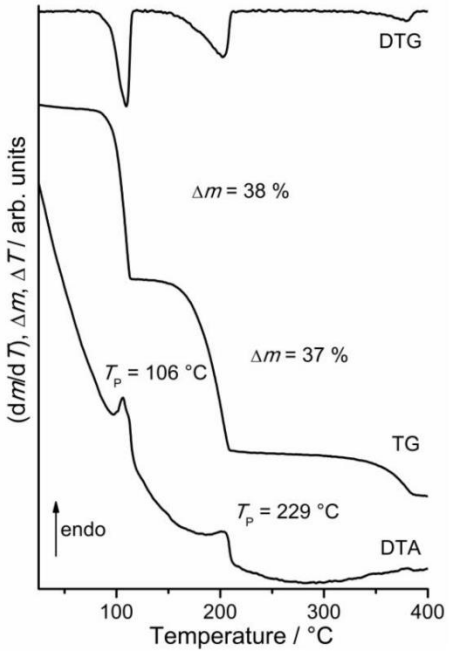

Figure S26. DTG, TG and DTA curves of compound **2-Ni**. Heating rate 1 °C / min; given are the mass change / % and the peak temperature T_P / °C.

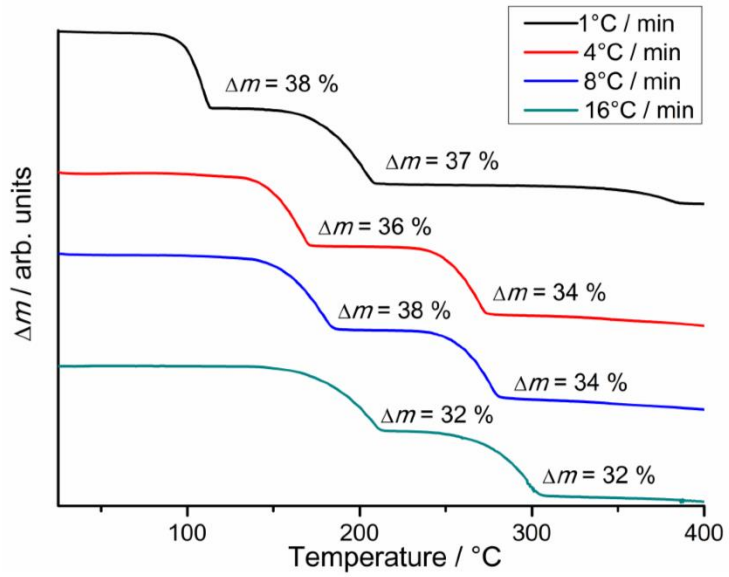

Figure S27. TG curves of **2-Ni** at different heating rates (1, 4, 8, 16 °C/min).

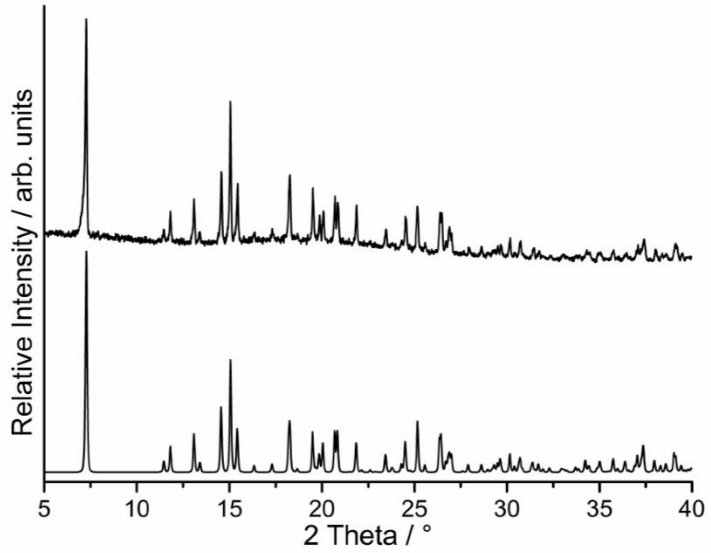

Figure S28. Experimental XRPD pattern of the residue obtained after the first TG step in the thermogravimetric measurement of **2-Ni** at 4 °C/min (top) and calculated XRPD pattern of **3-Ni/I** (bottom).

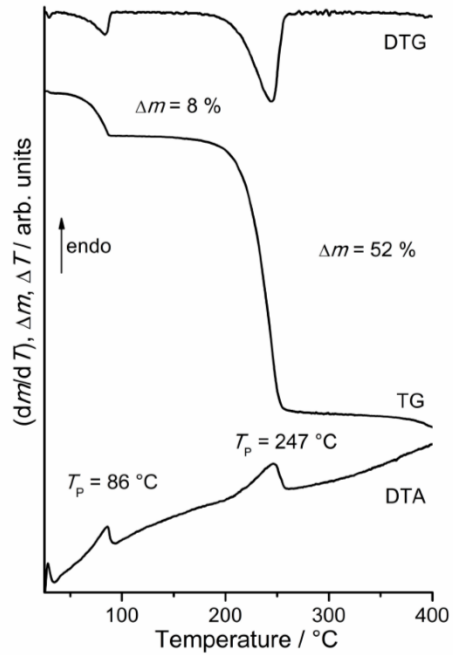

Figure S29. DTG, TG and DTA curves of compound **1-Ni**. Heating rate 1 °C / min; given are the mass change / % and the peak temperature T_P / °C.

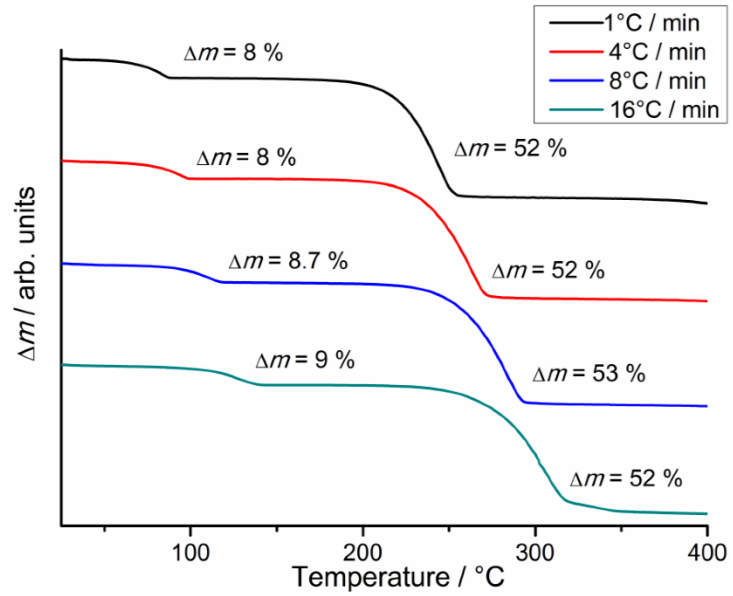

Figure S30. TG curves of **1-Ni** at different heating rates (1, 4, 8, 16 °C/min).

20

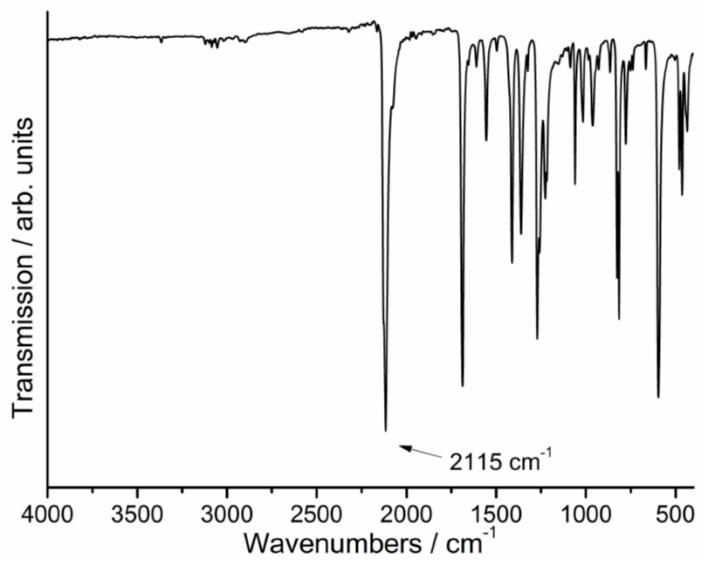

Figure S31. IR spectra of the residue obtained by thermal decomposition of **1-Ni** at 1°C/min.

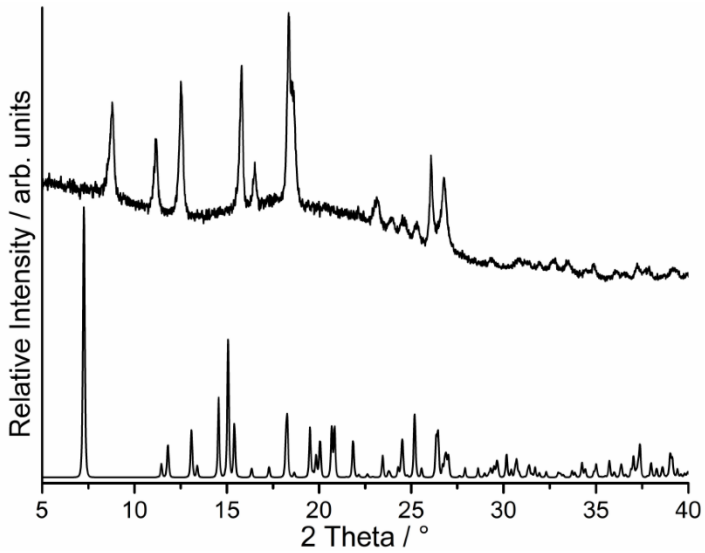

Figure S32. Experimental XRPD pattern of **3-Ni/I** obtained by thermal decomposition of **1-Ni** at 167°C and calculated pattern for **3-Ni/I**.

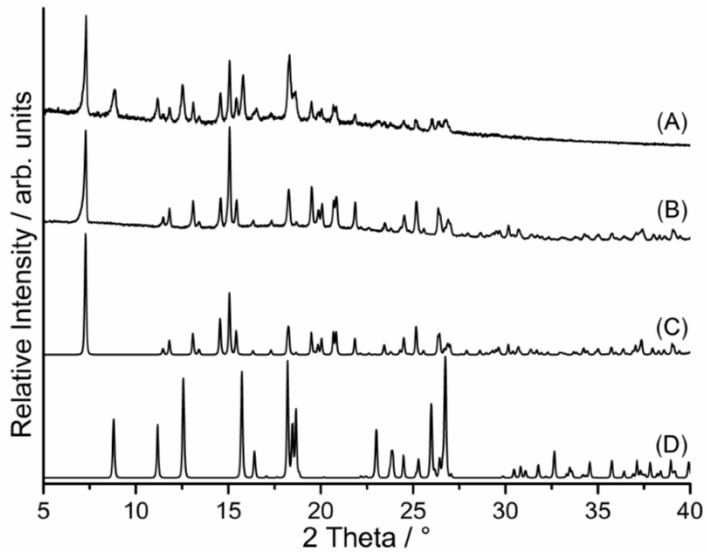

Figure S33. Experimental XRPD pattern of a mixture of **3-Ni/I** and **3-Ni/II** (A) and of the residue obtained after stirring this mixture for several days in acetonitrile (B), together with the calculated pattern for **3-Ni/I** (C) and $[Co(NCS)_2(4\text{-Acpy})_2]_n$ 1D (D).

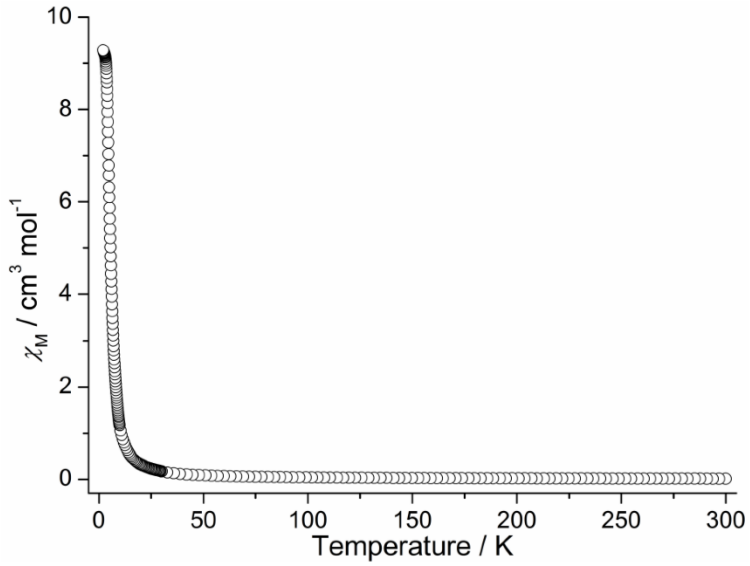

Figure S34. Temperature dependence of the susceptibility of **3-Fe** at 1000 Oe shown in the temperature range 2- 300 K.

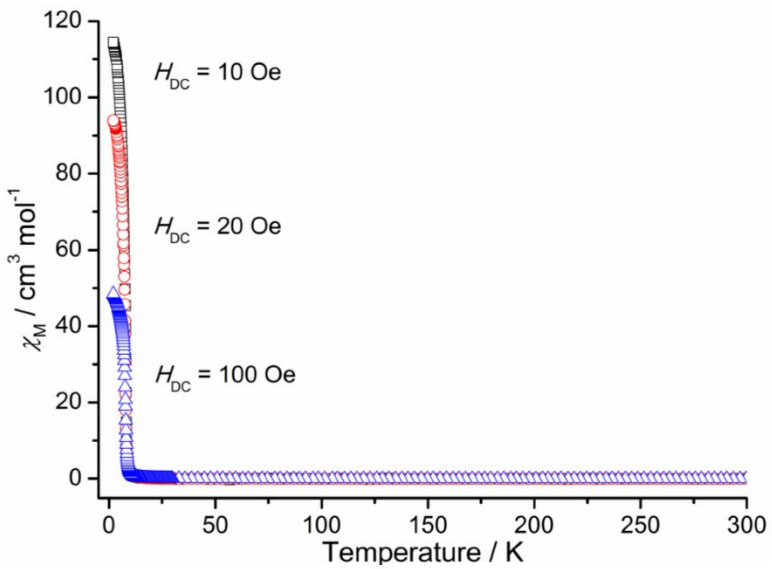

Figure S35. Temperature dependence of the susceptibility of **3-Ni/I** at 10, 20, and 100 Oe.

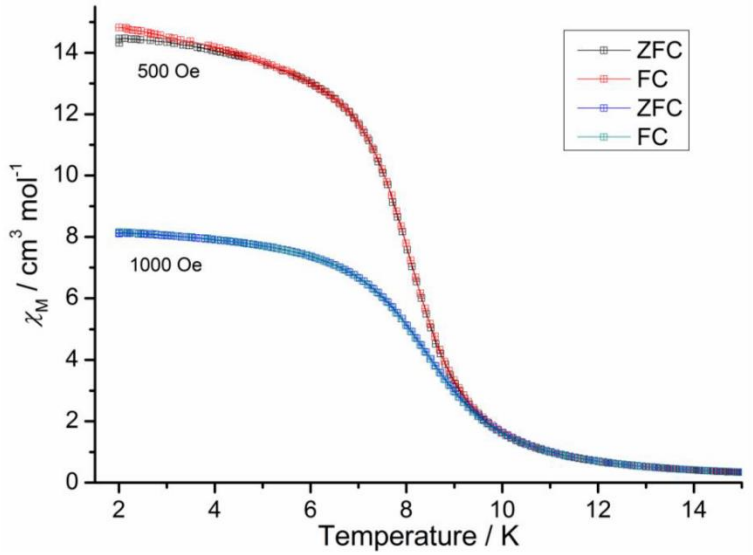

Figure S36. Susceptibility as function of temperature at different DC fields measured in FC and ZFC conditions.

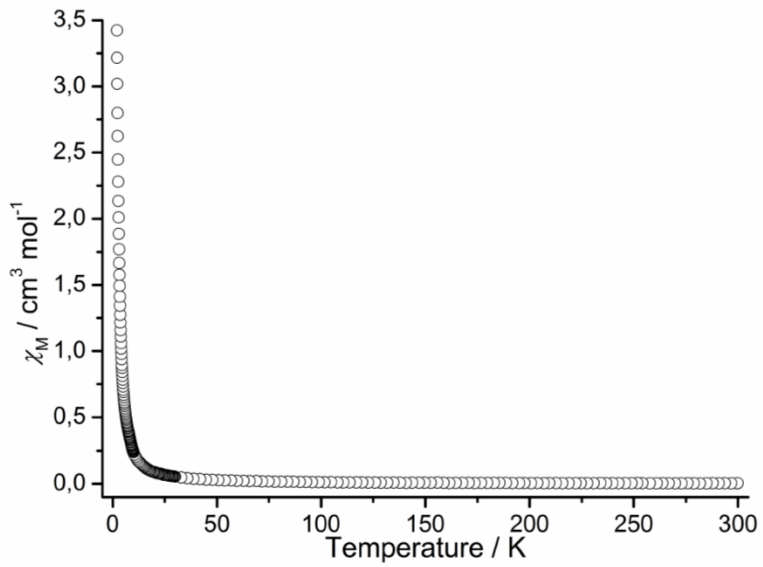

Figure S37. Temperature depence of the susceptibility of **3-Ni/II** at 1000 Oe.

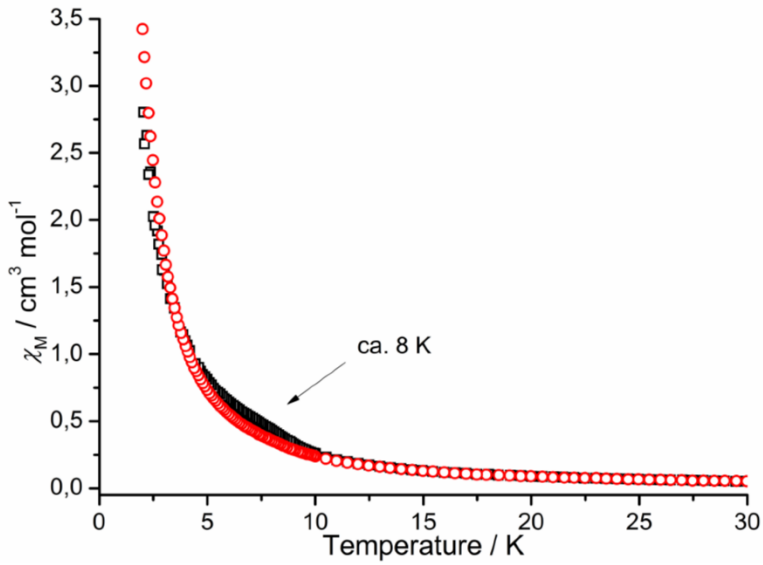

Figure S38. Comparison of the susceptibility curves of two different batches of **3-Ni/II** at 1000 Oe.

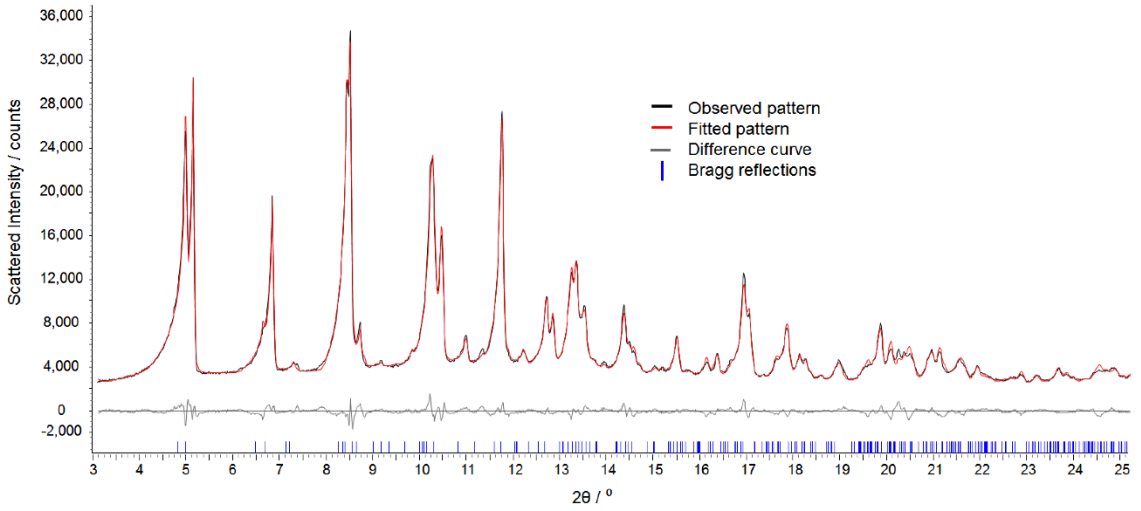

Figure S39. Rietveld plot of the scattered X-ray intensity of **1-Ni** presented as a function of 2θ angle, collected at room temperature with Mo$K\alpha_1$ radiation.

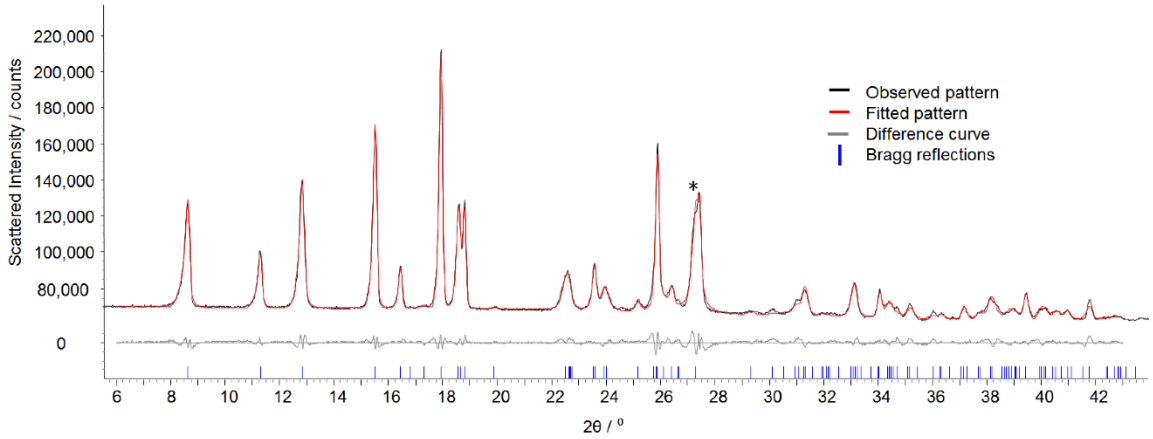

Figure S40. Rietveld plot of the scattered X-ray intensity of **3-Fe/II** presented as a function of 2θ angle, collected at room temperature with Cu$K\alpha_1$ radiation source. The star presents the position of an additional non-Bragg reflection due to stacking faults in the structure.

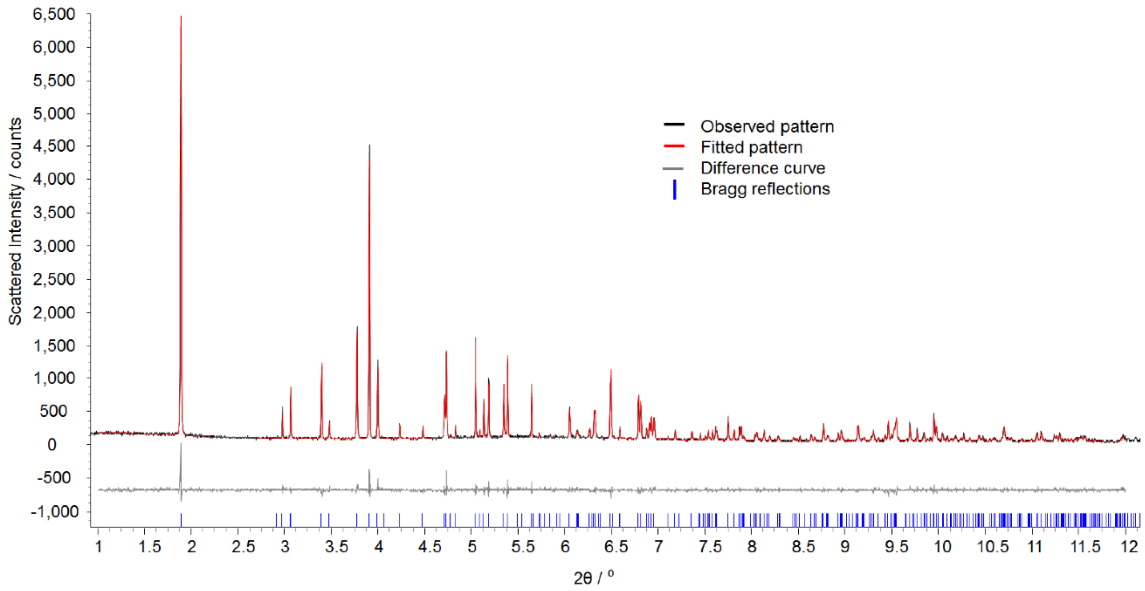

Figure S41. Rietveld plot of the scattered X-ray intensity of **3-Ni/I** presented as a function of 2θ angle, collected at room temperature at the ESRF with X-ray wavelength of 0.4 Å.

8.7. Supporting Information: Synthesis, Structures, and Magnetic Properties of New Thiocyanato Coordination Polymers with 4-(3-Phenylpropyl)pyridine as Ligand

Supporting Information

Synthesis, Structures and Magnetic Properties of New Thiocyanato Coordination Polymers with 4-(3-Phenylpropyl)pyridine

Julia Werner, Inke Jess and Christian Näther

Content

1

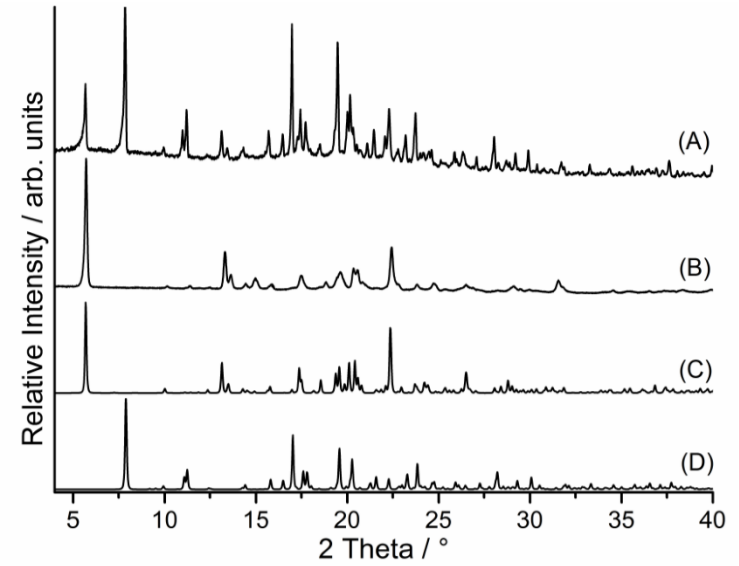

Figure S1. Experimental XRPD pattern for **Mn-2/3** (A), **Ni-2** (B) and calculated XRPD pattern for compound **Mn-2** (C) and **Mn-3** (D).

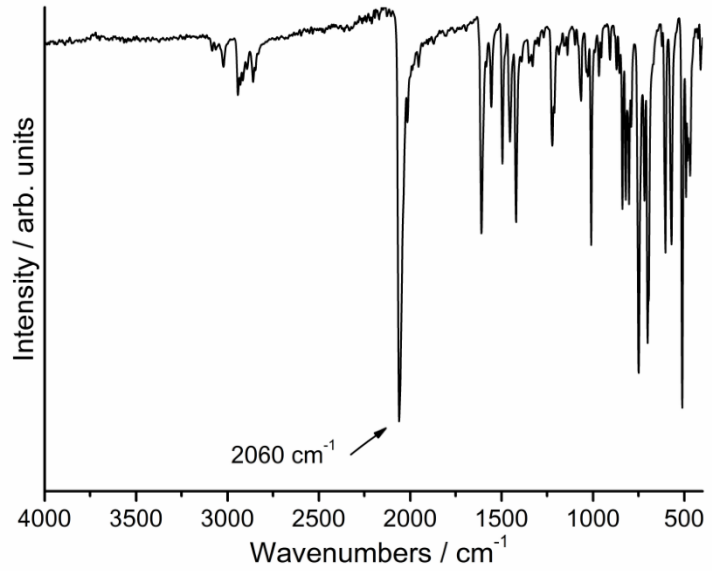

Figure S2. IR spectra of **Mn-1**. The CN stretching vibration is given.

2

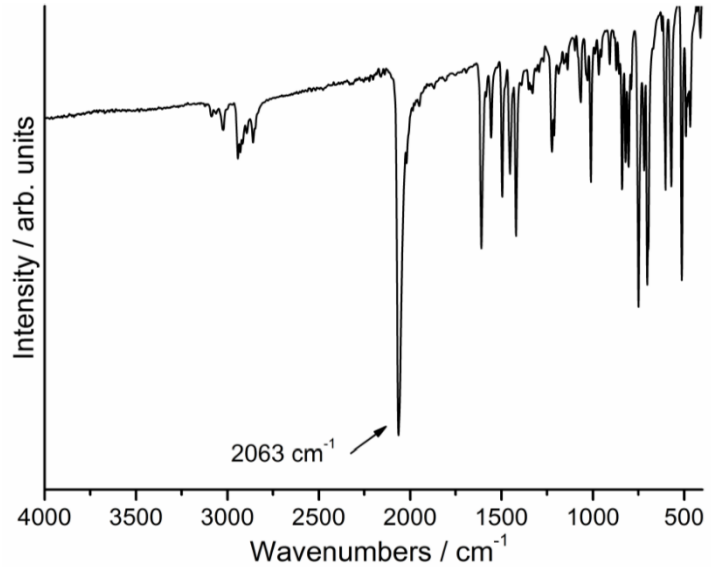

Figure S3. IR spectra of **Fe-1**. The CN stretching vibration is given.

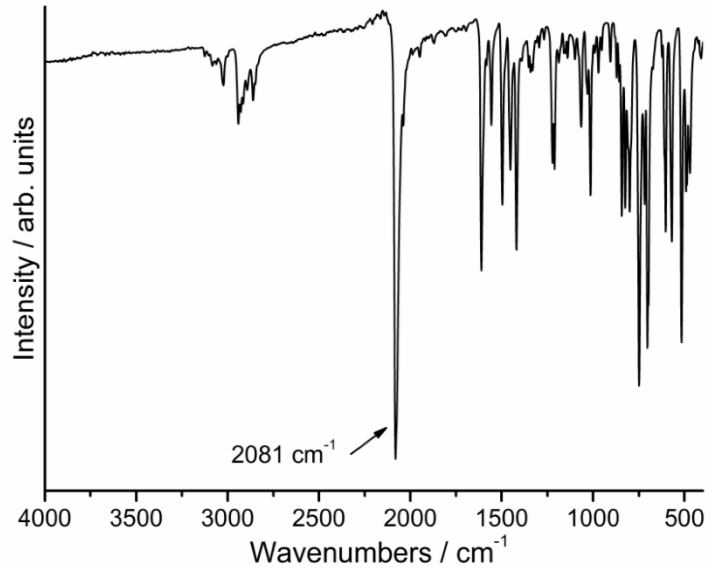

Figure S4. IR spectra of **Ni-1**. The CN stretching vibration is given.

3

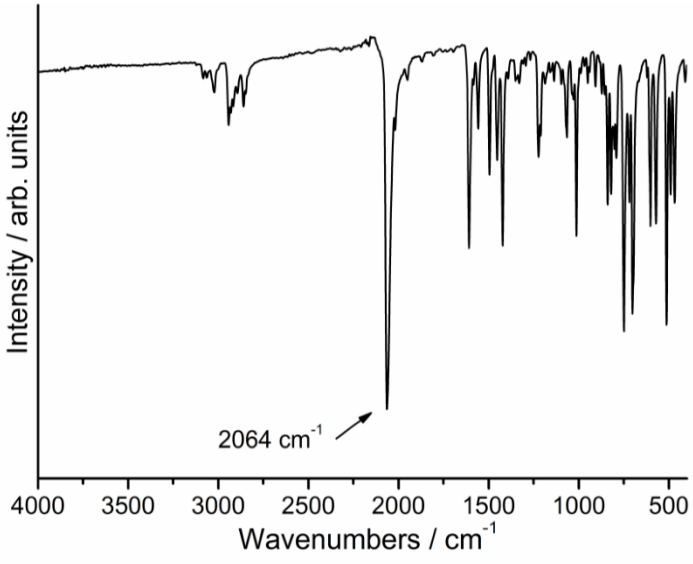

Figure S5. IR spectra of **Cd-1**. The CN stretching vibration is given.

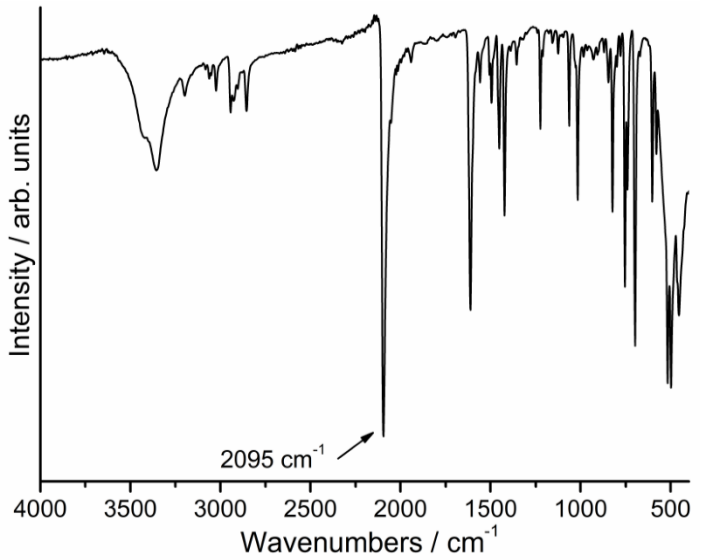

Figure S6. IR spectra of **Mn-2**. The CN stretching vibration is given. The IR spectra was measured using selected single crystals.

4

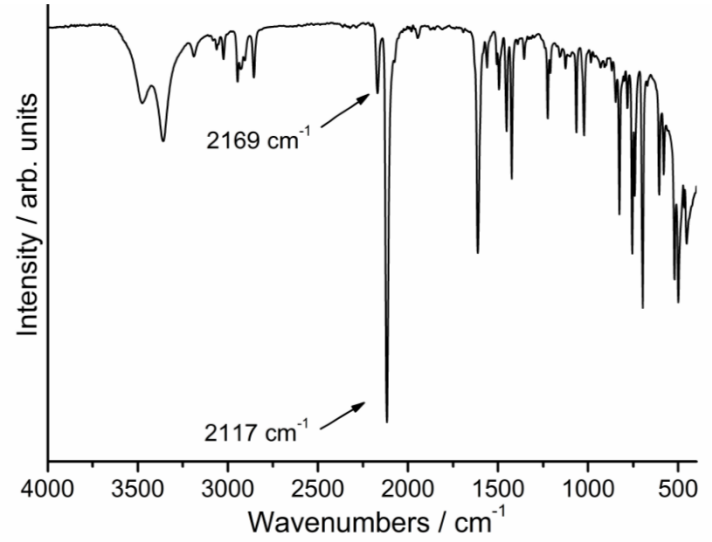

Figure S7. IR spectra of **Ni-2**. The CN stretching vibration is given.

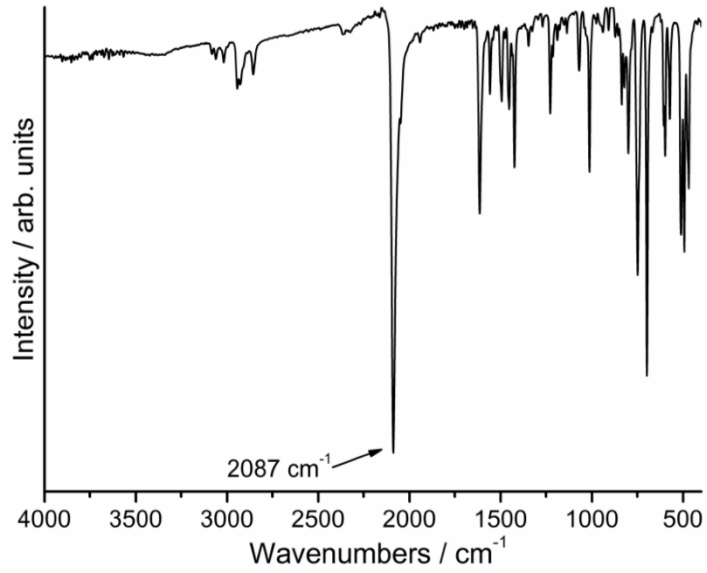

Figure S8. IR spectra of **Mn-3**. The CN stretching vibration is given.

5

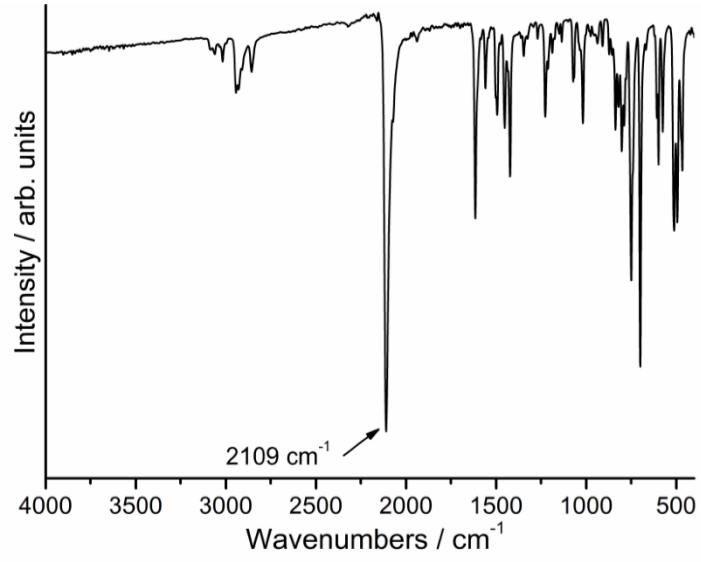

Figure S9. IR spectra of **Ni-3**. The CN stretching vibration is given.

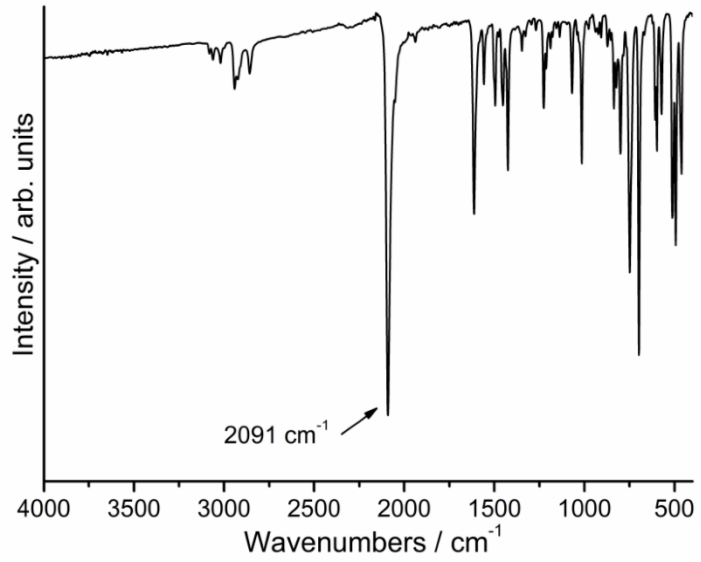

Figure S10. IR spectra of **Cd-3**. The CN stretching vibration is given.

6

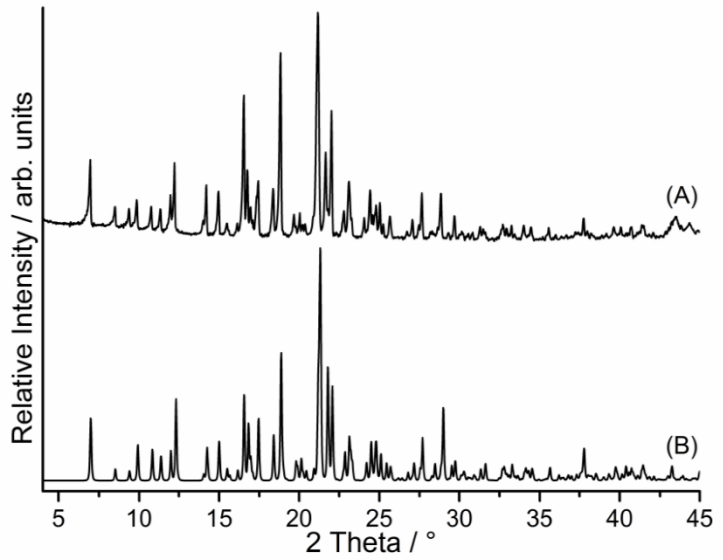

Figure S11. Experimental (A) and calculated (B) XRPD pattern for compound **Mn-1**.

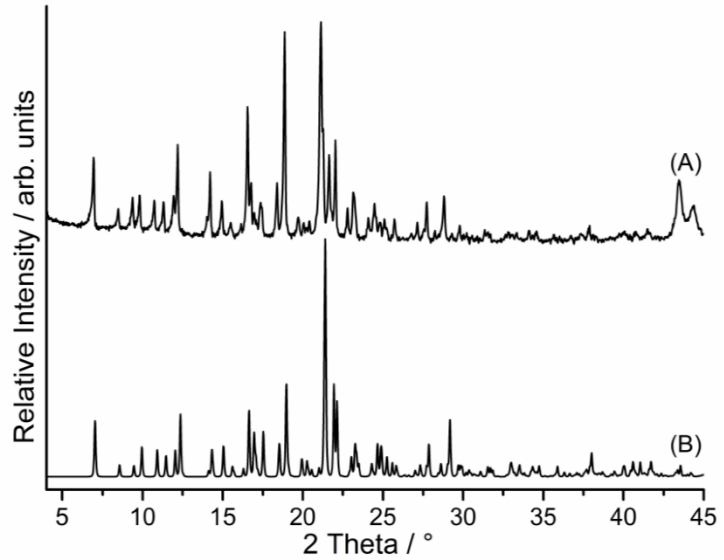

Figure S12. Experimental (A) and calculated (B) XRPD pattern for compound **Fe-1**.

7

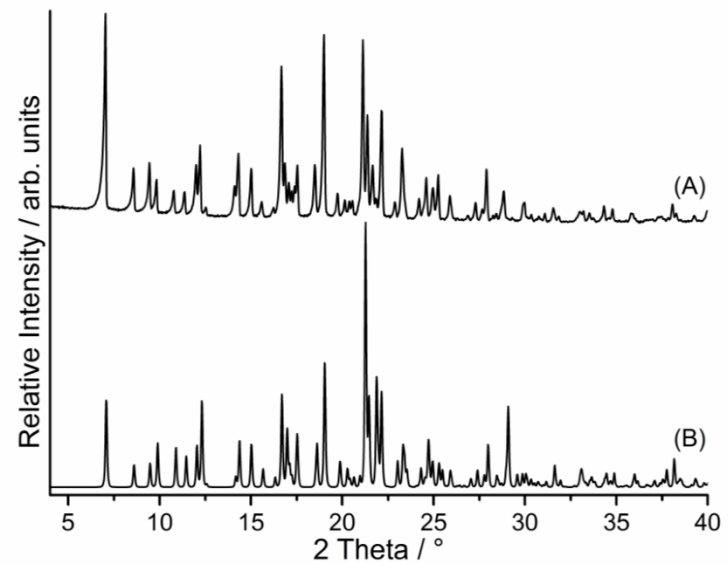

Figure S13. Experimental (A) and calculated (B) XRPD pattern for compound **Ni-1**.

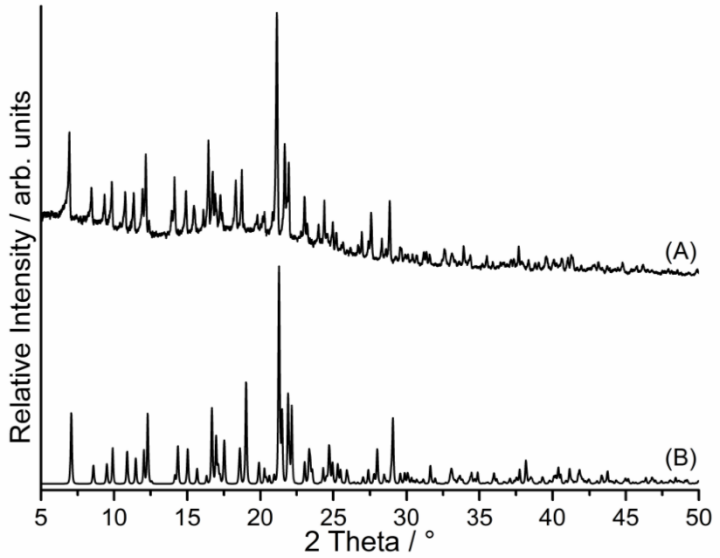

Figure S14. Experimental (A) for compound **Cd-1** and calculated (B) XRPD pattern for compound **Ni-1**.

8

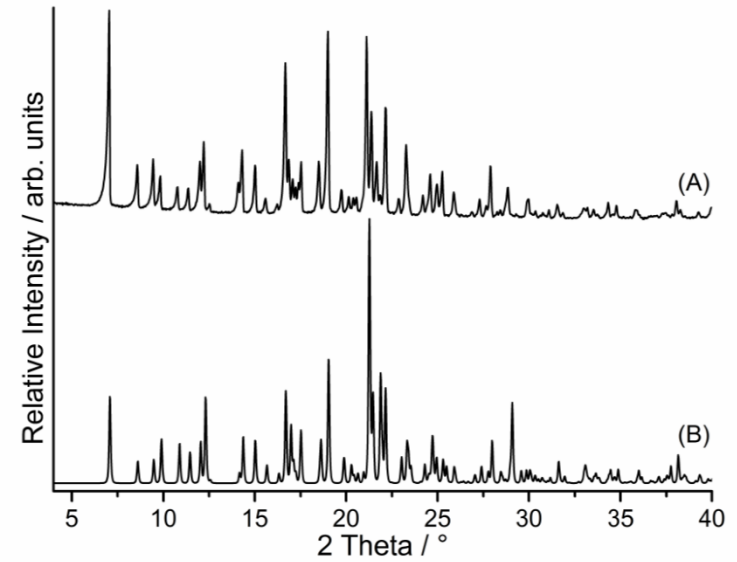

Figure S15. Experimental (A) for compound **Ni-2** and calculated (B) XRPD pattern for compound **Mn-2**. This powder pattern was measured from a few handpicked crystals.

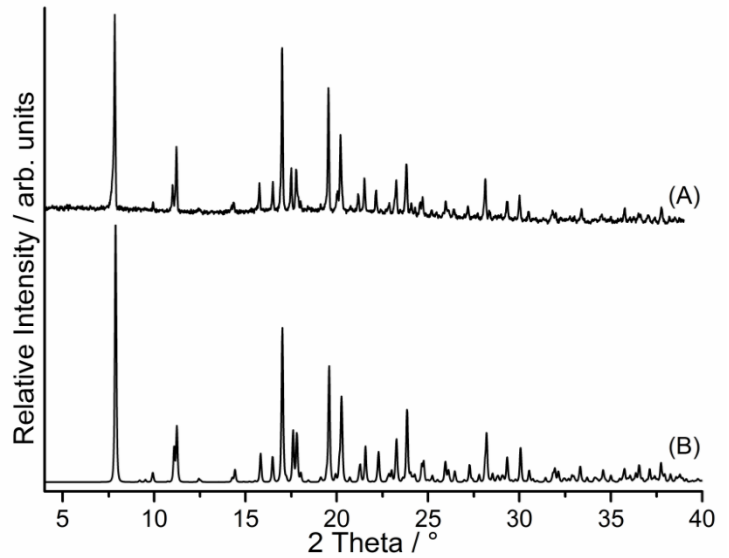

Figure S16. Experimental (A) and calculated (B) XRPD pattern for compound **Mn-3.**

9

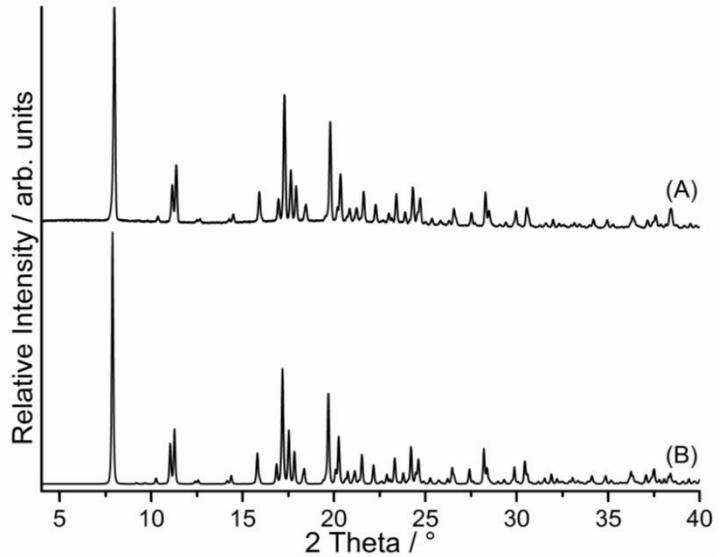

Figure S17. Experimental (A) and calculated (B) XRPD pattern for compound **Ni-3**.

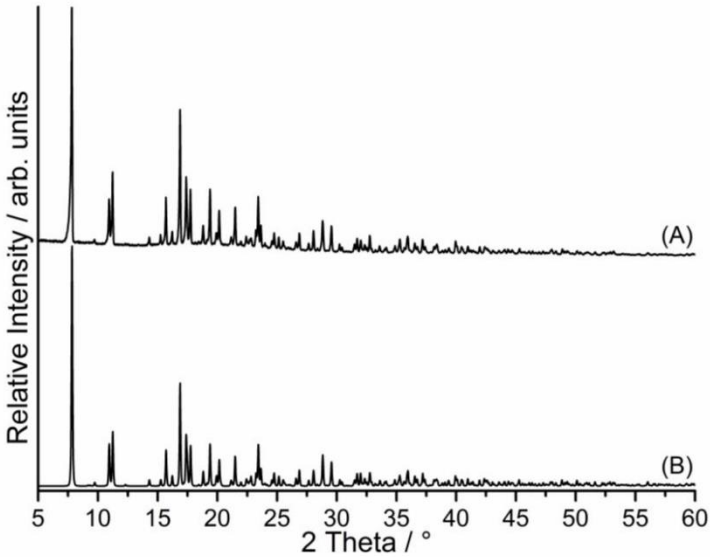

Figure S18. Experimental (A) and calculated (B) XRPD pattern for compound **Cd-3**.

10

Table S1. Selected bond lengths (Å) and angles (°) for **Mn-1**. Symmetry code: A: -x+1,-y+1,-z+1.

$Mn(NCS)_2$(4-(3-Phenylpropyl)pyridine)$_4$ (**Mn-1**)			
Mn(1)-N(1)	2.174(2)	Mn(1)-N(31)	2.306(2)
Mn(1)-N(11)	2.344(2)		
N(1)-Mn(1)-N(1A)	180.0	N(1)-Mn(1)-N(11)	87.97(9)
N(1)-Mn(1)-N(31A)	88.64(10)	N(31)-Mn(1)-N(11)	91.66(9)
N(1)-Mn(1)-N(31)	91.36(10	N(31)-Mn(1)-N(11A)	88.34(9)
N(1)-Mn(1)-N(11A)	92.03(9)		

Table S2. Selected bond lengths (Å) and angles (°) for **Fe-1**. Symmetry code: A: -x+1,-y+1,-z+1.

$Fe(NCS)_2$(4-(3-Phenylpropyl)pyridine)$_4$ (**Fe-1**)			
Fe(1)-N(1)	2.1313(15)	Fe(1)-N(31)	2.2345(14)
Fe(1)-N(11)	2.2804(15)		
N(1)-Fe(1)-N(1A)	180.0	N(1)-Fe(1)-N(11A)	91.62(6)
N(1)-Fe(1)-N(31A)	88.88(6)	N(31)-Fe(1)-N(11)	91.67(5)
N(1)-Fe(1)-N(31)	91.12(6)	N(31)-Fe(1)-N(11A)	88.33(5)
N(1)-Fe(1)-N(11)	88.38(6)		

Table S3. Selected bond lengths (Å) and angles (°) for **Ni-1**. Symmetry code: A: -x+1,-y+1,-z+1.

$Ni(NCS)_2$(4-(3-Phenylpropyl)pyridine)$_4$ (**Ni-1**)			
Ni(1)-N(1)	2.067(2)	Ni(1)-N(31)	2.154(2)
Ni(1)-N(11)	2.206(2)		
N(1)-Ni(1)-N(1A)	180.0	N(1)-Ni(1)-N(11A)	91.16(9)
N(1)-Ni(1)-N(31A)	88.97(8)	N(31)-Ni(1)-N(11)	91.90(8)
N(1)-Ni(1)-N(31)	91.03(8)	N(31)-Ni(1)-N(11A)	88.10(8)
N(1)-Ni(1)-N(11)	88.84(9)		

11

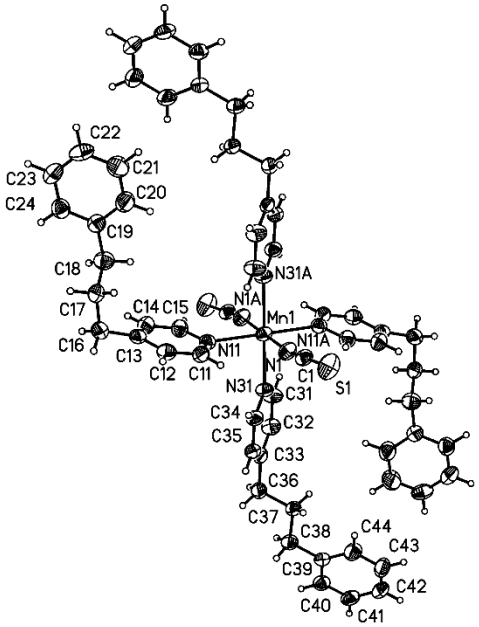

Figure S19. Crystal structure of compound **Mn-1** with labeling and displacement ellipsoids drawn at the 50 % probability level. Symmetry transformation used to generate equivalent atoms: A: -x+1,-y+1,-z+1.

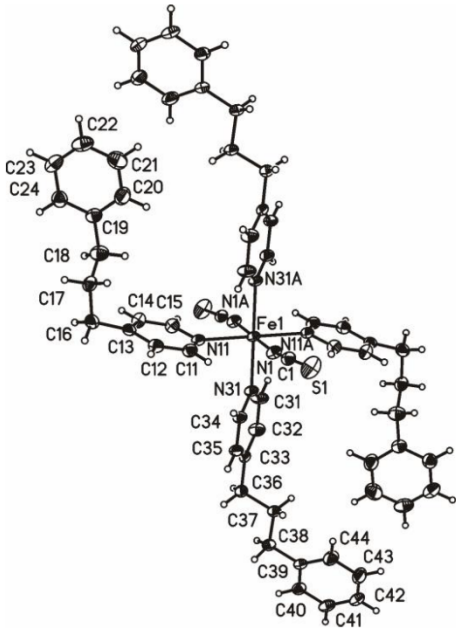

Figure S20. Crystal structure of compound **Fe-1** with labeling and displacement ellipsoids drawn at the 50 % probability level. Symmetry transformation used to generate equivalent atoms: A: -x+1,-y+1,-z+1.

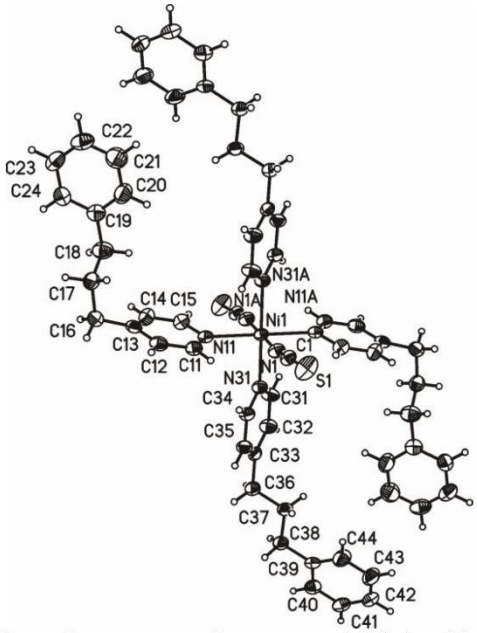

Figure S21. Crystal structure of compound **Ni-1** with labeling and displacement ellipsoids drawn at the 50 % probability level. Symmetry transformation used to generate equivalent atoms: A: -x+1,-y+1,-z+1.

Table S4. Selected bond lengths (Å) and angles (°) for **Mn-2**. Symmetry code: A: -x,-y+1,-z+1; B: -x+1,-y,-z+1.

$Mn(NCS)_2(4\text{-}(3\text{-Phenylpropyl})pyridine)_2(H_2O)_2$ (**Mn-2**)			
Mn(1)-N(1)	2.187(2)	Mn(2)-N(2)	2.191(2)
Mn(1)-O(1)	2.2176(17)	Mn(2)-O(2)	2.2152(16)
Mn(1)-N(11)	2.2628(19)	Mn(2)-N(31)	2.2710(18)
N(1A)-Mn(1)-N(1)	180.0	N(2B)-Mn(2)-N(2)	180.0
N(1)-Mn(1)-O(1A)	92.84(8)	N(2)-Mn(2)-O(2B)	92.95(8)
N(1)-Mn(1)-O(1)	87.16(8)	N(2)-Mn(2)-O(2)	87.05(7)
N(1)-Mn(1)-N(11A)	89.49(7)	N(2)-Mn(2)-N(31)	89.47(7)
N(1)-Mn(1)-N(11)	90.51(7)	N(2)-Mn(2)-N(31B)	90.53(7)
O(1)-Mn(1)-N(11)	88.60(7)	O(2)-Mn(2)-N(31)	89.16(6)
O(1)-Mn(1)-N(11A)	91.40(7)	O(2)-Mn(2)-N(31B)	90.84(7)

13

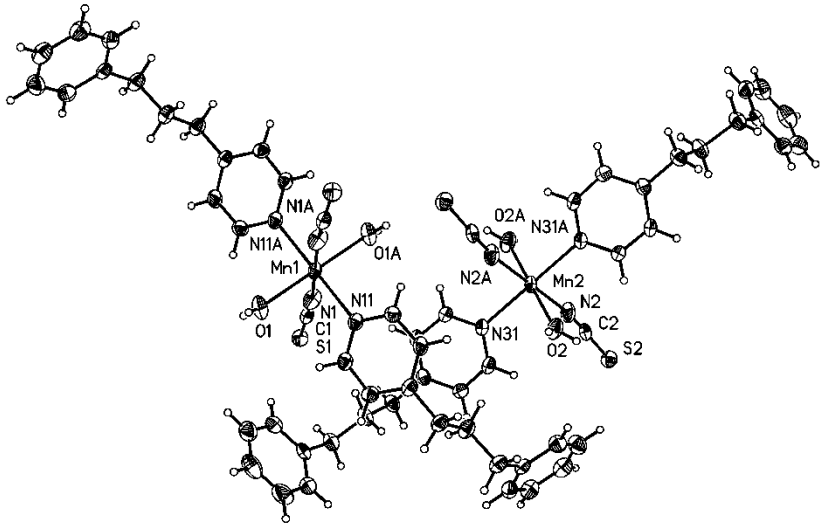

Figure S22. Crystal structure of compound **Mn-2** with labeling and displacement ellipsoids drawn at the 50 % probability level. Symmetry transformation used to generate equivalent atoms: Λ: -x,-y+1,-z+1; B: -x+1,-y,-z+1.

Table S5. Selected bond lengths (Å) and angles (°) for **Mn-3**. Symmetry code: A: -x,-y+1,-z; B: -x+1,-y+1,-z.

[Mn(NCS)$_2$(4-(3-Phenylpropyl)pyridine)]$_n$ (**Mn-3**)			
Mn(1)-N(1)	2.1748(13)	Mn(2)-N(2)	2.1446(14)
Mn(1)-N(11)	2.2658(12)	Mn(2)-N(31)	2.2887(14)
Mn(1)-S(2)	2.6809(4)	Mn(2)-S(1)	2.7311(4)
N(1A)-Mn(1)-N(1)	180.00(6)	N(2)-Mn(2)-N(2B)	180.00(7)
S(2A)-Mn(1)-S(2)	180.000(18)	S(1B)-Mn(2)-S(1)	180.0
N(1)-Mn(1)-N(11)	90.00(5)	N(2)-Mn(2)-N(31)	90.14(5)
N(1)-Mn(1)-S(2)	93.17(4)	N(2)-Mn(2)-S(1)	93.85(4)
N(1)-Mn(1)-S(2A)	86.83(4)	N(2)-Mn(2)-S(1B)	86.15(4)
N(11)-Mn(1)-S(2)	93.02(3)	N(31)-Mn(2)-S(1)	92.86(4)
N(11)-Mn(1)-S(2A)	86.98(3)	N(31)-Mn(2)-S(1B)	87.14(4)

Table S6. Selected bond lengths (Å) and angles (°) for **Ni-3**. Symmetry code: A: -x,-y+1,-z; B: -x+1,-y+1,-z.

[Ni(NCS)$_2$(4-(3-Phenylpropyl)pyridine)]$_n$ (**Ni-3**)			
Ni(1)-N(1)	2.047(3)	Ni(2)-N(2)	2.028(3)
Ni(1)-N(11)	2.125(3)	Ni(2)-N(31)	2.126(3)
Ni(1)-S(2)	2.5266(10)	Ni(2)-S(1)	2.5679(10)
N(1A)-Ni(1)-N(1)	180.00(17)	N(2)-Ni(2)-N(2B)	180.00(16)
S(2)-Ni(1)-S(2A)	180.0	S(1)-Ni(2)-S(1B)	180.0
N(1)-Ni(1)-N(11)	89.88(12)	N(2)-Ni(2)-N(31)	89.95(12)
N(1)-Ni(1)-S(2)	93.69(9)	N(2)-Ni(2)-S(1)	93.26(9)
N(1)-Ni(1)-S(2A)	86.31(9)	N(2)-Ni(2)-S(1B)	86.74(9)
N(11)-Ni(1)-S(2)	91.84(9)	N(31)-Ni(2)-S(1)	91.26(9)

Table S7. Selected bond lengths (Å) and angles (°) for **Cd-3**. Symmetry code: A: -x,-y+1,-z, B: -x+1,-y+1,-z.

[Cd(NCS)$_2$(4-(3-Phenylpropyl)pyridine)]$_n$ (**Cd-3**)			
Cd(1)-N(1)	2.316(2)	Cd(2)-N(2)	2.284(2)
Cd(1)-N(11)	2.339(2)	Cd(2)-N(31)	2.351(2)
Cd(1)-S(2)	2.7265(7)	Cd(2)-S(1)	2.7714(8)
N(1A)-Cd(1)-N(1)	180.00(15)	N(2)-Cd(2)-N(2B)	180.00(15)
S(2)-Cd(1)-S(2A)	180.0	S(1B)-Cd(2)-S(1)	180.0
N(1)-Cd(1)-N(11)	90.12(8)	N(2)-Cd(2)-N(31)	89.74(9)
N(1)-Cd(1)-S(2)	92.54(6)	N(2)-Cd(2)-S(1)	94.49(6)
N(1)-Cd(1)-S(2A)	87.46(6)	N(2)-Cd(2)-S(1B)	85.51(6)
N(11)-Cd(1)-S(2)	93.39(6)	N(31)-Cd(2)-S(1)	92.63(6)

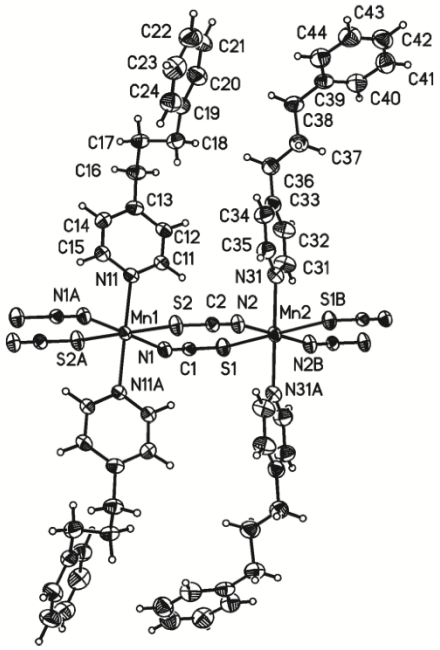

Figure S23. Crystal structure of compound **Mn-3** with labeling and displacement ellipsoids drawn at the 50 % probability level. Symmetry transformation used to generate equivalent atoms: A: -x,-y+1,-z, B: -x+1,-y+1,-z.

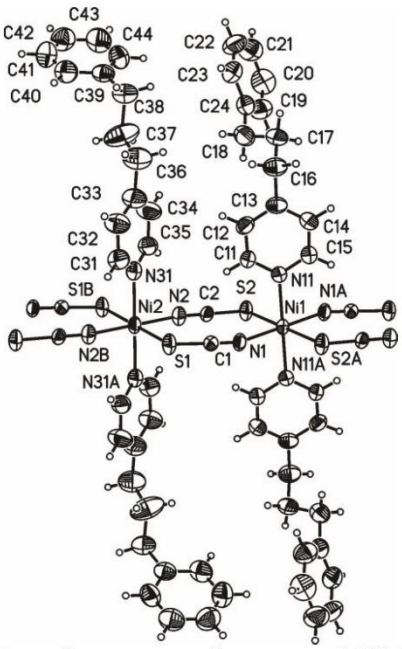

Figure S24. Crystal structure of compound **Ni-3** with labeling and displacement ellipsoids drawn at the 50 % probability level. Symmetry transformation used to generate equivalent atoms: A: -x,-y+1,-z; B: -x+1,-y+1,-z.

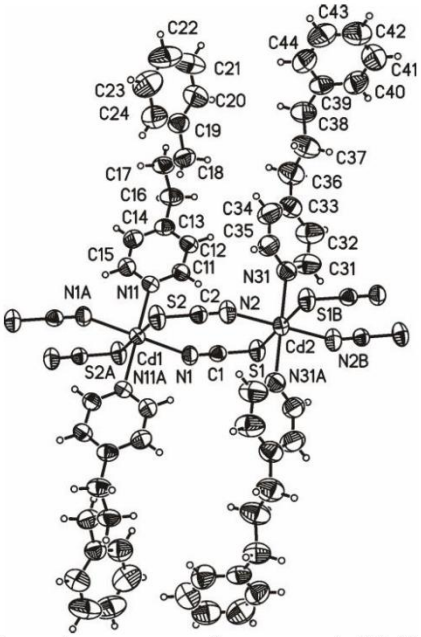

Figure S25. Crystal structure of compound **Cd-3** with labeling and displacement ellipsoids drawn at the 50 % probability level. Symmetry transformation used to generate equivalent atoms: A: -x,-y+1,-z, B: -x+1,-y+1,-z.

16

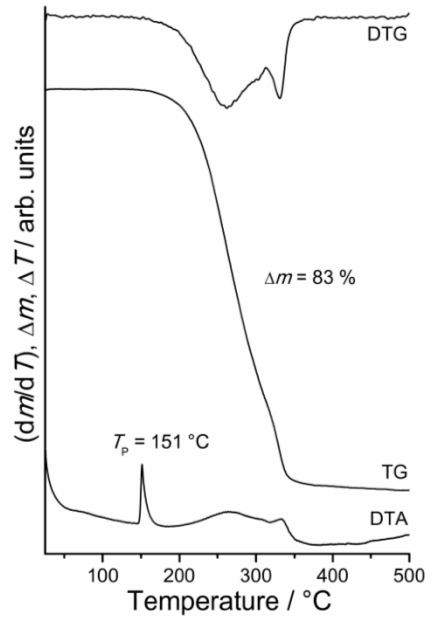

Figure S26. DTG, TG and DTA curves for **Mn-1**. Heating rate = 4 °C/min. Given are the ‚ass change in % and the peak temperature in T_P in °C.

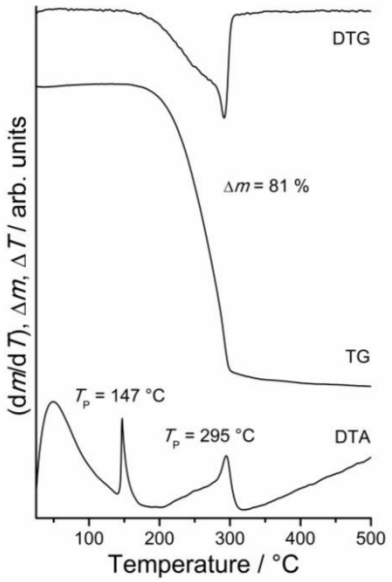

Figure S27. DTG, TG and DTA curves for **Fe-1**. Heating rate = 4 °C/min. Given are the ‚ass change in % and the peak temperature in T_P in °C.

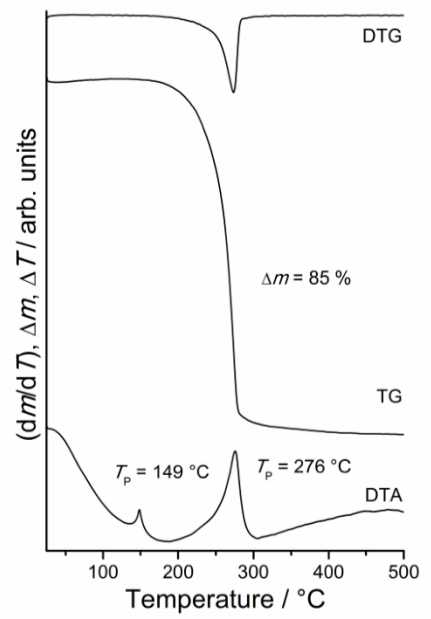

Figure S28. DTG, TG and DTA curves for **Ni-1**. Heating rate = 4 °C/min. Given are the ‚ass change in % and the peak temperature in T_P in °C.

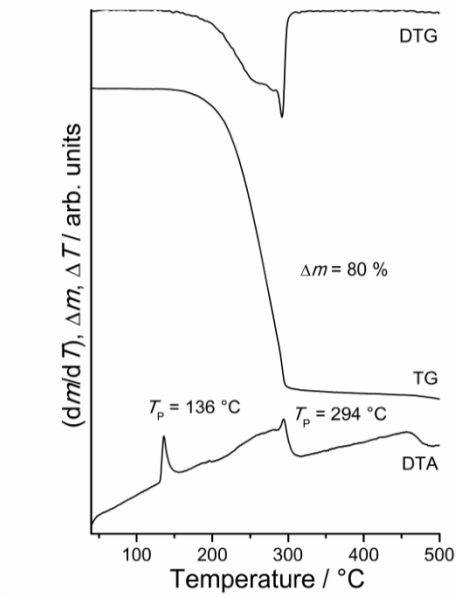

Figure S29. DTG, TG and DTA curves for **Cd-1**. Heating rate = 4 °C/min. Given are the ‚ass change in % and the peak temperature in T_P in °C.

18

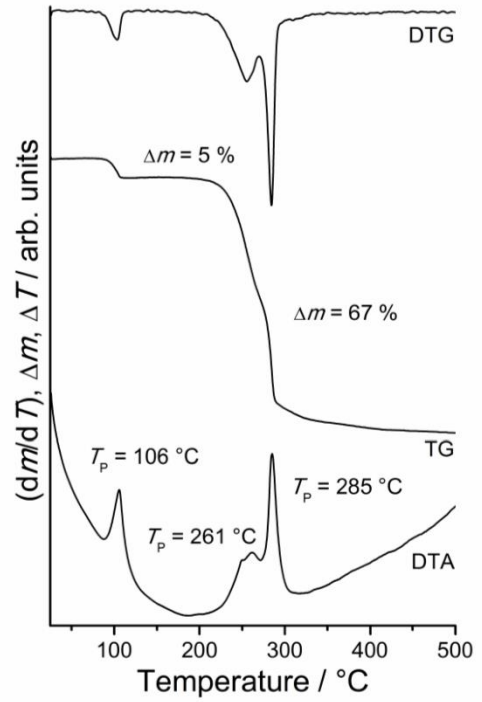

Figure S30. DTG, TG and DTA curves for **Ni-2**. Heating rate = 4 °C/min. Given are the ‚ass change in % and the peak temperature in T_P in °C.

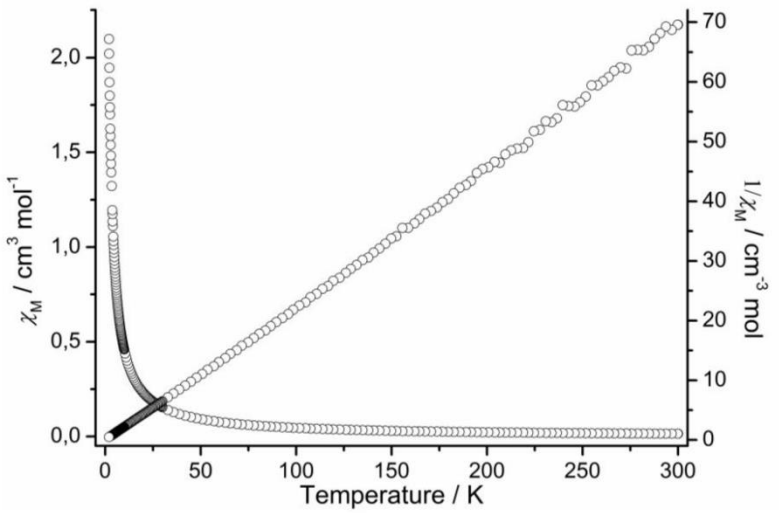

Figure S31. χ and 1/χ as function of temperature for **Mn-1** measured at H_{DC} = 1 kOe.

19

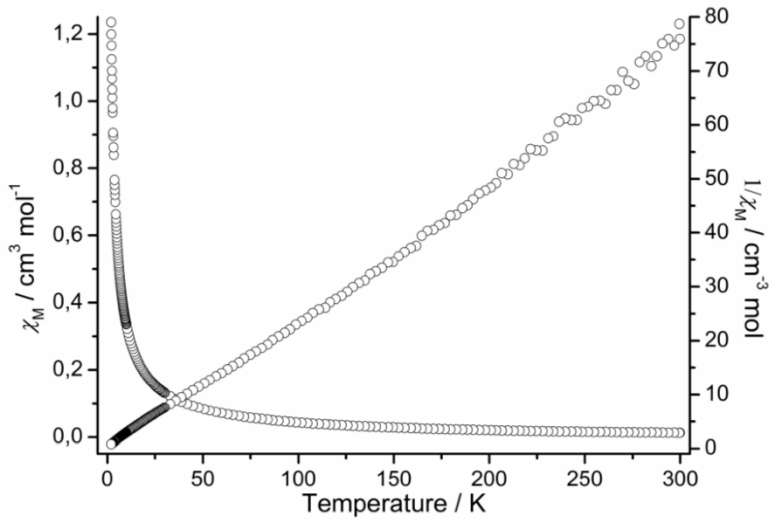

Figure S32. χ and 1/χ as function of temperature for **Fe-1** measured at H_{DC} = 1 kOe.

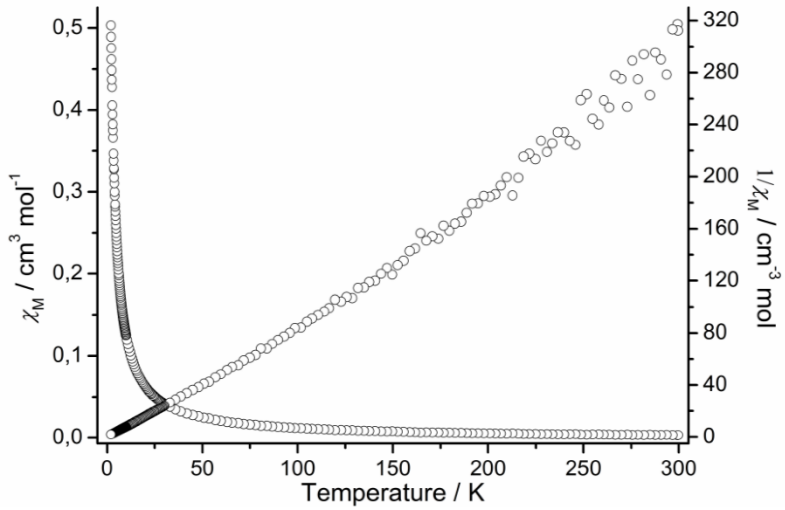

Figure S33. χ and 1/χ as function of temperature for **Ni-1** measured at H_{DC} = 1 kOe.

20

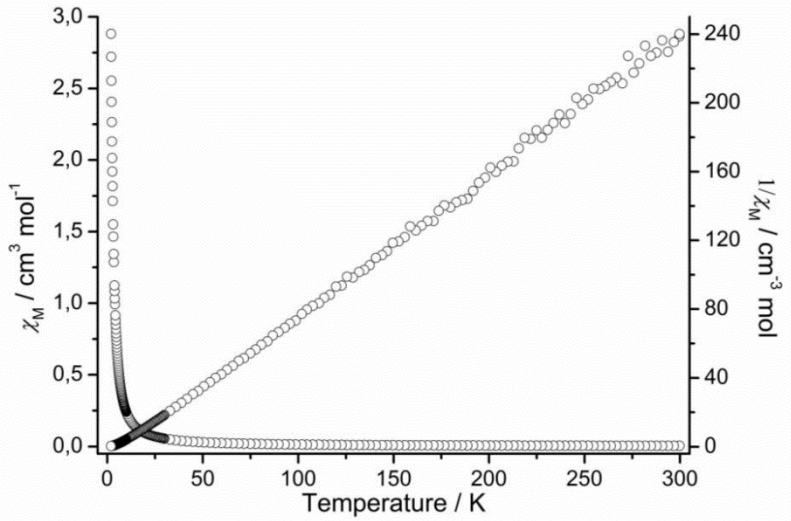

Figure S34. χ and $1/\chi$ as function of temperature for **Ni-3** measured at H_{DC} = 1 kOe.

8.8. Supporting Information: Synthesis, Structures, and Properties of Transition Metal Thiocyanato Coordination Compounds with 4-(4-Chlorobenzyl)pyridine as Ligand

Supporting Information

Synthesis, Structures and Properties of Transition Metal Thiocyanato Coordination Compounds with 4-(4-Chlorobenzyl)pyridine as Ligand

Julia Werner[a], Tristan Neumann[a], and Christian Näther*[a]

[a] Institut für Anorganische Chemie, Christian-Albrechts-Universität zu Kiel, Max-Eyth-Str. 2, 24118 Kiel

4

Table S1. Crystalline phases that are obtained if different ratios of the metal salts are reacted with Clbp in water, ethanol, methanol or acetonitrile.

Molar ratio		Compound			
Metal salt	Clbp	Mn	Fe	Ni	Cd
1	12	**Mn-1**	**Fe-1/I**	**Ni-1**	**Cd-1**
1	10	**Mn-1**	**Fe-1/I**	**Ni-1**	**Cd-1**
1	8	**Mn-1**	**Fe-1/I**	**Ni-1**	**Cd-1**
1	4	**Mn-1**	**Fe-1/II**	**Ni-1**	**Cd-1**
1	2	**Mn-1**	**Fe-1/I**	**Ni-1/2**	**Cd-1**
1	1	**Mn-1**	-	**Ni-1/2**	**Cd-2**
2	1	**Mn-1/2**	-	**Ni-1/2**	**Cd-2**
4	1	**Mn-1/2**	-	**Ni-2**	**Cd-2**

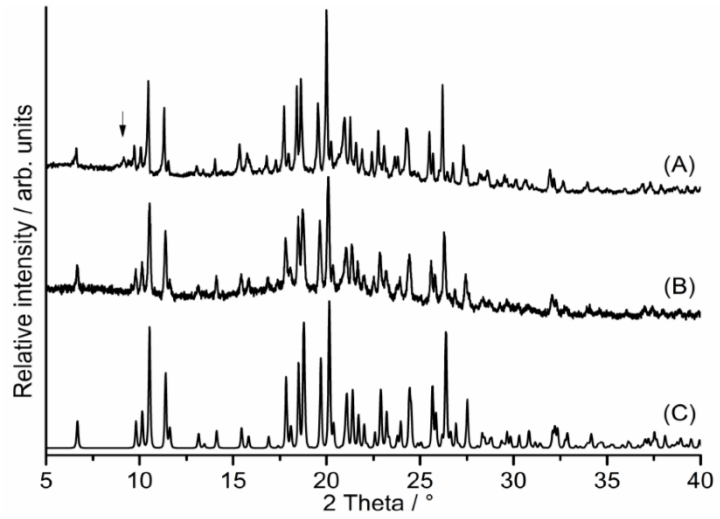

Figure S1. XRPD pattern of a mixture of **Fe-1/I** and **Fe-1/II** (A) and after stirring this mixture in water for 1 h (B) as well as calculated XRPD pattern for compound **Fe-1/I**.

5

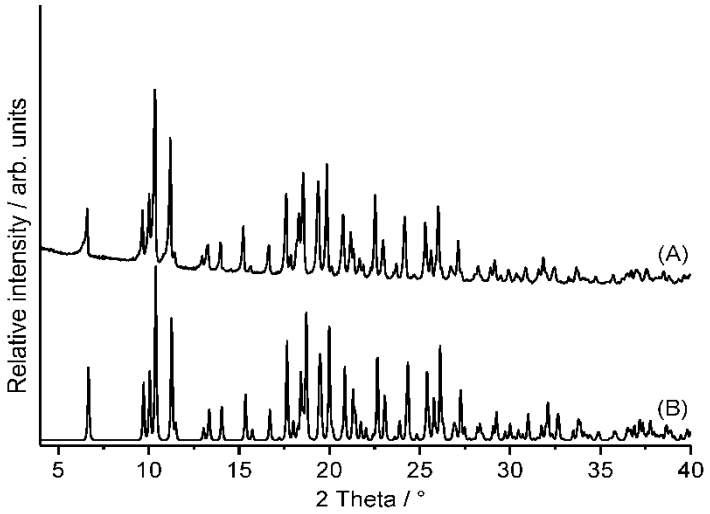

Figure S2. Experimental (A) and calculated (B) XRPD pattern for compound **Cd-1**.

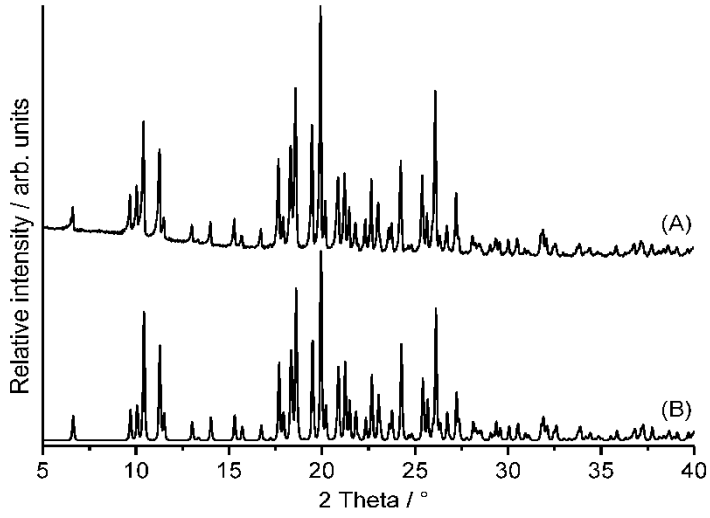

Figure S3. Experimental (A) and calculated (B) XRPD pattern for compound **Mn-1**.

6

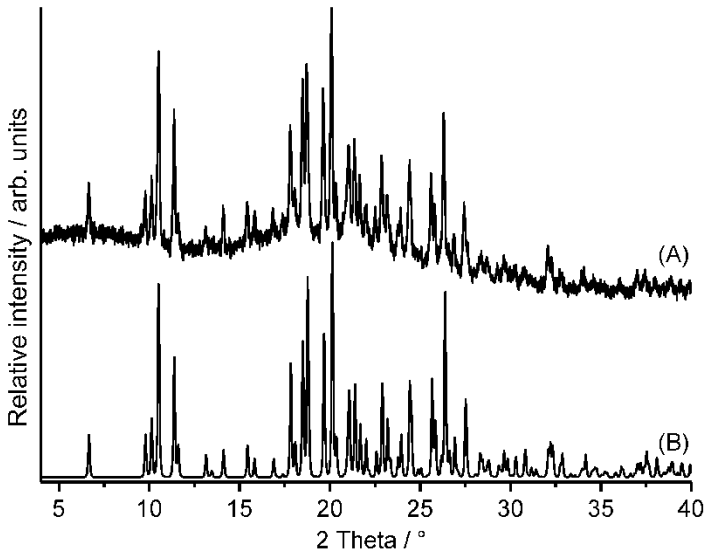

Figure S4. Experimental (A) and calculated (B) XRPD pattern for compound **Fe-1**.

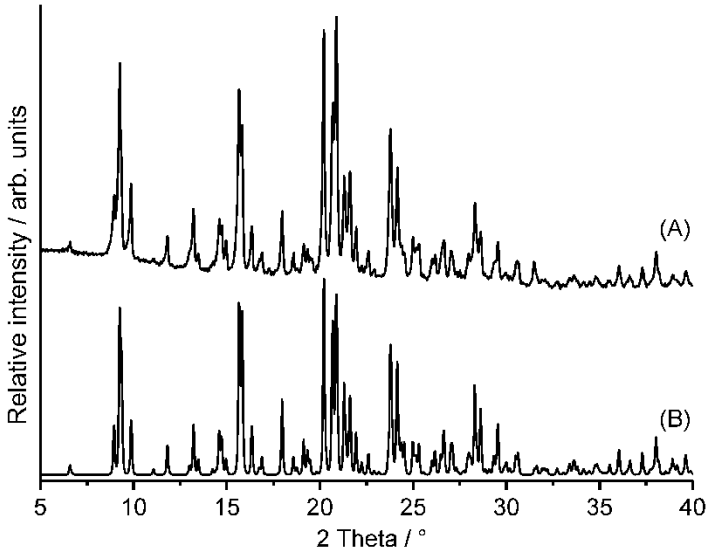

Figure S5. Experimental (A) and calculated (B) XRPD pattern for compound **Ni-1**.

7

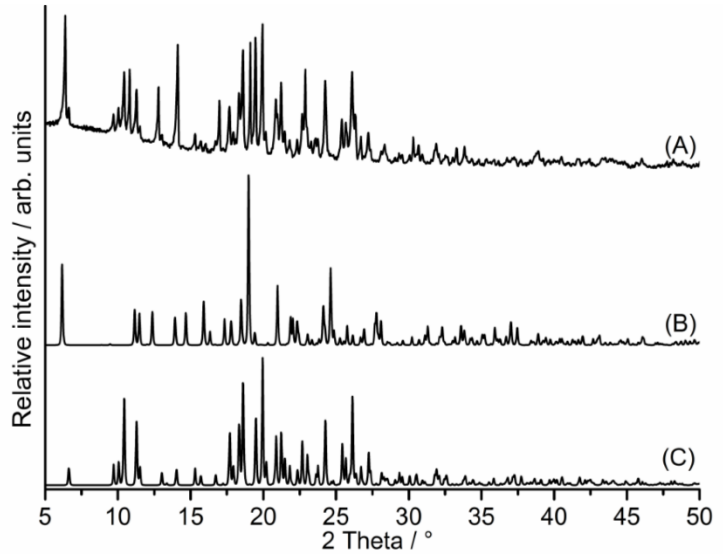

Figure S6. Experimental (A) and calculated XRPD patterns for compound **Mn-2** (B) and **Mn-1** (C).

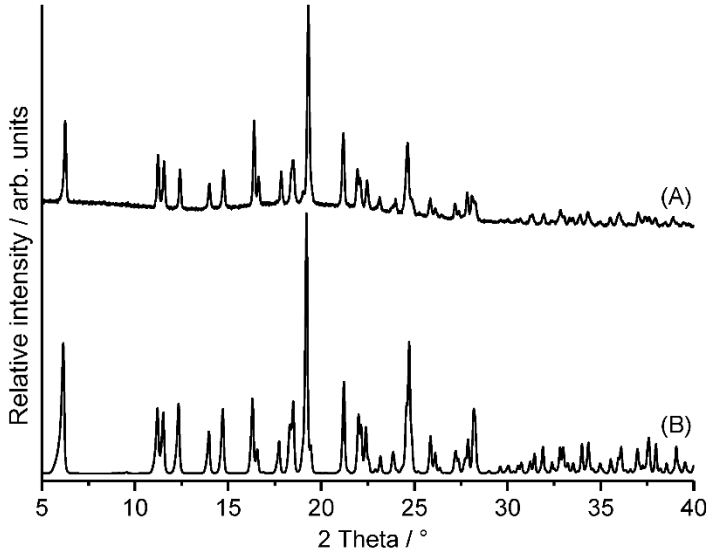

Figure S7. Experimental (A) and calculated (B) XRPD pattern for compound **Ni-2**.

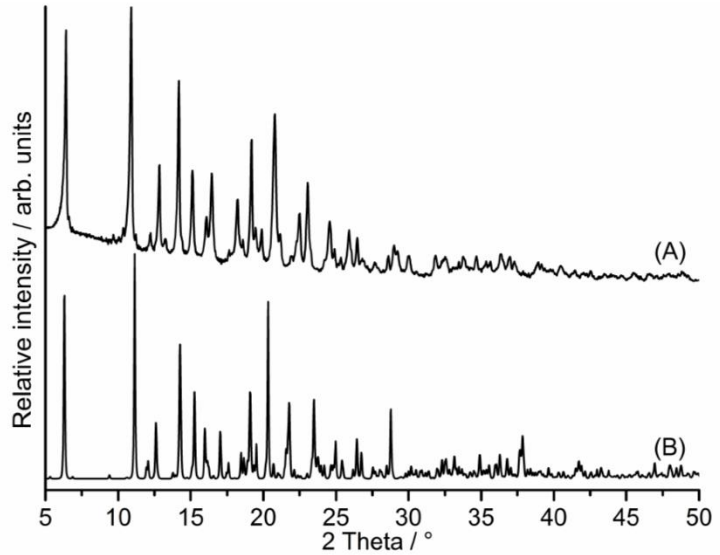

Figure S8. Experimental (A) and calculated (B) XRPD pattern for compound **Cd-2**.

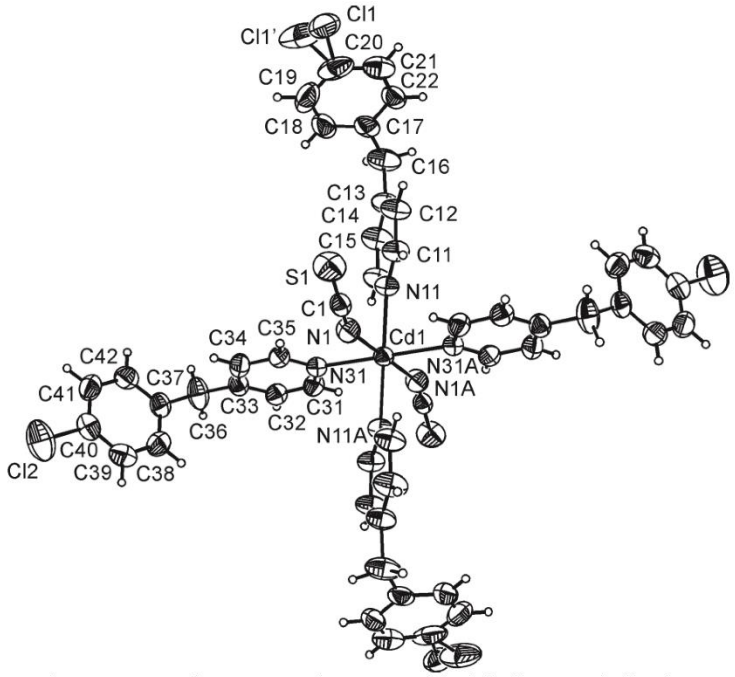

Figure S9. Crystal structure of compound **Cd-1** with labeling and displacement ellipsoids drawn at the 50 % probability level. Symmetry transformation used to generate equivalent atoms: A: -x+1/2, -y+1/2, -z+1.

9

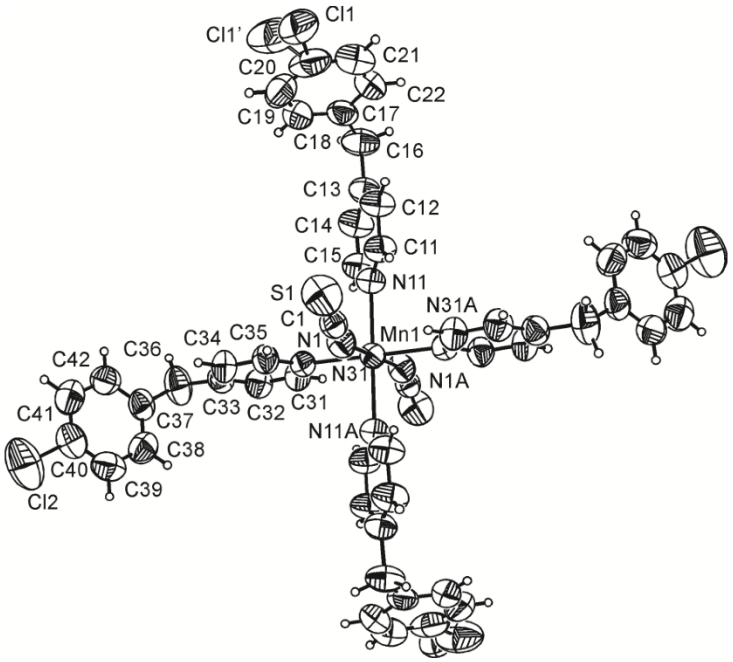

Figure S10. Crystal structure of compound **Mn-1** with labeling and displacement ellipsoids drawn at the 50 % probability level. Symmetry transformation used to generate equivalent atoms: A: -x+3/2, -y+1/2, -z+1.

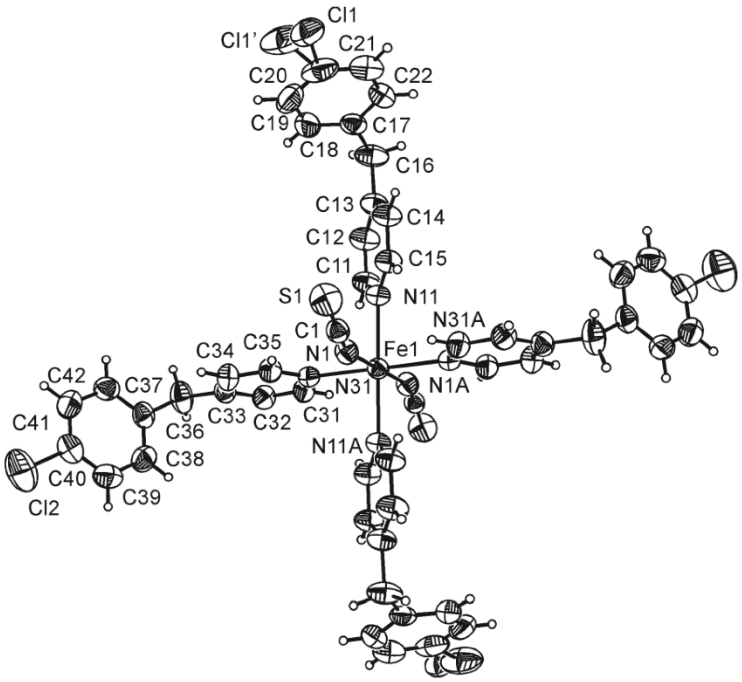

Figure S11. Crystal structure of compound **Fe-1** with labeling and displacement ellipsoids drawn at the 50 % probability level. Symmetry transformation used to generate equivalent atoms: A: -x+3/2, -y+1/2, -z+1.

10

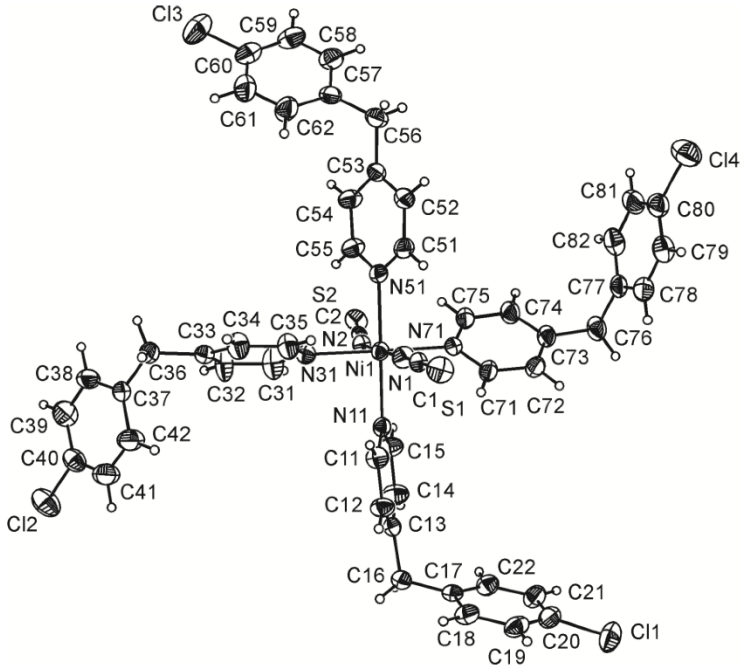

Figure S12. Crystal structure of compound **Ni-1** with labeling and displacement ellipsoids drawn at the 50 % probability level.

Table S2. Selected bond lengths (Å) and angles (°) for **Mn-1**. Symmetry code:

Mn(1)-N(1)	2.178(2)	N(1)-Mn(1)-N(11)	89.31(8)
Mn(1)-N(11)	2.2778(19)	N(1)-Mn(1)-N(31)	91.20(7)
Mn(1)-N(31)	2.3324(19)	N(11)-Mn(1)-N(31)	90.45(7)

Table S3. Selected bond lengths (Å) and angles (°) for **Fe-1**. Symmetry code:

Fe(1)-N(1)	2.1127(18)	N(1)-Fe(1)-N(11)	89.14(7)
Fe(1)-N(11)	2.2067(17)	N(1)-Fe(1)-N(31)	90.98(7)
Fe(1)-N(31)	2.2714(17)	N(11)-Fe(1)-N(31)	90.37(6)

11

Table S4. Selected bond lengths (Å) and angles (°) for **Ni-1**. Symmetry code:

Ni(1)-N(2)	2.040(3)	N(1)-Ni(1)-N(11)	90.65(16)
Ni(1)-N(1)	2.060(3)	N(1)-Ni(1)-N(31)	91.15(16)
Ni(1)-N(11)	2.137(4)	N(2)-Ni(1)-N(11)	89.75(17)
Ni(1)-N(31)	2.138(4)	N(2)-Ni(1)-N(31)	91.24(18)
Ni(1)-N(51)	2.153(4)	N(1)-Ni(1)-N(51)	90.01(16)
Ni(1)-N(71)	2.150(4)	N(1)-Ni(1)-N(71)	88.33(17)
N(2)-Ni(1)-N(71)	89.28(19)	N(2)-Ni(1)-N(51)	89.60(17)

Table S5. Selected bond lengths (Å) and angles (°) for **Cd-1**. Symmetry code:

Cd(1)-N(1)	2.300(2)	N(1)-Cd(1)-N(11)	89.34(9)
Cd(1)-N(11)	2.341(2)	N(1)-Cd(1)-N(31)	91.39(8)
Cd(1)-N(31)	2.381(2)	N(11)-Cd(1)-N(31)	90.47(8)

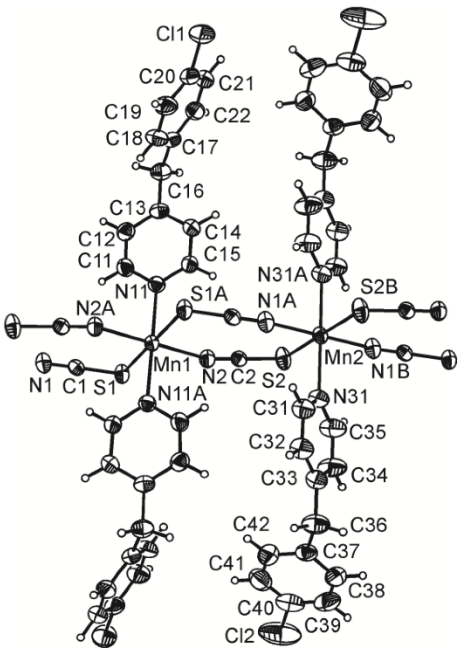

Figure S13. Crystal structure of compound **Mn-2** with labeling and displacement ellipsoids drawn at the 50 % probability level. Symmetry transformation used to generate equivalent atoms: A: -x+1,-y+1,-z+1; B: x-1,y+1,z; C: -x,-y+2,-z+1; D: x+1,y-1,z.

12

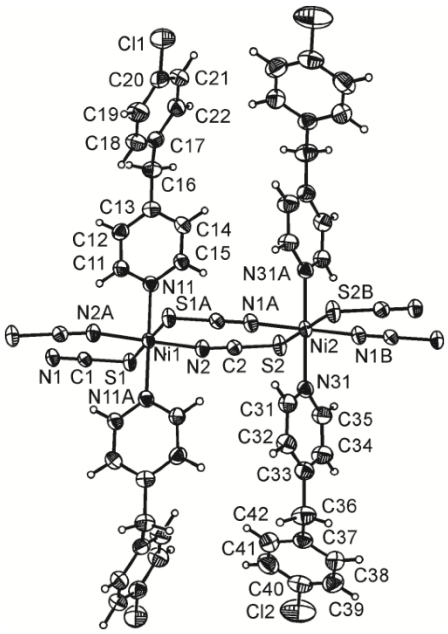

Figure S14. Crystal structure of compound **Ni-2** with labeling and displacement ellipsoids drawn at the 50 % probability level. Symmetry transformation used to generate equivalent atoms: A: -x+1, -y+1, -z+1; B: x-1, y+1, z; C: -x, -y+2, -z+1; D: x+1, y-1, z.

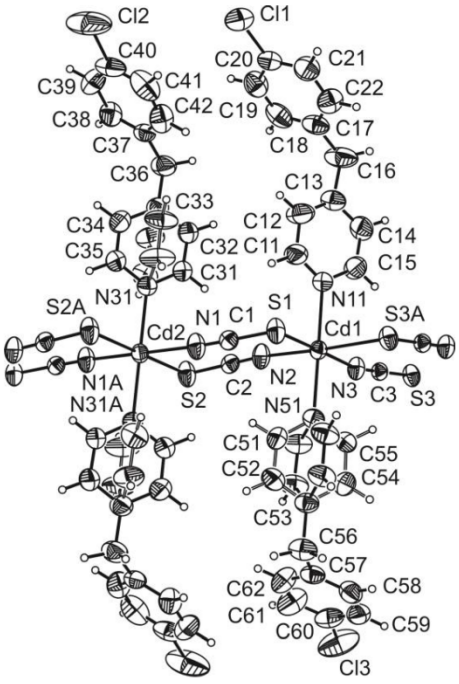

Figure S15. Crystal structure of compound **Cd-2** with labeling and displacement ellipsoids drawn at the 50 % probability level.

Table S6. Selected bond lengths (Å) and angles (°) for **Mn-2**. Symmetry code:

Mn(1)-N(2)	2.1519(15)	Mn(2)-N(1A)	2.1600(16)
Mn(1)-N(11)	2.2685(14)	Mn(2)-S(2)	2.7119(7)
Mn(1)-S(1)	2.6721(7)	Mn(2)-N(31)	2.2528(15)
N(2)-Mn(1)-N(11)	89.74(6)	N(1A)-Mn(2)-N(31)	89.86(6)
N(2)-Mn(1)-N(11A)	90.26(6)	N(1B)-Mn(2)-N(31)	90.14(6)
N(2)-Mn(1)-S(1)	86.31(4)	N(1A)-Mn(2)-S(2)	94.53(4)
N(2)-Mn(1)-S(1A)	93.69(4)	N(1A)-Mn(2)-S(2C)	85.47(4)
N(11)-Mn(1)-S(1A)	88.22(4)	N(31)-Mn(2)-S(2C)	90.08(4)
N(11)-Mn(1)-S(1)	91.78(4)	N(31)-Mn(2)-S(2)	89.92(4)

Table S7. Selected bond lengths (Å) and angles (°) for **Ni-2**. Symmetry code:

Ni(1)-N(2)	2.027(2)	Ni(2)-N(1A)	2.033(2)
Ni(1)-N(11)	2.120(2)	Ni(2)-N(31)	2.105(2)
Ni(1)-S(1)	2.5151(6)	Ni(2)-S(2)	2.5498(7)
N(2)-Ni(1)-N(11)	89.92(8)	N(1B)-Ni(2)-N(31)	89.95(8)
N(2)-Ni(1)-N(11A)	90.08(8)	N(1A)-Ni(2)-N(31)	90.05(8)
N(2)-Ni(1)-S(1)	86.12(6)	N(1B)-Ni(2)-S(2)	86.27(6)
N(2)-Ni(1)-S(1A)	93.88(6)	N(1A)-Ni(2)-S(2)	93.73(6)
N(11)-Ni(1)-S(1)	91.06(6)	N(31)-Ni(2)-S(2)	90.08(6)
N(11)-Ni(1)-S(1A)	88.94(6)	N(31)-Ni(2)-S(2C)	89.92(6)

Table S8. Selected bond lengths (Å) and angles (°) for **Cd-2**. Symmetry code:

Cd(1)-N(2)	2.296(3)	Cd(1)-N(51)	2.335(3)
Cd(1)-N(3)	2.306(3)	Cd(2)-N(1)	2.322(3)
Cd(1)-S(1)	2.7384(10)	Cd(2)-S(2)	2.7438(10)
Cd(1)-N(11)	2.352(3)	Cd(2)-N(31)	2.332(3)
N(2)-Cd(1)-S(1)	93.54(8)	N(51)-Cd(1)-S(1)	87.14(8)
N(2)-Cd(1)-N(11)	90.30(12)	N(51)-Cd(1)-S(3A)	91.68(9)
N(3)-Cd(1)-N(11)	91.66(12)	N(1)-Cd(2)-S(2B)	87.57(8)
N(3)-Cd(1)-S(3A)	91.67(8)	N(1B)-Cd(2)-S(2B)	92.43(8)
S(1)-Cd(1)-S(3A)	83.86(3)	N(31)-Cd(2)-S(2)	89.86(9)
N(11)-Cd(1)-S(1)	91.75(9)	N(31)-Cd(2)-S(2B)	90.14(9)
N(11)-Cd(1)-S(3A)	87.93(9)		

14

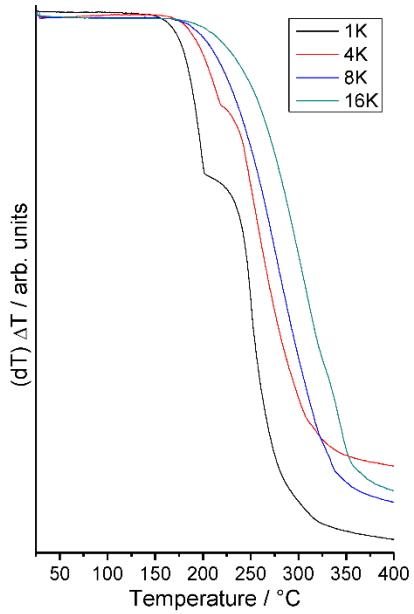

Figure S16. TG curves for compound [Mn(NCS)$_2$(4,4-Chlorobenzylpyridine)$_4$] (**Mn-1**). Heating rate = 1 °C; 4 °C, 8 °C and 16 °C·min^{-1}.

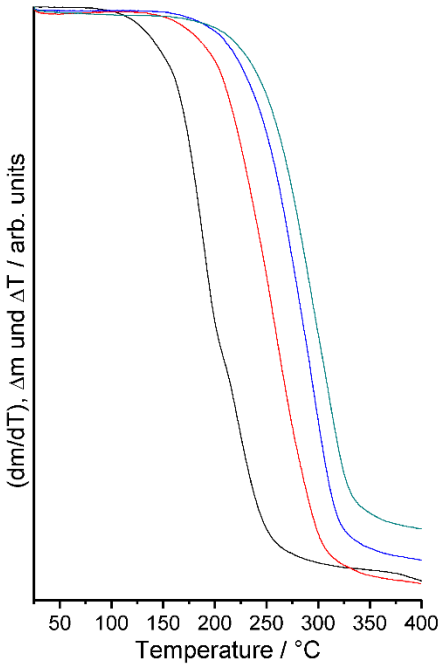

Figure S17. TG curves for compound [Fe(NCS)$_2$(4,4-Chlorobenzylpyridine)$_4$] (**Fe-1**). Heating rate = 1 °C; 4 °C, 8 °C and 16 °C·min^{-1}.

15

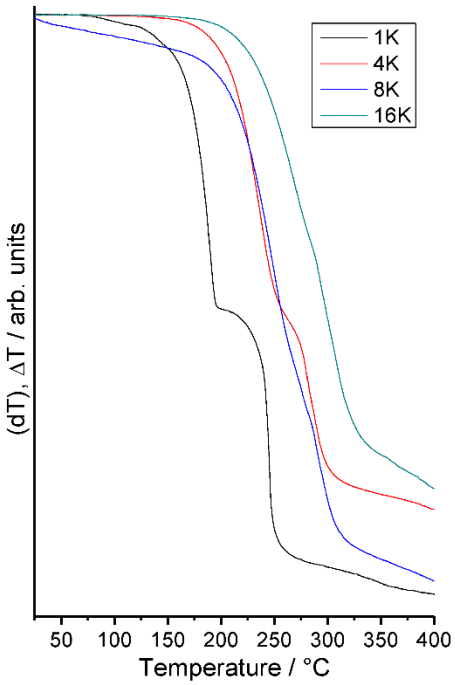

Figure S18. TG curves for compound [Ni(NCS)$_2$(4,4-Chlorobenzylpyridine)$_4$] (**Ni-1**). Heating rate = 1 °C; 4 °C, 8 °C and 16 °C·min^{-1}.

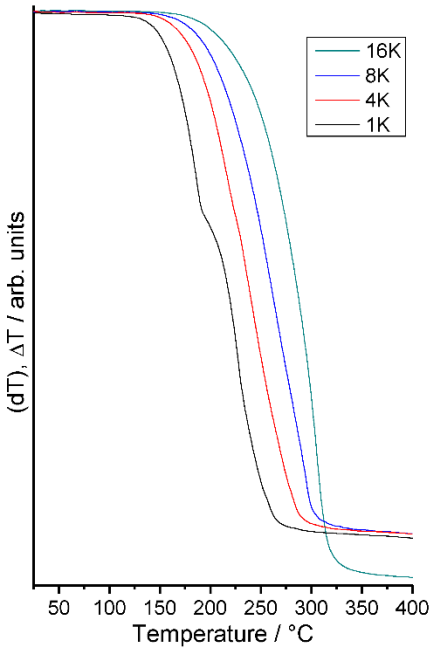

Figure S19. TG curves for compound [Cd(NCS)$_2$(4,4-Chlorobenzylpyridine)$_4$] (**Cd-1**). Heating rate = 1 °C; 4 °C, 8 °C and 16 °C·min^{-1}.

16

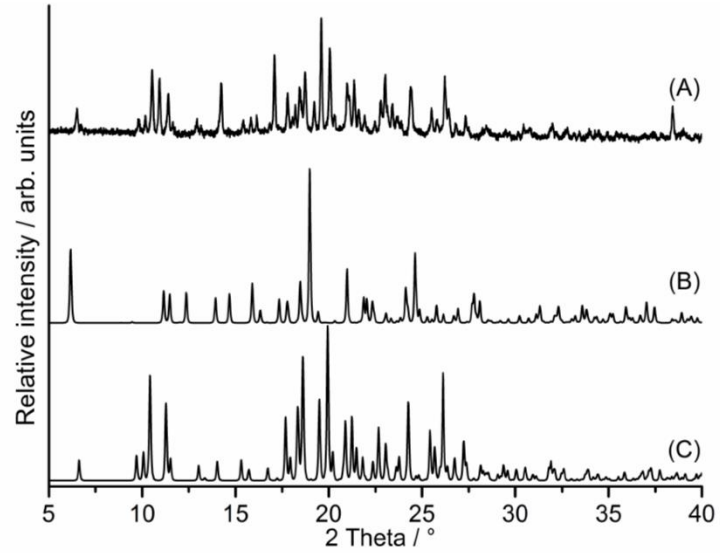

Figure S20. XRPD pattern of the residue obtained after the first mass loss of **Mn-1** (A) and the calculated XRPD pat*t*ern for **Mn-2** (B) and **Mn-1** (C).

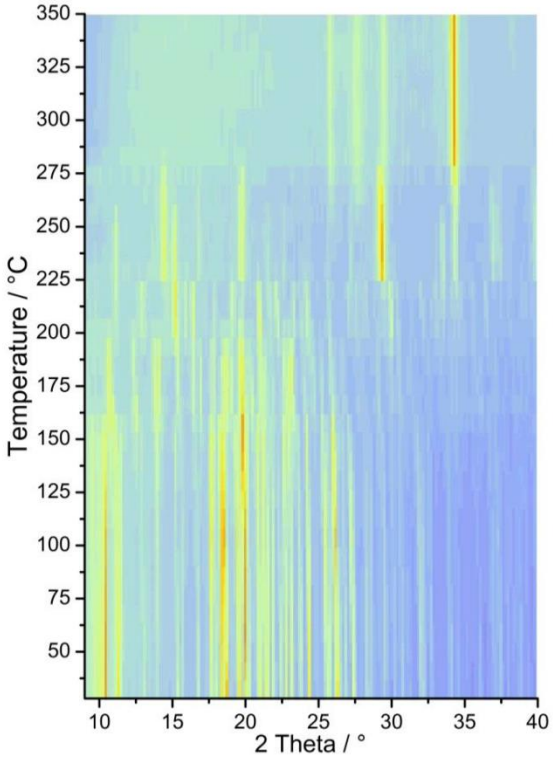

Figure S21. Temperature-resolved in-situ XRD of **Mn-1** from28 to 350 °C, (heatingrate: 5 °C/min).

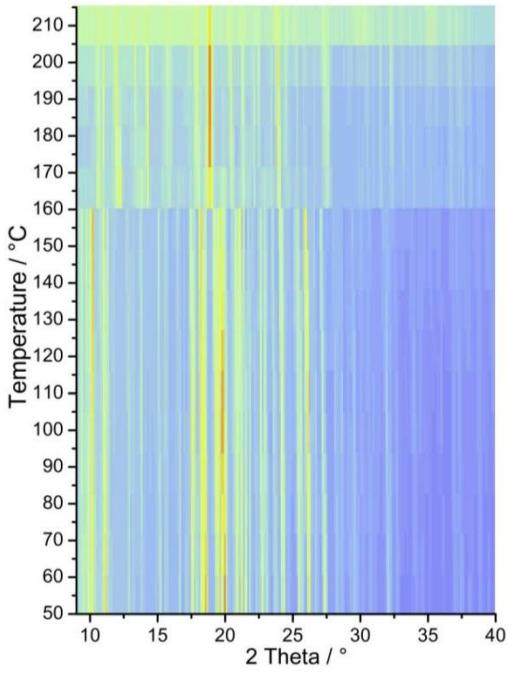

Figure S22. Temperature-resolved in-situ XRD of **Fe-1** from 50 to 215 °C, (heatingrate: 5 °C/min).

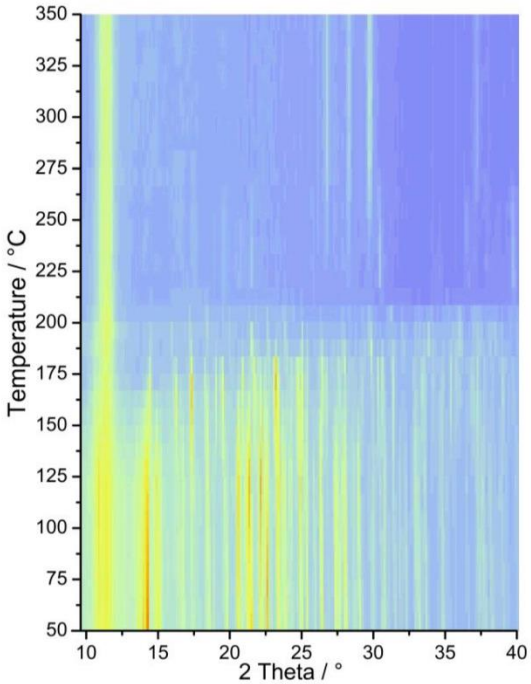

Figure S23. Temperature-resolved in-situ XRD of **Cd-1** from 50 to 350 °C, (heatingrate: 5 °C/min).

18

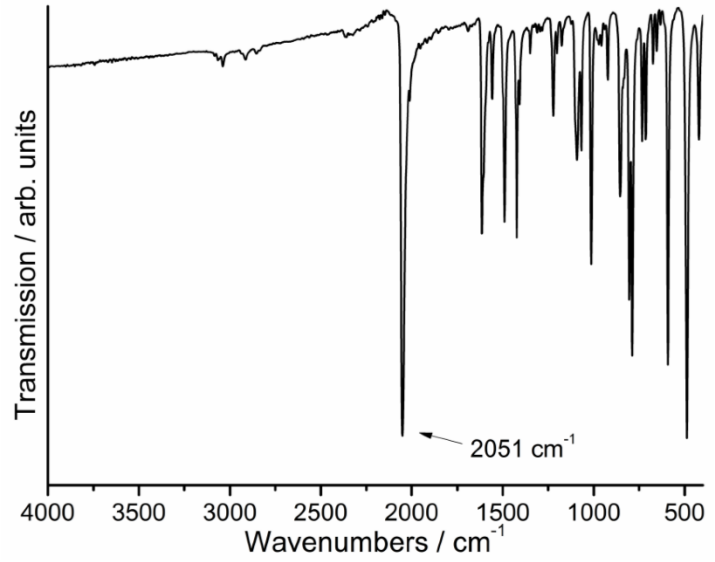

Figure S24. IR spectra of **Mn-1**. The value of the CN stretching vibration is given.

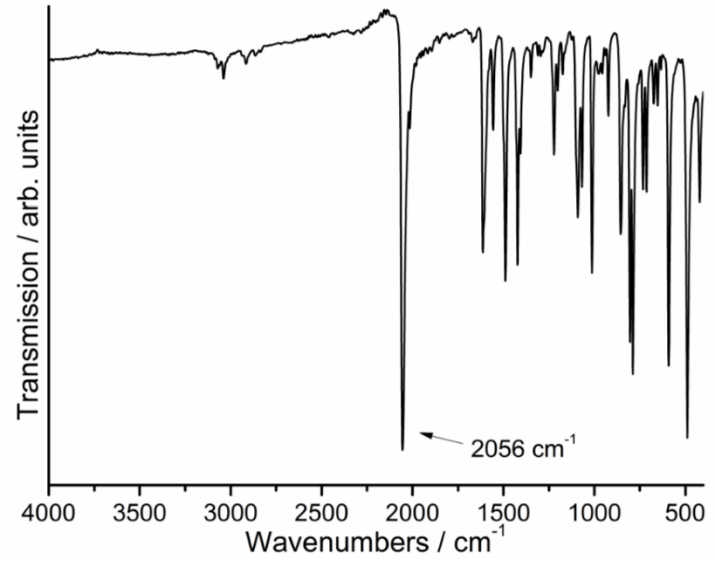

Figure S25. IR spectra of **Fe-1/I**. The value of the CN stretching vibration is given.

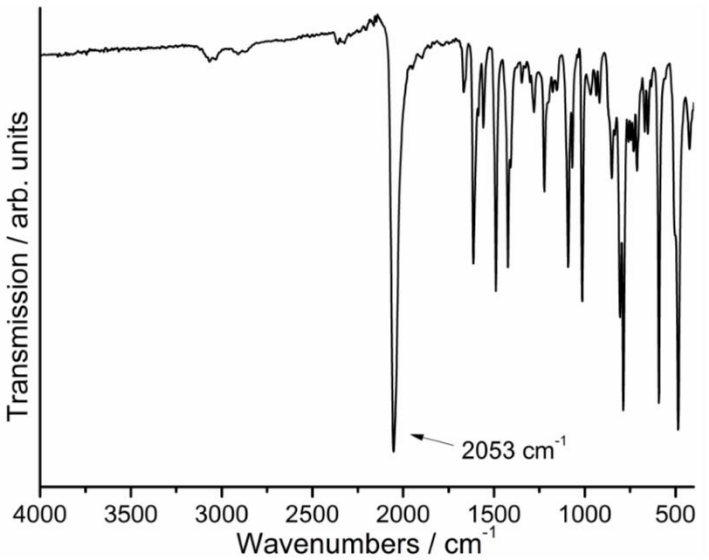

Figure S26. IR spectra of **Fe-1/II**. The value of the CN stretching vibration is given.

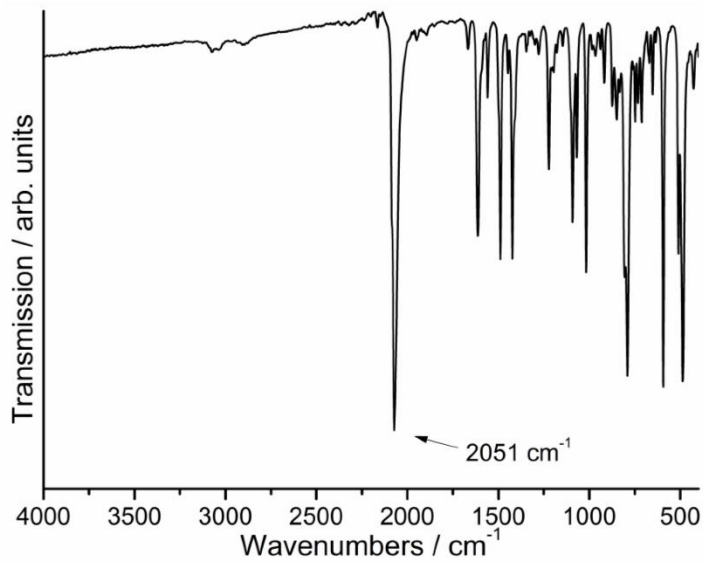

Figure S27. IR spectra of **Ni-1**. The value of the CN stretching vibration is given.

20

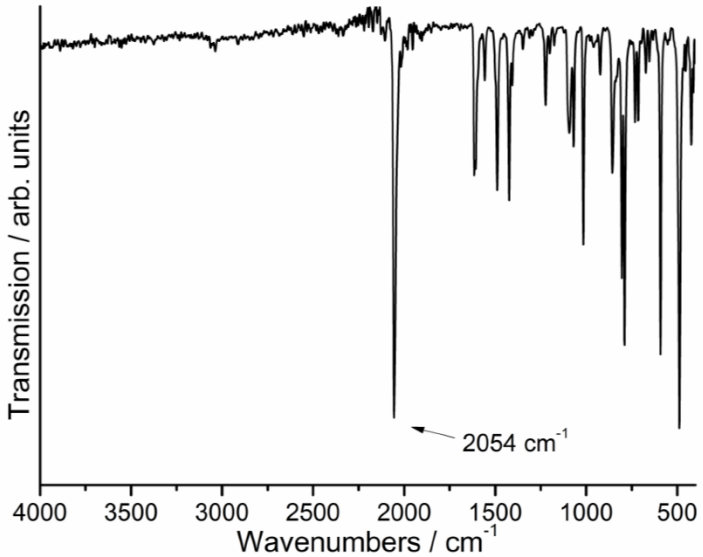

Figure S28. IR spectra of **Cd-1**. The value of the CN stretching vibration is given

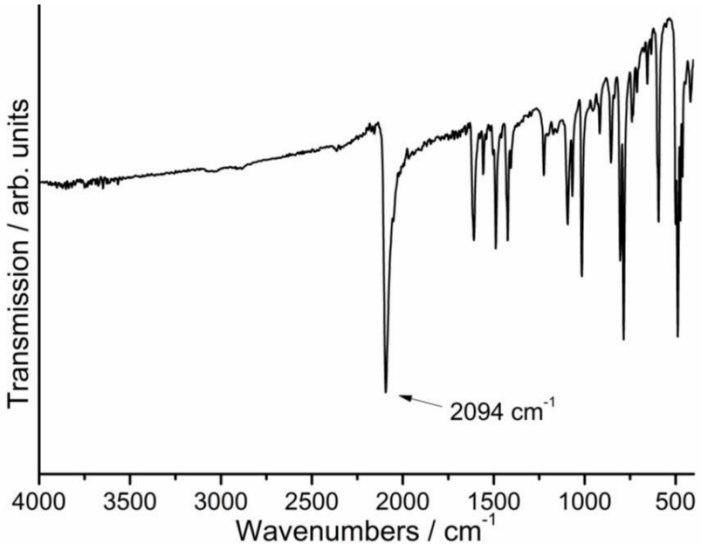

Figure S29. IR spectra of **Mn-2**. The value of the CN stretching vibration is given.

21

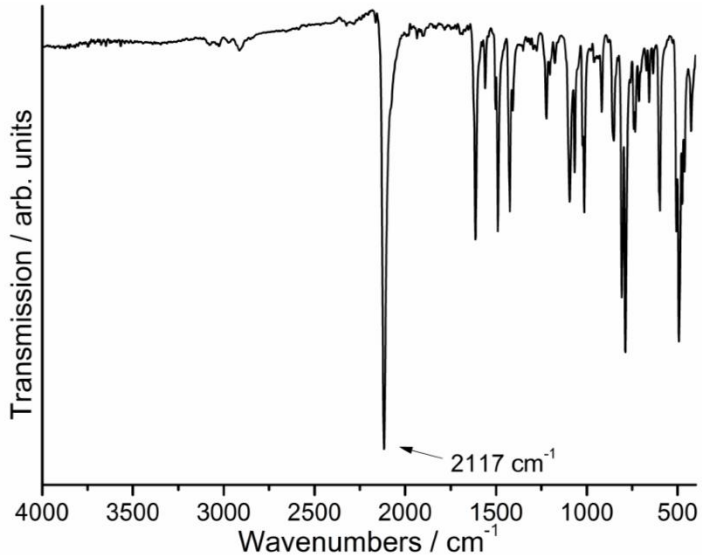

Figure S30. IR spectra of **Ni-2**. The value of the CN stretching vibration is given.

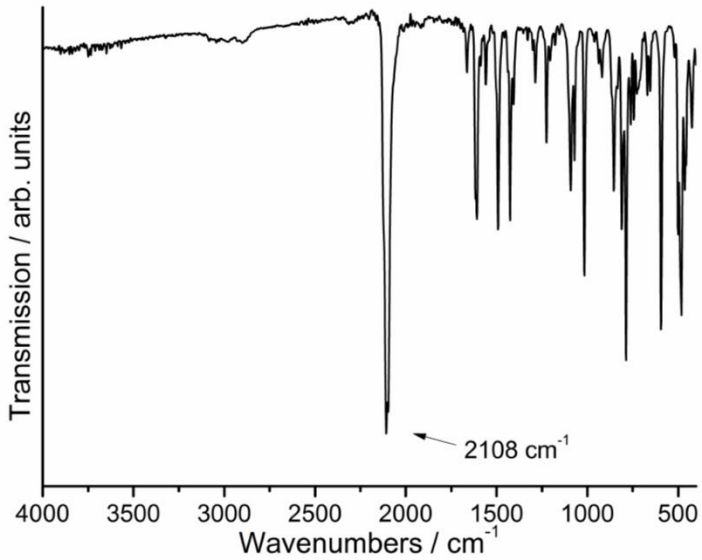

Figure S31. IR spectra of **Cd-2**. The value of the CN stretching vibration is given.

8.9. Supporting Information: Synthesis, Crystal Structures and Properties of $Ni(NCS)_2$-4-(hydroxymethyl)pyridine Coordination Compounds

Supplementary Material

Synthesis, Crystal Structures and Properties of $Ni(NCS)_2$-4-(hydroxymethyl)pyridine Coordination Compounds

Julia Werner and Christian Näther

3

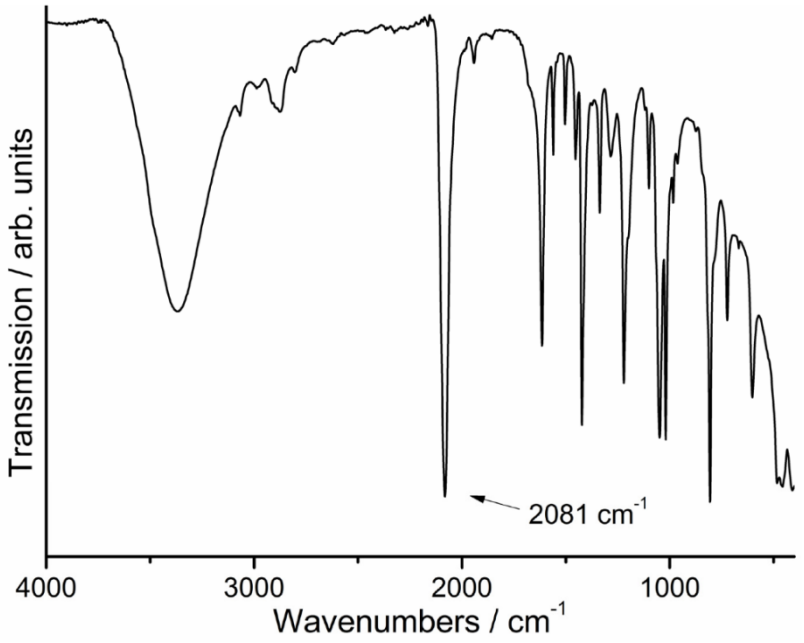

Figure S1: IR spectra of **1-H_2O**. The value of the CN stretching vibration is given.

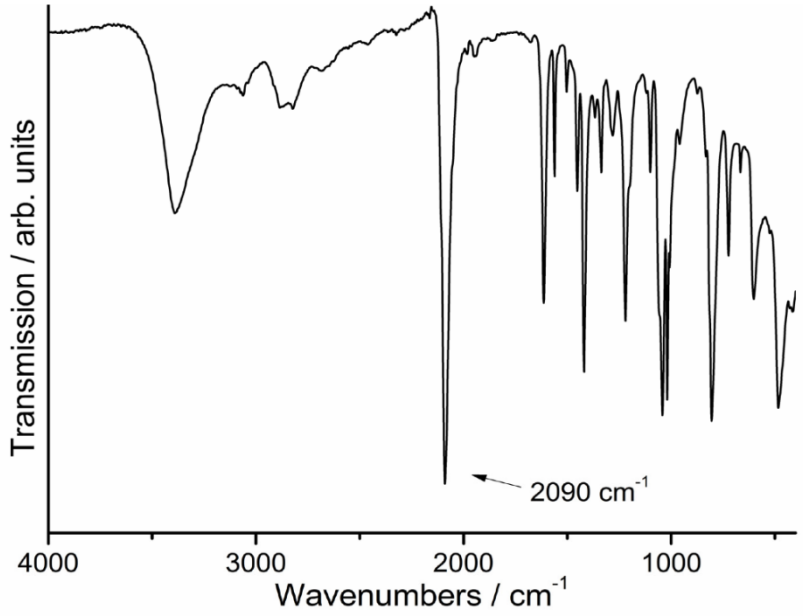

Figure S2: IR spectra of **1**. The value of the CN stretching vibration is given.

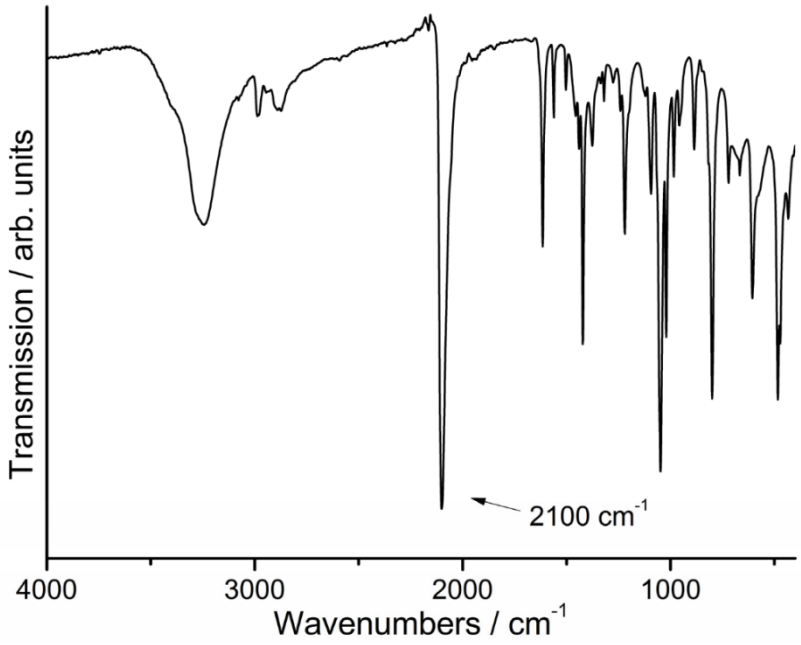

Figure S3. IR spectra of **2**. The value of the CN stretching vibration is given.

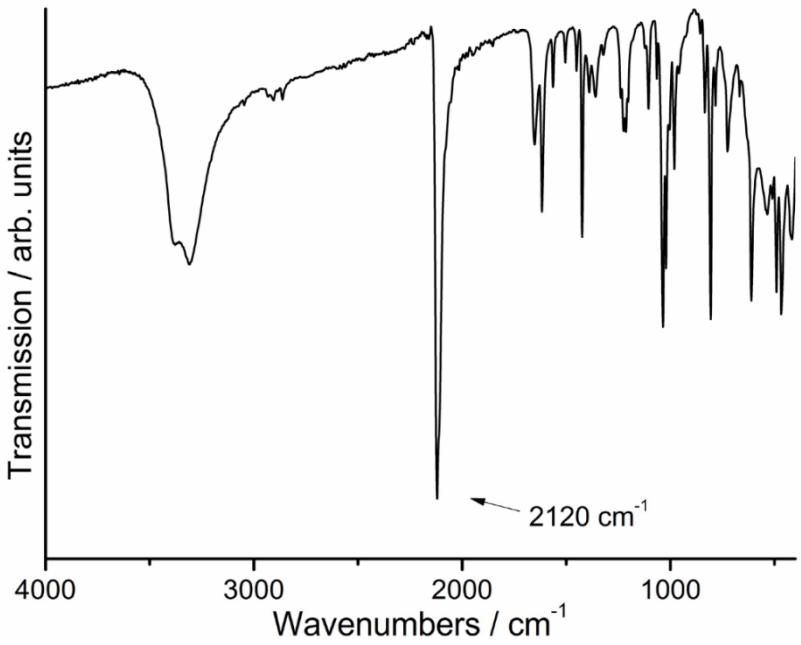

Figure S4. IR spectra of **3**. The value of the CN stretching vibration is given.

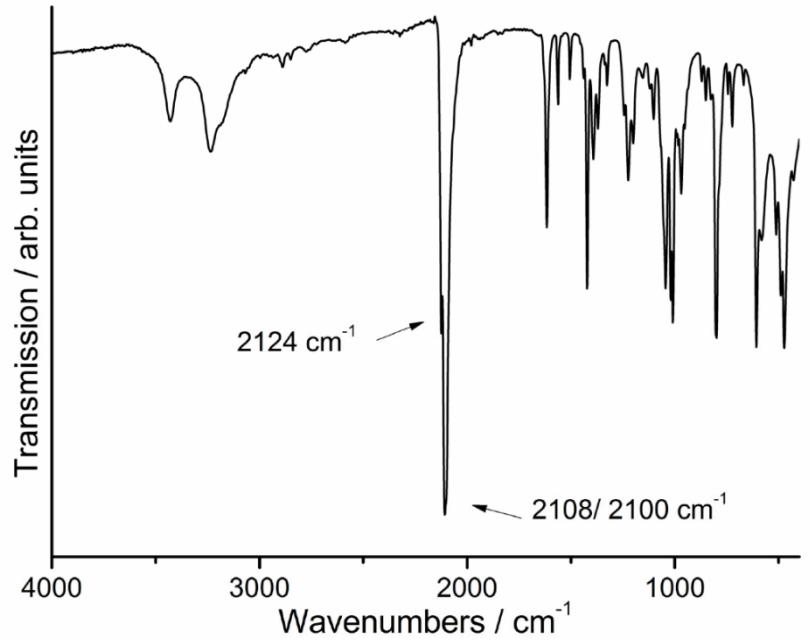

Figure S5. IR spectra of **4**. The values of the CN stretching vibrations are given.

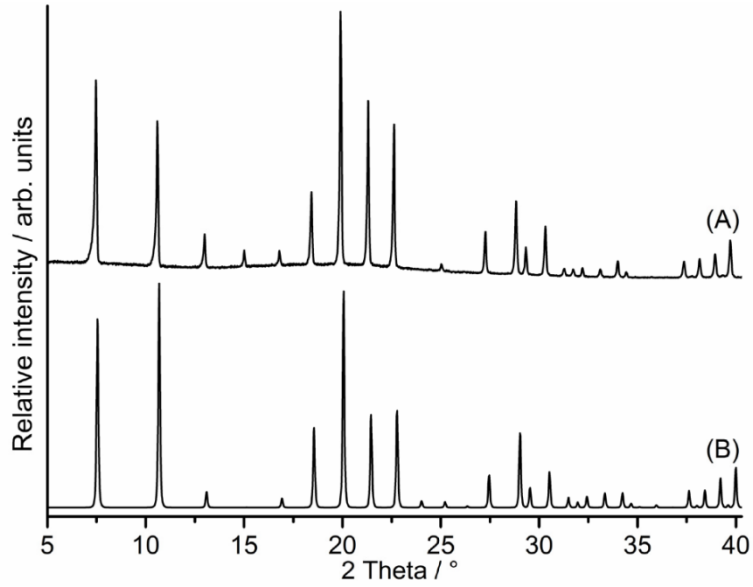

Figure S6. Experimental (A) and calculated (B) XRPD pattern for compound **1-H_2O**.

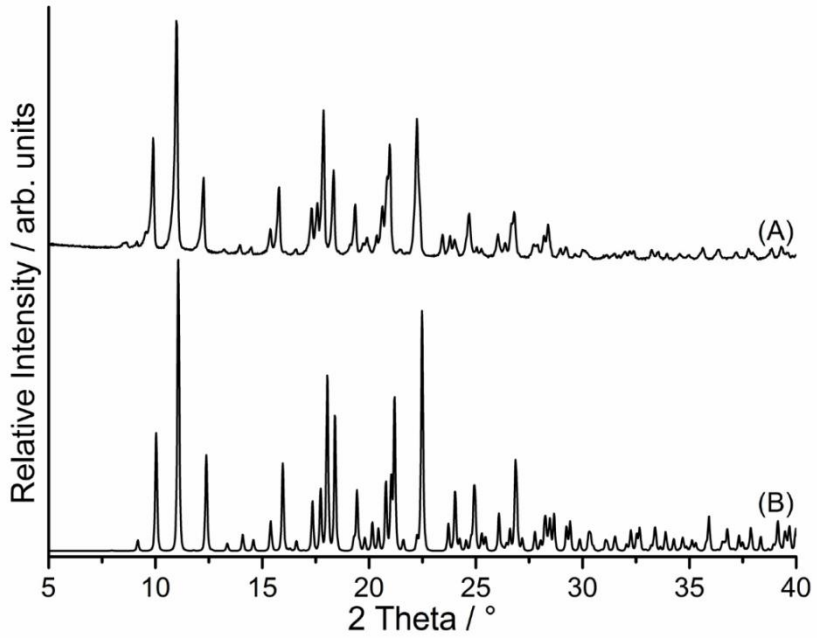

Figure S7. Experimental (A) and calculated (B) XRPD pattern for compound **1**.

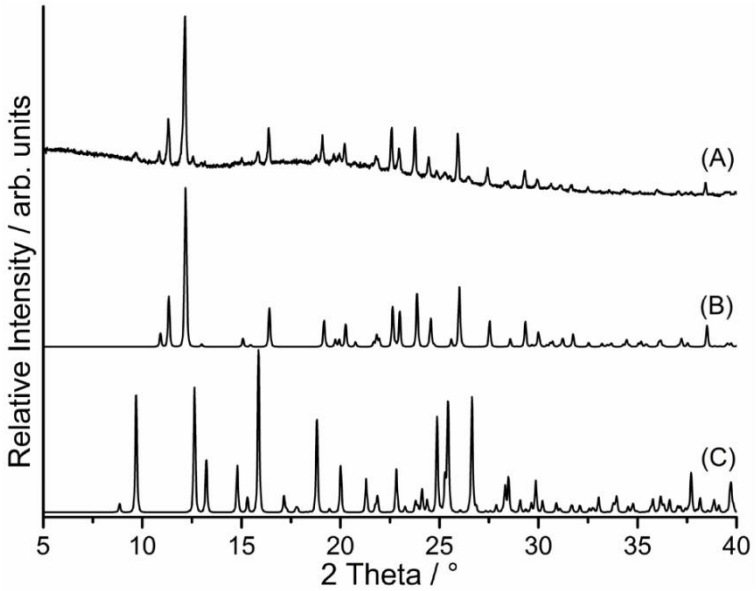

Figure S8. Experimental (A) and calculated (B) XRPD pattern for compound **2** and calculated XRPD pattern for **4**.

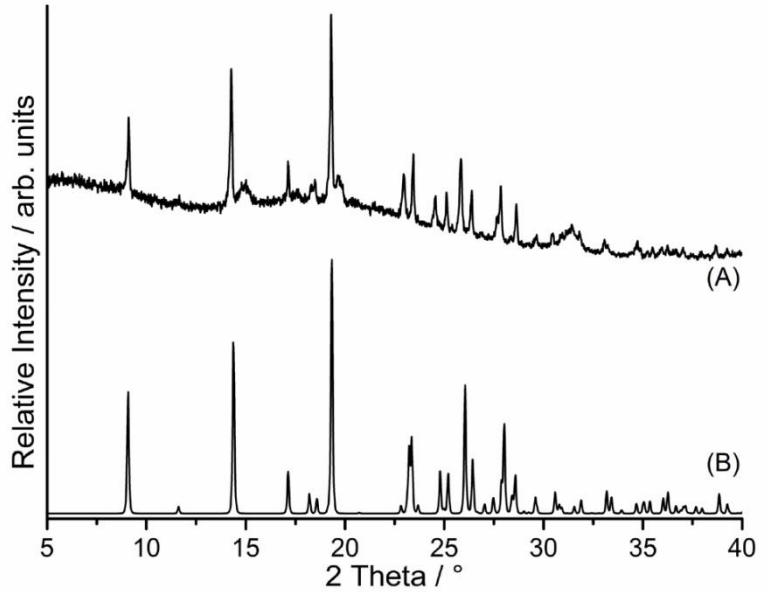

Figure S9. Experimental (A) and calculated (B) XRPD pattern for compound **3**.

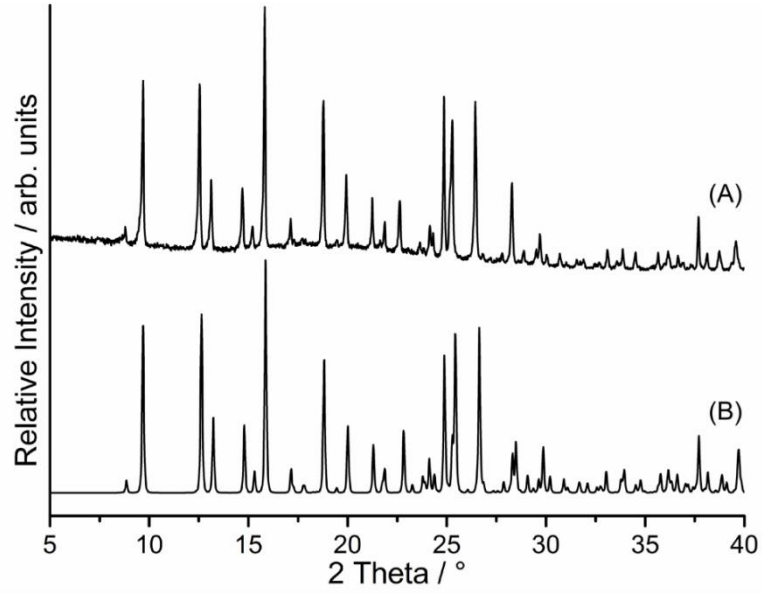

Figure S10. Experimental (A) and calculated (B) XRPD pattern for compound **4**.

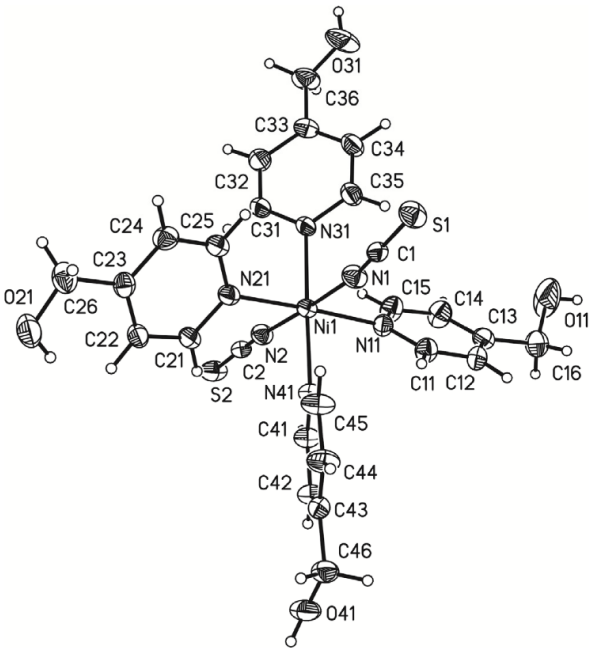

Figure S11. Crystal structure of compound **1** with labeling and displacement ellipsoids drawn at the 50 % probability level.

Table S1. Selected bond lengths (Å) and angles (°) for **1**.

Ni(1)-N(1)	2.075(2)	Ni(1)-N(2)	2.071(2)
Ni(1)-N(11)	2.139(2)	Ni(1)-N(31)	2.124(2)
Ni(1)-N(21)	2.121(2)	Ni(1)-N(41)	2.128(2)
N(1)-Ni(1)-N(11)	89.36(9)	N(2)-Ni(1)-N(41)	91.77(9)
N(1)-Ni(1)-N(21)	89.85(10)	N(21)-Ni(1)-N(11)	176.84(9)
N(1)-Ni(1)-N(31)	88.36(9)	N(21)-Ni(1)-N(31)	92.44(9)
N(1)-Ni(1)-N(41)	90.72(10)	N(21)-Ni(1)-N(41)	88.64(9)
N(2)-Ni(1)-N(1)	177.50(10)	N(31)-Ni(1)-N(11)	90.59(9)
N(2)-Ni(1)-N(11)	90.99(9)	N(31)-Ni(1)-N(41)	178.58(9)
N(2)-Ni(1)-N(21)	89.92(9)	N(41)-Ni(1)-N(11)	88.31(9)
N(2)-Ni(1)-N(31)	89.16(9)		

Table S2. Hydrogen bonding for **1**. Symmetry transformations used to generate equivalent atoms: A -x+2,y-1/2,-z+3/2, B: x+1,y,z, C: x-1,y,z, D: -x+1,y+1/2,-z+3/2

D-H…A	d(D-H)	d(H...A)	d(D...A)	<(DHA)
O(11)-H(11O)...S(1D)	0.84	2.51	3.320(4)	161.7
O(21)-H(21O)...S(2A)	0.84	2.54	3.337(3)	158.0
O(31)-H(31O)...S(2C)	0.84	2.47	3.292(4)	166.5
O(41)-H(41O)...S(1B)	0.84	2.49	3.298(4)	161.2

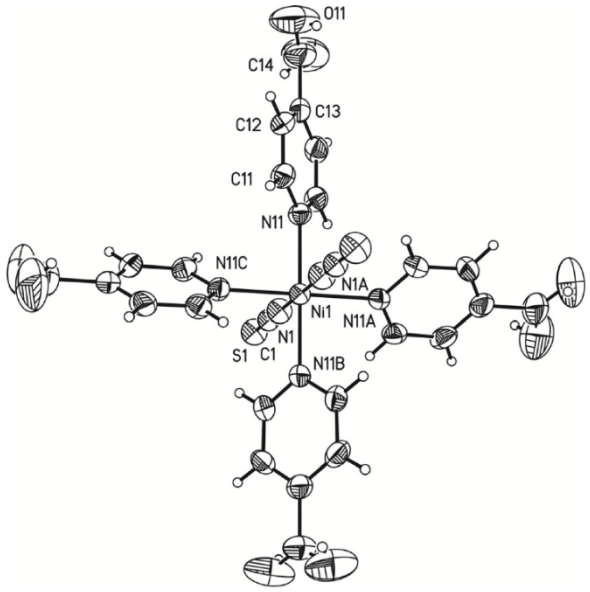

Figure S12. Crystal structure of compound **1-H_2O** with labeling and displacement ellipsoids drawn at the 50 % probability level. Symmetry transformation used to generate equivalent atoms:
A: -x+1/2,-y+3/2,z; B: x,-y+3/2,-z+1/2 ; C: -x+1/2,y,-z+1/2 ; D: -z+1/2,-y+3/2,-x+1/2.

Table S3. Selected bond lengths (Å) and angles (°) for **1-H_2O**.

Ni(1)-N(1)	2.060(6)	Ni(1)-N(11)	2.113(4)
N(1**A**)-Ni(1)-N(1)	180.0	N(1)-Ni(1)-N(11)	90.0
N(1)-Ni(1)-N(11**B**)	90.000(1)		

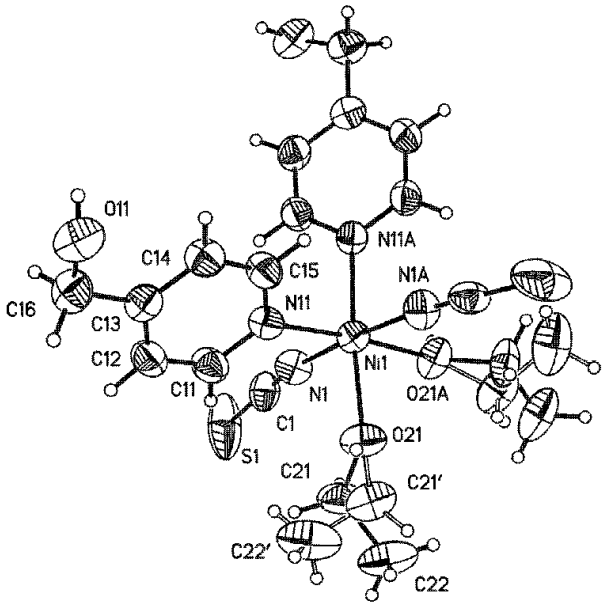

Figure S13. Crystal structure of compound **2** with labeling and displacement ellipsoids drawn at the 50 % probability level. The disorder of the ethanol molecule is shown as full and open bonds.

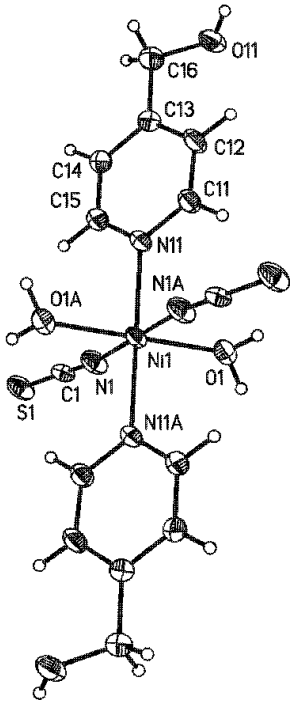

Figure S14. Crystal structure of compound **3** with labeling and displacement ellipsoids drawn at the 50 % probability level.

Table S4. Selected bond lengths (Å) and angles (°) for **2**.

Ni(1)-N(1)	2.041(3)	Ni(1)-O(21)	2.100(2)
Ni(1)-N(11)	2.101(3)		
N(1A)-Ni(1)-N(1)	176.20(18)	O(21)-Ni(1)-N(11)	89.78(10)
N(1)-Ni(1)-O(21A)	87.03(11)	N(1)-Ni(1)-N(11A)	90.79(11)
N (1)-Ni(1)-O(21)	90.18(11)	N(11A)-Ni(1)-N(11)	94.92(15)
N(1)-Ni(1)-N(11)	91.78(11)	O(21)-Ni(1)-O(21A)	85.54(14)
O(21)-Ni(1)-N(11A)	175.17(11)		

Table S5. Selected bond lengths (Å) and angles (°) for **3**.

Ni(1)-N(1)	2.0443(19)	Ni(1)-O(1)	2.0896(17)
Ni(1)-N(11)	2.1273(19)		
N(1A)-Ni(1)-N(1)	180.00(10)	N(11)-Ni(1)-N(11A)	180.0
N(1)-Ni(1)-O(1)	89.98(9)	O(1)-Ni(1)-N(11)	88.80(7)
N(1)-Ni(1)-O(1A)	90.02(9)	N(1)-Ni(1)-N(11A)	89.51(7)
N(1)-Ni(1)-N(11)	90.49(7)	O(1)-Ni(1)-N(11A)	91.20(7)
O(1A)-Ni(1)-O(1)	180.0		

Table S6. Hydrogen bonding for **2**. Symmetry transformations used to generate equivalent atoms: A: -x+1,y,-z+1/2 B: -x+3/2,y-1/2,-z+1/2

D-H…A	d(D-H)	d(H...A)	d(D...A)	<(DHA)
O(11)-H(11O)...S(1B)	0.84	2.34	3.178(3)	172.2

Table S7. Hydrogen bonding for **3**. Symmetry transformations used to generate equivalent atoms: A: -x+1,-y+1,-z+1; B: -x+3/2,y-1/2,z; C: x+1/2,-y+3/2,-z+1; D: x-1/2,-y+3/2,-z+1.

D-H…A	d(D-H)	d(H...A)	d(D...A)	<(DHA)
O(1)-H(2O1)...S(1C)	0.84	2.45	3.2891(17)	173.5
O(1)-H(1O1)...O(11D)	0.84	1.95	2.768(3)	173.5
O(11)-H(11O)...S(1B)	0.84	2.36	3.1964(19)	172.0

Table S8. Selected bond lengths (Å) and angles (°) for **4**.

Ni(1)-N(1)	2.0394(19)	Ni(1)-N(2A)	2.0417(19)
Ni(1)-S(2)	2.5269(6)	Ni(1)-O(21B)	2.1371(15)
Ni(1)-N(11)	2.1188(19)	Ni(1)-N(21)	2.1209(19)
N(1)-Ni(1)-N(2A)	176.61(8)	N(2A)-Ni(1)-S(2)	93.41(6)
N(1)-Ni(1)-N(11)	87.87(8)	N(11)-Ni(1)-S(2)	94.05(5)
N(1)-Ni(1)-N(21)	90.00(8)	N(11)-Ni(1)-N(21)	175.34(8)
N(1)-Ni(1)-O(21B)	86.91(7)	N(11)-Ni(1)-O(21B)	88.74(7)
N(1)-Ni(1)-S(2)	89.14(6)	N(21)-Ni(1)-O(21B)	87.01(7)
N(2A)-Ni(1)-N(11)	89.70(8)	N(21)-Ni(1)-S(2)	90.06(6)
N(2A)-Ni(1)-N(21)	92.24(9)	O(21B)-Ni(1)-S(2)	175.07(5)
N(2A)-Ni(1)-O(21B)	90.67(7)		

Table S9. Hydrogen bonding for **4**. Symmetry transformations used to generate equivalent atoms: A: -x+1,-y+1,-z+1; B: -x+2,-y+1,-z+1; C: x-1,-y+3/2,z-1/2; D: -x+2,y-1/2,-z+3/2.

D-H…A	d(D-H)	d(H...A)	d(D...A)	<(DHA)
O(11)-H(11O)...S(1C)	0.84	2.46	3.297(2)	177.7
O(21)-H(21O)...S(1D)	0.84	2.43	3.1924(16)	160.4

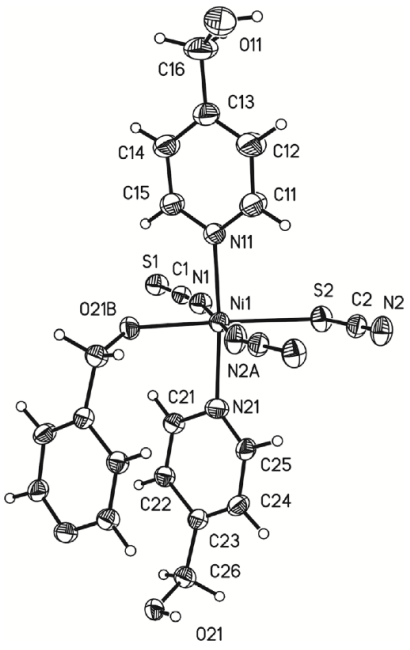

Figure S15. Crystal structure of compound **4** with labeling and displacement ellipsoids drawn at the 50 % probability level. The disordering of the 4-methanolypyridine ligand was omitted for clarity. Symmetry transformation used to generate equivalent atoms: A: -x+1,-y+1,-z+1, B: -x+2,-y+1,-z+1.

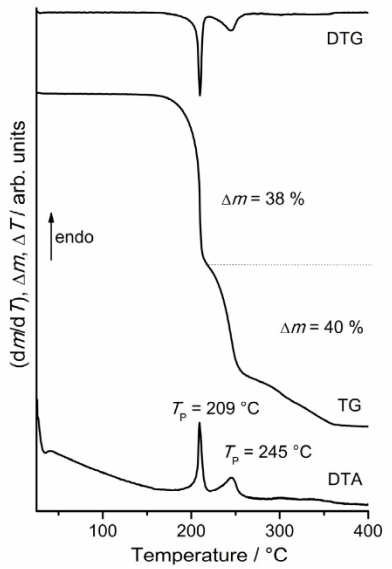

Figure S16. DTA, DTG and TG curves of compound **1**. Heating rate = 1 °C/min, mass change in %, and peak temperature T_P /°C.

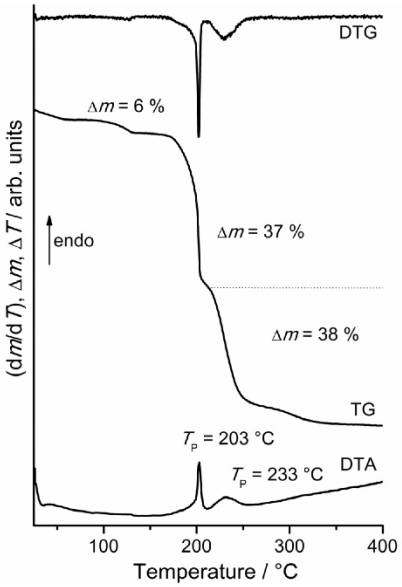

Figure S17. DTA, DTG and TG curves of compound **1-H_2O**. Heating rate = 1 °C/min, mass change in %, and peak temperature T_P /°C.

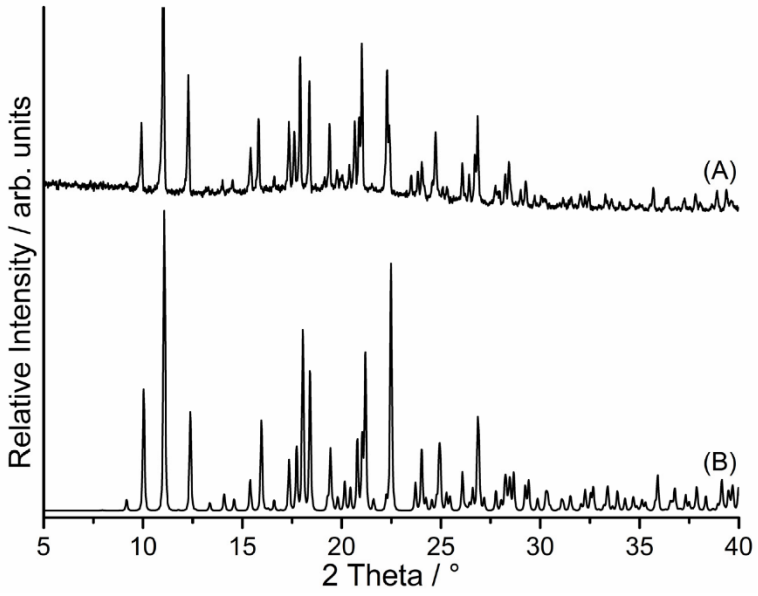

Figure S18. Residue obtained after the first mass step of **1**-H_2O (A) and calculated XRPD pattern for compound **1** (B).

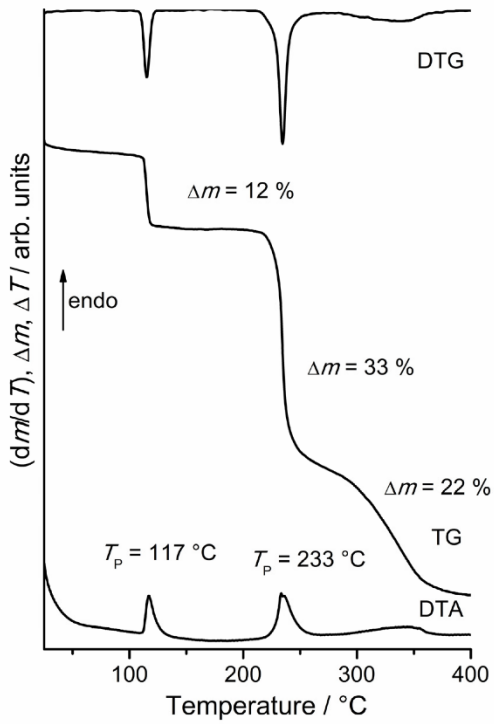

Figure S19. DTA, DTG and TG curves of compound **2**. Heating rate = 4 °C/min, mass change in %, and peak temperature T_P /°C.

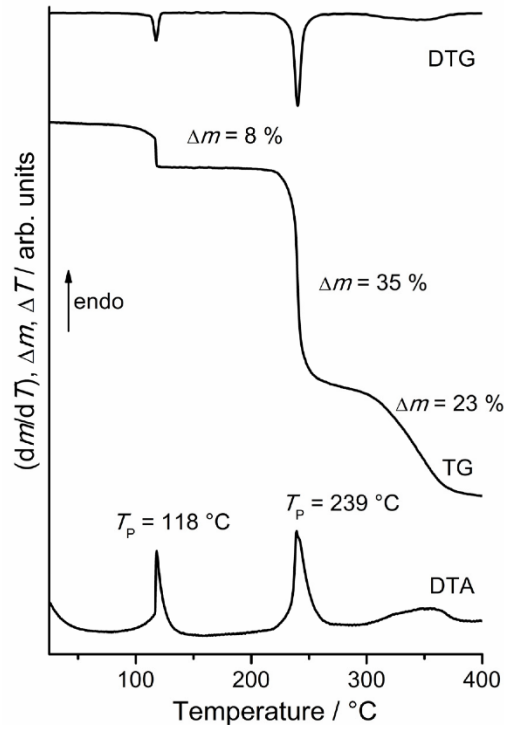

Figure S20. DTA, DTG and TG curves of compound **3**. Heating rate = 4 °C/min, mass change in %, and peak temperature T_P /°C.

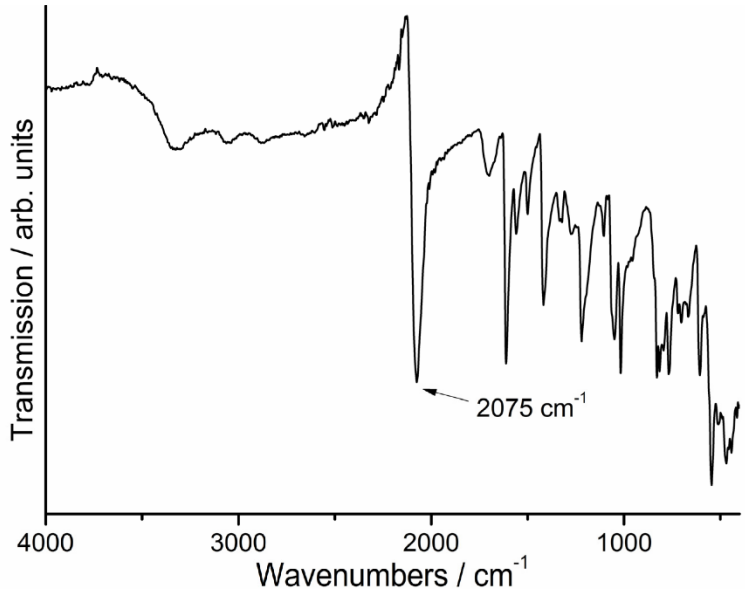

Figure S21. IR spectra of the residue obtained after the first mass step of compound **1**. The CN stretching vibration is given.

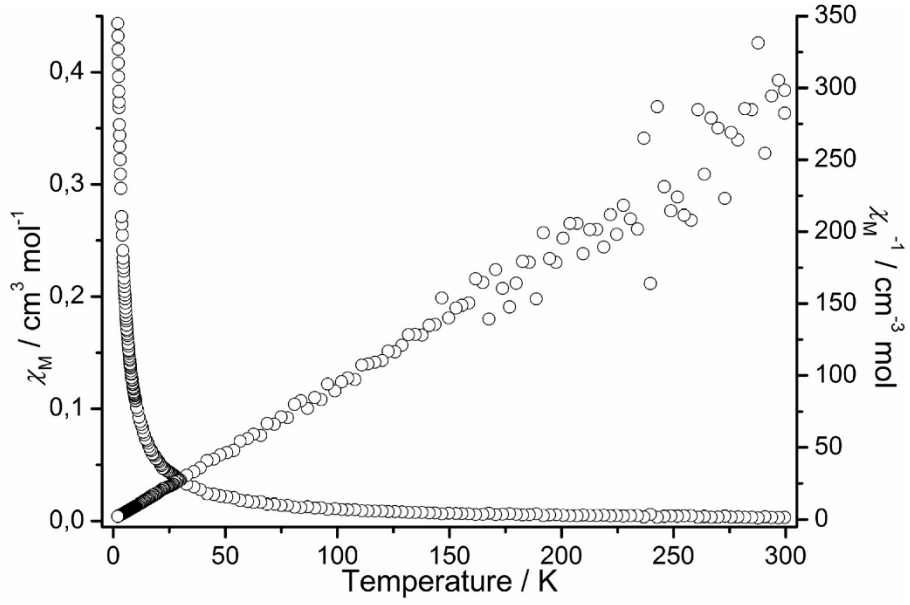

Figure S22. χ_M and χ_M^{-1} as function of the temperature of **1-H₂O** at H_{DC} = 1 kOe.

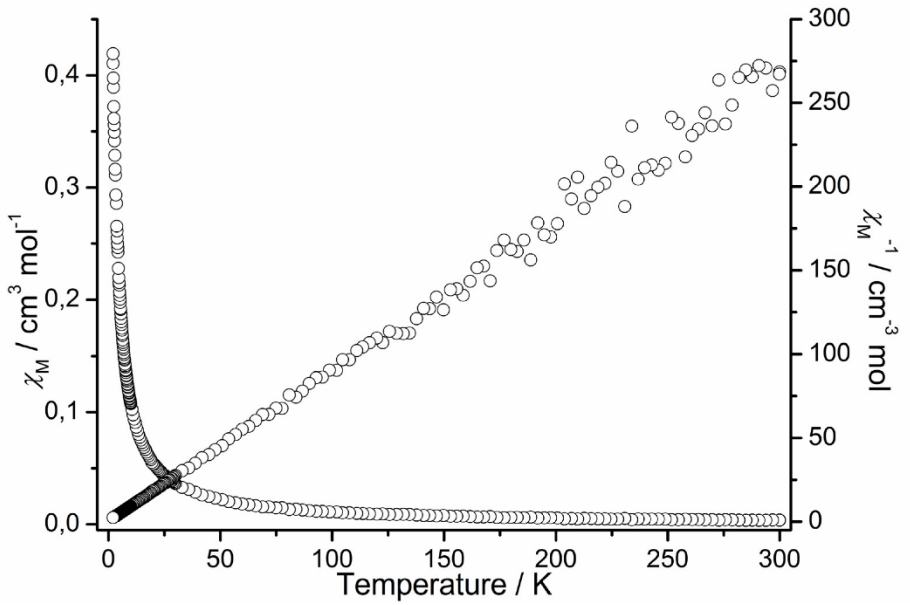

Figure S23. χ_M and χ_M^{-1} as function of the temperature of **1** at H_{DC} = 1 kOe.

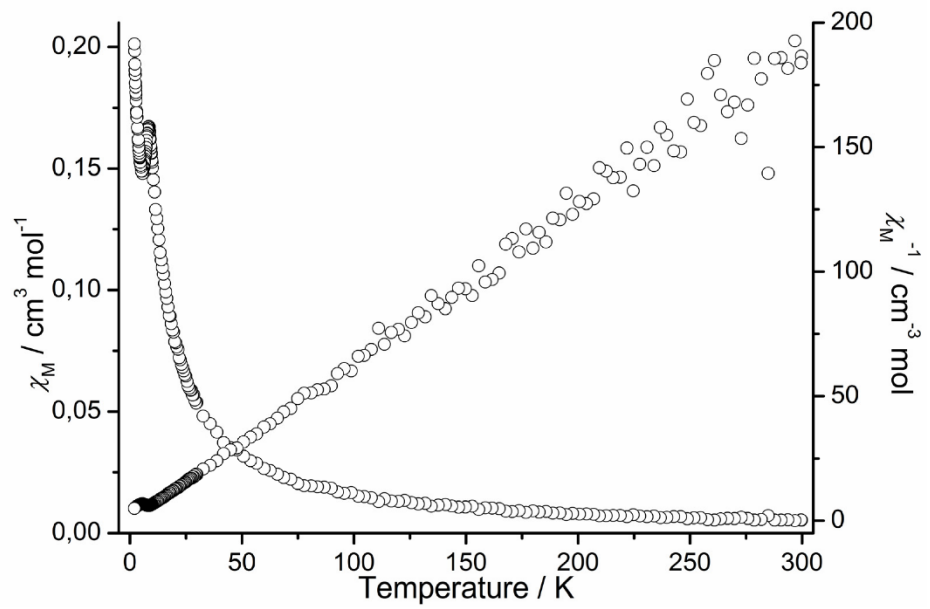

Figure S24. χ_M and χ_M^{-1} as function of the temperature of **2** at H_{DC} = 1 kOe.

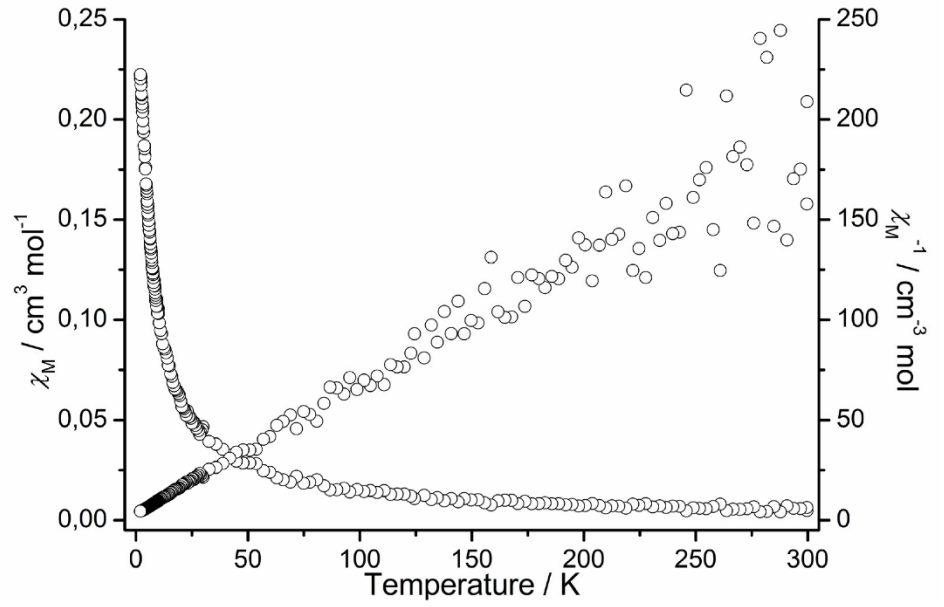

Figure S25. χ_M and χ_M^{-1} as function of the temperature of **3** at H_{DC} = 1 kOe.

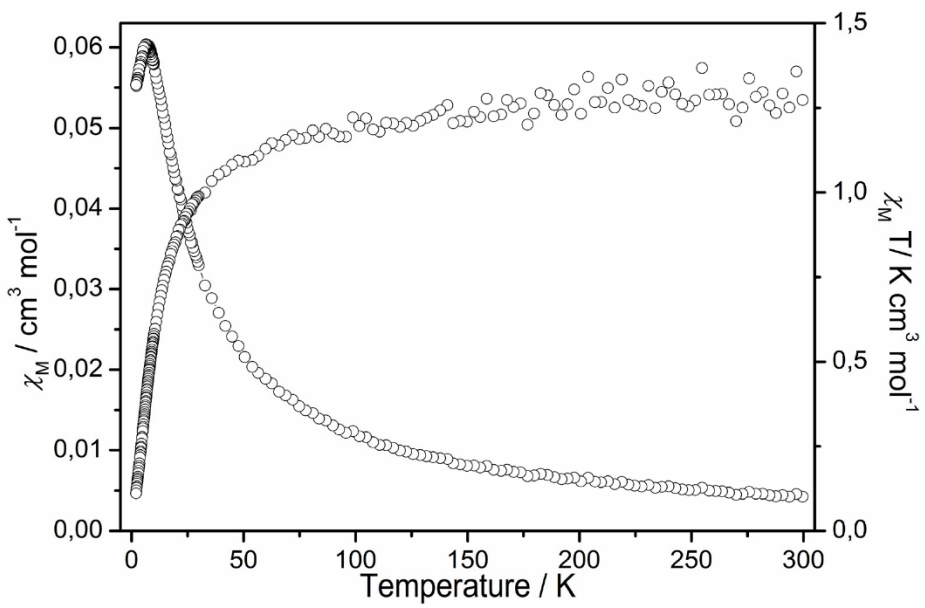

Figure S26. χ_M and χ_M T as function of the temperature of **4** at H_{DC} = 3 kOe.

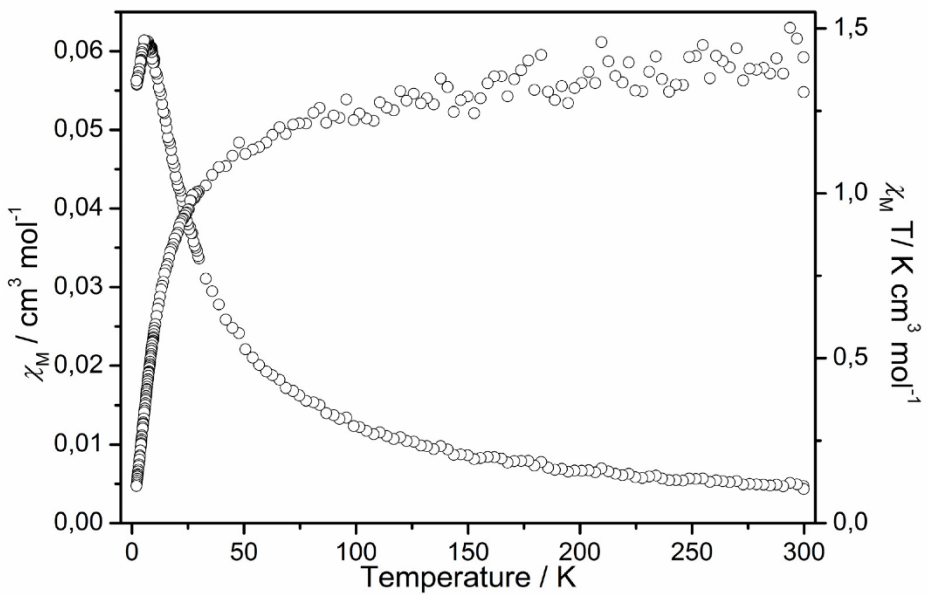

Figure S27. χ_M and χ_M T as function of the temperature of **4** at H_{DC} = 2 kOe.

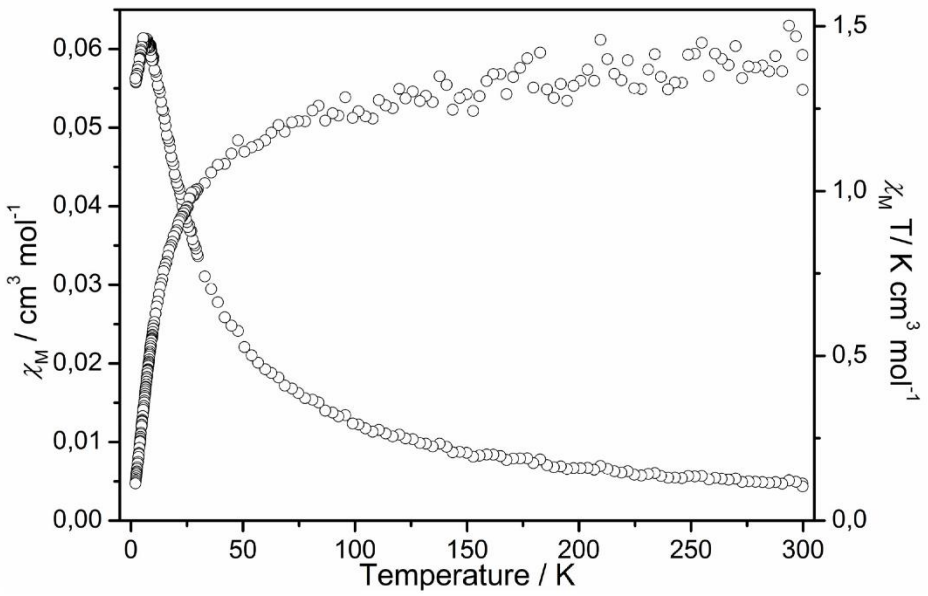

Figure S28. χ_M and χ_M T as function of the temperature of **4** at H_{DC} = 1.5 kOe.

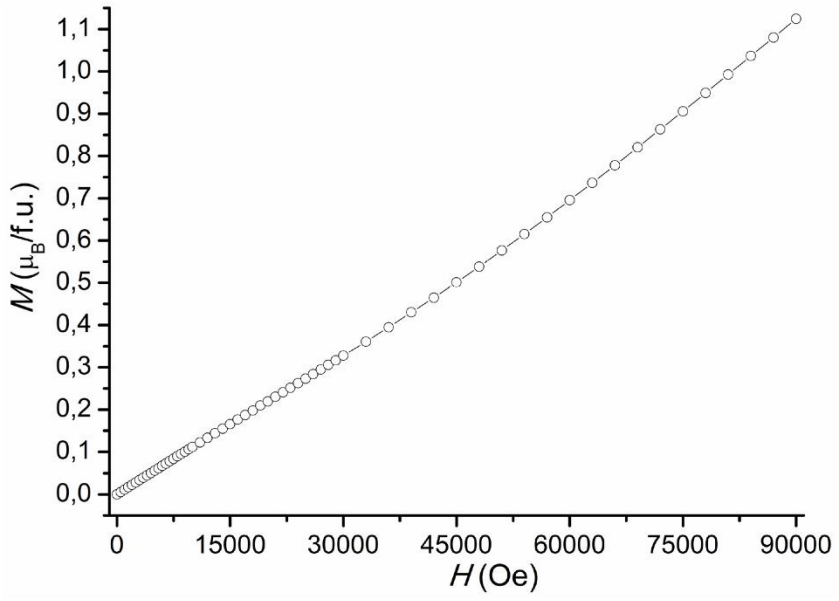

Figure S29. Virgin curve of **4** at 2 K.

8.10. Supporting Information: Investigations on the Structure Diversity and Thermal Degradation Behavior of Cd^{II} and Zn^{II} Thiocyanato Coordination Compounds based on 3-Acetylpyridine as Neutral Co-Ligand

Supporting Information

Investigations on the Structure Diversity and Thermal Degradation Behaviour of Cd^{II} and Zn^{II} Thiocyanato Coordination Compounds based on 3-Acetylpyridine as Neutral Co-Ligand

Julia Werner[a], Jan Boeckmann[a], and Christian Näther*[a]

[a] Institut für Anorganische Chemie, Christian-Albrechts-Universität zu Kiel, Max-Eyth-Str. 2, 24118 Kiel

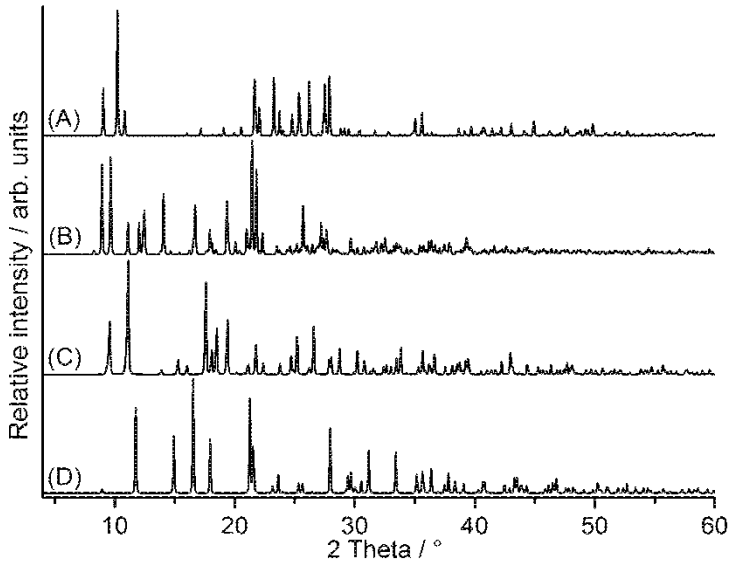

Figure S1. XRPD pattern for compound **2A** (A), **1A** (B), **1B** (C) and **1C** (D).

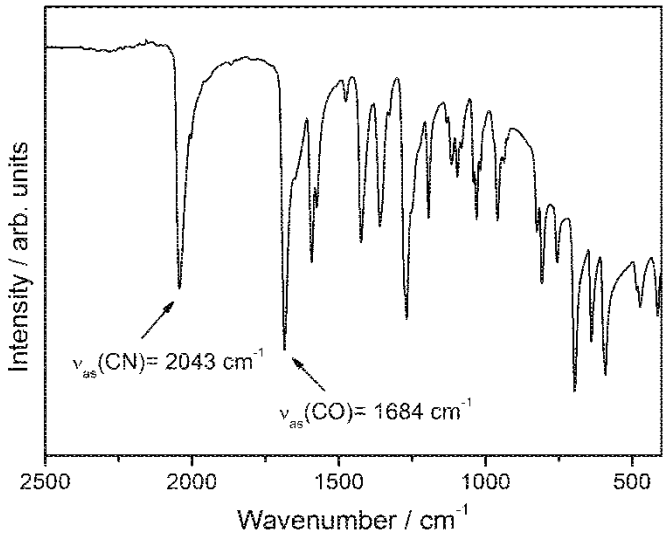

Figure S2. IR spectra of compound **1A**.

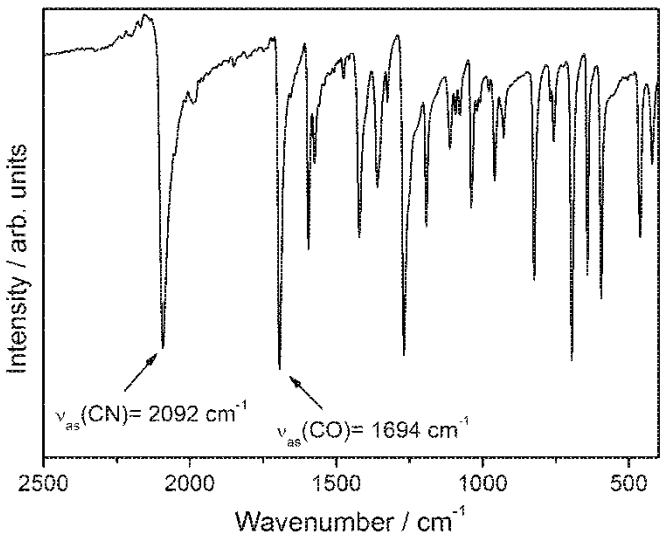

Figure S3. IR spectra of compound **1B**.

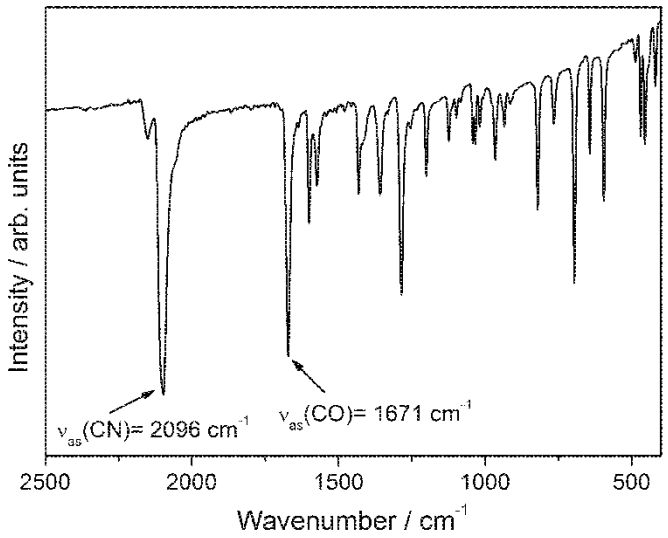

Figure S4. IR spectra of compound **1C**.

5

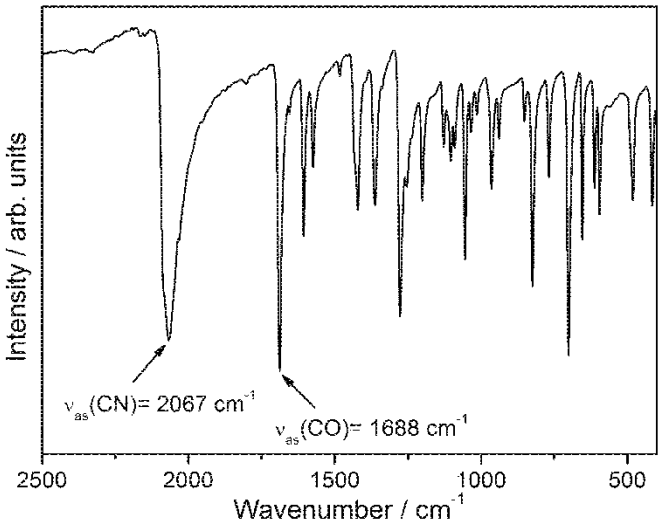

Figure S5. IR spectra of compound **2A**.

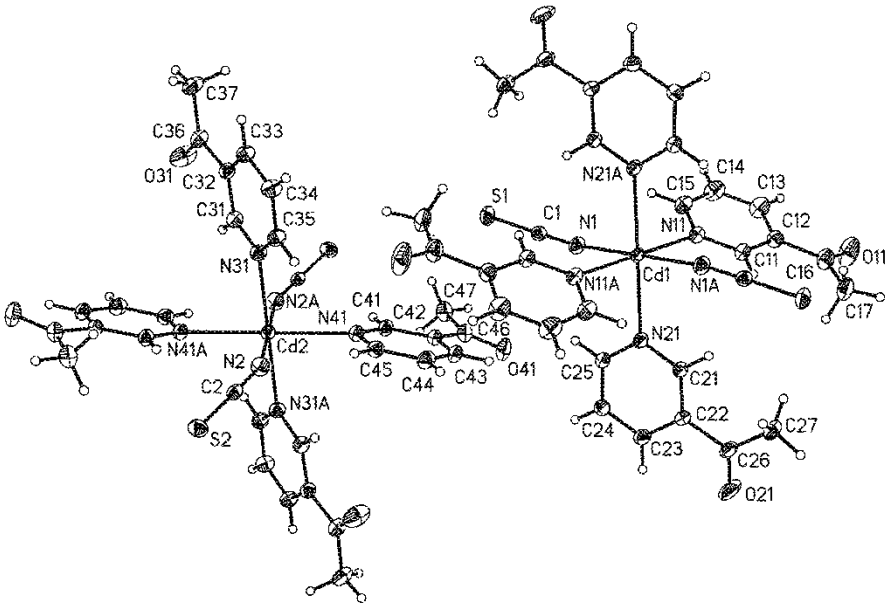

Figure S6. Crystal structure of compound **1A** with labeling and displacement ellipsoids drawn at the 30 % probability level. Symmetry transformation used to generate equivalent atoms: A: -x,-y+1,-z+1; B: -x+1,-y,-z.

6

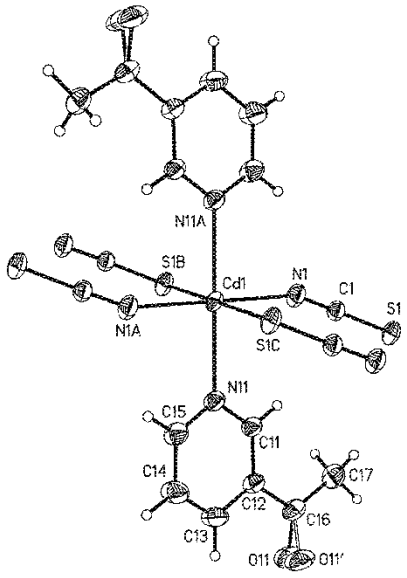

Figure S7. Crystal structure of compound **1B** with labeling and displacement ellipsoids drawn at the 30 % probability level. Symmetry transformation used to generate equivalent atoms: A: -x, -y+1, -z; B: x-1, y, z, C: -x+1, -y+1, -z.

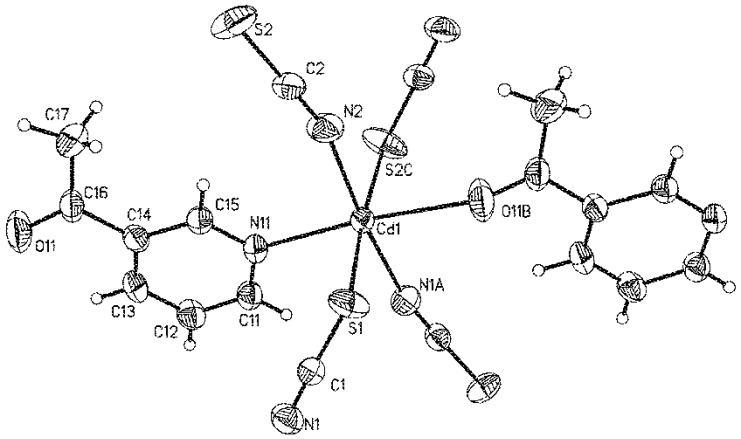

Figure S8. Crystal structure of compound **1C** with labeling and displacement ellipsoids drawn at the 50 % probability level. Symmetry transformation used to generate equivalent atoms: A: x,-y+1,z-1/2; B: x-1,y,z-1; C: x,-y,z-1/2.

7

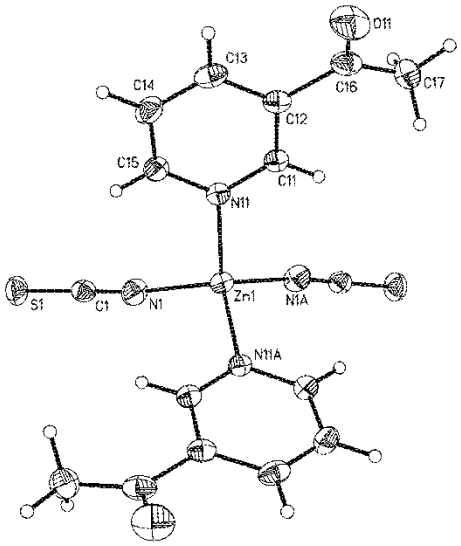

Figure S9. Crystal structure of compound **2A** with labeling and displacement ellipsoids drawn at the 50 % probability level. Symmetry transformation used to generate equivalent atoms: A: -x+1,y,-z+1/2.

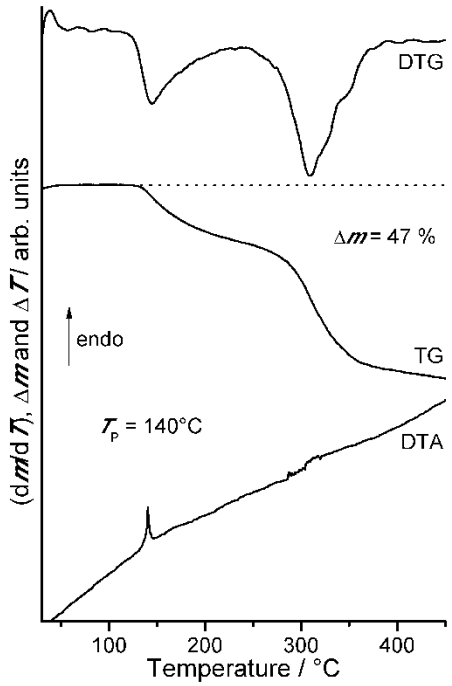

Figure S10. DTG, TG and DTA curves for compound $[Zn(NCS)_2(3\text{-Acpy})_2]$ (**2A**). Heating rate = 1 °C·min^{-1}; given are the mass changes [%] and the peak temperatures T_P [°C].

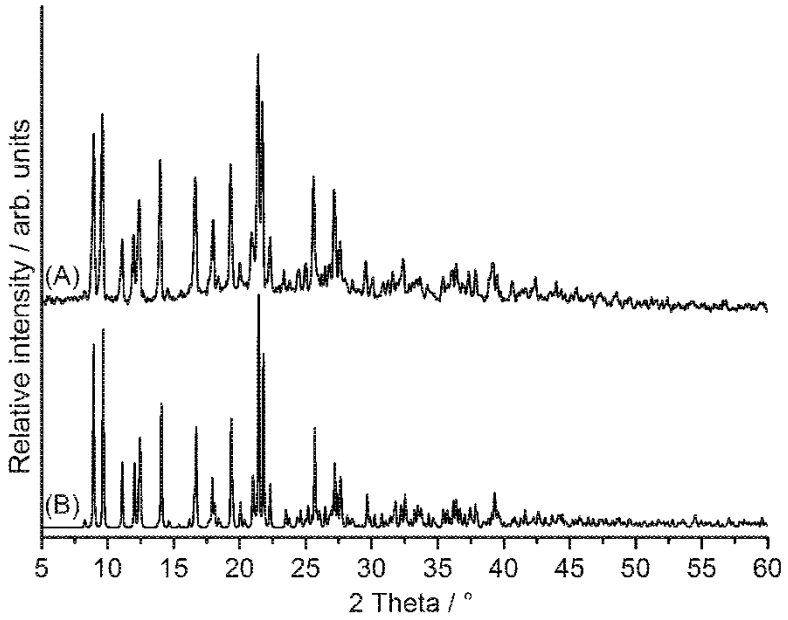

Figure S11. Experimental (A) and calculated (B) XRPD pattern for compound **1A**.

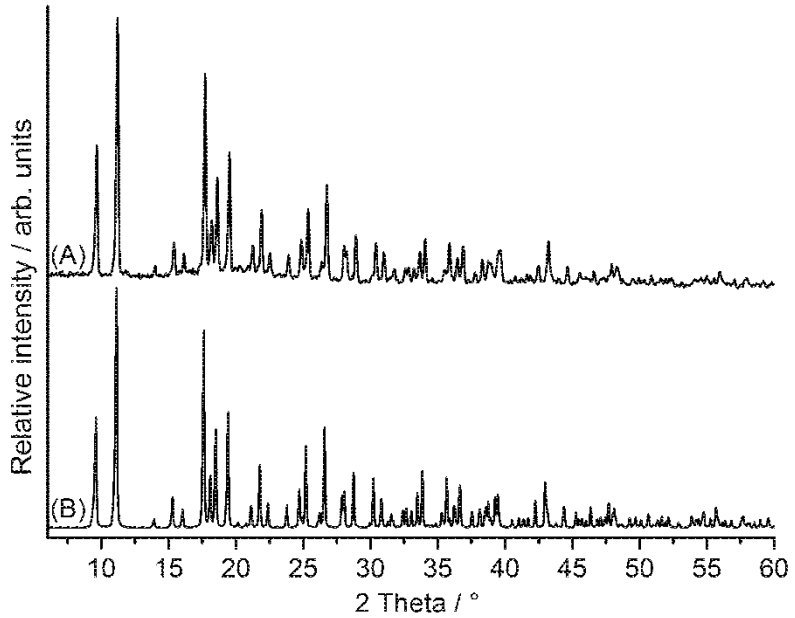

Figure S12. Experimental (A) and calculated (B) XRPD pattern for compound **1B**.

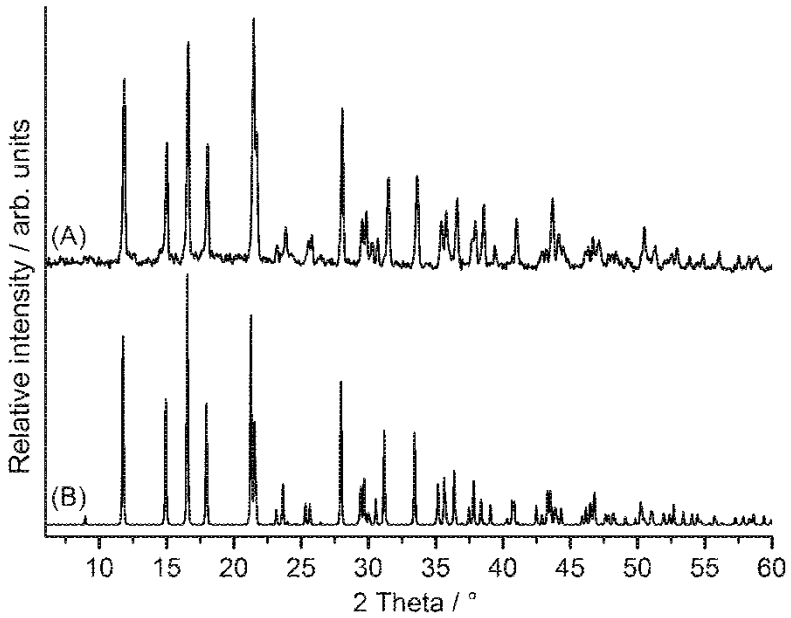

Figure S13. Experimental (A) and calculated (B) XRPD pattern for compound **1C**.

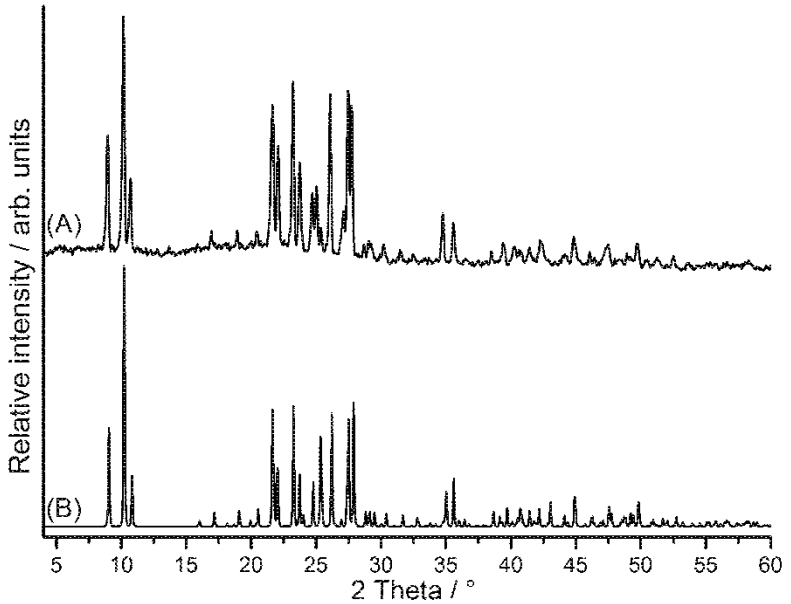

Figure S14. Experimental (A) and calculated (B) XRPD pattern for compound **2A**.

9. Erklärung

Hiermit versichere ich an Eides statt, dass ich, Julia Werner, die vorliegende Arbeit selbständig — abgesehen von der Beratung durch meinen wissenschaftlichen Lehrer — und nur unter Verwendung der angegebenen Hilfsmittel angefertigt habe. Die Arbeit ist unter Einhaltung der Regeln guter wissenschaftlicher Praxis der Deutschen Forschungsgesellschaft entstanden. Die Dissertation wird ausschließlich an dieser Stelle zur Promotion vorgelegt. Zusätzlich erkläre ich, dass ich noch keinen Promotionsversuch, weder an dieser noch an einer anderen Hochschule, unternommen habe.

Kiel, Juli 2015